Emissive Monocopper Amidophosphine Complexes

–and–

Lewis Acid-Assisted Reductive Coupling of Carbon Monoxide

Thesis by

Alexander J. M. Miller

In Partial Fulfillment of the Requirements for the

Degree of Doctor of Philosophy

CALIFORNIA INSTITUTE OF TECHNOLOGY
Pasadena, California
2011
(Defended November 12, 2010)

For my grandfathers.

Acknowledgements

During my time in Pasadena I have had the incredible fortune of being surrounded by a supportive and brilliant community of advisors, friends, students, and staff. In the interest of brevity, I can't thank everyone personally; but it takes a shocking number of people to grow a PhD from seed to fruit and I extend my gratitude to everyone who has been a part of my time at Caltech.

My first thanks must be directed at John Bercaw, who welcomed me without hesitation (as far as I know…) into his research group when I was hoping for a safe landing. John allowed me nearly limitless intellectual and creative freedom, and was always willing (OK, sometimes begrudgingly) to sit down on short notice and bounce ideas around. John's firm but *quiet* mentoring methods resonate with me; he guided our research like the group hikes he led, letting us discover the Sierras for ourselves instead of loudly leading the charge. Jay Labinger sat with me through more moments of scientific shock, confusion, and reassessment than either of us might care to admit. As I dug myself deeper into mechanistic conundrums and paradoxes, Jay was with me all the way, finding the perfect experiment to pull me out of the hole. It has been an honor to work with both of you.

Before joining John and Jay, I had a great experience in the Peters group. Jonas' enthusiasm for chemistry helped draw me to Caltech, and his support both during my time in the group and afterwards has been unwavering. It's good to have you and the group back West.

Caltech is a phenomenal academic environment, with a warmth and openness that fosters collaboration and the genesis of great ideas. My ever-expanding committee was a source of great guidance and advice on matters from optimizing synthetic strategies to contemplating career decisions. I owe great debts to my Committee Chair Brian Stoltz, as well as additional members Bob Grubbs and Theodor Agapie, who all gladly sat down with me individually and let me bounce ideas off of them. Outside of my committee, Harry Gray has been fantastic, sponsoring me as an honorary group member, and always exuding pure class. Jay Winkler and Bruce Brunschwig have both been sources of help in spectroscopic times of need.

Beyond the steering of my advisors, the amazing staff at Caltech has been instrumental in making the research possible. The NMR facilities are great and steadily reaching higher levels under the direction of David Vander Velde and Scott Ross. Dave in particular helped with 2-D, diffusion, and multinuclear NMR experiments. Mona Shahgholi and Naseem Torian in the Mass Spectrometry Facility did a great job handling air-sensitive compounds. Angelo Di Bilio guided me through an EPR GLA-ship and helped with experiments. Without Larry Henling and Mike Day, none of the crystal structures would have been obtained. Larry has spent many memorable hours patiently watching while I piddled around solving structures and learning just enough crystallography to be a danger to myself. Mike taught me the theory of crystallography, and then made sure all my poor quality data sets came out looking as good as they possibly could. Rick Gerhart was flexible when I broke a crucial piece of glassware at just the wrong time, or when I tried to design some fancy new apparatus; it was always a fun trip to the basement. As a Safety Officer I got to know Art Seiden, Larry Martinez, and Paul Carroad, who work hard to keep our labs safe

and running smoothly, and should not be forgotten. Without Rick Germond (the silky voice of the Central Warehouse), Joe Drew, and Tom Dunn all the chemistry groups would fall apart. Finally, Pat Anderson made dreaded paperwork enjoyable and the Division Office made that paperwork run smoothly: Anne Penney, Agnes Tong, and predecessors Laura Howe and Dian Buchness all deserve many thanks. Ernie catered much of my PhD affair, and Jerry and the staff at the Athenaeum served up libations.

In both research groups I have had the honor of working with brilliant chemists who doubled as talented, fun, kick ass people. A lot of my habits were formed in the Peters group, and I think most of them are good ones, thanks in particular to Dr. Bruce MacKay, who instinctively brought me under his wing as a postdoc, and Dr. Matt Whited, my "(g)lovebox mate" for a year in Box 1 and an awesome partner in chemistry and wine enthusiasm long after that. There was great leadership in the group, and Christine Thomas, Connie Lu, Mark Mehn, and Louise Berben and Xile Hu were fonts of knowledge (and entertainment), and Seth Harkins dropped by a few times to talk luminescence. Credit goes to Arjun Mendiratta for helping to keep me balanced, growing my wine habit and organizing adventures to quirky musical events. And for Halloween parties. Caroline, the brave solider who went there and back again with Jonas, has kept me in touch with the group and been a great resource and friend.

The transition between groups was seamless, and I can't thank the Bercaw group enough for welcoming me and collaborating on great science and "good times". I think I can safely say that fellow wanderers Valerie Scott, Paul Oblad, and Ted Weintrob got similar treatment. Dave Weinberg, my labmate, roommate, teammate, and nearly desk neighbor,

is a true legend, attacking life with a zeal that I remain in awe of. The kindness of Nilay Hazari, always available to talk science, cheer me up, and throw a ball around, will never be forgotten; nor will his ninja-like laboratory skills, as he stealthily and methodically completed project after project, inspiring the group. As I grew to a wise old graduate student age, and my habits became more and more entrenched (not to mention my need for caffeine), my good friends Ian Tonks, Steve Baldwin, and Ned West made a habit of taking a stroll for a soda precisely between 2 and 2:30 every afternoon. Those walks helped keep me sane and formed a strong bond with those fellows. Rachel Klet, my tail, evolved from a wide-eyed pupil as a first year to a trusted friend and chemical sparring partner. My collaborators on syngas chemistry were always a pleasure to work with: Paul Elowe, Aaron Wilson, Ned West, Sze-Man Yu, Amaruka Hazari, and Carl Laskowski. Lastly, I must mention the great sports teams of the Bercaw lab. Jeff Byers drafted me while I was still working for Jonas and from that time until my recent retirement the sense of team pride and effort put forth for Bearcaw Bulls basketball was inspiring, and the selfless fun-first attitude of the Cp All-Stars softball team led us to great successes. There are too many people to go into more depth here, without rambling on too long: Travis Williams, Bolin Lin, George Chen, Suzanne Golisz (football host extraordinaire!), Taylor Lenton, Ross Fu, Yan-Choi Lam, Matt Winston, and Emmanuelle Despagnet-Ayoub. Thanks to all, and all the best moving forward.

I've been fortunate to work with some great undergraduate students. They taught me as much as I taught them. Alexandra Velian and I were both first years at Caltech when we met, and I was so proud to watch her grow up as a scientist, and I'm sure she watched me develop as a mentor as well. Little Alex was a pleasure to mentor, and I won't forget the

transformation that took place as she learned to design her own experiments and interpret her own results, and *took hold* of her chemistry. Over 4 years, across two research groups, I always had a friend and colleague nearby. I'm excited to reunite with Dalina Thrift-Viveros, who I spent a shorter but similarly rewarding time working with, and see how far she has come since moving on to graduate school at the University of Washington.

None of this would be possible without my family. First and foremost, gratitude goes to my parents, who first inspired and then supported my academic pursuits. From sneaking my mother into conferences because she just *had* to see me speak, to plumbing the merits of scientific curricula at various institutions with my father, it has been a pleasure to share my science with you both. My grandparents always echoed this support; conversations and recipes from my grandmother Anne Minden helped get me through the tough times. In some ways it is that generation that I see more directly in myself: my father's father James Miller Jr. was a wordsmith and Professor of English; my mother's father Joseph Minden was a surgeon with stellar hands; I like to think I combine these genetic traits as I carry out and then write about my research. The last words go to Jillian Dempsey, the love of my life, who already feels like family, and who has made my time at Caltech enjoyable in every aspect. I am so lucky to have someone to bounce ideas off of, to take care of me when I fall ill in so many peculiar ways, and to go on adventures with all over Southern California. I can't wait for more adventures in the future.

Abstract

Two major themes are presented, in roughly chronological order: the synthesis and characterization of photoluminescent copper complexes are described, followed by studies on the selective conversion of synthesis gas (CO and H_2) to oxygenates. With the latter comprising the majority of the work, it is the subject of the introductory Chapter 1. In Chapter 2, the photoluminescent copper chemistry is introduced, and the synthesis and photophysics of monomeric amidophosphine complexes of copper is presented. The copper complexes are exceptional luminophores, with quantum efficiency up to 70% and lifetimes up to 150 μs. In Chapter 3, homogeneous CO hydrogenation is pursued using a strategy reliant on the incorporation of pendent Lewis acidic groups into the secondary coordination sphere of a metal carbonyl complex. This design feature promotes facile C–H and C–C bond formation, with transition metal hydrides as the hydrogen source. A structure-function study investigating the specific role of the Lewis acid determined that the first C–H bond formation is not particularly sensitive to the acid, whereas the second C–H bond formation and C–C coupling are both *highly* sensitive to the length of the tether between the metal and the borane. In Chapter 4, this chemistry is extended to utilize dihydrogen *directly* as a reductant, in a "frustrated Lewis pair" (FLP) mechanism. A strong phosphazene base is too bulky to interact with the pendent borane, but can heterolytically cleave dihydrogen in concert with the borane to generate a borohydride that transforms the carbonyl ligands into a metal-bound C_2 organic fragment. In Chapter 5, Lewis acidic boranes are again employed as promoters of reductive chemistry, this time for CO_2 reduction. The same late transition metal hydrides that were employed for CO reduction,

such as $[HNi(dmpe)_2][BF_4]$ (dmpe = 1,2-bis(dimethylphosphino)ethane), are able to reduce CO_2 gas when used in concert with the appropriate borane, affording a borane-formate adduct. In Chapter 6, the "frustrated Lewis pair" concept is extended to a different problem: the dehydrogenation of amine-boranes, which are candidates for hydrogen storage applications. Treatment of amine-boranes with the FLP $^t Bu_3P/B(C_6F_5)_3$ effects rapid and quantitative transfer of H_2 from the amine-borane, forming cyclic aminoborane products along with $[^t Bu_3PH][HB(C_6F_5)_3]$. Appendices are provided, including early work on Brønsted acid-assisted CO reduction, speciation of trialkylborohydrides, tabulating NMR impurities in deuterated solvents of interest to the organometallic chemist, and crystallographic tables.

Table of Contents

List of Figures

Chapter 2

Chapter 3

Chapter 4

Chapter 5

Chapter 6

Appendix A

Appendix B

List of Tables

Chapter 1

Introduction: Synthesis Gas as an Alternative Fuel and Chemical Feedstock

Adapted in part from:
West, N. M.; Miller, A. J. M.; Labinger, J. A.; Bercaw, J. E. *Coord. Chem. Rev.* **2010**, *In press*.

Chapter 1

Background

Faced with political and socioeconomical pressures to move away from petroleum-derived fuels and chemicals, various alternative feedstocks are currently the focus of intense research.[1] Synthesis gas (or syngas, a mixture of H_2 and CO) is an attractive feedstock, as it is readily obtained from natural gas, coal and biomass on industrial scales—albeit at a steep energy cost due to the high temperatures required to drive the uphill reaction.[2] Research in the field of syngas conversion received sparks in 1902, when Sabatier reported methanation over nickel,[3] and in 1926, when Fischer and Tropsch obtained liquid hydrocarbons.[4] While syngas conversion to a variety of C_1 products, notably methanol and acetic acid, is efficient and selective (and widely practiced on an industrial scale), conversion to more complex C_{2+} products (either hydrocarbons or oxygenates) is more problematic. The main issue is selectivity: the Fischer-Tropsch reaction generates a Schultz-Flory distribution of hydrocarbons, for which the ability to select for any particular desired range of products, such as diesel, is limited. The high costs of separation or refining make the Fischer-Tropsch process economically unfeasible in most cases, but there *are* some geopolitical climates where coal- or gas-to-liquids chemistry is financially viable, and large-scale plants have come online in places such as South Africa and Malaysia.[5] Only limited success in selective formation of higher alcohols and other oxygenates has ever been achieved.

Homogeneous catalysts, which often perform reactions faster and more selectively than their heterogeneous counterparts, are attractive alternatives to current Fischer-Tropsch technology. Homogeneous catalysts usually feature a single well-defined reactive site that can be "tuned" (by ligand design or alteration, for example) to tailor product distribution; such strategies are often guided by insights from mechanistic studies. Rational modification of heterogeneous catalysts is more difficult.

Homogeneous approaches to synthesis gas hydrogenation and oligomerization[6] were first reported by Dupont in the early 1950s, using cobalt catalysts operating under extremely high syngas pressures (1500-5000 atm).[7] Research efforts intensified during the oil crisis of the 1970s and early 1980s, and a number of other catalysts, including complexes of Rh, Fe, Ru, and Ir, were reported to similarly hydrogenate CO;[6b] high pressures are still required (generally over 1000 atm) and methanol is the major product, with low yields of C_{2+} products (mostly ethylene glycol). The mildest conditions for the homogeneous reaction were found using $Ru_3(CO)_{12}$ as the precatalyst, at pressures as low as 100 atm, but still affording methanol as the major product.[8]

The presence of a Lewis or Brønsted acid appears to be critical to C_{2+} product formation in the homogeneous systems as well as heterogeneously catalyzed Fischer-Tropsch reactions.[9] Ethane and higher hydrocarbons were obtained using $Ir_4(CO)_{12}$ in a $NaCl/AlCl_3$ melt;[10] Os and Rh carbonyl complexes display similar reactivity in the presence of BBr_3 or $AlBr_3$.[11] Carboxylic acid solvents help direct the reactivity of $Ru_3(CO)_{12}$ from methanol synthesis (observed in many organic solvents) to ethylene glycol (as the diester).[8] Rh carbonyl catalysts can give ethylene glycol selectivities up to 75% at 200-230 °C, under 2200-2400

psi of 1:1 H_2/CO, and with the addition of Lewis bases and alkali cations.[6b,c,12] There has been little improvement of these processes since their disclosure.

The extreme conditions required for these reactions might result from the difficulty of forming the first C–H bond. Mechanistically speaking, the C–H bond-forming step could involve (kinetically disfavored) intramolecular insertion of CO into an M–H bond or intermolecular attack of a (weakly nucleophilic) metal hydride on a metal carbonyl complex. The Lewis acidic additives could promote glycol formation by facilitating the insertion of CO into intermediate M–C (or even M–H) bonds by binding to the carbonyl oxygen. In combined Rh/Ru catalysis, 10 times more Ru than Rh was required and the C_1/C_2 product selectivity displayed concentration dependence on Rh but not Ru, suggesting that Ru serves as the hydride source while CO reduction and coupling occurs on the Rh center.[6c,13]

The mechanistic uncertainty surrounding homogeneous syngas conversion sparked interest in model compounds bearing more complex ligands. The following organometallic approaches to the development of new catalysts, spanning the periodic table, form the foundation of current syngas conversion chemistry.

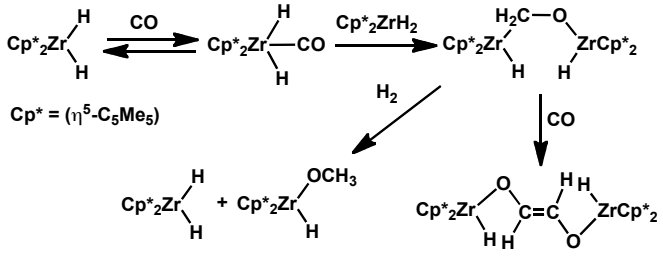

Scheme 1.1

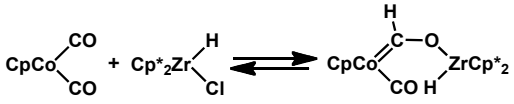

Scheme 1.2

In a seminal contribution, Bercaw and coworkers showed that $Cp^*_2ZrH_2$ (formed by H_2 addition to a highly reducing Zr^{II} precursor) would react with CO to form methoxide or bridging ene-diolate species (Scheme 1.1). A large number of early metal and f-block systems that carry out similar transformations have since been reported,[14] even though it is now well established that migratory insertion of CO into a M–H bond is highly endoenergetic.[15] Rather than migratory insertion, the mechanism of CO reduction (in all but one case[16]) relies on the nucleophilic character of early transition metal hydrides. Early transition metal hydrides can be extremely hydridic,[17] which has been exploited for a number of stoichiometric reductions of CO, such as the Zr–H reduction of a Co–CO species shown in Scheme 1.2.[18] The rather less nucleophilic Cp_2NbH_3 reacts with $Cr(CO)_6$, at only slightly elevated temperature, to produce ethane.[19] In a report of relevance to homogeneous syngas conversion catalysis, Dombek showed that the proposed intermediate $[HRu(CO)_4]^-$ can reduce $[CpRe(CO)_2NO]^+$ to the corresponding formyl.[20]

Electron-rich early metal complexes also react with CO in the absence of H_2 to give oligomerization products that could, in principle, be converted to organics. Early work on CO reductive coupling by Lippard (early transition metals)[21] and Evans (lanthanides)[22] has recently been complemented by Cloke (uranium)[23] to generate a wide range of metal-bound CO oligomers, such as ketenecarboxylate, deltate, and squarate complexes. The potent reducing agents required to activate the metals for reactivity with CO probably preclude applications for syngas conversion.

In general, early metal systems also are not viable candidates for catalytic processes involving oxygenates: extremely strong M–O bonds are invariably formed in these reactions with such electropositive metals, and these bonds cannot be cleaved to close a catalytic cycle. It is quite possible that some or all of the known catalytic reactions that produce alcohols proceed via the general M–H transfer to M–CO route; but those systems involve less nucleophilic late transition metal complexes — and probably as a result require fairly extreme conditions to induce hydride transfer (while avoiding the strong M–O bonds).

Elements from the middle of the transition series generally form much weaker bonds to oxygen, thereby avoiding one major drawback of CO reduction on early metals. While the first reported transition metal formyl complex, $[Fe(CO)_4(CHO)]^-$, was synthesized by addition of nucleophilic $[Fe(CO)_4]^{2-}$ to formic acetic anhydride,[24] it quickly became clear that M–CO reduction by strong hydride sources was a general route to formyl complexes.[25] The most studied formyl species are of the type Cp´Re(NO)(L)(CHO) (Cp´ = Cp, Cp*; L = CO, PPh_3) formed from the carbonyl cation and a borohydride reagent.[26]

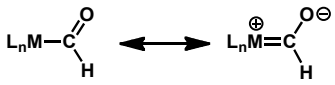

Scheme 1.3

Two resonance structures, one best described as a formyl and the other as a carbene, contribute to the stability and reactivity of these species (Scheme 1.3). Formyl species are generally regarded as quite potent hydride donors themselves,[27] transferring H^- and

reforming M–CO; carbene species render the oxygen nucleophilic,[25] capable of coordinating to electrophiles.

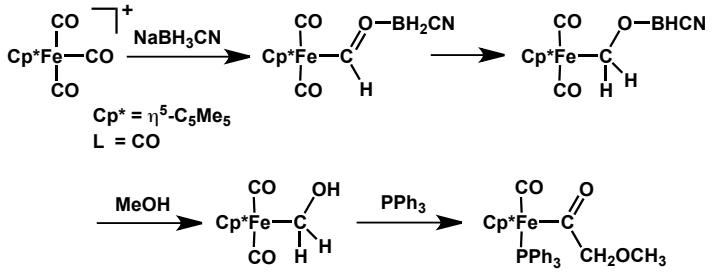

Scheme 1.4

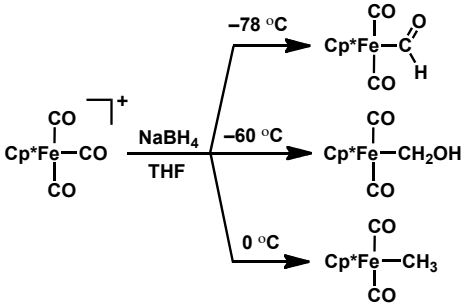

Scheme 1.5

Coordination of an electrophile to the formyl oxygen favors reduction at carbon, and use of reagents such as $NaBH_4$ or $LiAlH_4$ can result in multiple reductions of a carbonyl ligand: after the first hydride is delivered, Lewis acidic BH_3 or AlH_3 can coordinate to the formyl oxygen, activating the ligand towards futher reduction (Scheme 1.4). Species such as $CpRe(NO)(CO)_2^+$ and $CpFe(CO)_3^+$ can be reduced to a variety of products depending on conditions: formyl, hydroxymethyl, or methyl species (Scheme 1.5).[26b,26d,28]

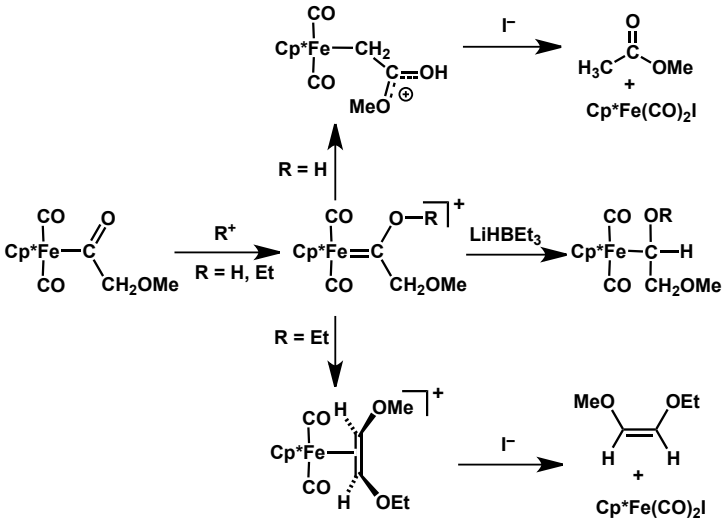

Scheme 1.6

Integration of stepwise reduction schemes, alternating strong reductants and electrophiles (Scheme 1.4) with chemistry to release reduced products from the metal (Scheme 1.6) enables stoichiometric formation of C_{2+} organics from CO and H^-/H^+.[29] Such schemes remain far from catalytic, however, as the reagents for each sequential step are incompatible with each other.

Late metals can also support CO reduction chemistry, usually by a very different mechanism involving radical chemistry. A wide body of work by Wayland and coworkers is typified by the reaction of (octaethylporphyrin)rhodium hydride with CO to afford a formyl:[30] the net CO insertion actually results from H-atom transfer (not H^- transfer) to a metalloradical Rh–CO species.[31] The chemistry can be modulated by alteration of the ligand and reaction conditions to selectively form Rh–CHO, Rh–C(O)–Rh, or Rh–C(O)C(O)–Rh species.[32] Organic products have not been released from these systems, however; one reason could be that the very strong Rh–C bonds are hard to cleave, reminiscent of the strong M–O bonds of early metals.

New strategies for homogeneous CO hydrogenation

Clearly, selective conversion of syngas to multicarbon products under mild homogeneous conditions faces a number of hurdles, and new tactics are required in the pursuit of a catalyst. Our approach in this area was initially guided by DuBois and coworkers' discovery that bis(diphosphine) hydride complexes of late transition metals (Co, Rh, Ni, Pd, and Pt) can be surprisingly nucleophilic, and can furthermore be formed by the heterolytic cleavage of dihydrogen in concert with an appropriate base (Scheme 1.7). The choice of metal along with a number of ligand steric parameters enables the "hydricity" or hydride donor strength (ΔG_{H^-}) to be tuned along a vast continuum: from neutral Rh^{I} hydrides, similar in strength to "Super-hydride" ($[HBEt_3]^-$), to cationic Ni^{II} hydrides better described as acids than hydrides.

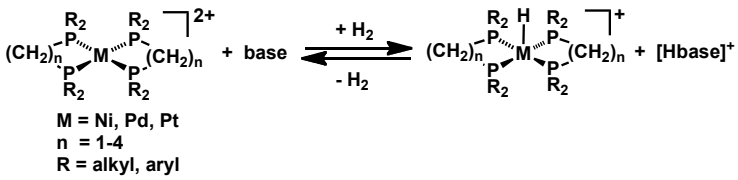

Scheme 1.7

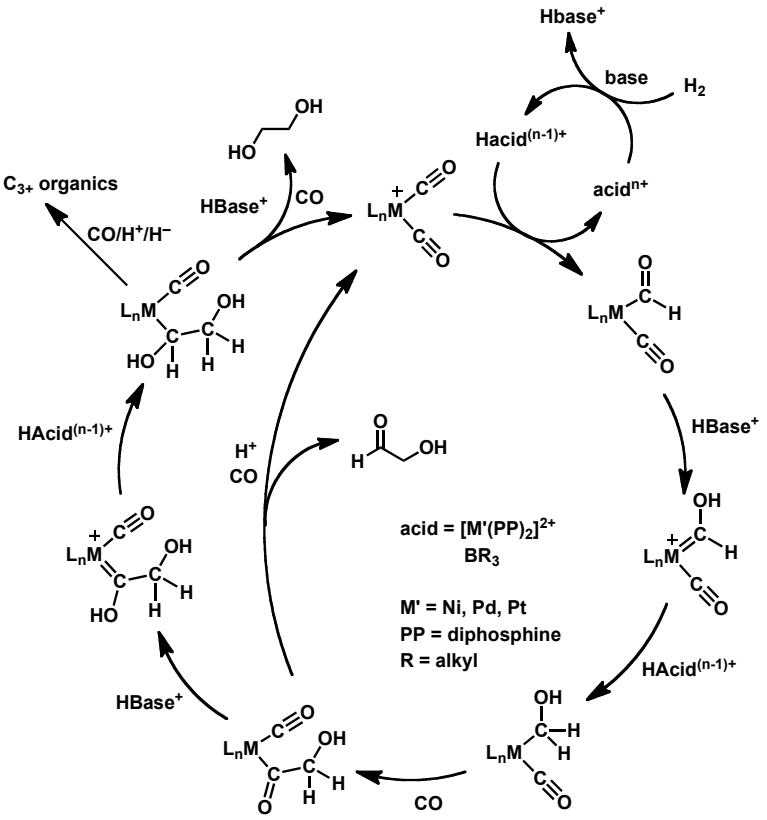

Scheme 1.8

In conjunction with DuBois' results, the work summarized above provides fairly clear guidelines for a viable approach to selective homogeneous syngas conversion based on a two-catalyst system, where one metal complex acts as a scaffold for CO reduction, while the other delivers hydride. The metal carbonyl must be sufficiently electrophilic to accept a hydride, and the metal hydride must be sufficiently nucleophilic, but neither can be so oxophilic that strong M–O bond formation would preclude catalysis. One vision for such a cycle is shown in Scheme 1.8. A stoichiometric version of this cycle was indeed established using a fairly hydridic platinum hydride;[33] but similar to earlier work using stronger main group hydrides, the electrophilic reagents of Scheme 1.9 were incompatible with the Pt–H bond.

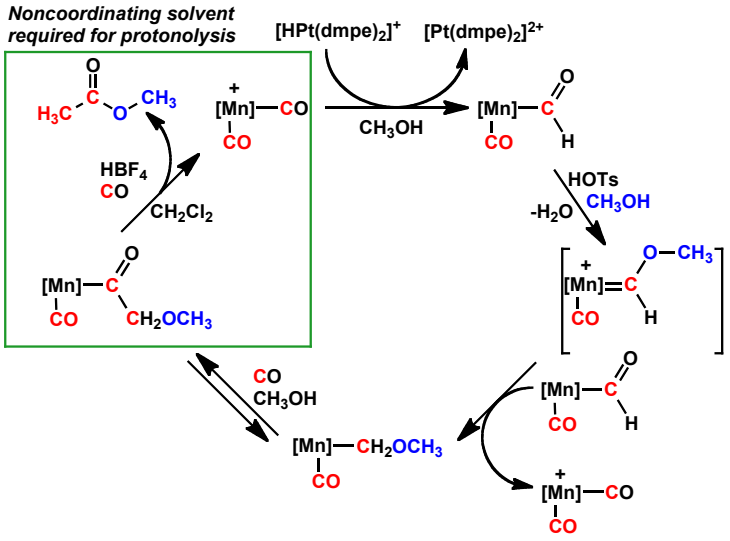

Scheme 1.9

In order to avoid such reactivity, we chose to add additional reactive centers. The combination of transition metal complexes with Lewis or Brønsted acids appears to be beneficial in several different ways, for example promoting both hydride transfer to CO and C–C bond forming reactions. Aiding these steps might permit the use of weaker hydrides or lower pressures of CO (to induce migratory insertion). Directly attaching the acidic center to the metal could bestow additional advantages, utilizing the chelate effect to enhance acid promotion.

With these goals in mind, we set out to synthesize bifunctional metal carbonyl complexes containing pendent alkylborane moieties, and investigate their reactivity with late transition metal hydride donors and H_2 itself. We find that Lewis acids indeed engender unique reactivity to a variety of metal centers and transformations. With a focus on CO reduction, we showed that — depending on the acid strength and length of tether — both C–H and C–C bond formation are promoted by pendent boranes. These boranes can even

participate in "frustrated Lewis pair" chemistry[34] (in which the acid and base are too sterically encumbered to form a traditional Lewis adduct) to utilize dihydrogen directly to reduce metal carbonyl complexes. We also show that Lewis acids can aid in another C–H bond-forming reaction, hydride transfer from a nickel hydride to CO_2. Finally, "frustrated Lewis pairs" are further explored, with studies on the dehydrogenation of potential hydrogen storage candidate amine-boranes.

References

1. World Energy Assessment Report: Energy and the Challenge of Sustainability. Program, U. N. D., Ed. United Nations: New York, 2000.
2. Navarro, R. M.; Pena, M. A.; Fierro, J. L. G. *Chem. Rev.* **2007**, *107*, 3952.
3. Sabatier, P.; Senderens, J. B. *C. R. Hebd. Seances Acad. Sci.* **1902**, *134*, 514.
4. Fischer, F.; Tropsch, H. *Ber. Dtsch. Chem. Ges.* **1926**, *59*, 830.
5. Khodakov, A. Y.; Chu, W.; Fongarland, P. *Chem. Rev.* **2007**, *107*, 1692.
6. (a) Dombek, B. D. *Adv. Catal.* **1983**, *32*, 325; (b) Marko, L. *Transition Met. Chem.* **1992**, *17*, 474; (c) Whyman, R.; Wright, A. P.; Iggo, J. A.; Heaton, B. T. *J. Chem. Soc., Dalton Trans.* **2002**, 771.
7. (a) Gresham, W. F.; Schweitzer, C. E. Homogeneous Co FT. 2534018, 1950; (b) Gresham, W. F. Homogenous Co FT-2. 2636046, 1953.
8. Dombek, B. D. *J. Am. Chem. Soc.* **1980**, *102*, 6855.
9. Maitlis, P. M.; Zanotti, V. *Chem. Commun.* **2009**, 1619.
10. (a) Demitras, G. C.; Muetterties, E. L. *J. Am. Chem. Soc.* **1977**, *99*, 2796; (b) Wang, H.-K.; Choi, H.-W.; Muetterties, E. L. *Inorg. Chem.* **1981**, *20*, 2661; (c) Collman, J. P.; Brauman, J. I.; Tustin, G.; Wann, G. S. *J. Am. Chem. Soc.* **1983**, *105*, 3913.
11. (a) Choi, H.-W.; Muetterties, E. L. *Inorg. Chem.* **1981**, *20*, 2664; (b) Lapidus, A. L.; Savelev, M. M.; Kondratev, L. T.; Yastrebova, E. V. *Izv. Akad. Nauk. SSSR, Ser. Khim.* **1981**, 1564.
12. (a) Pruett, R. L. *Ann. N. Y. Acad. Sci.* **1977**, *295*, 239; (b) Kiso, Y.; Tanaka, M.; Hayashi, T.; Saeki, K. *J. Organomet. Chem.* **1987**, *322*, C32.
13. Whyman, R.; Gilhooley, K.; Rigby, S.; Winstanley, D., In *Industrial Chemicals via C1 Processes, ACS Symposium Series No. 328*, Fahey, D. R., Ed. American Chemical Society: Washington, D. C., p 108.
14. West, N. M.; Miller, A., J. M.; Labinger, J. A.; Bercaw, J. E. *Coord. Chem. Rev.* **2010**, *In Press*.

15. Berke, H.; Hoffmann, R. *J. Am. Chem. Soc.* **1978**, *100*, 7224.
16. Fagan, P. J.; Moloy, K. G.; Marks, T. J. *J. Am. Chem. Soc.* **1981**, *103*, 6959.
17. Labinger, J. A.; Bercaw, J. E. *Organometallics* **1988**, *7*, 926.
18. Barger, P. T.; Bercaw, J. E. *Organometallics* **1984**, *3*, 278.
19. (a) Wong, K. S.; Labinger, J. A. *J. Am. Chem. Soc.* **1980**, *102*, 3652; (b) Labinger, J. A.; Wong, K. S.; Scheidt, W. R. *J. Am. Chem. Soc.* **1978**, *100*, 3254.
20. Dombek, B. D.; Harrison, A. M. *J. Am. Chem. Soc.* **1983**, *105*, 2485.
21. (a) Neithamer, D. R.; Lapointe, R. E.; Wheeler, R. A.; Richeson, D. S.; Vanduyne, G. D.; Wolczanski, P. T. *J. Am. Chem. Soc.* **1989**, *111*, 9056; (b) Carnahan, E. M.; Protasiewicz, J. D.; Lippard, S. J. *Acc. Chem. Res.* **1993**, *26*, 90.
22. (a) Evans, W. J.; Grate, J. W.; Hughes, L. A.; Zhang, H.; Atwood, J. L. *J. Am. Chem. Soc.* **1985**, *107*, 3728; (b) Evans, W. J.; Lee, D. S.; Ziller, J. W.; Kaltsoyannis, N. *J. Am. Chem. Soc.* **2006**, *128*, 14176; (c) Evans, W. J.; Davis, B. L. *Chem. Rev.* **2002**, *102*, 2119.
23. (a) Summerscales, O. T.; Cloke, F. G. N.; Hitchcock, P. B.; Green, J. C.; Hazari, N. *Science* **2006**, *311*, 829; (b) Summerscales, O. T.; Cloke, F. G. N., In *Organometallic and Coordination Chemistry of the Actinides*, Springer-Verlag Berlin: Berlin, 2008; Vol. 127, pp 87.
24. Collman, J. P.; Winter, S. R. *J. Am. Chem. Soc.* **1973**, *95*, 4089.
25. Gladysz, J. A. *Adv. Organomet. Chem.* **1982**, *20*, 1.
26. (a) Casey, C. P.; Andrews, M. A.; Rinz, J. E. *J. Am. Chem. Soc.* **1979**, *101*, 741; (b) Sweet, J. R.; Graham, W. A. G. *J. Organomet. Chem.* **1979**, *173*, C9; (c) Tam, W.; Wong, W.-K.; Gladysz, J. A. *J. Am. Chem. Soc.* **1979**, *101*, 1589; (d) Wong, W. K.; Tam, W.; Strouse, C. E.; Gladysz, J. A. *J. Chem. Soc., Chem. Commun.* **1979**, 530.
27. Wong, W.-K.; Tam, W.; Gladysz, J. A. *J. Am. Chem. Soc.* **1979**, *101*, 5440.
28. (a) Bodnar, T.; Coman, E.; Menard, K.; Cutler, A. *Inorg. Chem.* **1982**, *21*, 1275; (b) Tam, W.; Lin, G. Y.; Wong, W.-K.; Kiel, W. A.; Wong, V. K.; Gladysz, J. A. *J. Am. Chem. Soc.* **1982**, *104*, 141; (c) Lapinte, C.; Astruc, D. *J. Chem. Soc., Chem. Commun.* **1983**, 430.
29. Crawford, E. J.; Lambert, C.; Menard, K. P.; Cutler, A. R. *J. Am. Chem. Soc.* **1985**, *107*, 3130.
30. Wayland, B. B.; Woods, B. A. *J. Chem. Soc., Chem. Commun.* **1981**, 700.
31. Paonessa, R. S.; Thomas, N. C.; Halpern, J. *J. Am. Chem. Soc.* **1985**, *107*, 4333.
32. (a) Coffin, V. L.; Brennen, W.; Wayland, B. B. *J. Am. Chem. Soc.* **1988**, *110*, 6063; (b) Wayland, B. B.; Sherry, A. E.; Poszmik, G.; Bunn, A. G. *J. Am. Chem. Soc.* **1992**, *114*, 1673.
33. Elowe, P. R.; West, N. M.; Labinger, J. A.; Bercaw, J. E. *Organometallics* **2009**, *28*, 6218.
34. Stephan, D. W.; Erker, G. *Angew. Chem. Int. Ed.* **2010**, *49*, 46.

Chapter 2

Long-lived and Efficient Emission from Mononuclear Amidophosphine Complexes of Copper

Adapted in part from:
Miller, A. J. M.; Dempsey, J. L.; Peters, J. C. *Inorg. Chem.* **2007**, *46*, 7244.
http://dx.doi.org/10.1021/ic7009513

Chapter 2

Introduction

Highly luminescent transition metal complexes are widely studied[1] due to broad interest in their use for such applications as organic light-emitting diodes (OLEDs),[2] biological imaging,[3] photochemical catalysis,[4] and light-driven fuel production.[5] The best-studied luminophores are transition metal complexes of Ru, Re, and Pt. The large d-orbital splitting and high degree of spin-orbit coupling of second- and third-row transition metals are often cited as key factors in promoting excited state emission rather than non-radiative decay pathways[1a]—but such metals are often quite expensive. A general goal is to find alternative low cost emitters that also feature high quantum yields, long lifetimes, and tunable emission. To this end, the family of aluminum complexes exemplified by AlQ_3 ((8-quinolinolato)aluminum) warrants mention; these low cost complexes are commonly used as electroluminophores in organic light-emitting diodes (OLEDs).[2]

Copper luminophores[6] have been investigated as relatively inexpensive, biologically relevant[7] replacements for more ubiquitous Ru, Re, and Pt emitters. The most thoroughly studied Cu emitters are monomers supported by modified polypyridine and phenanthroline ligands, but these complexes often suffer from low quantum efficiencies and short luminescence lifetimes.[7] These deficiencies were assigned to multiple excited state processes: exciplex quenching, in which solvent binds the metal, and distortion of the ligands towards a square planar configuration could both be non-radiative processes. McMillin and

coworkers have demonstrated that bulky bidentate phosphines inhibit exciplex quenching, and mixed diphosphine-phenanthroline systems feature unusually long lifetimes and promising quantum efficiency (τ = 16 μs, ϕ = 0.16 in solution at 298 K).[8] Simple phosphine complexes of copper halides have also been reported,[9] and the effect of bulky diphosphine ligands on such complexes has recently been investigated.[10] While these complexes can be highly emissive in the solid state or in low-temperature solvent glasses, they display only faint, short-lived emission in solution at ambient temperatures.

The Peters group recently reported an amide-bridged dicopper complex, $\{(PNP)Cu^{I}\}_2$ ([PNP]$^-$ = bis(2-(diisopropylphosphino)phenyl)amide), that featured both long-lived and highly efficient emission (τ = 10.9(4) μs, ϕ = 0.67(4) in THF at 298 K).[11] The origin of the luminescence was elusive, however: isostructural complexes—with thioether donors in place of the phosphines ($\{(SNS)Cu^{I}\}_2$),[12] and with a phosphide bridging ligand in place of the amide ($\{(PPP)Cu^{I}\}_2$)[13]—show essentially no luminescence. One theory was that the specific dicopper structure (in the ground and excited state) was a key factor in promoting emissive relaxation processes. The distinct luminescence behavior of $\{(PNP)Cu^{I}\}_2$ thus motivated us to study related amidophosphine copper systems. Herein we report that *monomeric* amidophosphine copper complexes retain the general photophysical properties of $\{(PNP)Cu^{I}\}_2$, featuring high quantum efficiencies ($0.16 < \phi < 0.70$), long lifetimes (16-150 μs), and variable emission maxima (~ 500-550 nm) in solution at 298 K.[14]

Results and Discussion

Synthesis and physical characterization of [PN]Cu(L)$_2$

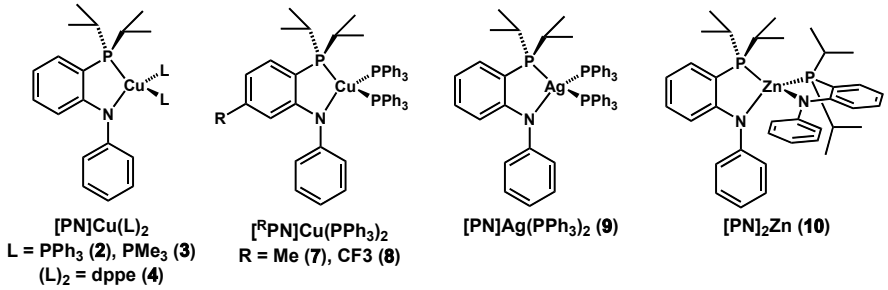

Scheme 2.1

A set of monomeric amidophosphine complexes of copper (general type [^{R}PN]Cu(L)$_2$), silver, and zinc was assembled (Scheme 2.1). The amidophosphine ligands used herein can be readily prepared in two steps. Buchwald-Hartwig coupling provided fluorine-substituted diarylamine precursors, and nucleophilic aromatic substitution by addition of Li$P^{i}Pr_2$ provided the desired ligands. The simplest precursor, 2-fluoro-diphenylamine, provides [PN]Li (**1**), which exhibits blue luminescence when irradiated with a UV lamp and features optical transitions at 411, 354, and 286 nm. A related ligand containing phenyl rather than isopropyl substituents at phosphorous has been reported by Liang.[15]

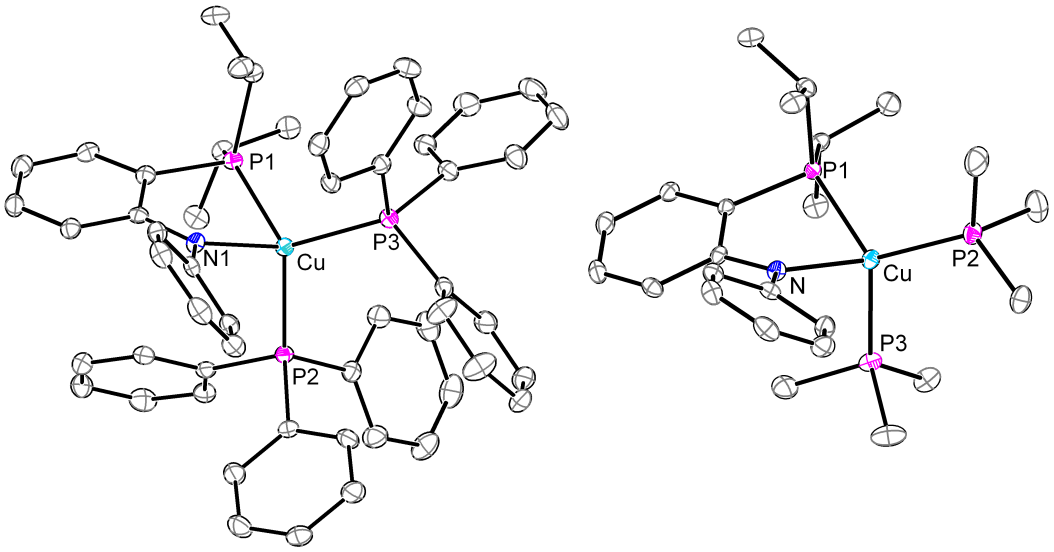

Figure 2.1. Structural representation of **2** (left) and **3** (right), with ellipsoids at 50% probability. Key bond lengths (Å) and angles (°) for **2**: Cu–N 2.083(1), Cu–P1 2.3173(5), Cu–P2 2.3319(5), Cu–P3 3.3261(6), N–Cu–P1 83.53(4). For **3**: Cu–N 2.086(1), Cu–P1 2.2744(5), Cu–P2 2.331(5), Cu–P3 2.2690(5), N–Cu–P1 82.54(4).

Addition of Et_2O solutions of [PN]Li to a stirring suspension of CuBr•Me_2S and the appropriate tertiary phosphine in Et_2O readily affords bright yellow Cu complexes [PN]Cu$(L)_2$ (Scheme 2.1; **2**, L = PPh_3; **3**, L = PMe_3; **4**, $(L)_2$ = dppe, 1,2-bis(diphenylphosphino)ethane). The expected monomeric, pseudotetrahedral structures were confirmed by X-Ray diffraction (XRD) analysis. The structures of **2** and **3** are shown in Figure 2.1; crystals of **4** suffered from severe twinning, but the overall connectivity was the same as **2** and **3**. $^{31}P\{^1H\}$ NMR spectra exhibited two broad resonances in a 2:1 ratio. Cyclic voltammetry of **2** shows a single reversible peak at –270 mV vs. Fc/Fc^+ (Figure 2.2), assigned to the $Cu^{II/I}$ couple.

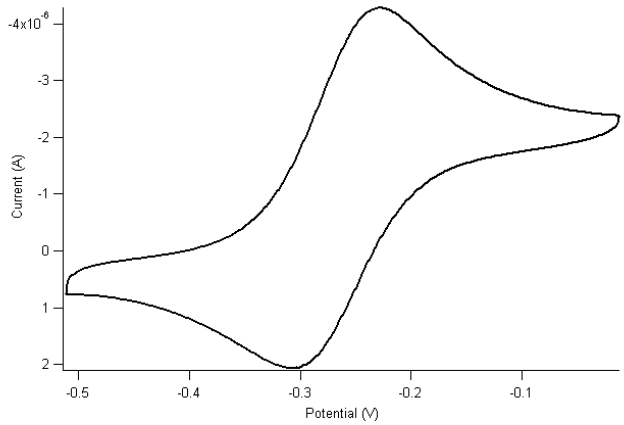

Figure 2.2. Cyclic voltammagram of $PNCu(PPh_3)_2$ (**2**).

Photophysical properties and comparisons

Absorption spectra of **2-4** in benzene feature similar peaks around 430 nm (ε = 2,000-2,500 $M^{-1}cm^{-1}$) and 350 nm (ε = 10,000-15,000 $M^{-1}cm^{-1}$), overlaid in Figure 2.3. Complexes **2-4** glow bright green under visible light, both in the solid state and in solution. Excitation into any absorption band leads to sharp, featureless emission at 298 K, with maxima at 504 nm for **2**, 497 nm for **3**, and 534 nm for **4** (Figure 2.4). The quantum efficiency of each complex in benzene solution at 298 K was assessed with excitation at 430 nm and 350 nm.[16] Quantum yields of the present complexes vary widely depending on the auxiliary ligand, from ϕ = 0.56 for **2**, to ϕ = 0.21 for **3** (Table 2.1). Such high solution quantum efficiency is unique among monomeric Cu systems,[17] as underscored in Table 2.1. When more polar solvents such as Et_2O or THF are employed, the luminescence efficiency is significantly attenuated, typically by ~50% (see Experimental Section for details).

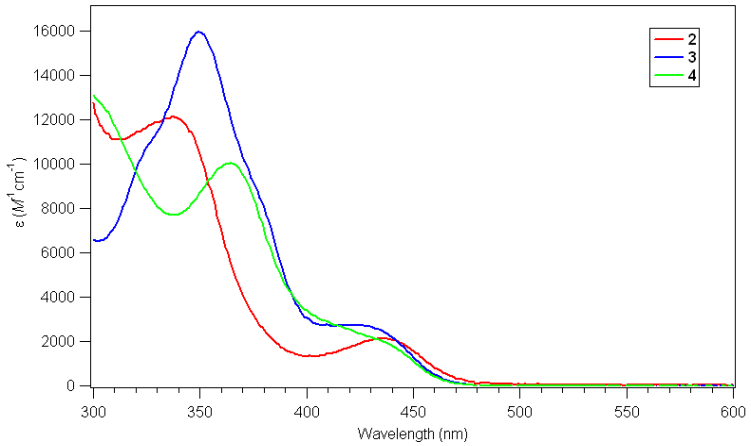

Figure 2.3. Overlay of absorption spectra of $PNCu(L)_2$ (L = PPh_3 (**2**), PMe_3 (**3**); $(L)_2$ = dppe (**4**) in benzene.

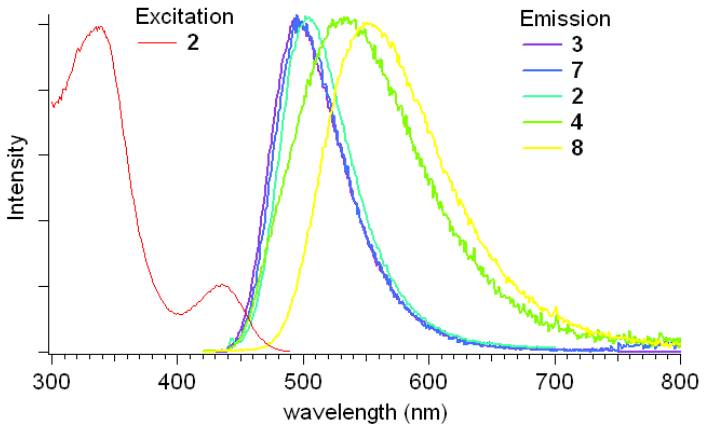

Figure 2.4. Excitation spectrum of **2** and normalized emission spectra of **2**, **3**, **4**, **7**, and **8**.

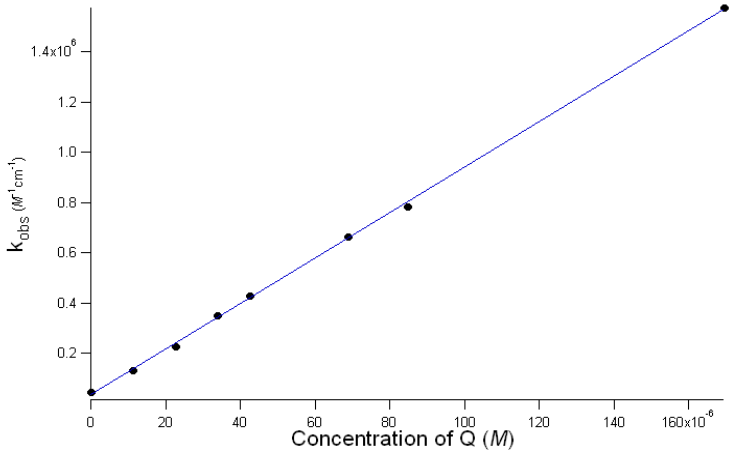

Figure 2.5. Oxidative quenching of [PN]Cu(PPh_3)$_2$ (2) with 2,6-dibenzoquinone (Q). y = $9.043x10^9$(x) + 36767, R^2 = 0.9997

The reducing power of excited-state complex **2*** can be estimated by taking the difference between E_{00} (2.65 eV, the emission/excitation crossover point) and the ground state $Cu^{II/I}$ couple, predicting a reduction potential of –2.9 V (vs. Cp_2Fe^+/Cp_2Fe). The excited state of **2** is extremely reducing compared to $[Ru(bpy)_3]^{2+*}$, –1.2 V, and [Cu(2,9-diphenyl-1,10-phenanthroline)$_2$]$^{+*}$, –1.5 V.[18] A quenching experiment showed that 2,6-dibenzoquinone oxidatively quenches **2***. A Stern-Volmer plot (luminescence decay rate vs concentration of quencher, Figure 2.5) shows a linear dependence; the slope is equal to the electron transfer rate, $k = 9.04x10^9$ M^{-1} s^{-1}, which indicates a diffusion-controlled electron-transfer process.

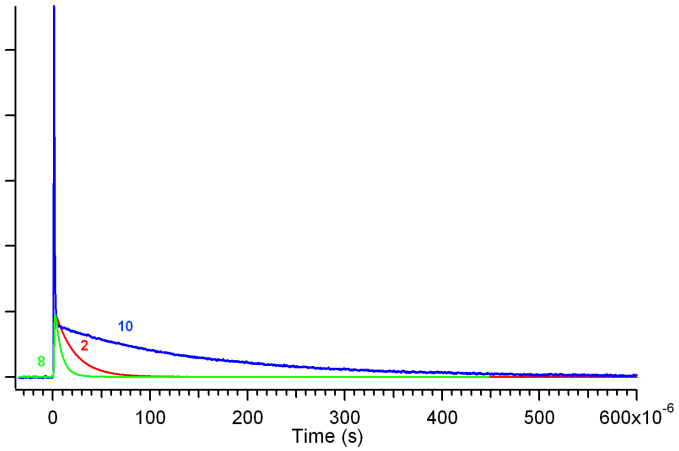

Figure 2.6. Luminescence decay traces of [^{Me}PN]Cu(PPh$_3$)$_2$ (7, green), PNCu(PPh$_3$)$_2$ (**2**, red) and [^{CF3}PN]Cu(PPh$_3$)$_2$ (**8**, blue) in C_6H_6 at 298 K (λ_{ex} = 430 nm).

Table 2.1. Photophysical Comparison of Cu Complexes at 298 K

Complex	Solvent	λ_{abs} (nm)	λ_{em} (nm)	ϕ_{em}[a]	τ (μs)
1	Et_2O	411	480	0.16	0.012(1)
2	C_6H_6	434	504	0.56	20.2(1)
3	C_6H_6	427	497	0.21	22.3(7)
4	C_6H_6	423	534	0.32	16.3(3)
7	C_6H_6	433	498	0.70	6.7(1)
8	C_6H_6	444	552	0.16	150(3)
[dbpCuPOP]$^+$	CH_2Cl_2	378	560	0.16	16.1
[dmpCudppe]$^+$	CH_2Cl_2	400	630	0.010	1.33
CuI(dppb)PPh$_3$	Me-THF	~380	550	0.01	<1

a. Quantum yields from this work are reported with confidence of ±5 on the last significant figure. b. Data reported in CH_2Cl_2. c. Data reported in 2-methyl-tetrahydrofuran. dbp = 2,9-di-*n*-butyl-1,10-phenanthroline; dmp = 2,9-dimethyl-1,10-phenanthroline; POP = bis[2-(diphenylphosphino)phenyl]ether; dppb = 1,2-bis[diphenylphosphino]benzene.

Complexes **2**, **3**, and **4** show long luminescence lifetimes in benzene solutions: 20.2(1) μs for **2** (Figure 2.6 and Table 2.1), 22.3(7) μs for **3**, and 16.3(3) μs for **4**. Interestingly, and in contrast to the quantum efficiency measurements, the lifetimes of **2**–**4** in Et_2O were virtually identical to those in benzene. We observe that the luminescence decay of PMe$_3$ adduct **3** has two components, with a small spike indicating the decay of a shorter-lived species (<10 ns).

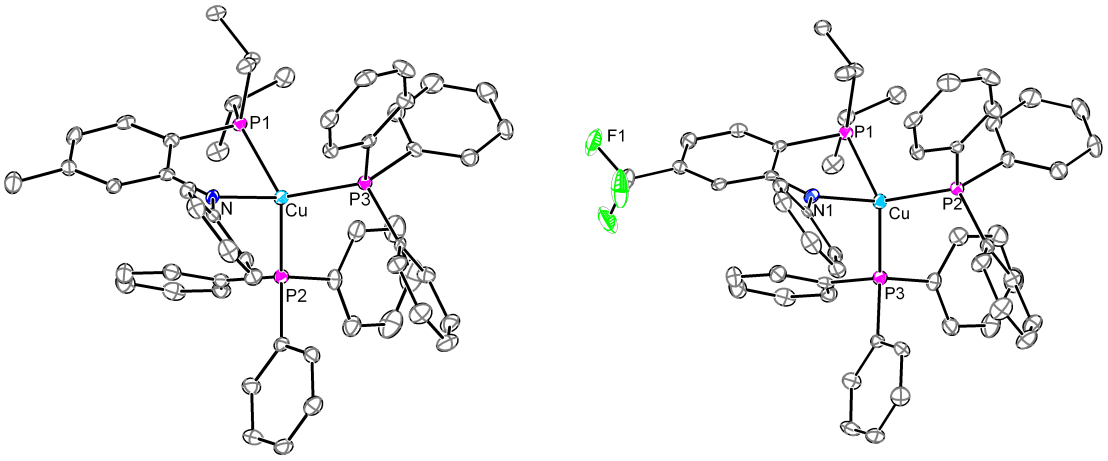

Figure 2.7. Structural representation of **7** (left) and **8** (right), with ellipsoids at 50% probability. Key bond lengths (Å) and angles (°) for **7**: Cu–N 2.076(2), Cu–P1 2.326(1), Cu–P2 2.3439(9), Cu–P3 2.3189(9), N–Cu–P1 82.24(7). For **8**, Cu–N 2.091(4), Cu–P1 2.347(3), Cu–P2 2.329(3), Cu–P3 2.363(3), N–Cu–P1 82.1(2).

In order to tune the emission wavelength, we prepared two [PN] ligands with donating and withdrawing groups on the arene backbone. Methyl- and trifluoromethyl-substituted amides [^{Me}PN]Li (**5**) and [^{CF3}PN]Li (**6**) were prepared analogously to **1**, with subsequent metallation in the presence of two equivalents of PPh_3 yielding [^{Me}PN]Cu(PPh_3)$_2$ (**7**) and [^{CF3}PN]Cu(PPh_3)$_2$ (**8**), as depicted in Scheme 2.1. Complexes **7** and **8** were fully characterized, including XRD studies (Figure 2.7). Methyl substitution does not greatly perturb the optical spectrum of **7** relative to **2**, and only a 6 nm blue shift is observed in the emission maximum (Figure 2.4). Complex **7** emits significantly brighter than **2**, with ϕ = 0.70, but exhibits a shorter luminescence lifetime of 6.7(1) μs.

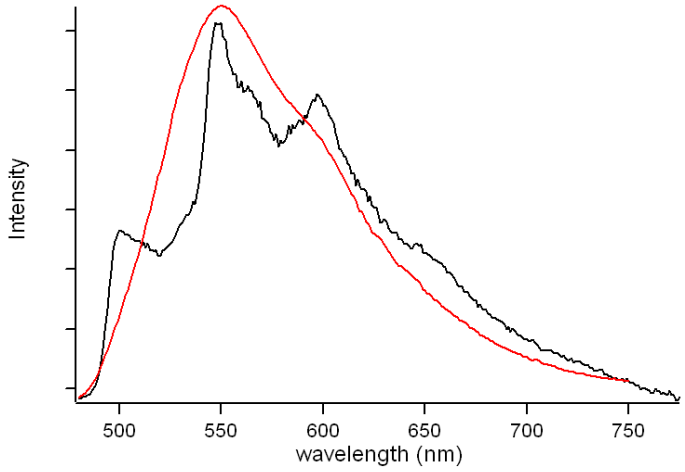

Figure 2.8. Emission spectra of polycrystalline [^{CF3}PN]Cu(PPh$_3$)$_2$ (**8**; λ_{ex} = 430 nm) at 77 K (black) and 298 K (red).

Relative to **2**, CF_3-substitution on the ligand backbone imparts a 10 nm red shift in the optical spectrum (λ_{max} = 444 nm) for **8**, which is matched by a 48 nm red shift in the emission maximum (Figure 2.4). The quantum efficiency of **8** in benzene at 298 K, with ϕ = 0.16, represents a substantial decrease compared to PPh_3 adducts **2** and **7**. Polycrystalline **8** displays broad emission at 298 K that closely resembles the solution data; cooling to 77 K the emission develops some structure (Figure 2.8).[19] Most interesting, however, is a dramatic increase in the measured luminescence lifetime, to 150(3) μs (Figure 2.6). As for the PMe_3 adduct **3**, there is a two-component decay profile, with a much more pronounced short-lived (<10 ns) species. These decay profiles appear to reflect independent singlet/triplet emission pathways.[20] The triplet excited state is nearly an order of magnitude longer-lived than dbpCu(POP),[8] and is to our knowledge the longest-lived monomeric Cu emitter presently known in solution at ambient temperature.

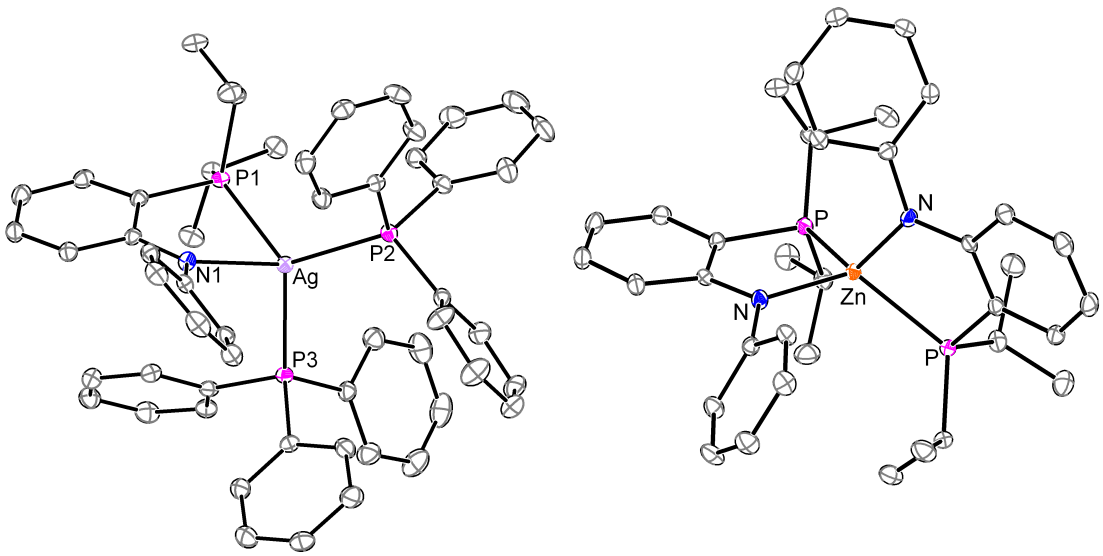

Figure 2.9. Structural representations of [PN]Ag(PPh_3)$_2$ (**9**, left) and [PN]$_2$Zn (**10**, right) with ellipsoids at 50% probability. Key bond lengths (Å) and angles (°): for **9**, Ag–N 2.369(1), Ag–P1 2.4881(4), Ag–P2 2.4919(4), Ag–P3 2.5028(4), N–Ag–P1 76.40(3); for **10**, Zn–N 1.969(2), Zn–P 2.372(1), N–Zn–P 85.72(4).

For comparison to the Cu complexes, **1** was added to AgOTf in the presence of two equivalents of PPh_3 in Et_2O, affording golden yellow [PN]Ag(PPh_3)$_2$ (**9**). An XRD study showed an analogous geometry to copper complex **2** (Figure 2.9). Compound **9** is a rare example of a mononuclear silver amide complex. While its absorption spectrum is similar to those of **2** and **3** (Figure 2.11), its emission spectrum exhibits a very broad peak centered at 544 nm, suggesting loss of energy via structural reorganization. The luminescence is extremely attenuated relative to the corresponding Cu complexes (ϕ = 0.0010), and it has a lifetime that is likewise much shorter (125(5) ns). Metathesis of two equivalents of **1** with $ZnCl_2$, followed by filtration and crystallization, provided yellow [PN]$_2$Zn (**10**). The tetrahedral geometry was confirmed by XRD (Figure 2.9). The optical spectrum of **10** differs substantially from the copper complexes (Figure 2.11); excitation at either absorption feature (λ_{max} = 324, 390 nm) led to aquamarine blue emission centered at 475 nm that was

substantially less efficient and shorter lived than for the Cu complexes (ϕ = 0.088, τ < 10 ns).

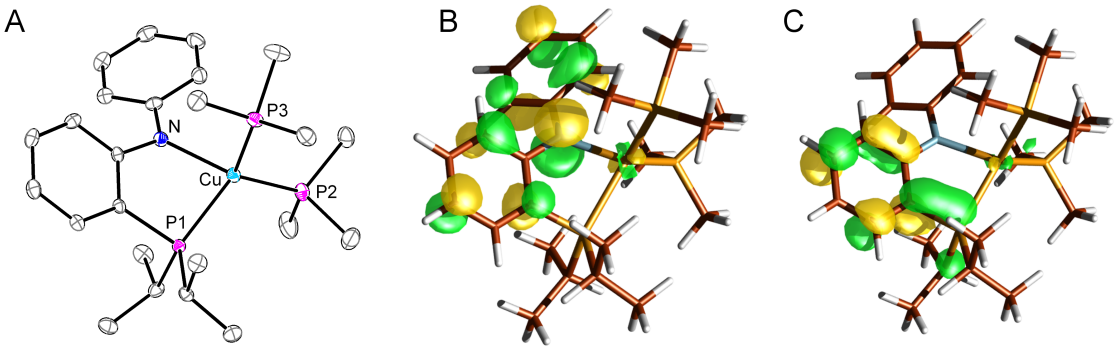

Figure 2.10. A: Alternate view of structural representation of **3** (see **Figure 2.1** for full details). B: The DFT calculated HOMO of **3**. C: The DFT calculated LUMO of **3**.

Understanding the luminescence mechanism

Similarities in the absorption profiles and the generality of the luminescent behavior lead us to tentatively suggest that intraligand charge transfer (ILCT) transitions are present in *all* of the compounds **1**-**10**. Copper appears critical to accessing the interesting long-lived triplet excited state, though, and in the absence of Cu only fluorescence is observed. DFT calculations on **3** show HOMO and LUMO orbitals consistent with excitation from the N lone pair to arene π* orbitals. The calculation on the full molecule **3** was performed using the hybrid DFT functional B3LYP/LACVP** as implemented in the Jaguar 6.5 program package, optimized starting from the crystallographic parameters. Substantial N lone pair character (mixed with non-bonding arene π character) is present in the HOMO, and a predominantly π* orbital (localized on the P-containing arene and perhaps involving a P σ* orbital) is depicted in the LUMO (Figure 2.10). The frontier orbitals display very little metal

character (HOMO: 5% Cu; 2% P; 36% N; 57% C), while the HOMO–1 and HOMO–2 orbitals feature appreciably more Cu d character (HOMO–1: 45% Cu; 13% P; 21% N; 20% C; HOMO–2: 46% Cu; 23% P; 15% N; 26% C). If the DFT-predicted intraligand π-π* transition is in fact operative, emission from this transition is manifested as short-lived fluorescence for non-copper-containing species **1**, **5**, **6**, and **10**. The more interesting Cu emitters (**2**, **3**, **4**, **7**, and **8**) seem to display both singlet and triplet emissions, indicative of additional luminescence processes. The presence of both triplet and singlet excited states is not uncommon. In a particularly similar case, a d^0 metal shows both charge transfer (LMCT) and N lone pair to arene π* excited states.[21]

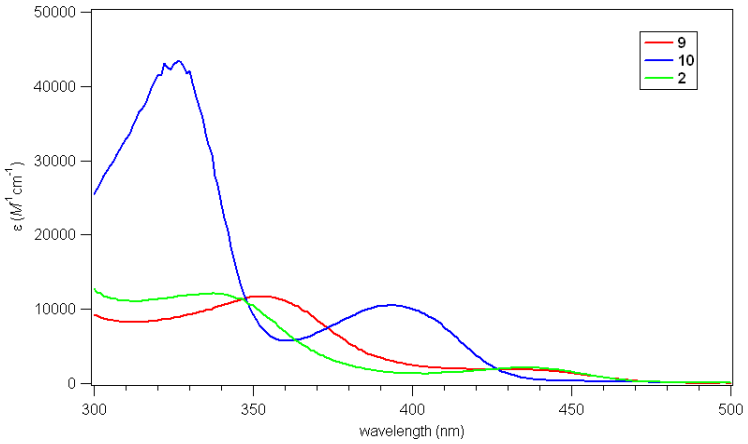

Figure 2.11. Overlay of [PN]Ag(PPh$_3$)$_2$ (**9**), [PN]$_2$Zn (**10**), [PN]Cu(PPh$_3$)$_2$ (**2**).

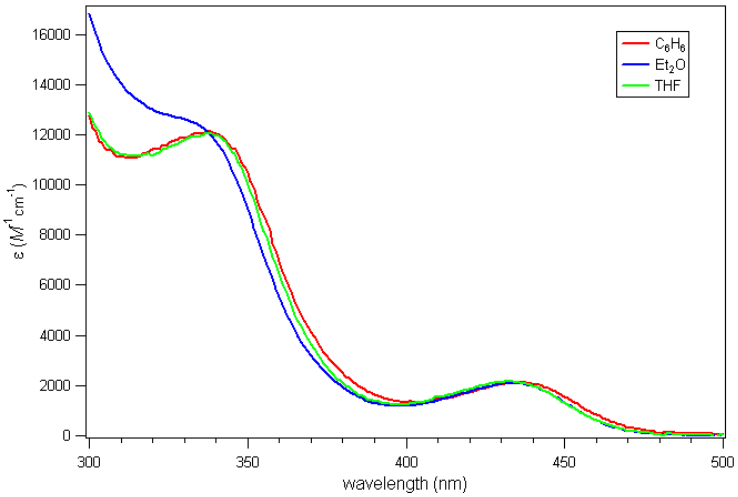

Figure 2.12. Optical spectra of [PN]Cu(PPh_3)$_2$ (**2**) in benzene (red), diethyl ether (blue), and tetrahydrofuran (green) solvent.

Perhaps the simplest description of the observed Cu phosphorescence is MLCT from a Cu d-orbital to the arene π* orbital. This explanation is inconsistent with the following data, however. First, only minor differences are observed in the absorption spectra of Cu and Ag complexes **2** and **9** (Figure 2.11)—rather than the often-striking shift in MLCT transition energy caused by moving to a 4d element.[22] Additionally, there is minimal solvent dependence on the ground state absorption spectrum of **2** (Figure 2.12), while significant solvent dependence is often observed in well-defined MLCT systems.[23] Further, MLCT states generally have large Stokes shifts, but the complexes here all have small Stokes shifts (Figure 2.4).

Finally, the Cu complexes do not appear to be drastically quenched by a five-coordinate exciplex, as is typical for MLCT.[6] If exciplex quenching played a significant role, the differences in steric bulk between **2**, **3**, and **4** might be expected to have a more significant effect on the phosphorescence lifetime. Electronic effects seem to play a more important

role when comparing **2**, **7**, and **8**, as the sterically similar (but electronically diverse) complexes have quite different lifetimes and quantum efficiencies. Given these data, we speculate that the Cu phosphorescence is derived from good orbital overlap and energetic matching between the Cu d-manifold and the ligand π* system, which allows facile intersystem crossing to a Cu-stabilized triplet, which is inaccessible in the other complexes.

Recent work probed the temperature-dependent luminescence of vapor-deposited $\{(PNP)Cu^{I}\}_2$, and an E-type fluorescence mechanism was suggested.[24] In E-type fluorescence an emissive singlet state lies at slightly higher energy than an emissive triplet state, and thermal equilibration between the two states occurs at room temperature. This could explain the multiple emission processes observed in the closely related monocopper complexes, and helps to explain the unusual "duality" at play: the Cu complexes exhibit long lifetimes typically reserved for triplet emitters, but also feature very small Stokes' shifts, a hallmark of singlet emitters. The solvent-dependent quantum efficiency and solvent-independent luminescence lifetimes are also consistent with this picture of multiple emissive states: perhaps the singlet state is affected by polar solvents (or spurious water therein), altering the emission intensity (which is a mixture of singlet and triplet states as a steady-state spectroscopy), while the triplet state (the only one observed in lifetime measurements) is not affected.

Another recent study investigated the sequential one-electron oxidations of $\{(PNP)Cu^{I}\}_2$.[25] The first oxidation can be thought of as an extreme model of an excited state species. These studies showed that the core structure was largely left unchanged (according to XRD studies) and that the ligand was non-innocent (according to XAS studies): the ligand-metal

core was oxidized as a whole unit, rather than oxidation being localized on the metals. These findings support a ligand-stabilized or -centered excited state that would be unperturbed by major structural distortions, consistent with the remarkable luminescence properties.

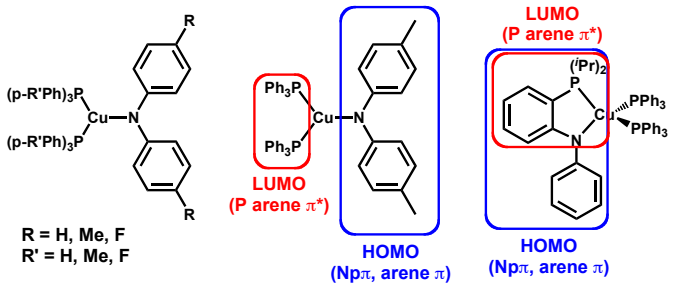

Scheme 2.2

Conclusions

In summary, we have reported the synthesis and luminescence properties of a series of amidophosphine complexes of copper, silver, and zinc. While all of the [PN]-containing complexes are emissive, the combination of arylamido and phosphine donors engenders copper species with emission properties that are distinct relative to previously studied classes of copper emitters, allowing access to both singlet and triplet emissive states, perhaps *via* an E-type fluorescence mechanism. Further studies in the group have focused on probing the constraints of luminescence: "disconnecting" the phosphine and the amide has allowed the synthesis of a more easily tunable series of three coordinate copper bis(phosphine) copper amides (Scheme 2.2), which retain their luminescence.[26] Interestingly, DFT calculations show similar HOMO and LUMO pictures to complex **2** (Scheme 2.2), suggesting a related luminescence mechanism.

Experimental Section

General Considerations

All manipulations were carried out using standard Schlenk or glovebox techniques under a dinitrogen atmosphere. Unless otherwise noted, solvents were deoxygenated and dried by thorough sparging with N_2 followed by passage through an activated alumina column. Non-halogenated solvents were tested with a standard solution of sodium benzophenone ketyl in tetrahydrofuran in order to confirm effective oxygen and moisture removal. Deuterated solvents were degassed and stored over activated 3 Å molecular sieves prior to use. THF-d_8 was dried by passage over activated alumina and stored over activated 3 Å sieves prior to use. $LiP(^iPr)_2$[27] was prepared according to a literature procedure. All other reagents were purchased from commercial vendors and used without further purification, unless explicitly stated. Elemental analysis was carried out at Desert Analytics, Tucson, Arizona. NMR spectra were recorded at ambient temperature on a Varian Mercury 300 MHz or Inova 500 MHz spectrometer. ^{1}H NMR chemical shifts were referenced to residual solvent. ^{31}P NMR chemical shifts are reported relative to an external standard of 85% H_3PO_4. ^{19}F NMR chemical shifts are reported relative to either a HCF_3 (0 ppm) or C_6F_6 (–164.9) standard. UV-vis measurements were taken on a Varian Cary 50 Bio Spectrophotometer, using a quartz crystal cell with a Teflon stopper. Electrochemical analysis was performed on a CHI 600B Potentiostat/Galvanostat using a glassy carbon working electrode, a platinum wire auxiliary electrode, and a $Ag/AgNO_3$ (0.01 M)

reference electrode filled with THF, with reference to Cp_2Fe/Cp_2Fe^+ as an internal standard. X-ray diffraction studies were carried out in the Beckman Institute Crystallographic Facility on a Bruker Smart 1000 CCD diffractometer. High resolution mass spectra (HRMS) were obtained at the California Institute of Technology Mass Spectral Facility. Luminescence measurements were carried out at the California Institute of Technology's Beckman Institute Laser Resource Center.

X-ray Crystallography Procedures

X-ray quality crystals were grown as indicated in the experimental procedures for each complex. The crystals were mounted on a glass fiber with Paratone-N oil. Structures were determined using direct methods with standard Fourier techniques using the Bruker AXS software package. In some cases, Patterson maps were used in place of the direct methods procedure. Full details are provided in Appendix D.

Lifetime measurements

A solution of analyte in diethyl ether or benzene was prepared in a nitrogen-filled glovebox. The quartz cuvettes (1 cm pathlength) were charged with this solution, and sealed with a Teflon stopper. Absorption spectra were acquired both before and after measurements to ensure the sample was not photodegrading. Generally, there was an insignificant amount (<1%) of photodecomposition under the experimental conditions, although there was more pronounced degradation under prolonged irradiation. Luminescence lifetime measurements were carried out as previously described[28] using 8 ns pulses (at a repetition rate of 10 Hz) from a Nd:YAG laser pumped OPO (Quanta Ray Pro, Spectra Physics).

The luminescence was dispersed through a monochromator (Instruments SA DH-10) onto a photomultiplier tube (PMT) (Hamamatsu R928). The PMT current was amplified and recorded with a transient digitizer (Lecroy 9354A). Measurements were performed at 298 K with two cuvettes of analyte solution, with excitation at λ_{ex} = 430 nm for **2**, **3**, **4**, **7**, and **8**; λ_{ex} = 440 nm for **9**; and λ_{ex} = 310 nm for **1** and **10**. Emission was collected at the wavelength, λ_{em}, specified in Table 2.2. The emission decay was averaged over at least 500 laser pulses, and fit to an exponential function from which k_{obs} and τ were determined. For **3** and **8**, the short-lived portion of the bi-exponential function was below the response time of the amplifier, and is approximated < 10 ns. The Zn complex **6** also had a lifetime that was too short to quantify, and so is estimated simply as < 10 ns.

Table 2.2. Data for Excited State Lifetime Measurements.

Sample	λ_{em} (nm)	k_{obs} (s^{-1})	Lifetime (τ) (μs)
223 μM **1** in Et_2O	480	8.64×10^7	0.012(1)
40.3 μM **2** in C_6H_6	504	4.94×10^4	20.2(1)
80.0 μM **3** in C_6H_6	503	(a) 4.44×10^4	22.3(7)
		(b) n/a	< 10 ns
77.7 μM **4** in C_6H_6	533	6.15×10^4	16.3(3)
49.6 μM **7** in C_6H_6	504	1.50×10^5	6.7(1)
57.4 μM **8** in C_6H_6[a]	555	(a) 6.76×10^3	150(3)
		(b) n/a	< 10 ns
98.1 μM **9** in C_6H_6[a]	517	8.76×10^6	0.125(5)

a. Sample was excited at 440 nm.

Oxidative Luminescence Quenching

Samples were prepared from two stock solutions: 34 μM **2** in C_6H_6, and a mixture of 34 μM **2** and 339 μM 2,6-dichlorobenzoquinone (DCQ). Using cuvettes with Teflon-separated 25 mL bulbs, solutions of varying concentrations were prepared in the cuvette,

with the stock solution of **2** in the bulbs. After measurements were made on the cuvette solution, the stock solution in the bulb was mixed with the cuvette solution, diluting the concentration by a half. Luminescence lifetime measurements were taken as above. The data measurements are reported in Table 2.3, and a Stern-Volmer plot of k_{obs} vs. concentration of DCQ is shown in Figure 2.5. The data is consistent with diffusion-limited electron transfer, with a rate constant, $k = 9.04 \times 10^9\ M^{-1}s^{-1}$.

Table 2.3. Stern-Volmer quenching data for **2**.

Concentration of DCQ	k_{obs} **(s^{-1})**	**Lifetime (τ, 1/ k$_{obs}$) (μs)**
0 μM	4.70×10^4	21.26
11.3 μM	1.34×10^5	7.48
22.6 μM	2.25×10^5	4.44
33.8 μM	3.51×10^5	2.84
42.4 μM	4.29×10^5	2.33
68.7 μM	6.65×10^5	1.50
84.7 μM	7.84×10^5	1.27
169.5 μM	1.57×10^6	0.635

Quantum yield experiments

Emission spectra were recorded on a Spex Fluorolog-2 spectro-fluorometer. A solution of analyte or reference compound in benzene, diethyl ether, tetrahydrofuran, or acetonitrile was prepared in a nitrogen filled glovebox. Cuvettes (1 cm path length) were charged with this solution and sealed with a teflon stopper. The absorption spectra were acquired both before and after fluorescence measurements to ensure the sample was not degrading. In some cases a very minor amount (<1%) of photodecomposition was observed, with more pronounced degradation under prolonged exposure to light. Fluorescence measurements

were performed at the specified wavelength and corrected for detector response after equilibration to 298 K. The area under the curve of the emission spectrum was determined using standard trapezoidal integration methods. Quantum yields (Table 2.4) were then calculated by the methods described by Demas and Crosby[16a] using Equation 2.1. Quinine sulfate in 0.1 $\mathcal{N}$ H_2SO_4 ($\phi = 0.54$)[16a] and $[Ru(bpy)_3][PF_6]_2$ in acetonitrile ($\phi = 0.075$)[16b] were used as reference standards. Quantum yields are reported with confidence of ±5 on the last significant figure for measurements in benzene, and ±10 on the last two significant figures for measurements in Et_2O and THF. Lithium salts of the ligands were prone to photodecomposition: **1** (10%), **5** (20%) and **6** (15%) all decomposed significantly after irradiation in the fluorimeter. The data is included here, but should be taken as a much more crude value.

$$\phi = (QR)(I / IR)(ODR / OD)\,(\eta^2 / \eta_R^2) \qquad \textbf{(2.1)}$$

ϕ: quantum yield of the sample.
QR: quantum yield of reference.
I: integrated intensity of analyte.
IR: integrated intensity of reference.
ODR: optical density of the reference in absorption units.
OD: optical density of the analyte in absorption units.
η: index of refraction of the solvent in which the analyte was dissolved.
η_R: index of refraction of the solvent in which the reference was dissolved.

Table 2.4. Data for Quantum Yield Measurements.

Sample (solvent)	λ_{ex}	ϕ
1 (Et_2O)	430	0.16
2 (C_6H_6)	430	0.56
	350	0.52
2 (Et_2O)	430	0.29
2 (THF)	430	0.27
3 (C_6H_6)	430	0.21
	350	0.17
3 (Et_2O)	430	0.10
3 (THF)	430	0.05
4 (C_6H_6)	430	0.31
	350	0.36
4 (Et_2O)	430	0.15
4 (THF)	430	0.05
5 (Et_2O)	430	0.12
6 (Et_2O)	430	0.05
7 (C_6H_6)	430	0.70
7 (Et_2O)	430	0.55
7 (THF)	430	0.30
8 (C_6H_6)	430	0.16
8 (Et_2O)	430	0.08
8 (THF)	430	0.07
9 (C_6H_6)	430	0.00106
10 (C_6H_6)	350	0.088

Preparation of complexes

2-Fluoro-diphenylamine. In the glovebox, a 200 mL Teflon-stopped high-pressure flask was charged with Pd_2dba_3 (315 mg, 0.344 mmol; dba = dibenzylideneacetone), DPPF (275 mg, 0.688 mmol; DPPF = 1,1'-bis(diphenylphosphino)ferrocene), NaO^tBu (4.62 g, 48.16

mmol), and 80 mL toluene. The reaction flask was removed from the glovebox, and 1-bromo-2-fluorobenzene (3.74 mL, 34.4 mmol) and aniline (3.14 mL, 34.4 mmol) were added by syringe under N_2 counterflow. The mixture was heated in an oil bath at 100 °C overnight. After verifying consumption of starting materials by GC–MS and ^{19}F NMR, the mixture was allowed to cool and filtered through a plug of silica, washing with copious petroleum ether to yield a light yellow solution. The solvents were removed *in vacuo*, yielding the desired product as a pale orange oil (5.49 g, 85%). **^{1}H NMR** (C_6D_6, 300 MHz): δ 7.15-6.95 (m, 3H, Ar–*H*), 6.89-6.65 (m, 4H, Ar–*H*), 6.5 (m, 2H, Ar–*H*), 5.36 (br, 1H, N*H*). **^{19}F NMR** (282 MHz): δ –132.5. **HRMS** (EI^+) *m/z* calcd. for $C_{12}H_{10}FN$: 187.0797. Found: 187.0796 [M^+], 168.0947 [M–F].

Lithium 2-(diisopropylphosphino)diphenylamide (1). To a 200 mL Teflon-stopped flask charged with 20 mL of a light brown THF solution of 2-Fluoro-diphenylamine (2.20 g, 11.76 mmol), was added a 1.6 M hexanes solution of *n*BuLi (7.75 mL, 12.35 mmol), after which the mixture turned orange and was stirred for 20 minutes. After concentration to 5 mL, a 50 mL solution of LiP(*i*Pr)$_2$ (2.92 g, 23.52 mmol) in THF was added, and the vessel was sealed and removed from the glovebox and heated to 65 °C for 8 days, monitoring by GC–MS and ^{19}F NMR. The mixture turned dark green over time, and was blue luminescent under a UV lamp. When no remaining starting materials were detected spectroscopically, the mixture was brought back into the glovebox, and quenched with 5 mL EtOH. After addition of 40 mL petroleum ether, the reaction mixture was filtered through celite, and the solvents were removed *in vacuo*. As it was concentrated, the oily residue formed large sticky bubbles, and the mixture was repeatedly treated with

diethyl ether and then re-concentrated to control the bubbling. The residual oil was extracted with petroleum ether, and filtered through a plug of silica. Removal of solvents left a brown oil that solidified when left at ambient temperatures overnight, and was determined to be ~ 80% [PN]H by NMR, with an unknown phosphine-containing product as an impurity. Addition of *n*BuLi (7.35 mL, 11.76 mmol) to a stirring solution of the brown solids resulted in immediate precipitation of **1**, which was isolated on a sintered glass frit, and washed with copious petroleum ether, before being collected as a spectroscopically pure, thermally unstable off-white powder (2.15 g, 64%). **^{1}H NMR** (300 MHz, THF-d_8): δ 7.04 (m, 1H, Ar–*H*), 6.88 (m, 3H, Ar–*H*), 6.73 (m, 3H, Ar–*H*), 6.26 (t, 1H, Ar–*H*), 6.12 (t, 1H, Ar–*H*), 2.02 (m, 2H, C*H*(CH_3)$_2$), 1.11, (q, 6H, CH(C*H*$_3$)$_2$), 0.98 (q, 6H, CH(C*H*$_3$)$_2$). **^{31}P{^{1}H} NMR** (120 MHz): δ –6.03 (q, 1P). **HRMS** (EI$^+$) *m*/*z* calcd. for $C_{18}H_{24}NP$ ([PN]H): 285.1646. Found: 285.1637 [M$^+$], 243.1072 [M–^{i}Pr], 200.0424 [M– 2 ^{i}Pr].

General Procedure for Cu complexes 2-4. Diethyl ether solutions (~ 3 mL) of CuBr•Me_2S and the appropriate tertiary phosphine were cooled to –35 °C. The phosphine-containing solution was added to the CuBr•Me_2S suspension and the mixture was stirred and protected from the light with aluminum foil. After 5 minutes, a cooled (– 35 °C) diethyl ether solution of **1** was added slowly to the reaction mixture, and the solution turned bright yellow immediately. After 2 hours of stirring the mixture was green-yellow, and the solvent was removed *in vacuo*. Extraction with benzene, followed by filtration through celite, yielded a bright yellow solution, which was lyophilized, affording spectroscopically pure product as a yellow powder.

[PN]Cu(PPh$_3$)$_2$ (2). X-Ray quality crystals were grown from vapor diffusion of petroleum ether into a solution of **2** in diethyl ether. **^{1}H NMR** (C_6D_6, 300 MHz): δ 7.3 (m, 30H, P(C_6H_5)$_3$), 7.02 (t, 2H, Ar–*H*), 6.92 (t, 3H, Ar–*H*), 6.79 (t, 1H, Ar–*H*), 6.72 (t, 1H, Ar–*H*), 6.59 (t, 1H, Ar–*H*), 6.17 (t, 1H, Ar–*H*), 2.26 (sept., 2H, C*H*(CH_3)$_2$), 1.08 (dd, 6H, CH(C*H*$_3$)$_2$), .99 (dd, 6H, CH(C*H*$_3$)$_2$). **^{13}C{^{1}H} NMR** (C_6D_6, 75 MHz): δ 166.41, 158.39, 136.03 (d, $\mathcal{J}_{PC}$ = 12.6 Hz), 134.61 (d, $\mathcal{J}_{PC}$ = 16.9 Hz), 133.34, 132.43, 129.81, 129.76, 129.14 (d, $\mathcal{J}_{PC}$ = 8.3 Hz), 128.93, 126.05, 119.70, 113.40 (d, $\mathcal{J}_{PC}$ = 156 Hz), 23.85 (d, $\mathcal{J}_{PC}$ = 12.31 Hz), 20.22 (d, $\mathcal{J}_{PC}$ = 10.87 Hz), 19.02 (d, $\mathcal{J}_{PC}$ = 3.0 Hz). **^{31}P{^{1}H} NMR** (C_6D_6, 120 MHz): δ –1.2 (br, 2P), –3.7 (br, 1P). **Anal. calcd.** for $C_{54}H_{53}CuNP_3$ C, 74.34; H, 6.12; N, 1.61; Found: C, 74.31; H, 5.94; N, 1.60.

[PN]Cu(PMe$_3$)$_2$ (3). X-Ray quality crystals were grown from vapor diffusion of petroleum ether into a diethyl ether solution of **3**. **^{1}H NMR** (C_6D_6, 300 MHz,): δ 7.72 (q, 1H, Ar–*H*), 7.4 (m, 2H, Ar–*H*), 7.29 (t, 2H, Ar–*H*), 7.2–7.0 (m, 2H, Ar–*H*), 6.78 (tt, 1H, Ar–*H*), 6.54 (t, 1H, Ar–*H*), 1.95 (sept., 2H, C*H*(CH_3)$_2$), 1.10 (q, 6H, CH(C*H*$_3$)$_2$), 1.00 (q, 6H, CH(C*H*$_3$)$_2$), 0.85 (br. 18H, P(C*H*$_3$)$_3$). **^{13}C{^{1}H} NMR** (C_6D_6, 125 MHz): δ 163.40, 158.20, 131.80, 130.65, 128.79, 128.19, 121.20, 117.63 (d, $\mathcal{J}_{PC}$ = 34.9 Hz), 114.95, 114.07 (dd, JPC = 478.5 Hz, 3.7 Hz), 22.45 (d, $\mathcal{J}_{PC}$ = 8.8 Hz), 19.63 (d, $\mathcal{J}_{PC}$ = 11.6 Hz), 18.41 (d, $\mathcal{J}_{PC}$ = 3.3 Hz), 16.63 (d, $\mathcal{J}_{PC}$ = 13.0 Hz). **^{31}P{^{1}H} NMR** (C_6D_6, 120 MHz): δ 7.0 (br, 1P, [*P*N]), –46.3 (br, 2P, *P*(CH_3)$_3$). **Anal. calcd.** for $C_{24}H_{41}CuNP_3$ C, 57.64; H, 8.26; N, 2.80; Found: C, 57.61; H, 8.00; N, 2.84.

[PN]CuDPPE (4). Crystals used for X-Ray diffraction were grown from vapor diffusion of petroleum ether into a solution of **4** in THF. **^{1}H NMR** (C_6D_6, 300 Mhz,): δ 7.65 (q, 2H, Ar–*H*), 7.44 (m, 8H, DPPE), 7.2-7.1 (m, 2H, Ar–*H*), 7.02 (d, 12H, DPPE), 6.9 (m, 3H, Ar–*H*), 6.55 (m, 2H, Ar–*H*), 2.18 (t, 4H, DPPE), 2.08 (sept., 2H, C*H*$(CH_3)_2$), 1.15 (q, 6H, CH(C*H*$_3)_2$), 0.89 (q, 6H, CH(C*H*$_3)_2$). **^{13}C{^{1}H} NMR** (125 MHz): δ 159.27, 136.06, 133.82 (t, $\mathcal{J}_{PC}$ = 8.1 Hz), 133.18, 131.53, 129.26, 129.09 (t, $\mathcal{J}_{PC}$ = 4.3 Hz), 124.15, 117.03, 114.20 (dd, $\mathcal{J}_{PC}$ = 571.3 Hz, 4.7 Hz), 68.16 (THF), 27.36 (td $\mathcal{J}_{PC}$ = 17.1 Hz, 5.5 Hz), 26.16 (THF), 23.09 (d, $\mathcal{J}_{PC}$ = 11.9 Hz), 19.89 (d, $\mathcal{J}_{PC}$ = 11.1 Hz), 17.97. **^{31}P{^{1}H} NMR** (120 Mhz): δ 8.7 (br, 1P, [*P*N]), –1.4 (br 2P, DPPE). **Anal. calcd.** for $C_{44}H_{47}CuNP_3$ C, 70.81; H, 6.35; N, 1.88; Found: C, 70.52; H, 6.46; N, 1.60.

2-Fluoro-5-methyl-diphenylamine. A 200 mL high-pressure reaction vessel was charged with 30 mL toluene, Pd_2dba_3 (91.7 mg, 0.10 mmol), and 2-(dicyclohexylphosphino)biphenyl (140.2 mg, 0.40 mmol). The reaction flask was then removed from the box and stirred, with the dark red mixture turning more orange. As the reaction flask was stirring, 2-Fluoro-5-methylaniline (3.01 g, 24.05 mmol), iodobenzene (4.09 g, 20.04 mmol), and dry toluene were added to a 50 mL Schlenk flask, which was then boil-degassed. After subsequent cannula transfer of the organics into the high-pressure vessel, NaO^{t}Bu (2.70 g, 28.05 mmol) was added under N_2 counterflow, and the flask was sealed with a Teflon stopper. The mixture was heated to 110 °C for 20 hours, was allowed to cool to room temperature, then was filtered through a plug of silica in air, washing with copious petroleum ether (~250 mL). The solvent was removed under vacuum, yielding an orange-brown oil. The crude product was purified by column chromatography on silica gel

with petroleum ether eluent, affording the title compound as a pale yellow oil (3.01 g, 70%). **^{1}H NMR** ($CDCl_3$, 300 MHz): δ 7.31 (t, 2H), 7.12 (d, 3H), 7.00 (m, 2H), 6.64 (t, 1H), 6.75 (bs, 1H, N*H*), 2.27 (s, 3H, –CH_3). **^{19}F NMR** (282 MHz): δ –137.59 (s, 1F). **HRMS** (EI^+) *m/z* calcd. for $C_{13}H_{12}FN$: 201.0954. Found: 201.0957 [M^+].

[^{Me}PN]Li (5). A 10 mL THF solution of 2-fluoro-5-methyldiphenylamine (1.452 g, 5.19 mmol) was cooled to – 35 °C and added to a 100 mL high pressure flask. To this vessel was added a 1.6 M solution of *n*BuLi in hexanes (3.41 mL, 5.45 mmol), dropwise with stirring. The clear colorless solution turned yellow, then orange, as it was warmed to room temperature, after which it was stirred for 2 hours. A 10 mL THF solution of $LiP(iPr)_2$ (1.611 g, 12.99 mmol) was added slowly to the mixture, and the vessel was sealed with a Teflon stopper, removed from the glovebox, and heated to 80 °C for 7 days. After this time, a GC–MS trace showed complete consumption of starting material and growth of one other peak corresponding to product. The flask was brought back into the glovebox, and the reaction was quenched with 5 mL EtOH, resulting in a pale green color, before removal of solvents. Filtration of the residue through silica, washing with copious petroleum ether, followed by removal of solvents in vacuo and another filtration through celite, yielded [^{Me}PN]Li as a mixture with another phosphorous-containing product (80% by ^{31}P NMR integration). Addition of *n*BuLi (3.41 mL, 5.45 mmol) to a cooled (–35 °C) solution of this crude product in a solution of 10 mL petroleum ether resulted in immediate precipitation of beige solids. The mixture was stirred 2.5 hrs before collecting the solids on a frit, and washing with 60 mL petroleum ether, afforing pure **5**. **^{1}H NMR** (THF-d_8, 300 Mhz): δ 6.7-6.9 (m, 6H), 6.25 (t, 1H), 5.98 (d, 1H), 1.96-2.06 (m, 5H, Ar-CH_3, CH(CH_3)$_2$), 1.10 (dd,

6H), 0.95 (d, 6H). **^{31}P{^{1}H} NMR** (THF-d_8, 120 MHz): δ -7.07 (m, 1H). **HRMS** (EI$^+$) *m/z* calcd. for $C_{19}H_{26}NP$: 299.1805. Found: 299.1803 [M$^+$], 257.1387 [M-^{i}Pr], 214.0860 [M- 2 ^{i}Pr].

2-Fluoro-5-trifluormethyl-diphenylamine. In the glovebox, a 200 mL Teflon-stopped reaction vessel was charged with Pd_2dba_3 (44.9 mg, 0.049 mmol), 2-(dicyclohexylphosphino)biphenyl (68.7 mg, 0.196 mmol), NaOtBu (1.32 g, 13.7 mmol), and 15 mL toluene. This vessel was removed from the box, and stirred for 10 minutes, wherein the dark red mixture took on a more orange appearance. Under a purge of N_2, 2-Fluoro-4-trifluoromethyl-aniline (1.53 mL, 11.76 mmol) and iodobenzene (1.09 mL, 9.8 mmol) were added to the vessel by syringe. The mixture was then sealed with the Teflon stopper, and heated to 100 °C in an oil bath overnight. After 18 hours, the reaction was shown to be complete by GC–MS, at which point the mixture was filtered through a large plug of silica in air, and washed with copious (~200 mL) petroleum ether, yielding a pale orange solution. The solvents were removed by rotary evaporation, yielding an orange oil. Upon storage at –30 °C overnight, crystalline orange needles of pure compound were obtained (1.939 g, 78%). **^{1}H NMR** ($CDCl_3$, 300 MHz): δ 7.53 (dd, 1H), 7.4-7.33 (m, 2H), 7.2-7.05 (m, 4H), 5.82 (br N*H*). **^{19}F NMR** ($CDCl_3$, 282 MHz): δ –58.8 (3F), –125.5 (1F). **HRMS** (FAB$^+$) *m/z* calcd. for $C_{13}H_9F_4N$: 255.0671. Found: 255.0682 [M$^+$].

[^{CF3}PN]Li (6). In the glovebox, 1-Fluoro-4-trifluoromethyl-diphenylamine (1.94 g, 7.63 mmol) was dissolved in 20 mL THF, and added to a 200 mL Teflon-stopped glass vessel equipped with a stirbar. The vessel was cooled to –78 °C, at which point a 1.6 M hexanes

solution of *n*BuLi (4.8 mL, 7.71 mmol) was added dropwise by syringe. The reaction mixture was allowed to warm with stirring for 30 minutes, during which time the solution darkened from pale orange to a darker orange-brown. At this point a 10 mL THF solution of LiP(*i*Pr)$_2$ (1.90 g, 15.33 mmol) was added to the reaction mixture, and the vessel was heated to 70 °C for 4 days, while monitoring the reaction for completion by GC–MS and ^{31}P NMR. The reaction mixture, which had darkened to a red-brown, was luminescent yellow under a UV lamp. The vessel was cooled to room temperature, and was brought into the glovebox. The mixture was then quenched with 10 mL EtOH, and 10 mL of petroleum ether were added, yielding a golden-brown solution. The solvents were removed *in vacuo*. The oily residue was treated with 10 mL of diethyl ether, which was subsequently removed under reduced pressure; this procedure was repeated as necessary to reduce bubbling. The residue was extracted with petroleum ether, filtered through celite, and concentrated to a brown oil, which was left under dynamic vacuum overnight. The residue contained a mixture of [^{CF3}PN]H (~85-90%) and one unknown P-containing side-product (δ +4 ppm). Crude [^{CF3}PN]H was dissolved in 20 mL of petroleum ether, added to a 100 mL round-bottom flask, and cooled to –35 °C. A 1.6 M hexanes solution of *n*BuLi (4.8 mL, 7.71 mmol) was then added dropwise by syringe, yielding a beige precipitate. The flask was warmed to room temperature and stirred overnight, at which point the solids were collected on a sintered glass frit, and washed with 40 mL petroleum ether, yielding spectroscopically pure **6** (1.61 g, 59%). **^{1}H NMR** (THF-d_8, 300 MHz): δ 7.15 (d, 1H), 7.05-6.94 (m, 3H), 6.82 (dd, 2H), 6.45 (t, 1H), 6.24 (dd, 2H), 2.09 (sept, 2H, C*H*(CH$_3$)$_2$), 1.14 (q, 6H, CH(C*H*$_3$)$_2$), 1.00 (q, 6H, CH(C*H*$_3$)$_2$). **^{31}P{^{1}H} NMR** (THF-d_8, 120 MHz): δ –6.6 (br q, 1P).

^{19}F NMR (THF-d_8, 282 MHz): δ –60.5 (s, 3F). **HRMS** (EI^+) m/z calcd. for $C_{19}H_{23}F_3NP$: 353.1520. Found: 353.1506 [M^+], 311.1105 [M – ^{i}Pr], 268.0594 [M – 2 ^{i}Pr], 235.0692 [M–(^{i}Pr)$_2$P].

[MePN]Cu(PPh$_3$)$_2$ (7). Diethyl ether solutions of **5** (67.7 mg, 0.222 mmol), CuBr•Me_2S (45.6 mg, 0.222 mmol), and PPh_3 (116.3 mg, 0.444 mmol) were cooled to – 35 °C. PPh_3 was added to the cold suspension of CuBr•Me_2S with stirring, and the scintillation vial was covered with aluminum foil. After 5 minutes amide **5** was added slowly, and the reaction mixture was stirred for 2.5 hrs. After removal of solvent in vacuo, the residue was extracted with benzene, filtered through celite, and lyophilized, yielding **7** in quantitative yield as a yellow powder. X-Ray quality crystals were grown from a diethyl ether solution of **7** layered with petroleum ether and cooled to –30 °C. **^{1}H NMR** (C_6D_6, 300 MHz): δ 7.48-7.35 (m, 12H, P(C_6H_5)$_3$), 7.26 (d, Ar–*H*), 7.2-7.1 (m), 7.08-7.0 (m, 18H, P(C_6H_5)$_3$), 6.86 (t, 1H, Ar–*H*), 6.42 (d, 1H, Ar–*H*), 2.11 (s, 3H, [C*H*3PN]), 2.06 (sept, 2H, C*H*(CH_3)$_2$), 1.1-0.94 (m, 12H, CH(C*H*$_3$)$_2$). **^{13}C{^{1}H} NMR** (C_6D_6, 75 MHz): δ 166.54, 158.34, 141.69, 135.80 (d, $\mathcal{J}_{PC}$ = 12.0 Hz), 134.18 (d, $\mathcal{J}_{PC}$ = 17.2 Hz), 132.98, 129.51, 128.87 (d, $\mathcal{J}_{PC}$ = 8.3 Hz), 125.88, 119.35, 114.05 (dd, $\mathcal{J}_{PC}$ = 75.3 Hz, 4.9 Hz), 23.51 (d, $\mathcal{J}_{PC}$ = 13.1 Hz), 22.15, 19.92 (d, $\mathcal{J}_{PC}$ = 11.2 Hz), 18.67 (d, $\mathcal{J}_{PC}$ = 3.7 Hz). **^{31}P{^{1}H} NMR** (C_6D_6, 120 MHz): δ 1.1 (2P), –3.9 (1P). **Anal. calcd.** for $C_{55}H_{55}CuNP_3$ C, 74.52; H, 6.25; N, 1.58. Found: C, 74.42; H, 6.45; N, 1.57.

[^{CF3}PN]Cu(PPh$_3$)$_2$ (8). Diethyl ether solutions of **6** (97.8 mg, 0.273 mmol), CuBr•Me_2S (56.0 mg, 0.273 mmol), and PPh_3 (142.9 mg, 0.545 mmol) were cooled in scintillation vials

to –35 °C. The PPh_3 solution was added to the slurry of $CuBr•Me_2S$, before the vial was covered with aluminum foil and stirred for 5 minutes. Amide **6** was slowly added to the slurry via pipette, which immediately resulted in a clear yellow solution. The reaction was stirred 2 hr, at which point the solvents were removed *in vacuo*. The residues were extracted with benzene, and filtered through celite, yielding a bright yellow solution. The benzene was removed by lyophilization overnight, affording spectroscopically pure yellow powder (254.6 mg, 99%). X-Ray quality crystals were grown from a cooled (–30 ºC) layering of petroleum ether upon a diethyl ether solution of **8**. **^{1}H NMR** (C_6D_6, 300 Mhz): δ 7.65 (d, 1H, [PN]Ar–*H*), 7.4 (m, 12H, P(C_6H_5)$_3$), 7.29 (d, 2H, [PN]Ar–*H*), 7.08 (t, 3H, [PN]Ar–*H*), 7.0 (m, 18 H, P(C_6H_5)$_3$), 6.83 (t, 1H, [PN]Ar–*H*), 6.76 (d, 1H, [PN]Ar–*H*), 1.933 (sept., 2H, C*H*(CH_3)$_2$), 0.977 (dd, 6H, CH(C*H*$_3$)$_2$), 0.873 (dd, 6H, CH(C*H*$_3$)$_2$). **^{13}C{^{1}H} NMR** (C_6D_6, 125 MHz): δ 135.64 (d, $\mathcal{J}_{PC}$ = 15.6 Hz), 134.54 (d, $\mathcal{J}_{PC}$ = 17.09), 133.35, 129.59, 129.97 (d, $\mathcal{J}_{PC}$ = 0.9 Hz), 129.20 (d, $\mathcal{J}_{PC}$ = 8.3 Hz), 128.92 (d, $\mathcal{J}_{PC}$ = 0.4 Hz), 125.42, 120.57, 109.41, 106.95, 23.86 (d, $\mathcal{J}_{PC}$ = 12.4 Hz), 20.11 (d, $\mathcal{J}_{PC}$ = 11.1 Hz), 18.91 (d, $\mathcal{J}_{PC}$ = 3.1 Hz). **^{31}P{^{1}H} NMR** (C_6D_6, 120 MHz): δ 0.19 (br, 2P, *P*(C_6H_5)$_3$), –3.98 (br, 1P, [*P*N]). **^{19}F NMR** (C_6D_6, 470 MHz): δ –63.4 (3F). **Anal. calcd.** for $C_{55}H_{52}CuF_3NP_3$ C, 70.24; H, 5.57; N, 1.49. Found: C, 70.10; H, 5.84; N, 1.45.

[PN]Ag(PPh_3)$_2$ (9). A 20 mL scintillation vial protected from the light was charged with AgOTf and 3 mL diethyl ether. To the stirring solution was added a diethyl ether solution of PPh_3, and five minutes subsequently was added a solution of **1**. After 2 hours, the reaction mixture was filtered, and the bright yellow solution was dried *in vacuo*. Analytically pure crystals were grown from a THF solution layered with petroleum ethers, and cooled to

–30 °C. **^{1}H NMR** (C_6D_6, 300 MHz): δ 7.71 (t, 1H, Ar–*H*), 7.49 (d, 2H, Ar–*H*), 7.38 (m, 12H, P(C_6H_5)$_3$), 7.2-7.1 (m, 4H, Ar–*H*), 7.05 (m, 18H, P(C_6H_5)$_3$), 6.77 (t, 1H, Ar–*H*), 6.55 (t, 1H, Ar–*H*), 2.02 (sept., 2H, C*H*(CH_3)$_2$), 1.08 (q, 6H, CH(C*H*$_3$)$_2$), 0.93 (q, 6H, CH(C*H*$_3$)$_2$). **^{13}C{^{1}H} NMR** (C_6D_6, 75 MHz): δ 159.2, 135.49 (d, $\mathcal{J}_{PC}$ = 12.9 Hz), 134.70 (d, $\mathcal{J}_{PC}$ = 17.5 Hz), 133.58, 131.82, 130.02, 129.70, 129.24 (d, $\mathcal{J}_{PC}$ = 8.59 Hz), 123.67, 116.88, 113.43 (d, $\mathcal{J}_{PC}$ = 33.2 Hz), 114.04 (d, $\mathcal{J}_{PC}$ = 342.2 Hz), 23.92 (d, $\mathcal{J}_{PC}$ = 7.44 Hz), 20.48 (d, $\mathcal{J}_{PC}$ = 12.31), 19.23 (d, $\mathcal{J}_{PC}$ = 4.87 Hz). **^{31}P{^{1}H} NMR** (C_6D_6, 120 MHz): δ 7.7 (1P), 5.5 (2P). **Anal. Calcd.** for $C_{54}H_{53}AgNP_3$ C, 70.74; H, 5.83; N, 1.53. Found: C, 70.67; H, 6.03; N, 1.51.

[PN]$_2$Zn (10). To a THF solution of $ZnCl_2$ (16.0 mg, 0.1174 mmol in 3 mL) chilled to –35 °C in a scintillation vial, was added two equivalents of **1** (68.4 mg, 0.235 mmol) in 5 mL cold THF solution, while stirring. The mixture was allowed to warm to room temperature while stirring for 3 hours. The golden reaction solution was then filtered through celite, dried by evaporation, and extracted with diethyl ether. Filtration through celite, followed by washing with 2 mL ether, yielded a golden yellow solution that was layered with petroleum ether and cooled to –30 °C, affording golden crystals of analytically pure **10**. **^{1}H NMR** (C_6D_6, 300 MHz): δ 7.2-7.1 (m, 4H), 7.08-6.9 (m, 10H), 6.61 (t, 2H), 6.25 (m, 2H), 2.36 (sept, 4H, C*H*(CH_3)$_2$), 1.28 (q, 6H, CH(C*H*$_3$)$_2$), 1.18 (q, 6H, CH(C*H*$_3$)$_2$), 1.02 (q, 6H, CH(C*H*$_3$)$_2$), 0.36 (q, 6H, CH(C*H*$_3$)$_2$). **^{13}C{^{1}H} NMR** (C_6D_6, 75 MHz): δ 162.87 (t, $\mathcal{J}_{PC}$ = 7.8 Hz), 154.62, 132.77 (d, $\mathcal{J}_{PC}$ = 6.4 Hz), 129.87, 124.62, 120.69, 115.14, 113.26, 107.85 (t, $\mathcal{J}_{PC}$ = 21.2 Hz), 23.46 (t, $\mathcal{J}_{PC}$ = 7.4 Hz), 21.19 (t, $\mathcal{J}_{PC}$ = 10.5 Hz), 19.35 (t, $\mathcal{J}_{PC}$ = 3.6 Hz), 18.86 (t, $\mathcal{J}_{PC}$ = 4.1 Hz), 17.96 (t, br), 16.69 (s, br). **^{31}P{^{1}H} NMR** (C_6D_6, 120 MHz): δ –

12.23 (2P). **Anal calcd.** for $C_{36}H_{46}ZnN_2P_2$ C, 68.19; H, 7.31; N, 4.42. Found: C, 68.47; H, 7.50; N, 4.04.

Table 2.5. Assorted photophysical properties of all reported complexes.

		λ_{em} (nm)				
Compound	**λ_{abs} (nm)**	**C_6H_6**	**Et_2O**	**THF**	**Stokes Shift, Solvent (nm)**	**λ (cm^{-1})[a]**
1	411, 354, 298	--	480	--	69, Et_2O	8970
2	434, 339	504	500	504	70, C_6H_6	2810
3	427, 350	497	495	501	70, C_6H_6	3080
4	423, 365	534	530	555	111, C_6H_6	7400
5	407, 355	--	465	--	58, Et_2O	4930
6	421, 354	--	550	--	129, Et_2O	6470
7	433, 342	498	499	506	65, C_6H_6	3000
8	444, 332	552	546	563	108, C_6H_6	5120
9	431, 353	544	--	--	113, C_6H_6	12460
10	394, 326	473	--	--	79, C_6H_6	5270

a. The reorganization energy $\lambda = (\Delta\nu_{1/2})^2 / (16RT \ln 2)$.
$\Delta\nu_{1/2}$ = Full width at half max.
R = 8.31451 J mol^{-1} K^{-1}
T = 298 K

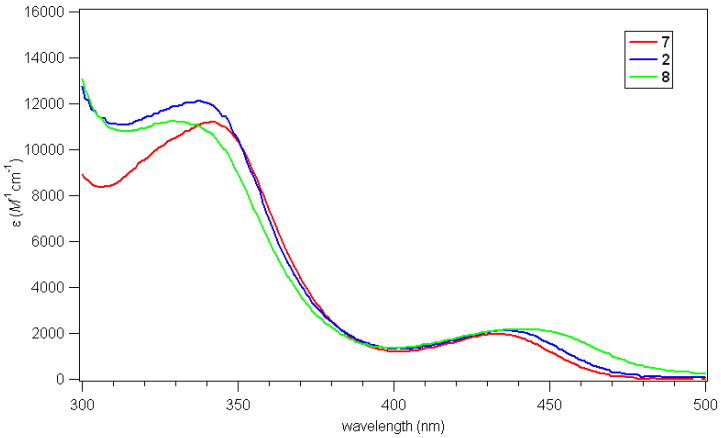

Figure 2.13. Overlay of [PN]Cu(PPh3)2 (**2**), [^{Me}PN]Cu(PPh3)2 (**7**), and [^{CF3}PN]Cu(PPh3)2 (**8**).

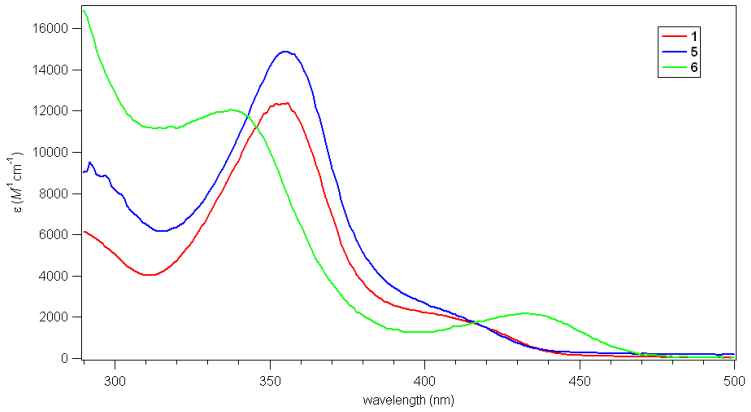

Figure 2.14. Overlay of [PN]Li (**1**), [^{Me}PN]Li (**5**), and [^{CF3}PN]Li (**6**).

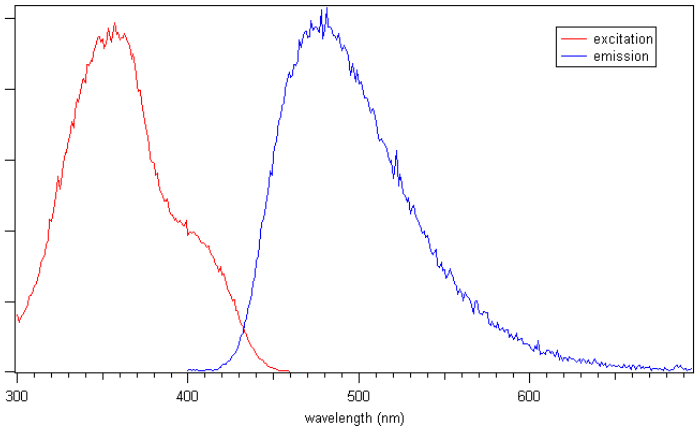

Figure 2.15. Emission/Excitation Spectra of [PN]Li (**1**; λ_{ex} = 350 nm).

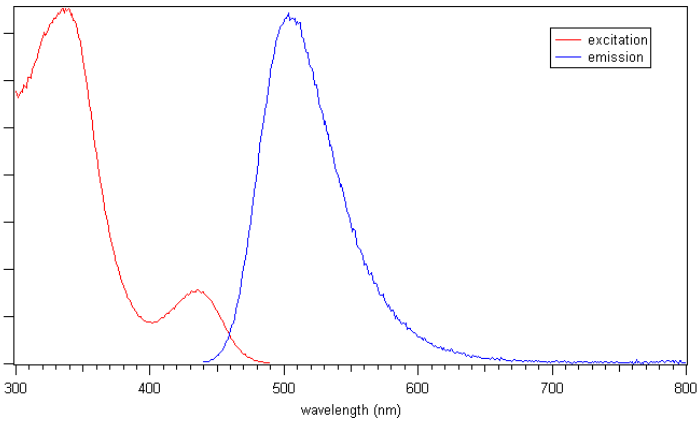

Figure 2.16. Emission/Excitation spectra of [PN]Cu(PPh$_3$)$_2$ (**2**; λ_{ex} = 430 nm).

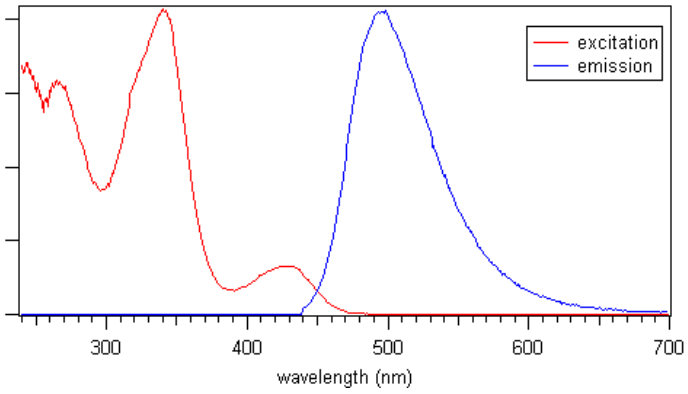

Figure 2.17. Emission/Excitation spectra of [PN]Cu(PMe_3)$_2$ (**3**; λ_{ex} = 430 nm).

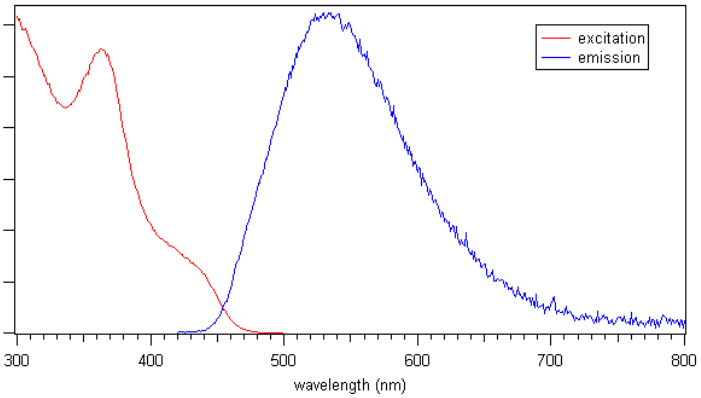

Figure 2.18. Emission/Excitation spectra of [PN]Cu(dppe) (**4**; λ_{ex} = 430 nm).

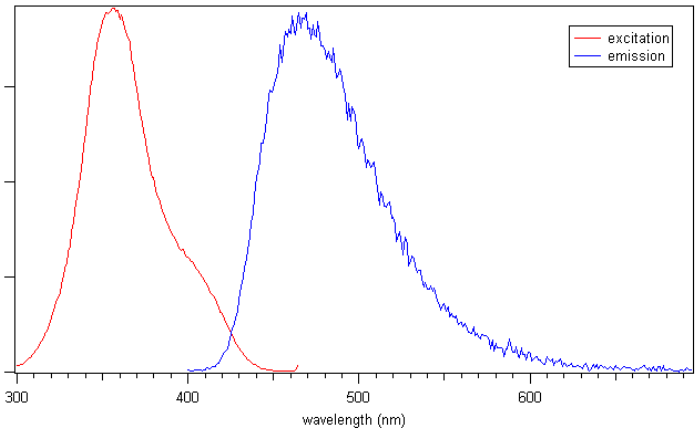

Figure 2.19. Emission/Excitation spectra of [^{Me}PN]Li (**5**; λ_{ex} = 350 nm).

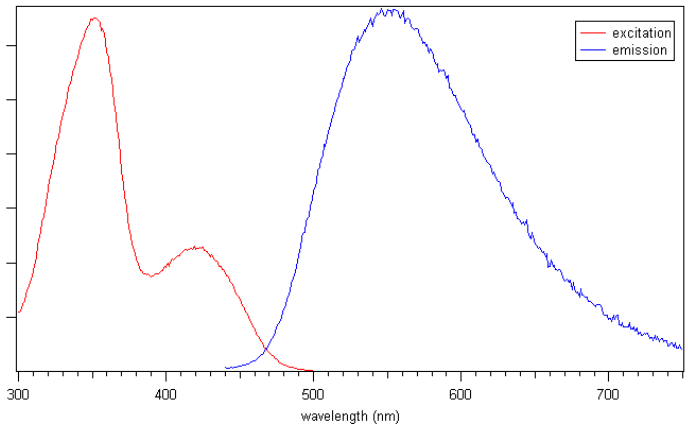

Figure 2.20. Emission/Excitation spectra of [^{CF3}PN]Li (**6**; λ_{ex} = 350 nm).

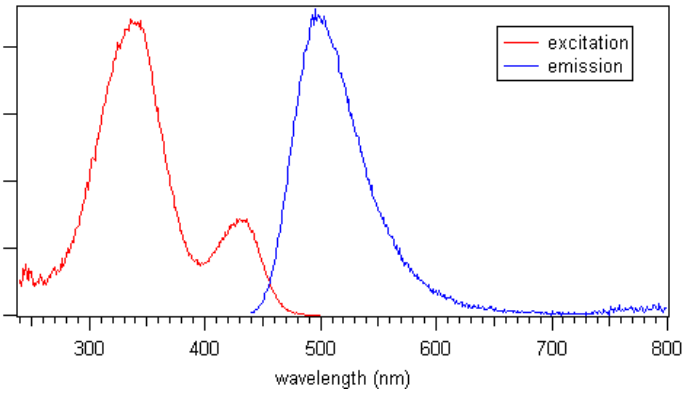

Figure 2.21. Emission/Excitation spectra of [^{Me}PN]Cu(PPh$_3$)$_2$ (**7**; λ_{ex} = 430 nm).

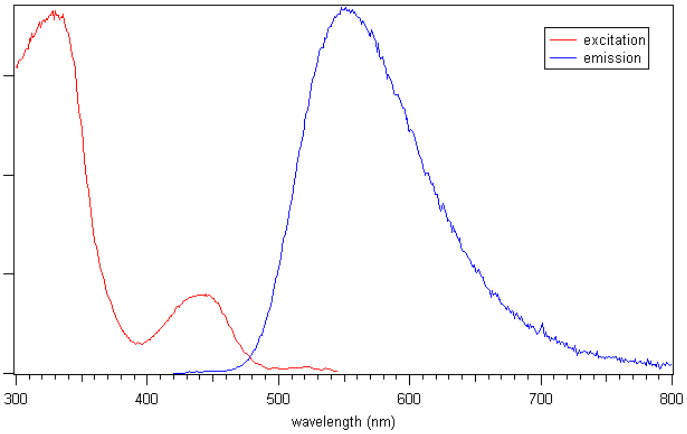

Figure 2.22. Emission/Excitation spectra of [^{CF3}PN]Cu(PPh$_3$)$_2$ (**8**; λ_{ex} = 430 nm).

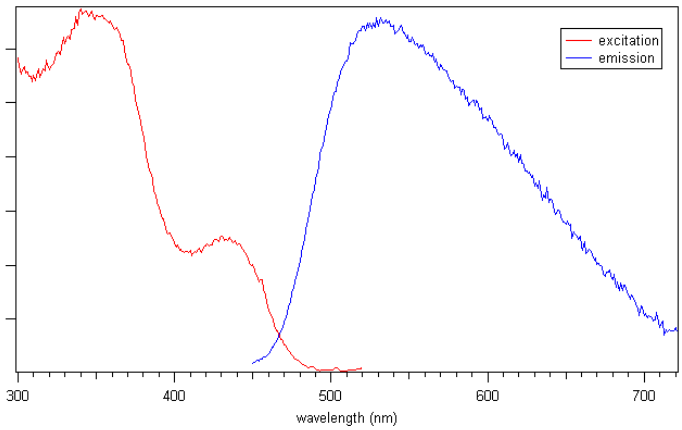

Figure 2.23. Emission/Excitation Spectra of [PN]Ag(PPh_3)$_2$ (**9**; λ_{ex} = 430 nm).

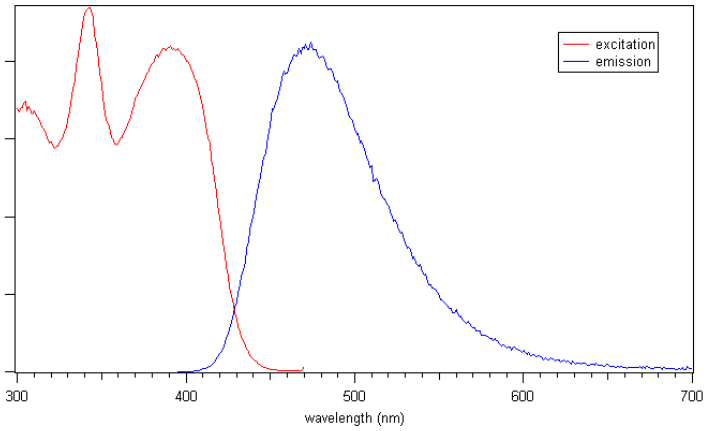

Figure 2.24. Emission/Excitation Spectra of [PN]$_2$Zn (**10**; λ_{ex} = 350 nm).

References

1. (a) Vlcek, A. *Coord. Chem. Rev.* **2000**, *200-202*, 933; (b) Bargossi, C.; Fiorini, M. C.; Montalti, M.; Prodi, L.; Zaccheroni, N. *Coord. Chem. Rev.* **2000**, *208*, 17; (c) de Silva, A. P.; Fox, D. B.; Huxley, A. J. M.; Moody, T. S. *Coord. Chem. Rev.* **2000**, *205*, 41.
2. Chen, C. H.; Shi, J. *Coord. Chem. Rev.* **1998**, *171*, 161.
3. Riegler, J.; Nann, T. *Analytical and Bioanalytical Chemistry* **2004**, *379*, 913.
4. Ciesla, P.; Kocot, P.; Mytych, P.; Stasicka, Z. *J. Mol. Catal. A: Chem.* **2004**, *224*, 17.
5. Brown, G. M.; Brunschwig, B. S.; Creutz, C.; Endicott, J. F.; Sutin, N. *J. Am. Chem. Soc.* **1979**, *101*, 1298.

6. (a) Ford, P. C.; Cariati, E.; Bourassa, J. *Chem. Rev. (Washington, D. C.)* **1999**, *99*, 3625; (b) Horvath, O. *Coord. Chem. Rev.* **1994**, *135/136*, 303; (c) Balzani, V.; Juris, A.; Venturi, M.; Campagna, S.; Serroni, S. *Chem. Rev. (Washington, D. C.)* **1996**, *96*, 759.
7. McMillin, D. R.; McNett, K. M. *Chem. Rev.* **1998**, *98*, 1201.
8. Cuttell, D. G.; Kuang, S.-M.; Fanwick, P. E.; McMillin, D. R.; Walton, R. A. *J. Am. Chem. Soc.* **2002**, *124*, 6.
9. (a) Ziolo, R. F.; Lipton, S.; Dori, Z. *Journal of the Chemical Society D: Chemical Communications* **1970**, 1124; (b) Kutal, C. *Coord. Chem. Rev.* **1990**, *99*, 213.
10. Tsuboyama, A.; Kuge, K.; Furugori, M.; Okada, S.; Hoshino, M.; Ueno, K. *Inorg. Chem. (Washington, DC, U. S.)* **2007**, *46*, 1992.
11. Harkins, S. B.; Peters, J. C. *J. Am. Chem. Soc.* **2005**, *127*, 2030.
12. Harkins, S. B.; Peters, J. C. *J. Am. Chem. Soc.* **2004**, *126*, 2885.
13. Mankad, N. P.; Rivard, E.; Harkins, S. B.; Peters, J. C. *J. Am. Chem. Soc.* **2005**, *127*, 16032.
14. Peters, J. C.; Miller, A. J. M.; Dempsey, J. L. US Patent 7,683,183 B2. 2010.
15. Liang, L.-C.; Lee, W.-Y.; Hung, C.-H. *Inorg. Chem.* **2003**, *42*, 5471.
16. (a) Crosby, G. A.; Demas, J. N. *The Journal of Physical Chemistry* **1971**, *75*, 991; (b) Wallace, W. L.; Bard, A. J. *J. Phys. Chem.* **1979**, *83*, 1350.
17. Scaltrito, D. V.; Thompson, D. W.; O'Callaghan, J. A.; Meyer, G. J. *Coord. Chem. Rev.* **2000**, *208*, 243.
18. Armaroli, N. *Chem. Soc. Rev.* **2001**, *30*, 113.
19. Similar emission from crystalline and solution samples is consistent with unchanged structure in solution.
20. Kirchhoff, J. R.; Gamache, R. E., Jr.; Blaskie, M. W.; Del Paggio, A. A.; Lengel, R. K.; McMillin, D. R. *Inorg. Chem.* **1983**, *22*, 2380.
21. Da Re, R. E.; Jantunen, K. C.; Golden, J. T.; Kiplinger, J. L.; Morris, D. E. *J. Am. Chem. Soc.* **2005**, *127*, 682.
22. McMillin, D. R., *Physical Methods in Bioinorganic Chemistry: Spectroscopy and Magnetism*. University Science Books: Sausalito, CA, 2000.
23. Timpson, C. J.; Bignozzi, C. A.; Sullivan, B. P.; Kober, E. M.; Meyer, T. J. *J. Phys. Chem.* **1996**, *100*, 2915.
24. Deaton, J. C.; Switalski, S. C.; Kondakov, D. Y.; Young, R. H.; Pawlik, T. D.; Giesen, D. J.; Harkins, S. B.; Miller, A. J. M.; Mickenberg, S. F.; Peters, J. C. *J. Am. Chem. Soc.* **2010**, *132*, 9499.
25. Harkins, S. B.; Mankad, N. P.; Miller, A. J. M.; Szilagyi, R. K.; Peters, J. C. *J. Am. Chem. Soc.* **2008**, *130*, 3478.
26. Lotito, K. J.; Peters, J. C. *Chem. Commun.* **2010**, *46*, 3690.
27. Cowley, A. H.; Jones, R. A.; Mardones, M. A.; Nunn, C. M. *Organometallics* **1991**, *10*, 1635.
28. Wenger, O. S.; Henling, L. M.; Day, M. W.; Winkler, J. R.; Gray, H. B. *Inorg. Chem.* **2004**, *43*, 2043.

Chapter 3

Lewis Acid-Assisted Reductive Coupling of Carbon Monoxide

Adapted in part from:
Miller, A. J. M.; Labinger, J. A.; Bercaw, J. E. *J. Am. Chem. Soc.* **2008**, *130*, 11874.
http://dx.doi.org/10.1021/ja805108z
–and–
Miller, A. J. M.; Labinger, J. A.; Bercaw, J. E. *Organometallics* **2010**, *29*, 4499.
http://dx.doi.org/10.1021/om100638d

Chapter 3

Introduction

Many of the approaches under active investigation for obtaining fuels and commodity chemicals from coal, methane, or biomass follow an indirect route via synthesis gas (syngas, CO/H_2), typified by the Fischer-Tropsch (F–T) process.[1] Selective conversion of syngas to discrete multi-carbon hydrocarbons or oxygenates could offer substantial improvements over non-selective F–T.[2] The possibility that homogeneous catalysis might provide more promising opportunities for selective transformations has intrigued organometallic chemists for several decades.[3] While sequential reduction and protonation of mid-to-late transition metal carbonyls resulted in the release of C_2 and higher organics,[3a,4] the hydrides used are not readily obtainable from H_2 and are incompatible with the strong acids required, precluding catalysis. Some early transition metal species (and their f-block congeners) that *can* be formed directly from H_2,[5] such as $Cp^*_2ZrH_2$,[3d] can effect both CO reduction and C–C coupling, but the extremely strong M–O bonds thus generated will again preclude catalysis. A few examples of homogeneous catalytic conversion of syngas to methanol and C_2 products (EtOH, ethylene glycol) have been reported, but extremely high pressures and temperatures are required.[6]

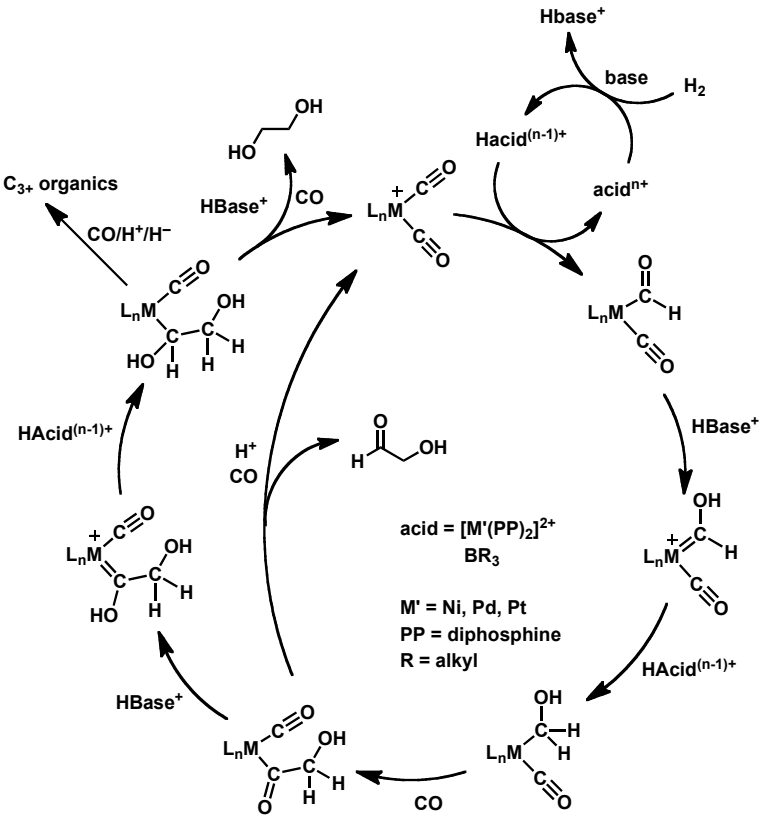

Scheme 3.1

Our renewed interest in this approach[7] was inspired by the discovery that late transition metal hydrides $[HM(PP)_2]^+$ (M = Ni, Pd, Pt; PP = chelating diphosphine ligand), which may be formed directly from H_2 by heterolytic activation, can form C–H bonds by facile nucleophilic attack on metal carbonyl complexes.[8] Because these metals should not form prohibitively strong M–O bonds, we proposed that a dual system, consisting of the late transition metal hydrogen activator along with a relatively electrophilic metal carbonyl complex (probably from the middle of the transition series, where C–H bond formation is well documented[3b,3d,8a,9]) could lead to catalytic conversion, perhaps as shown in Scheme 3.1. We[7b] and others[10] have demonstrated stoichiometric versions of Scheme 3.1, but the various steps operate under conditions that are mutually incompatible; in particular, some

steps require very strong acids or other electrophiles that would react with hydride sources. The difficulty of forming a C–H bond from coordinated CO therefore appears to be a major obstacle to this approach; another challenge is the facile formation of a C–C bond from a reduced carbonyl species.

We have sought to address both of these challenges with a single design element: the incorporation of a Lewis acidic borane in the secondary coordination sphere of a rhenium carbonyl complex. Lewis acid promotion of reductions of organic carbonyls[11] and alkyl migratory insertions of coordinated CO[12] is well known; participation of Lewis acids in homogeneous catalytic CO reduction[6a] and heterogeneous F–T chemistry[13] has also been proposed. The additional advantage of intramolecular attachment could make conversion possible with a relatively weak acidic center, which might not be sufficiently activating as a separate promoter. We report here that this pendent Lewis acid facilitates the delivery of multiple hydride equivalents — from both main group and late transition metal hydrides — to a CO ligand, followed by spontaneous alkyl migration to form a C–C bond.

Results and Discussion

CO reductive coupling promoted by pendent boranes

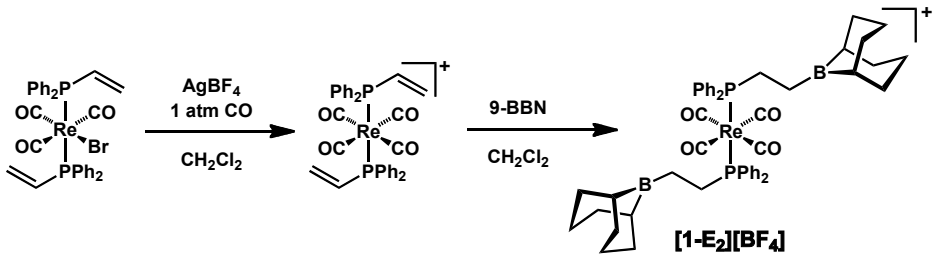

Scheme 3.2

Our first attempts to incorporate a Lewis acid into the secondary coordination sphere of a transition metal carbonyl utilized a templated ligand synthesis to access a weakly Lewis acidic trialklyborane (Scheme 3.2). Commercially available diphenylvinylphosphine was metallated with $Re(CO)_5Br$ at 120 °C in toluene in a sealed vessel, yielding *trans,mer*-$(Ph_2PC_2H_3)_2Re(CO)_3Br$ as a white powder in good yield. Subsequent treatment with $AgBF_4$ under 1 atm of CO afforded cationic $[(Ph_2PC_2H_3)_2Re(CO)_4][BF_4]$. Hydroboration with 9-BBN (9-borabicyclo[3.3.1]nonane) proceeded over 48 hours at 70 °C to afford the desired product $[(Ph_2P(CH_2)_2B(C_8H_{14}))_2Re(CO)_4][BF_4]$ ([**1-E$_2$**][BF_4]). The phosphinoborane ligand can be independently synthesized,[14] but metallation is nontrivial due to thermal decomposition.

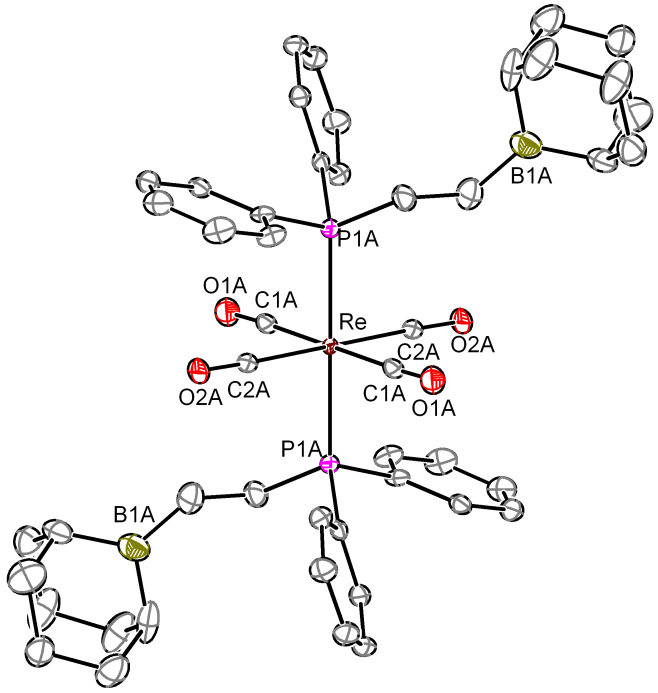

Figure 3.1. Structural representation (50% ellipsoids) of complex [**1-E$_2$**][BF$_4$]. Hydrogen atoms, BF$_4$ counterion, and solvent molecules of crystallization omitted for clarity. Selected bond lengths (Å) and angles (°): Re–C1A, 1.984(3); Re–C2A, 2.003(3); Re–P1A, 2.4377(8); P1A–Re–P1A#1, 180.0; C1A–Re–C2A, 86.7(1).

An X-Ray diffraction (XRD) study confirmed the expected structure of [**1-E$_2$**][BF$_4$] (Figure 3.1). As strongly donating solvents were avoided throughout the synthesis of [**1-E$_2$**]$^+$, the boron centers in the 9-BBN groups remain three-coordinate. The IR spectrum of [**1-E$_2$**][BF$_4$] shows a single CO stretch at 1998 cm^{-1}, similar to the PPh$_3$ analogue [(PPh$_3$)$_2$Re(CO)$_4$][BF$_4$] (ν_{CO} = 2000 cm^{-1}).[15] CO stretching frequency can be roughly correlated with hydride acceptor ability: e.g., [Cp*Re(CO)$_2$NO]$^+$ (ν_{CO} = 2092, 2036 cm^{-1}) readily reacts with group 10 hydrides, while [(PPh$_3$)$_2$Re(CO)$_4$]$^+$ (ν_{CO} = 2000 cm^{-1}) does not.

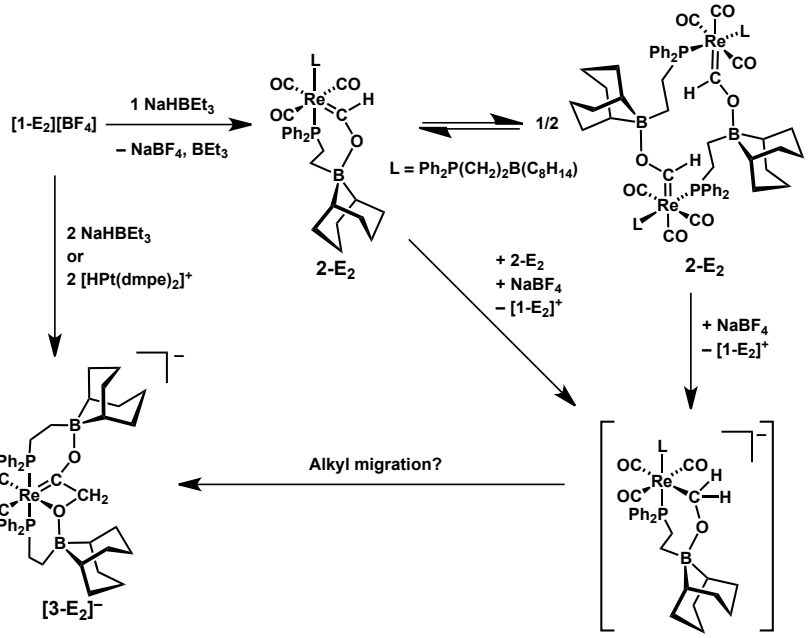

Scheme 3.3

Despite similar CO stretching frequencies, the pendent borane has a strong impact on the hydride acceptor ability of [**1-E2**]$^+$. Addition of one equivalent of [HPt(dmpe)$_2$][PF$_6$] ([**HPt**][PF$_6$]) in either C_6D_5Cl or 1,2-$C_6H_4F_2$ leads to a new proton resonance at δ 13.95 and precipitation of [Pt(dmpe)$_2$][BF$_4$]$_x$[PF$_6$]$_{2-x}$ ([**Pt**]$^{2+}$). [(PPh$_3$)$_2$Re(CO)$_4$]$^+$ does not readily react with [**HPt**]$^+$. We attribute the downfield NMR signal to a neutral boroxycarbene such as **2-E2** (Scheme 3.3), formed in 60-70% yield. In hopes of achieving complete conversion, one equivalent of the stronger hydride donor NaHBEt$_3$ (1.0 M in toluene) was added to a PhCl solution of [**1-E2**][BF$_4$], affording a yellow solution that showed quantitative formation of **2-E2**, as assessed by ^{31}P{^{1}H} NMR, IR, and the unique ^{1}H NMR resonance at δ 13.95. Decomposition with formation of the starting material [**1-E2**]$^+$ and an unknown species took place over several days in solution. Performing the hydride addition in CD_2Cl_2 also gave the NMR signal (along with additional products that may

include Re–Cl species), and colorless crystals grew overnight. An XRD study verified that the boroxycarbene feature was present, but the structure so obtained is bimetallic, with the oxygen of the carbene on one Re interacting with the boron from the other, generating a 14-membered cycle (Figure 3.2).

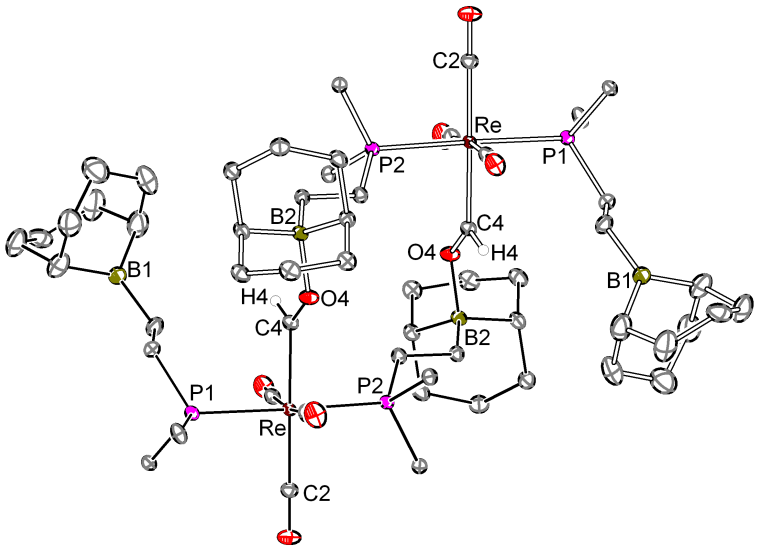

Figure 3.2. XRD structural representation (50% ellipsoids) of complex **2-E$_2$**. Most hydrogens omitted and phenyl rings trimmed for clarity. Selected bond legnths (Å) and angles (°), **2-E$_2$**: Re–C4 2.118(1), C4–O4 1.253(1), O4–B2 1.612(1), Re–C4–O4 126.12(8), C4–O4–B1 126.87(8).

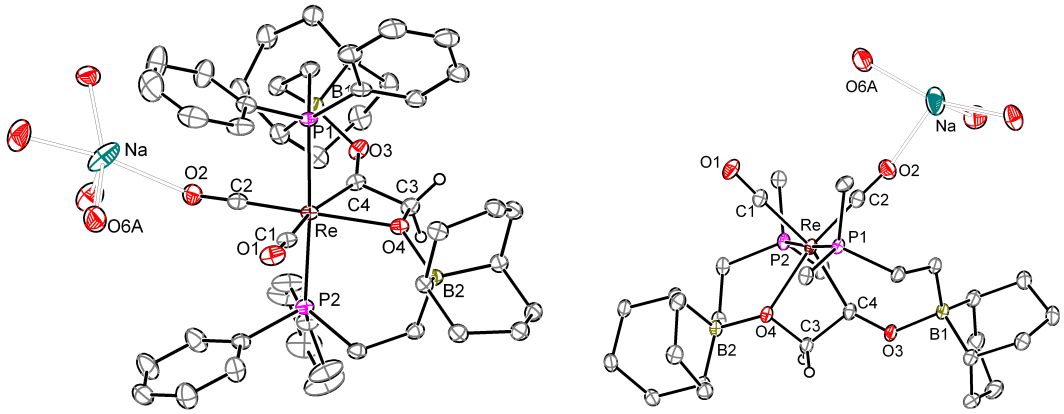

Figure 3.3. Structural representation (two views) of [Na•3.5THF•0.5Et_2O][**3-E$_2$**], ellipsoids at 50% probability. Most hydrogen atoms and carbons from disordered Na-coordinated THF (and most phenyl C atoms in top view) are omitted for clarity. Selected bond legnths (Å) and angles (°): Re–C4 2.0960(9), Re–O4 2.2322(7), C4–O3 1.271(1), C3–C4 1.513(1), C3–O4 1.423(1), Re–C4–O3 147.27(7), C4–C3–O4 102.79(7).

Attempts to crystallize **2-E$_2$** by vapor diffusion of Et_2O into a PhCl solution took days, but eventually yielded colorless plates; XRD revealed transformation to complex [**3-E$_2$**]$^-$ (Scheme 3.3), a novel boroxy(boroxymethyl)carbene generated by formation of a new C–C bond. The oxygen of the boroxymethyl group coordinates to Re, forming three rhenacycles of 7, 4, and 6 members; a sodium cation bound by ether molecules interacts with one of the two remaining CO ligands (Figure 3.3). The structure shown in Figure 3.3 was obtained from isolated [Na][**3-E$_2$**], which yielded the solvate [Na•3.5THF•0.5Et_2O][**3-E$_2$**] from THF/Et_2O vapor diffusion. (Other solvent systems for crystallization yielded different solvates, with structures of lower quality; details in the Experimental Section).

A plausible mechanism for the production of [Na][**3-E$_2$**] begins with disproportionation of **2-E$_2$**, forming a boroxyalkyl via intra- or intermolecular hydride transfer (the two boroxycarbene carbons are ~5 Å apart), with concomitant formation of tetracarbonyl cation [**1-E$_2$**]$^+$ (Scheme 3.3). Boroxyalkyl migration to CO would generate [**3-E$_2$**]$^-$. The

decanted supernatant after crystallization of [Na][**3-E$_2$**] indeed contained predominantly [**1-E$_2$**]$^+$, along with some residual [Na][**3-E$_2$**]. The reaction could also be intermolecular, as the dimer might dissociate in solution. It is notable that no additional CO or other ligand is needed to induce alkyl migration.

Addition of *two* equivalents $NaHBEt_3$ to a PhCl solution of [**1-E$_2$**][BF_4] resulted in the immediate precipitation of [Na][**3-E$_2$**] in 80-95% isolated yield. (In contrast, $[(PPh_3)_2Re(CO_4)]^+$ yields a formyl with one equivalent $NaHBEt_3$,[15] but does not react further with excess borohydride.) This preparation allowed full characterization of [Na][**3-E$_2$**]. The asymmetry shown in the crystal structure is evident by NMR as well, with two doublets (δ 12.0, 17.7) in the $^{31}P\{^1H\}$ NMR, and complex aromatic and aliphatic regions in the ^1H NMR; the [C*H*$_2$O] group resonates as two doublets at δ 4.55 and 4.64. The infrared spectrum of [Na][**3-E$_2$**] exhibits two CO stretches at 1848 and 1933 cm^{-1}, consistent with a relatively electron rich species. The carbenoid nature of [Na][**3-E$_2$**] is apparent in the $^{13}C\{^1H\}$ NMR spectrum, with a characteristic doublet of doublets at 303.4 ppm.

It is noteworthy that the conversion of [**1-E$_2$**]$^+$ to [**3-E$_2$**]$^-$ can also be carried out with two equivalents [**HPt**]$^+$, in slightly lower yield (~70%). Since the Pt hydride can be preformed externally by heterolytic cleavage of H_2 in the presence of a suitable base (KOPh or tetramethylguanidine),[8b] this transformation amounts to the net formation of a C_2 species from intermediates directly obtainable from CO and H_2.

Ligand effects on the reductive coupling of CO

Our initial findings revealed that incorporation of a borane into the secondary coordination sphere of a Re carbonyl complex fundamentally alters reactivity by facilitating hydride transfer, permitting a group 10 transition metal hydride generated from H_2 to serve as hydride source, and promoting C–C bond formation by alkyl migration, even in the absence of a strong donor.

While alkylborane-based systems are probably not viable catalysts because of strong B–O bonding, they do provide an excellent framework for investigating some of the key issues arising from this approach. In particular, what factors affect how the chelate effect operates? How does reactivity depend on the length of the tether connecting the borane to the metal center? Can an external borane promote the same transformations? What happens if there is only one Lewis acid center attached instead of two? We would also like to learn something about the fundamental mechanism of this transformation: how is hydride transferred from Pt to C, and how does C–C bond formation take place? We report here on our findings.

Reduction of $[(PPh_3)_2Re(CO)_4]^+$ ($[1\text{-}Ph_2]^+$)

To further probe the role of pendent (internal) boranes, we explored the chemistry of $[(PPh_3)_2Re(CO)_4]^+$ ($[\mathbf{1\text{-}Ph_2}]^+$) with ($[\mathbf{HPt}]^+$; see Scheme 3.6 below for system used for abbreviations) in the absence and presence of added external Lewis acids, as summarized in Scheme 3.4. A solution of $[\mathbf{1\text{-}Ph_2}][BPh_4]$ and $[\mathbf{HPt}][PF_6]$ in C_6D_5Cl shows no discernible reaction over 24 hours, although it should be noted that $[\mathbf{1\text{-}Ph_2}][BPh_4]$ is only slightly

soluble in C_6D_5Cl.[7a] In addition, the choice of anion can play an important role in reductions using [**HPt**]$^+$: as previously reported, the equilibrium shown in Scheme 3.5 lies far toward the left side (unreduced [**1-E$_2$**]$^+$), but can be driven to the right by precipitation of [**Pt**][BF_4]$_x$[PF_6]$_{2-x}$.[7c] Suspensions of [**1-Ph$_2$**][BF_4] (also fairly insoluble) and [**HPt**][PF_6] in C_6D_5Cl or THF slowly convert to a mixture of $(PPh_3)_2Re(CO)_3(CHO)$ (**2-Ph$_2$**; ^{1}H NMR ReC*H*O, δ 15.22 in C_6D_5Cl), $(PPh_3)_2Re(CO)_3(H)$ (**4-Ph$_2$**) and $(PPh_3)Re(CO)_4(H)$ (**4-Ph$_1$**). The half-life for consumption of [**HPt**]$^+$ is 2-4 d, and the yield of **2-Ph$_2$** never exceeds ~5% (by NMR, relative to [**HPt**]$^+$). Therefore, while the unassisted transfer of a hydride from [**HPt**]$^+$ to [**1-Ph$_2$**]$^+$ can be observed, it appears to be thermodynamically unfavorable unless driven by precipitation of the [**Pt**]$^{2+}$ salt, and is kinetically so slow that decarbonylation to the Re–H products dominates, preventing formation of more than a very small amount of formyl complex.

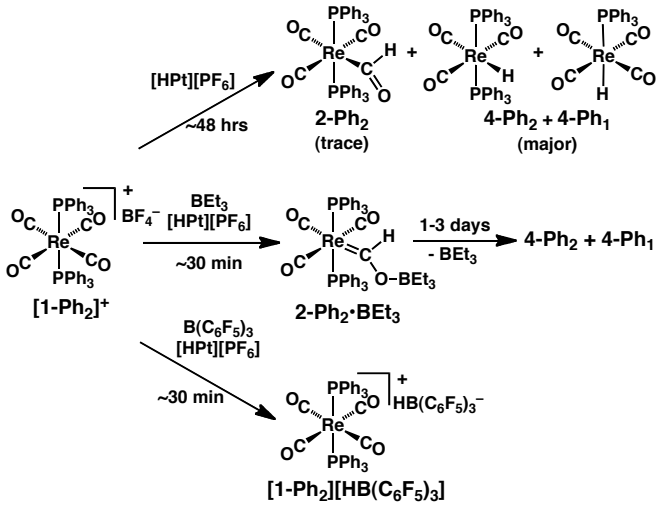

Scheme 3.4

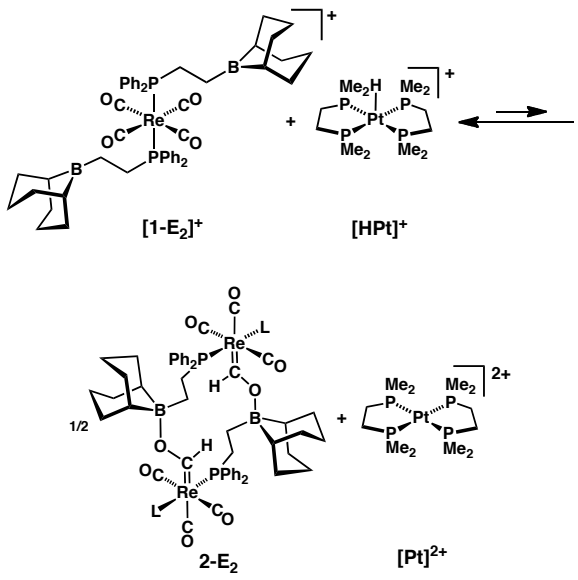

Scheme 3.5

Addition of isopropyl pinacol borate, a weak Lewis acid, has no effect on the above reaction: only traces of the characteristic ^{1}H NMR formyl signal for **2-Ph$_2$** are observed, at an essentially unchanged chemical shift (ReC*H*O, δ 15.21) that indicates no interaction between the formyl oxygen and the boron center. In contrast, a solution of [**1-Ph$_2$**][BF_4] with [**HPt**][PF_6] and two equivalents ^{t}Bu(CH_2)$_2$B(C_8H_{14}) in C_6D_5Cl shows clean conversion to a formyl species in a couple of hours. (When [**1-Ph$_2$**][BAr^F_4] was treated with [**HPt**][PF_6] in the presence of 2 or 10 equivalents of BEt_3 (1.0 M in hexanes), only ~1% boroxycarbene was detected, and no further reaction was observed over ~24 h, consistent with inhibition of reduction by small amounts of [**Pt**][BAr^F_4]$_2$ in solution. The Re–C*H*O resonance (δ 14.60) is shifted well upfield from that observed for the Lewis acid-free reaction, and the ^{31}P NMR resonance also differs (δ 14.5, vs. δ 15.8 in the absence of borane), indicating significant interaction between the borane and the formyl ligand.

Treatment of [**1-Ph$_2$**]$^+$ with NaHBEt$_3$ gave a spectroscopically similar product which was structurally characterized by X-Ray diffraction (XRD) as the boroxycarbene (PPh$_3$)$_2$Re(CO)$_3$(CHOBEt$_3$) (**2-Ph$_2$•BEt$_3$**) (Figure 3.4). In comparison to analogous adducts of the stronger Lewis acids BF$_3$ and B(C$_6$F$_5$)$_3$,[7b] the boroxycarbene moiety in **2-Ph$_2$•BEt$_3$** has longer B–O and Re–C bonds and a shorter C–O bond, consistent with less carbene character and a weaker B–O interaction. Accordingly, the BEt$_3$ can be removed under vacuum to afford **2-Ph$_2$**.

Complexes such as **2-Ph$_2$•BEt$_3$** can be regarded as either borane-stabilized formyls or as boroxycarbenes. There is a continuum, and M–CHO–BR$_3$ species are probably best considered intermediate between formyl and boroxycarbene. For simplicity, we choose to describe them as boroxycarbenes here, due to the lack of observed C=O stretch in the IR and the relatively upfield Re–*C*HO ^{13}C chemical shift. Solid-state structures are intermediate between carbene and formyl.

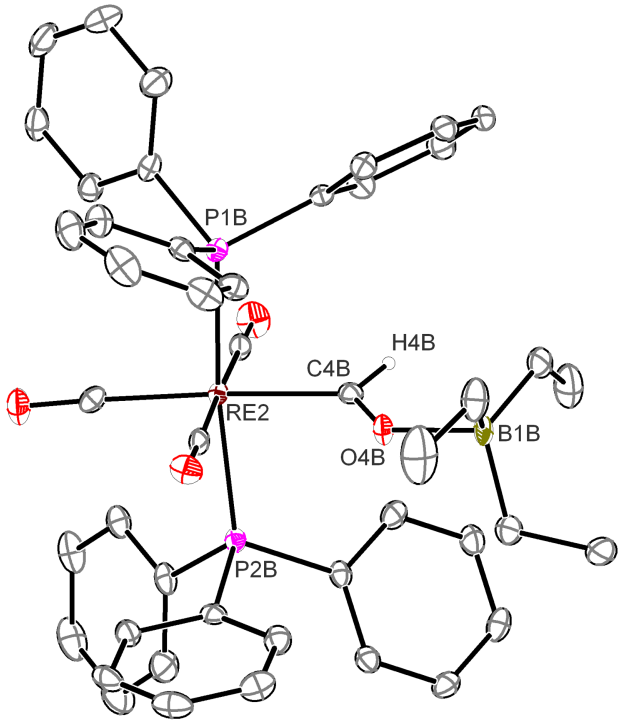

Figure 3.4. Structural representation of **(2-Ph$_2$•**BEt$_3$)•($C_6H_5CH_3$) with thermal ellipsoids at 50% probability. Only one of the two independent molecules in the asymmetric unit is portrayed; the bond lengths and angles are similar. H-atoms (except on the carbene) and two toluene solvent molecules of crystallization are omitted for clarity. Selected bond lengths (Å) and angles (°): Re2–C4B 2.126(3), Re–CO(avg) 1.985, C4B–O4B 1.252(3), O4B–B1B 1.638(3), Re2–C4B–O4B 125.2(2), C4B–O4B–B1B 129.2(2).

On titration of $(PPh_3)_2Re(CO)_3(CHO)$ with a solution of ^{t}Bu$(CH_2)_2$B(C_8H_{14}) in THF-*d*$_8$ the formyl ^{1}H NMR resonance showed a steady upfield shift, with no change in lineshape, consistent with fast, reversible adduct formation. The equilibrium constant for adduct formation was estimated from a Benesi-Hildebrand plot[16] as K_{eq} = 100 M^{-1}, corresponding to a free energy of B–O bond formation of 11.4 kcal mol^{-1}. Notably, ^{t}Bu$(CH_2)_2$B(C_8H_{14}) prefers to bind to $(PPh_3)_2Re(CO)_3(CHO)$ over THF (K_{eq} = 0.19 M^{-1})[7c] by roughly three orders of magnitude.

The BEt_3-stabilized formyl **2-Ph$_2$•BEt$_3$** is somewhat longer-lived than **2-Ph$_2$**, but still decomposes over the course of a few days to Re–H species **4-Ph$_2$** and **4-Ph$_1$** (Scheme 3.4; decomposition times tend to vary widely, as has been observed for other formyls[17]). No further reduction was observed when **2-Ph$_2$•BEt$_3$** was treated with additional $NaHBEt_3$ or [**HPt**][PF_6], even in the presence of excess trialkylborane.

The stronger Lewis acid $B(C_6F_5)_3$ does not promote C–H bond formation from [**1-Ph$_2$**][BF_4] and [**HPt**][PF_6]. Instead, hydride is transferred from [**HPt**]$^+$ to B, forming the stable salt [**1-Ph$_2$**][$HB(C_6F_5)_3$] along with precipitated [**Pt**]$^{2+}$. $B(C_6F_5)_3$ forms a stable boroxycarbene when added to pre-formed $(PPh_3)_2Re(CO)_3(CHO)$,[7b] but gentle heating of **2-Ph$_2$•B(C$_6$F$_5$)$_3$** provides the same tetracarbonyl borohydride salt [**1-Ph$_2$**][$HB(C_6F_5)_3$],[18] suggesting that $[HB(C_6F_5)_3]^-$ is a weaker hydride donor than **2-Ph$_2$**. Similar to **2-Ph$_2$•BEt$_3$**, **2-Ph$_2$•B(C$_6$F$_5$)$_3$** shows no further reaction with hydride sources.[18]

In summary, while small amounts of an unstable formyl can be generated slowly from [**1-Ph$_2$**]$^+$ and [**HPt**]$^+$ alone, high yields of a boroxycarbene (stabilized formyl) species were generated rapidly from [**1-Ph$_2$**]$^+$ and [**HPt**]$^+$ in the presence of the *appropriate* external Lewis acid. Trialkylborate Lewis acids are too weak to have an effect; the strong Lewis acid $B(C_6F_5)_3$ diverts the hydride transfer to make a stable borohydride; intermediate acid strength trialkylboranes greatly accelerate the first hydride transfer reaction, and increase the lifetime of the reduced product. However, none of the external Lewis acids promote the further reduction or C–C coupling chemistry achieved by the pendent Lewis acid in [**1-E$_2$**]$^+$.[7b]

Synthesis of Complexes with Pendent Boranes

Given the importance of intramolecular interactions, a structure-function study on pendent Lewis acid assistance was designed, requiring complexes in which the number of phosphinoborane ligands and the length of the hydrocarbon chain connecting P and B are varied. Complexes with one or two phosphinoborane ligands with $(CH_2)_{1\text{-}3}$ linkers were synthesized, along with a mixed complex containing one phosphinoborane and one simple tertiary phosphine ligand. A system which identifies the phosphine ligand(s) and the class of complex will be used, as depicted in Scheme 3.6. The ligands will be identified by the specific hydrocarbon linker (methylene, 1,2-ethanediyl, 1,3-propanediyl): **M** = $Ph_2PCH_2B(C_8H_{14})$, **E** = $Ph_2P(CH_2)_2B(C_8H_{14})$, **P** = $Ph_2P(CH_2)_3B(C_8H_{14})$, and **Ph** = PPh_3. The cationic rhenium carbonyl fragment is designated [**1**]$^+$, with the first reduction Re–CHO products designated **2**, and the doubly-reduced C–C coupled products designated [**3**]$^-$. The number of phosphine ligands dictates the number of carbonyl ligands on the metal complexes: for [**1-M**$_1$]$^+$, [**1**]$^+$ = $[Re(CO)_5]^+$; for [**1-M$_2$**]$^+$, [**1**]$^+$ = $[Re(CO)_4]^+$.

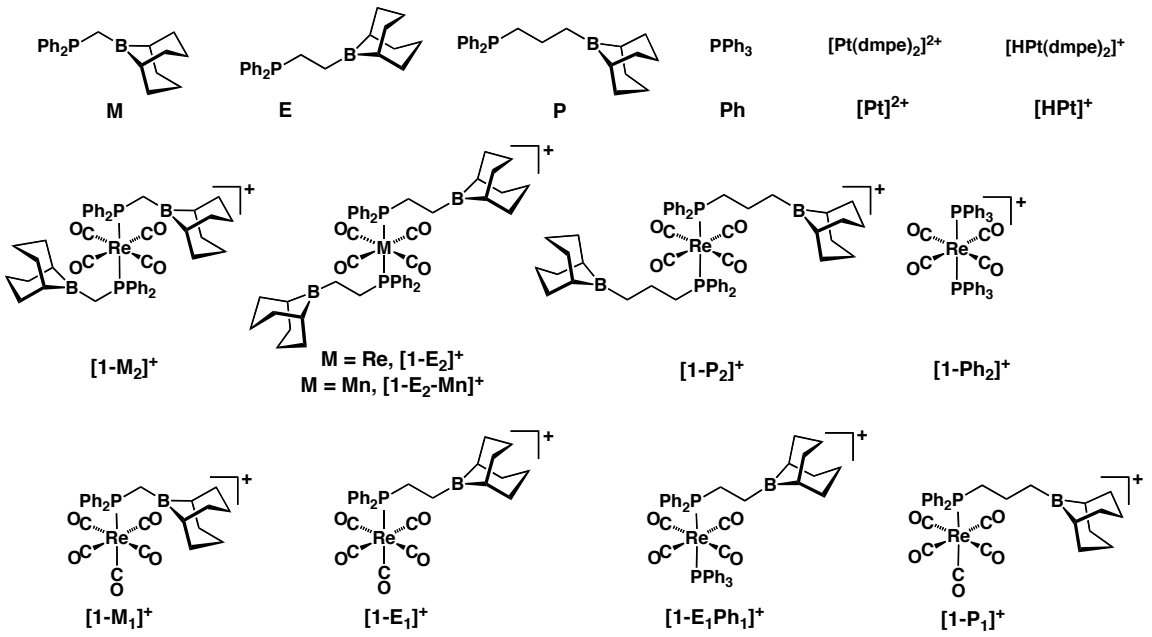

Scheme 3.6

Two routes are available for bis(phosphinoborane) complexes: prior generation of the entire ligand followed by coordination, or hydroboration of a pre-coordinated alkenylphosphine (Scheme 3.7). The ethylene-linked cation [**1-E$_2$**][BF$_4$] was described above;[7a] the Mn analogue [**1-E$_2$-Mn**][BF$_4$] was obtained in good yield by a similar procedure, as was the complex with a propylene-linked phosphinoborane ligand ([**1-P$_2$**][BF$_4$]). Hydroboration of the allylphosphine with 9-BBN proceeded significantly more readily than the vinyl analogue, possibly reflecting reduced conjugation of the double bond with the electron-deficient metal center.

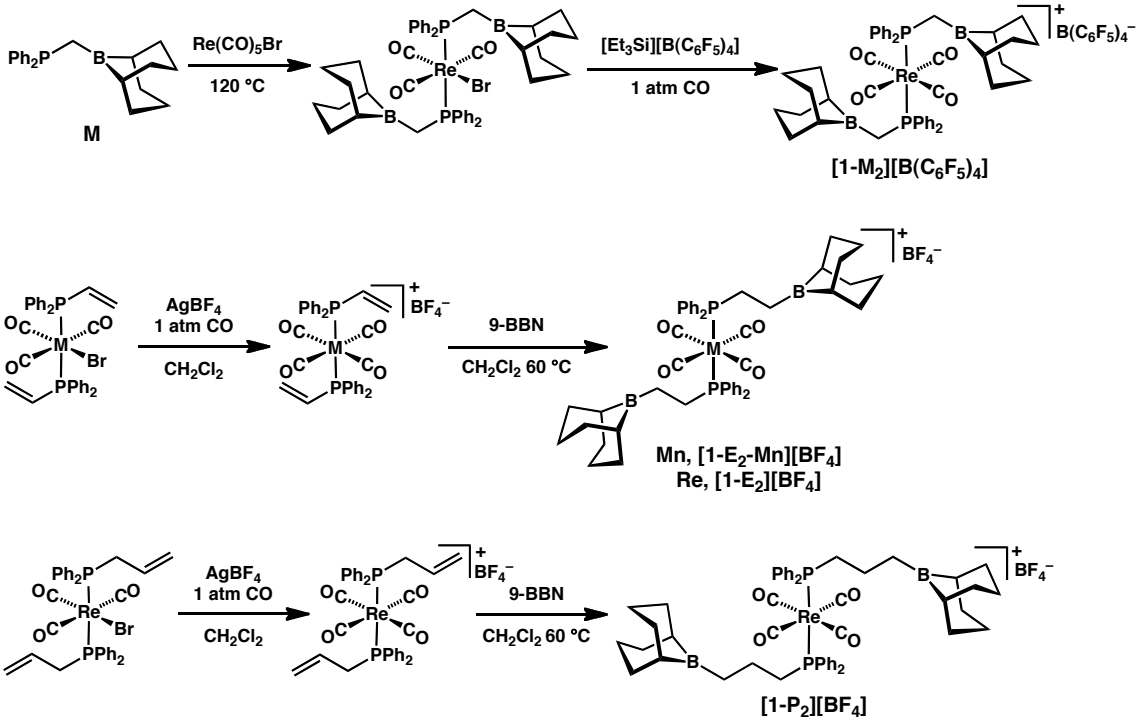

Scheme 3.7

The ligand with a methylene spacer is inaccessible by hydroboration; the reaction of Ph_2PCH_2Li and $ClB(C_8H_{14})$ in cold pentane affords an insoluble white powder from which $Ph_2PCH_2B(C_8H_{14})$ is obtained. Treatment of $Re(CO)_5Br$ with two equivalents of $Ph_2PCH_2B(C_8H_{14})$ produced *trans,mer*-$(Ph_2PCH_2B(C_8H_{14}))_2Re(CO)_3Br$, from which halide abstraction could not be achieved with Ag^+ (which reacts with trialkylboranes)[19] or Tl^+ salts; but addition of $[Et_3Si][B(C_6F_5)_4]$[20] to a C_6H_5Cl solution under 1 atm CO gave the desired cation, *trans*-$[(Ph_2PCH_2B(C_8H_{14}))_2Re(CO)_4][B(C_6F_5)_4]$ ($[\mathbf{1\text{-}M_2}][B(C_6F_5)_4]$), whose structure was confirmed by XRD (Figure 3.5). As in $[\mathbf{1\text{-}E_2}][BF_4]$, no intramolecular CO···B interaction is observed (although there are close contacts between the $[B(C_6F_5)_4]$ anion and nearby CO's: O3–F19 2.867 Å, O4–F19 3.042 Å).

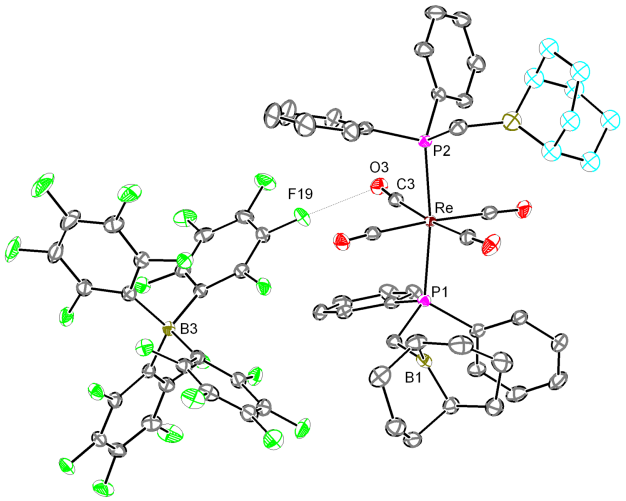

Figure 3.5. Structural representation of [**1-M$_2$**][B(C_6F_5)$_4$], with ellipsoids shown at 50% probability. One of the B(C_8H_{14}) groups was disordered by a rotation around the B–C bond; only the major component (66%) is shown (represented as light blue isotropic atoms). All H atoms and a disordered dichloroethane solvent molecule of crystallization are omitted for clarity. Selected bond lengths (Å) and angles (°): Re–P1 2.4521(5), Re–P2 2.4509(5), Re–C(avg) = 1.99, P1–Re–P2 172.34(2).

Reaction of [(PPh_3)Re($CO)_5$]OTf with $Ph_2P(CH_2)_2B(C_8H_{14})$ seemed an obvious route to an asymmetric cation with only one Lewis acid, but under both thermal and photolytic conditions only intractable mixtures were obtained. Instead, the reaction of *trans*-Re(PPh_3)(I)($CO)_4$[21] with AgOTf followed by $Ph_2P(CH_2)_2B(C_8H_{14})$ under gentle heating gives *trans*-[($Ph_2P(CH_2)_2B(C_8H_{14})$($PPh_3$)Re($CO)_4$][OTf] (**1-E$_1Ph_1$**) in good yield (Scheme 3.8).

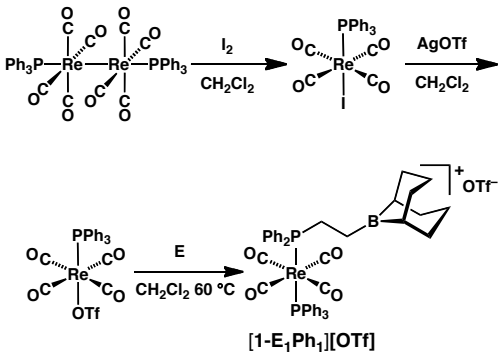

Scheme 3.8

Complexes with a single phosphine ligand were synthesized starting with $Re(CO)_5OTf$ (Scheme 3.9). Both $Ph_2PCH_2B(C_8H_{14})$ and $Ph_2P(CH_2)_2B(C_8H_{14})$[14a] displace triflate from $Re(CO)_5OTf$ at 60 °C to give $[(Ph_2PCH_2B(C_8H_{14}))Re(CO)_5][OTf]$ ([**1-M$_1$**][OTf]), which was characterized crystallographically (Figure 3.6), and $[(Ph_2P(CH_2)_2B(C_8H_{14}))Re(CO)_5][OTf]$ ([**1-E$_1$**][OTf]), respectively. The propylene-linked analogue was obtained by reaction of $Ph_2PCH_2CHCH_2$ with $Re(CO)_5OTf$ at 60 °C, affording $[(Ph_2PCH_2CHCH_2)Re(CO)_5][OTf]$; hydroboration with 9-BBN gave $[(Ph_2P(CH_2)_3B(C_8H_{14}))Re(CO)_5][OTf]$ ([**1-P$_1$**][OTf]).

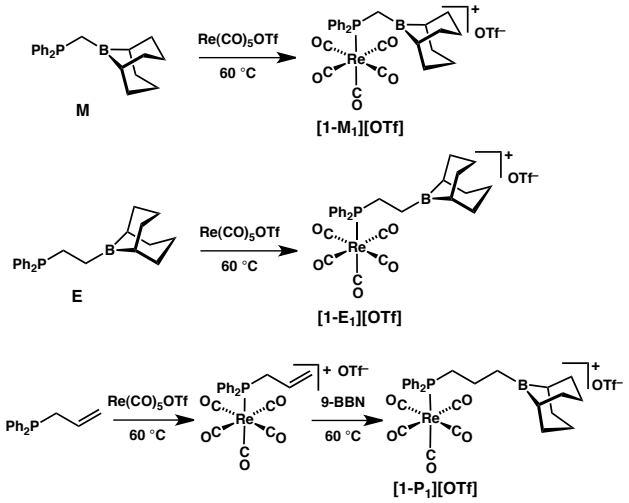

Scheme 3.9

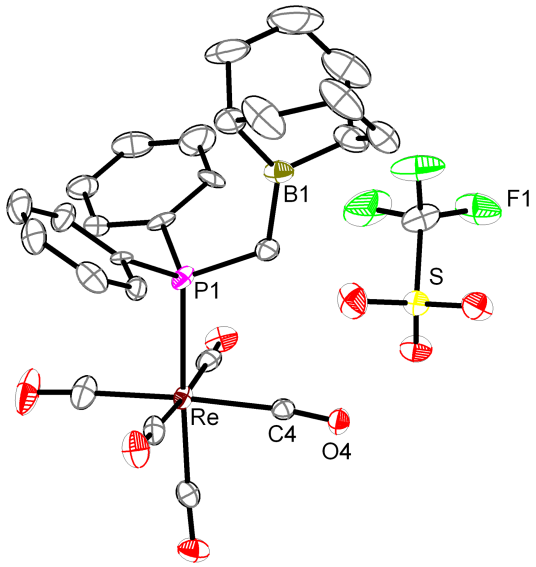

Figure 3.6. Structural representation of [**1-M$_1$**][OTf], ellipsoids at 50% probability. A highly disordered solvent molecule was omitted for clarity. The two phenyl groups were disordered by rotation about the P–C bond, and only the major contributor is included for clarity. Selected bond lengths (Å) and angles (°): Re–C1 2.027(2), Re–C2 2.000(2), Re–C3 2.016(2), Re–C4 2.021(2), Re–C5 1.973(2), Re–P 2.4846(5), P–Re–C5 176.54(6), C1–Re–C3 176.96(8).

Reduction of [(Ph$_2$PCH$_2$B(C$_8$H$_{14}$))$_2$Re(CO)$_4$]$^+$ ([1-M$_2$]$^+$)

[**1-M$_2$**]$^+$ was readily synthesized only as the [B(C$_6$F$_5$)$_4$]$^-$ salt, which complicated reductions with [**HPt**]$^+$: reduction with [**HPt**][PF$_6$] proceeded very slowly to ~90% conversion (by NMR) over 6 days. Partially soluble [**Pt**][B(C$_6$F$_5$)$_4$]$_2$, visible by NMR in small amounts throughout the reaction, may inhibit reduction according to the equilibrium in Scheme 3.5 (precipitation of [**Pt**]$^{2+}$ cannot drive the reaction). To circumvent this problem, [**1-M$_2$**][B(C$_6$F$_5$)$_4$] was treated with both [hept$_4$N][BF$_4$] (or NaBF$_4$) and [**HPt**][PF$_6$] in C$_6$D$_5$Cl, which led to complete consumption of [**1-M$_2$**]$^+$ and formation of a new Re species over ~3 hours in > 95% yield (by NMR), with concomitant precipitation of [**Pt**][BF$_4$]$_x$[PF$_6$]$_{2-x}$. At room temperature the ^{1}H NMR spectrum of the product exhibits a diagnostic triplet at δ 13.89 ($\mathcal{J}_{PH}$ = 5.9 Hz) but is otherwise broad and nondescript, while the ^{31}P{^{1}H} NMR spectrum shows two very broad resonances. (Similar reactivity and spectroscopy was observed in THF-*d$_8$*). Variable temperature NMR studies showed fluxional behavior; at low temperatures both the ^{1}H and ^{31}P NMR spectra display sharp doublets indicating nonequivalent P and CH$_2$ groups. These results strongly indicate the boroxycarbene structure **2-M$_2$** (Scheme 3.10), although we were unable to obtain an analytically pure sample. (See Experimental Section for details of the NMR and assignment; a related intramolecular boroxycarbene has been obtained for a CpFe system.[22])

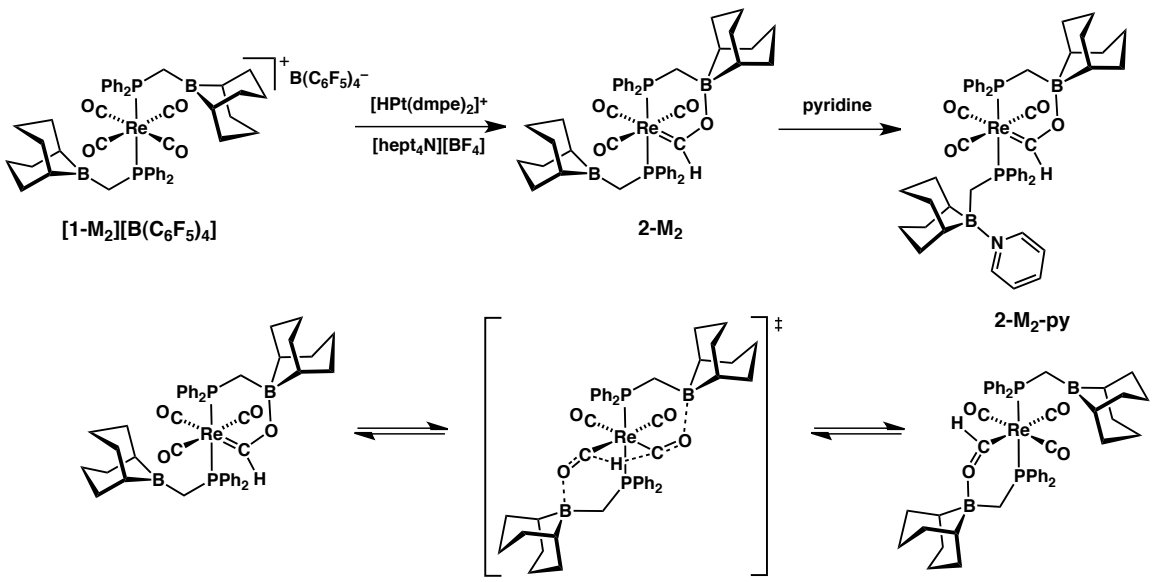

Scheme 3.10

The fluxional process in **2-M$_2$** interconverts the two phosphinoborane ligands ($\Delta G^{\ddagger}$ = 13.6 ± 0.2 kcal mol^{-1}, estimated from the coalescence temperature of 323 K). A sequence of B–O bond breaking, rotation, and B–O bond formation with the other ligand seems a plausible mechanism. $^{13}C\{^1H\}$ NMR spectroscopy is not entirely consistent with this, however, as the CO carbon signals are very broad at room temperature, suggesting their involvement in the exchange process. Hydride transfer from a formyl to an adjacent carbonyl (Scheme 3.10, bottom) has been observed previously ($\Delta G^{\ddagger}$ = 11.7 kcal mol^{-1});[23] that may be more consistent with our observations. Furthermore, treatment of **2-M$_2$** with up to 100 equivalents of pyridine leads to *no B–O cleavage*; only coordination of pyridine to the free B center is observed (Scheme 3.10, top), resulting in sharp NMR resonances expected for a non-fluxional product. If reversible B–O cleavage were occurring rapidly on the NMR time scale, pyridine binding might be expected to intervene. This observation stands in stark contrast to B–O bonds involving intermolecular Lewis acids as well as

phosphinoboranes with longer linkers, which are readily broken in the presence of pyridine (*vide infra*). Similarly, carbene **2-M$_2$** is remarkably stable in comparison to **2-Ph$_2$** and **2-Ph$_2$•BEt$_3$**: no decomposition is observed over short periods at 95 °C or weeks at room temperature.

Treatment of [**1-M$_2$**][B(C$_6$F$_5$)$_4$] with two equivalents each of [hept$_4$N][BF$_4$] and [**HPt**][PF$_6$] in THF-*d$_8$* led to formation of a single new Re-containing product (~70% yield by NMR, relative to [hept$_4$N]$^+$), again with precipitation of [**Pt**]$^{2+}$. Because the presence of soluble salts such as [hept$_4$N][B(C$_6$F$_5$)$_4$] prevented isolation and structural determination by XRD, the product was characterized spectroscopically. Two sharp doublets are found in the ^{31}P{^{1}H} NMR spectrum at δ 22.2 and 37.3 ($\mathcal{J}_{PP}$ = 127 Hz), and two slightly broadened doublets are also found in the ^{1}H NMR spectrum, δ 3.12 and 4.63 ($\mathcal{J}_{HH}$ = 13.0 Hz). The downfield ^{31}P NMR shift is consistent with a 5-membered ring,[24] as expected for a structure analogous to the C–C coupled product [**3-E$_2$**]$^-$ (Scheme 3.3), but a number of other spectroscopic features rule out this assignment, including the absence of a downfield ^{13}C NMR signal for a carbene carbon, and the *mer*-tricarbonyl geometry assigned by ^{13}C NMR and IR. A simple alkyl is also ruled out by the 5-membered ring structure, no observed P coupling to the CH$_2$ group, and no 3-coordinate ^{11}B NMR signals. All the spectroscopic data are consistent with the doubly reduced "confused" alkyl species [**5**]$^-$ (Scheme 3.11), in which the CH$_2$ is bound to one B, and O is bound to Re and the other B, forming a bicyclic ring system. The very broad C signal and slightly broad H signals of the CH$_2$ group point to coordination to quadrupolar B; the B–O–Re fragment would provide the expected downfield ^{31}P NMR shift due to a 5-membered ring; and two ^{11}B NMR signals consistent

with 4-coordinate BR_4^- and $BR_3(OR')^-$ are observed. In addition, high-resolution mass spectrometry (HRMS) gives the expected mass for [**5**]$^-$. Thus although a second reduction was facilitated by the pendent Lewis acid, an entirely different product was obtained than in the complex supported by ethylene-linked ligands: no C–C bond formation occurred, and an unusual isomerization was instead observed, presumably driven by formation of 4-coordinate B in favorable ring sizes. The pendent acid is clearly required for this transformation: whereas **2-M$_2$** (preformed *in situ*) reacted with [**HPt**][PF_6] and [$hept_4N$][BF_4] to give [**5**]$^-$, similar treatment of **2-M$_2$•py** produced no observable reaction.

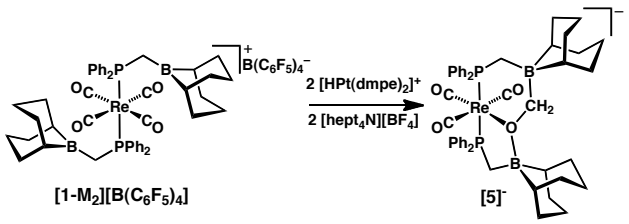

Scheme 3.11

Reduction of [(Ph$_2$P(CH$_2$)$_2$B(C$_8$H$_{14}$))$_2$Re(CO)$_4$]$^+$ ([1-E$_2$]$^+$)

Initial studies found that treatment of [**1-E$_2$**][BF_4] in C_6D_5Cl with one equivalent of $NaHBEt_3$ or [**HPt**][BF_4] affords boroxycarbene **2-E$_2$** (Scheme 3.3). The carbene is identified by a characteristic downfield signal in the ^{1}H NMR spectrum (δ 13.96) and a closely separated pair of doublets in the $^{31}P\{^1H\}$ NMR spectrum (δ 9.9). Boroxycarbene **2-E$_2$** spontaneously crystallizes from CD_2Cl_2, and XRD revealed a binuclear structure in which the pendent borane from one Re center acts as an *intermolecular* Lewis acid for the other; the two carbene carbons are separated by ~5 Å. Pulsed gradient spin-echo (PGSE) diffusion NMR experiments[25] on **2-E$_2$**, using $(PPh_3)_2Re(CO)_3Br$ (**6**) as an internal standard

of similar size and shape to the proposed monomer, suggest that significant intermolecular interactions are maintained in solution. Initial measurements provided a ratio of hydrodynamic volumes of **2-E$_2$**:**6**; then excess pyridine was added to the NMR tube, and the experiment was repeated. If **2-E$_2$** were strictly monomeric in solution, the ratio would be expected to increase, since pyridine binding would increase the hydrodynamic volume; if **2-E$_2$** were strictly dimeric, the second ratio should be close to 0.5 times the first, as the monomer should have roughly half the hydrodynamic volume of the dimer. The values of the ratio were 2.34(7) before pyridine addition and 1.6(1) after; the decrease by a factor of 0.69(5) could reflect a monomer-dimer equilibrium, giving a time-averaged PGSE value.[26] The broad ^{1}H and ^{31}P NMR resonances of **2-E$_2$** at 298 K support such a conclusion, although full variable-temperature NMR experiments could not be carried out due to the thermal instability (*vide infra*). Perhaps owing to its fluxional solution behavior, **2-E$_2$** is quite reactive: C_6D_5Cl solutions of **2-E$_2$** disproportionate (at a rate dependent on the concentration of **2-E$_2$**) to a 1:1 mixture of [**1-E$_2$**]$^+$ and [**3-E$_2$**]$^-$ (Scheme 3.12).

The same reduction chemistry is operative in THF, although the carbene is quite short-lived in this solvent: disproportionation is complete after a few minutes at room temperature, in stark contrast to the extremely stable methylene-linked analogue **2-M$_2$**. This rate enhancement might be due to the more polar solvent facilitating transformation to the ionic products [**1-E$_2$**]$^+$ and [**3-E$_2$**]$^-$, the enhanced solubility of $NaBF_4$ in THF (with Na^+ being incorporated into the product), or the ability of THF to break intermolecular B–O bonds in **2-E$_2$**. The ^{31}P{^{1}H} NMR signal for **2-E$_2$** in THF appears as a singlet (δ 10.3), probably a result of competitive borane binding by THF and formyl, implying relatively

weak B–O bonds in **2-E$_2$** when compared to **2-M$_2$**. The aforementioned PGSE experiment is consistent with this description, as reaction of pyridine with carbene **2-E$_2$** (in C_6D_5Cl) displaces the formyl group from the borane, forming an unstabilized formyl ($^{31}P\{^1H\}$ singlet at δ 11.7, ^1H Re–C*H*O signal at δ 15.21) that decomposes *without disproportionation* to give Re–H by decarbonylation (the normal pathway for formyl decomposition).[3b]

While **2-E$_2$** is stable for a number of hours at room temperature in C_6D_5Cl, it decomposes as the temperature is raised: up to 40 °C, disproportionation is the main path followed, but heating at 90 °C for a few minutes converts **2-E$_2$** to a single new product whose $^{31}P\{^1H\}$ NMR spectrum shows two doublets, δ 12.6 and 39.9 ($\mathcal{J}_{PP}$ = 124.8 Hz); the uncommonly downfield-shifted doublet is consistent with a 5-membered phosphorus-containing ring.[24] In the ^1H NMR spectrum, the downfield carbene resonance has been replaced by a new broad resonance at δ 5.85. These observations along with 2-D NMR experiments support structure **7** (Scheme 3.12) in which a B–C bond has been cleaved, and the ethylene linker has added to the carbene carbon, giving a (boroxyalkyl)metal complex.

Boroxycarbene **2-E$_2$** acts as a strong hydride donor, liberating H_2 with reagents such as H_2O and $[HNMe_3][BPh_4]$ (Scheme 3.12). In the latter case, the parent cationic tetracarbonyl $[\mathbf{1\text{-}E_2}]^+$ re-forms; with water the binuclear B-O(H)-B-bridged complex **8**, which contains a 20-membered ring, was formed and characterized by XRD (Figure 3.7). $[^tBu_3PH][HB(C_6F_5)_3]$, which is a potential hydride source as well as a protic reagent (and which can be formed directly, without any metal complex required, from H_2[27]) was tested to see if further reduction and C–C coupling could be obtained with such a weak hydride.

Instead, H_2 release was observed again, and the ion pair [**1-E$_2$**][HB(C_6F_5)$_3$] was obtained, in addition to free P^{t}Bu$_3$. Thus [HB(C_6F_5)$_3$]$^-$ is too weak a hydride to reduce the rhenium carbonyl cation,[7b] consistent with the stability of [**1-Ph$_2$**][HB(C_6F_5)$_4$] (Scheme 3.4) and despite the presence of a pendent acid group.

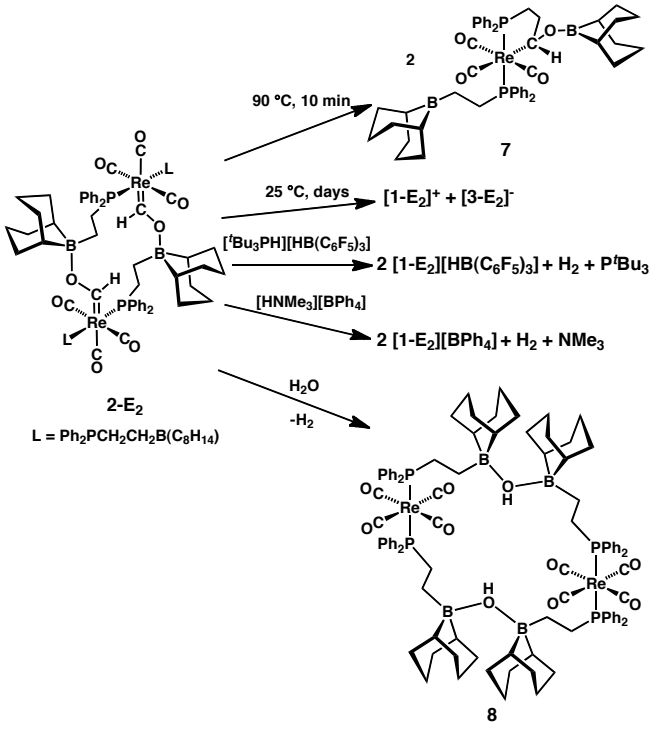

Scheme 3.12

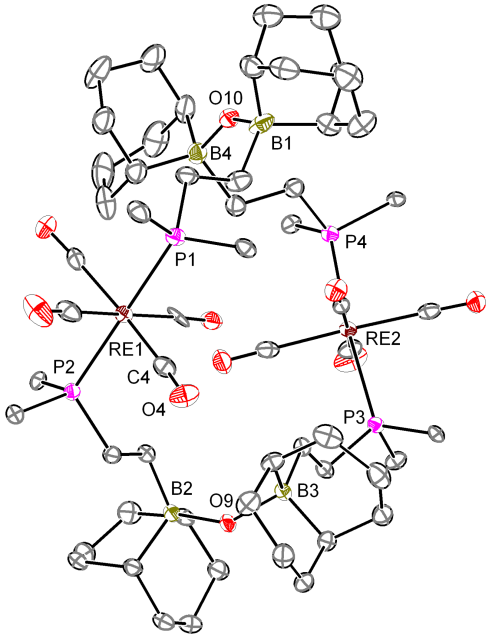

Figure 3.7. Structural representation of **8•**$(C_6H_6)_{2.5}(C_5H_{12})_{0.5}$, ellipsoids at 50% probability. H atoms and (disordered) solvents of crystallization omitted, and Ph groups truncated for clarity. Selected bond distances (Å) and angles (°): Re1–CO(avg) 1.988, Re1–P1 2.4437(6), Re1–P2 2.4490(6), B1–O10 1.609(4), B2–O9 1.597(3), B1–O10–B4 143.0(2). B2–O9–B3 141.7(2).

Carbene **2-E$_2$** can be directly reduced (before disproportionation occurs) to [**3-E$_2$**]$^-$ with a second equivalent of $NaHBEt_3$ or [**HPt**][BF_4] (*vide supra*). In contrast to **2-E$_2$**, [**3-E$_2$**]$^-$ is thermally stable up to 70 °C in THF solution, as well as towards further reduction with excess $NaHBEt_3$, presumably because a dianionic product would be disfavored. The B–O bonds of [**3-E$_2$**]$^-$ appear to be much stronger than those of **2-E$_2$**; they are not cleaved by addition of pyridine. Unlike **2-E$_2$**, treatment of [**3-E$_2$**]$^-$ with [**Pt**][$BAr^F{}_4$]$_2$ did not lead to any reaction, implying that its formation is essentially irreversible. [**3-E$_2$**]$^-$ reacts with strong acids (HBF_4, HOTf) to give a single product before going on to multiple species, and addition of MeOTf cleanly yields a stable neutral product, but none of these have been reliably characterized.

Plausible pathways for the transfer of hydride from [**HPt**]$^+$ to Re–CO in [**1-E$_2$**]$^+$ include (Scheme 3.13): Path A) hydride transfer to the pendent borane, followed by intramolecular hydride transfer from boron to carbon; Path B) hydride transfer from [**HPt**]$^+$ directly to the Re–CO fragment, yielding a formyl which is trapped by the pendent borane; Path C) transient borane coordination to a Re–CO oxygen, activating the carbon for nucleophilic attack.

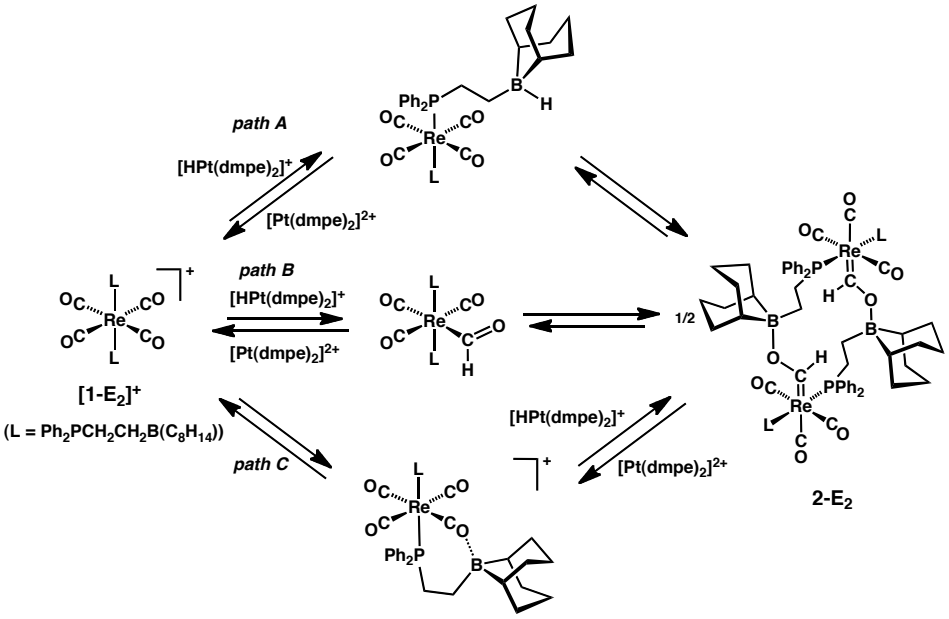

Scheme 3.13

When the reaction was monitored by $^{31}P\{^1H\}$ NMR spectroscopy at –40 °C, a new broad resonance was observed at δ –6, near the sharper signal for [**HPt**]$^+$ at δ –7. Both signals disappear as the reaction goes on, although the broad resonance is consumed first. The appearance of a broad Pt–H signal suggests the possibility of a Pt–H–B bridged intermediate, which would be most consistent with pathway A. In further support, reaction

of [**HPt**][PF_6] with BEt_3 led to precipitation of [**Pt**][PF_6]$_2$ and the appearance of a broad ^{31}P resonance at δ –2.4, along with a broadened resonance for [**HPt**]$^+$ at δ –7.1. Fluxionality was also apparent in a broad ^{1}H NMR signal in the hydride region at δ –11.7, and a ^{11}B NMR signal at 14.8 (compare Li[Et_3BHBEt_3], δ 8.7[28]). At –40 °C the signals sharpened and separated into two sets. The ^{31}P NMR spectrum showed two singlets, one corresponding to [**HPt**]$^+$ (δ –7.4, $^1\mathcal{J}_{PtP}$ = 2240 Hz), and one conspicuously lacking Pt satellites (δ –1.6). The ^{1}H NMR spectrum showed the hydride signal expected for [**HPt**]$^+$ (δ –12.02, pent, $^2\mathcal{J}_{PH}$ = 29.3 Hz, $^1\mathcal{J}_{PtH}$ = 694 Hz) along with another broad doublet with Pt satellites at δ –3.25 ($\mathcal{J}_{PH}$ = 166 Hz, $\mathcal{J}_{PtH}$ = 958 Hz), downfield of most Pt hydrides, but closer to the chemical shift expected for [$HBEt_3$]$^-$ ($\delta \sim$ –0.5) or [Et_3BHBEt_3]$^-$ ($\delta \sim$ –2.7).[28] ^{11}B NMR at this temperature showed signals for free BEt_3 and another close to that of [$HBEt_3$]$^-$.

These observations strongly indicate that H has been transferred (partly or entirely) to B; we tentatively assign the broad Pt–H signal to [$(dmpe)_2$Pt–H–BEt_3]$^+$ or the borane adduct [$(dmpe)_2$Pt($HBEt_3$)(BEt_3)]$^+$ (Scheme 3.14), since the large $\mathcal{J}_{PH}$ would be consistent with a phosphine *trans* to the hydride,[29] and the broadening with quadrupolar interaction with boron. The added bulk of the coordinated BEt_3 group(s) could favor a trigonal bipyramidal geometry; phosphines in such systems have been observed to undergo rapid interchange, leading to loss of Pt satellites in the ^{31}P NMR.[30] Precipitation of [**Pt**]$^{2+}$ is consistent with the stoichiometry required to form [Et_3BHBEt_3]$^-$. The reaction of preformed [Li][Et_3BHBEt_3] with [**Pt**]$^{2+}$ afforded multiple products; the major product was Pt$(dmpe)_2$, but some of the

trans hydride was also observed. Similar chemistry has been previously reported for $HRh(dmpe)_2$.[28]

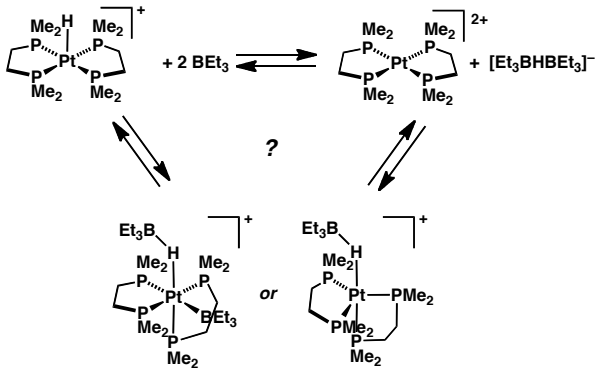

Scheme 3.14

While hydride transfer between B and Pt appears facile when the $[PF_6]$ anion is employed, no reaction is observed when [**HPt**]$[BAr^F{}_4]$ is treated with BEt_3. This difference is consistent with our previous observation that [**1-E$_2$**]$[BAr^F{}_4]$ is not reduced by [**HPt**]$[BAr^F{}_4]$ in C_6D_5Cl,[7c] and suggests that an equilibrium involving hydride transfer from Pt to B could be driving the chemistry of Scheme 3.5. Furthermore, we recently reported that the combination of a suitably strong and bulky base and H_2 is sufficient to directly reduce [**1-E$_2$**]$^+$;[7c] that reduction must go through a pendent borohydride intermediate. All of this evidence supports the "hydride shuttle" mechanism of path A (Scheme 3.13), wherein formation of a small amount of trialkylborohydride is followed by rapid intramolecular carbonyl reduction. Note also that [**1-Ph$_2$**]$^+$ *does* react with [**HPt**]$^+$ to give an (unstable) formyl (*vide supra*), but that reaction is very slow and is strongly accelerated by the addition of BEt_3, suggesting that direct transfer of hydride to carbonyl carbon as in path B is possible but much slower than the shuttle route.

Mechanism of C–C bond formation: Evidence for a bis(carbene) intermediate.

Reaction of [**1-E$_2$**][BF$_4$] with two equivalents of NaHBEt$_3$ or [**HPt**][PF$_6$], or of preformed **2-E$_2$** with one equivalent of either reductant, affords [**3-E$_2$**]$^-$ rapidly at room temperature. The reaction is irreversible and, in contrast to the first hydride transfer, is not driven by precipitation ([**3-E$_2$**]$^-$ does precipitate from C_6D_5Cl, but remains in solution in THF-*d$_8$*), as evidenced by the lack of observed reaction when [**3-E$_2$**]$^-$ is treated with [**Pt**][BAr$^F{}_4$]$_2$. The second reduction and subsequent C–C coupling necessarily involves a number of elementary steps. The mononuclear form of **2-E$_2$** (accessible according to the PGSE NMR data, *vide supra*), containing intramolecular borane coordination, is proposed to be an intermediate in the transformation to mononuclear product [**3-E$_2$**]$^-$. Two reasonable pathways for the formation of [**3-E$_2$**]$^-$ are shown in Scheme 3.15: Path A, reduction at the carbene center to give an anionic boroxyalkyl species, which undergoes Lewis acid-assisted migratory insertion; or Path B, reduction at a second CO to give an anionic bis(carbene) (or doubly stabilized bis(formyl): [CpRe(NO)(CHO)$_2$]$^-$ has been previously reported,[9a,9d]) species, followed by carbene coupling and hydrogen shift to give the observed product. Related hydrogen shifts have been previously observed in Fe[31] and Mn[7b] systems.

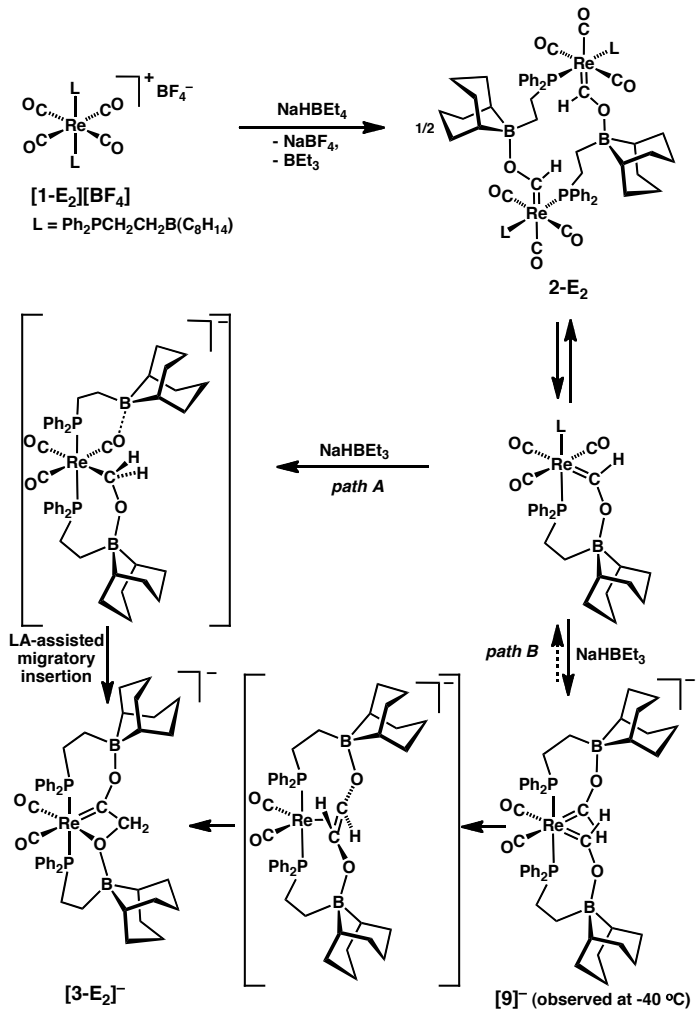

Scheme 3.15

Evidence for pathway B is provided by low temperature NMR studies. When one equivalent of $NaHBEt_3$ is added to an NMR tube containing a frozen solution of **2-E2** in C_6D_5Cl and the solution is warmed to –40 °C, clean conversion to a new symmetric species is observed. This species features a sharp singlet at δ 10.0 in the $^{31}P\{^1H\}$ NMR spectrum, a new downfield singlet at δ 16.43 in the ^1H NMR, which integrates as two protons, and only one CO resonance and one boroxycarbene resonance in the $^{13}C\{^1H\}$ NMR, all consistent with the bis(carbene) structure [**9**]$^-$. Upon slowly warming the sample, no new species were

observed by NMR spectroscopy; instead, the signal-to-noise decreased until essentially no signals attributable to Re species were visible, and a large amount of white precipitate was found upon removal of the tube from the probe. The precipitate was isolated and dissolved in THF-d_8, and NMR showed it to be [**3-E$_2$**]$^-$.

It should be noted that the observation of [**9**]$^-$ in C_6D_5Cl does not necessarily rule out a migratory insertion mechanism, since bis(carbene) formation could be reversible. Migratory insertion of a carbonyl into a Re–C bond has been reported to proceed with assistance from a (much stronger) Lewis acid.[32] The reduction of [**1-M$_1$**]$^+$ (*vide infra*) appears unambiguously to proceed via migratory insertion as well, but that reaction is quite slow.

Reduction of [(Ph$_2$P(CH$_2$)$_2$B(C$_8$H$_{14}$))$_2$Mn(CO)$_4$]$^+$ ([1-E$_2$-Mn]$^+$)

Treatment of [**1-E$_2$-Mn**][BF_4] with one equivalent of $NaHBEt_3$ in C_6D_5Cl showed significant conversion to a Mn–CHO species, with broad singlets at δ 13.81 (^{1}H NMR) and δ 61.0 (^{31}P NMR). When [**1-E$_2$-Mn**][BF_4] was similarly treated with one equivalent $NaHBEt_3$ in THF-d_8, a mixture of products formed, showing no downfield ^{1}H NMR signal (consistent with disproportionation chemistry as **2-E$_2$**); however, addition of two equivalents of $NaHBEt_3$ in THF-d_8 led to rapid and clean conversion to a single species that exhibits NMR signals — in particular, two doublets each in the ^{1}H and ^{31}P{^{1}H} NMR spectra, and correlation between the two proton doublets (δ 4.32 and 4.82) and a carbene carbon signal (δ 332) by ^{1}H–^{13}C gHMBC spectroscopy — very similar to those of the Re C–C coupling product [**3-E$_2$**]$^-$. Accordingly we assign the two products as **2-E$_2$-Mn** and [**3-E$_2$-Mn**]$^-$ (Scheme 3.16). **2-E$_2$-Mn** is presumed to be dimeric like the Re analog, although we have

no direct evidence for that. The $\mathcal{J}_{PP}$ value of 27 Hz in [**3-E$_2$-Mn**]$^-$ is much smaller than that in [**3-E$_2$**]$^-$, suggesting the former has *cis* phosphines (one possible isomer is drawn in Scheme 3.16). Both **2-E$_2$-Mn** and [**3-E$_2$-Mn**]$^-$ appear to be considerably less stable than their Re analogues; attempts to isolate [**3-E$_2$-Mn**]$^-$ by concentration led only to decomposition.

Treatment of [**1-E$_2$-Mn**][BF$_4$] with two equivalents [**HPt**][PF$_6$] in THF-d_8 also led to formation of [**3-E$_2$-Mn**]$^-$, although the reaction did not go to completion. Manganese, an inexpensive first-row alternative to rhenium, is thus capable of effecting the same reductive coupling chemistry, albeit with decreased product stability.

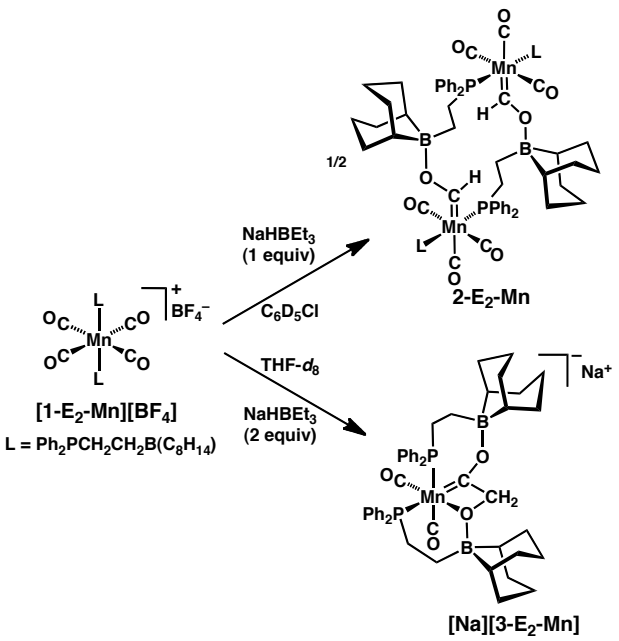

Scheme 3.16

Reduction of [(Ph$_2$P(CH$_2$)$_3$B(C$_8$H$_{14}$))$_2$Re(CO)$_4$]$^+$ ([1-P$_2$]$^+$)

Treatment of [**1-P$_2$**][BF$_4$] with one equivalent of NaHBEt$_3$ in C$_6$D$_5$Cl appears to afford a single product in good yield by NMR spectroscopy. The ^{1}H NMR spectrum includes a singlet at δ 14.10, characteristic of a formyl or boroxycarbene proton. The ^{31}P{^{1}H} NMR spectrum shows a broad singlet (δ 6.6), in contrast to the AB pattern of **2-E$_2$** and the widely spaced broad resonances in **2-M$_2$**. The same species is obtained using [**HPt**]$^+$, with essentially identical NMR signals, indicating that free BEt$_3$ does not play a role in the broadening of the ^{31}P signal.

A white solid precipitates from this solution over a few hours; it is insoluble in common organic solvents and water, but can be re-dissolved by addition of excess pyridine. The resulting solution exhibits a [Re–C*H*O] resonance, shifted downfield by ~1 ppm (δ 14.99) from the original position, while the ^{31}P{^{1}H} NMR resonance is slightly shifted (δ 6.2) and significantly sharpened; the ^{11}B{^{1}H} NMR shows a single resonance at δ 2.2, consistent with non-fluxional 4-coordinate boron.

Based on these results structure [**2-P$_2$**]$_n$ is assigned to the initially formed soluble species (Scheme 3.17). This species presumably contains only weak B–O interactions, consistent with the shift of the formyl proton and the broadness of the ^{31}P resonance (attributed to moderately fast B–O bond breaking/forming). As the linker length is increased, the chemical shift of the formyl in C$_6$D$_5$Cl moves downfield, which may indicate less B–O interaction. A similar trend is observed upon titration of (PPh$_3$)$_2$Re(CO)$_3$(CHO) with trialkylboranes, as the formyl shifts upfield with added borane. Complex [**2-P$_2$**]$_n$

precipitates as an oligomer; addition of pyridine re-dissolves it by coordinating to boron and breaking the B–O bonds, generating complex **2-P$_2$•2py**. Because the "bare" formyl **2-P$_2$•2py** is not stabilized by any Lewis acid interaction, it decomposes over a period of hours, resulting in two new Re–H ^{1}H NMR signals, one a triplet and the other a doublet, which can be assigned to **4-P$_2$•2py** and **4-P$_1$•py** (Scheme 3.17), respectively. These products were not isolated; the pyridine adduct of the free ligand ($Ph_2P(CH_2)_3B(C_8H_{14})$·pyridine) was also observed by $^{31}P\{^1H\}$ NMR spectroscopy.

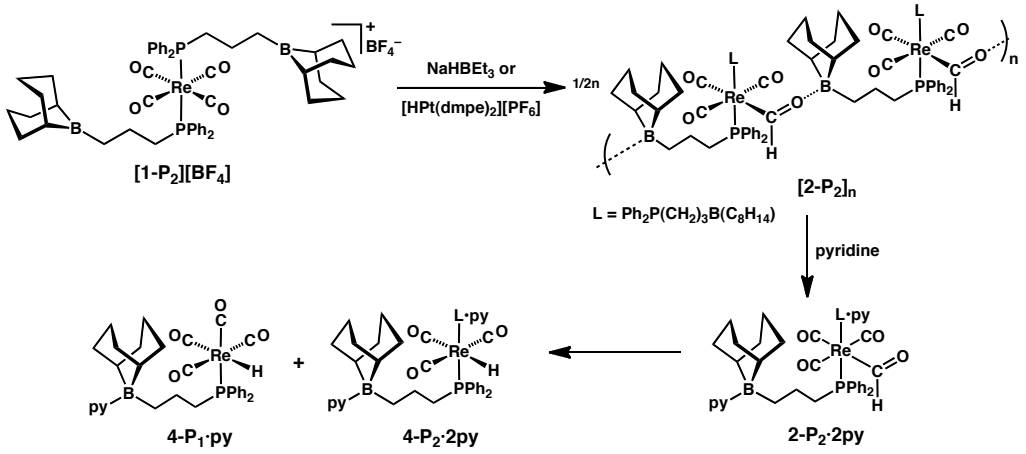

Scheme 3.17

Treatment of [**1-P$_2$**][BF$_4$] with two equivalents of NaHBEt$_3$ led to NMR spectra that indicated the formation of multiple asymmetric species, possibly including one or more with new C–C bonds, but they could not be separated or fully characterized. Treatment of [**1-P$_2$**][BF$_4$] with two equivalents of [**HPt**][PF$_6$] gave only boroxycarbene [**2-P$_2$**]$_n$ and unreacted [**HPt**][PF$_6$]. This failure to undergo a second hydride addition may support our hypothesis that intramolecular facilitation is required for multiple reductions by [**HPt**]$^+$: an

intramolecular B–O interaction in **2-P$_2$** would require an 8-membered ring, which is probably too large for effective stabilization.

Overview of (Ph$_2$P(CH$_2$)$_n$B(C$_8$H$_{14}$))$_2$Re complexes: Ring size effects

Only methylene-linked boroxycarbene **2-M$_2$** clearly exhibits *intramolecular* interaction of the pendent borane with the [Re–CHO] moiety, forming a favorable 6-membered ring. The corresponding 7-and 8-membered rings that would result from intramolecular coordination in the ethylene- and propylene-linked analogues are not observed; instead *intermolecular* coordination leads to a dimer or an insoluble oligomer respectively. In the absence of significant intramolecular interactions in the ethylene- and propylene-linked systems, the two boroxycarbenes are expected to exhibit similar stability and hydride strength. Indeed, mixing preformed **2-E$_2$** with [**1-P$_2$**]$^+$ (or **2-P$_2$** with [**1-E$_2$**]$^+$) gives an equilibrium mixture (Scheme 3.18), with $K_{eq} \approx 1$. Similarly, addition of carbene **2-E$_2$** to simple phosphine complex [**1-Ph$_2$**]$^+$, or of simple formyl complex **2-Ph$_2$** to B-linked carbonyl complex [**1-E$_2$**]$^+$, establishes an equilibrium, also with $K_{eq} \approx 1$.

In contrast, mixing preformed **2-E$_2$** with the methylene-linked [**1-M$_2$**]$^+$ results in *complete* hydride transfer, giving only the intramolecularly-stabilized carbene **2-M$_2$**, which does not react with [**1-E$_2$**][BF$_4$]. Furthermore, **2-M$_2$** is able to accept a second hydride from **2-E$_2$**, affording the "confused" alkyl [**5**]$^-$ (Scheme 3.11) as the major product. Clearly the favorability of intramolecular coordination with the methylene linker effects a substantial difference in stability and reactivity. The fact that ethylene-linked boroxycarbene **2-E$_2$** *can* undergo a second hydride addition and C–C coupling, which in general does not appear to

be well facilitated by external Lewis acids, is further evidence that **2-E$_2$** exists in solution as an equilibrium between the dimer and an intramolecularly coordinated monomer.

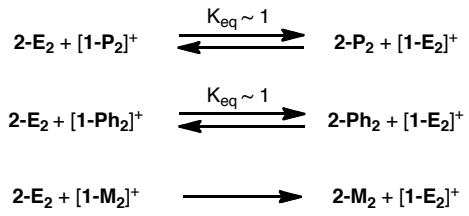

Scheme 3.18

Reduction of [(Ph$_3$P)Re(CO)$_5$]$^+$ ([1-Ph$_1$]$^+$)

In general we would expect monophosphine rhenium pentacarbonyl cations to be more electrophilic than their bis(phosphine) counterparts, rendering them better hydride acceptors, and indeed, in contrast to [**1-Ph$_2$**]$^+$, [(PPh$_3$)Re(CO)$_5$]$^+$ ([**1-Ph$_1$**]$^+$) is readily reduced by [**HPt**]$^+$ in the absence of any Lewis acid assistance.[7b] Furthermore, precipitation of a [**Pt**]$^{2+}$ salt is not required to drive the reaction, although reduction of [**1-Ph$_1$**][OTf] with [**HPt**][PF$_6$] (which results in precipitation of [**Pt**][OTf]$_x$[PF$_6$]$_{2-x}$) is more rapid than that of [**1-Ph$_1$**][BAr$^F{}_4$] with [**HPt**][BAr$^F{}_4$] (in which case [**Pt**][BAr$^F{}_4$]$_2$ remains in solution). One possibility for this kinetic discrepancy could be tighter ion pairing for the smaller ions, which may aid in the transfer of hydride between two cationic species. The resultant monophosphine formyl species (PPh$_3$)Re(CO)$_4$(CHO) (**2-Ph$_1$**) is much less stable than **2-Ph$_2$**;[15,33] it quickly ($t_{1/2}$ ~ 30 min) de-inserts to give Re–H,[17] and cannot easily be further reduced (unless a strong electrophile such as MeOTf is added, to afford an electrophilic methoxycarbene[7b]).

Reduction of [(Ph$_2$PCH$_2$B(C$_8$H$_{14}$))Re(CO)$_5$]$^+$ ([1-M$_1$]$^+$)

Reaction of [**1-M$_1$**][OTf] with one equivalent of [**HPt**][PF$_6$] in C$_6$D$_5$Cl gives boroxycarbene **2-M$_1$** as the major (~90% isolated yield) product in ~10 minutes at room temperature (Scheme 3.19). The minor (~10%) side product was tentatively assigned as an alkyl species bridging two Re centers, a hypothesis later solidified by spectroscopic analogy to related reduced monophosphine-ligated species (*vide infra*). Treatment with stronger hydrides such as NaHBEt$_3$ generally resulted in much more Re–H formation and was thus avoided. These reactions were sometimes accompanied by intense color changes consistent with reduction processes, which would labilize CO and lead to reactivity at Re itself. Similar results were obtained in CD_2Cl_2, although a slow background reaction of [**HPt**]$^+$ with the solvent gives some CD_2HCl. In both solvents [**Pt**][OTf]$_x$[PF$_6$]$_{2-x}$ precipitates, but that is not a requisite driving force: treatment of [**1-M$_1$**][BAr$^F_4$] with [**HPt**][BAr$^F_4$] (which forms soluble [**Pt**][BAr$^F_4$]$_2$) led to complete reduction as well (albeit more slowly, as with the [**1-Ph$_1$**]$^+$ salts above; also see below). **2-M$_1$** exhibits the characteristic downfield ^{1}H NMR signal (δ 14.07, d, $^3\mathcal{J}_{PH}$ = 2.5 Hz in C$_6$D$_5$Cl); a broad ^{13}C{^{1}H} resonance at δ 283 is attributed to the carbene carbon. In contrast to most of the other boroxycarbenes studied, which show either broad or no ^{11}B resonances, **2-M$_1$** displays a relatively sharp ^{11}B{^{1}H} signal at δ 11.2, consistent with 4-coordinate boron.[34]

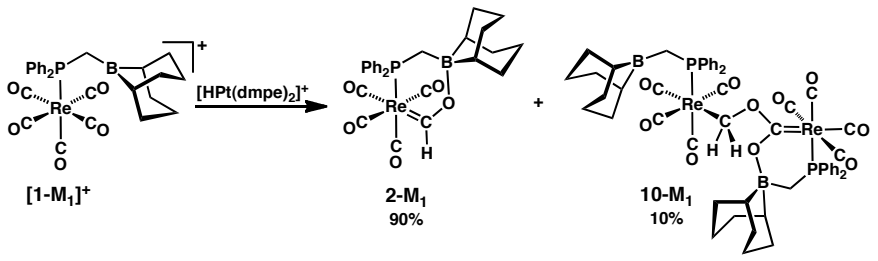

Scheme 3.19

Reaction of **2-M1** with pyridine led after ~30 minutes to complete disappearance of the carbene resonance and growth of a new doublet at 4.91 ($\mathcal{J}_{PH}$ = 5.8 Hz, 2H) in the ^{1}H NMR spectrum; two equal intensity singlets were observed in the ^{31}P{^{1}H} NMR spectrum. These spectroscopic characteristics are quite similar to those of the product of [**HPt**]$^{+}$ reduction of the ethylene-linked analogue **1-E1** (*vide infra*), as well as of the minor side product that accompanied formation of **2-M1**; accordingly we assign it as the bridging alkyl-carbene dirhenium species **10-M1•py** (Scheme 3.20), formed *via* disproportionation. It is noteworthy that the B–O bond of **2-M1** can be cleaved by pyridine, in contrast to that in **2-M2** (Scheme 3.10); perhaps the more electrophilic nature of the monophosphine complexes places more of the negative charge at C instead of O.

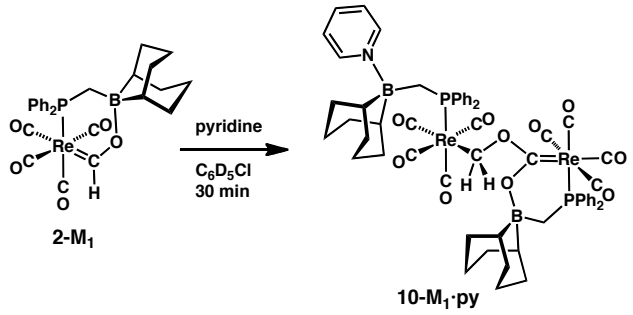

Scheme 3.20

By itself, **2-M$_1$** is quite stable in solution: there is no observable decarbonylation over a month, indicating a particularly strong B–O interaction that inhibits the normal formyl de-insertion path. This stability is far greater than **2-Ph$_2$**, **2-E$_2$**, and **2-Ph$_1$**, in line with that of **2-M$_2$**. There is eventually some decomposition after two months to a new species (Scheme 3.21), identified by XRD as the alkoxy-boroxy-carbene complex **11** (Figure 3.8), whose formation likely involves B–C cleavage to extrude 9-BBN, coupling of the methylene fragment to the formyl carbon, and addition of the resulting alkoxy oxygen to a carbonyl carbon on another Re center, although the exact mechanistic sequence is not known. **11** exhibits an unusually upfield $^{31}P\{^1H\}$ NMR signal, δ –54.0, typical of P in a 4-membered ring;[24] the alkoxyboroxycarbene $^{13}C\{^1H\}$ resonance is observed at δ 210.2 (d, $\mathcal{J}_{PC}$ = 9.4 Hz).

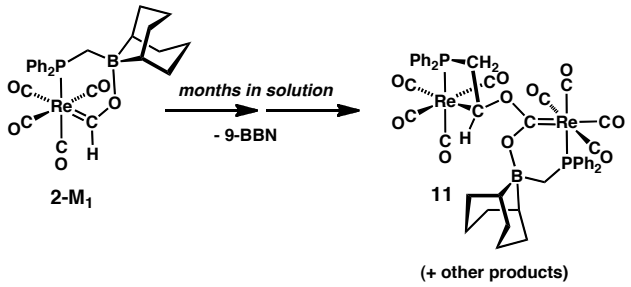

Scheme 3.21

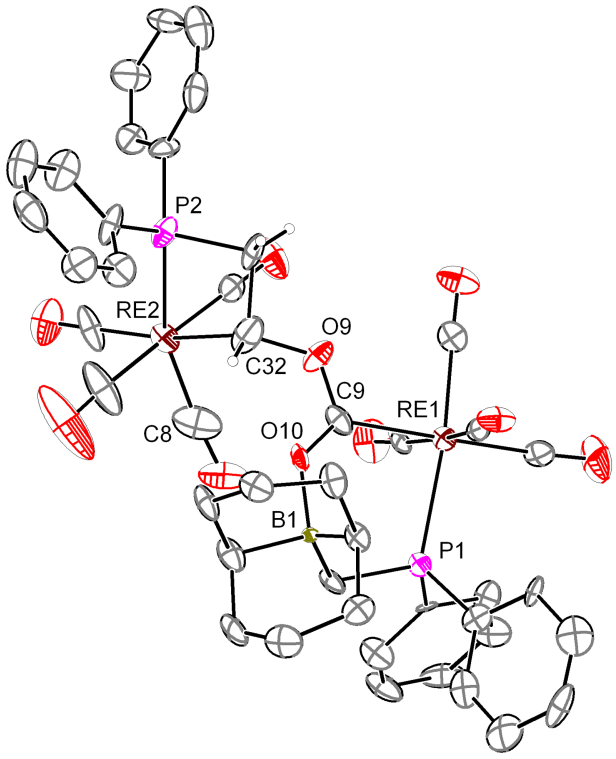

Figure 3.8. Structural representation of **11** with ellipsoids at 50% probability. Most H atoms omitted for clarity. Selected bond distances (Å) and angles (°): Re1–C9 2.20(1) C9–O9 1.33(1), C9–O10 1.25(1), O10–B1 1.59(2), O9–C32 1.49(1), Re2–C32 2.28(1), P2–Re2–C8 159.0(5), P1–Re1–C2 172.2(4).

Addition of a second equivalent of [**HPt**][PF_6] to **2-M$_1$** produces two new species over a period of hours. At early stages the major species exhibits a ^{1}H doublet at δ 4.54 ($^3\mathcal{J}_{PH}$ = 2.6 Hz), which in ^{1}H–^{13}C and ^{1}H-^{31}P gHMBC NMR experiments showed 3-bond coupling (through Re) to CO and P ligands; these and other multinuclear and multidimensional NMR experiments support assignment as the mononuclear Re alkyl complex **12**. Over 48 hours **12** is converted quantitatively (by NMR) to the second species, assigned as Re-acyl [**3-M$_1$**]$^-$ (Scheme 3.22), based on (*inter alia*) the following NMR evidence: 1) an AB pattern ($\mathcal{J}_{HH}$ = 16 Hz) corresponding to geminal CH_2 protons, further coupled to an acyl carbon at 275 ppm (by ^{1}H–^{13}C-gHMBC, which also shows that there is no longer any 2 or 3 bond

coupling between the CH_2 group and CO ligands); 2) a single $^{31}P\{^1H\}$ NMR resonance with a downfield shift, δ 38.1, consistent with a 5-membered ring structure,[24] which is weakly coupled to one of the CH_2 protons.

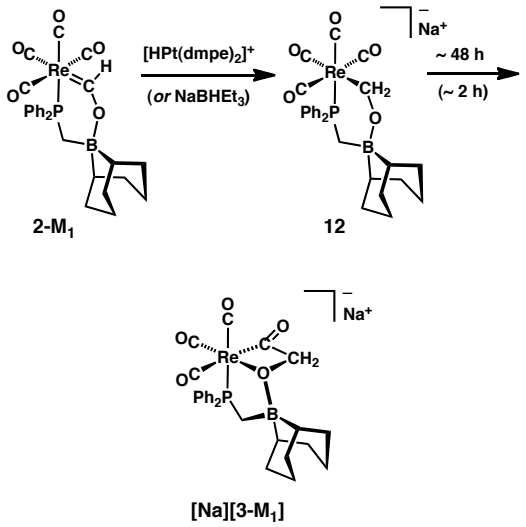

Scheme 3.22

It is unclear whether the migratory insertion leading from **12** to [**3-M$_1$**]$^-$ is Lewis acid-assisted (which would require B–O cleavage). Migratory insertion on Re in the absence of a Lewis acid is very rare and usually slow,[32,35] but the reaction here *is* quite slow compared to the insertions observed following reduction of **2-E$_2$** and **2-E$_2$-Mn**. (The analogous reaction in the **2-E$_1$Ph$_1$** system is also faster*; vide infra*). Reaction of **2-M$_1$** with the stronger hydride $NaHBEt_3$ led to [**3-M$_1$**]$^-$ much more rapidly. Acceleration could be due to BEt_3- or Na^+-assisted migratory insertion or product stabilization, but separate experiments probing any additive effect of BEt_3 or $NaBF_4$ (on [**HPt**]$^+$-mediated reductions) were inconclusive.

Reduction of [**1-M$_1$**][BAr$^F{}_4$] using [**HPt**][BAr$^F{}_4$] resulted in a change in the rate-limiting step, as reduction of the carbene was slower than migratory insertion. Therefore, no alkyl intermediate was observed, and the reaction took about 1 week to reach completion.

The presence of the Na^+ counterion in the synthesis of [**3-M$_1$**]$^-$ allowed for crystallization of single crystals of [Na(THF)$_3$][**3-M$_1$**] from a cold THF/pentane mixture, with an XRD study confirming the structure assigned by NMR (Figure 3.9). A B–O bond is formed between the cyclic alkoxide and the borane in the secondary coordination sphere; the bond distances are consistent with an acyl functionality as illustrated, with a relatively short C=O distance of 1.218(5) Å. The Na^+ counterion bridges an acyl O of one molecule and a carbonyl O of another molecule, forming a zig-zagging network in the crystal lattice.

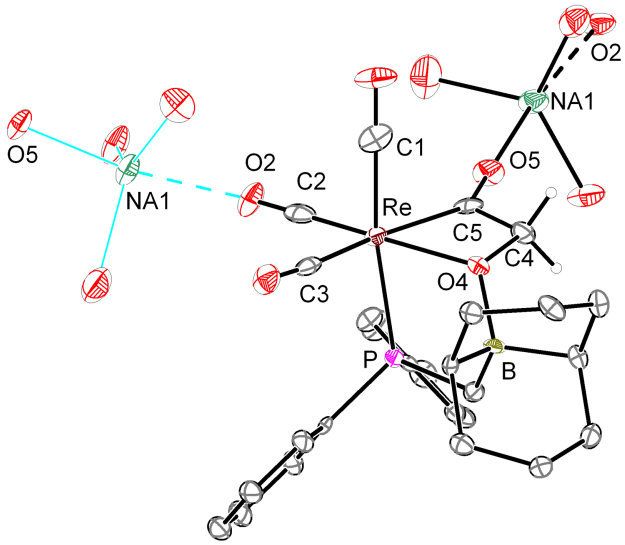

Figure 3.9. Structural representation of [Na(THF)$_3$][**3-M$_1$**] with ellipsoids at 50% probability. Most H atoms, and C atoms of THF molecules, omitted for clarity. Selected bond lengths (Å) and angles (°): Re–C1 1.935(5), Re–C2 1.849(5), Re–C3 1.951(5), Re–C5 2.130(4), Re–O4 2.206(3), O4–C4 1.440(4), O4–B 1.575(5), C4–C5 1.532(6), C5–O5 1.218(5), O5–Na 2.238(3), O2#1–Na 2.411(3), Re–C5–O5 143.2(3).

Reduction of [(Ph$_2$P(CH$_2$)$_2$B(C$_8$H$_{14}$))Re(CO)$_5$]$^+$ ([1-E$_1$]$^+$)

The reaction of [**1-E$_1$**][OTf], with one equivalent of [**HPt**][PF$_6$] in C_6D_5Cl proceeds readily at ambient temperature, but the expected boroxycarbene product is not observed; instead a single species is formed in good yield, whose NMR properties (in particular, a ^{1}H doublet at δ 5.06 ($^3\mathcal{J}_{PH}$ = 6.9 Hz, 2H); two ^{31}P peaks in a 1:1 ratio, one of which correlates to ^{1}H δ 5.06 in ^{1}H–^{31}P gHMBC; a ^{13}C resonance at δ 209.6) are reminiscent of the dioxycarbene linkage in **11** and suggest the related structure **10-E$_1$** (Scheme 3.23). The expected carbene species **2-E$_1$** can be observed as an intermediate at low temperature: NMR spectroscopic monitoring of the reaction in a thawing C_6D_5Cl solution at –40 °C showed nearly complete conversion to a carbene species, which at 25 °C is cleanly and quickly converted to **10-E$_1$**.

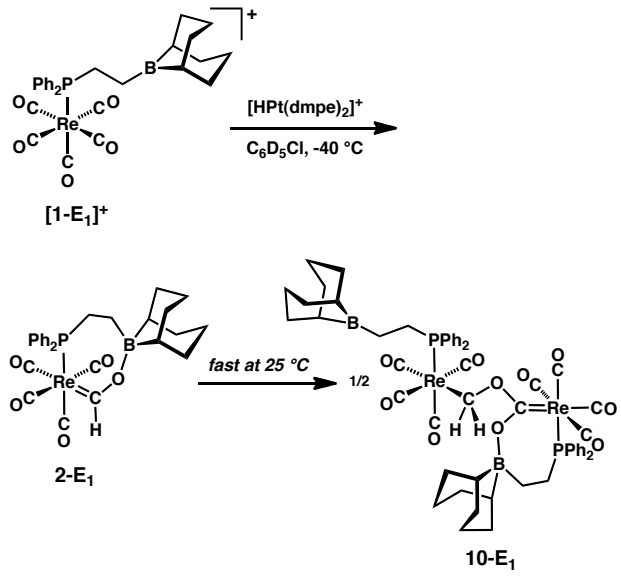

Scheme 3.23

Two pathways can be envisioned for disproportionation of **2-E$_1$** to **10-E$_1$**: 1) hydride donation from one Re–CHO group (exposed by B–O cleavage) to a second Re=CHOBR$_3$

to give a Re–CH_2O^- fragment capable of nucleophilic attack on the M–CO of re-formed [**1-E$_1$**]$^+$, or 2) nucleophilic attack by the O of the Re–CHO group (again exposed by B–O cleavage) on another carbene, followed by a hydride shift. The first would require breaking a bond between Re–CH_2O^- and B, which is expected to be quite strong (recall the inability of pyridine to break the B–O bond in [**3-E$_2$**]$^-$), perhaps favoring the second. The two alternatives can be distinguished by reaction of **2-M$_1$** with **2-P$_1$**, in which the routes beginning with hydride transfer (left, Scheme 3.24) and O attack (right, Scheme 3.24) would produce different products. Only one mixed-ligand dinuclear complex, **10-M$_1$P$_1$**, in which the alkyl group is bound to the Re ligated by the propylene linked ligand, is observed by NMR (>90%), supporting the preferred nucleophilic O attack mechanism. The same mechanism is likely operating in the reaction of methylene-linked **2-M$_1$** with pyridine (*vide supra*), with the Lewis base inducing B–O bond cleavage, exposing a formyl O that attacks unperturbed **2-M$_1$** to afford the related **10-M$_1$**. Very similar mechanisms have been proposed for the formation of related metalloesters (lacking borane stabilization).[9a,36]

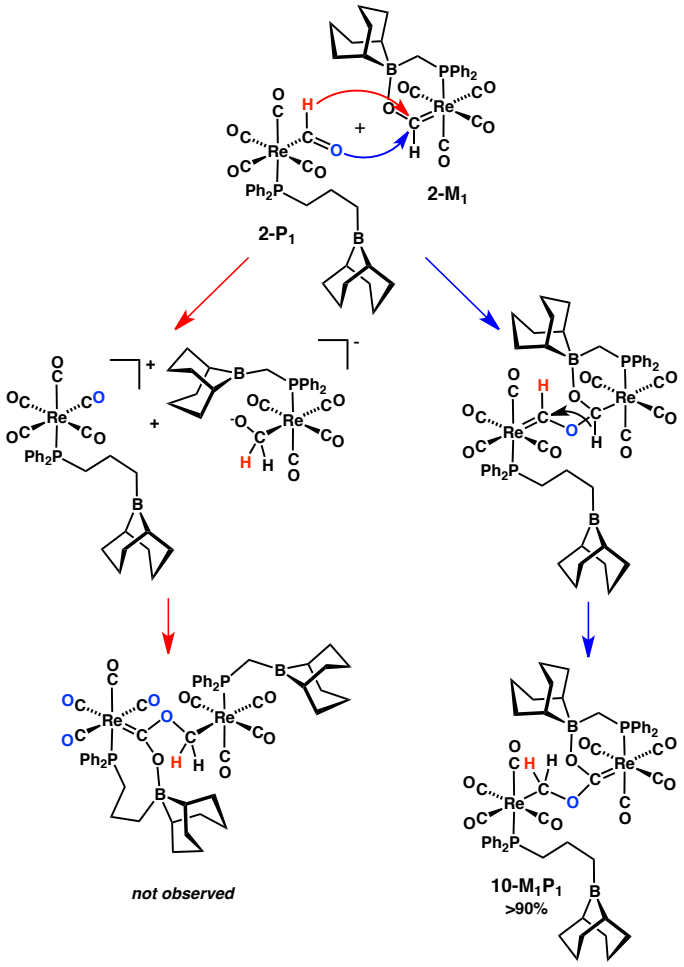

Scheme 3.24

Reduction of [(Ph2P(CH2)2B(C8H14))(Ph3P)Re(CO)4]+ ([1-E1Ph1]+)

When [**1-E$_1$Ph$_1$**][OTf] was treated with NaHBEt$_3$ in C_6D_5Cl, a single species formed immediately, which exhibited a downfield ^{1}H NMR singlet, δ 13.74, and two ^{31}P{^{1}H} NMR doublets, δ 9.3 and 15.4 ($\mathcal{J}_{PP}$ = 97 Hz); but after a few minutes solids precipitated, which could be re-dissolved by adding pyridine, suggesting that the initial product is **2-E$_1$Ph$_1$** (Scheme 3.25), which rearranges to an insoluble oligomer (similar to propylene-linked **2-P$_2$**). No evidence of disproportionation or any other transformation of [**1-E$_1$Ph$_1$**]$^+$ was observed before precipitation.

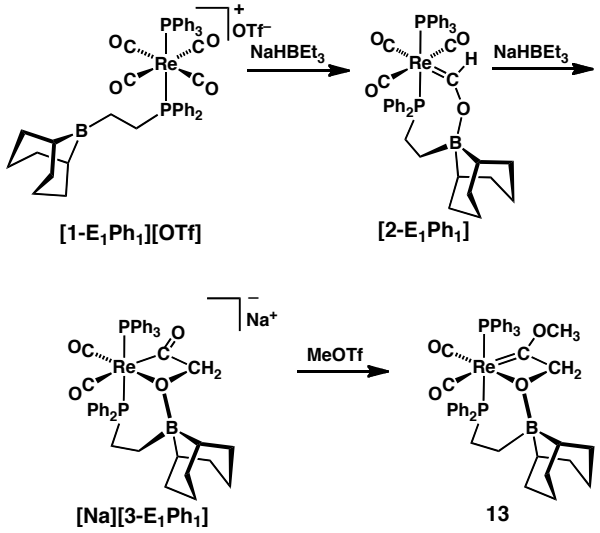

Scheme 3.25

Treatment of [**1-E$_1$Ph$_1$**][OTf] with two equivalents of NaHBEt$_3$ in THF cleanly afforded a new reduced species whose NMR and IR data are consistent with C–C bond formation analogous to that found in [**3-E$_2$**]$^-$, except for an IR band at 1572 cm^{-1} suggesting structure [**3-E$_1$Ph$_1$**]$^-$ (Scheme 3.25), with a free acyl group (in contrast to the boroxycarbene functionality in [**3-E$_2$**]$^-$, Scheme 3.3). [Na(THF)$_3$][**3-E$_1$Ph$_1$**] was crystallized and the structure confirmed by XRD (Figure 3.10); the single borane is bound to the alkoxide oxygen, leaving a free acyl whose O interacts with the sodium counterion, which also interacts with a CO of a neighboring molecule, forming long chains of repeating units in the crystal lattice. These chains are more linear than the zig-zag network of [Na(THF)$_3$][**3-M$_1$**], due to Na$^+$ bridging *trans*-disposed ligands rather than *cis*-disposed ones. The metrical parameters are also quite similar to [Na(THF)$_3$][**3-M$_1$**].

Reaction of [**3-E$_1$Ph$_1$**]$^-$ with MeOTf gives the neutral methoxycarbene complex **13** (Scheme 3.25). Large yellow blocks of **13** grew from chlorobenzene solutions upon diffusion

of pentane vapors, allowing for structural characterization (Figure 3.10). A smooth trend in the Re–C and C–O bond distances, reflecting decreased acyl and increased carbene character, can be seen on comparing the "free" acyl group in the sodium salt of [**3-E$_1$Ph$_1$**]$^-$, 2.133(1) and 1.251(2); the boroxycarbene in the sodium salt of [**3-E$_2$**]$^-$, 2.0960(9) and 1.271(1); and the methoxycarbene in **13**, 2.0250(6) and 1.3079(7) Å, respectively. The Re–C and C–O bonds in [**3-E$_1$Ph$_1$**]$^-$ are only ~0.02 Å shorter and longer, respectively, than that of structurally similar anionic Re-acyl species,[37] indicating that the O–Na interaction does not much perturb the acyl bonding. Notably, the B–O distances in these three species, which presumably are related to B–O bond strength, are quite similar — 1.593(1) (boroxycarbene) and 1.580(1) Å in [**3-E$_2$**]$^-$, 1.574(2) Å in [**3-E$_1$Ph$_1$**]$^-$, and 1.5897(8) Å in **13** — and shorter than the (easily broken) boroxycarbene B–O bond in **2-E$_2$**, 1.612(1) Å.

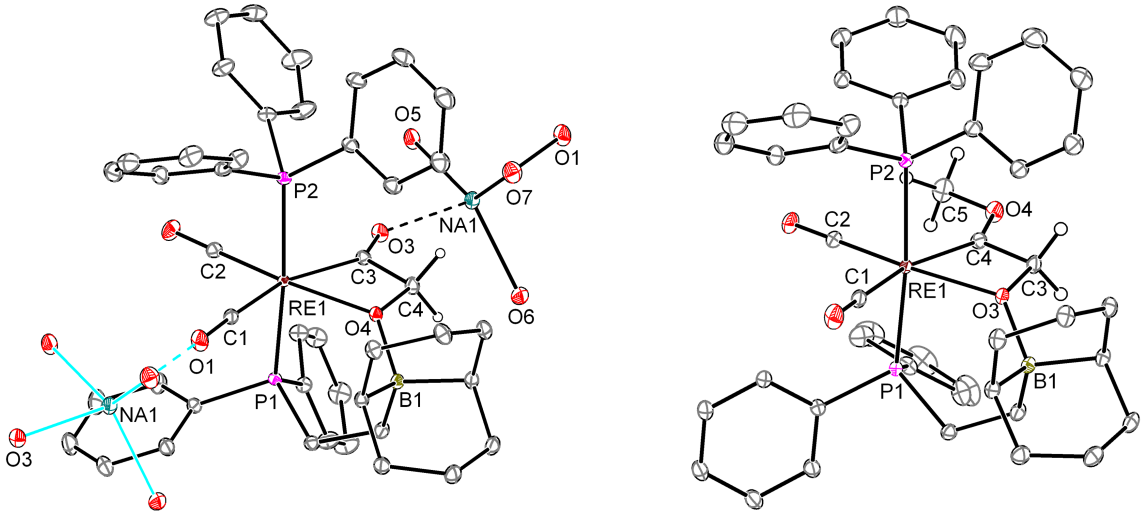

Figure 3.10. Structural representation of [Na(THF)$_3$][**3-E$_1$Ph$_1$**] (left) and **13**•(C$_6$H$_5$Cl)$_{0.5}$ (right), with thermal ellipsoids at 50% probability. Most H atoms, C atoms of THF molecules, and solvent molecules of crystallization omitted for clarity. The chlorobenzene molecule cocrystallized with 13 was disordered and sat near a center of symmetry. Selected bond distances (Å) and angles (°): [Na(THF)$_3$][**3-E$_1$Ph$_1$**]: Re–C1 1.9428(6), Re–C2 1.8799(6), Re–C3 2.1361(6), Re–O4 2.2470(5), O4–C4 1.4379(8), O4–B1 1.5731(9), C4–C3 1.5181(9), C3–O3 1.2416(8), O3–Na 2.2935(6), Re–O3–C3 143.20(5). **13**•(C$_6$H$_5$Cl)$_{0.5}$: Re–C1 1.9902(6), Re–C2 1.8772(7), Re–C4 2.0250(6), Re–O3 2.2263(5), O3–C3 1.4359(8), O3–B1 1.5897(8), C3–C4 1.496(1), C4–O4 1.3079(7), O4–C5 1.457(1), Re–C4–O4 145.15(6).

In contrast to the result when two equivalents of NaHBEt$_3$ are employed, treatment of [**1-E$_1$Ph$_1$**][OTf] with two equivalents [**HPt**][PF$_6$] in THF-*d$_8$* does *not* afford C–C bond formation: after initial rapid formation of the carbene species **2-E$_1$Ph$_1$**, no further reaction was observed before precipitation of the carbene (which occurs over a few hours under these conditions). This may be compared to the reaction of [**1-E$_2$**][BF$_4$] with [**HPt**][PF$_6$] which proceeds to [**3-E$_2$**]$^-$ within a few minutes, suggesting that a major role of the second pendent Lewis acid in the latter system is to promote hydride transfer from the weaker hydride source [**HPt**]$^+$, besides aiding the CO insertion step. Further comparison can be made to **2-M$_2$•py**, which also effectively has only one Lewis acid, and also is not reduced

by [**HPt**]$^+$. It is somewhat surprising that CO coupling proceeds so readily in the formation of [**3-E$_1$Ph$_1$**]$^-$ from [**1-E$_1$Ph$_1$**][OTf] and two equivalents of $NaHBEt_3$, as unassisted migratory insertion is not generally observed in simple alkyl species of rhenium under such mild conditions (especially without added ligand);[32,35] perhaps BEt_3 (the byproduct of reduction by $[HBEt_3]^-$) provides the needed assistance as an external Lewis acid.

Reduction of [(Ph$_2$P(CH$_2$)$_3$B(C$_8$H$_{14}$))Re(CO)$_5$]$^+$ ([1-P$_1$]$^+$)

Treatment of 1,3-propanediyl-linked phosphinoborane cation [**1-P$_1$**][OTf] with one equivalent of [**HPt**][PF_6] in C_6D_5Cl gives a new species with a ^{1}H NMR resonance at δ 13.74, a ^{31}P{^{1}H} resonance at δ 1.7, and a broad ^{11}B resonance at δ 85. The ^{11}B chemical shift indicates 3-coordinate boron,[34] suggesting the unstabilized formyl structure **2-P$_1$** (Scheme 3.26). Consistent with this formulation, and unlike all of the other [Re–CHO] species with pendent boranes reported here, **2-P$_1$** undergoes CO loss and Re–H formation over a period of several hours, similar to the behavior of $(PPh_3)Re(CO)_4(CHO)$ (**2-Ph$_1$**). A small amount (<5% by NMR) of an additional species, possibly an alkyl, formed initially and remained through the reaction, but no C–C coupling was observed before complete decomposition, even with excess [**HPt**][PF_6]. Apparently an 8-membered ring is too large for intramolecular stabilization of the formyl; the absence of any effective intermolecular stabilization may reflect lower basicity of the formyl O for this monophosphine complex, compared to the bis(phosphine) complexes where dimeric and oligomeric species are observed.

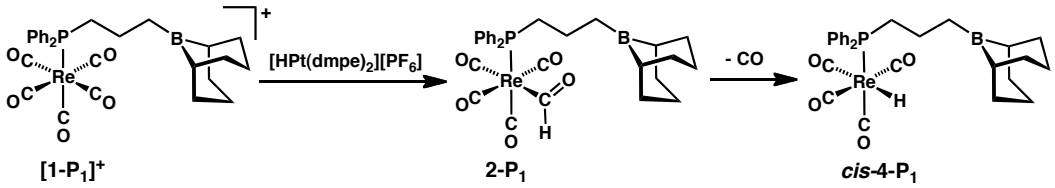

Scheme 3.26

Overview of ($Ph_2P(CH_2)_nB(C_8H_{14})$)Re complexes: Ring size effects

The effect of changing chelate ring size is summarized in Scheme 3.27; remarkably, each system exhibits different reduction chemistry. With a methylene spacer, boroxycarbene **2-M$_1$** is stable, and can be further reduced by [**HPt**]$^+$ to undergo C–C coupling; with an ethylene spacer, the less stabilized **2-E$_1$** rapidly disproportionates to dinuclear alkyl **10-E$_1$** (which *does not* undergo spontaneous C–C coupling); with a propylene spacer, neither stabilization *nor* novel reactivity of the Re–CHO species is observed, and the formyl rapidly decarbonylates, similar to borane-free systems.[15] Addition of pyridine to **2-M$_1$** disrupts the B–O bond and leads to **10-M$_1$•py**, a product very similar to that obtained in the ethylene-linked case, showing that under appropriate conditions the selectivity can be tailored.

The chain-length effect may be attributed to the relative stability of the intramolecular B–O interaction; the 6-membered ring in **2-M$_1$** is quite favorable, and the resulting stable boroxycarbene readily undergoes further reduction. For **2-E$_1$** there is an apparently rapid equilibrium between free formyl and boroxycarbene (an intramolecular 7-membered ring), leading to disproportionation; the potential 8-membered ring in **2-P$_1$** is not at all favorable, and the species behaves as a simple, unstabilized formyl.

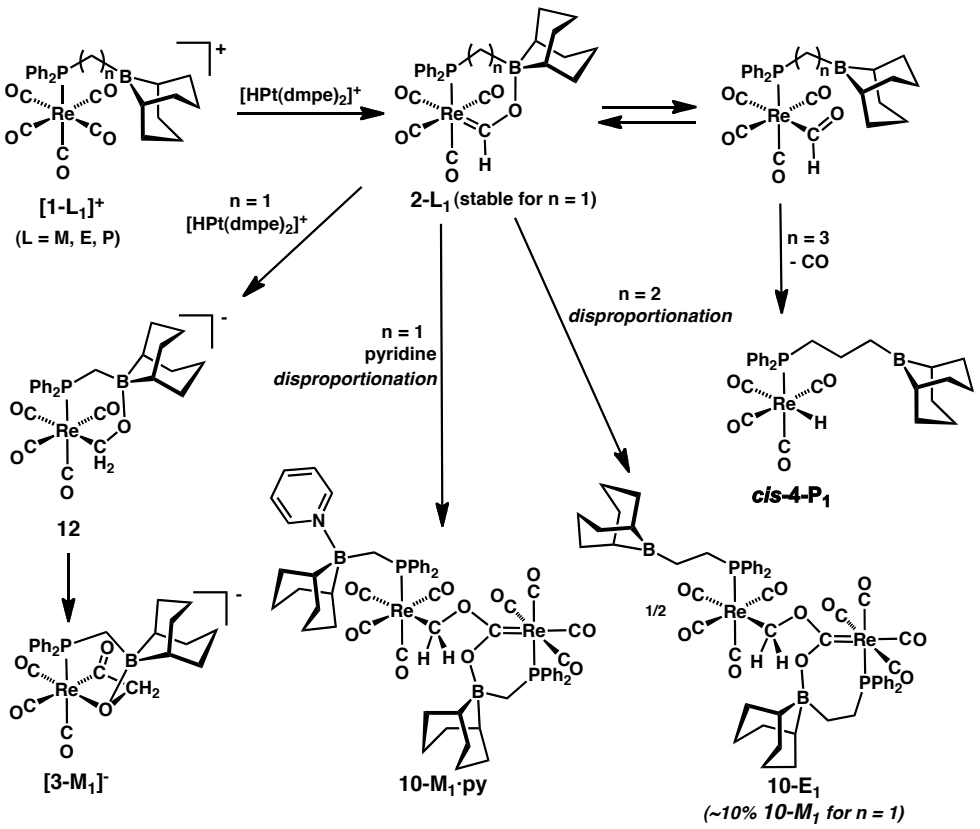

Scheme 3.27

Conclusions

Appending a trialkylborane moiety in the secondary coordination sphere of transition metal carbonyl complexes enhances CO reduction and C–C bond formation. The precise nature of the Lewis acid additives has a large impact on the reductive coupling of CO. External trialkylborane additives can facilitate reduction of $[(PPh_3)_2Re(CO)_4]^+$ by [**HPt**]$^+$ and stabilization of the resultant formyl, but no further reduction or C–C bond formation is observed. To achieve the latter transformation, intramolecular interaction between boron and oxygen appears to be required, which is possible when the phosphine ligand contains a pendent alkylborane. We hypothesize that the size of the ring formed by intramolecular B–

O interaction determines speciation, as shown in Scheme 3.28: shorter chain lengths give smaller, more stable rings, giving monomeric boroxycarbenes, while longer chain lengths give larger rings, which are destabilized, leading to either more formyl character (little interaction) or *intermolecular* interactions being dominant (with the pendent borane from one molecule binding oxygen on another). The monomeric species which contain *intramolecular* borane coordination appear to be readily reduced by [**HPt**]$^+$ (although bis(phosphine) complexes require a second pendent acid to shuttle the Pt–H), while oligomeric or externally borane-coordinated species do not show reductive coupling chemistry. This could be due to a geometric change of the boroxycarbene, imposed by the rigid ring structure (Figure 3.11). When the geometry is constrained in the P–Re plane, the backbonding is competing with 3 CO ligands, whereas the more favored geometry, essentially 90° out of plane, only competes with 2 CO ligands. This subtle change would render the chelated boroxycarbene more electrophilic, and perhaps more prone to nucleophilic attack.

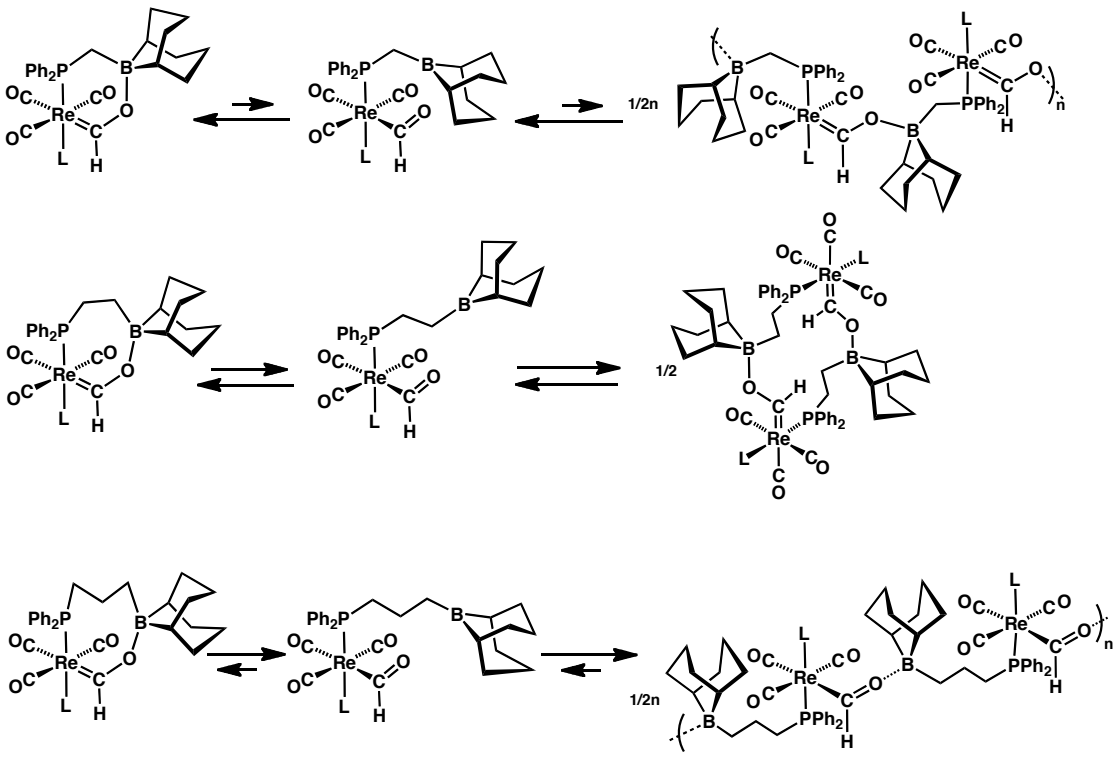

Scheme 3.28

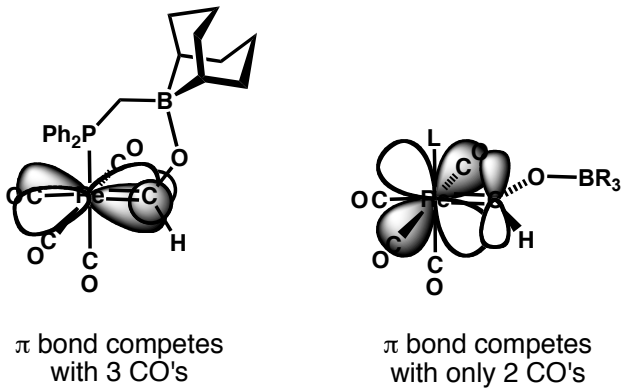

Figure 3.11. Orbital overlap diagrams for two orthogonal boroxycarbene orientations.

The number of Lewis acids is also important. Reductive coupling in systems with only one Lewis acid was observed in only two cases ($[\mathbf{1\text{-}M_1}]^+$ and $[\mathbf{1\text{-}E_1Ph_1}]^+$), although in the case of the less electrophilic bis(phosphine) complex, strong hydride sources were required. This implies that the C–C bond forming step does not require Lewis acid-assistance, and may be

driven more by ring-strain arguments. A second acid is required to shuttle a hydride from Pt to B in the case of bis(phosphine) complexes, if [**HPt**]$^+$ is used as the reductant.

We have identified key requirements for successful integration of pendent boranes, and have a preliminary understanding of the key steps of Lewis acid facilitated CO hydrogenation. The number of Lewis acids and their strength are both important factors, and having a favorable ring size for intramolecular B–O coordination is essential. Work still remains in understanding the mechanistic subtleties of this system, and in closing the cycle on rhenium by liberating the organic fragment.

Experimental Section

General Considerations

All air- and moisture-sensitive compounds were manipulated using standard vacuum line or Schlenk techniques, or in a glovebox under a nitrogen atmosphere. Under standard glovebox conditions, petroleum ether, diethyl ether, benzene, toluene, and tetrahydrofuran were used without purging, such that traces of those solvents were in the atmosphere, and could be found intermixed in the solvent bottles. When non-coordinating (ether-free) conditions were necessary, the glovebox was purged before use, and separate, rigorously ether-free solvent bottles were used. The solvents for air- and moisture-sensitive reactions were dried over sodium benzophenone ketyl, calcium hydride, or by the method of Grubbs.[38] All NMR solvents were purchased from Cambridge Isotopes Laboratories, Inc.

Benzene-d_6 was distilled from sodium benzophenone ketyl or titanocene. Dichloromethane-d_2 and chlorobenzene-d_5 were distilled from calcium hydride and run through a small column of activated alumina. Tetrahydrofuran-d_8 was purchased in a sealed ampoule, and dried by passage through activated alumina. Unless noted, other materials were used as received. $Re(CO)_5Br$ was purchased from Strem Chemicals, Inc. $Re(CO)_5OTf$,[39] *trans*-$Re(PPh_3)(CO)_4I$,[21] *trans*-$[(PPh_3)_2Re(CO)_4][BF_4]$,[15] $Ph_2P(CH_2)_2B(C_8H_{14})$,[14a] Cl-9-BBN,[40] Ph_2PCH_2Li,[41] $^tBu(CH_2)_2B(C_8H_{14})$,[42] $[Pt(dmpe)_2][PF_6]_2$ ($[\mathbf{Pt}][PF_6]_2$),[8a] and $NaBAr^F{}_4$[43] ($BAr^F{}_4$ = $[B(C_6H_3(3,5\text{-}(CF_3)_2)_4]$) were synthesized according to literature procedures. Elemental analyses were performed by Robertson Microlit Laboratories, Madison, NJ or Desert Analytics, Tuscon, AZ. ^1H and ^{13}C NMR spectra were recorded on Varian Mercury 300, 400-MR, INOVA-500 or -600 MHz spectrometers at room temperature, unless indicated otherwise. Chemical shifts are reported with respect to residual internal protio solvent for ^1H and $^{13}C\{^1H\}$ spectra. Other nuclei were referenced to an external standard: H_3PO_4 (^{31}P), 15% $BF_3{\bullet}Et_2O/CDCl_3$ (^{11}B), $CFCl_3$ (^{19}F), all at 0 ppm. High resolution mass spectra (HRMS) were obtained at the California Institute of Technology Mass Spectrometry Facility.

X-ray Crystallography Procedures

X-ray quality crystals were grown as indicated in the experimental procedures for each complex. The crystals were mounted on a glass fiber with Paratone-N oil. Structures were determined using direct methods with standard Fourier techniques using the Bruker AXS software package. In some cases, Patterson maps were used in place of the direct methods procedure. Full details are provided in Appendix D.

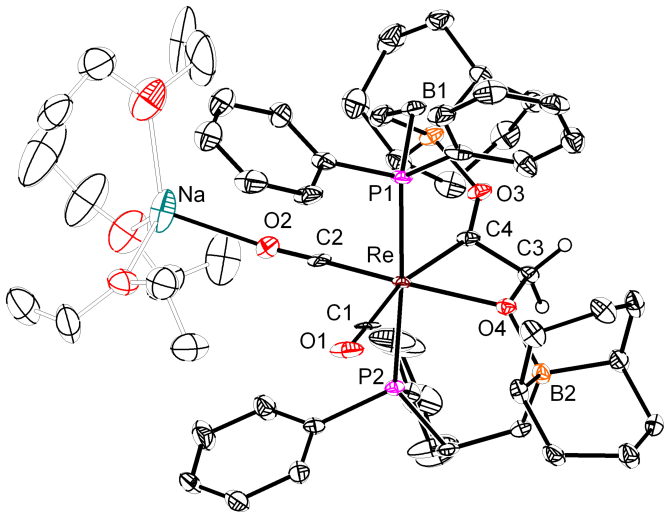

Figure 3.12. Structural representation of [Na•3Et$_2$O][**3-E$_2$**]. Ellipsoids are shown at 50% probability. Most hydrogen atoms omitted for clarity. Selected bond lengths (Å) and angles (°): Re–C2, 1.858(6); Re–C1, 1.955(5); Re–C4, 2.101(5); Re–O4, 2.227(3); Re–P2 2.4153(15); Re–P1 2.4188(15). O1–C1, 1.164(6); O2–C2, 1.167(6); O2–Na1 2.279(5); O3–C4, 1.264(6); O3–B1, 1.601(7); O4–C3, 1.426(5); O4–B2, 1.588(7); C3–C4, 1.510(7); C4–Re–O4, 63.84(17); O3–C4–Re, 147.1(4); C3–C4–Re 97.5(3).

Synthesis and reductive coupling of [1-E$_2$][BF$_4$]

(Ph$_2$PC$_2$H$_3$)$_2$Re(CO)$_3$Br. A 100 mL Teflon-stoppered tube was charged with 2.15 g (5.30 mmol) Re(CO)$_5$Br, 40 mL toluene, and a stirbar. A 10 mL toluene solution of diphenylvinylphosphine (2.25 g, 10.60 mmol) was added to the reaction vessel, at which point it was sealed and heated at 120 °C. The reaction was monitored by obtaining ^{31}P{^{1}H} NMR spectra of aliquots. After 5 days the reaction was complete, and the flask was allowed to cool to room temperature. Solvents were removed on a Schlenk line, leaving a white powder. The vessel was brought back into the glovebox, and the solids collected on a fritted glass funnel, washing with Et$_2$O. The spectroscopically pure white powder was collected and dried, yielding 3.52 g (90%) of (Ph$_2$PC$_2$H$_3$)$_2$Re(CO)$_3$Br. **^{1}H NMR** (500 MHz, CD$_2$Cl$_2$): δ 5.25 (m, 2H, Ph$_2$C$_2$*H*$_3$), 5.99 (br dd, $\mathcal{J}_{HH}$ = 20 Hz; $\mathcal{J}_{PH}$ = 36 Hz, 2H, Ph$_2$C$_2$*H*$_3$),

7.17 (m, 2H, $Ph_2C_2H_3$), 7.46 (br s, 12H, $Ph_2C_2H_3$), 7.65 (br s, 8H, $Ph_2C_2H_3$). **$^{31}P\{^1H\}$ NMR** (CD_2Cl_2, 121 MHz): δ –1.1. **$^{13}C\{^1H\}$ NMR** (CD_2Cl_2, 126 MHz): δ 128.9 ($Ph_2PC_2H_3$), 130.8 ($Ph_2PC_2H_3$), 130.9 ($Ph_2PC_2H_3$), 133.8 (t, $\mathcal{J}_{PC}$ = 22.5 Hz, $Ph_2PC_2H_3$), 133.9 ($Ph_2PC_2H_3$), 134.8 (t, $\mathcal{J}_{PC}$ = 22.9 Hz, $Ph_2PC_2H_3$), 190.2 (br t, CO), 192.2 (br t, $\mathcal{J}_{PC}$ = 8.4 Hz, CO). **IR** (toluene) ν_{CO}, 2036, 1955, 1902 cm^{-1}.

$[(Ph_2PC_2H_3)_2Re(CO)_4][BF_4]$. To a 60 mL Teflon-stoppered tube were added 0.518 g (2.680 mmol) $AgBF_4$, 1.509 g (2.048 mmol) $(Ph_2PC_2H_3)_2Re(CO)_3Br$, 15 mL CH_2Cl_2, and a stirbar. Without allowing the mixture to stir, the flask was sealed, removed from the glovebox, and immediately frozen in liquid N_2. The headspace was removed, and the flask was filled with 1 atm CO while warming to ambient temperature with stirring. The reaction was protected from light using aluminum foil while it was stirred. After 13 hours, the mixture was degassed by boiling the solvent at reduced pressure, brought into the glovebox, and filtered through celite, washing with 4 mL CH_2Cl_2. The colorless solution was evaporated to dryness, yielding a white powder that was triturated in THF (10 mL) for 90 minutes before collecting the solids on a fritted glass filter. The solids were washed with ether, and the white powder was collected and dried under vacuum to yield 1.31 g (79%) of $[(Ph_2PC_2H_3)_2Re(CO)_4][BF_4]$. If residual Ag-containing salts are present, the white powder will become colored upon prolonged light exposure, and subsequent reactions with boranes will yield dark solutions and Ag metal. If the material becomes colored, it can be extracted in CH_2Cl_2, filtered, and the solvents removed to yield a white powder, with minimal mass loss (~1%). Analytically pure material was obtained by growing crystals from CH_2Cl_2/Et_2O vapor diffusion. **^1H NMR** (CD_2Cl_2, 300 MHz): δ 5.39 (dd, 2H, $\mathcal{J}_{HH}$ = 17.8; $\mathcal{J}_{PH}$ = 21.1 Hz,

$Ph_2PC_3H_3$), 6.20 (dd, 2H, $\mathcal{J}_{HH}$ = 12.1; $\mathcal{J}_{PH}$ = 41.2 Hz, $Ph_2PC_2H_3$), 6.95 (ddd, 2H, $\mathcal{J}_{HH}$ = 11.0, 16.9 Hz; $\mathcal{J}_{PH}$ = 27.9, $Ph_2PC_2H_3$), 7.45-7.55 (m, 8H, $Ph_2PC_2H_3$), 7.56-7.66 (m, 12H, $Ph_2PC_2H_3$). **^{13}C{^{1}H} NMR** (CD_2Cl_2, 125 Mhz): δ 130.2 (t, $\mathcal{J}_{PC}$ = 5.5 Hz, Ph_2PCHCH_2), 131.0 (t, $\mathcal{J}_{PC}$ = 28.0 Hz, Ph_2PCHCH_2), 132.6 (t, $\mathcal{J}_{PC}$ = 24.5 Hz, $Ph_2PCH_2H_3$), 132.8 ($Ph_2PCH_2H_3$), 132.8 (t, $\mathcal{J}_{PC}$ = 5.9 Hz, $Ph_2PCH_2H_3$), 134.1 ($Ph_2PCH_2H_3$), 185.2 (t, $\mathcal{J}_{PC}$ = 7.5 Hz, $Re(CO)_4$). **^{31}P{^{1}H} NMR** (CD_2Cl_2, 121 MHz): δ –1.37. **IR** (CH_2Cl_2) ν_{CO}, 2005 cm^{-1}. **Anal. calcd.** for $C_{32}H_{26}BF_4O_4P_2Re$: C, 47.48; H, 3.24. Found: C, 47.56; H, 3.46; N, <0.05.

[($Ph_2PCH_2CH_2B(C_8H_{14})$)$_2$Re(CO)$_4$][BF$_4$] ([1-E$_2$][BF$_4$]). A glovebox was purged for 10 minutes before dissolving 0.660 g (0.811 mmol) **2** in 4 mL ether-free CH_2Cl_2. Solid 9-BBN dimer (0.594 g, 4.87 mmol, 6 equivalents of monomer) was added to the Teflon-stoppered flask, and the mixture was stirred, and an additional 2 mL CH_2Cl_2 was added. The flask was sealed, removed from the box, and heated to 70 °C. After 64 hours, the reaction was cooled to room temperature, pumped into the glovebox, and filtered, leaving some black and silver solids. The colorless solution was concentrated under vacuum to 1 mL of solvent, and 15 mL ether-free petroleum ether was added. The mixture was triturated for 1 hour, and the white powder was collected on a fritted glass filter. The powder was washed with petroleum ether, collected, and dried *in vacuo*, yielding 0.720 g (84%) analytically pure [**1-E$_2$**][BF_4]. X-Ray quality crystals were grown from a solution of [**1-E$_2$**][BF_4] in CH_2Cl_2 layered with petroleum ether at – 35 °C. **^{1}H NMR** (CD_2Cl_2, 300 MHz): δ 1.14 (br m, 4H, 9-BBN), 1.33 (br m, 4H, $Ph_2PCH_2CH_2BR_2$), 1.55 (m, 8H, 9-BBN), 1.66 (m, 4H, 9-BBN), 1.8-1.75 (m, 12H, 9-BBN), 2.95 (br m, 4H,

$Ph_2PCH_2CH_2BR_2$), 7.5-7.65 (m, 20H, Ph_2PR). **$^{31}P\{^1H\}$ NMR** (CD_2Cl_2, 121 MHz): δ 0.25 ppm. **$^{11}B\{^1H\}$ NMR** (CD_2Cl_2, 160 MHz): δ –1.0 (s, BF_4^-), 87.7 (br s, 9-BBN). **$^{13}C\{^1H\}$ NMR** (CD_2Cl_2, 126 MHz): δ 21.0, 23.5, 28.8 (t, $\mathcal{J}_{PC}$ = 15.5 Hz), 32.0, 33.7, 130.2, 132.3, 132.5, 132.9 (t, $\mathcal{J}_{PC}$ = 25.9 Hz), 185.8 (br t, $\mathcal{J}_{PC}$ = 7.2 Hz, CO). **$^{19}F\{^1H\}$ NMR** (CD_2Cl_2): δ –153.2. **IR** (CH_2Cl_2): ν_{CO}, 1998 cm^{-1}. **Anal. calcd.** for $C_{48}H_{56}B_3F_4O_4P_2Re$: C, 54.72; H, 5.36. Found: C, 54.45; H, 5.40; N, <0.05.

Boroxycarbene 2-E_2. Rhenium cation [**1-E_2**][BF_4] (0.084 g, 0.0798 mmol) was dissolved in 1 mL C_6D_5Cl, and 79.8 μL (0.0798 mmol) of a toluene solution of $NaHBEt_3$ (1.0 M) was added by syringe. The mixture turned clear yellow immediately. At low concentrations (<0.02 mmol) the carbene is stable for ~18 hours before disproportionation products become apparent. Isolation was not possible, as concentration led to increased rates of disproportionation. **^1H NMR** (C_6D_5Cl, 300 MHz): δ 0.5 (br s), 1.5-2.0 (br m), 2.5 (br m), 2.7 (br m), 7.2 (br m), 7.7 (br m), 13.96 (br s). The spectrum also contained toluene (2.23 s, 7.05-7.25 m) and BEt_3 (1.0 t, 1.2 q). **$^{31}P\{^1H\}$ NMR** (C_6D_5Cl, 121 MHz): δ 9.0 (br d). The broad doublet is attributed to two doublets with very close chemical shifts, such that the outer pair of signals has been reduced into the noise of the ^{31}P spectrum.

Disproportionation of 2-E_2. Following the above synthesis of **2-E_2**, an aliquot was inspected by ^1H NMR spectroscopy, showing complete conversion to carbene **2-E_2**. A vapor diffusion was carried out, with Et_2O diffusion into the remaining reaction mixture. After 1 hour, some solids had crashed out. The pale yellow Et_2O/C_6D_5Cl mixture was decanted and cooled in a separate vial to –35 °C. After two days, colorless plates of [Na][**3-**

E$_2$] formed, which were identified by XRD. NMR spectroscopy of the undiffracted crystals was consistent with the structure, and matched the large-scale preparation of [Na][**3-E$_2$**]. NMR of the solids yielded from evaporation of the mother liquor showed predominantly starting cation [**1-E$_2$**]$^+$, with some residual [Na][**3-E$_2$**].

Reaction of [1-E$_2$][BF$_4$] with 1 equiv [HPt(dmpe)$_2$][PF$_6$]. A J-Young NMR tube was charged with 17.0 mg (0.016 mmol) [**1-E$_2$**][BF$_4$], 10.3 mg (0.016 mmol) [HPt(dmpe)$_2$][PF$_6$], and 0.5 mL C_6D_5Cl in a glovebox. The tube was sealed and vigorously shaken, providing a slightly cloudy yellow solution. After 15 minutes, NMR revealed ~65% conversion to **2-E$_2$**. After 4 days, carbene **2-E$_2$** had begun to disproportionate to [**3-E$_2$**]$^-$ and [**1-E$_2$**]$^+$. The reaction was similarly carried out in 1,2-$C_6H_4F_2$, and NMR studies showed the same product in similar conversion.

Boroxy(boroxymethyl)carbene [Na][3-E$_2$]. A 1.0 M solution of $NaHBEt_3$ in toluene (0.695 mL, 0.695 mmol, 2 equiv) was added dropwise by syringe to a stirring colorless solution of [**1-E$_2$**][BF$_4$] (0.3662 g, 0.348 mmol, 1 equiv) in 5 mL PhCl. The reaction mixture turned yellow and clarified after 1 equiv was added, and immediately precipitated to form a thick slurry as the second equiv was added. The mixture was stirred 1 hr, at which point 2 mL each of Et_2O and pet. ether were added, and the solvents all removed. The pale yellow solids were triturated briefly with 3 mL of pet. ether and collected by filtration. The solids were washed with 10 mL Et_2O, then extracted with 5 mL THF. The THF was removed *in vacuo* to afford [Na][**3-E$_2$**] as a pale yellow powder (0.280 g, 88%). If residual $NaBF_4$ or other minor impurities (between 0-20%) were present, the crude product

was crystallized from 1,2-Difluorobenzene / pet. ether layer at –35 °C to yield pale yellow crystals. X-Ray quality crystals were grown from THF/Et_2O vapor diffusion. **^{1}H NMR** (500 MHz, THF-*d*$_8$): 0.29 (br s, 1H, BBN), 0.61 (m, 1H, BBN), 0.8-1.0 (m, 2H, BBN), 1.1-1.38 (m, 4H, BBN), 1.42 (br s, 5H, BBN), 1.56 (br s, 5H, BBN), 1.63-1.72 (m, 5H, BBN), 1.8 (br, 5H, BBN), 2.18 (m, 1H, $Ph_2PCH_2CH_2$BBN), 2.83 (m, 2H, $Ph_2PCH_2CH_2$BBN), 3.02 (m, 1H, $Ph_2PCH_2CH_2$BBN), 4.55 (d, $\mathcal{J}_{HH}$ = 15.5, 1H, Re=C(OBBN)CH_2OBBN), 4.64 (d, $\mathcal{J}_{HH}$ = 16.1, 1H, Re–C(OBBN)CH_2OBBN), 7.0-7.4 (m, 14H), 7.53 (m, 2H), 7.62 (t, 2H), 7.89 (t, 2H). **^{31}P{^{1}H} NMR** (THF-*d*$_8$, 121 MHz): 12.0 (d, $\mathcal{J}_{PP}$ = 144 Hz, 1P), 17.7 (d, $\mathcal{J}_{PP}$ = 145 Hz, 1P). **^{13}C{^{1}H} NMR** (THF-*d*$_8$, 125 MHz): 12.7, 15.6, 26.5, 26.6, 27.1 (d, $\mathcal{J}_{PC}$ = 23.7 Hz), 27.3, 31.3 (d, $\mathcal{J}_{PC}$ = 29.8 Hz), 31.9, 32.2, 32.7, 33.0, 34.7 (d, $\mathcal{J}_{PC}$ = 17.1 Hz), 35.1 (d, $\mathcal{J}_{PC}$ = 17.1 Hz), 96.6 (Re=C(OBBN)*C*H$_2$OBBN), 128.0 (dd, $\mathcal{J}_{PC}$ = 8.9, 24.9 Hz), 128.6 (t, $\mathcal{J}_{PC}$ = 8.6 Hz), 129.0 (d, $\mathcal{J}_{PC}$ = 9.7 Hz), 129.2, 129.9, 132.3 (d, $\mathcal{J}_{PC}$ = 8.3 Hz), 133.7 (t, $\mathcal{J}_{PC}$ = 8.8 Hz), 135.2 (d, $\mathcal{J}_{PC}$ = 11.5 Hz), 138.7 (d, $\mathcal{J}_{PC}$ = 37.0 Hz), 142.4 (d, $\mathcal{J}_{PC}$ = 46.4 Hz), 143.3 (d, $\mathcal{J}_{PC}$ = 31.0 Hz), 143.8 (d, $\mathcal{J}_{PC}$ = 46.0 Hz), 203.4 (t, $\mathcal{J}_{PC}$ = 9.2 Hz; CO), 211.4 (dd, $\mathcal{J}_{PC}$ = 5.86, 9.2 Hz; CO), 303.4 (dd, $\mathcal{J}_{PC}$ = 7.8, 11.4 Hz; Re=*C*(OBBN)CH$_2$OBBN). **IR** (THF): ν_{CO}, 1848, 1933 cm^{-1}. **HRMS** (FAB$^-$) m/z calcd. for $C_{48}H_{58}O_4P_2B_2Re$: 969.3554. Found: 969.3539 [M$^-$], 791.2480 [M–(CO)CH$_2$(BBN)]. Elemental analysis yielded widely variable results based on triplicate analysis. Calcd. for $C_{52}H_{70}O_5P_2B_2ReNa$(5•$Et_2O$): C, 58.49; H, 6.61. Found: C, 57.43/59.34/60.07 (Avg. 58.95); H, 6.13/6.42/6.41(Avg. 6.32); N, 0.33/0.28/0.20.

Reaction of [1-E$_2$][BF$_4$] with 2 equiv [HPt(dmpe)$_2$][PF$_6$]. A J-Young NMR tube was charged with 16.8 mg (0.0159 mmol) [**1-E$_2$**][BF_4], 20.5 mg (0.0319 mmol)

$[HPt(dmpe)_2][PF_6]$, and 0.5 mL C_6D_5Cl. The tube was sealed and vigorously shaken, providing a slightly cloudy yellow solution. After 30 minutes ^{31}P NMR revealed a mixture of $[\mathbf{3\text{-}E_2}]^-$:$\mathbf{2\text{-}E_2}$ in a 2.8:1 ratio. After 3 hours, the ratio settled to 4.2:1, along with some unknown Re products. The total yield of C–C coupled product was 67%.

Reductions of trans-$[(PPh_3)_2Re(CO)_4]^+$ ($[1\text{-}Ph_2]^+$)

Synthesis of $[HPt(dmpe)_2][PF_6]$ ($[HPt][PF_6]$). While the published literature procedure is serviceable,[8a] certain alterations improved the yield in our hands. In particular, the reaction was run more dilute to ensure that all $[\mathbf{HPt}]^+$ remained in solution, and the use of EtOH (which appeared to decompose $[\mathbf{HPt}]^+$ reasonably quickly) was avoided. A 500 mL round bottom flask was charged with 1.96 g (2.49 mmol) $[Pt(dmpe)_2][PF_6]_2$, 200 mL acetonitrile, and a stir bar. With the acetonitrile solution stirring, 0.189 g (4.99 mmol, 2 equiv) $NaBH_4$ (as a 10 wt% mixture in basic alumina) was added as a solid. The mixture was stirred for ~12 hours, filtered through a fine frit, and the filtrate was dried under vacuum to afford an off-white powder. The crude material contained only $[\mathbf{HPt}][PF_6]$ and excess $NaBH_4$. The desired $[\mathbf{HPt}][PF_6]$ was extracted with 15 mL C_6H_5Cl, and filtered away from the insoluble white $NaBH_4$. The solvent was removed from the filtrate under vacuum, and the very pale yellow solids were washed with 3 x 5 mL Et_2O to afford 1.414 g (88% yield) spectroscopically pure $[\mathbf{HPt}][PF_6]$. This procedure provided material with spectroscopic characteristics that matched the published values well, and also matched samples of $[\mathbf{HPt}][PF_6]$ prepared using the literature procedure.

Reaction of [HPt][PF_6] with CD_2Cl_2. A J-Young NMR tube was charged with 16 mg (0.0234 mmol) [**HPt**][PF_6] and ~0.5 mL CD_2Cl_2. The tube was sealed and monitored by ^1H and $^{31}P\{^1H\}$ NMR spectroscopy over 1 week. Colorless crystals of [**Pt**]Cl_2 formed in the tube over the course of the week, and spectroscopic analysis revealed steady disappearance of the hydride resonances of [**HPt**]$^+$ (–11.62, pent, $\mathcal{J}_{PH}$ = 29.4 Hz, $\mathcal{J}_{PtH}$ = 705 Hz) with concomitant growth of a peak at 2.98 (pent, $\mathcal{J}_{HD}$ = 1.6 Hz) assigned to CHD_2Cl.

Reaction of [$HPt(dmpe)_2$][PF_6] with [$(PPh_3)_2Re(CO)_4$][BPh_4]. A J-Young NMR tube was charged with 7.4 mg (0.0116 mmol) solid [$HPt(dmpe)_2$][PF_6] and 13.2 mg (0.0116 mmol) [$(PPh_3)_2Re(CO)_4$][BPh_4]. Chlorobenzene-d_5 was added to the tube, and the mixture was shaken vigorously for 3 minutes. Some of the Re did not dissolve. The reaction was monitored by ^1H and $^{31}P\{^1H\}$ NMR. The solution ratio of starting materials was roughly 2:1 Pt–H:Re^+. There was no observed reaction over time: neither formation of a formyl or other reduced CO species nor any consumption of the [$HPt(dmpe)_2$][PF_6] was observed.

Reaction of [$HPt(dmpe)_2$][PF_6] with [$(PPh_3)_2Re(CO)_4$][$B(3,5\text{-}C_6H_3(CF_3)_2)_4$] and BEt_3. A resealable J-Young NMR tube was charged with 21.4 mg (0.0127 mmol) [$(PPh_3)_2Re(CO)_4$][$B(C_6H_3(3,5\text{-}(CF_3)_2))_4$], 8.1 mg (0.0127 mmol) [$HPt(dmpe)_2$][PF_6], and 0.5 mL C_6D_5Cl. The tube was sealed and shaken; NMR studies showed that no reaction had occurred. The tube was returned to the glovebox, where 25 μL (0.025 mmol, 2 equiv) BEt_3 was added by syringe. After 20 minutes, a small formyl peak at 13.9 ppm, integrating to ~1% conversion, was observed. The peak did not change over 3 hours, at which point

another 100 μL (0.1 mmol, 8 equiv) BEt_3 was added. No further changes were observed, and the conversion to formyl remained at roughly 1%.

Reaction of excess $NaHBEt_3$ with $[(PPh_3)_2Re(CO)_4][BF_4]$. 27.2 μL (0.027 mmol) $NaHBEt_3$ (1.0 M in toluene) was added dropwise to a slurry of $[(PPh_3)_2Re(CO)_4][BF_4]$ in ~0.6 mL C_6D_5Cl with vigorous stirring. After 5 minutes, the solution was transferred to an NMR tube, and examined by ^1H and $^{31}P\{^1H\}$ NMR. The known formyl complex $(PPh_3)_2Re(CO)_3(CHO)$ was observed, and no precipitation or spectral evidence for further reactivity was noted. Over a few hours the formyl decomposed with generation of Re–H peaks (as expected for the unstabilized formyl).

Reaction of $[\mathbf{1\text{-}Ph_2}][BF_4]$ with $[\mathbf{HPt}][PF_6]$. A J-Young NMR tube was charged with 7.9 mg (0.0087 mmol) [**1-Ph$_2$**][BF_4], 5.6 mg (0.0087 mmol) [**HPt**][PF_6], and ~0.6 mL C_6D_5Cl. After 1 hour, a small resonance for formyl $(PPh_3)_2Re(CO)_3(CHO)$ (**2-Ph$_2$**) was observed at d 15.22. After ~35 hours, a mixture of $(PPh_3)_2Re(CO)_3H$ and $(PPh_3)Re(CO)_4H$ was observed, which grew as the $[\mathbf{HPt}]^+$ was consumed. The reaction was monitored for 7 days, during which time the formyl did not accumulate to any significant extent; eventually only the two Re–H species remained.

Reaction of $[\mathbf{1\text{-}Ph_2}][BF_4]$ with $[\mathbf{HPt}][PF_6]$ in presence of $B(OR)_3$. A ~0.6 mL C_6D_5Cl solution of 6.3 mg (0.0329 mmol) isopropyl pinacol borate was added to 10.9 mg (0.0169 mmol) [**HPt**][PF_6], and the solution was then added to 15.4 mg (0.0169 mmol) [**1-Ph$_2$**][BF_4]. The resulting slurry was added to a J-Young NMR tube, and monitored by ^1H and ^{31}P NMR. The reaction proceeded slowly, with small amounts of formyl persisting over

the course of 6 days and large amounts of Re–H species being formed. Significant variation in the ratio of Re hydride species formed was observed in multiple experiments. The rate of the reaction was roughly the same as that with no added acid.

Reaction of [1-Ph$_2$][BF$_4$] with [HPt][PF$_6$] in presence of B(C$_6$F$_5$)$_3$. A vial was charged with 17.9 mg (0.0197 mmol) [**1-Ph$_2$**][BF$_4$], 10.1 mg (0.0197 mmol) B(C$_6$F$_5$)$_3$, and 12.6 mg (0.0197 mmol) [**HPt**][PF$_6$]. C$_6$D$_5$Cl (~0.6 mL) was added to the vial, and the slurry was moved to a J-Young NMR tube, where it was shaken well. NMR spectroscopy revealed complete consumption of [**HPt**]$^+$ and small amounts of [**Pt**]$^{2+}$ in solution (with the majority precipitating), affording only one Re-containing species, assigned as [(PPh$_3$)$_2$Re(CO)$_4$][HB(C$_6$F$_5$)$_3$]. The same reactivity was observed when 2 equiv B(C$_6$F$_5$)$_3$ were added. **^{1}H NMR** (C$_6$D$_5$Cl, 300 MHz): δ 7.19-7.29 (m, 12H), 7.32-7.40 (m, 8H). **^{31}P{^{1}H} NMR** (C$_6$D$_5$Cl, 121 MHz): δ 4.2. **^{19}F NMR** (C$_6$D$_5$Cl, 282 MHz): δ –134.19 (m, 6F), –161.32 (t, $\mathcal{J}_{FF}$ = 20.5 Hz, 3F), –165.77 (m, 6F). **^{11}B NMR** (C$_6$D$_5$Cl, 160 MHz): with 2 equiv added B(C$_6$F$_5$)$_3$, δ ~ 0 (br), consistent with exchange between B(C$_6$F$_5$)$_3$ and [HB(C$_6$F$_5$)$_3$]$^-$. **IR** (C$_6$D$_5$Cl): ν_{CO} 2003 (s); ν_{BH} 1644 (m), ν_{CF} 1514 (m), 1466 (s).

NMR Scale Reaction of [1-Ph$_2$][BF$_4$] with [HPt][PF$_6$] in presence of trialkylborane. A ~0.6 mL C$_6$D$_5$Cl solution of 6.3 mg (0.0300 mmol) ^{t}Bu(CH$_2$)$_2$B(C$_8$H$_{14}$) was added to 9.7 mg (0.00152 mmol) [**HPt**][PF$_6$], and the mixture was added to 13.8 mg (0.0152 mmol) solid [**1-Ph$_2$**][BF$_4$]. The reaction mixture was transferred to a J-Young NMR tube, and monitored by multinuclear NMR. After 15 minutes, high conversion to a boroxycarbene species (δ 14.60) was observed; the reaction was complete within 3 hours.

NMR parameters of the ~2:1 mixture of $^{t}Bu(CH_2)_2B(C_8H_{14})$: **2-Ph$_2$** (reversible adduct formation leads to chemical shifts dependent on the amount of borane present). The product displayed spectral parameters very similar to the product of reduction of [**1-Ph$_2$**][BF_4] with 1 equiv $NaHBEt_3$ (1.0 M in toluene). **^{1}H NMR** (C_6D_5Cl, 300 MHz): δ 0.91 (s, ^{t}*Bu*$CH_2CH_2B(C_8H_{14})$, 18H), 1.15-1.38 (m, $^{t}BuCH_2CH_2B(C_8$*H*$_{14}$), 16H), 1.59 (br m, $^{t}BuCH_2C$*H*$_2B(C_8H_{14})$, 4H), 1.65-1.95 (m, ^{t}BuC*H*$_2CH_2B(C_8$*H*$_{14}$), 24H), 7.07-7.21 (m, PPh_3, 12H), 7.58-7.64 (m, PPh_3, 8H), 14.60 (s, Re–CHO, 1H). **^{31}P{^{1}H} NMR** (C_6D_5Cl, 121 MHz): δ 14.5.

Synthesis of *mer,trans*-(PPh$_3$)$_2$Re(CO)$_3$(CHO) (2-Ph$_2$). A 20 mL scintillation vial was charged with 95 mg (0.083 mmol) *trans*-[$(PPh_3)_2Re(CO)_4$][BPh_4] and 5 mL THF. With stirring, 83 μL (0.083 mmol) $LiHBEt_3$ (1.0 M in THF) was added dropwise, during which time the colorless solution turned yellow. The reaction was stirred for 5 minutes, filtered, and the solvents concentrated to 1 mL under vacuum. A layer of 2 mL pentane was added, and the mixture placed in the freezer at –35 °C. A yellow powder formed overnight, which contained a mixture of **2-Ph$_2$** and $LiBPh_4$. Another 10 mL pentane was added to the mother liquor of the first crystallization, which upon cooling yielded a second crop of powder, which yielded ~30 mg pure **2-Ph$_2$** (45% yield). As previously reported, the product reacts with CH_2Cl_2 and was sparingly soluble in most solvents; an IR spectrum (KBr/nujol mull) matched the literature values well.[15]

Single crystals of the BEt_3 adduct **2-Ph$_2$**•BEt_3 were obtained in a separate reaction by adding 10 equiv BEt_3 (1.0 M in hexanes) to a THF solution of **2-Ph$_2$** (prepared as above),

which was then layered 1:1 with pentane and cooled to −35 °C. Long colorless needles suitable for XRD needles grew over a few days.

Titration of 2-Ph$_2$ with ^{t}Bu(CH$_2$)$_2$B(C$_8$H$_{14}$). The equilibrium constant for adduct formation between formyl **2-Ph$_2$** and a ^{t}Bu(CH$_2$)$_2$B(C$_8$H$_{14}$) (Scheme 3.29) was carried out by titration, with monitoring by ^{1}H NMR. Due to the insolubility of **2-Ph$_2$**, an internal standard was used to quantify the concentration. A sample of 15.2 mg (0.0185 mmol) was weighed and 0.6 mL THF-*d*$_8$ was added. The slurry was filtered into a J-Young NMR tube, and a 2.8 mg crystal (0.0106 mmol) 18-crown-6 was added to the tube. An initial NMR spectrum showed 1.01:1.00 18-crown-6:formyl, and the concentration of Re was determined to be 17.5 mM. Aliquots of a 1.0 M solution of ^{t}Bu(CH$_2$)$_2$B(C$_8$H$_{14}$) in THF-*d*$_8$ were then added: 0.13, 0.33, 0.89, 1.33, and 1.68 equiv. The chemical shift change of the formyl was recorded at each concentration of borane, and a Benesi-Hildebrand-type analysis[16] gave a linear plot of $1/\Delta\delta$ vs. $1/[^t\text{Bu(CH}_2)_2\text{B(C}_8\text{H}_{14})]$ (Figure 3.13), providing an estimate of the equilibrium constant of Scheme 3.29, K_{eq} = 100 M^{-1} favoring adduct formation. A correction was made for the background equilibrium of THF binding the borane, as less borane would be available to interact with the formyl.

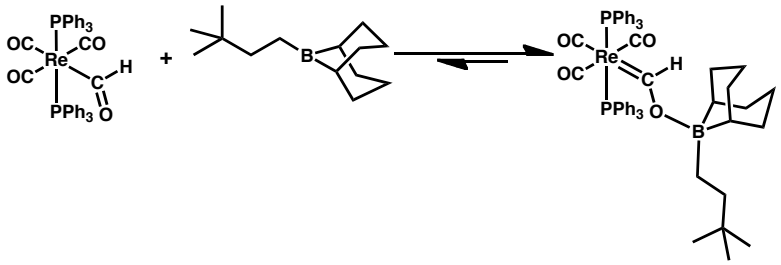

Scheme 3.29

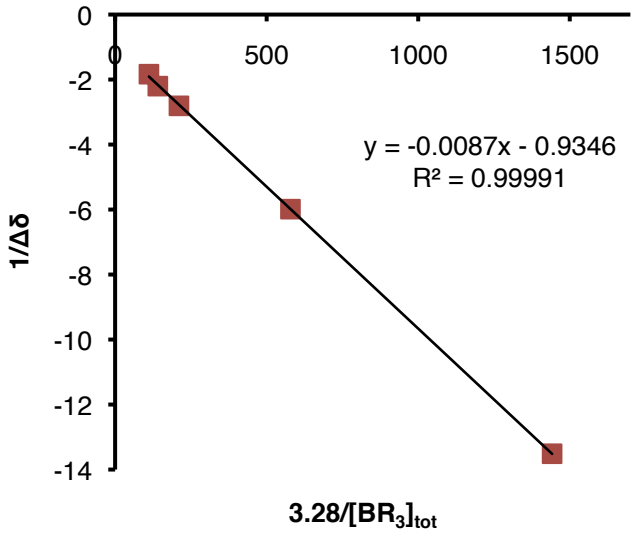

Figure 3.13. Benesi-Hildebrand plot showing borane binding to formyl.

Synthesis of Complexes with Pendent Boranes

Synthesis of Crude $Ph_2PCH_2B(C_8H_{14})$. A slurry of 1.42 g (6.87 mmol) Ph_2PCH_2Li in 50 mL pentane was frozen in the cold well of a glovebox. As the slurry thawed, a thawing 20 mL pentane solution of Cl-9-BBN was added. The mixture was allowed to warm with stirring, and was stirred for 18 hours. White solids remained throughout the reaction, which were collected on a frit, and washed with 3 x 5 mL THF. The solids were dried, giving 1.97 g (6.15 mmol, 90%) of white powder assigned as oligomeric $Ph_2PCH_2B(C_8H_{14})$. These solids are insoluble in common organic solvents. The crude phosphinoborane ligand could be used at this stage, but better results were obtained when the ligand was treated successively with pyridine and BF_3•Et_2O, as follows.

Synthesis of $Ph_2PCH_2B(C_8H_{14})$•pyridine. A 20 mL scintillation vial was charged with 0.756 g (2.36 mmol) $Ph_2PCH_2B(C_8H_{14})$, in the form of crude white insoluble solids as described above. A stirbar and 10 mL toluene was added, giving a thick white slurry. A 5

mL toluene solution of 0.242 g (3.07 mmol) pyridine was added, and over a few minutes the slurry steadily became less cloudy, although there were still some solids that did not dissolve over the course of the reaction. After 6 hours, the cloudy reaction mixture was filtered, and the filtrate evaporated to dryness *in vacuo*. The white solids where washed with 3 x 4 mL pentane, and dried to give 0.700 g (1.75 mmol, 74%) white microcrystalline $Ph_2PCH_2B(C_8H_{14})$•pyridine. The pyridine adduct was soluble in most organic solvents (except pentane). **^{1}H NMR** (THF-d_8, 500 MHz): δ 1.14-1.25 (m, 3H, $Ph_2PCH_2B(C_8H_{14})$), 1.38 (d, $\mathcal{J}_{PH}$ = 4.7 Hz, 2H, $Ph_2PCH_2B(C_8H_{14})$), 1.38-1.44 (m, 2H, $Ph_2PCH_2B(C_8H_{14})$), 1.60 (m, 3H, $Ph_2PCH_2B(C_8H_{14})$), 1.73-1.79 (m, 2H, $Ph_2PCH_2B(C_8H_{14})$), 1.90 (m, 2H, $Ph_2PCH_2B(C_8H_{14})$), 2.16 (br m, 2H, $Ph_2PCH_2B(C_8H_{14})$), 7.07 (m, 6H, $Ph_2PCH_2B(C_8H_{14})$), 7.20 (m, 4H, $Ph_2PCH_2B(C_8H_{14})$), 7.35 (t, $\mathcal{J}_{HH}$ = 7.0 Hz, 2H, *m*-C_5H_5N), 7.75 (t, $\mathcal{J}_{HH}$ = 7.6 Hz, 1H, *p*-C_5H_5N), 8.45 (d, $\mathcal{J}_{HH}$ = 5.2 Hz, 2H, *o*-C_5H_5N). **^{31}P{^{1}H} NMR** (THF-d_8, 121 MHz): δ –17.1. **^{11}B NMR** (THF-d_8, 160 MHz): δ –0.2. **^{13}C{^{1}H} NMR** (THF-d_8, 125 MHz): δ 23.30 (br), 25.57, 25.84, 31.24, 33.35, 126.29 (*m*-C_5H_5N), 127.97 (*p*-Ph), 128.53 (d, $^3\mathcal{J}_{PC}$ = 6.3 Hz, *m*-Ph), 133.45 (d, $^2\mathcal{J}_{PC}$ = 19.2 Hz, *o*-Ph), 140.57 (*p*-C_5H_5N), 144.86 (d, $^1\mathcal{J}_{PC}$ = 18.2 Hz, *ipso*-Ph), 146.57 (*o*-C_5H_5N). **HRMS** (FAB$^+$): m/z calcd. for $C_{26}H_{31}BNP$: 399.2287. Found: 399.2284 (M^+), 320.1907 (M–C_5H_5N), 200.1611 (M–Ph_2PCH_2).

Synthesis of $Ph_2PCH_2B(C_8H_{14})$. A 20 mL scintillation vial was charged with 615 mg (1.5 mmol) $Ph_2PCH_2B(C_8H_{14})$•pyridine, 18 mL Et_2O, and a stirbar. With stirring, 195 μL BF_3•OEt_2 was added dropwise by syringe. As the BF_3•OEt_2 was added, fluffy white precipitates formed, eventually giving a thick white slurry. After stirring for 20 minutes, the solids were collected on a frit, and washed with 3 x 5 mL Et_2O, and 4 x 4 mL CH_2Cl_2,

yielding 369 mg (1.15 mmol, 77%) $Ph_2PCH_2B(C_8H_{14})$. This material was quite insoluble, precluding full characterization, but yielded clean metallation reactions. **Anal. Calcd.** for $C_{21}H_{26}BP$: C, 78.77; H, 8.18. Found: C, 78.52; H, 8.45.

Synthesis of *mer,trans*-$(Ph_2PCH_2B(C_8H_{14}))_2Re(CO)_3Br$. A pressure vessel equipped with a Teflon valve was charged with 1.33 g (4.16 mmol, 2 equiv) $Ph_2PCH_2B(C_8H_{14})$, 0.85 g (2.08 mmol, 1 equiv) $Re(CO)_5Br$, 30 mL toluene, and a stirbar. The vessel was sealed and heated to 120 °C with stirring. The two mostly-insoluble white powders dissolved quickly upon heating, and the solution turned pale yellow as the reaction proceeded. After 18 hours, the reaction mixture was cooled and degassed under vacuum. After backfilling with argon the vessel was sealed and re-heated to 120 °C. After 4 days the mixture was cooled, degassed, put under argon, and re-heated again. After heating for another 48 hours, the reaction mixture was allowed to cool, and the solvents were removed to dryness, yielding 2.2 g crude product (90% pure by NMR). The crude material was purified by crystallization from a toluene/pentane mixture at –35 °C. **^{1}H NMR** (CD_2Cl_2, 500 MHz): δ 1.21-1.29 (m, 8H, $Ph_2PCH_2B(C_8\mathit{H}_{14})$), 1.64-1.84 (br m, 20H, $Ph_2PCH_2B(C_8\mathit{H}_{14})$), 2.94 (m, 4H, $Ph_2PC\mathit{H}_2B(C_8H_{14})$), 7.35-7.43 (m, 12H, Ph), 7.65 (m, 8H, Ph). **^{31}P{^{1}H} NMR** (C_6D_5Cl, 121 MHz): δ 8.2. **^{13}C{^{1}H} NMR** (CD_2Cl_2, 126 MHz): δ 24.08 ($Ph_2PCH_2B(\mathit{C}_8H_{14})$), 27.05 (br t, ($Ph_2P\mathit{C}H_2B(C_8H_{14})$), 32.34 (br, ($Ph_2PCH_2B(\mathit{C}_8H_{14})$), 34.72 ($Ph_2PCH_2B(\mathit{C}_8H_{14})$), 128.81 (m, (*m*-$Ph_2PCH_2B(\mathit{C}_8H_{14})$), 130.33 ((*p*-$Ph_2PCH_2B(\mathit{C}_8H_{14})$), 132.47 (m, (*o*-$Ph_2PCH_2B(\mathit{C}_8H_{14})$), 139.04 (m, (*ipso*-$Ph_2PCH_2B(\mathit{C}_8H_{14})$), 192.77 (t, $\mathcal{J}_{PC}$ = 8.5 Hz, CO), 192.87 (t, $\mathcal{J}_{PC}$ = 6.8 Hz, CO). **^{11}B NMR** (CD_2Cl_2, 160 MHz): δ 67.8 (v br). **IR**

(CD_2Cl_2): 2012 (w), 1958 (vs), 1899 (s) cm^{-1}. **Anal. Calcd.** for $C_{45}H_{52}B_2BrO_3P_2Re$: C, 54.56; H, 5.29. Found: C, 54.39; H, 5.05.

Synthesis of *trans*-[($Ph_2PCH_2B(C_8H_{14})$)$_2$Re(CO)$_4$][B(C_6F_5)$_4$] ([1-M$_2$][B(C_6F_5)$_4$]). A 20 mL scintillation vial was charged with 0.145 g (0.157 mmol) [Ph_3C][B(C_6F_5)$_4$] and 5 mL C_6H_5Cl. To the stirring solution was added 25.1 μL (0.157 mmol) Et_3SiH dropwise. The orange-brown mixture was stirred for 25 minutes, after which time the mixture was added to a 60 mL Teflon-stoppered pressure vessel charged with a suspension of 0.156 g (0.157 mmol) *mer,trans*-($Ph_2PCH_2B(C_8H_{14})$)$_2$Re(CO)$_3$Br in 5 mL C_6H_5Cl. The vessel was sealed, removed from the box, and the contents frozen in a liquid nitrogen bath. After two freeze-pump-thaw cycles, 1 atm CO gas (treated by passage through a column of activated Mn oxide and sieves) was introduced to the vessel. The reaction vessel was sealed and stirred overnight. After ~12 hours, the mixture had a lighter, more yellow color. At this time the vessel was degassed, and the solvents were concentrated *in vacuo* to 2 mL. Treatment with 10 mL pentane prompted immediate precipitation of copious amounts of pale yellow solids. After stirring a few hours, the solids were collected on a frit, and washed with more pentane. The solids were dried, affording 0.228 g (90%, 0.141 mmol) spectroscopically pure [**1-M$_2$**][B(C_6F_5)$_4$]. X-Ray quality crystals were obtained by crystallization from 1,2-dichloroethane / pentane mixtures. **^{1}H NMR** (CD_2Cl_2, 500 MHz): δ 0.95 (m, 4H), 1.35-1.43 (m, 8H), 1.48 (br, 4H), 1.63-1.75 (m, 12H), 3.24 (m, 4H), 7.54 (s, 20H). **^{31}P{^{1}H} NMR** (CD_2Cl_2, 202 MHz): δ –13.7. **^{13}C{^{1}H} NMR** (CD_2Cl_2, 125 MHz): δ 22.97, 31.51 (br), 34.00, 35.48, 124.5 (v. br, *ipso*-C_6F_5), 130.07 (t, $\mathcal{J}_{PC}$ = 5.3 Hz, *m*-Ph), 131.62 (t, $\mathcal{J}_{PC}$ = 5.6 Hz, *o*-Ph), 132.44 (t, $\mathcal{J}_{PC}$ = 1.0 Hz, *p*-Ph), 135.27 (dd, $\mathcal{J}_{PC}$ = 25.9, 26.7

Hz, *ipso*-Ph), 136.88 (dm, $\mathcal{J}_{PF}$ = 241.4 Hz), 138.82 (dm, $\mathcal{J}_{PF}$ = 245.7 Hz), 148.74 (dm, 239.1 Hz), 186.37 (t, $\mathcal{J}_{PC}$ = 7.4 Hz). **^{11}B NMR** (CD_2Cl_2, 160 MHz): δ 88.6 (br), −16.8 (BAr^F_4). **IR** (C_6D_5Cl): 1998 cm^{-1}. **HRMS** (TOF ES$^+$): m/z calcd for $C_{46}H_{52}B_2O_4P_2Re$: 939.3102. Found: 939.3076.

Synthesis of *mer,trans*-$(Ph_2PCHCH_2)_2Mn(CO)_3Br$. A 100 mL Teflon-stoppered pressure vessel was charged with 1.612 g (5.86 mmol) $Mn(CO)_5Br$, 2.49 g (11.7 mmol) diphenylvinylphosphine, 25 mL toluene, and a magnetic stirbar. The orange solution with some undissolved solids was sealed and heated to 120 °C, and the mixture darkened, with almost all of the solids dissolved. After 24 hours, the reaction mixture was allowed to cool to room temperature, during which time yellow powder precipitated and brown crystals grew, leaving an orange solution. The solids were collected on a frit, and washed with 10 mL toluene and 10 mL pentane, and then dried under vacuum. When the brown crystals were pulverized, they yielded yellow powder. Drying the powder afforded 2.48 g (66%) *mer,trans*-$(Ph_2PCHCH_2)_2Mn(CO)_3Br$. **^{1}H NMR** ($CD_2Cl_2$, 500 MHz): δ 5.18 (t, $\mathcal{J}$ = 17.6 Hz, 2H, $Ph_2PCHC\mathit{H}_2$), 6.01 (dd, $\mathcal{J}$ = 12.0, 35.2, 2H, $Ph_2PCHC\mathit{H}_2$), 7.24 (m, 2H, $Ph_2PC\mathit{H}CH_2$), 7.47 (br, 12H, 2H, Ph_2PCHCH_2), 7.68 (br, 8H, Ph_2PCHCH_2). **^{31}P{^{1}H} NMR** (THF-d_8, 121 MHz): δ 49.0. **^{13}C{^{1}H} NMR** (CD_2Cl_2, 126 MHz): δ 128.77 (t, $\mathcal{J}_{PC}$ = 4.7 Hz), 130.03, 130.72, 133.87 (t, $\mathcal{J}_{PC}$ = 4.8 Hz), 134.01 (m), 135.23 (m), 217.21 (br m, *trans*-CO), 223.39 (CO). **IR** (CH_2Cl_2): ν_{CO} 2039 (w), 1954 (s), 1912 (m) cm^{-1}. **HRMS** (FAB$^+$): m/z calcd for $C_{31}H_{26}BrMnO_3P_2$: 641.9921. Found: 641.9866.

Synthesis of *trans*-[$(Ph_2PCHCH_2)_2Mn(CO)_4$][BF_4]. A 100 mL Teflon-stoppered pressure vessel was charged with 1.515 g (2.35 mmol) *mer,trans*-$(Ph_2PCHCH_2)_2Mn(CO)_3Br$, 0.596 g (3.06 mmol) $AgBF_4$, and a stirbar. 40 mL of CH_2Cl_2 was added, and the vessel was sealed and protected from light. The reaction mixture was boil-degassed, and 1 atm CO was introduced to the vessel. The dark orange turbid mixture was stirred for 20 hours, at which point it was boil-degassed to remove excess CO, and filtered through celite, affording a bright yellow solution. The filtrate was dried *in vacuo*, affording 1.6 g (100%) of yellow product. **^{1}H NMR** (CD_2Cl_2, 500 MHz): δ 5.40 (t, $\mathcal{J}$ = 18.8 Hz, 2H, $Ph_2PCHC\mathit{H}_2$), 6.30 (dd, $\mathcal{J}$ = 10.9, 40.5 Hz $Ph_2PCHC\mathit{H}_2$), 7.02 (m, 2H, $Ph_2PC\mathit{H}CH_2$), 7.55-7.65 (m, 20H, Ph_2PCHCH_2). **^{31}P{^{1}H} NMR** (CD_2Cl_2, 121 MHz): δ 44.2. **^{13}C{^{1}H} NMR** (CD_2Cl_2, 126 MHz): δ 130.29 (dd, $\mathcal{J}_{PC}$ = 2.1, 51.8 Hz), 130.32 (m, *o*-Ph_2PCHCH_2), 131.33 (dd, $\mathcal{J}_{PC}$ = 2.2, 46.8 Hz), 132.87 (m, *m*-Ph_2PCHCH_2), 132.91, 134.12, 211.3 (br, CO). **IR** (CH_2Cl_2): ν_{CO} 2003 cm^{-1}. **HRMS (FAB$^+$)**: m/z cald for $[C_{32}H_{26}MnO_4P_2]^+$: 591.0687. Found: 591.0672, 563.0756 (–CO).

Synthesis of *trans*-[$(Ph_2P(CH_2)_2B(C_8H_{14}))_2Mn(CO)_4$][$BF_4$] ([1-$E_2$-Mn][$BF_4$]). A 20 mL scintillation vial was charged with 641 mg (0.945 mmol) *trans*-[$(Ph_2PCHCH_2)_2Mn(CO)_4$][BF_4], and 20 mL CH_2Cl_2 was added. If any residual silver salts were present, as black insoluble solids, the solution was filtered. The solution was added to a 100 mL Teflon-stoppered pressure vessel, to which was then added 692 mg (5.67 mmol) 9-BBN and a stirbar. The yellow solution turned dark orange quickly. The reaction vessel was sealed and moved to a 60 ˚C oil bath, where it was heated with stirring for 10 days. At this time the reaction was allowed to cool to room temperature, and the mixture was filtered

through celite, giving a bright yellow solution. The filtrate was concentrated to 3 mL, and 15 mL pentane was added, producing an orange oil with yellow solution above it. The solvent was decanted from the oil, and the oil was washed with 3 x 5 mL pentane, and then dried under vacuum, giving 700 mg (80%) crude [**1-E$_2$-Mn**][BF_4], ~90% pure by NMR spectroscopy. Further purification was achieved by dissolving the solids in 7 mL toluene, and letting the solution stand overnight, which yielded analytically pure yellow polycrystalline [**1-E$_2$-Mn**][BF_4] (460 mg, 53%). **^{1}H NMR** (THF-d_8, 300 MHz): δ 0.54 (m, 4H), 0.70 (4H), 1.23 (m, 4H), 1.48 (16H), 1.68 (m, 4H), 2.74 (m, 4H), 7.52 (m, 12H), 7.71 (m, 8H). **^{31}P{^{1}H} NMR** (THF-d_8, 121 MHz): δ 51.5. **^{13}C{^{1}H} NMR** (CD_2Cl_2, 126 MHz): δ 20.83 (br, $Ph_2PCH_2CH_2B(C_8H_{14})$), 23.51 ($Ph_2PCH_2CH_2B(C_8H_{14})$), 28.14 (dd, $\mathcal{J}_{PC}$ = 2.8, 28.6 Hz, $Ph_2PCH_2CH_2B(C_8H_{14})$), 31.91 (br, $Ph_2PCH_2CH_2B(C_8H_{14})$), 33.71 ($Ph_2PCH_2CH_2B(C_8H_{14})$), 130.30 (m, *m*-Ph), 131.91 (dd, $\mathcal{J}_{PC}$ 1.7, 47.6 Hz, *ipso*-Ph), 132.25 (m, *o*-Ph), 132.54 (*p*-Ph), 212.18 (br, CO). **^{11}B NMR** (CD_2Cl_2, 160 MHz): δ −1.2 (BF_4), 86.9 (br, $-B(C_8H_{14})$). **^{19}F NMR** (CD_2Cl_2, 282 MHz): δ −152.5 (br). **IR** (THF): ν_{CO} 1995 cm^{-1}.

Synthesis of *mer,trans*-($Ph_2PCH_2CHCH_2$)$_2$Re(CO)$_3$Br. A 60 mL Teflon-stoppered pressure tube was charged with 741 mg (1.82 mmol) $Re(CO)_5Br$, 825 mg (3.64 mmol, 2 equiv) $Ph_2PCH_2CHCH_2$, 15 mL toluene, and a stirbar. The tube was sealed, removed from the glovebox, and heated to 120 °C. After 5 days, the reaction was cooled to ambient temperature, degassed to remove liberated CO, and brought into a glovebox. All solvents were removed under vacuum, the solids were washed with 25 mL pentane, and collected on a frit. The white powder was dried, giving 1.28 g (1.59 mmol, 88%) pure *mer,trans*-($Ph_2PCH_2CHCH_2$)$_2$Re(CO)$_3$Br. **^{1}H NMR** (CD_2Cl_2, 300 MHz): δ 3.62 (m, 4H,

$Ph_2PCH_2CHCH_2$), 4.85 (dd, $^4J_{PH}$=1.8 Hz, J_{HH}=17.3 Hz, 2H, $Ph_2PCH_2CHCH_2$), 4.98 (dd, $^4J_{PH}$=1.7 Hz, J_{HH}=10.3 Hz, 2H, $Ph_2PCH_2CHCH_2$), 5.63 (m, 2H, $Ph_2PCH_2CHCH_2$), 7.40-7.48 (m, 12H, $Ph_2PCH_2CHCH_2$), 7.56-7.65 (m, 8H, $Ph_2PCH_2CHCH_2$). **$^{31}P\{^1H\}$ NMR** (CD_2Cl_2, 121 MHz): δ –0.9 (s). **$^{13}C\{^1H\}$ NMR** (CD_2Cl_2, 125 MHz): δ 35.88 (t, $^1J_{PC}$ = 14.4 Hz, $Ph_2PCH_2CHCH_2$), 120.53 (t, $^3J_{PC}$ = 5.4 Hz, $Ph_2PCH_2CHCH_2$), 128.76 (t, J_{PC} = 4.7 Hz, *m*-$Ph_2PCH_2CHCH_2$), 130.58 (t, $^2J_{PC}$ = 2.6 Hz, $Ph_2PCH_2CHCH_2$), 130.68 (br t, J_{PC} < 1 Hz, *p*-$Ph_2PCH_2CHCH_2$), 133.36 (t, J_{PC} = 5.0 Hz, *o*-$Ph_2PCH_2CHCH_2$), 135.21 (t, $^1J_{PC}$ = 23.3 Hz, *ipso*-$Ph_2PCH_2CHCH_2$), 190.38 (t, $^2J_{PC}$ = 6.7 Hz, *C*O *trans* to Br), 192.25 (t, $^2J_{PC}$ = 8.5 Hz, *C*O). **IR (CD_2Cl_2):** ν_{CO}, 2060, 1958, 1899 cm^{-1}. **Anal. Calcd.** for $C_{33}H_{30}BrO_3P_2Re$: C, 49.38; H, 3.77. Found: C, 49.32; H, 3.38.

Synthesis of *trans*-[$(Ph_2PCH_2CHCH_2)_2Re(CO)_4$][$BF_4$]. An 80 mL Teflon-stoppered pressure vessel was charged with 1.2 g (1.49 mmol) *mer,trans*-$(Ph_2PCH_2CHCH_2)_2Re(CO)_3Br$, 0.378 g (1.94 mmol, 1.3 equiv) $AgBF_4$, 20 mL CH_2Cl_2, and a stirbar. The mixture started to become cloudy. The vessel was quickly sealed and removed from the glovebox, whereupon it was frozen in liquid nitrogen. Two freeze-pump-thaw sequences were followed by addition of 1 atm CO. The vessel was sealed (at room temperature), protected from light, and stirred overnight (8-12 hours). The reaction mixture was then boil-degassed on a Schlenk line, and brought into a glovebox. The mixture was filtered through celite and dried, giving 0.832 g (0.99 mmol, 67%) of off-white solids, of ~95% purity (^{31}P NMR). This crude material was crystallized from CH_2Cl_2/pentane to afford 0.55 g (0.657 mmol, 44%) white *trans*-[$(Ph_2PCH_2CHCH_2)_2Re(CO)_4$][$BF_4$]. **$^1H$ NMR** (CD_2Cl_2, 300 MHz): δ 3.56-3.66 (m, 4H), 5.12-5.32 (m, 4H), 5.34-5.49 (m, 4H), 7.44-7.62

(m, 20H). **^{31}P{^{1}H} NMR** (CD_2Cl_2, 121 MHz): δ –5.7. **^{13}C{^{1}H} NMR** (CD_2Cl_2, 151 MHz). δ 38.99 (t, $^{1}\mathcal{J}_{PC}$ = 16.0, $Ph_2PCH_2CHCH_2$), 123.89 (t, $^{3}\mathcal{J}_{PC}$ = 6.1 Hz, $Ph_2PCH_2CHCH_2$), 127.97 (t, $^{2}\mathcal{J}_{PC}$ = 2.6 Hz, $Ph_2PCH_2CHCH_2$), 130.15 (t, $\mathcal{J}_{PC}$ = 5.2 Hz, *m*-$Ph_2PCH_2CHCH_2$), 132.39 (t, $\mathcal{J}_{PC}$ = 5.2 Hz, *o*-$Ph_2PCH_2CHCH_2$), 132.63 (br t, $\mathcal{J}$ < 2 Hz, *p*-$Ph_2PCH_2CHCH_2$), 132.6 (t, $\mathcal{J}_{PC}$ = 25.2 Hz, *ipso*-$Ph_2PCH_2CHCH_2$), 185.22 (t, $^{2}\mathcal{J}_{PC}$ = 7.5 Hz, Re–*C*O). **^{19}F NMR** (CD_2Cl_2): δ –152.5. IR (CD_2Cl_2): ν_{CO}, 2004 cm^{-1}. **HRMS** (TOF ES$^+$): m/z calcd. for $C_{34}H_{30}O_4P_2Re$: 751.1179. Found: 751.1177 (M^+).

Synthesis of *trans*-[$(Ph_2P(CH_2)_3B(C_8H_{14}))_2Re(CO)_4$][$BF_4$] ([1-$P_2$][$BF_4$]). A 60 mL Teflon-stoppered pressure vessel was charged with 239 mg (0.285 mmol) *trans*-[$(Ph_2PCH_2CHCH_2)_2Re(CO)_4$][$BF_4$], 69.6 mg (0.576 mmol) 9-BBN, and 15 mL CH_2Cl_2. A stirbar was added, and the vessel was sealed and the reaction vessel was heated to 60 °C. After 8 hours, the reaction mixture was cooled, and returned to the glovebox. After filtration, the solvent was removed to give 301 mg (0.278 mmol, 97%) crude white [**1-P_2**][BF_4]. The purity of this material was >95% (assessed by ^{1}H and ^{31}P NMR), and was used without further purification. If protic impurities appear to be present, [**1-P_2**][BF_4] can be treated with TMSCl (10 equiv. in CH_2Cl_2). After stirring for one hour, the mixture was filtered, the solvents removed, and the white solids washed with pentane. Crystallization from THF/pentane layer (–35 °C) afforded spectroscopically pure material. **^{1}H NMR** (CD_2Cl_2, 500 MHz): δ 1.15 (m, 4H), 1.46 (br, 4H), 1.5-1.6 (m, 16H), 1.75-1.85 (m, 12H), 2.76 (br, 4H), 7.50-7.54 (m, 8H), 7.58 (m, 12H). **^{31}P{^{1}H} NMR** (CD_2Cl_2, 202 MHz): δ –4.3. **^{11}B{^{1}H} NMR** (CD_2Cl_2, 160 MHz): –0.5 (BF_4), 88.5 ($Ph_2P(CH_2)_3B(C_8H_{14})$). **^{13}C{^{1}H} NMR** (CD_2Cl_2, 126 MHz): δ 20.31, 23.64, 29.0 (br), 31.5 (br), 33.61, 36.28 (t, $\mathcal{J}_{PC}$ = 15.5

Hz), 130.1 (t, $\mathcal{J}_{PC}$ = 5.2 Hz), 132.2 (t, $\mathcal{J}_{PC}$ = 5.2 Hz), 132.16 (t, $\mathcal{J}_{PC}$ = 5.4 Hz), 132.43, 132.85 (dd, $\mathcal{J}_{PC}$ = 25.7, 26.5 Hz), 185.58 (t, $\mathcal{J}_{PC}$ = 7.4 Hz). **IR** (CH_2Cl_2): ν_{CO}, 1999 cm^{-1}. **HRMS** (TOF HR–ESI$^+$): Calcd for $C_{50}H_{60}B_2O_4P_2Re$: 995.3802. Found: 995.3804.

Synthesis of [($Ph_2PCH_2B(C_8H_{14})$)$Re(CO)_5$][OTf] ([1-M_1][OTf]). Either isolated or in situ generated $Re(CO)_5OTf$ could be used in this synthesis. A representative experiment did not isolate $Re(CO)_5OTf$, which was formed by adding 800 mg (3.1 mmol, 1.25 equiv) solid AgOTf to a 30 mL stirring solution of 1.01 g (2.50 mmol) $Re(CO)_5Br$ in CH_2Cl_2. The mixture was protected from light and allowed to stir for 6 hours, over which time a large amount of precipitates formed. The mixture was filtered into a 100 mL Teflon-stoppered glass pressure vessel charged with 800 mg (2.50 mmol, 1 equiv) $Ph_2PCH_2B(C_8H_{14})$. The vessel was sealed after addition of a stirbar and removed from the glovebox and heated to 60 °C. After 5 days heating, the reaction was allowed to cool to ambient temperature, returned to the glovebox, where it was filtered, and the solvent removed from the clear colorless filtrate under vacuum to give white solid [**1-M_1**][OTf] in 93% purity. The material was washed with 5x15 mL Et_2O, and dried in vacuo to give analytically pure [**1-M_1**][OTf] (1.45 g, 74%). **^{1}H NMR** (CD_2Cl_2, 300 MHz): δ 0.92-1.01 (m, 2H), 1.37-1.44 (m, 6H), 1.65-1.75 (m, 6H), 3.37 (d, 11.7 Hz, 2H, $Ph_2PCH_2B(C_8H_{14})$), 7.58-7.65 (m, 10H, $Ph_2PCH_2B(C_8H_{14})$). **^{31}P{^{1}H} NMR** (CD_2Cl_2, 121 MHz): δ –14.7. **^{19}F NMR** (CD_2Cl_2, 282 MHz): δ –78.1. **^{13}C{^{1}H} NMR** (CD_2Cl_2, 125 MHz): δ 22.95, 29.66 (br d, $\mathcal{J}_{PC}$ = 24.3 Hz), 33.91, 35.11 (br), 121.61 (q, $\mathcal{J}_{FC}$ = 321 Hz, $CF_3SO_3^-$), 130.37 (d, $\mathcal{J}_{PC}$ = 10.8 Hz), 131.91 (d, $\mathcal{J}_{PC}$ = 10.6 Hz), 132.89 (d, $\mathcal{J}_{PC}$ = 2.6 Hz), 133.08 (d, $\mathcal{J}_{PC}$ = 53.1 Hz), 175.9 (v. br d, axial *C*O), 179.3 (br, equatorial *C*O). **^{11}B{^{1}H} NMR** (CD_2Cl_2, 160 MHz): δ 88.3. **IR** (C_6D_5Cl):

ν_{CO}, 2156 (w), 2099 (w), 2041 (vs) cm^{-1}. **Anal. Calcd.** for $C_{27}H_{26}BF_3O_8PReS$: C, 40.76; H, 3.29. Found: C, 40.49; H, 3.16.

Synthesis of [($Ph_2P(CH_2)_2B(C_8H_{14})$)$Re(CO)_5$][OTf] ([1-$E_1$][OTf]). A glass pressure vessel with a Teflon valve was charged with 0.402 g (0.844 mmol) $Re(CO)_5OTf$, 0.282 g (0.844 mmol) $Ph_2P(CH_2)_2B(C_8H_{14})$, 15 mL CH_2Cl_2 and a stirbar. The phosphinoborane did not fully dissolve. The flask was sealed and heated to 60 °C. After 15 minutes, all of the ligand had dissolved. After 48 hours, the reaction mixture was cooled to ambient temperature, at which point the vessel was pumped into the glovebox. The solution was filtered, and the solvents removed, giving a white powder: 0.670 g (0.827 mmol, 98% yield) of pure [**1-E_1**][OTf]. **^{1}H NMR** (CD_2Cl_2, 600 MHz): δ 1.15 (m, 2H), 1.34 (m, 2H), 1.57-1.63 (m, 4H), 1.69 (br, 2H), 1.78-1.88 (m, 6H), 2.99 (m, 2H), 7.54-7.58 (m, 4H), 7.62-7.64 (m, 6H)**. ^{31}P{^{1}H} NMR** (C_6D_5Cl, 121 MHz): δ 0.14 (s). **^{19}F NMR** (C_6D_5Cl, 282 MHz): δ –78.0. **^{11}B{^{1}H} NMR** (CD_2Cl_2, 160 MHz): δ 86.5 (br, s). **^{13}C{^{1}H} NMR** (CD_2Cl_2, 126 MHz): δ 20.8 (br), 23.51, 27.5 (d, $\mathcal{J}_{PC}$ = 29.8), 32.0, 33.7, 121.6 (q, $\mathcal{J}_{FC}$ = 321 Hz, $CF_3SO_3^-$), 130.5 (d, $\mathcal{J}_{PC}$ = 10.6), 130.6 (d, $\mathcal{J}_{PC}$ = 52.6), 132.5 (d, $\mathcal{J}_{PC}$ = 9.9 Hz), 133.1 (d, $\mathcal{J}_{PC}$ = 2.5 Hz), 175.8 (br s, *C*O), 179.0 (br s, *C*O)**. IR (CD_2Cl_2):** ν_{CO}, 2156 (m), 2096 (w), 2064 (vs) cm^{-1}; ν_{SO}, 1274 cm^{-1}; ν_{CF}, 1161 cm^{-1}. **HRMS** (TOF ES$^+$): m/z calcd for $[C_{27}H_{28}BO_5PRe]^+$: 661.1331. Found: 661.1349.

Synthesis of *trans*-[(PPh_3)($Ph_2P(CH_2)_2B(C_8H_{14})$)$Re(CO)_4$][OTf] ([1-$E_1$$Ph_1$][OTf]). A 20 mL scintillation vial was charged with 819 mg (1.19 mmol) *trans*-(PPh_3)$Re(CO)_4I$ and 10 mL CH_2Cl_2. Solid AgOTf (382 mg, 1.49 mmol, 1.25 equiv) was

added, and the reaction mixture was stirred for 2 hours with protection from light. The resulting cloudy mixture was filtered through celite to give a clear, pale yellow solution. A 100 mL Teflon-stoppered pressure tube was charged with the filtrate, and a solution of 398 mg (1.19 mmol) $Ph_2P(CH_2)_2B(C_8H_{14})$ in 5 mL CH_2Cl_2 was added, along with a stirbar. The tube was sealed, removed from the glovebox, and heated in an oil bath to 60 °C for 24 hours. After the allotted time, the reaction was cooled to ambient temperature and returned to the box. The reaction mixture was filtered and the solvent were removed *in vacuo*, giving 1.21 g (1.15 mmol, 97%) pure white [**1-E$_1$Ph$_1$**][OTf]. **^{1}H NMR** (CD_2Cl_2, 500 Mhz): δ 1.10-1.18 (m, 2H), 1.34 (dd, $\mathcal{J}$ = 10.2, 16.4, 2H, $Ph_2PCH_2CH_2B(C_8H_{14})$), 1.52-1.62 (m, 4H), 1.68 (br s, 2H), 1.77-1.88 (m, 6H), 3.00 (dd, $\mathcal{J}$ = 7.3, 15.6, 2H $Ph_2PCH_2CH_2B(C_8H_{14})$,7.46-7.52 (m, 6H), 7.54-7.62 (m, 19H). **^{31}P{^{1}H} NMR** (CD_2Cl_2, 121 MHz): δ 0.6 (d, $\mathcal{J}_{PP}$ = 80.6 Hz, 1P), 5.7 (d, $\mathcal{J}_{PP}$ = 80.0 Hz, 1P). **^{19}F NMR** (CD_2Cl_2, 282 MHz): δ –77.9. **^{11}B{^{1}H} NMR** (CD_2Cl_2, 160 MHz): δ 88.5. **^{13}C{^{1}H} NMR** (CD_2Cl_2, 125 MHz): δ 20.97 (br, $Ph_2PCH_2CH_2B(C_8H_{14})$), 23.51, 28.68 (d, $\mathcal{J}_{PC}$ = 30.6 Hz $Ph_2PCH_2CH_2B(C_8H_{14})$), 32.0 (br), 33.71, 121.55 (q, $\mathcal{J}_{CF}$ = 320 Hz, $CF_3SO_3^-$), 129.72 (d, $\mathcal{J}_{PC}$ = 10.5 Hz), 130.07 (d, $\mathcal{J}_{PC}$ = 11.0 Hz), 130.20, 132.26 (dd, $\mathcal{J}_{PC}$ = 2.1, 22.1 Hz), 132.35 (d, $\mathcal{J}_{PC}$ = 9.8 Hz), 132.54 (dd, $\mathcal{J}_{PC}$ = 2.4, 12.2 Hz), 132.76, 133.23 (d, $\mathcal{J}_{PC}$ = 11.3 Hz), 133.81 (d, $\mathcal{J}_{PC}$ = 11.0 Hz), 185.96 (t, $\mathcal{J}_{PC}$ = 7.5 Hz, *C*O). **IR (CH_2Cl_2):** ν_{CO}, 2000 cm^{-1}. **HRMS** (TOF ES^+): m/z cald for $C_{44}H_{43}BO_4P_2Re$: 895.2297. Found: 895.2271.

Synthesis of [$Ph_2PCH_2CHCH_2Re(CO)_5$][OTf]. A ¼ cup glass pressure vessel fitted with a Teflon valve was charged with 0.247 g (1.09 mmol) allyldiphenylphosphine ($Ph_2PCH_2CHCH_2$), 0.518 g (1.09 mmol) $Re(CO)_5OTf$, 1 Tbs CH_2Cl_2, and a stirbar. The

vessel was sealed and heated to 60 °C for 11 hours with stirring, after which time the vessel was cooled to ambient temperature, and moved to a glovebox. The colorless solution was filtered, and the solvents removed *in vacuo*, affording 0.730 g (1.04 mmol, 95%) spectroscopically pure white powder. **^{1}H NMR** (CD_2Cl_2, 300 MHz): δ 3.68 (dd, $\mathcal{J}_{HH}$ = 5.8 Hz, $\mathcal{J}_{PH}$ = 10.34 Hz, 2H, $Ph_2PC\mathit{H}_2CHCH_2$), 5.25-5.5 (m, 3H, $Ph_2PCH_2C\mathit{H}C\mathit{H}_2$), 7.5-7.67 (m, 10H, $\mathit{Ph}_2PC\mathit{H}_2CHCH_2$). **^{31}P{^{1}H} NMR** (CD_2Cl_2, 121 MHz) δ: –5.0 (br s). **^{19}F NMR** (CD_2Cl_2, 282 MHz): δ –79.4. **^{13}C{^{1}H} NMR** (CD_2Cl_2, 126 MHz): δ 37.41 (d, $\mathcal{J}_{PC}$ = 31.2 Hz, $Ph_2P\mathit{C}H_2CHCH_2$), 121.60 (q, $\mathcal{J}_{FC}$ = 321.1 Hz, $[\mathit{C}F_3SO_3]^-$), 124.85 (d, $\mathcal{J}_{PC}$ = 12.8 Hz, $Ph_2PCH_2\mathit{C}HCH_2$), 127.09 (d, $\mathcal{J}_{PC}$ = 5.9 Hz, $Ph_2PCH_2CH\mathit{C}H_2$), 130.37 (d, $\mathcal{J}_{PC}$ = 52.7 Hz, *ipso*-$\mathit{Ph}_2PCH_2CHCH_2$), 130.49 (d, $\mathcal{J}_{PC}$ = 10.8 Hz, *m*-$\mathit{Ph}_2PCH_2CHCH_2$), 132.51 (d, $\mathcal{J}_{PC}$ = 10.2 Hz, *o*-$\mathit{Ph}_2PCH_2CHCH_2$), 133.24 (d, $\mathcal{J}_{PC}$ = 2.5 Hz, *p*-$\mathit{Ph}_2PCH_2CHCH_2$), 175.68 (br d, $\mathcal{J}_{PC}$ = 38 Hz, axial *C*O), 178.69 (br s, eq. *C*O). **IR** (CD_2Cl_2): ν_{CO}, 2157 (m), 2098 (w), 2048 (vs) cm^{-1}; ν_{SO}, 1270 (m) cm^{-1}; ν_{CF}, 1161 (w) cm^{-1}. **HRMS** (FAB$^+$): m/z calcd. for $[C_{20}H_{15}ReO_5P]^+$: 553.0215. Found: 553.0222 (M^+), 525.0161 (M–CO), 497.0260 (M–2CO), 469.0208 (M–3CO).

Synthesis of [($Ph_2P(CH_2)_3B(C_8H_{14})$)$Re(CO)_5$][OTf] ([1-P$_1$][OTf]). A 20 mL glass pressure vessel fitted with a Teflon valve was charged with 0.710 g (1.01 mmol) $[Ph_2PCH_2CHCH_2Re(CO)_5][OTf]$, 0.124 g (1.01 mmol) 9-BBN, 5 mL CH_2Cl_2, and a magnetic stirbar. The vessel was sealed, removed from the box and heated to 60 °C for 12 hours. After this time the clear colorless solution was cooled to ambient temperature, brought back into the glovebox, and filtered. Removal of solvents from the filtrate yielded 0.747 g (0.91 mmol, 90%) of a white powder, which was ~95% pure by ^{1}H NMR, with the

other 5% being unreacted starting material. Treatment under the same conditions with slightly more 9-BBN gave spectroscopically pure [**1-P$_1$**][OTf] after washing with pentane. Analytically pure material was obtained by crystallization from a THF solution layered (1:1) with pentane at –35 °C. **^{1}H NMR** (C_6D_5Cl, 300 MHz): δ 1.08 (br m, 2H), 1.48 (br m, 8H), 1.70 (br m, 6H), 1.84 (br s, 2H), 2.82 (br m, 2H), 7.16-7.23 (m, 2H), 7.26-7.33 (m, 4H), 7.45-7.54 (m, 4H). **^{31}P{^{1}H} NMR** (C_6D_5Cl, 121 MHz): δ –6.2. **^{19}F NMR** (C_6D_5Cl, 282 MHz): δ –78.2. **^{13}C{^{1}H} NMR** (CD_2Cl_2, 125 Hz): δ 20.3, 23.6, 26.1, 29.0 (br), 31.6 (br), 33.6, 34.6 (d, $\mathcal{J}_{PC}$ = 30.0 Hz), 121.6 (q, $\mathcal{J}_{FC}$ = 321.0 Hz, $SO_3CF_3^-$), 130.5 (d, $\mathcal{J}_{PC}$ = 53.5 Hz), 130.5 (d, $\mathcal{J}_{PC}$ = 10.7 Hz), 132.2 (d, $\mathcal{J}_{PC}$ = 10.2 Hz), 133.1 (d, $\mathcal{J}_{PC}$ = 2.2 Hz), 175.8 (br, axial CO), 178.9 (br, equatorial CO). **^{11}B{^{1}H} NMR** (CD_2Cl_2, 160 MHz): δ 87.4. **IR** (CH_2Cl_2): ν_{CO}, 2156 (m), 2095 (w), 2047 (vs) cm^{-1}. **Anal. Calcd.** for $C_{29}H_{30}BF_3O_8PReS$: C, 42.29; H, 3.74. Found: C, 42.08; H, 3.74.

General procedure for preparation of BAr$^F_4$ salts of rhenium complexes. The appropriate rhenium cation, bearing either a BF_4 or OTf counter anion, was dissolved in CH_2Cl_2 solution (affording roughly 20 mM concentration) with stirring. Solid $NaBArF_4$ (1 equiv relative to Re complex) was added, and the mixture stirred for at least 2 hours. Following filtration, the solvents were removed from the filtrate *in vacuo* to afford powders or oils of the rhenium BAr$^F_4$ salts. If the product was oily, it was triturated with pentane to give a powder, and the pentane was removed under vacuum. Yields were essentially quantitative, and spectroscopic analysis correlated very favorably with the BF_4 or OTf starting materials, indicating that the structure had not changed. ^{19}F NMR unequivocally showed removal of BF_4 or OTf, and incorporation of BAr$^F_4$ anion.

NMR-scale Reaction of [1-M$_2$][B(C$_6$F$_5$)$_4$] with 1 equiv [HPt][PF$_6$]. To a stirring ~0.6 mL C_6D_5Cl solution of 31.3 mg (0.0194 mmol) [**1-M$_2$**][B(C$_6$F$_5$)$_4$] was added 12.4 mg (0.0194 mmol) [**HPt**][PF$_6$]. Monitoring by NMR spectroscopy showed a slow reaction, with ~50% conversion after 12 hours, ~70% conversion after 24 hours, and ~90% conversion after 6 days.

Reaction of [1-M$_2$][B(C$_6$F$_5$)$_4$] with 1 equiv [HPt][PF$_6$] in the presence of [Na][BF$_4$]. A 20 mL scintillation vial was charged with 103.0 mg (0.0637 mmol) [**1-M$_2$**][B(C$_6$F$_5$)$_4$], 35.0 (0.319 mmol, 5 equiv) $NaBF_4$, and 2 mL C_6H_5Cl. With stirring, 49.0 mg (0.0764, 1.2 mmol) [**HPt**][PF$_6$] was added slowly as a solid. The mixture turned yellow and developed precipitates over a few minutes, and was stirred overnight. The reaction mixture was filtered, and the solvent removed from the filtrate under vacuum. The solids were extracted with C_6H_6, filtered, and the solvents removed from the filtrate to afford 59 mg (99%) **2-M**$_2$ as a pale yellow powder in ~95% purity ([**HPt**]$^+$ was the other observed species, along with small amounts of residual C_6H_5Cl). **^{1}H NMR** (C_6D_6, 300 MHz): δ 1.49 (br, Ph$_2$PC*H$_2$*B(C$_8$H$_{14}$)), 1.88 (br, Ph$_2$PCH$_2$B(C$_8$*H$_{14}$*)), 7.16 (*Ph$_2$*PCH$_2$B(C$_8$H$_{14}$), 12H), 7.53 (br, *Ph$_2$*PCH$_2$B(C$_8$H$_{14}$), 8H), 13.96 (t, $\mathcal{J}_{PH}$ = 6.0 Hz, Re–C*H*O, 1H). **^{31}P{^{1}H} NMR** (C_6D_6, 121 MHz): δ –2 (br, 1P), 6.0 (br, 1P). **IR** (heptane): ν_{CO} 1999 (s), 1950 (s), 1938 (s) cm^{-1}.

NMR-scale reaction of [1-M$_2$][B(C$_6$F$_5$)$_4$] with 1 equiv [HPt][PF$_6$] in the presence of [hept$_4$N][BF$_4$]. A small vial was charged with 29.1 mg (0.0180 mmol) [**1-M$_2$**][B(C$_6$F$_5$)$_4$], 17.7 mg (0.0360 mmol, 2 equiv) tetraheptylammonium tetrafluoroborate,

and ~0.6 mL C_6D_5Cl. With stirring, 11.6 mg (0.0180 mmol, 1 equiv) [**HPt**][PF_6] was added as a solid. The mixture was moved to a J-Young tube, and allowed to sit for about 3 hours, at which point NMR spectroscopy showed near complete conversion to the desired boroxycarbene. As in the isolated product, at room temperature many resonances were quite broad, including the ^{31}P NMR. Variable temperature NMR studies were therefore undertaken.

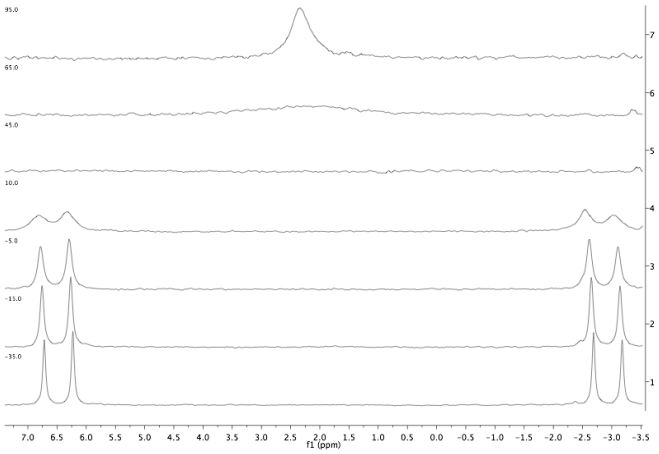

Figure 3.14. $^{31}P\{^1H\}$ NMR from −35 to 95 C.

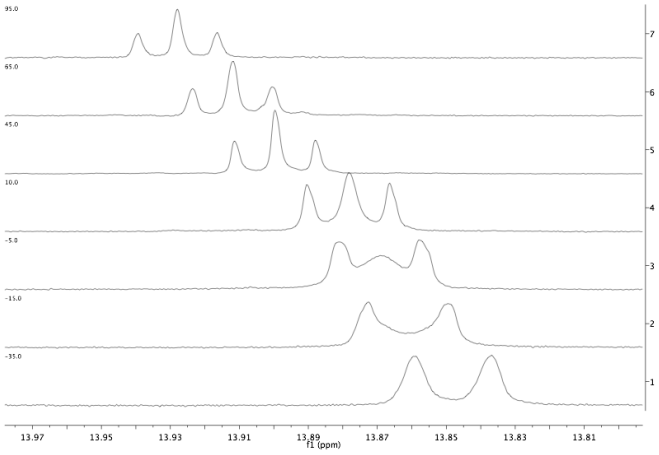

Figure 3.15. ^1H NMR (formyl region) from −35 to 95 C.

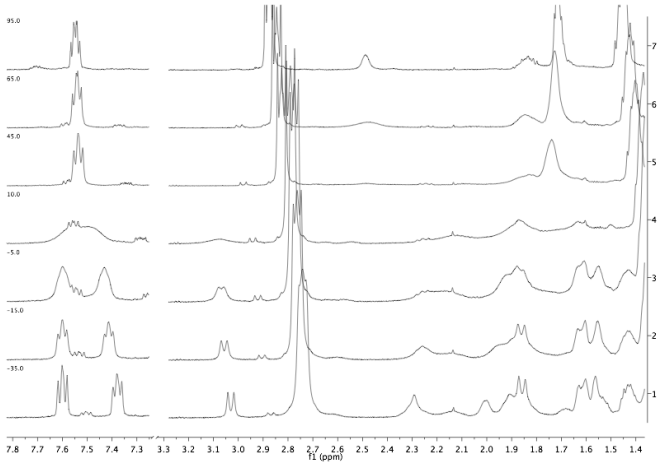

Figure 3.16. ^{1}H NMR (aryl, alkyl regions from –35 to 95 C).

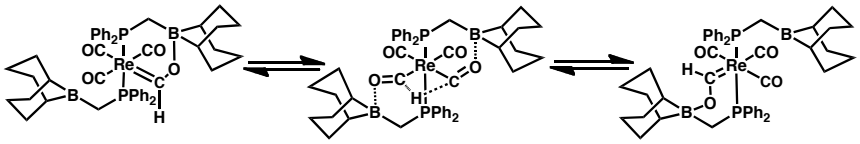

Scheme 3.30

Variable temperature NMR studies of **2-M$_2$** between –35 °C and +95 °C in C_6D_5Cl revealed fluxional processes. The ^{31}P NMR spectrum of **2-M$_2$** displays two sharp doublets (δ –2.9, $^{2}\mathcal{J}_{PP}$ = 99.1 Hz; δ 6.5, $^{2}\mathcal{J}_{PP}$ = 99.2 Hz) at low temperatures, which coalesce into a singlet (δ 2.3) at ~50 °C. The ^{1}H NMR spectrum shows similar sharpening upon cooling to –35 °C, with two sharp doublets at δ 3.07 ($\mathcal{J}_{PH}$ = 12.1 Hz) and δ 1.87 ($\mathcal{J}_{PH}$ = 13.1 Hz) emerging for two inequivalent CH_2 groups on the ligands. Near 50 °C these doublets coalesce into one broad singlet, consistent with the fluxional processes that give a more symmetric ligand environment. Interestingly, the carbene proton triplet collapses into a doublet as it is cooled, δ 13.85, $\mathcal{J}_{PH}$ = 11.1 Hz. This is consistent with a static structure with *intramolecular* coordination of one pendent borane to the carbene oxygen, in contrast to ethylene-linker-containing complex **2-E$_2$**, which has intermolecular coordination and is

dimeric. The restricted rotation of the carbene affords favorable angles for P–H coupling to the phosphinoborane that is binding the oxygen, while the other phosphine has an undetectable coupling constant due to the unfavorable coupling angles. The phosphine resonance at δ –2.9 is assigned as the intramolecularly coordinated phosphinoborane, due to the slight upield shift consistent with a 6-membered ring structure, and from ^{1}H–^{31}P gHMBC correlation to the carbene proton, as well as the downfield-shifted methylene protons of that ligand (also consistent with a constrained ring geometry).

From the coalescence temperature the barrier for the fluxtional process can be estimated, $\Delta G^{\ddagger} = 13.6 \pm 0.2$ kcal mol^{-1}. The exact process that creates equivalent ligand environments could be B–O bond breaking, rotation, and B–O bond formation with the other ligand. $^{13}C\{^{1}H\}$ NMR spectroscopy is not entirely consistent with this, however, as the CO carbons are very broad at room temperature, implicating exchange of H between the various CO groups of the complex. Further, treatment of carbene **2-M$_2$** with up to 100 equivalents of pyridine leads to *no B–O cleavage*, contrasting the easily broken B–O bonds of external Lewis acids and other linkers. If B–O cleavage were occurring rapidly on the NMR time scale, pyridine binding would be expected to be favored. Transfer of hydride from a formyl to an adjacent carbonyl ligand has been observed before, and that process, which would lead to broadening of CO signals in the ^{13}C NMR, is consistent with our observations (Scheme 3.30).[23]

NMR-scale Reaction of [1-M$_2$][B(C$_6$F$_5$)$_4$] with 2 equiv [HPt][PF$_6$] in the presence of [hept$_4$N][BF$_4$]. To a stirring ~0.6 mL THF-*d*$_8$ solution of 35.4 mg (0.0219 mmol) [**1-M**$_2$][B(C$_6$F$_5$)$_4$] was added 28.1 mg (0.0438 mmol, 2 equiv) [**HPt**][PF$_6$] partwise

slowly. The mixture was stirred for an addition 5 minutes before being transferred to a J-Young NMR tube and monitored by NMR spectroscopy. In the first few hours mainly boroxycarbene **2-M**$_2$ was observed, in addition to the asymmetric doubly-reduced product. The tube was affixed to a rotating motor to ensure good mixing, and spun overnight, at which point only doubly-reduced [**5**]$^-$ and unreacted [**HPt**]$^+$ were observed. A ~70% yield of [**5**]$^-$ from **2-M$_1$** was established by two methods, i) simple NMR integration of Re species relative to [hept$_4$N]$^+$ (assuming a constant amount of [hept$_4$N]$^+$ in solution) and ii) integration against an internal standard (capillary containing P(2,4,6-$C_6H_2Me_3)_3$). No other Re-containing products were observed in solution or when the precipitates were extracted with CD_3CN (only [**Pt**]$^{2+}$ precipitated). Spectroscopic analysis was consistent with an anionic "confused" alkyl species, containing 2 B–O bonds. Separation from the ammonium salts proved challenging, limiting identification to solution methods. Very similar reactivity was observed when C_6D_5Cl was used as the solvent. **^{1}H NMR** (THF-*d*$_8$, 600 MHz): δ 0.28 (br, 2H), 0.54 (br, 1H), 0.69 (br, 1H), 1.1-1.9 (m, overlapping with [hept$_4$N]$^+$), 2.13 (m, 1H), 2.27 (m, 1H), 3.12 (br d, $\mathcal{J}_{HH}$ = 13.0, 1H), 4.63 (br d, $\mathcal{J}_{HH}$ = 13.2 Hz, 1H), 7.20-7.35 (m, 12H), 7.52 (t, $\mathcal{J}$ = 8.3 Hz, 2H), 7.74 (t, $\mathcal{J}$ = 8.5 Hz, 2H), 7.85-7.92 (m, 4H). **^{31}P{^{1}H} NMR** (THF-*d*$_8$, 121 MHz): δ 22.3 (d, $\mathcal{J}_{PP}$ = 127.5 Hz, 1P), 37.3 (d, $\mathcal{J}_{PP}$ = 128.4 Hz). **^{13}C{^{1}H} NMR** (THF-*d*$_8$, 151 MHz): δ 21.00 (br), 23.32, 25.94, 26.81, 26.87, 27.07, 28.24 (br), 31.50 (d, $\mathcal{J}_{PC}$ = 16.7 Hz, $Ph_2PCH_2B(C_8H_{14})$), 33.07 (d, $\mathcal{J}_{PC}$ = 16.1 Hz, $Ph_2PCH_2B(C_8H_{14})$), 34.14, 34.34, 34.94, 35.20, 37.88, 82.2 (v br, Re–O–CH_2–BR_3), 125.3 (v br, *ipso*-$B(C_6F_5)_4$), 127.86, 127.98 (d, $\mathcal{J}_{PC}$ = 9.0 Hz), 128.59 (d, $\mathcal{J}_{PC}$ = 9.2 Hz), 128.66, 128.29, 129.69, 131.73 (d, $\mathcal{J}_{PC}$ = 8.9 Hz), 131.83 (d, $\mathcal{J}_{PC}$ = 9.5 Hz), 133.86 (d, $\mathcal{J}_{PC}$ = 11.1 Hz), 136.31 (d, $\mathcal{J}_{PC}$ = 11.3

Hz), 137.28 (dm, $\mathcal{J}_{FC}$ = 247.4 Hz, $B(C_6F_5)_4$), 139.28 (d, $\mathcal{J}_{FC}$ = 243.6 Hz, $B(C_6F_5)_4$), 139.68 (d, $\mathcal{J}_{PC}$ = 41.7 Hz), 141.10 (d, $\mathcal{J}_{PC}$ = 45.7 Hz), 144.80 (d, $\mathcal{J}_{PC}$ = 37.8 Hz), 148.17 (d, $\mathcal{J}_{PC}$ = 36.6 Hz), 149.33 (d, $\mathcal{J}_{FC}$ = 240.0 Hz, $B(C_6F_5)_4$), 197.36 (t, $\mathcal{J}_{PC}$ = 8.3 Hz, CO), 198.27 (t, $\mathcal{J}_{PC}$ = 8.9 Hz, CO), 199.91 (t, $\mathcal{J}_{PC}$ = 4.2 Hz, CO). **IR** (C_6D_5Cl): ν_{CO} 2020 (w), 1932 (s), 1867 (m) cm^{-1}. **HRMS (TOF MS ES$^-$):** m/z calcd for $C_{46}H_{54}B_2O_4P_2Re$, 941.3259. Found, 941.3212.

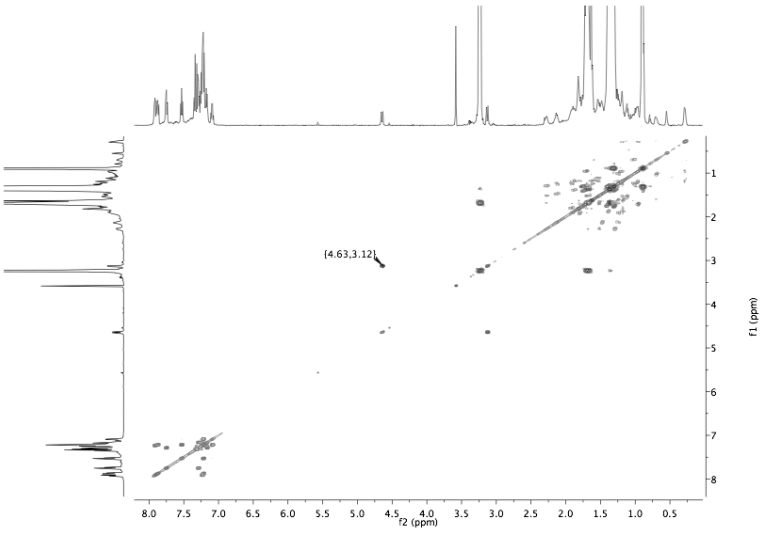

Figure 3.17. ^1H–^1H gCOSY of [**5**]$^-$. Correlation between Re–OC*H*$_2$–OBR$_3$ protons highlighted.

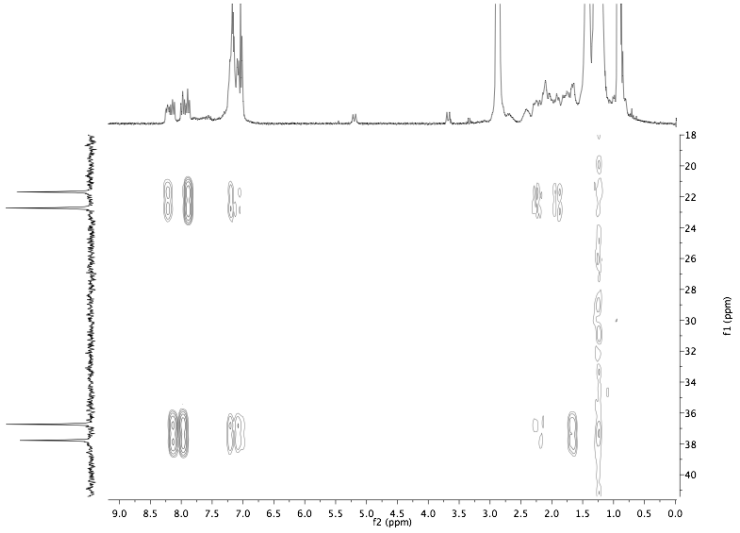

Figure 3.18. ^{1}H–^{31}P gHMBC of [**5**]$^{-}$ (C_6D_5Cl).

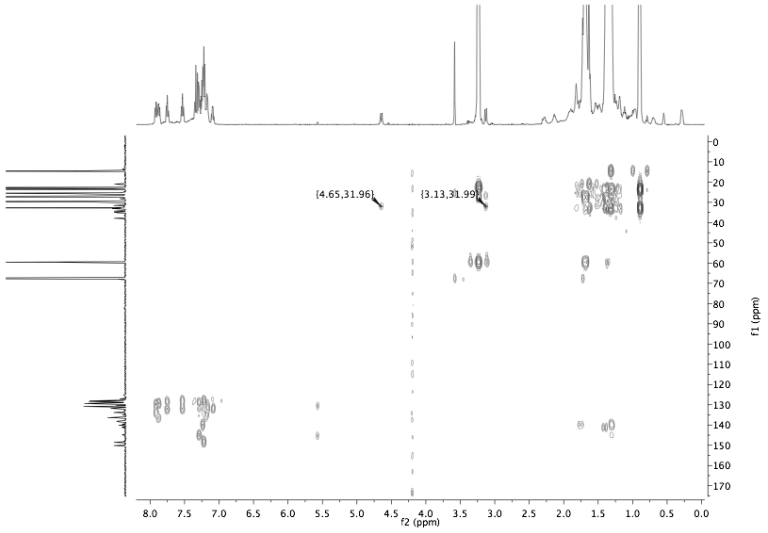

Figure 3.19. ^{1}H–^{13}C gHMBC of [**5**]$^{-}$. Correlation between Re–OC*H*$_2$–OBR$_3$ and $Ph_2PCH_2B(C_8H_{14})$ highlighted.

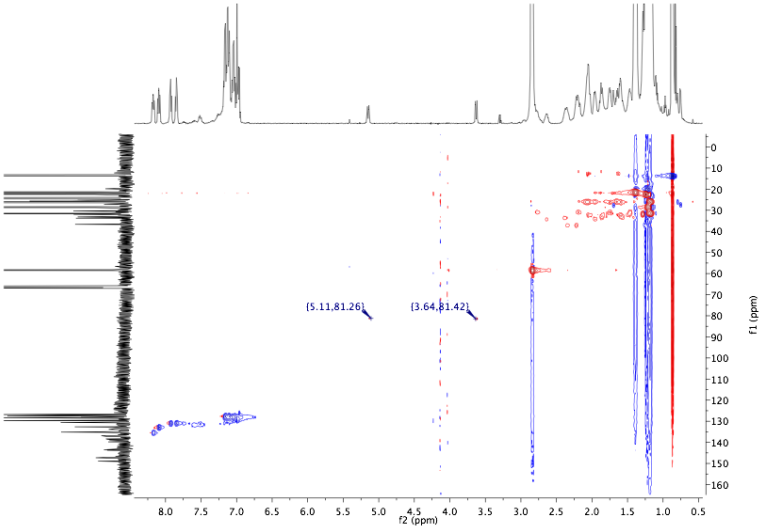

Figure 3.20. $^{1}H–^{13}C$ gHSQC of [**5**]$^{-}$ (C_6D_5Cl). Correlation between Re–OC*H*$_2$BR$_3$ and Re–O*C*H$_2$BR$_3$ is highlighted.

Reaction of 2-M$_2$ with pyridine. A vial was charged with 39.6 mg (0.0245 mmol) [**1-M**$_2$][B(C_6F_5)$_4$], 24.0 mg (0.0490 mmol) tetraheptylammonium tetrafluoroborate, and ~0.6 mL C_6D_5Cl. Solid [**HPt**][PF_6] (15.7 mg, 0.0245 mmol) was added in portions to the C_6D_5Cl solution with stirring, and the contents were added to a J-Young NMR tube. The tube was mixed by rotary motor overnight, at which point NMR spectroscopy showed clean conversion to boroxycarbene **2-M$_2$**. The NMR tube was returned to the glovebox, and the contents of the tube were poured onto an internal standard, 20 mg (0.0228 mmol) (PPh_3)$_2$Re(CO)$_3$Br. The mixture was filtered into a J-Young NMR tube, and NMR studies were carried out (there was no reaction or interaction with the Re–Br). Later, pyridine (6 μL, 0.0735, 3 equiv) was added. Instead of the expected B–O bond cleavage and downfield shift of the Re–CHO peak, a doublet at essentially unchanged chemical shift was observed. The ^{1}H NMR resonances sharpened and were consistent with two inequivalent ligands (two $Ph_2PCH_2BR_2$ groups). Two sharp ^{31}P NMR resonances were observed. Even with

addition of a few drops (~100 equiv) pyridine, no significant spectral change was observed. Based on comparisons to the boroxycarbene spectra, the product is assigned as intramolecularly coordinated boroxycarbene with the second pendent borane binding pyridine. The spectral characteristics are quite similar to the low temperature spectra of **2-M$_2$** in the absence of pyridine, suggesting an analogous structure. **^{1}H NMR** (C_6D_5Cl, 300 MHz): δ 1.4-2.5 (br, m, $Ph_2PCH_2B(C_8H_{14})$), 1.83 (d, 13.7 Hz), 2.50 (d, 11.2 Hz), 6.9-7.1 (m, pyridine and Ph), 7.27 (br t, $\mathcal{J}$ = 7.01, pyridine), 7.39 (m, 6H, Ph), 7.58 (m, 6H), 8.61 (br, pyridine), 13.66 (d, J = 10.3 Hz, Re–C*H*O). **^{31}P{^{1}H} NMR** (C_6D_5Cl, 121 MHz): δ 2.56 (d, $\mathcal{J}_{PP}$ = 96.0 Hz, 1P), 7.41 (d, $\mathcal{J}_{PP}$ = 95.8 Hz, 1P).

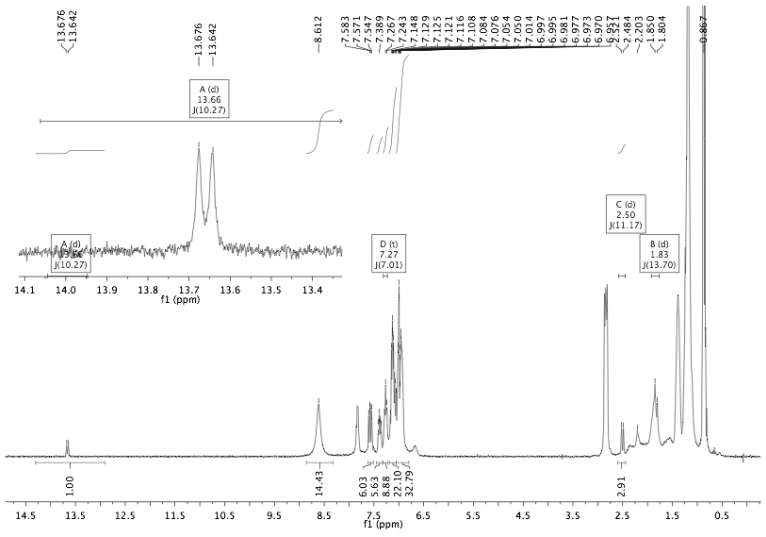

Figure 3.21. ^{1}H NMR of **2-M$_2$•py**.

Pulsed Gradient Spin-Echo Diffusion NMR Studies on 2-E$_2$

^{1}H NMR pulsed gradient spin-echo (PGSE) NMR measurements were performed using the standard echo pulse sequence on a Varian INOVA 500 MHz spectrometer at 298.15 K without spinning. The gradient shape was rectangular, with gradient length 2-4.2 ms, and

the gradient strength was varied during the experiment. The spectra were processed with 2.0 Hz line broadening, and single exponential fits of selected resonances provided values for the diffusion coefficient D_t. The experimental diffusion coefficient was used to obtain values of hydrodynamic radii and volumes using Chen's modification[44] of the Stokes-Einstein equation (3.1):

$$D_t = \frac{kT}{c\pi\eta r_H}$$

$$c = \frac{6}{1 + 0.695\left(\frac{r_{\text{solv}}}{r_{\text{H}}}\right)^{2.234}} \qquad (\mathbf{3.1})$$

$c = 6$ is the Stokes-Einstein equation.

The measurements were carried out in C_6D_5Cl (an atypical solvent for diffusion studies), due to low solubility of **2-E2** in nonpolar solvents, reactivity with halogenated alkane solvents such as CD_2Cl_2, and interaction of the borane groups with strong donor solvents such as CD_3CN. The value for r_{solv} (2.69 x 10^{-10} m)[45] in equation 3.1 is that of C_6H_5Cl, a reasonably good approximation. The viscosity, η (0.008 Pa s^{-1})[46] is that of C_6D_5Cl. The classical Stokes-Einstein equation has c = 6, whereas the Chen modification corrects for molecules that are not much larger than the solvent they are in. As expected for a moderately sized organometallic molecule, the experimental values of c were not 6, but varied from roughly 5.75-5.85. The molecules were assumed to be roughly spherical, and no further corrections were applied.

The PGSE NMR experiments were carried out in two phases, one with unknown aggregation, the other assumed to be strictly monomeric, and the size of the species compared. First, an NMR tube was charged with a C_6D_5Cl solution of **2-E$_2$** and $(PPh_3)_2Re(CO)_3Br$ (**6**) (internal standard of similar size and shape). The **2-E$_2$** solution was prepared either A) *in situ* (by treating [**1-E$_2$**][BF_4] with 1 equiv $NaHBEt_3$), or B) by dissolution of crudely isolated **2-E$_2$** (by precipitation of a C_6H_5Cl solution as prepared *in situ*, collection on a frit, and drying under vacuum). ^1H and $^{31}P\{^1H\}$ NMR experiments confirmed that **2-E$_2$** and **6** were the major species. A ^1H PGSE NMR experiment was carried out on this mixture, under which conditions the speciation of **2-E$_2$** was in question. After the first PGSE experiment was complete, the tube was returned to a nitrogen-filled glovebox, and an excess of pyridine (3-12 equiv) was added by syringe, and the tube sealed. ^1H and $^{31}P\{^1H\}$ NMR experiments confirmed that **2-E$_2$** had been converted to the bis(pyridine) adduct **2-E$_2$•**(pyridine)$_2$, which has a significantly downfield-shifted formyl resonance, and a single ^{31}P resonance. There was no change in chemical shift or lineshape of **6** upon addition of pyridine, confirming that no interaction occurs with the internal standard. The excess pyridine appeared close to the expected shift of free pyridine in C_6D_5Cl,[47] indicating any exchange of bound and free pyridine must be slow on the NMR time-scale. A second ^1H PGSE NMR experiment was then carried out, and in these conditions the Re formyl was assumed to be strictly monomeric.

The data was processed as described above, providing D_t values for all species in the presence and absence of pyridine. The number of units in an aggregate, N, can be calculated by comparing the ratio of the hydrodynamic volumes of **2-E$_2$•**(pyridine)$_2$:**6** (N =

1) and **2-E$_2$**:**6** (N unknown). Hydrodynamic volumes were calculated using equation 3.1. The ratio of hydrodynamic volumes of **2-E$_2$**:**6** was *1.5(1) times larger* than the ratio of hydrodynamic volumes of **2-E$_2$**•(pyridine)$_2$:**6**. For a monomeric species N = 1, while for a dimeric species (as observed by XRD) N = 2. The data in this case are intermediate between 1 and 2 units, reflecting significant intermolecular aggregation in solution; a simple monomeric system would have N very close to 1, and probably *less than* 1, due to the increased size of a bis(pyridine) adduct. The intermediate value of N, and the broad signals of **2-E$_2$** observed in ^{1}H NMR spectra at room temperature, are consistent with a *fluxional monomer-dimer equilibrium*, occurring rapidly on the NMR time-scale. The D_t value of a rapidly equilibrating mixture is reflective of the equilibrium distribution, as a time-weighted average of the equilibrating species.[26] Variable-temperature NMR experiments showed a subtle sharpening of the ^{1}H and ^{31}P resonances of **2-E$_2$** at low temperatures, but warming the solution led to decomposition, confounding complete analysis.

The uncertainty in the hydrodynamic volumes obtained from PGSE NMR experiments is significant; therefore no quantitative analysis was undertaken. The qualitative results are quite certain, however: the intermediate values for the speciation of **2-E$_2$** are reproducible under two different conditions (two runs of each experiment A and B) and are *inconsistent* with a strictly *monomeric solution structure* (in which case **2-E$_2$**•(pyridine)$_2$:**6** would be expected to be slightly *larger* than **2-E$_2$**:**6**). Furthermore, the observed *reactivity* of **2-E$_2$** is also consistent with a monomer-dimer equilibrium.

Reaction of 2-E_2 with pyridine. As part of a diffusion NMR experiment, 26.0 mg (0.0247 mmol) [**1**][BF_4] was treated with 24.7 μL (0.0247 mmol) $NaHBEt_3$ (1.0 M in toluene) by syringe in ~0.6 mL C_6D_5Cl to form carbene **2**. 21.6 mg (0.0247 mmol) $(PPh_3)_2Re(CO)_3Br$ was added as an internal standard, and an NMR was taken. Roughly 45 minutes later, 6.0 μL (0.0741 mmol, 3 equiv) pyridine was added by syringe, and the reaction was monitored by NMR. High initial conversion to one formyl product was observed, followed by slow decomposition to Re–H species over a few days. **^{1}H NMR** (C_6D_5Cl, 500 MHz): δ 0.48 (br m, 4H), 0.96 (br, 4H), 1.33 (6H), 1.57 (2H), 1.67 (4H), 1.8-2.0 (br m, 18H), 6.92 (pyridine), 7.20 (pyridine), 7.44 (m, 8H), 8.09 (pyridine), 15.21 (s, 1H, Re–C*H*O). **^{31}P{^{1}H} NMR** (C_6D_5Cl, 202 MHz): δ 11.8 (s).

Thermolysis of 2-E_2. A vial was charged with 53.2 mg (0.051 mmol) cation [**1-E_2**][BF_4] and 0.5 mL C_6D_5Cl. 50.5 μL $NaHBEt_3$ (1.0 M in toluene) was added dropwise to afford carbene **2-E_2** as a pale yellow solution. The solution was transferred to a J-Young NMR tube and the carbene was formed quantitatively as assessed by NMR spectroscopy. The tube was submerged in a 90 °C oil bath for 30 minutes, after which time ^{1}H and ^{31}P{^{1}H} NMR showed ~80% conversion to a new species as a mixture with ~10% each [**1-E_2**]$^+$ and C–C coupled product [**3**]$^-$. The tube was brought into a glovebox, filtered, and the solvents removed under vacuum. The solids were extracted with benzene, filtered, and the solvents were removed, yielding 41 mg (0.042 mmol, 84%) ligand-activated product **7**, in ~90% purity. The product could be fully characterized by multinuclear NMR studies, but the undesired product was not further purified. **^{1}H NMR** (C_6D_6, 500 MHz): δ 1.01-1.09

(m, 3H), 1.4-1.6 (m, 12H), 1.6-1.8 (m, 12H), 1.9-2.1 (m, 12H), 2.4-2.6 (m, 3H), 2.94 (m, 1H), 3.09 (m, 1H), 5.85 (br m, 1H), 6.9-7.1 (m, 12H), 7.75 (dt, $\mathcal{J}$ = 9.1, 17.9 Hz, 6H), 7.88 (t, $\mathcal{J}$ = 7.9 Hz, 2H). **^{31}P{^{1}H} NMR** (C_6D_6, 202 MHz): δ 12.6 (d, $^{2}\mathcal{J}_{PP}$ = 124.8 Hz, 1P), 39.9 (d, $^{2}\mathcal{J}_{PP}$ = 124.8 Hz, 1P). **^{13}C{^{1}H} NMR** (C_6D_6, 125 MHz): δ 22.2 (br, $Ph_2PCH_2\mathit{C}H_2B(C_8H_{14})$), 23.78, 24.33, 24.8 (br), 27.61 (d, $^{1}\mathcal{J}_{PC}$ = 27.2 Hz, $Ph_2P\mathit{C}H_2CH_2B(C_8H_{14})$), 31.38 (d, $^{1}\mathcal{J}_{PC}$ = 31.3 Hz, $Ph_2P\mathit{C}H_2CH_2CH(OBR_2)Re$), 31.93, 33.78, 33.84, 34.41, 34.64, 45.87 (dd, $\mathcal{J}_{PC}$ = 14.4, 5.3 Hz, $Ph_2PCH_2\mathit{C}H_2CH(OBR_2)Re$), 76.66 (dd, $\mathcal{J}_{PC}$ = 7.0, 2.2 Hz, $Ph_2PCH_2CH_2\mathit{C}H(OBR_2)Re$), 128.81 (d, $^{3}\mathcal{J}_{PC}$ = 9.3 Hz, *m*-Ph), 128.90 (d, $^{3}\mathcal{J}_{PC}$ = 9.3 Hz, *m*-Ph), 129.08 (d, $^{3}\mathcal{J}_{PC}$ = 9.7 Hz, *m*-Ph), 129.12 (d, $^{3}\mathcal{J}_{PC}$ = 9.5 Hz, *m*-Ph), 129.93 (d, $^{4}\mathcal{J}_{PC}$ = 1.8 Hz, *p*-Ph), 130.17 (d, $^{4}\mathcal{J}_{PC}$ = 1.9 Hz, *p*-Ph), 130.25 (d, $^{4}\mathcal{J}_{PC}$ = 1.9 Hz, *p*-Ph), 130.32 (d, $^{4}\mathcal{J}_{PC}$ = 2 Hz, *p*-Ph), 132.07 (d, $^{2}\mathcal{J}_{PC}$ = 10.5 Hz, *o*-Ph), 132.67 (d, $^{2}\mathcal{J}_{PC}$ = 11.0 Hz, *o*-Ph), 132.68 (d, $^{2}\mathcal{J}_{PC}$ = 10.2 Hz, *o*-Ph), 133.99 (d, $^{2}\mathcal{J}_{PC}$ = 9.9 Hz, *o*-Ph), 137.37 (d, $^{1}\mathcal{J}_{PC}$ = 43.6 Hz, *ipso*-Ph), 137.71 (d, $^{1}\mathcal{J}_{PC}$ = 45.7 Hz, *ipso*-Ph), 137.90 (d, $^{1}\mathcal{J}_{PC}$ = 44.5 Hz, *ipso*-Ph), 139.54 (d, $^{1}\mathcal{J}_{PC}$ = 42.2 Hz, *ipso*-Ph), 195.17 (t, $^{2}\mathcal{J}_{PC}$ = 9.3 Hz, Re–*C*O), 198.65 (t, $^{2}\mathcal{J}_{PC}$ = 5.7 Hz, Re–*C*O), 199.12 (t, $^{2}\mathcal{J}_{PC}$ = 9.4 Hz, Re–*C*O). **^{11}B{^{1}H} NMR** (C_6D_6, 160 MHz): δ 54.9, 88.0. Assignments were made using ^{1}H–^{31}P gHMBC, ^{1}H–^{13}C gHMQC, ^{1}H–^{13}C gHMBC, and ^{1}H–^{1}H gCOSY 2-D NMR experiments.

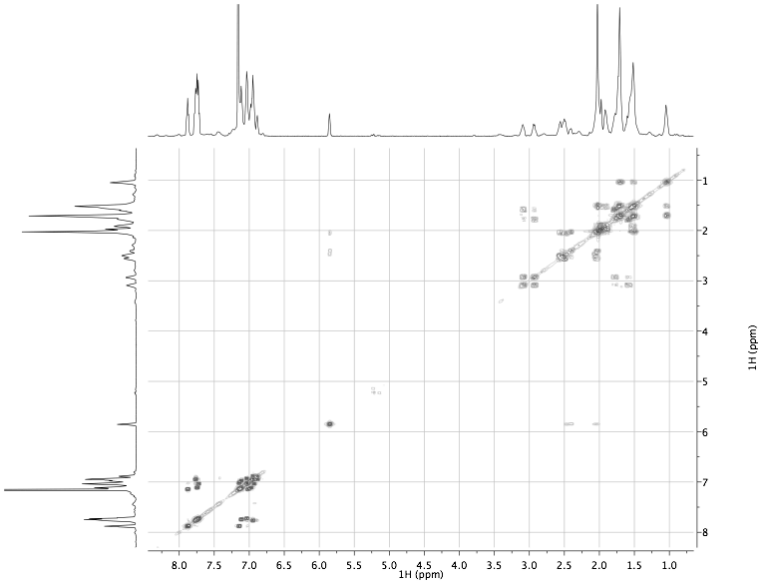

Figure 3.22. $^{1}H–^{1}H$ gCOSY of **7**.

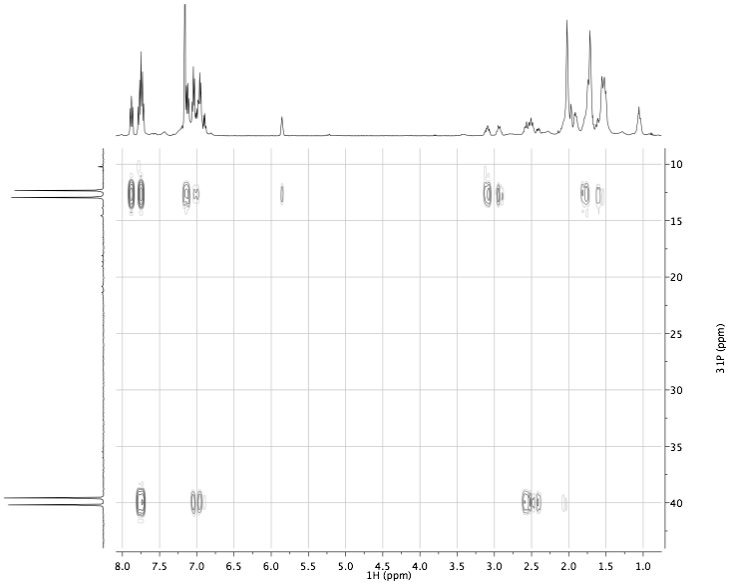

Figure 3.23. $^{1}H–^{31}P$ gHMBC of **7**.

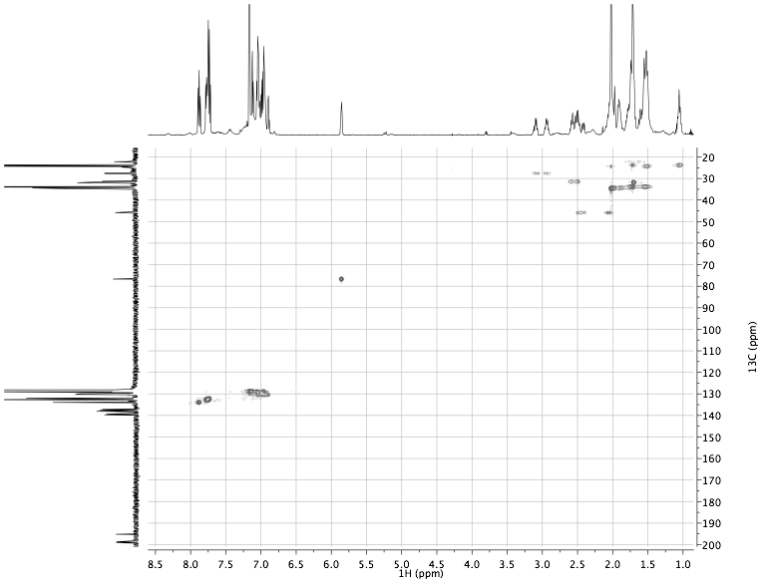

Figure 3.24. $^{1}H–^{13}C$ gHMQC of **7**.

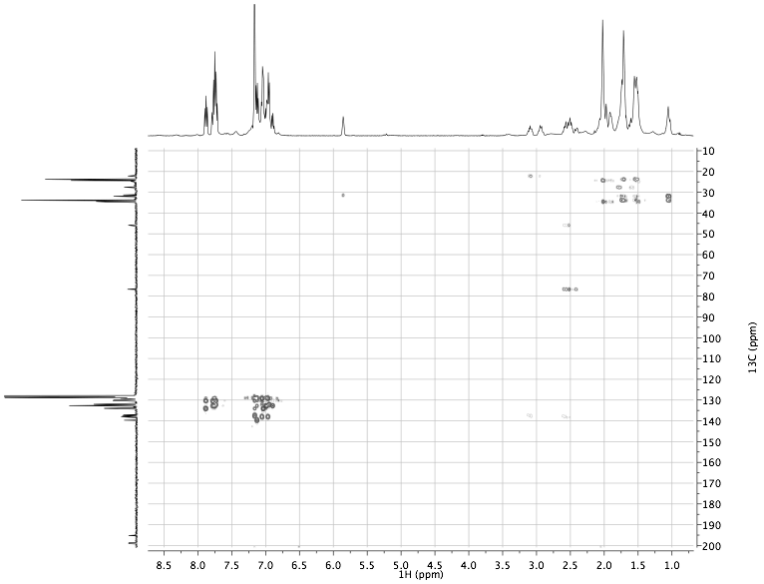

Figure 3.25. $^{1}H–^{13}C$ gHMBC of **7**.

Reaction of 2-E_2 with H_2O. Carbene **2-E_2** was prepared in the usual manner by dropwise addition of 21.8 μL (0.0218 mmol) $NaHBEt_3$ (1.0 M in toluene) to a rapidly stirring C_6D_5Cl solution of 23.0 mg (0.0218 mmol) cation [**1-E_2**]$^+$. ^{1}H and $^{31}P\{^{1}H\}$ NMR studies showed clean formation of the carbene. 30 minutes after preparation, 0.4 μL

(0.0218 mmol) degassed deionized H_2O was added by syringe. After addition, the solution immediately began bubbling, the yellow color of the carbene bleached, and some precipitates formed. A $^{31}P\{^1H\}$ NMR experiment showed one prominent singlet at δ 1.4, in a similar location as the cation [**1-E$_2$**]$^+$ (δ 0.3), along with minor impurities. The ^1H NMR spectrum showed complete consumption of the carbene resonance at δ 13.96, and a conspicuous resonance for H_2 gas at δ 4.49. The rest of the spectrum was rather broad and non-descript, but matched the spectrum of crystals obtained from a separate reaction of carbene **2-E$_2$** with wet CO.

Reaction of 2-E$_2$ with [Me$_3$NH][BPh$_4$]. Carbene **2-E$_2$** was prepared in the usual manner by dropwise addition of 21.2 μL (0.0212 mmol) $NaHBEt_3$ (1.0 M in toluene) to a rapidly stirring C_6D_5Cl solution of 22.3 mg (0.0212 mmol) [**1-E$_2$**][BF_4]. After stirring for 3 minutes, the mixture was added to a J-Young NMR tube already charged with 8.0 mg (0.0212 mmol) [Me_3NH][BPh_4]. Although the acid is not very soluble, and some solids remained at the bottom of the tube, the yellow color of the carbene disappeared and bubbles were observed. The single $^{31}P\{^1H\}$ NMR signal at δ 0.5 (s) and ^1H NMR pattern is indicative of a symmetric cationic bisphosphine tetracarbonyl species. Although a small amount of carbene remained after 30 minutes, no remaining carbene was detected 24 hours later. Hydrogen was observed in the ^1H NMR spectrum.

Reaction of 2-E$_2$ with [^{t}Bu$_3$PH][HB(C$_6$F$_5$)$_4$]. Boroxycarbene **2-E$_2$** was prepared in the usual manner by dropwise addition of 17.3 μL (0.0173 mmol) $NaHBEt_3$ (1.0 M in toluene) to a rapidly stirring C_6D_5Cl solution of 18.2 mg (0.0173 mmol) [**1-E$_2$**][BF_4]. After

stirring for 3 minutes, the mixture was added to a J-Young NMR tube already charged with 12.4 mg (0.0173 mmol) [^{t}Bu$_3$PH][HB(C$_6$F$_5$)$_4$]. The tube was sealed and shaken, and bubbles immediately started forming, along with a bleach of the yellow color of the carbene. A ^{1}H NMR experiment showed a peak for H_2 gas at δ 4.49, and aryl and Ph$_2$PC*H$_2$*C*H$_2$*B(C$_8$H$_{14}$) resonances at similar – but slightly different—chemical shifts from [**1-E$_2$**][BF$_4$]. A very broad peak near δ 4 is consistent with a BH functionality, and the presence of [HB(C$_6$F$_5$)$_3$] was further confirmed by ^{19}F NMR, δ –133.0, –164.3, –167.0. A ^{31}P{^{1}H} NMR experiment showed two singlets: free P^{t}Bu$_3$ at δ 62.1 and a rhenium species at δ 0.3, in the same location as [**1-E$_2$**][BF$_4$]. Thus we assign the product as closely related to cation **1**, [(Ph$_2$P(CH$_2$)$_2$B(C$_8$H$_{14}$))$_2$Re(CO)$_4$][HB(C$_6$F$_5$)$_4$]. Heating at 50 °C for one week resulted in no discernable reaction. Elevated temperatures (135 °C) led to decomposition of the ligands, including the presence of cyclooctene.

NMR-scale reaction of [Na][3-E$_2$] with [Pt][BAr$^F{}_4$]$_2$. To a ~0.6 mL THF-*d$_8$* solution of 21.0 mg (0.0199 mmol) [**1-E$_2$**][BF$_4$] was added 39.9 μL (0.0399 mmol, 2 equiv) NaHBEt$_3$ (1.0 M in toluene) dropwise with stirring. The mixture was filtered into a J-Young NMR tube, and NMR spectroscopy showed clean formation of [**3-E$_2$**]$^-$. The tube was returned to the glovebox, and the contents poured onto 88.6 mg (0.0199 mmol) [**Pt**][BAr$^F{}_4$]$_2$, which was dissolved and the reaction mixture returned to the tube. NMR spectroscopic monitoring revealed no detectable reaction of [**3-E$_2$**]$^-$ or formation of [**HPt**]$^+$ over 24 hours.

Reaction of [Na][3-E_2] with MeOTf. To a 5 mL toluene suspension of 35.8 mg (0.0341 mmol) [Na][**3-E_2**] was added 3.9 μL (0.0341 mmol) MeOTf by syringe, with stirring. The reaction mixture was stirred 30 minutes, filtered, washing with 0.5 mL toluene and 1 mL pentane, affording clear yellow filtrate (white solids left on filter). The solvents were removed under vacuum, giving 27 mg (80%) yield of yellow product. **^{1}H NMR** (THF-d_8, 300 MHz) showed a characteristic pair of doublets at 3.97 (d, $\mathcal{J}_{HH}$ = 18.8 Hz) and 4.61 (d, $\mathcal{J}_{HH}$ = 18.8 Hz), along with a singlet at 3.18 (3H) for the new methyl group. Integration of the crowded alkyl and aryl regions was not satisfactory, however. **^{31}P NMR** (THF-d_8, 300 MHz) showed only one product, 5.5 (d, $\mathcal{J}_{PP}$ = 110.2 Hz) and 14.1 (d, $\mathcal{J}_{PP}$ = 109.7 Hz). Crystallographic characterization, which would determine which oxygen was methylated, has been thus far elusive, and the material was not further purified or characterized.

Mechanistic Studies on the Reduction of [1-E_2]$^+$

Reaction of [1-E_2][BF_4] with [HPt][PF_6] at −40 °C. A J-Young NMR tube was charged with a ~0.2 mL C_6D_5Cl solution of 22.4 mg (0.0213 mmol) [**1-E_2**][BF_4]. The solution was frozen in a liquid nitrogen cooled cold well in the glovebox. A ~0.1 mL layer of C_6D_5Cl was added, and the tube was cooled to freeze the solvents again. Finally, a layer of ~0.3 mL C_6D_5Cl solution of 13.6 mg (0.0213 mmol) [**HPt**][PF_6] was added, and the solution frozen. The tube was sealed, removed from the glovebox, and inserted into a dry ice / acetone bath to keep the contents of the tube frozen. Meanwhile, the NMR probe was cooled to –40 °C. The tube was allowed to just start to thaw, at which point it was shaken vigorously for a few seconds, and then inserted into the –40 °C probe. NMR spectra were

obtained at various times and temperatures, with the temperature slowly being raised to 0 °C, at which point the reaction was complete. In separate experiments a broad ^{31}P signal at –5.9, slightly downfield of [**HPt**][PF_6] (δ –7.2) was always observed (sometimes an additional sharp peak for [**HPt**][PF_6] was observed), appearing to be an intermediate of hydride transfer from Pt to [**1-E$_2$**]$^+$. A set of two doublets at δ 1.15 ($\mathcal{J}_{PP}$ = 71 Hz) and δ 4.5 ($\mathcal{J}_{PP}$ = 75 Hz) were also observed, which disappeared at roughly the same rate as the broad hydride signal.

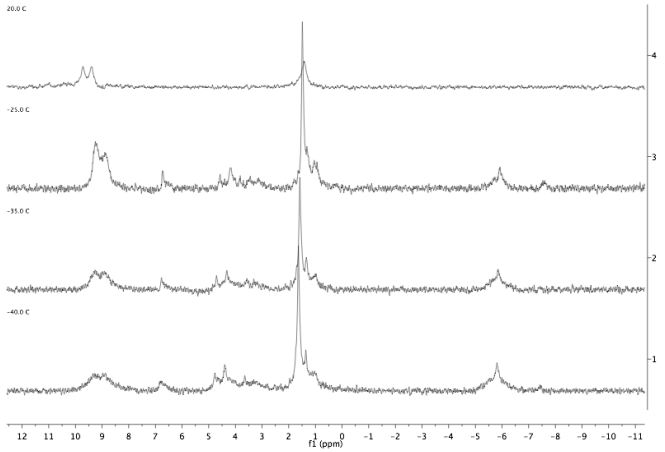

Figure 3.26. $^{31}P\{^1H\}$ NMR of reaction of [**1-E$_2$**]$^+$ with [**HPt**]$^+$ while warming.

Reaction of [1-E$_2$][BF$_4$] with 2 equiv NaHBEt$_3$ in C$_6$D$_5$Cl at − 40 °C. Boroxycarbene **2-E$_2$** was formed by dropwise addition of 28.4 μL (0.0284 mmol) $NaHBEt_3$ (1.0 M in toluene) to a rapidly stirring ~0.6 mL C_6D_5Cl solution of 29.9 mg (0.0284 mmol) [**1-E**$_2$][BF_4]. ^1H and ^{31}P NMR spectroscopy after formation of **2-E**$_2$ showed essentially quantitative conversion to the desired boroxycarbene. The NMR tube (J-Young) was returned to the glovebox, and placed in a liquid nitrogen cooled well to freeze the contents. A small amount (~100 μL) of C_6D_5Cl was layered on top, and the contents were frozen

again. Finally, 28.4 μL (0.0284 mmol) $NaHBEt_3$ (1.0 M in toluene) was added to the tube, and the contents were frozen. The tube was sealed and removed from the box, and inserted into a dry ice / acetone bath to keep the contents frozen. Meanwhile, the NMR spectrometer probe was cooled to – 40 °C. The tube was removed from the cold bath and allowed to just start to thaw, at which point the tube was shaken vigorously, and re-frozen. The tube was then inserted into the pre-cooled (– 40 °C) probe while still frozen, and was allowed to thaw in the probe. Upon thawing, a single Re-containing species was observed by multinuclear NMR experiments, characterized spectroscopically as the anionic bis-boroxycarbene species [**9**]$^-$. The species was quite stable at – 40 °C, but as the probe was warmed to 0 °C the intensity of the signals of [**9**]$^-$ steadily decreased until no Re-containing products were present in solution. Ejecting the NMR tube showed large amounts of pale yellow precipitates; extraction with THF-d_8 proved these solids to be the ultimate double-reduction product [**3-E$_2$**]$^-$. Spectroscopic characterization of [**9**]$^-$: **^{1}H NMR** (C_6D_5Cl, 500 MHz, – 40 °C, all peaks were broad): δ –0.15 (4H), 0.39 (4H), 0.66 (2H), 1.42 (2H), 1.57 (4H), 1.73 (16H), 1.98 (2H), 2.34 (2H), 2.64 (4H), 3.07 (4H), 7.58 (10H), 7.62 (10H), 16.43 (2H). **^{31}P{^{1}H} NMR** (C_6D_5Cl, 202 MHz, – 40 °C): δ 10.0 (s). **^{13}C{^{1}H} NMR** (C_6D_5Cl, 126 MHz, – 40 °C): δ 13.35 (br), 25.57, 26.02, 28.02 (br), 30.29, 38.23, 39.71, 130.79, 132.11, 142.82 (br m; other aromatic peaks are obscured by toluene and C_6D_5Cl peaks), 198.31 (m, Re–*C*O), 291.57 (Re–*C*HO).

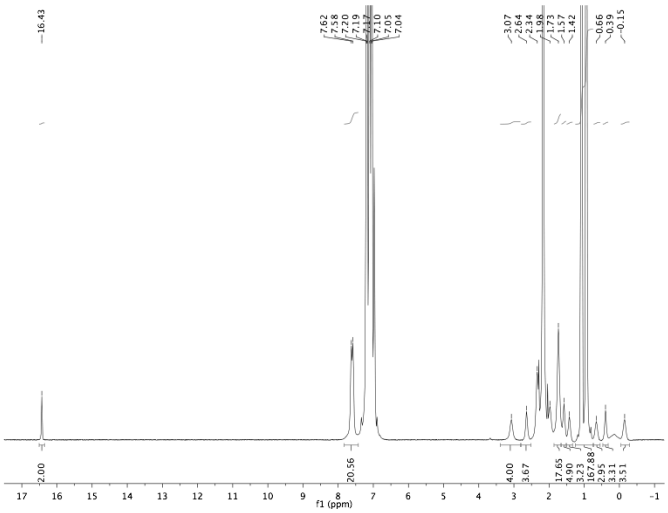

Figure 3.27. ^{1}H NMR of [**9**]$^{-}$.

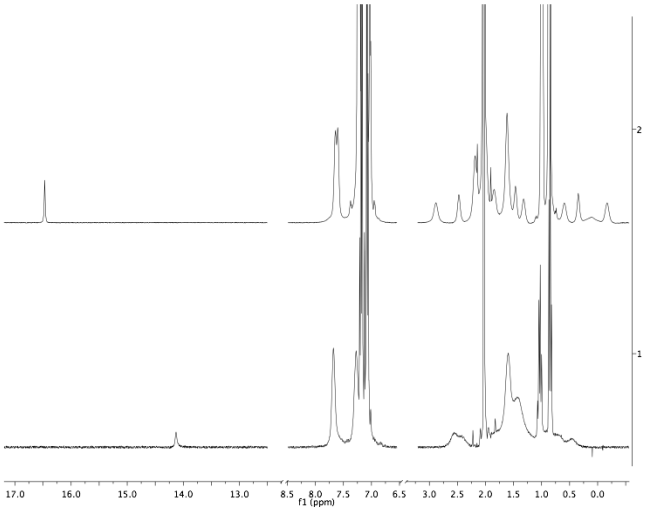

Figure 3.28. ^{1}H NMR overlay of **2-E$_2$** (bottom) and [**9**]$^{-}$ (top).

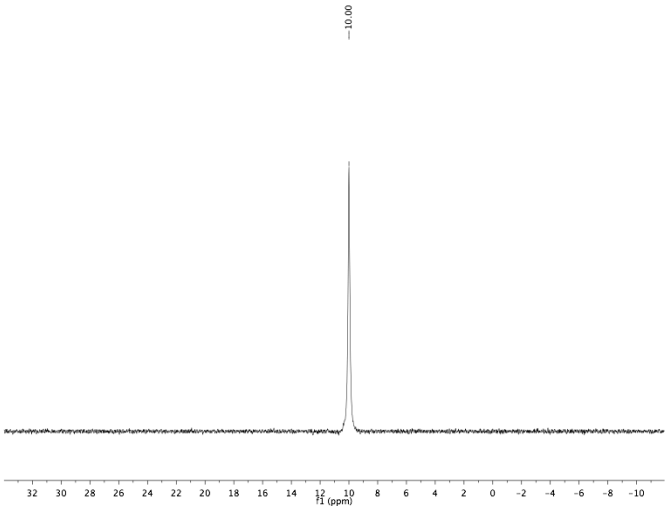

Figure 3.29. $^{31}P\{^{1}H\}$ NMR of [**9**]$^{-}$.

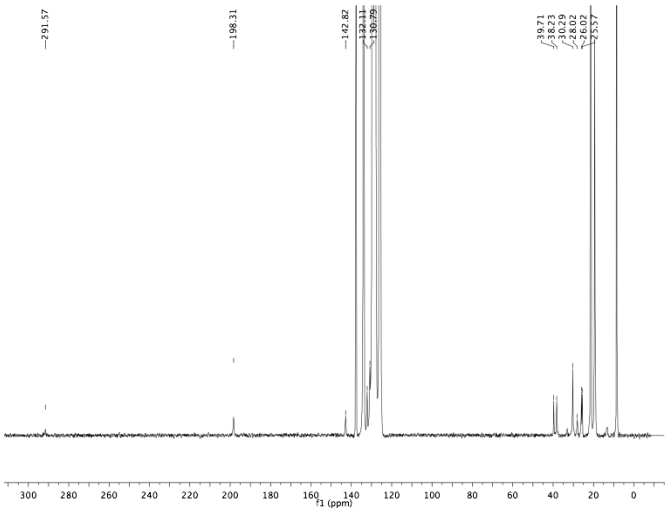

Figure 3.30. $^{13}C\{^{1}H\}$ NMR of [**9**]$^{-}$.

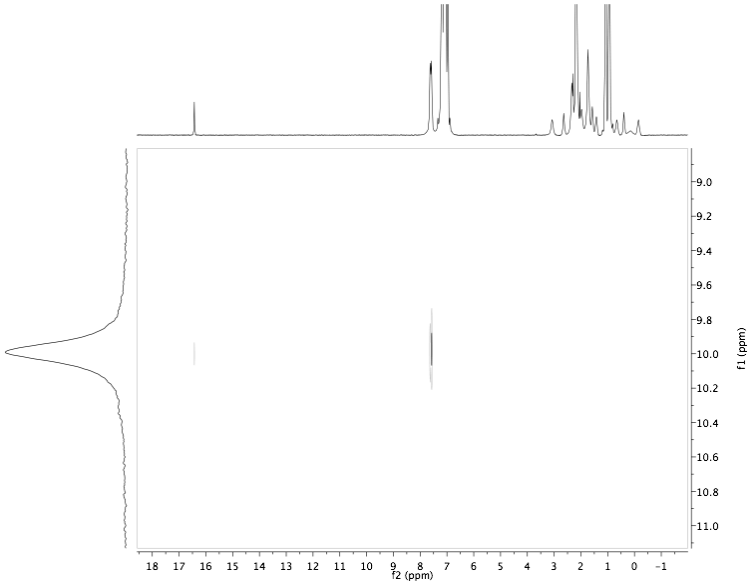

Figure 3.31. $^{1}H–^{31}P$ gHMBC of [**9**]$^{-}$.

Reaction of [HPt(dmpe)$_2$][PF$_6$] with BEt$_3$. A J-Young NMR tube was charged with 23.5 mg (0.0366 mol) [**HPt**][PF$_6$] and ~0.6 mL C_6D_5Cl. 36.6 μL (0.0366 mmol) BEt_3 (1.0 M in hexanes) was added by syringe, which prompted some precipitation. The tube was removed from the box and variable temperature NMR experiments were undertaken, showing dynamic fluxional spectra that changed with temperature. At room temperature only a broad signal for [**HPt**]$^{+}$ was observed in the ^{1}H NMR spectrum at –11.7. Upon cooling to –40 °C that signal sharpened into a pentet and an additional broad doublet at –3.23 ($\mathcal{J}_{PH}$ = 165 Hz, $\mathcal{J}_{PtH}$ = 952 Hz) was observed. The latter signal is consistent with a bridging Pt–H–B species. Similar results were obtained when $Ph_2PCH_2CH_2B(C_8H_{14})$ was used in place of BEt_3. The $^{31}P\{^{1}H\}$ NMR showed broad signals at –7.3 and –2.4. Cooling to –40 °C led to sharpening of the signals: –7.3 ($\mathcal{J}_{PtP}$ = 2230 Hz) and –1.6 (slightly broadened, no Pt coupling observed).

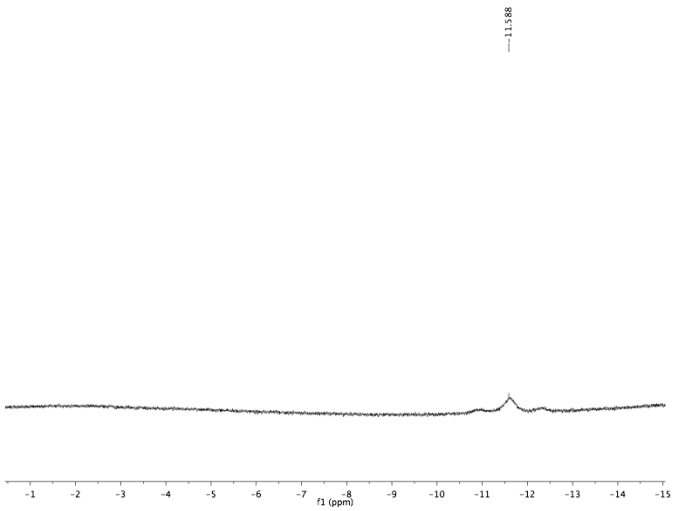

Figure 3.32. ^{1}H NMR (20 °C), hydride region, after mixing [**HPt**]$^{+}$ and BEt_3.

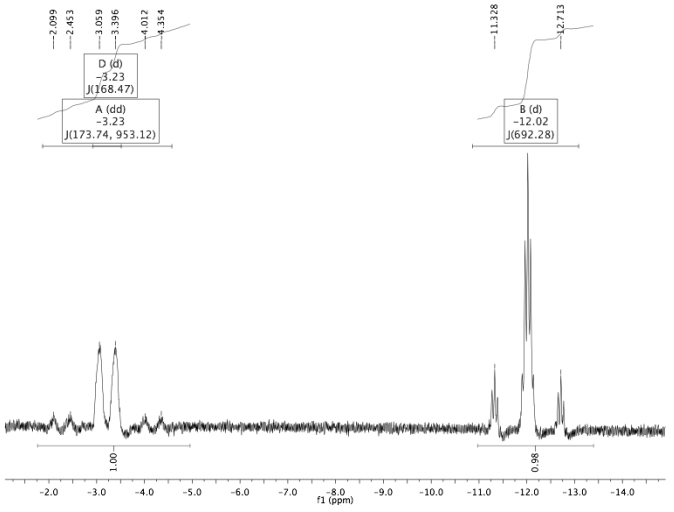

Figure 3.33. ^{1}H NMR (–40 °C), hydride region, after mixing [**HPt**]$^{+}$ and BEt_3.

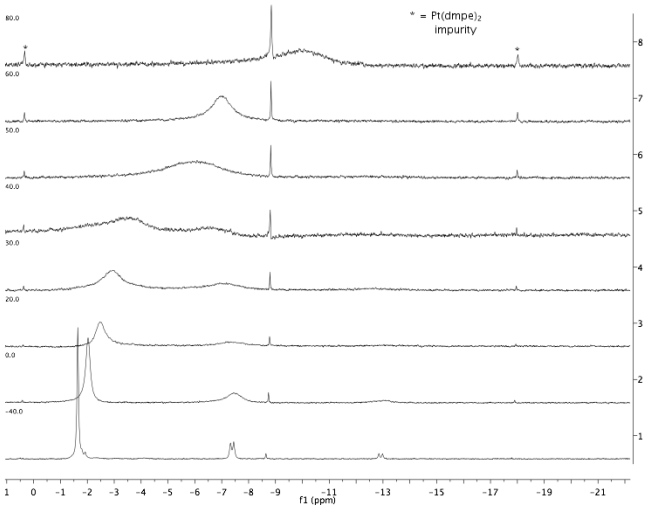

Figure 3.34. $^{31}P\{^{1}H\}$ NMR of [**HPt**]$^{+}$/BEt_3 from –40 to 80 °C.

Reaction of [HPt][BAr$^{F}_{4}$] with BEt_3. A J-Young NMR tube was charged with 21.5 mg (0.0158 mmol) [**HPt**][BAr^{F}_{4}] and ~0.6 mL C_6D_5Cl. 15.8 μL (0.0158 mmol) BEt_3 (1.0 M in hexanes) was added by syringe, and the tube was sealed. No precipitation was observed upon addition of the borane. NMR spectroscopy revealed no detectable change in line shape or chemical shift of the hydride.

Reaction of [Li][$Et_3BHBHEt_3$] + [Pt]$^{2+}$. A small vial was charged with ~0.6 mL THF-d_8, 25.5 μL (0.0255 mmol) BEt_3 (1.0 M in hexanes), and 25.5 μL (0.0255 mmol) $LiHBEt_3$ (1.0 M in THF-d_8). The mixture was added to solid [**Pt**][PF_6]$_2$, and the reaction mixture transferred to a J-Young tube. NMR spectroscopy showed that $Pt^0(dmpe)_2$ was the major product (consistent with observed bubbling, presumably of H_2), with the other P-containing product being a singlet at δ –0.7 with no Pt satellites. The ^{1}H NMR was mostly obscured by hexanes and THF, but the diagnostic broad doublet (–3.58, d, $\mathcal{J}_{PH}$ = 170 Hz)

was observed in the reaction of [**HPt**]$^+$ with boranes was observed, consistent with the bridging borohydride perhaps playing a role in the reaction.

Reduction of trans-[(Ph$_2$P(CH$_2$)$_2$B(C$_8$H$_{14}$))$_2$Mn(CO)$_4$][BF$_4$] ([1-E$_2$-Mn][BF$_4$])

Reaction of [1-E$_2$-Mn][BF$_4$] with 1 equiv NaHBEt$_3$. To a rapidly stirring solution of 32 mg (0.034 mmol) [**1-E$_2$-Mn**][BF$_4$] in ~0.6 mL C_6D_5Cl was added 34 μL (0.034 mmol) NaHBEt$_3$ (1.0 M in toluene). The solution darkened slightly, and the mixture was transferred to an NMR tube. Spectroscopic analysis revealed conversion to a putative boroxycarbene species (^{1}H NMR δ 13.81, ^{31}P{^{1}H} NMR δ 61.0.). This species was not further characterized. When the reaction was run in THF-*d*$_8$, only a mixture of starting material and doubly reduced species (see below) was observed, indicating fast disproportionation is operative.

Reaction of [1-E$_2$-Mn][BF$_4$] with 1 equiv [HPt(dmpe)$_2$]$^+$. To a stirring solution of 17.6 mg (0.0191 mmol) [**1-E$_2$-Mn**][BF$_4$] was added 12.2 mg [**HPt**][PF$_6$] partwise as a solid. The mixture was stirred for two minutes before being transferred to a J-Young NMR tube, at which time NMR spectroscopic analysis showed a mixture of the same boroxycarbene as in the preceding reaction, and cation starting material.

Reaction of [1-E$_2$-Mn][BF$_4$] with 2 equiv NaHBEt$_3$. To a rapidly stirring solution of 37 mg (0.040 mmol) [**1-E$_2$-Mn**][BF$_4$] in ~0.6 mL THF-*d*$_8$ was added 80 μL (0.080 mmol, 2 equiv) NaHBEt$_3$ (1.0 M in toluene). The color of the reaction mixture changed from pale yellow to orange over the course of the addition, and became cloudy. The mixture was filtered through a sintered glass filter into an NMR tube, and the resulting spectra revealed

one major asymmetric species. Some impurity, with small, broad resonances, was apparent. Attempts to isolate and purify the material were met with failure, as removal of solvents and redissolution in THF showed marked decomposition. The nature of this decomposition remains unknown. The general structure of the product, containing a C–C bond and *cis*-oriented phosphines, was deduced by multinuclear and multidimensional NMR techniques. **^{1}H NMR** (THF-d_8, 600 MHz): δ 0.25 (1H), 0.55 (dd, $\mathcal{J}$ = 13.8, 27.7 Hz), 1.1-2.0 (m, overlapping with THF-d_8), 2.64 (dd, $\mathcal{J}$ = 13.0, 24.7 Hz, 1H), 2.8 (m, 1H), 2.93 (t, $\mathcal{J}$ = 13.3 Hz, 1H), 4.32 (d, $\mathcal{J}_{HH}$ = 16.6 Hz, 1H), 4.82 (d, $\mathcal{J}_{HH}$ = 16.6 Hz, 1H), 7.34 (m, 2H), 7.40 (t, $\mathcal{J}$ = 7.1 Hz, 2H), 7.64 (t, $\mathcal{J}$ = 8.1 Hz, 2H), 7.68 (m, 2H), 8.11 (t, $\mathcal{J}$ = 8.4 Hz, 2H). **^{31}P{^{1}H} NMR** (THF-d_8, 121 MHz): δ 52.8 (d, $\mathcal{J}_{PP}$ = 27.0 Hz), 60.1 (d, $\mathcal{J}_{PP}$ = 26.8 Hz). **^{13}C{^{1}H} NMR** (THF-d_8, 151 MHz): δ 13.05 (br), 15.38 (br), 23.35, 26.74, 27.25 (br), 27.55, 31.48 (d, $\mathcal{J}_{PC}$ = 26.5 Hz), 31.87, 32.95, 33.61 (br), 33.92, 34.13 (d, $\mathcal{J}_{PC}$ = 14.2 Hz), 34.45 (br), 34.85, 34.98, 35.20, 92.85 (Mn=C(O–)*C*H$_2$O–), 127.77 (d, $\mathcal{J}_{PC}$ = 8.0 Hz), 127.94 (d, $\mathcal{J}_{PC}$ = 8.3 Hz), 128.13, 128.47 (d, $\mathcal{J}_{PC}$ = 8.0 Hz), 128.64, 129.63, 132.45 (d, $\mathcal{J}_{PC}$ = 7.4 Hz), 133.93 (d, $\mathcal{J}_{PC}$ = 8.2 Hz), 134.20 (d, $\mathcal{J}_{PC}$ = 8.7 Hz), 134.92 (d, $\mathcal{J}_{PC}$ = 10.5 Hz), 139.15 (d, $\mathcal{J}_{PC}$ = 25.9 Hz), 142.99 (d, $\mathcal{J}_{PC}$ = 37.0), 143.44 (d, $\mathcal{J}_{PC}$ = 20.0 Hz), 143.9 (d, $\mathcal{J}_{PC}$ = 38.3 Hz), 229.49 (dd, $\mathcal{J}_{PC}$ = 15.0, 17.8 Hz, CO), 231.11 (dd, $\mathcal{J}_{PC}$ = 23.6, 30.6 Hz, CO), 331.45 (m, Mn=*C*(O–)CH$_2$O–). **IR** (THF). 1935 (m), 1852 (s) cm^{-1}. A broad stretch at 1902 cm^{-1} appeared to be an impurity.

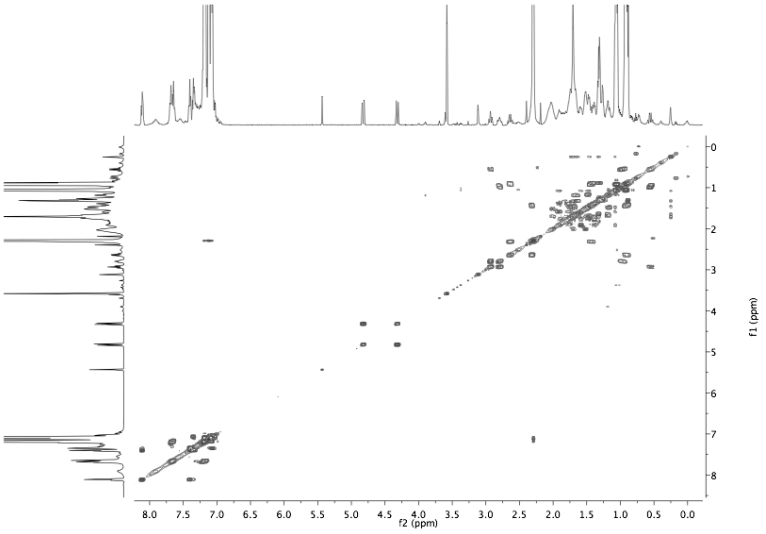

Figure 3.35. ^{1}H-^{1}H gCOSY of [**3-E$_2$-Mn**]$^{-}$.

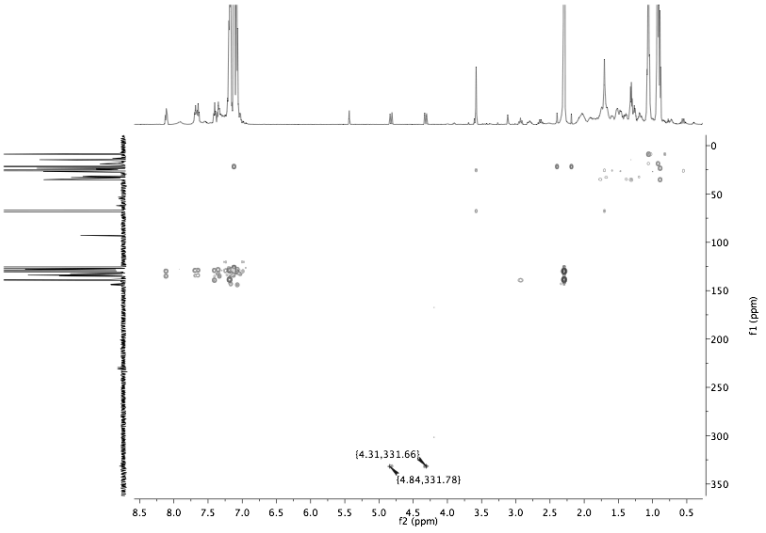

Figure 3.36. ^{1}H–^{13}C gHMBC of [**3-E$_2$-Mn**]$^{-}$.

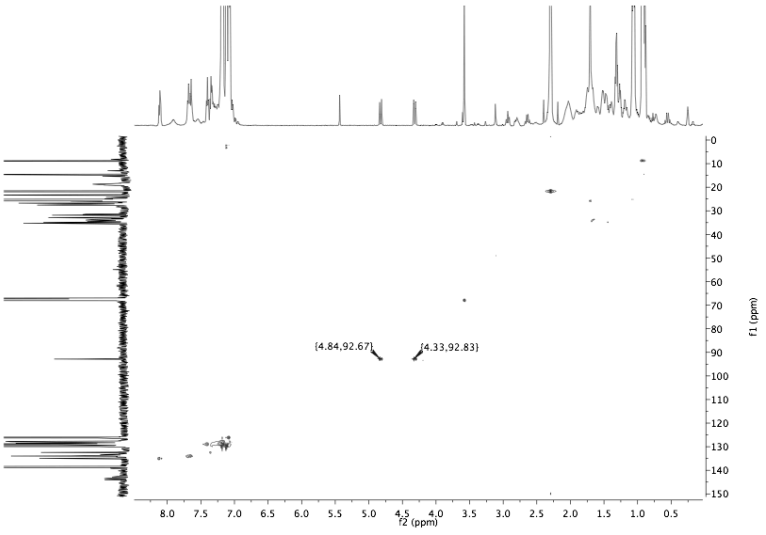

Figure 3.37. $^{1}H–^{13}C$ gHSQC of [**3-E$_2$-Mn**]$^-$.

Reaction of [1-E$_2$-Mn][BF$_4$] with 2 equiv [HPt][PF$_6$]. To a stirring ~0.6 mL THF-*d*$_8$ solution of 27.7 mg (0.030 mmol) was added 38.5 mg (0.060 mmol, 2 equiv) [**HPt**][PF$_6$] slowly as a solid. The solution darkened from yellow to orange with precipitation. After 30 minutes a mixture of C–C bond formed product [**3-E$_2$-Mn**]$^-$, starting cation, and unreacted [**HPt**]$^+$ were observed, closely resembling the spectra obtained using NaHBEt$_3$. Some minor variability in the chemical shifts is expected when changing the cation from Na^+ to [**Pt**]$^{2+}$ or [**HPt**]$^+$. Interestingly, the reaction did not proceed to completion overnight, possibly because monocationic [**HPt**]$^+$ was favored as the countercation over insoluble [**Pt**]$^{2+}$.

Reduction of trans-[(Ph$_2$P(CH$_2$)$_3$B(C$_8$H$_{14}$))$_2$Re(CO)$_4$][BF$_4$] ([1-P$_2$][BF$_4$])

Reaction of [1-P$_2$][BF$_4$] with 1 equiv NaHBEt$_3$. A scintillation vial was charged with 40.7 mg (0.0376 mmol) cation [**1-P$_2$**][BF$_4$] and 0.5 mL C_6D_5Cl. With rapid stirring, 37.6 μL (0.0376 mmol) NaHBEt$_3$ (1.0 M in toluene) was added dropwise. The colorless solution

turned yellow. The reduced species synthesized *in situ* in this manner was stable for ~ 24 hours, after which time a significant amount of white precipitates had formed. The formyl could be characterized by NMR spectroscopy in the presence of toluene and BEt_3 from the borohydride reagent. **^{1}H NMR** (C_6D_5Cl, 300 MHz): δ 1.36 (br, 12H), 1.7-2.1 (br m, 24H), 2.65 (br, 4H, $Ph_2PCH_2CH_2CH_2B(C_8H_{14})$), (7.0-7.2 m, toluene obscures $Ph_2PCH_2CH_2CH_2B(C_8H_{14})$ peak), 7.5 (m, 8H, $Ph_2PCH_2CH_2CH_2B(C_8H_{14})$), 14.09 (s, 1H, Re–C*H*O). **^{31}P{^{1}H} NMR** (C_6D_5Cl, 121 MHz): δ 6.7 (br). **^{13}C{^{1}H} NMR** (C_6D_5Cl, 125 MHz): 19.4 (br), 20.3, 24.7, 26.4, 28.7 (br), 32.9, 128.6 (t, $\mathcal{J}_{PC}$ = 4.6 Hz), 130.3, 132.0 (t, $\mathcal{J}_{PC}$ = 4.4 Hz), 136.4 (br m, *i-Ph*), 194.0 (m, Re–*C*O), 196.4 (m, Re–*C*O), 282.7 (v. br, Re–*C*HO).

The solids that precipitate over time are assigned as oligomeric isomers of the same compound. While these solids are insoluble in most common organic solvents, they do dissolve upon addition of pyridine, giving a formyl complex wherein the pendent boranes are bound by pyridine. This species was characterized by NMR, but decomposition (~80% Re–H after 18 hours) precluded isolation. **^{1}H NMR** (C_6D_5Cl, 300 MHz): δ 1.00 (br, 6H), 1.36 (br, 8H), 1.6-2.1 (br m, 22H), 2.47 (m, 4H), 7.47 (m, 8H), 8.12 (4H, BR_3-*py*), 15.00 (1H, Re–C*H*O). Some aryl peaks are obscured by toluene. **^{31}P{^{1}H} NMR** (C_6D_5Cl, 121 MHz): δ 6.2.

Reaction of [1-P$_2$][BF$_4$] with 2 equiv NaHBEt$_3$. A variety of hydride sources and conditions were screened, and after workup there were always at least two products. A representative preparation involved dissolving 120 mg (0.110 mmol) cation [**1-P$_2$**][BF_4] in 2

mL C_6H_5Cl with stirring, followed by dropwise addition of 110 μL (0.110 mmol, 1 equiv) $NaHBEt_3$ (1.0 M in toluene). The mixture was stirred briefly, then allowed to stand for 10 minutes. After filtration, to the yellow solution was added 38 mg (0.105 mmol, 0.95 equiv) dibenzo-18-crown-6, followed by another (0.110 mmol, 1 equiv) $NaHBEt_3$ (1.0 M in toluene), dropwise by syringe. The clear yellow solution was stirred for two hours, filtered again, and the solvents removed *in vacuo*. After washing with Et_2O, the solids were extracted in THF and the solvents removed *in vacuo*. The crude THF fraction included a number of products, including two doublets in the ^{1}H NMR at δ 4.63 ($\mathcal{J}_{HH}$ = 17.3 Hz) and 4.78 ($\mathcal{J}_{HH}$ = 16.8 Hz), similar to those observed in other C–C bond-formed products. Isolation of the desired product was unsuccessful, however.

NMR-scale Reaction of [1-P$_2$][BF$_4$] with 1 equiv [HPt][PF$_6$]. Under a nitrogen atmosphere, 28.5 mg (0.026 mmol) cation [**1-P$_2$**][BF_4] was dissolved in 0.5 mL C_6D_5Cl in a 10 mL scintillation vial with stirring. Solid [**HPt**]$^+$ (16.9 mg, 0.026 mmol) was added as a solid portionwise. After stirring for ten minutes, the cloudy solution was filtered through microporous glass into an NMR tube, and spectra acquired, showing relatively high conversion to carbene **2-P$_2$** (spectroscopic details above) in ~90% yield by ^{31}P integration.

Reaction of [1-P$_2$][BF$_4$] with 2 equiv [HPt][PF$_6$]. 19.3 mg (0.017 mmol) [**1-P$_2$**][BF_4], 22.9 mg (0.0357 mmol, 2 equiv) [**HPt**]$^+$, 4.5 mg (0.017 mmol) 18-crown-6, and 2.9 mg (0.017 mg) $NaPF_6$ were added to a small vial, and dissolved in C_6D_5Cl. The mixture was transferred to a J-Young NMR tube, and the reaction was monitored by ^{1}H and ^{31}P NMR. After initial formation of carbene **2-P$_2$**, no further reduction was observed over 3

days. The crown ether and $NaPF_6$ were added in an attempt to favor formation of soluble coupled products. In a separate experiment, only cation [**1-P$_2$**][BF_4] and 2 equiv [**HPt**]$^+$ were mixed, and the same results were observed.

Equilibrium Studies of Bis(phosphine) Complexes

Reaction of 2-E$_2$ with [Pt][PF$_6$]$_2$. To a stirring solution of 22.2 mg (0.021 mmol) [**1-E$_2$**][BF_4] in ~0.6 mL C_6D_5Cl was added 21 μL (0.021 mmol) $NaHBEt_3$ (1.0 M in toluene) dropwise by syringe. After stirring for a roughly one minute, the pale yellow solution was transferred to a J-Young NMR tube that had been charged with 16.5 mg (0.021 mmol) [Pt(dmpe)$_2$][PF_6]$_2$. The white Pt salt did not appear to dissolve. Monitoring by NMR showed no reaction over 24 hours.

Reaction of 2-M$_2$ with [1-E$_2$]$^+$. Boroxycarbene **2-M$_2$** was prepared by addition of solid [**HPt**][PF_6] (12.4 mg, 0.0194 mmol) to a stirring 0.6 mL C_6D_5Cl solution of 31.3 mg (0.0194 mmol) [**1-M$_2$**][$B(C_6F_5)_4$] and 8 mg (0.075 mmol, 3.75 equiv) $NaBF_4$. The mixture was transferred the a J-Young NMR tube, and monitored by multinuclear NMR spectroscopy. After 22 hours, all [**1-M$_2$**]$^+$ had been converted to **2-M$_2$** in good yield. Once the reaction had run to completion, the contents of the NMR tube were, under a N_2 atmosphere, filtered through sintered glass onto 20.4 mg (0.0194 mmol) solid [**1-E$_2$**][BF_4]. NMR spectroscopy showed only unreacted **2-M$_2$** and [**1-E$_2$**]$^+$ over 4 hours.

Reaction of 2-E$_2$ with [1-M$_2$]$^+$. Boroxycarbene **2-E$_2$** was prepared by dropwise addition of 21.8 μL (0.0218 mmol) $NaHBEt_3$ (1.0 M in toluene) to a stirring ~0.6 mL C_6D_5Cl solution of 23.0 mg (0.0218 mmol) [**1-E$_2$**][BF_4]. ^1H and ^{31}P NMR spectroscopy

showed clean conversion to **2-E$_2$**. The tube was returned to the glovebox, where it was poured onto 36.6 mg (0.0227 mmol, 1.04 equiv) [**1-M$_2$**]$^+$. Multinuclear NMR spectroscopy revealed complete hydride transfer had occurred, with no **2-E$_2$** remaining, and instead a mixture of **2-M$_2$**, unreacted [**1-M$_2$**]$^+$, and [**1-E$_2$**]$^+$. The observed hydride transfer is consistent with the preceding experiment in which the reverse reaction did not proceed to any appreciable extent.

Reaction of 2-E$_2$ with [1-P$_2$]$^+$. Boroxycarbene **2-E$_2$** was prepared by dropwise addition of 25.6 μL (0.0256 mmol) NaHBEt$_3$ (1.0 M in toluene) to a stirring ~0.6 mL C_6D_5Cl solution of 27.0 mg (0.0256 mmol) [**1-E$_2$**][BF_4]. After stirring for 5 minutes after hydride addition, the solution was added to solid [**1-P$_2$**][BF_4], and the mixture was transferred to a J-Young NMR tube. After 30 minutes, ^{1}H and ^{31}P{^{1}H} NMR spectroscopy revealed a mixture of all possible constituents, [**1-E$_2$**]$^+$, **2-E$_2$**, [**1-P$_2$**]$^+$, and **2-P$_2$**, in similar quantities. The ^{31}P NMR signals of **2-P$_2$** and [**1-E$_2$**]$^+$ were slightly broadened, and the Re–C*H*O signal of **2-P$_2$** in the ^{1}H NMR was significantly broadened, possibly signifying an intermolecular interaction between these species. The precise speciation is unknown, as probably fluxional, involving different species coordinating to the Re–CHO oxygen. Due to the broadness and uncertainty in ^{31}P NMR delay times, rigorous integration was not pursued; $K_{eq} \sim 1$ was obtained by ^{31}P NMR integration. The equilibrium mixture was stable for at least 4.5 hours.

Reaction of 2-P$_2$ with [1-E$_2$]$^+$. Boroxycarbene **2-P$_2$** was prepared by dropwise addition of 26.4 μL (0.0264 mmol) NaHBEt$_3$ (1.0 M in toluene) to a stirring ~0.6 mL C_6D_5Cl

solution of 28.5 mg (0.0264 mmol) [**1-P$_2$**][BF$_4$]. The solution was added to a J-Young NMR tube and multinuclear NMR spectroscopy showed clean conversion to **2-P$_2$**. The tube was returned to the glovebox, the contents poured onto 27.8 mg (0.0264 mmol) solid [**1-E$_2$**][BF$_4$], and the reaction mixture returned to the NMR tube. After 30 minutes, an equilibrium mixture of all the constituents was achieved ([**1-E$_2$**]$^+$, **2-E$_2$**, [**1-P$_2$**]$^+$, and **2-P$_2$**). The spectra were essentially the same as in the preceding reaction, with K_{eq} again roughly 1 (^{31}P NMR integration). The equilibrium mixture was stable for at least 3.5 hours.

Reaction of 2-E$_2$ with [1-Ph$_2$][BAr$^F_4$]. A vial was charged with 25.2 mg (0.0239 mmol) [**1-E$_2$**][BF$_4$] and ~0.6 mL C_6D_5Cl. With stirring, 15.3 mg (0.0239 mmol) [**HPt**][PF$_6$] was added as a solid, partwise. The colorless solution turned yellow with precipitation and was stirred for ~10 min, after which time the reaction mixture was added to 40.3 mg (0.0239 mmol) solid [**1-Ph$_2$**][BAr$^F_4$]. NMR spectroscopy revealed a mixture of all the possible constituents, in roughly equal parts, with a estimated $K_{eq} \sim 1$. As in the case of **2-P$_2$**, **2-Ph$_2$** showed shifted resonances in the ^{1}H NMR (Re–CHO) and ^{31}P NMR, with the ^{31}P NMR signal for [**1-E$_2$**]$^+$ being broadened, perhaps suggesting some interaction of **2-Ph$_2$** with one of the pendent boranes.

Reaction of 2-Ph$_2$ with [1-E$_2$][BF$_4$]. To a stirring solution of 41.4 mg (0.0246 mmol) [**1-Ph$_2$**][BAr$^F_4$] in C_6D_5Cl was added 24.6 μL (0.0246 mmol) NaHBEt$_3$ (1.0 M in toluene) dropwise. The mixture turned yellow and was stirred for 5 min, then added to 25.9 mg (0.0246 mmol) [**1-E$_2$**][BF$_4$]. The mixture was transferred to a J-Young tube and shaken well. NMR spectroscopy showed a mixture of both Re–CHO species and both cations, in

roughly equal amounts, giving a rough $K_{eq} \sim 1$. As in the preceding reaction, the resonances of **2-Ph$_2$** did not match previous syntheses exactly, suggesting some interaction with the pendent boranes of [**1-E$_2$**]$^+$.

Reaction of 2-E$_2$ with 2-M$_2$. Boroxycarbene **2-E$_2$** was first prepared, by addition of 21.0 mg (0.0327 mmol) solid [**HPt**]$^+$ to a stirring ~0.6 mL C_6D_5Cl solution of 52.8 mg (0.0327 mmol) [**1-M$_2$**][$B(C_6F_5)_4$] and 16.0 mg (0.0327 mmol) tetraheptylammonium tetrafluoroborate. The solution was transferred to a J-Young NMR tube, and was allowed to react overnight. A few days later, boroxycarbene **2-E$_2$** was prepared by dropwise addition of 32.7 μL (0.0327 mmol) $NaHBEt_3$ (1.0 M in toluene) to a stirring ~0.4 mL C_6D_5Cl solution of 34.5 mg (0.0327 mmol) [**1-E$_2$**][BF_4]. The preformed **2-M$_2$** was returned to the glovebox (NMR spectroscopy showed no decomposition during the days after preparation), and the contents of the tube were poured onto the solution containing **2-E$_2$**. The reaction mixture was filtered through sintered glass into a J-Young NMR tube, and multinuclear NMR spectra were obtained, showing high conversion to the further reduced confused alkyl [**5**]$^-$ and cation [**1-E$_2$**]$^+$ (resulting from hydride transfer from **2-E$_2$**). A small amount of carbene **2-E$_2$** remained, along with small amounts of residual [**HPt**]$^+$ from the synthesis of **2-M$_2$**.

Reduction of [(PPh$_3$)Re(CO)$_5$][OTf] ([1-Ph$_1$][OTf])

Reaction of [1-Ph$_1$][OTf] with 1 equiv [HPt][PF$_6$]. A small vial was charged with 16.7 mg (0.0225 mmol) [**1-Ph$_1$**][OTf] and ~0.6 mL C_6D_5Cl. With stirring, 14.4 mg (0.0225 mmol) [**HPt**][PF_6] was slowly added, and the reaction mixture transferred to a J-

Young NMR tube. After 20 minutes, ^{1}H NMR spectroscopy revealed a mixture of ~2:1 formyl:hydride, which converted almost entirely to hydride after 1.5 hours (~1:21 formyl:hydride). All formyl was consumed after 4 hours.

Reaction of [1-Ph$_1$][BAr$^F_4$] with 1 equiv [HPt][BAr$^F_4$]. A J-Young tube was charged with 31.3 mg (0.0215 mmol) [**1-Ph$_1$**][BAr$^F_4$], 29.2 mg (0.0215 mmol) [**HPt**][BAr$^F_4$], and ~0.6 mL C_6D_5Cl. Monitoring by NMR spectroscopy revealed no detectable reaction after 15 minutes, and only partial conversion to **2-Ph$_1$** after 3 hours. After 30 hours, complete conversion to the Re hydride *trans*-$(PPh_3)Re(CO)_4H$ [^{1}H NMR δ –4.65 (d, $\mathcal{J}_{PH}$ = 22.5 Hz); ^{31}P{^{1}H} NMR δ 15.7] was observed.

Reduction of [(Ph$_2$PCH$_2$B(C$_8$H$_{14}$))Re(CO)$_5$][OTf] ([1-M$_1$][OTf])

Reaction of [1-M$_1$][OTf] with 1 equiv [HPt][PF$_6$]. A 20 mL scintillation vial was charged with 99.1 mg (0.124 mmol) [**1-M$_1$**][OTf] and 2 mL C_6H_5Cl. With rapid stirring, 79.8 mg (0.124 mmol) [**HPt**][PF_6] was added in ~10 mg portions slowly over ~5 minutes. The mixture was allowed to stir overnight, at which point it was filtered through celite (washing with 1 mL C_6H_5Cl and 2 mL pentane), and the solvents were removed under vacuum. The oily residue was triturated briefly with pentane and the solvents were again removed under vacuum. The white solids were extracted with 5 mL pentane, filtered, and the solvents removed under vacuum to give 70 mg (87%) ~95% pure **2-M$_1$**. The side product was an Re–C*H*$_2$-containing species (δ 5.18 d, $\mathcal{J}_{PH}$ = 6.3 Hz) which had spectral characteristics (^{31}P NMR, δ –8.9 (1P), 2.3 (1P)) similar to more completely characterized dirhenium alkyl-dioxycarbene species **10-E$_1$**. **^{1}H NMR** (C_6D_6, 300 MHz): δ 1.16 (br, 2H,

$Ph_2PCH_2B(C_8H_{14})$), 1.3-1.8 (br, $Ph_2PCH_2B(C_8H_{14})$), 1.65 (d, $\mathcal{J}_{PH}$ = 12.9 Hz, $Ph_2PCH_2B(C_8H_{14})$), 2.02 (br, $Ph_2PCH_2B(C_8H_{14})$), 2.30 (br, $Ph_2PCH_2B(C_8H_{14})$; integration of all broad peaks from 1.3-2.6 is 16H as expected), 6.89-6.98 (m, 6H, $Ph_2PCH_2B(C_8H_{14})$), 7.25-7.32 (m, 4H, $Ph_2PCH_2B(C_8H_{14})$), 13.72 (d, JPH = 2.5 Hz, 1H, Re–C*H*O). **^{31}P{^{1}H} NMR** (C_6D_6, 121 MHz): δ –0.2. **^{13}C{^{1}H} NMR** (C_6D_6, 125 MHz): δ 14.76 (br), 25.41 (br), 26.90 (br), 31.54 (br), 32.49 (br), 128.77 (d, $\mathcal{J}_{PC}$ = 9.9 Hz), 130.31 (d, $\mathcal{J}_{PC}$ = 1.9 Hz), 132.02 (d, $\mathcal{J}_{PC}$ = 10.4 Hz), 137.75 (d, $\mathcal{J}_{PC}$ = 46.8 Hz), 186.93 (br, eq. COs), 189.80 (br, axial CO), 282.48 (br, Re–*C*HO). **^{11}B NMR** (C_6D_5Cl, 160 MHz): δ 11.2. **IR** (heptane): ν_{CO} 2096 (m), 2003 (s), 1975 (s), 1945 (m), ν_{CHO} 1517 cm^{-1}. **IR** (CH_2Cl_2): 2097 (m), 2000 (s), 1972 (s), 1942 (sh), 1507 cm^{-1}.

Variable temperature NMR experiments were undertaken as some of the –B(C_8H_{14}) resonances were broad. As the probe was cooled, the broad –B(C_8H_{14}) resonances sharpened significantly but otherwise remained relatively featureless. The carbene proton shifted slightly with temperature, although the coupling constant remained ~2 Hz at all temperatures. The broad ^{11}B NMR resonance disappeared at low temperatures. The broadening could be due to B–O de-coordination, as further evidenced by the reactivity of **2-M$_1$** with pyridine (see below).

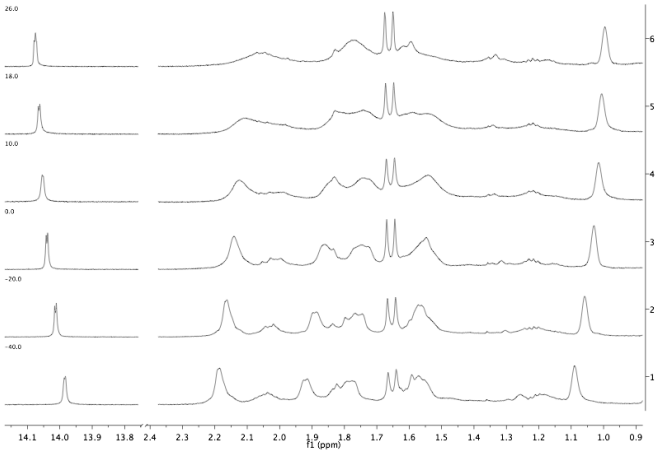

Figure 3.38. Variable temperature ^{1}H NMR of **2-M$_1$**.

Decomposition of 2-M$_1$ to 11. While searching for ideal conditions to reduce [**1-M$_1$**][OTf], a J-Young tube was charged with 19.3 mg (0.0242 mmol) [**1-M$_1$**][OTf], 4.0 mg (0.031 mmol) $NaHB(OMe)_3$, and ~0.6 mL C_6D_5Cl. The mixture turned yellow and was monitored by NMR spectroscopy, which showed conversion to two products in a ~2:1 ratio, with the major product being the boroxycarbene **2-M$_1$**. The product distribution was largely stable for weeks, but after 1 month NMR spectra showed nearly complete consumption of the carbene and formation of a new species containing three diagnostic multiplets at 3.94, 5.30, and 6.39. A separate reaction was carried out in C_6H_5Cl under similar conditions, from which the solvents were removed under vacuum, followed by extraction with pentane and crystallization from slow pentane evaporation. Crystals grew only after a few months, and turned out to be the decomposition product. Although the reaction was fairly clean, the undesired product was not isolated or purified, and was only characterized as a mixture in the NMR experiments and by X-Ray crystallography. Partial NMR spectroscopic details: **^{1}H NMR** (C_6D_5Cl, 500 MHz): 3.95 (ddd, $\mathcal{J}_{HH}$ = 8.7 Hz, 14.5 Hz, $\mathcal{J}_{PH}$ = 12.0 Hz, $Ph_2PCH_2C(O–)(H)–Re$), 5.30 (dt, $\mathcal{J}_{HH}$ = 8.6 Hz, $\mathcal{J}_{PH}$ = 14.5 Hz,

$Ph_2PCH_2C(O–)(H)–Re$), 6.40 (td, $\mathcal{J}_{HH}$ = 8.7 Hz, $\mathcal{J}_{PH}$ = 5.5, $Ph_2PCH_2C(O–)(H)–Re$). **$^{31}P\{^1H\}$ NMR** (C_6D_5Cl, 121 MHz): –54.0 (1P), 1.8 (1P, 4-membered ring). **$^{13}C\{^1H\}$ NMR** (C_6D_5Cl, 75 MHz): 44.13 ($\mathcal{J}_{PC}$ = 6.3 Hz, $Ph_2PCH_2C(O–)(H)–Re$), 52.24 ($\mathcal{J}_{PC}$ = 39.3 Hz, $Ph_2PCH_2C(O–)(H)–Re$), 210.20 (d, $\mathcal{J}_{PC}$ = 9.4 Hz, $Re=C(O–)O–C(R)H–Re$).

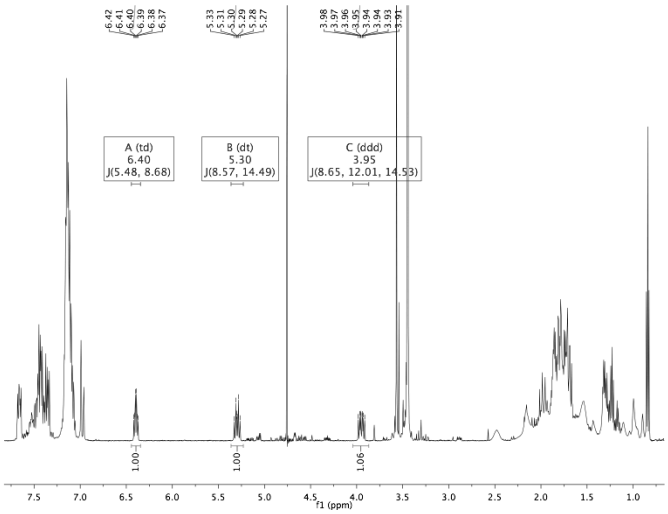

Figure 3.39. ^1H NMR of **11**.

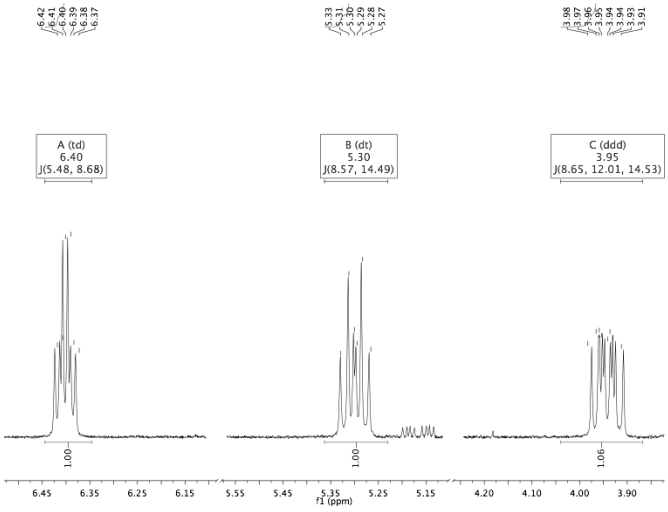

Figure 3.40. ^1H NMR of **11** (blow-up of cyclic alkyl region).

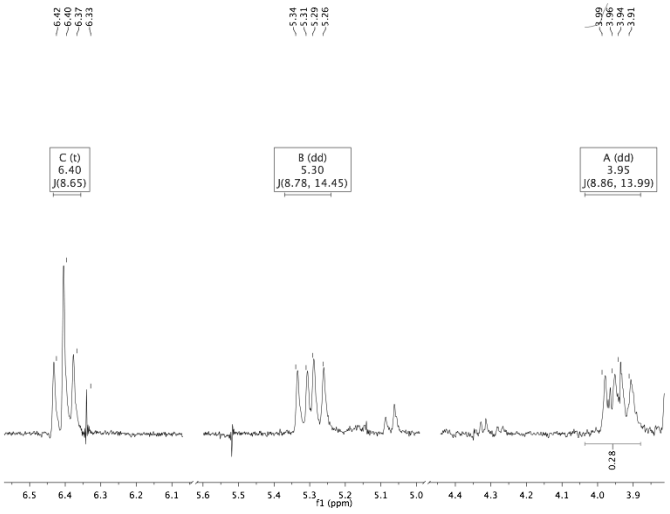

Figure 3.41. $^{1}H\{^{31}P\}$ NMR of **11**.

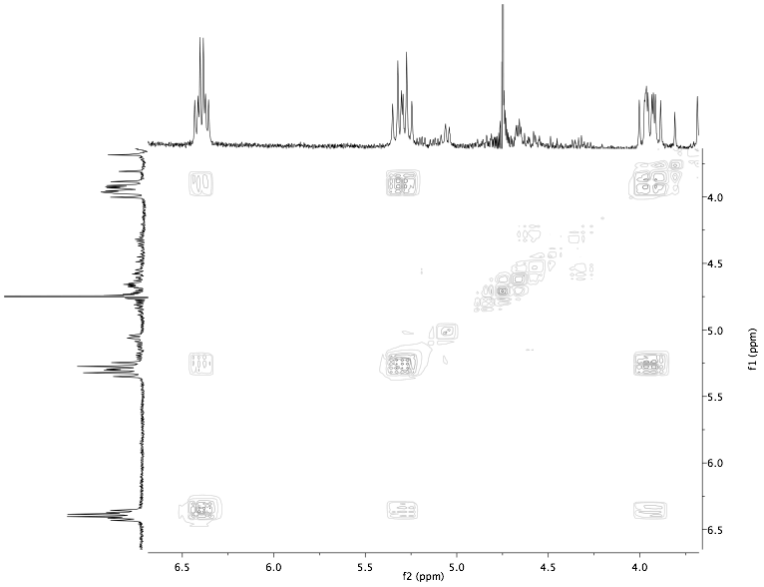

Figure 3.42. ^{1}H–^{1}H gCOSY of **11**.

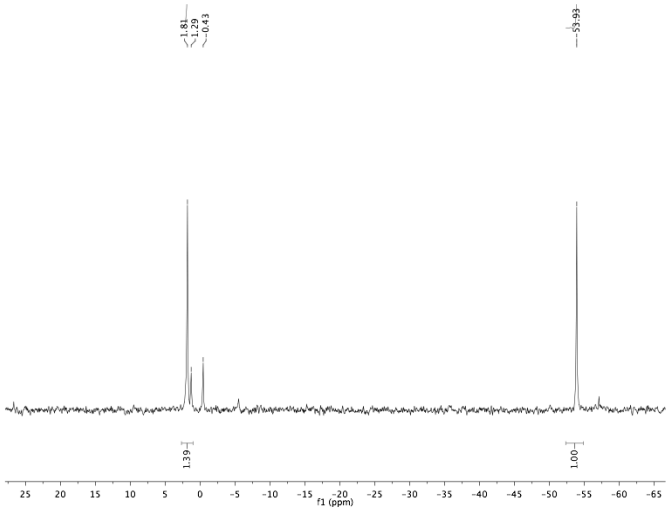

Figure 3.43. $^{31}P\{^{1}H\}$ NMR of **11**.

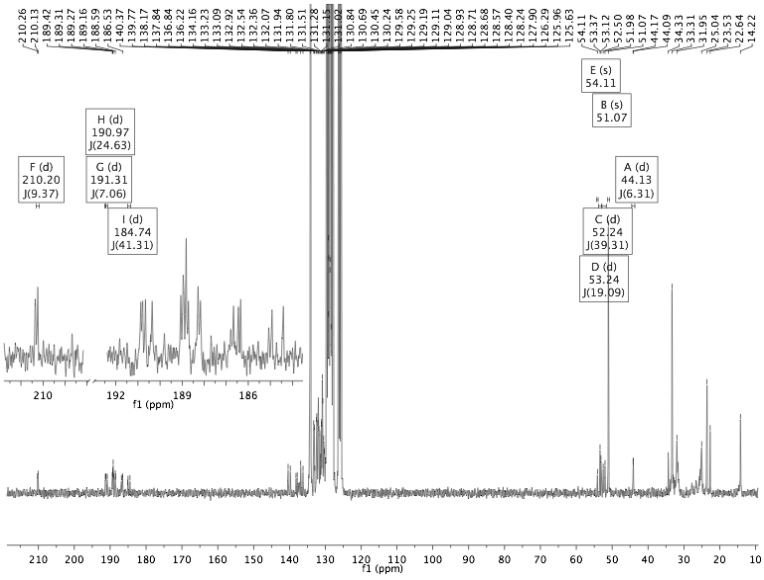

Figure 3.44. $^{13}C\{^{1}H\}$ NMR of **11**.

Reaction of [1-M$_1$][BAr$^F_4$] with [HPt][BAr$^F_4$]. Reaction of 2-M$_1$ with pyridine. A small vial was charged with 38.0 mg (0.0254 mmol) [**1-M$_1$**][BAr$^F_4$] and ~0.6 mL C_6D_5Cl. With stirring, 34.5 mg (0.0254 mmol) [**HPt**][BAr$^F_4$] was added as a solid, and the mixture was transferred to a J-Young NMR tube and monitored by NMR spectroscopy. After about 30 minutes, only a small resonance for **2-M$_1$** was observed. The reaction slowly

proceeded over ~24 hours, eventually consuming all [**HPt**]$^+$ and affording spectra matching previous syntheses of **2-M$_1$** (using OTf/PF_6 salts).

To the tube containing **2-M$_1$** was added 4 μL pyridine (0.0503 mmol, 2 equiv), and the tube was sealed and shaken to mix. NMR spectroscopy revealed consumption of the carbene with formation of a new bridging alkyl species. Multinuclear NMR spectroscopy was very similar to analytically characterized **10-E$_1$** (see below), confirming the analogous structure **10-M$_1$•py**. For **10-M$_1$•py**: **^{1}H NMR** (C_6D_6, 300 MHz): δ 0.92 (br, 2H, $Ph_2PCH_2B(C_8H_{14})$), 1.17 (br, 4H, $Ph_2PCH_2B(C_8H_{14})$), 1.71 (br m, 6H, $Ph_2PCH_2B(C_8H_{14})$), 1.81 (d, $\mathcal{J}_{PH}$ = 13.0 Hz, 2H $Ph_2PCH_2B(C_8H_{14})$), 1.9-2.2 (br m, 12H, $Ph_2PCH_2B(C_8H_{14})$), 2.32 (d, $\mathcal{J}_{PH}$ = 11.5 Hz, 2H, $Ph_2PCH_2B(C_8H_{14})$), 2.39 (br, 4H, $Ph_2PCH_2B(C_8H_{14})$), 5.05 (d, $\mathcal{J}_{PC}$ = 5.7 Hz, 2H, Re–CH_2O–), 6.22 (br, 2H, pyridine), 6.55 (br, 1H, pyridine), 6.9-7.0 (m, 12H, Ph), 7.31 (m, 4H, Ph), 7.48 (m, 4H, Ph), 7.72 (br, 2H, pyridine). **^{31}P{^{1}H} NMR** (C_6D_6, 121 MHz): δ –4.4 (1P), 2.4 (1P). **^{13}C{^{1}H} NMR** (C_6D_6, 126 MHz): 15.08 (d, $\mathcal{J}_{PC}$ = 11.8 Hz, $Ph_2PCH_2B(C_8H_{14})$), 24.41 ($Ph_2PCH_2B(C_8H_{14})$), 25.57 ($Ph_2PCH_2B(C_8H_{14})$), 26.22 (br, $Ph_2PCH_2B(C_8H_{14})$) 27.18 (d, $\mathcal{J}_{PC}$ = 10.6 Hz, $Ph_2PCH_2B(C_8H_{14})$), 30.45 ($Ph_2PCH_2B(C_8H_{14})$), 32.01 ($Ph_2PCH_2B(C_8H_{14})$), 32.85 ($Ph_2PCH_2B(C_8H_{14})$), 33.16 ($Ph_2PCH_2B(C_8H_{14})$), 54.39 (d, $\mathcal{J}_{PC}$ = 6.1 Hz, Re–CH_2O–C(O)–Re), 125.07 (pyridine), 128.34 (d, $\mathcal{J}_{PC}$ = 9.3 Hz, *m*-$Ph_2PCH_2B(C_8H_{14})$), 128.64 (d, $\mathcal{J}_{PC}$ = 9.8 Hz, *m*-$Ph_2PCH_2B(C_8H_{14})$), 129.85 (d, $\mathcal{J}_{PC}$ = 1.9 Hz, *p*-$Ph_2PCH_2B(C_8H_{14})$), 130.00 (d, $\mathcal{J}_{PC}$ = 2.1 Hz, *p*-$Ph_2PCH_2B(C_8H_{14})$), 132.35 (d, $\mathcal{J}_{PC}$ = 10.4 Hz, *o*-$Ph_2PCH_2B(C_8H_{14})$), 132.47 (d, $\mathcal{J}_{PC}$ = 10.0 Hz, *o*-$Ph_2PCH_2B(C_8H_{14})$), 137.36 (d, $\mathcal{J}_{PC}$ = 42.1 Hz, *ipso*-$Ph_2PCH_2B(C_8H_{14})$), 138.77 (d, $\mathcal{J}_{PC}$ = 46.1 Hz, *ipso*-$Ph_2PCH_2B(C_8H_{14})$), 139.39 (pyridine), 145.85 (pyridine), 184.89 (d, $\mathcal{J}_{PC}$ =

41.7 Hz, *C*O *trans* to P), 187.82 (d, $\mathcal{J}_{PC}$ = 8.5 Hz, 2 CO), 188.98 (d, $\mathcal{J}_{PC}$ = 45.5 Hz, CO *trans* to P), 189.41 (d, $\mathcal{J}_{PC}$ = 8.4 Hz, CO), 189.81 (d, $\mathcal{J}_{PC}$ = 6.7 Hz, CO), 191.08 (d, $\mathcal{J}_{PC}$ = 9.0 Hz, 2 CO), 211.60 (d, JPC = 9.4 Hz, Re–CH_2O–*C*(O)–Re). **IR** (C_6D_6): ν_{CO} 2095 (m), 2082 (m), 1997 (br s), 1960 (br s), 1935 (br s) cm^{-1}.

Reaction of 2-M_1 with 2-P_1 (Crossover Experiment). To a stirring ~0.6 mL C_6D_5Cl solution of 19.3 mg (0.0240 mmol) [**1-M$_1$**][OTf] was added 15.6 mg (0.0240 mmol) [**HPt**]$^+$ partwise as a solid. The solution was transferred to a J-Young NMR tube, and showed ~90% conversion to **2-M$_1$** by NMR spectroscopy. The side product was the bridging alkyl as discussed in the synthesis of **2-M$_1$**. Meanwhile, **2-P$_1$** was prepared by addition of 15.6 mg (0.0240 mmol) solid [**HPt**]$^+$ to 20.0 mg (0.024 mmol) [**1-P$_1$**][OTf] with stirring. After one minute of stirring, the contents of the tube containing **2-M$_1$** were poured into the vial containing **2-P$_1$**, and the reaction mixture was filtered into a J-Young NMR tube. After ~20 minutes, a mixture of both Re–CHO species and a bridging alkyl-metalloester species were observed. After 3 hours, no Re–CHO species remained, and the major species (~90%) was identified by ^{1}H–^{31}P gHMBC NMR as **10-M$_1$P$_1$**, with the minor product being the initially formed impurity containing only 1C ligands. The 2-D NMR shows correlation of the CH_2 group to the ^{31}P signal at 0.1, which also correlates to two multiplets in the ^{1}H NMR at 2.46 and 1.56, belonging to the **P** ligand, and confirming that the CH_2 is bound the same metal as the **P** ligand. The other ^{31}P signal of the major species and the impurity overlap at 2.1 ppm (the amount of impurity stayed roughly the same through the reaction). This resonance correlates to Ph protons and a doublet at 1.75, consistent with the other Re of both bimetallic species being ligated by **M**. As discussed in

the text, this assignment allows for the mechanistic pathway of formation of the bridging alkyl to be identified as nucleophilic attack by oxygen.

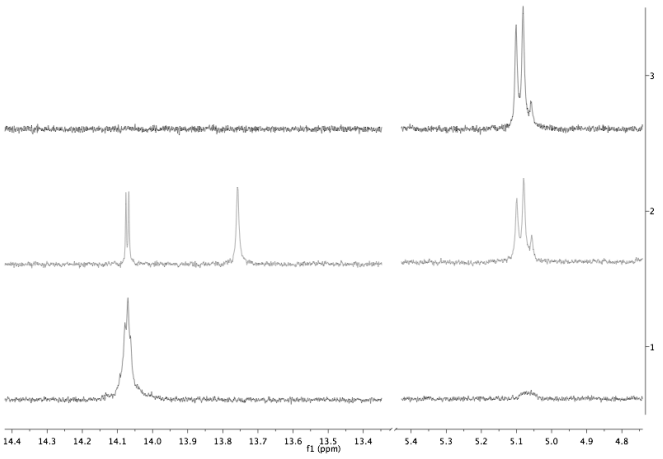

Figure 3.45. ^{1}H NMR time course. Bottom spectrum is **2-M$_1$** before addition of **2-P$_1$** (poor shimming due to solid Pt^{2+} salts formed during reaction). Middle spectrum is ~20 minutes after addition of **2-P$_1$** (after filtration). Top spectrum is upon completion of the reaction.

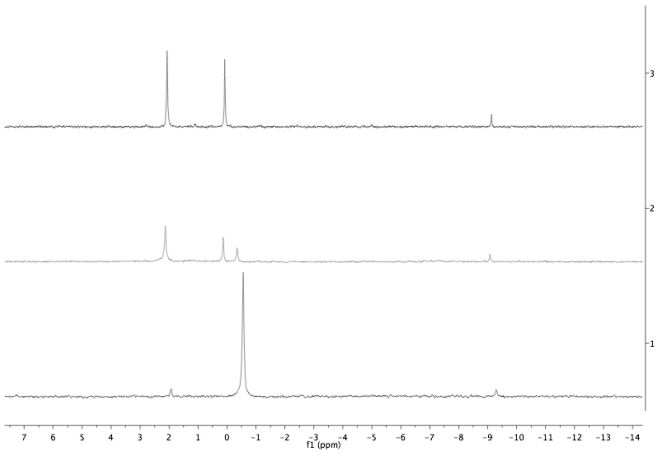

Figure 3.46. ^{1}H NMR time course. Bottom spectrum is **2-M$_1$** before addition of **2-P$_1$**. Middle spectrum is ~20 minutes after addition of **2-P$_1$** (after filtration). Top spectrum is upon completion of the reaction.

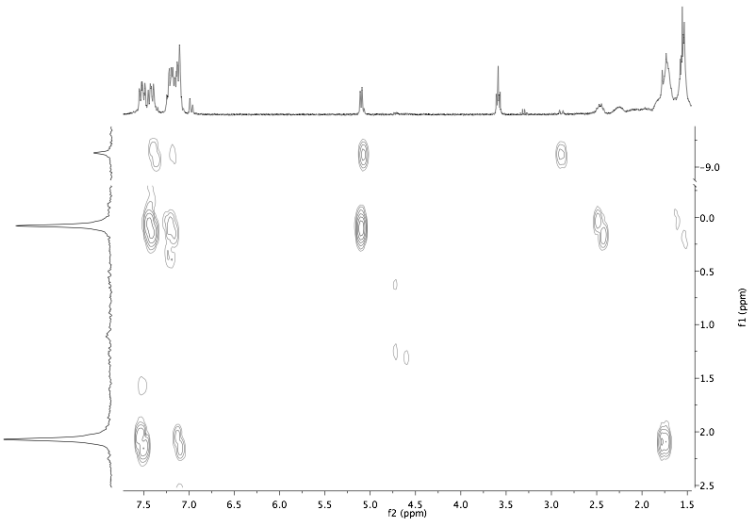

Figure 3.47. $^{1}H–^{31}P$ gHMBC NMR confirming the product as **10-M$_1$P$_1$**.

Reduction of [(Ph$_2$PCH$_2$B(C$_8$H$_{14}$))Re(CO)$_5$][OTf] ([1-M$_1$][OTf]) with 2 equiv hydride. A number of conditions, including changes in hydride source, solvent, anion, and countercation were varied. The results were generally similar; depending on the countercation of the product ([**HPt**]$^+$, [**Pt**]$^{2+}$, etc) the peaks shifted subtly, including the Re–C(O)C*H*$_2$O– group, the two doublets of which were sometimes more well resolved than others (moving to a singlet with Na^+ present). Typical procedure using two equiv [**HPt**][PF_6]: to a stirring ~0.6 mL C_6D_5Cl solution of 26.5 mg (0.0333 mmol) [**1-M$_1$**][OTf] was added 21.3 mg (0.0333 mmol, 1 equiv) [**HPt**][PF_6] partwise as a solid. The reaction was allowed to stir for 15 minutes, at which point the reaction mixture was filtered into a small vial charged with another 21.3 mg (0.0333 mmol, 1 equiv) of [**HPt**][PF_6]. Despite measuring 1 equiv of hydride, ~2 equiv was actually delivered, as the filtration left some carbene behind. The mixture was then transferred to a J-Young tube, and monitored by multinuclear NMR spectroscopy. After 20 minutes, carbene **2-M$_1$** was essentially the only Re species, but after 2.5 hours a mixture of **2-M$_1$**, and two new species were observed,

identified as a Re alkyl and as the migratory insertion product [**3-M$_1$**]$^-$. After 2.5 hours, there was more alkyl present than the final product (^{1}H NMR δ 5.14 (d, $\mathcal{J}_{PH}$ = 1.9 Hz); ^{31}P{^{1}H} NMR δ 3.4). After 24 hours, the starting carbene had been almost entirely consumed, and the major species was the acyl. After 48 hours, the reaction was complete, with only the acyl and residual [**HPt**]$^+$ remaining. 2D NMR experiments were performed on a reaction carried out in CD_2Cl_2, which contained a mixture of [**3-M$_1$**]$^-$, the alkyl intermediate, and small amounts of bridging alkyl impurities. Details of the crucial correlations that led to the structural assignment of the products are supplied by the appropriate figures. Typical procedure using $NaHBEt_3$: To a stirring ~0.6 mL C_6D_5Cl solution of 21.1 mg (0.0265 mmol) [**1-M$_1$**][OTf] was added 17.0 mg (0.0265 mmol) [**HPt**][PF_6] slowly as a solid. The mixture turned yellow with precipitation while it was allowed to stir for 10 minutes. After 10 minutes, the mixture was filtered through sintered glass, and 26.5 μL $NaHBEt_3$ (1.0 M in toluene) was added dropwise. Use of the stronger hydride source led to a much faster reaction, with complete conversion to in 2.5 hours. The ^{1}H and ^{31}P resonances were at approximately the same chemical shift, but were dramatically broadened relative to the [**HPt**]$^+$ reactions. Addition of pyridine directly following $NaHBEt_3$ (in a separate experiment) led to a moderate decrease in reaction rate, and a sharpening of the signals, suggesting BEt_3 is leading to broadening, and perhaps rate enhancement. Single crystals suitable for X-Ray diffraction were grown from this latter experiment, from a THF/pentane mixture at –35 °C. Characterization of acyl product [**3-M$_1$**]$^-$: **^{1}H NMR** (mix of [**Pt**]$^{2+}$ and [**HPt**]$^+$ salts, which obscure some $Ph_2PCH_2B(C_8H_{14})$ resonances, THF-*d*$_8$, 600 MHz): δ 0.43 (br, 1H, $Ph_2PCH_2B(C_8H_{14})$), 0.63 (br, 1H,

$Ph_2PCH_2B(C_8H_{14})$), 0.71 (dd, $\mathcal{J}_{PH}$ = 9.8 Hz, $\mathcal{J}_{HH}$ = 14.4 Hz, 1H, $Ph_2PCH_2B(C_8H_{14})$), 1.29 (m, 1H), 1.37-1.43 (m, 3H), 1.53 (m, 1H), 4.64 (dd, $\mathcal{J}_{PH}$ = 1.9 Hz, $\mathcal{J}_{HH}$ = 15.1 Hz, 1H, Re-C(O)CH_2O–), 4.71 (d, $\mathcal{J}_{HH}$ = 15.0 Hz, 1H, Re–C(O)CH_2O–), 7.17-7.25 (m, 4H, Ph), 7.30 (m, 2H, Ph), 7.69 (m, 2H, Ph), 7.75 (m, 2H, Ph). **^{31}P{^{1}H} NMR** (THF-d_8, 121 MHz): δ –5.9 ($\mathcal{J}_{PtP}$ = 2214 Hz, [**HPt**]$^+$), 34.9 ($\mathcal{J}_{PtP}$ = 2184 Hz, [**Pt**]$^{2+}$), 38.8 (s, Re). **^{13}C{^{1}H} NMR** (CD_2Cl_2, 126 MHz): δ 13.79 (br, [Pt($Me_2PCH_2CH_2PMe_2$)$_2$]$^{2+}$), 21.34 (m, [HPt($Me_2PCH_2CH_2PMe_2$)$_2$]$^+$), 26.14 ($Ph_2PCH_2B(C_8H_{14})$), 26.37 (br, overlapping ($Ph_2PCH_2B(C_8H_{14})$), 28.41 (br, [Pt($Me_2PCH_2CH_2PMe_2$)$_2$]$^{2+}$), 30.61 ($Ph_2PCH_2B(C_8H_{14})$), 32.21 ($Ph_2PCH_2B(C_8H_{14})$), 32.88(m, [HPt($Me_2PCH_2CH_2PMe_2$)$_2$]$^+$), 33.78 ($Ph_2PCH_2B(C_8H_{14})$), 35.38 ($Ph_2PCH_2B(C_8H_{14})$), 102.67 (ReC(O)CH$_2$O–), 128.38 (d, $\mathcal{J}_{PC}$ = 9.4 Hz, *m*-$Ph_2PCH_2B(C_8H_{14})$), 128.40 (d, $\mathcal{J}_{PC}$ = 9.3 Hz, *m*-$Ph_2PCH_2B(C_8H_{14})$), 129.34 (d, $\mathcal{J}_{PC}$ = 1.5 Hz, *p*-$Ph_2PCH_2B(C_8H_{14})$, 129.53 (d, $\mathcal{J}_{PC}$ = 1.3 Hz, *p*-$Ph_2PCH_2B(C_8H_{14})$), 132.63 (d, $\mathcal{J}_{PC}$ = 11.2 Hz, *o*-$Ph_2PCH_2B(C_8H_{14})$), 133.49 (d, $\mathcal{J}_{PC}$ = 10.7 Hz, *o*-$Ph_2PCH_2B(C_8H_{14})$), 139.78 (d, $\mathcal{J}_{PC}$ = 40.5 Hz, *ipso*-$Ph_2PCH_2B(C_8H_{14})$), 141.17 (d, $\mathcal{J}_{PC}$ = 39.2 Hz, *ipso*-$Ph_2PCH_2B(C_8H_{14})$), 200.79 (d, $\mathcal{J}_{PC}$ = 53.3 Hz, CO *trans* to P), 202.26 (d, $\mathcal{J}_{PC}$ = 7.6 Hz, CO), 203.87 (d, $\mathcal{J}_{PC}$ = 8.3 Hz, CO), 274.74 (d, $\mathcal{J}_{PC}$ = 12.0 Hz, ReC(O)CH$_2$O–). ^{11}B NMR (CD_2Cl_2, 160 MHz): δ 6.5 (br). **IR** (CH_2Cl_2): ν_{CO} 1997 (s), 1906 (s), 1861 (s), $\nu_{C=O}$ 1615 (m). **HRMS (TOF MS ES$^-$):** Calcd for $C_{26}H_{28}BO_5PRe$, 649.1311. Found, 649.1325.

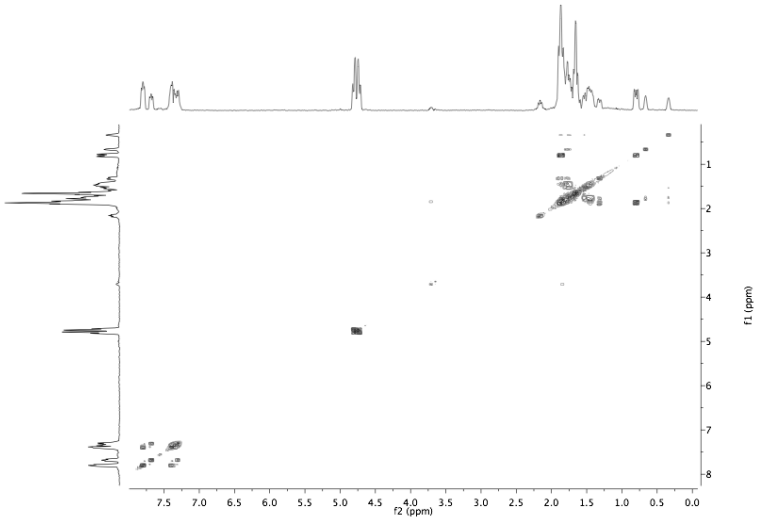

Figure 3.48. $^{1}H–^{1}H$ gCOSY of [**3-M$_1$**]$^-$.

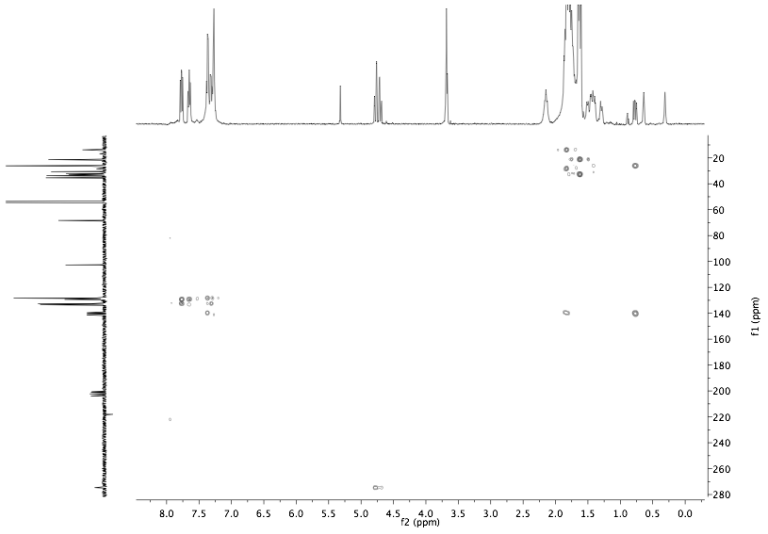

Figure 3.49. $^{1}H–^{13}C$ gHMBC of [**3-M$_1$**]$^-$.

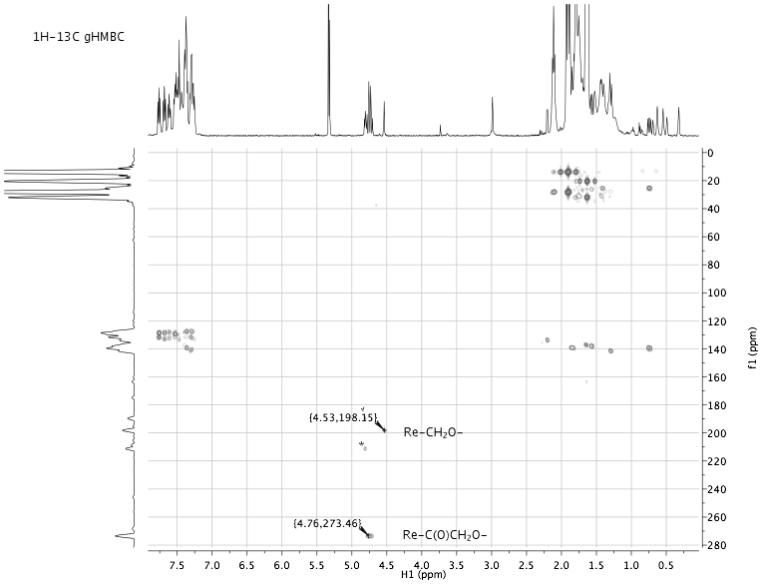

Figure 3.50. $^{1}H–^{13}C$ gHMBC during reaction of [**1-M$_1$**]$^+$ with [**HPt**]$^+$. Mixture of boroxyalkyl, [**3-M$_1$**]$^-$; bridging alkyl impurity marked with star.

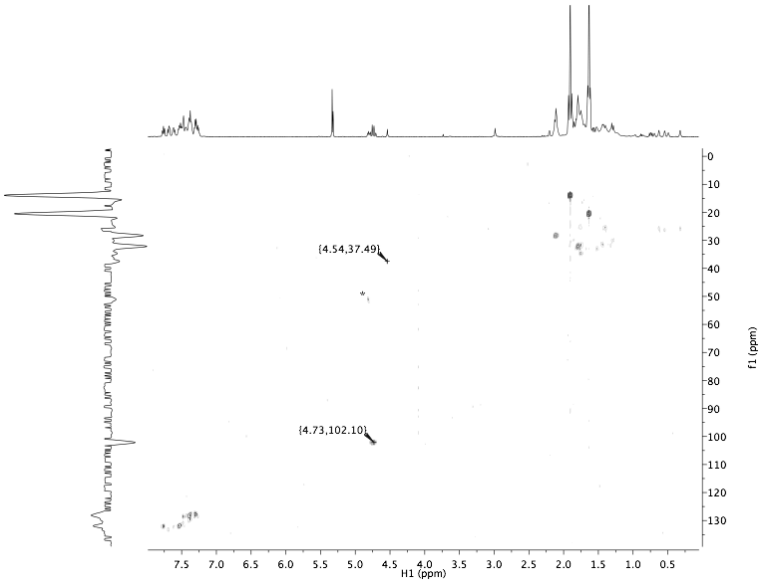

Figure 3.51. $^{1}H–^{13}C$ gHSQC during reaction of [**1-M$_1$**]$^+$ with [**HPt**]$^+$. Mixture of boroxyalkyl, [**3-M$_1$**]$^-$; bridging alkyl impurity marked with star.

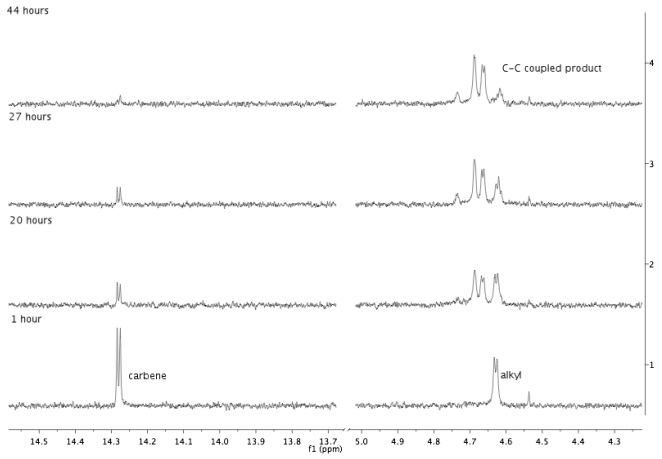

Figure 3.52. Time couse of reaction of [**1-M$_1$**]$^+$ with [**HPt**]$^+$ (2 equiv [HPt]$^+$ in THF-d_8).

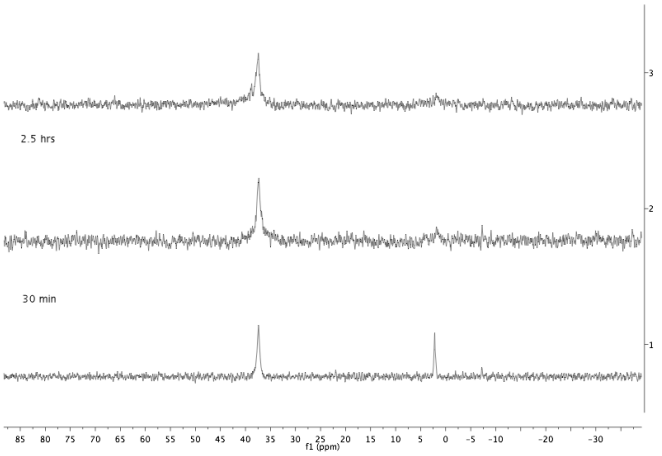

Figure 3.53. Time couse of reaction of [**1-M$_1$**]$^+$ with [**HPt**]$^+$ (1 equiv [HPt]$^+$, 1 equiv $NaHBEt_3$).

Reductions of [(Ph$_2$P(CH$_2$)$_2$B(C$_8$H$_{14}$))Re(CO)$_5$][OTf] ([1-E$_1$][OTf])

Reaction of [(Ph$_2$P(CH$_2$)$_2$B(C$_8$H$_{14}$))Re(CO)$_5$][OTf] ([1-E$_1$][OTf]) with [HPt][PF$_6$]. To a stirring solution of 27.5 mg (0.034 mmol) [**1-E$_1$**][OTf] in ~0.6 mL C_6D_5Cl was added 24.0 mg (0.037 mmol) [HPt(dmpe)$_2$][PF_6] as a solid in small portions. After stirring for a minute, the reaction mixture was added to a J-Young NMR tube. After 20 minutes, essentially quantitative conversion to a new species was observed, identified as

dinuclear bridging alkyl-dioxycarbene **10-E$_1$**. Filtration followed by removal of solvents gave analytically pure white solids. **^{1}H NMR** (600 MHz, C_6D_5Cl): δ 1.04-1.11 (m, 4H, $Ph_2PCH_2CH_2B(C_8H_{14})$), 1.21 (br, 2H, $Ph_2PCH_2CH_2B(C_8H_{14})$), 1.41 (m, 2H, $Ph_2PCH_2CH_2B(C_8H_{14})$), 1.53-1.58 (m, 6H, $Ph_2PCH_2CH_2B(C_8H_{14})$), 1.65 (br, 2H, $Ph_2PCH_2CH_2B(C_8H_{14})$), 1.70-1.77 (m, 6H, $Ph_2PCH_2CH_2B(C_8H_{14})$), 1.90 (m, 4H, $Ph_2PCH_2CH_2B(C_8H_{14})$), 2.11 (m, 6H, $Ph_2PCH_2CH_2B(C_8H_{14})$), 2.54 (m, 2H, $Ph_2PCH_2CH_2B(C_8H_{14})$), 2.73 (m, 2H, $Ph_2PCH_2CH_2B(C_8H_{14})$), 5.05 (d, $\mathcal{J}_{PH}$ = 6.9 Hz, 2H, Re–CH_2O–), 7.14-7.20 (m, 8H, $Ph_2PCH_2CH_2B(C_8H_{14})$), 7.24 (m, 4H, $Ph_2PCH_2CH_2B(C_8H_{14})$), 7.45 (m, 8H, $Ph_2PCH_2CH_2B(C_8H_{14})$). **^{31}P{^{1}H} NMR** (C_6D_5Cl, 121 MHz): δ 3.7 (1P), 13.3 (1P). **^{13}C{^{1}H} NMR** (C_6D_5Cl, 125 MHz): 13.95 (br, $Ph_2PCH_2CH_2B(C_8H_{14})$), 20.59 (br, $Ph_2PCH_2CH_2B(C_8H_{14})$), 23.16 ($Ph_2PCH_2CH_2B(C_8H_{14})$), 23.91 (d, $\mathcal{J}_{PC}$ = 17.4 Hz, $Ph_2PCH_2CH_2B(C_8H_{14})$), 25.39 ($Ph_2PCH_2CH_2B(C_8H_{14})$), 25.87 (d, $\mathcal{J}_{PC}$ = 27.8 Hz, $Ph_2PCH_2CH_2B(C_8H_{14})$), 26.97 (br, $Ph_2PCH_2CH_2B(C_8H_{14})$), 31.34 (br, $Ph_2PCH_2CH_2B(C_8H_{14})$), 32.78 ($Ph_2PCH_2CH_2B(C_8H_{14})$), 33.21 ($Ph_2PCH_2CH_2B(C_8H_{14})$), 49.88 (d, $\mathcal{J}_{PC}$ = 6.6 Hz, Re–CH_2O–), 128.69 (d, JPC = 9.6 Hz, Ph), 130.51 (d, $\mathcal{J}_{PC}$ = 24.9 Hz), 132.17 (d, $\mathcal{J}_{PC}$ = 9.6 Hz), 132.21 (d, $\mathcal{J}_{PC}$ = 9.6 Hz), 133.49 (d, $\mathcal{J}_{PC}$ = 44.9 Hz), 135.59 (d, $\mathcal{J}_{PC}$ = 46.3 Hz), 184.98 (d, $\mathcal{J}_{PC}$ = 44.0 Hz, CO), 187.23 (d, $\mathcal{J}_{PC}$ = 8.4 Hz, CO), 187.68 (d, $\mathcal{J}_{PC}$ = 6.9 Hz, CO), 187.69 (d, $\mathcal{J}_{PC}$ = 7.6 Hz, CO; overlap with preceding peak leads to one broad doublet), 188.27 (d, $\mathcal{J}_{PC}$ = 48.2 Hz, CO), 189.94 (d, $\mathcal{J}_{PC}$ = 9.4 Hz, CO), 209.61 (d, $\mathcal{J}_{PC}$ = 10.5 Hz, Re–$C(O–BR_3)OCH_2$–). **IR** (C_6D_5Cl): ν_{CO}, 2090 (w), 2084 (w), 2013 (s), 1997 (s), 1965 (s), 1939 (s) cm^{-1}. **Anal. Calcd.** for $C_{54}H_{58}B_2O_{10}P_2Re_2$: C, 49.02; H, 4.42. Found: C, 48.74; H, 4.32.

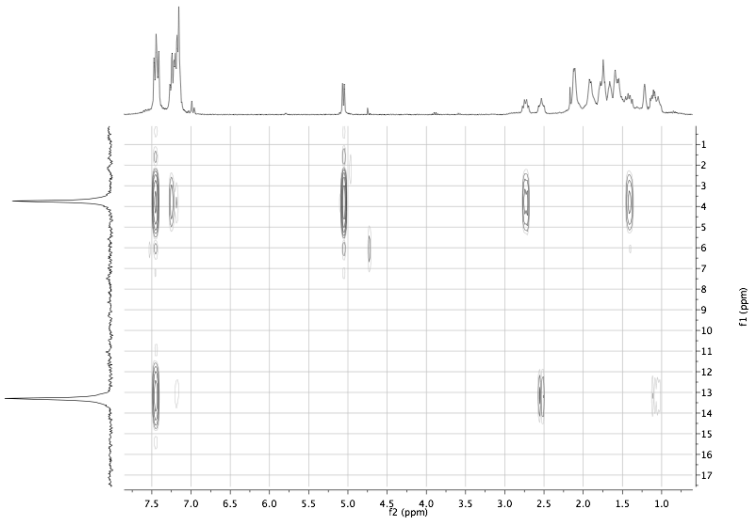

Figure 3.54. $^{1}H–^{31}P$ gHMBC of **10-E$_1$**.

Low temperature monitoring of the reaction of [1-E$_1$][OTf] with [HPt][PF$_6$]. A J-Young tube was charged with 25.8 mg (0.0318 mmol) cation [**1-E$_1$**][OTf]. Roughly 0.1 mL C_6D_5Cl was added, dissolving the cation. The tube was placed in a cold well chilled with liquid nitrogen, freezing the solution. A small amount of C_6D_5Cl was layered atop the frozen solution as a buffer, and the contents again were frozen. Roughly 0.3 mL of a C_6D_5Cl solution of 20.4 mg (0.0318 mmol) [**HPt**][PF_6] was added to the tube, which was then sealed and the contents frozen again. The tube was then removed from the box and the contents kept frozen in a dry ice/ acetone bath. At the NMR spectrometer, the tube was removed from the bath, and warmed until just thawing, at which point it was vigorously shaken and inserted into the probe (held at 25 °C). NMR spectra were acquired over ~30 minutes. Initial, spectra showed a mixture of starting materials and a carbene. Shortly thereafter the starting materials were consumed and a mixture of the carbene intermediate and the final alkyl product were observed. Over a few minutes at room temperature the carbene disappears, giving way to alkyl species **10-E$_1$** as the only observed

product, as monitored by $^{31}P\{^{1}H\}$ NMR. Carbene NMR data: **^{1}H NMR** (C_6D_5Cl, 500 MHz –40 °C): δ 0.66 (br), 0.96 (br), 1.32 (br), 1.5-2.1 (br m), 2.32 (br), 7.00 (br), 7.1-7.3 (br m), 7.52 (br), 13.75 (br, Re–C*H*O). **^{31}P{^{1}H} NMR** (C_6D_5Cl, 202 MHz, –40 °C): δ 7.4 (s).

Reductions of trans-[(PPh$_3$)(Ph$_2$P(CH$_2$)$_2$B(C$_8$H$_{14}$))Re(CO)$_4$][OTf] ([1-E$_1$Ph$_1$][OTf])

Reaction of *trans*-[(PPh$_3$)(Ph$_2$P(CH$_2$)$_2$B(C$_8$H$_{14}$))Re(CO)$_4$][OTf] ([1-E$_1$Ph$_1$][OTf]) with 1 equiv NaHBEt$_3$. Attempts to monitor the reduction of [**1-E$_1$Ph$_1$**][OTf] by a single hydride were thwarted by the precipitation of the product only a few minutes after reaction. A vial charged with 23.7 mg (0.0227 mmol) [**1-E$_1$Ph$_1$**][OTf] and ~0.6 mL THF-*d*$_8$ was stirred rapidly, and 22.7 μL $NaHBEt_3$ (1.0 M in toluene) was added dropwise. After ~10 minutes, significant precipitates had formed, and NMR spectroscopy revealed a mixture of boroxycarbene [^{1}H δ 13.42, $^{31}P\{^{1}H\}$ δ 9.3 ($\mathcal{J}_{PP}$ = 97 Hz) and 15.4 ($\mathcal{J}_{PP}$ = 97 Hz)] and Re–H (–4.94, d, $\mathcal{J}_{PH}$ = 22.6 Hz). The large coupling constant of the Re–H signal suggests it *trans*-$(PPh_3)Re(CO)_4H$, probably formed from a small amount of *trans*-$Re(CO)_4I$ remaining from the synthesis of [**1-E$_1$Ph$_1$**][OTf] (and not from decarbonylation, which would give a *cis*-hydride exclusively). No further reduction products were observed before complete precipitation of the boroxycarbene, suggesting that disproportionation is at least slower than precipitation in THF (significant disproporationation of **2-E**$_2$ is observed in 15 minutes in THF).

Reaction of *trans*-[(PPh$_3$)(Ph$_2$P(CH$_2$)$_2$B(C$_8$H$_{14}$))Re(CO)$_4$][OTf] ([1-E$_1$Ph$_1$][OTf]) with 2 equiv NaHBEt$_3$. 0.130 g (0.125 mmol) [**1-E$_1$Ph$_1$**][OTf] was dissolved in 2 mL THF with stirring. To the rapidly stirring clear colorless solution was

added dropwise 250 μL $NaHBEt_3$ (1.0 M in toluene). The solution turned bright yellow as the addition proceeded. The mixture was allowed to stir for 17 hours (note: NMR scale reactions showed the reaction is complete within minutes), after which time the solvents were removed. A small amount (<1 mL) of benzene was added to the oily residues before drying again. The crude mixture was washed with benzene, and extracted with THF. Removal of the THF filtrate *in vacuo* yielded 0.098 g (0.1 mmol, 85%) C–C coupled acyl anion [**3-E$_1$Ph$_1$**]$^-$. Analytically pure single crystals suitable for X-Ray diffraction were grown from vapor diffusion of pentane into a THF solution of [Na][**3-E$_1$Ph$_1$**]. **^{1}H NMR** (THF-d_8, 600 MHz): δ 0.19 (1H), 0.69 (q, $\mathcal{J}_{PH}$ = 13.7 Hz, 1H), 1.12 (m, 2H), 1.4 (m, 2H), 1.5 (m, 2H), 1.53 (m, 1H), 1.64 (m, 1H), 1.7-1.9 (m, 5H), 2.1 (m, 1H), 2.71 (br t, $\mathcal{J}_{PH}$ = 14.0 Hz, 1H), 3.1 (m, 1H), 3.86 (d, $^2\mathcal{J}_{HH}$ = 15.3 Hz), 4.10 (d, $^2\mathcal{J}_{HH}$ = 15.3 Hz), 7.11-7.14 (m, 4H), 7.23-7.33 (m, 10H), 7.39 (dd, J = 7.5, 10.5 Hz, 4H), 7.64 (m, 5H), 8.03 (t, J = 8.4 Hz, 2H). **^{31}P{^{1}H} NMR**. δ 11.4 (d, $\mathcal{J}_{PP}$ = 159.7 Hz, 1P), 17.4 (d, $\mathcal{J}_{PP}$ = 159.8 Hz, 1P). **^{11}B{^{1}H} NMR**. No signal observed apart from borosilicate in Varian probe. **^{13}C{^{1}H} NMR** (THF-d_8, 125 MHz): δ 13.63 (br), 26.09 (d, $\mathcal{J}_{PC}$ = 23.8 Hz, $Ph_2PCH_2CH_2BR_2$), 26.74, 27.16, 32.32, 32.87, 34.76, 34.85, 98.93, 128.00 (d, $\mathcal{J}_{PC}$ = 8.9 Hz, *m*-$Ph_2PCH_2CH_2BR_2$), 128.35 (d, $\mathcal{J}_{PC}$ = 9.2 Hz, *m*-$Ph_2PCH_2CH_2BR_2$), 128.44 (d, $\mathcal{J}_{PC}$ = 9.2 Hz, *m*-PPh_3), 128.59 (d, $\mathcal{J}_{PC}$ = 1.5 Hz, *p*-$Ph_2PCH_2CH_2BR_2$), 129.52 (d, $\mathcal{J}_{PC}$ = 1.4 Hz, *p*-PPh_3), 129.86 (d, $\mathcal{J}_{PC}$ = 1.3 Hz, *p*-$Ph_2PCH_2CH_2BR_2$), 132.50 (d, $\mathcal{J}_{PC}$ = 9.0 Hz, *o*-$Ph_2PCH_2CH_2BR_2$), 135.31 (d, $\mathcal{J}_{PC}$ = 10.6 Hz, *o*-PPh_3), 135.35 (d, $\mathcal{J}_{PC}$ = 9.8 Hz, *o*-$Ph_2PCH_2CH_2BR_2$), 137.33 (dd, $\mathcal{J}_{PC}$ = 38.5, 2.1 Hz, *ipso*-$Ph_2PCH_2CH_2BR_2$), 139.85 (d, $\mathcal{J}_{PC}$ = 40.8 Hz, *ipso*-PPh_3), 142.99 (d, $\mathcal{J}_{PC}$ = 46.4 Hz *ipso*-$Ph_2PCH_2CH_2BR_2$), 203.58 (dd, $\mathcal{J}_{PC}$ = 8.9, 9.6 Hz, Re–*C*O), 210.16 (dd, $\mathcal{J}_{PC}$ = 5.9, 7.2 Hz,

Re–*C*O), 297.45 (dd, $\mathcal{J}_{PC}$ = 10.6, 12.0, Re*C*(O)CH_2OBR_3). **IR** (THF): ν_{CO}, 1934, 1841; ν_{acyl} 1572 cm^{-1}. **Anal. Calcd.** for $C_{44}H_{45}BNaO_4P_2Re$: C, 57.46; H, 4.93. Found: C, 57.56; H, 4.95.

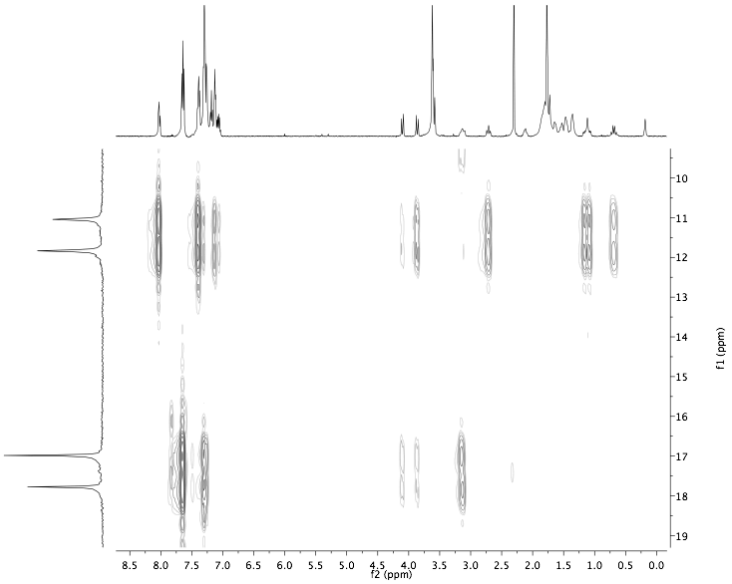

Figure 3.55. ^1H–^{31}P gHMBC of [**3-E$_1$Ph$_1$**]$^-$.

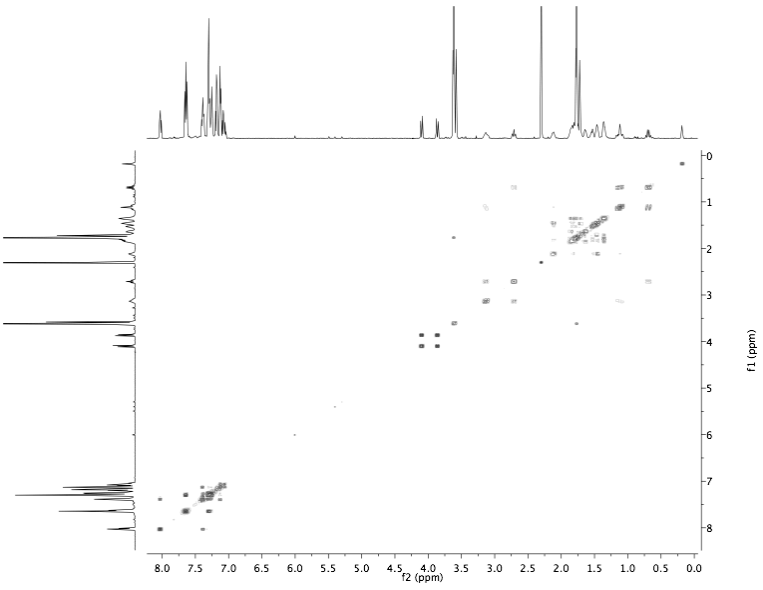

Figure 3.56. ^1H–^1H gCOSY of [**3-E$_1$Ph$_1$**]$^-$.

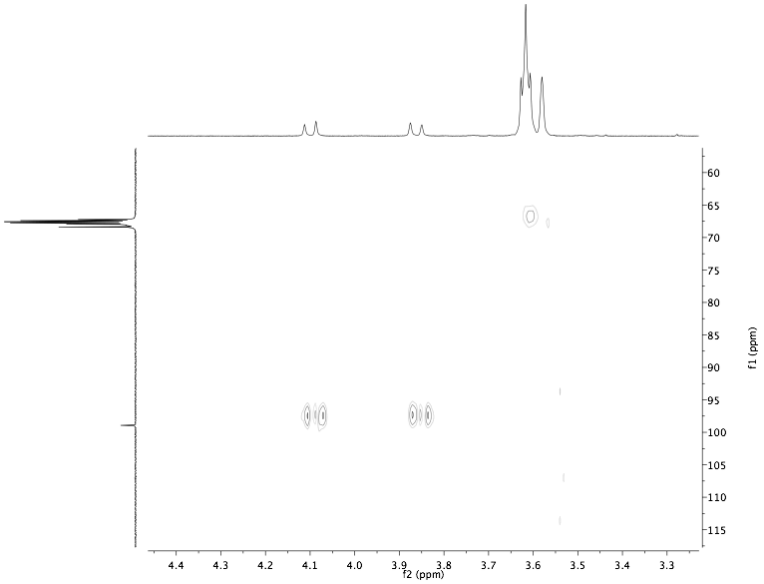

Figure 3.57. $^{1}H–^{13}C$ gHMQC NMR of [**3-E$_1$Ph$_1$**]$^-$ showing correlation between Re–C(O)*C*H$_2$O– and Re–C(O)C*H$_2$*O–.

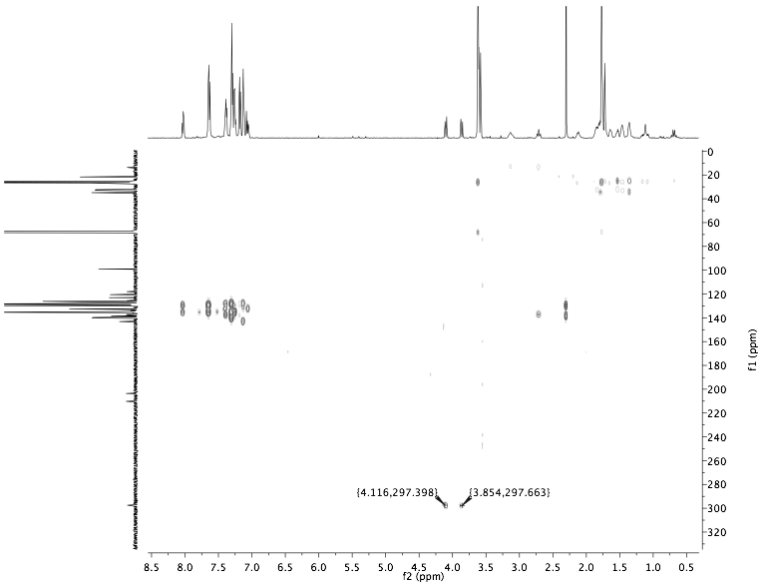

Figure 3.58. $^{1}H–^{13}C$ gHMBC NMR of [**3-E$_1$Ph$_1$**]$^-$ with 2-bond correlation to acyl carbon highlighted.

Reaction of *trans*-[(PPh$_3$)(Ph$_2$P(CH$_2$)$_2$B(C$_8$H$_{14}$))Re(CO)$_4$][OTf] ([1-E$_1$Ph$_1$][OTf]) with 2 equiv [HPt][PF$_6$] (with and without triethylborane). A vial was charged with 31.9 mg (0.0306 mmol) [**1-E$_1$Ph$_1$**][OTf] and ~0.6 mL THF-*d$_8$*. With

stirring, solid [**HPt**][PF_6] (39.2 mg, 0.0611, 2 equiv) was added, and the mixture was transferred to a J-Young NMR tube. Before monitoring by NMR could begin, most of the Re-containing material had precipitated as boroxycarbene (see above). No further reduction or C–C bond formation products were observed by NMR or when the precipitates were extracted with pyridine.

Separate experiments were carried out under similar conditions, only with 1 and 10 equiv BEt_3 (1.0 M in hexanes) added after the hydride had been added to the Re. Precipitation still occurred, although in the case of 1 equiv, trace C–C coupled products were observed after ~4 hours.

Reaction of [Na][(PPh_3)($Ph_2P(CH_2)_2B(C_8H_{14})$)$Re(CO)_2$($C(O)CH_2O$—)] with MeOTf. A 20 mL scintillation vial was charged with 55.3 mg (0.0485 mmol) [$Na(THF)_3$][**3-E$_1$Ph$_1$**] and 2 mL C_6H_5Cl. With stirring, 5.5 μL (0.0485 mmol) MeOTf was added by syringe. The reaction was stirred overnight (NMR studies show reaction to be complete in as little as 30 minutes, however), at which time it was filtered, washed with C_6H_6, and the solvent removed from the filtrate under vacuum, affording 33 mg (0.0362 mmol, 75%) **12** as a yellow powder. Single crystals (large yellow blocks) were grown from vapor diffusion of pentane into a C_6H_5Cl (or C_6H_6) solution of **12**. **^{1}H NMR** (C_6D_6, 500 MHz): δ 1.00 (br, 1H, $Ph_2PCH_2CH_2B(C_8H_{14})$), 1.24 (m, 1H $Ph_2PCH_2CH_2B(C_8H_{14})$), 1.31 (br, 1H, $Ph_2PCH_2CH_2B(C_8H_{14})$), 1.66-1.77 (m, 1H, $Ph_2PCH_2CH_2B(C_8H_{14})$), 1.96-2.47 (m, 12H, $Ph_2PCH_2CH_2B(C_8H_{14})$), 2.74 (m, 1H, $Ph_2PCH_2CH_2B(C_8H_{14})$), 2.80 (3H, $Re{=}C(OCH_3)CH_2O$–), 3.30 (m, 1H, $Ph_2PCH_2CH_2B(C_8H_{14})$), 6.8-6.9 (m, 2H,

Ph$_2$PCH$_2$CH$_2$B(C$_8$H$_{14}$)), 6.99 (m, 4H, *Ph*$_2$PCH$_2$CH$_2$B(C$_8$H$_{14}$)), 7.08 (m, 9H, P*Ph*$_3$), 7.65 (m, 2H, *Ph*$_2$PCH$_2$CH$_2$B(C$_8$H$_{14}$)), 7.71 (m, 6H, P*Ph*$_3$), 7.84 (m, 2H, *Ph*$_2$PCH$_2$CH$_2$B(C$_8$H$_{14}$)). **^{31}P{^{1}H} NMR** (C$_6$D$_6$, 202 MHz): δ 5.7 (d, $^2\mathcal{J}_{PP}$ = 114.2 Hz, 1P), 13.5 (d, $^2\mathcal{J}_{PP}$ = 114.3 Hz, 1P). **^{13}C{^{1}H} NMR** (C$_6$D$_6$, 126 MHz): δ 15.00 (br), 24.39 (br), 24.90 (br), 26.06 (Ph$_2$PCH$_2$CH$_2$B(*C*$_8$H$_{14}$)), 26.51 (Ph$_2$PCH$_2$CH$_2$B(*C*$_8$H$_{14}$)), 27.96 (d, $\mathcal{J}_{PC}$ = 26.1 Hz, Ph$_2$P*C*H$_2$CH$_2$B(C$_8$H$_{14}$)), 32.00 (Ph$_2$PCH$_2$CH$_2$B(*C*$_8$H$_{14}$)), 32.25 (Ph$_2$PCH$_2$CH$_2$B(*C*$_8$H$_{14}$)), 34.05 (Ph$_2$PCH$_2$CH$_2$B(*C*$_8$H$_{14}$)), 34.51 (Ph$_2$PCH$_2$CH$_2$B(*C*$_8$H$_{14}$)), 66.55 (Re=C(O*C*H$_3$)CH$_2$O–), 90.99 (Re=C(OCH$_3$)*C*H$_2$O–), 128.55 (d, JPC = 9.1 Hz, *m*-*Ph*$_2$PCH$_2$CH$_2$B(C$_8$H$_{14}$)), 128.74 (d, $\mathcal{J}_{PC}$ = 9.7 Hz, *m*-P*Ph*$_3$), 130.36 (*p*-PPh$_3$), 130.79 (d, $\mathcal{J}_{PC}$ = 8.7 Hz, *p*-*Ph*$_2$PCH$_2$CH$_2$B(C$_8$H$_{14}$)), 133.72 (d, $\mathcal{J}_{PC}$ = 9.2 Hz, *o*-*Ph*$_2$PCH$_2$CH$_2$B(C$_8$H$_{14}$)), 133.86 (d, $\mathcal{J}_{PC}$ = 10.7 Hz, *o*-PPh$_3$), 136.73 (d, $\mathcal{J}_{PC}$ = 45.2 Hz, *ipso*-P*Ph*$_3$), 144.75 (d, $\mathcal{J}_{PC}$ = 46.6 Hz, *ipso*-*Ph*$_2$PCH$_2$CH$_2$B(C$_8$H$_{14}$)), 203.43 (br t, $\mathcal{J}_{PC}$ ~ 7.9 Hz, *C*O), 209.03 (br t, $\mathcal{J}_{PC}$ ~ 9.9 Hz, *C*O), 307.18 (br, Re=*C*(OCH$_3$)CH$_2$O–). **IR** (C$_6$H$_6$): ν_{CO}, 1989, 1857 cm^{-1}. Anal. calcd. for C$_{45}$H$_{48}$BO$_4$P$_2$Re: C, 59.27; H, 5.31. Found: C, 59.54; H, 5.26; N, <0.02.

Reductions of [(Ph$_2$P(CH$_2$)$_3$B(C$_8$H$_{14}$))Re(CO)$_5$][OTf] ([1-P$_1$][OTf])

Reaction of [1-P$_1$][OTf] with [HPt][PF$_6$]. A 10 mL scintillation vial was charged with 24.6 mg (0.0299 mmol) [**1-P$_1$**][OTf], which was dissolved in ~0.6 mL C$_6$D$_5$Cl. To the stirring solution was added 19.2 mg (0.0299 mmol) [**HPt**]$^+$ as a solid portionwise. After stirring for a couple minutes, the mixture was transferred to a J-Young NMR tube, and monitored by ^{1}H and ^{31}P{^{1}H} NMR. After 30 minutes, the ratio of formyl: Re–H was 1.00:0.03. After 1.5 hours, the ratio was 1.00:0.61. After 2.5 hours the ratio was 1.00:28.68. After 5.5 hours, all of the formyl was consumed. During the course of the reaction what

appeared to be a Re-alkyl (4.72, d, $\mathcal{J}_{PH}$ = 6.6 Hz) was present; the small (~10 %) amount remained constant over the course of the reaction. NMR spectra data for Re–CHO species: **^{1}H NMR** (C_6D_5Cl, 300 MHz): δ 0.89 (br, 2H, $Ph_2PCH_2CH_2CH_2B(C_8H_{14})$), 1.04 (br, 2H, $Ph_2PCH_2CH_2CH_2B(C_8H_{14})$), 1.52-1.86 (m, 12H, $Ph_2PCH_2CH_2CH_2B(C_8H_{14})$), 1.98 (m, 2H, $Ph_2PCH_2CH_2CH_2B(C_8H_{14})$), 2.51 (m, 2H, $Ph_2PCH_2CH_2CH_2B(C_8H_{14})$), 7.19 (m, 6H, $Ph_2PCH_2CH_2CH_2B(C_8H_{14})$), 7.42-7.49 (m, 4H, $Ph_2PCH_2CH_2CH_2B(C_8H_{14})$), 13.71 (1H, Re–C*H*O). **^{31}P{^{1}H} NMR** (C_6D_5Cl, 121 MHz): δ 1.7.

In a separate reaction, 5.2 mg (0.0063 mmol) [**1-P$_1$**][OTf] was dissolved in 0.5 mL CH_2Cl_2 and treated with 4.1 mg (0.0063 mmol) [**HPt**][PF_6]. The reaction mixture was transferred to a solution IR cell for analysis, which showed nearly complete reaction to a formyl species (small amounts of residual starting material were observed). **IR** (CH_2Cl_2): ν_{CO} 2100 (m), 2018 (m), 1983 (s), 1939 (sh), ν_{CHO} 1508 cm^{-1}.

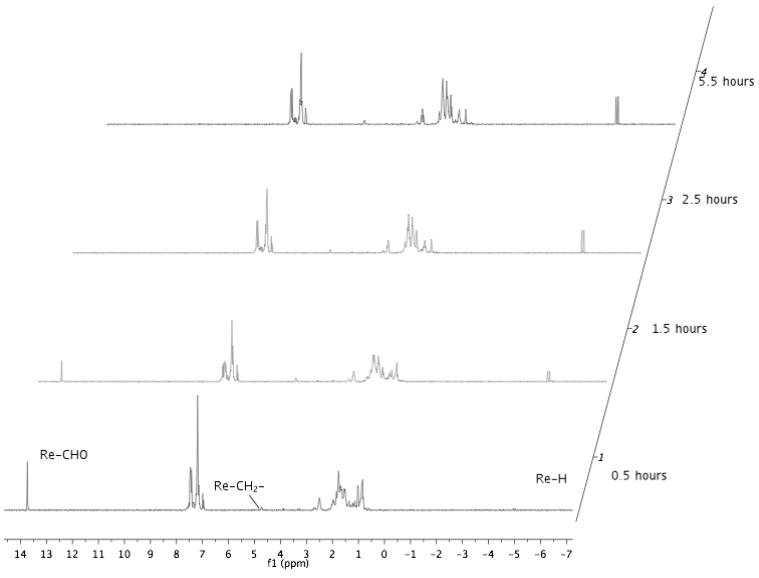

Figure 3.59. ^{1}H NMR time course of [**1-P$_1$**]$^+$ + [**HPt**]$^+$.

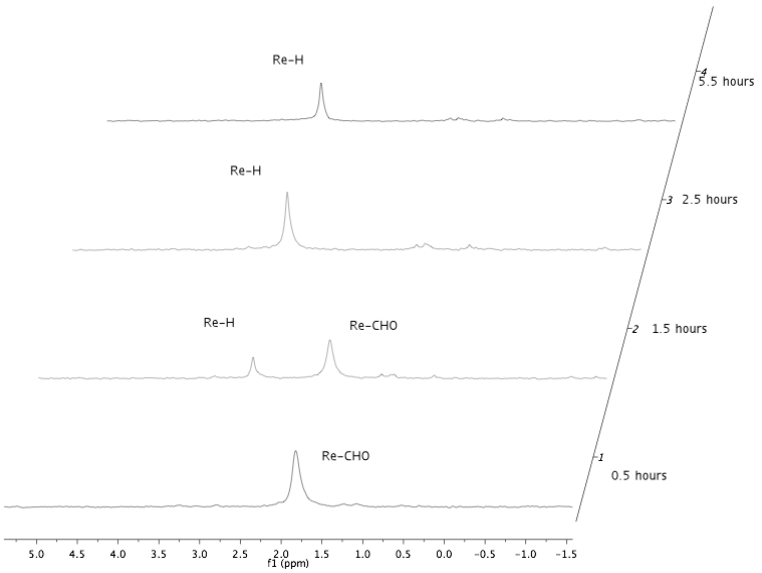

Figure 3.60. $^{31}P\{^{1}H\}$ NMR time course of [**1-P$_1$**]$^+$ + [**HPt**]$^+$.

References

1. (a) Khodakov, A. Y.; Chu, W.; Fongarland, P. *Chem. Rev.* **2007**, *107*, 1692; (b) Rofer-DePoorter, C. K. *Chem. Rev.* **1981**, *81*, 447.
2. World Energy Assessment Report: Energy and the Challenge of Sustainability. Program, U. N. D., Ed. United Nations: New York, 2000.
3. (a) Cutler, A. R.; Hanna, P. K.; Vites, J. C. *Chem. Rev.* **1988**, *88*, 1363; (b) Gladysz, J. A. *Adv. Organomet. Chem.* **1982**, *20*, 1; (c) Herrmann, W. A. *Angew. Chem. Int. Ed.* **1982**, *21*, 117; (d) Wolczanski, P. T.; Bercaw, J. E. *Acc. Chem. Res.* **1986**, *13*, 121.
4. Brown, S. L.; Davies, S. G. *J. Chem. Soc., Chem. Commun.* **1986**, 84.
5. (a) Evans, W. J.; Grate, J. W.; Doedens, R. J. *J. Am. Chem. Soc.* **1985**, *107*, 1671; (b) Fagan, P. J.; Moloy, K. G.; Marks, T. J. *J. Am. Chem. Soc.* **1981**, *103*, 6959; (c) Gambarotta, S.; Floriani, C.; Chiesivilla, A.; Guastini, C. *J. Am. Chem. Soc.* **1983**, *105*, 1690; (d) Manriquez, J. M.; McAlister, D. R.; Sanner, R. D.; Bercaw, J. E. *J. Am. Chem. Soc.* **1978**, *100*, 2716; (e) Miller, R. L.; Toreki, R.; LaPointe, R. E.; Wolczanski, P. T.; Van Duyne, G. D.; Roe, D. C. *J. Am. Chem. Soc.* **1993**, *115*, 5570; (f) Werkema, E. L.; Maron, L.; Eisenstein, O.; Andersen, R. A. *J. Am. Chem. Soc.* **2007**, *129*, 2529; (g) Shima, T.; Hou, Z. *J. Am. Chem. Soc.* **2006**, *128*, 8124.
6. (a) Demitras, G. C.; Muetterties, E. L. *J. Am. Chem. Soc.* **1977**, *99*, 2796; (b) Dombek, B. D. *Adv. Catal.* **1983**, *32*, 325.

7. (a) Miller, A. J. M.; Labinger, J. A.; Bercaw, J. E. *J. Am. Chem. Soc.* **2008**, *130*, 11874; (b) Elowe, P. R.; West, N. M.; Labinger, J. A.; Bercaw, J. E. *Organometallics* **2009**, *28*, 6218; (c) Miller, A. J. M.; Labinger, J. A.; Bercaw, J. E. *J. Am. Chem. Soc.* **2010**, *132*, 3301.
8. (a) Miedaner, A.; DuBois, D. L.; Curtis, C. J.; Haltiwanger, R. C. *Organometallics* **1993**, *12*, 299; (b) Curtis, C. J.; Miedaner, A.; Ellis, W. W.; DuBois, D. L. *J. Am. Chem. Soc.* **2002**, *124*, 1918; (c) DuBois, M. R.; DuBois, D. L. *Chem. Soc. Rev.* **2009**, *38*, 62.
9. (a) Casey, C. P.; Andrews, M. A.; McAlister, D. R.; Rinz, J. E. *J. Am. Chem. Soc.* **1980**, *102*, 1927; (b) Casey, C. P.; Neumann, S. M. *J. Am. Chem. Soc.* **1976**, *98*, 5395; (c) Collman, J. P.; Winter, S. R. *J. Am. Chem. Soc.* **1973**, *95*, 4089; (d) Tam, W.; Wong, W.-K.; Gladysz, J. A. *J. Am. Chem. Soc.* **1979**, *101*, 1589.
10. Crawford, E. J.; Bodnar, T. W.; Cutler, A. R. *J. Am. Chem. Soc.* **1986**, *108*, 6202.
11. Yamamoto, H., *Lewis acids in organic synthesis*. Wiley-VCH: Weinheim ; New York, 2000.
12. (a) Butts, S. B.; Holt, E. M.; Strauss, S. H.; Alcock, N. W.; Stimson, R. E.; Shriver, D. F. *J. Am. Chem. Soc.* **1979**, *101*, 5864; (b) Butts, S. B.; Strauss, S. H.; Holt, E. M.; Stimson, R. E.; Alcock, N. W.; Shriver, D. F. *J. Am. Chem. Soc.* **1980**, *102*, 5093; (c) Grimmett, D. L.; Labinger, J. A.; Bonfiglio, J. N.; Masuo, S. T.; Shearin, E.; Miller, J. S. *J. Am. Chem. Soc.* **1982**, *104*, 6858; (d) Labinger, J. A.; Miller, J. S. *J. Am. Chem. Soc.* **1982**, *104*, 6856; (e) Labinger, J. A.; Bonfiglio, J. N.; Grimmett, D. L.; Masuo, S. T.; Shearin, E.; Miller, J. S. *Organometallics* **1983**, *2*, 733.
13. Maitlis, P. M.; Zanotti, V. *Chem. Commun.* **2009**, 1619.
14. (a) Fischbach, A.; Bazinet, P. R.; Waterman, R.; Tilley, T. D. *Organometallics* **2008**, *27*, 1135; (b) Vergnaud, J.; Grellier, M.; Bouhadir, G.; Vendier, L.; Sabo-Etienne, S.; Bourissou, D. *Organometallics* **2008**, *27*, 1140.
15. Gibson, D. H.; Owens, K.; Mandal, S. K.; Sattich, W. E.; Franco, J. O. *Organometallics* **1989**, *8*, 498.
16. (a) Baldwin, S. M.; Bercaw, J. E.; Brintzinger, H. H. *J. Am. Chem. Soc.* **2008**, *130*, 17423; (b) Benesi, H. A.; Hildebrand, J. H. *J. Am. Chem. Soc.* **1949**, *71*, 2703; (c) Rose, N. J.; Drago, R. S. *J. Am. Chem. Soc.* **1959**, *81*, 6138.
17. (a) Narayanan, B. A.; Amatore, C.; Kochi, J. K. *Organometallics* **1987**, *6*, 129; (b) Narayanan, B. A.; Amatore, C. A.; Kochi, J. K. *Organometallics* **1984**, *3*, 802; (c) Sumner, C. E.; Nelson, G. O. *J. Am. Chem. Soc.* **1984**, *106*, 432.
18. Elowe, P. R. The Selective Oligomerization of Ethylene Using Chromium Diphosphine Catalysts and The Synthesis and Reactivity of Group 7 Carbonyl Derivatives Relevant to Synthesis Gas Conversion. Ph.D. Thesis, California Institute of Technology, Pasadena, CA, 2009.
19. (a) Brown, H. C.; Verbrugge, C.; Snyder, C. H. *J. Am. Chem. Soc.* **1961**, *83*, 1001; (b) Brown, H. C.; Hébert, N. C.; Snyder, C. H. *J. Am. Chem. Soc.* **1961**, *83*, 1001; (c) Brown, H. C.; Snyder, C. H. *J. Am. Chem. Soc.* **1961**, *83*, 1002.
20. Lambert, J. B.; Zhang, S.; Ciro, S. M. *Organometallics* **1994**, *13*, 2430.
21. Ingham, W. L.; Coville, N. J. *Organometallics* **1992**, *11*, 2551.

22. Kubo, K.; Nakazawa, H.; Nakahara, S.; Yoshino, K.; Mizuta, T.; Miyoshi, K. *Organometallics* **2000**, *19*, 4932.
23. Luan, L.; Brookhart, M.; Templeton, J. L. *Organometallics* **1992**, *11*, 1433.
24. Garrou, P. E. *Chem. Rev.* **1981**, *81*, 229.
25. Li, D. Y.; Keresztes, I.; Hopson, R.; Williard, P. G. *Acc. Chem. Res.* **2009**, *42*, 270.
26. (a) Cohen, Y.; Avram, L.; Frish, L. *Angew. Chem. Int. Ed.* **2005**, *44*, 520; (b) Macchioni, A.; Ciancaleoni, G.; Zuccaccia, C.; Zuccaccia, D. *Chem. Soc. Rev.* **2008**, *37*, 479.
27. (a) Stephan, D. W.; Erker, G. *Angew. Chem. Int. Ed.* **2010**, *49*, 46; (b) Welch, G. C.; Stephan, D. W. *J. Am. Chem. Soc.* **2007**, *129*, 1880.
28. DuBois, D. L.; Blake, D. M.; Miedaner, A.; Curtis, C. J.; DuBois, M. R.; Franz, J. A.; Linehan, J. C. *Organometallics* **2006**, *25*, 4414.
29. Miedaner, A.; Raebiger, J. W.; Curtis, C. J.; Miller, S. M.; DuBois, D. L. *Organometallics* **2004**, *23*, 2670.
30. Lin, W. B.; Wilson, S. R.; Girolami, G. S. *Inorg. Chem.* **1997**, *36*, 2662.
31. Crawford, E. J.; Lambert, C.; Menard, K. P.; Cutler, A. R. *J. Am. Chem. Soc.* **1985**, *107*, 3130.
32. Lindner, E.; von Au, G. *Angew. Chem. Int. Ed.* **1980**, *19*, 824.
33. Tam, W.; Lin, G.-Y.; Gladysz, J. A. *Organometallics* **1982**, *1*, 525.
34. Eaton, G. R. *J. Chem. Ed.* **1969**, *46*, 547.
35. (a) Mckinney, R. J.; Kaesz, H. D. *J. Am. Chem. Soc.* **1975**, *97*, 3066; (b) Casey, C. P.; Scheck, D. M. *J. Am. Chem. Soc.* **1980**, *102*, 2723; (c) Casey, C. P.; Jones, W. D. *J. Am. Chem. Soc.* **1980**, *102*, 6154; (d) Warner, K. E.; Norton, J. R. *Organometallics* **1985**, *4*, 2150; (e) Martin, B. D.; Warner, K. E.; Norton, J. R. *J. Am. Chem. Soc.* **1986**, *108*, 33.
36. (a) Casey, C. P.; Andrews, M. A.; McAlister, D. R. *J. Am. Chem. Soc.* **1979**, *101*, 3371; (b) Berke, H.; Weiler, G. *Angew. Chem. Int. Ed.* **1982**, *21*, 150.
37. (a) Djukic, J. P.; Dotz, K. H.; Pfeffer, M.; De Cian, A.; Fischer, J. *Inorg. Chem.* **1998**, *37*, 3649; (b) Lenhert, P. G.; Lukehart, C. M.; Sotiropoulos, P. D.; Srinivasan, K. *Inorg. Chem.* **1984**, *23*, 1807; (c) Padolik, L. L.; Gallucci, J. C.; Wojcicki, A. *J. Am. Chem. Soc.* **1993**, *115*, 9986.
38. Pangborn, A. B.; Giardello, M. A.; Grubbs, R. H.; Rosen, R. K.; Timmers, F. J. *Organometallics* **1996**, *15*, 1518.
39. Schmidt, S. P.; Nitschke, J.; Trogler, W. C.; Huckett, S. I.; Angelici, R. J. *Inorg. Synth.* **1989**, *26*, 113.
40. Brown, H. C.; Kulkarni, S. U. *J. Organomet. Chem.* **1979**, *168*, 281.
41. Schore, N. E.; LaBelle, B. E. *J. Org. Chem.* **1981**, *46*, 2306.
42. Hirano, K.; Yorimitsu, H.; Oshima, K. *Org. Lett.* **2005**, *7*, 4689.
43. Yakelis, N. A.; Bergman, R. G. *Organometallics* **2005**, *24*, 3579.
44. Chen, H.-C.; Chen, S.-H. *J. Phys. Chem.* **1984**, *88*, 5118.
45. Gabler, T.; Paschke, A.; Schuurmann, G. *J. Chem. Eng. Data* **1996**, *41*, 33.
46. Wolfram Alpha (www.wolframalpha.com).
47. Fulmer, G. R.; Miller, A. J. M.; Sherden, N. H.; Gottlieb, H. E.; Nudelman, A.; Stoltz, B. M.; Bercaw, J. E.; Goldberg, K. I. *Organometallics* **2010**, *29*, 2176.

Chapter 4

Homogeneous CO Hydrogenation: Dihydrogen Activation Involves a Frustrated Lewis Pair Instead of a Platinum Complex

Adapted in part from:
Miller, A. J. M.; Labinger, J. A.; Bercaw, J. E. *J. Am. Chem. Soc.* **2010**, *132*, 3301.
http://dx.doi.org/10.1021/ja100574n

Chapter 4

Introduction

Since the oil crisis of the 1970s there has been interest in developing selective, homogeneously catalyzed conversion of synthesis gas (syngas; CO/H_2) to valuable hydrocarbons and oxygenates, as an alternative to the nonselective Fischer-Tropsch (F–T) process.[1] Our approach to homogeneous CO hydrogenation involves a multicomponent catalyst system, consisting of a metal carbonyl complex where CO is coordinated and activated, a late transition metal complex that heterolytically cleaves H_2 to form a nucleophilic metal hydride,[2] and a (Lewis or Brønsted) acid site to promote hydride transfer to CO and/or C–C bond formation steps.[3] A stoichiometric example was achieved using the carbonyl cation $[(Ph_2P(CH_2)_2B(C_8H_{14}))_2Re(CO)_4][BF_4]$ ([**1**][BF_4]), which features pendent Lewis acidic borane moieties that facilitate hydride transfer from $[HPt(dmpe)_2][PF_6]$ ([**HPt**][PF_6]; dmpe = 1,2-bis(dimethylphosphino)ethane) as well as further reduction and C–C bond formation (Scheme 4.1).[3b,c]

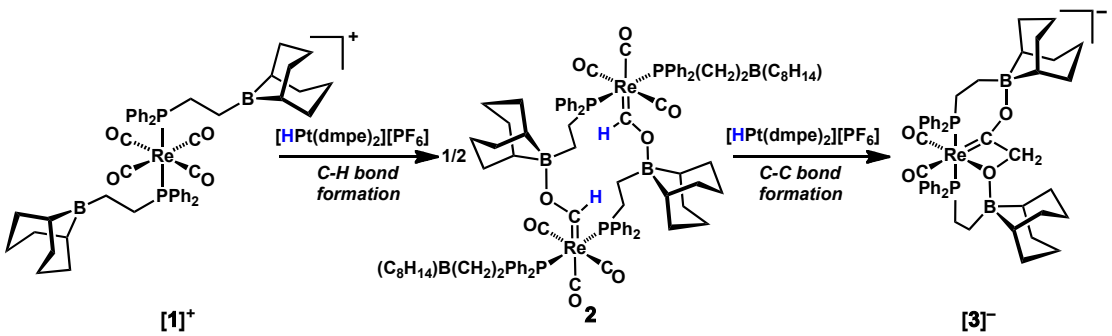

Scheme 4.1

The transformation of Scheme 4.1 used preformed [**HPt**]$^+$. In principle it could be carried out with H_2 and catalytic amounts of [Pt(dmpe)$_2$]$^{2+}$ ([**Pt**]$^{2+}$, Scheme 4.2), but the strong bases (conjugate acid pK_a > 23 in MeCN[4]) that are required in order to produce [**HPt**]$^+$ from H_2 are very likely to attack the carbonyls and/or interact strongly with the Lewis acid sites, disrupting the intended pathway. Instability of the resultant formyl species has also confounded related efforts,[5] but Lewis acids can greatly stabilize reduced CO species.

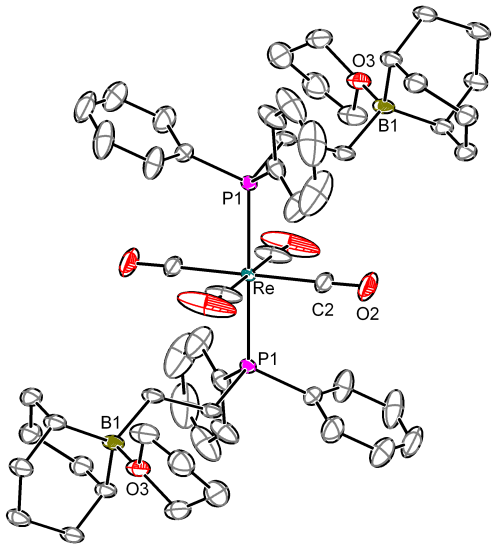

Figure 4.1. Structural representation of [**1**•(THF)$_2$][BF$_4$] (ellipsoids at 50% probability), with BF$_4$ group and hydrogen atoms omitted for clarity. Selected bond distances (Å): Re–C1 1.983(1), Re–C2 1.990(1), Re–P1 2.4324(2), O1–C1 1.127(2), O2–C2 1.135(2), O3–B1 1.683(2).

Results and Discussion

Interaction with Lewis bases

The weak Lewis base THF coordinates to [**1**][BF$_4$] at boron only weakly and reversibly, and does not interfere with the chemistry of Scheme 4.1. The K_{eq} of THF adduct formation with one of the pendent boranes was determined to be 0.19(2) M^{-1} by NMR

titration experiments (presumably, the K_{eq} for binding to the second borane is similar, but the bis(THF) adduct would be only a minor contributor). Consistent with the weak binding, [**1**•(THF)$_2$][BF_4], which was characterized crystallographically (Figure 4.1), readily loses THF on exposure to vacuum. On the other hand, addition of two equivalents pyridine resulted in strong Lewis pair adduct formation, evidenced by a substantial upfield shift of the ^{11}B resonance of [**1**][BF_4] and complete inhibition of the reaction of [**1**][BF_4] with [**HPt**][PF_6]. Interestingly, however, addition of two equivalents of the stronger Lewis base NEt_3 to [**1**][BF_4] shifts the ^{11}B NMR resonance only slightly, indicating minimal interaction, and [**HPt**][PF_6] does reduce [**1**][BF_4] to [**3**]$^-$ in the presence of added NEt_3. This observation suggested to us that [**Pt**]$^{2+}$, in combination with a strong but sterically bulky Lewis base, might catalyze H_2 activation and hydride transfer to a carbonyl of [**1**]$^+$ (Scheme 4.2).

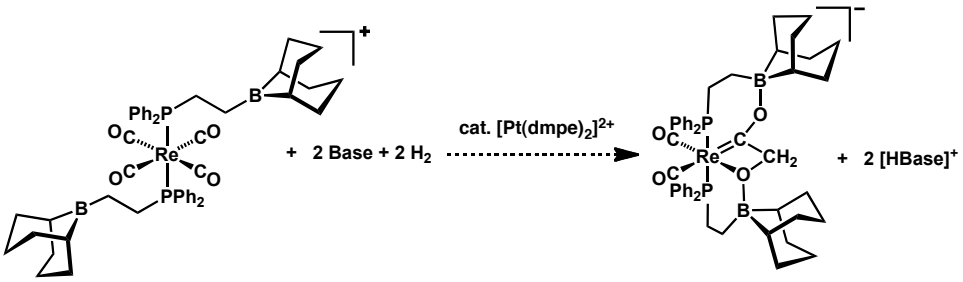

Scheme 4.2

The bulky, strong phosphazene base ^{t}BuNP(pyrrolidinyl)$_3$ (**P$_1$**)[6] seemed a promising candidate. Addition of two equivalents **P$_1$** to a solution of [**1**][BF_4] causes only slight changes in chemical shift and lineshape in ^{1}H, ^{31}P and ^{11}B NMR resonances, indicating weak, reversible interaction. Consequently, [**1**][BF_4] was smoothly reduced by [**HPt**][PF_6] in THF in the presence of **P$_1$**, albeit with concomitant precipitation of [**Pt**][PF_6]$_2$.

Reductions using dihydrogen and substoichiometric platinum.

The insolubility of [**Pt**][PF_6]$_2$ in THF necessitated a change from [BF_4] and [PF_6] salts to the more solubilizing [BAr^F_4] anion (BAr^F_4 = tetrakis(3,5-trifluoromethylphenyl)borate) before attempting catalysis. Gratifyingly, [**1**][BAr^F_4] underwent reductive coupling to form [**3**]$^-$ in the presence of substoichiometric amounts of [**Pt**][BAr^F_4]$_2$, along with excess $\mathbf{P_1}$ and H_2. Presumably steric repulsion prevents $\mathbf{P_1}$ from tightly binding the borane or attacking the carbonyl, even though [$\mathbf{HP_1}$]$^+$ has a pK_a of 28.4 in MeCN,[7] making $\mathbf{P_1}$ a far stronger base than pyridine (which deactivates the system by binding the borane) and similar to KOPh (pK_a 26.6[8]), which reacts irreversibly with [**1**][BF_4]. Furthermore, as expected for such a strong base,[4] THF solutions of $\mathbf{P_1}$ and [**Pt**][BAr^F_4]$_2$ readily react with H_2 to afford [$\mathbf{HP_1}$][BAr^F_4] and [**HPt**][BAr^F_4], with $t_{1/2}$ ~ 10.2 h.

When an NMR tube was charged with cation [**1**][BAr^F_4], 4 equivalents $\mathbf{P_1}$, and 15 mol% [Pt(dmpe)$_2$][BAr^F_4]$_2$ in THF-d_8, no significant reaction was observed; subsequent introduction of 1-4 atm H_2 led to formation of [$\mathbf{HP_1}$][BAr^F_4] and [**HPt**][BAr^F_4] over a few hours. Curiously, no reduction of [**1**]$^+$ was seen as the hydride built up; but after this induction period, the doubly-reduced C–C coupled anion [**3**]$^-$ formed in high yield over a few days at 23 °C (Scheme 4.3).

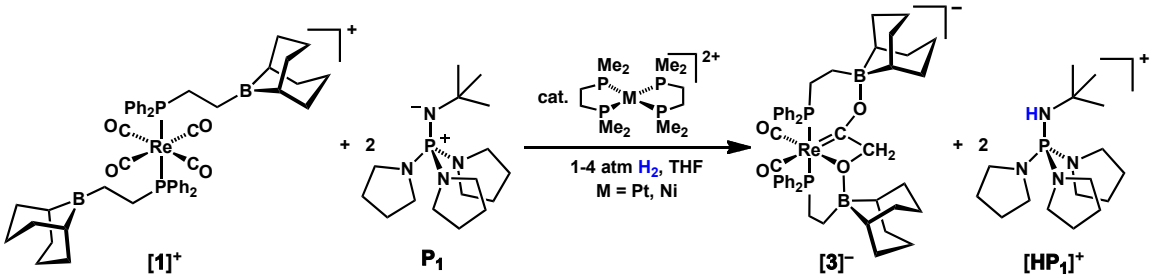

Scheme 4.3

The observed induction period was unexpected, since [**HPt**][PF_6] reacts with [**1**][BF_4] quickly and in high yields;[3b] this turns out to be a consequence of the choice of counterion. The seemingly innocuous substitution of [BAr^F_4] for [BF_4]/[PF_6] to keep [**Pt**]$^{2+}$ soluble in THF has the unintended effect of *completely inhibiting* the stoichiometric reaction of [**1**][BAr^F_4] with [**HPt**][BAr^F_4]. Hydride transfer thus appears to be an equilibrium that lies far towards unreacted [**1**]$^+$ (Scheme 4.4), but can be pushed towards carbene **2** by precipitation of [**Pt**][BF_4]$_x$[PF_6]$_{2-x}$, as in our original report.[3b] Indeed, when carbene **2** was independently prepared in C_6D_5Cl and [**Pt**][BAr^F_4]$_2$ was added, [**1**]$^+$ and [**HPt**]$^+$ formed rapidly. The presence of [**Pt**][BAr^F_4]$_2$ thus inhibits reduction of [**1**]$^+$ to [**3**]$^-$, according to the equilibrium in Scheme 4.4, accounting for the induction period. Hydride transfer cannot proceed until all [**Pt**]$^{2+}$ is converted to [**HPt**]$^+$. A measurable equilibrium could not be established because of the limited solubility of [**Pt**][BAr^F_4]$_2$ in C_6D_5Cl and the instability of carbene **2** toward irreversible disproportionation in THF. Nonetheless, the equilibrium could be inferred by driving it completely to one side or the other under various conditions.

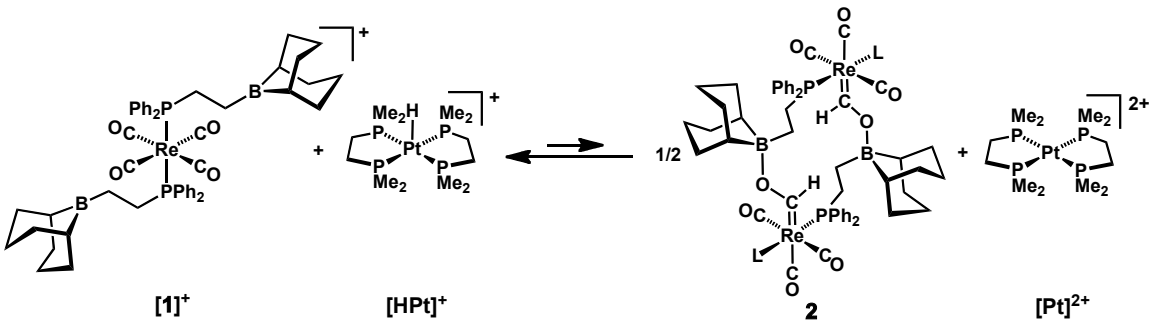

Scheme 4.4

Dihydrogen cleavage and delivery by a frustrated Lewis pair.

The above observations appeared consistent with catalytic H_2 activation by [**Pt**][BAr^F_4]$_2$ and reduction of [**1**]$^+$ to [**3**]$^-$ by [**HPt**][BAr^F_4], proceeding only after all of the [**Pt**][BAr^F_4]$_2$ has been converted to hydride. However, additional observations did not seem to support our hypothesis. While changing the catalyst loading altered the length of the induction period as expected, it did not significantly change the *rate* of reduction of [**1**]$^+$ to [**3**]$^-$ (Figure 4.2). Furthermore, [Ni(dmpe)$_2$][BAr^F_4]$_2$ appeared to catalyze reduction of [**1**]$^+$ by H_2 with rates similar to the Pt analog — despite the observation that [HNi(dmpe)$_2$][PF_6] *does not react* with [**1**][BF_4]. Finally, [**HPt**]$^+$ formed markedly *faster* under the catalytic conditions ($t_{1/2}$ ~ 2.8 h) than in the absence of [**1**]$^+$ ($t_{1/2}$ ~ 10.2 h) (Figure 4.3).

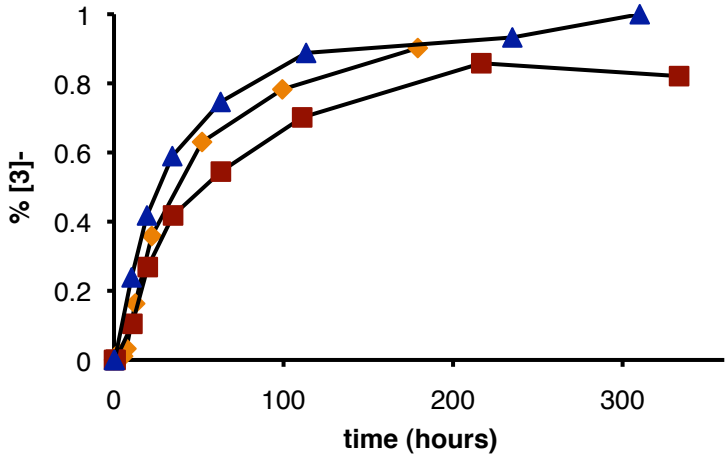

Figure 4.2. Time course of formation of [**3**]$^-$ in the presence of 15 mol % [**Pt**]$^{2+}$ (red squares), 55 mol % [**Pt**]$^{2+}$ (orange diamonds), and 5 mol % [**Ni**]$^{2+}$ (blue triangles). Between 4 and 5.5 equiv phosphazene base were used in each case (non-pseudo first order).

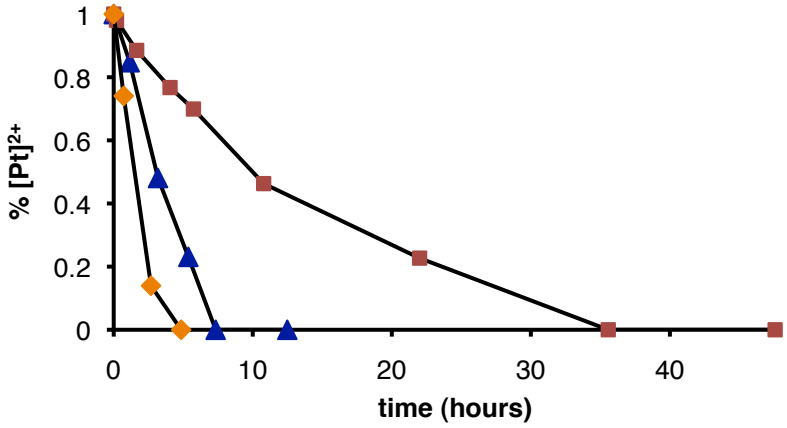

Figure 4.3. Consumption of [**Pt**]$^{2+}$ as it cleaves H_2 with $\mathbf{P_1}$, with and without Lewis acid additives. Red squares, 1 equiv [**Pt**]$^{2+}$, 10 equiv $\mathbf{P_1}$, no [**1**]$^+$; blue triangles, 1 equiv [**Pt**]$^{2+}$, 10 equiv $\mathbf{P_1}$, 1.8 equiv [**1**]$^+$; orange diamonds, 1 equiv [**Pt**]$^{2+}$, 10 equiv P_1, 4 equiv ^{t}Bu$(CH_2)_2$B(C_8H_{14}).

These observations suggest the possibility of activation of H_2 and reduction of [**1**]$^+$ by some species that does not involve the group 10 metal "catalyst" at all. When a mixture of [**1**][BAr^F_4] and $\mathbf{P_1}$ – *but no Pt complex* – was exposed to H_2, reduction to [**3**]$^-$ began immediately, with no induction period, and proceeded to high yields (~92% after 8 days) of

$[\mathbf{3}]^-$, with concomitant formation of $[\mathbf{HP_1}]^+$. We propose that in our "catalytic" reaction H_2 cleavage and hydride delivery is actually mediated by a "frustrated Lewis pair" (FLP). FLPs consist of sterically demanding Lewis acids and bases that cannot form stable Lewis pairs;[9] they have been found to carry out a number of interesting transformations,[10] most notably the cleavage of H_2[11] and metal-free hydrogenation of bulky imines[12] by a number of $B(C_6F_5)_3$/base pairs. Here the FLP would consist of $\mathbf{P_1}$ and the BBN group appended to the ligands of $[\mathbf{1}]^+$.

According to this proposal the (net stoichiometric) reaction proceeds as shown in Scheme 4.5. First, FLP-mediated H_2 cleavage generates small equilibrium amounts of the conjugate acid of $\mathbf{P_1}$ and a pendent borohydride (not observed), which can rapidly transfer H^- to CO to afford **2**. The subsequent transformation involves disproportionation of **2** to give $[\mathbf{3}]^-$ and $[\mathbf{1}]^+$ (rapid in THF relative to the reduction by H_2) and/or reduction of **2** to $[\mathbf{3}]^-$ by another FLP-mediated H_2 cleavage and hydride transfer involving the second appended borane. The small amounts of **2** usually observed at early reaction times are consistent with this mechanism; other minor impurities were also observed, especially when large a excess of $\mathbf{P_1}$ was used.

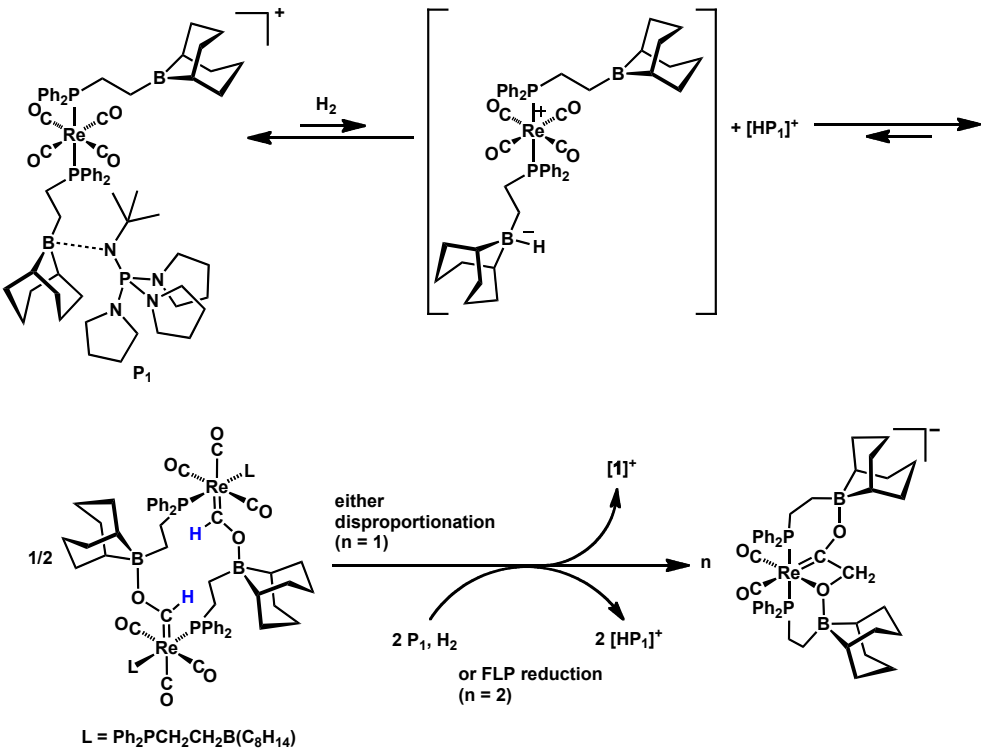

Scheme 4.5

A number of observations support our revised proposal of FLP mediation. Firstly, the Lewis acid and base are both essential: the Lewis acidity can be quenched with two equivalents of pyridine (which coordinate tightly to the boron centers of $[\mathbf{1}]^+$), and under these conditions no formation of $[\mathbf{3}]^-$ under H_2 is observed; if the Lewis base $\mathbf{P_1}$ is removed from the system, $[\mathbf{1}]^+$ alone is not reduced under H_2 alone. Addition of D_2 instead of H_2 resulted in >95% deuterium incorporation at the expected site in $[\mathbf{3}]^-$ (=C(O–)C*D*$_2$O–), confirming that dihydrogen is the source of hydride. The rate of reduction did not change much between H_2 and D_2 (small kinetic isotope effect). The rate of reduction of $[\mathbf{1}]^+$ does increase with increasing amounts of $\mathbf{P_1}$, such that with 20 equivalents $\mathbf{P_1}$ ~70% yield of $[\mathbf{3}]^-$ was obtained after 22 h. Without the need to dissolve $[\mathbf{Pt}]^{2+}$, the requirement to use the solubilizing $[BAr^F{}_4]$ anion was lifted, and indeed $[\mathbf{1}][BF_4]$ is readily reduced by H_2 in the presence of $\mathbf{P_1}$

in similar fashion. If spurious [**Pt**]$^{2+}$ was involved, addition of [BF_4] would likely cause precipitation and reduce activity; no such effect is observed.

The accelerated formation of [**HPt**][BAr^F_4] in the "catalytic" reaction (Figure 4.3) is also understandable under the revised mechanistic hypothesis, if H_2 activation is faster by the FLP than by [**Pt**]$^{2+}$ and $\mathbf{P_1}$. The FLP would cleave H_2 to give first borohydride and then **2**, as in Scheme 4.5; but before irreversible formation of [**3**]$^-$ could occur, the fast equilibrium in Scheme 4.4 would take over, with [**Pt**]$^{2+}$ abstracting a hydride to produce [**HPt**]$^+$. The Lewis acid is the key feature of [**1**]$^+$ that enables this acceleration: addition of ^{t}Bu(CH_2)$_2$B(C_8H_{14}) (**4**, a Lewis acid of similar structure and strength as those in [**1**]$^+$) to mixtures of [**Pt**]$^{2+}$ and $\mathbf{P_1}$ under H_2 also accelerated formation of [**HPt**]$^+$ (Figure 4.3). The reaction rates are broadly consistent with the proposed mechanism, as stoichiometric formation of **2** by $NaHBEt_3$ and production of [**HPt**]$^+$ by hydride abstraction from **2** are both much faster processes than the heterolytic cleavage of H_2 by [**Pt**]$^{2+}$ and $\mathbf{P_1}$. This alternate pathway for formation of [**HPt**]$^+$ (as opposed to direct heterolytic cleavage of H_2 in conjunction with $\mathbf{P_1}$) explains the rate enhancement in the presence of [**1**]$^+$.

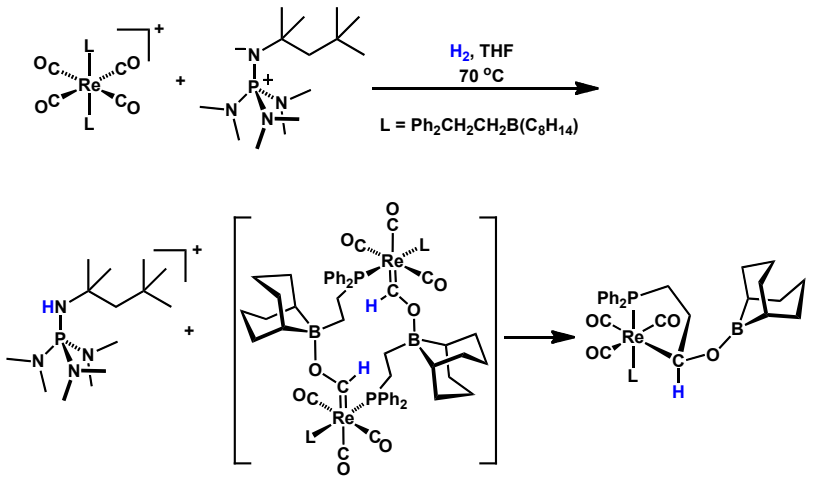

Scheme 4.6

Substitution of the phosphazene base for a bulkier — but less basic — analogue led to diminished reactivity. Hydride transfer only occurred upon mild heating (70 °C), consistent with diminished basicity (by 1-2 units); but at elevated temperatures the boroxycarbene intermediate **2** is not stable. Instead, the major Re-containing product was a ligand-activated variant of **2** (Scheme 4.6); the same product is obtained when **2** is formed in situ, and subsequently heated (See Chapter 3). The choice of Re carbonyl is also critical. Both phosphazene bases react (in the absence of H_2) with less sterically protected metal carbonyls, such as $[(PPh_3)Re(CO)_5]^+$ and $[Cp^*Re(CO)_2(NO)]^+$, presumably by nucleophilic attack at Re–CO.

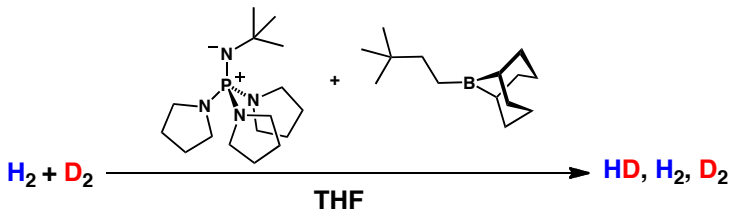

Scheme 4.7

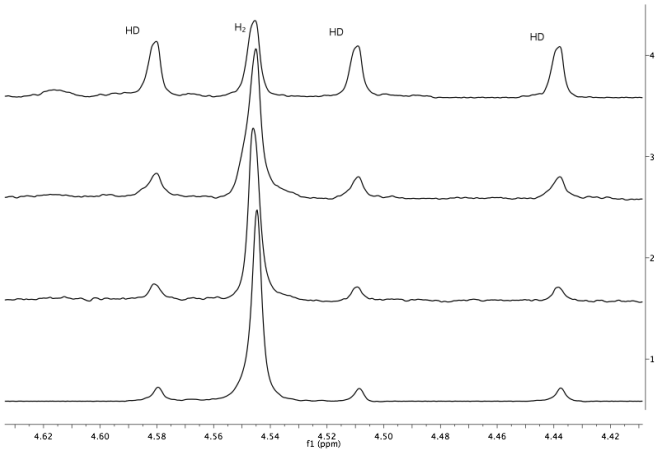

Figure 4.4. ^{1}H NMR of H_2/D_2 comproportionation to HD, monitored at 30 minutes, 24 hours, 2 days, 12 days.

Reductions catalytic in borane.

The mechanism proposed in Scheme 4.5 suggests that an external borane could mediate a similar hydride transfer from H_2 to CO. A metal-free FLP was generated by mixing ^{t}Bu$(CH_2)_2$B(C_8H_{14}) (**4**) and $\mathbf{P_1}$. No reaction of $\mathbf{4/P_1}$ with H_2 was observed by NMR, but the pair does catalyze isotopic comproportionation of H_2 and D_2 to HD, implicating reversible H_2 activation with an equilibrium that lies far towards the FLP. H_2 activation was also implicated from the rapid formation of [**HPt**]$^+$ in the presence of $\mathbf{4/P_1}$ (Figure 4.3). Estimates extrapolated from previous calculations[13] suggest that H_2 cleavage by such a FLP should be close to thermoneutral.

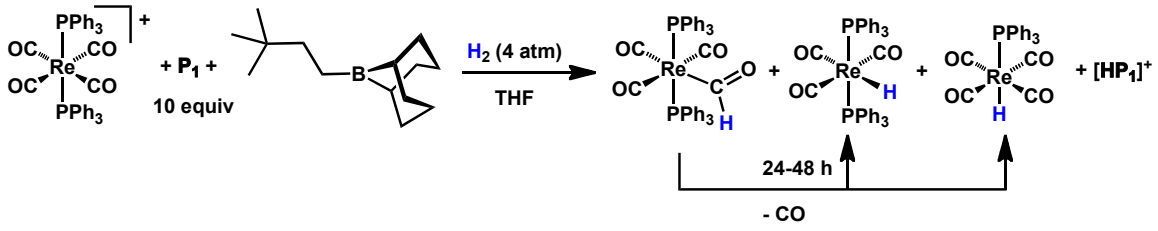

Scheme 4.8

The **4**/**P**$_1$ FLP was next investigated for intermolecular hydride transfer ability (Scheme 4.8). A solution of cation [(PPh$_3$)$_2$Re(CO)$_4$][BAr$^F_4$] (the unadorned analogue of [**1**]$^+$), 10 equivalents **P**$_1$, and one equivalent **4** in THF-d_8 under an H_2 atmosphere showed good conversion (~70% after 24 h at 23 °C) to (PPh$_3$)$_2$Re(CO)$_3$(CHO), along with (PPh$_3$)$_2$Re(CO)$_3$H and (PPh$_3$)Re(CO)$_4$H, the products of decarbonylation of the relatively unstable formyl complex[14] (formyl:hydride, 1.0:0.7).

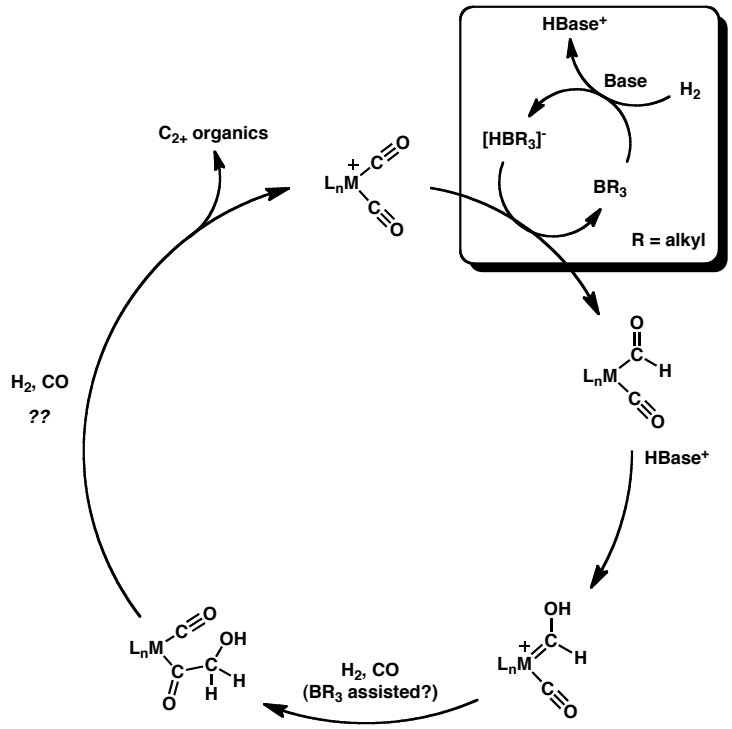

Scheme 4.9

The lability of trialkylborane adducts of (PPh$_3$)$_2$Re(CO)$_3$(CHO) (Chapter 3) suggested that H_2 reductions *catalytic* in borane might be feasible. Indeed, mixtures of [(PPh$_3$)$_2$Re(CO)$_4$][BAr$^F_4$], 10 equivalents **P**$_1$, and 0.2 equivalents ^{t}Bu(CH$_2$)$_2$B(C$_8$H$_{14}$) (**4**) in THF-d_8 under an H_2 atmosphere produced a mixture of Re–CHO and Re–H species. After 18 hours, conversion to 6% formyl and 7% hydrides was observed; the amount of

formyl remained roughly constant over one week, while the amount of hydride steadily increased. Upon complete consumption of $[(PPh_3)_2Re(CO)_4][BAr^F{}_4]$, 52% yield of a mixture of Re–CHO and Re–H species (1:25 ratio) was observed, indicating 2.6 turnovers in **4** (Scheme 4.8). The mediocre yield of formyl and hydride products, as compared to the high 92% yield of [**HP1**]$^+$, perhaps indicates additional uncharacterized reduction processes ongoing. The modest *catalytic* utilization of dihydrogen as a CO reductant nonetheless represents an important proof-of-principle of the proposed two catalyst cycle, involving a FLP catalyst instead of platinum one (Scheme 4.9). As underscored in Chapter 3, however, external trialkylboranes are unsuitable for promoting the steps beyond initial hydride transfer. No further reduction or C–C coupling steps were observed; those transformations require the assistance of a pendent Lewis acid in [**1**]$^+$. Further limitations are provided by the very weak acidity of [$\mathbf{HP_1}$]$^+$, which would have to protonate a reduced CO species in order to represent complete transfer of H_2, and allow catalytic transfer in both borane and base.

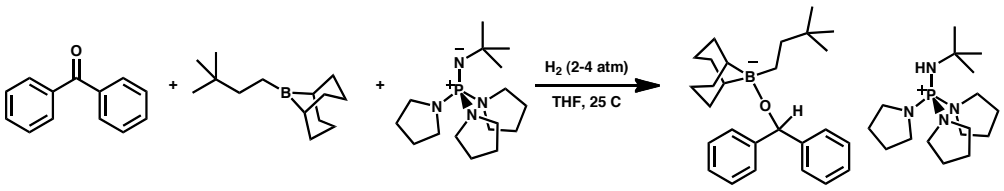

Scheme 4.10

Conclusions

The simple metal-free pair **4**/$\mathbf{P_1}$ constitutes the first example of a trialkylborane-derived FLP that activates H_2. Such FLPs appear quite different from those previously reported: their equilibrium constants for formation lie much further towards free H_2 rather than the

[**HP$_1$**]$^+$/borohydride salts, but they provide a borohydride (generated directly from H_2) that is significantly more potent than the commonly used $[HB(C_6F_5)_3]^-$. This novel FLP has allowed the use of dihydrogen directly to reduce rhenium-bound CO to a C_2 organic fragment. The implementation of an external FLP demonstrates that this novel type of FLP may be generally applicable in hydride transfers to CO ligands and, perhaps, a wider variety of substrates that require strong hydride donors, directly utilizing H_2 as hydride source. In fact, preliminary investigations suggest that treatment of benzophenone with **4**/**P$_1$** and H_2 produces a reduced species, probably containing a B–O bond (Scheme 4.10).

Experimental Section

General Considerations

All air- and moisture-sensitive compounds were manipulated using standard vacuum line or Schlenk techniques, or in a glovebox under a nitrogen atmosphere. Under standard glovebox conditions, petroleum ether, diethyl ether, benzene, toluene, and tetrahydrofuran were used without purging, such that traces of those solvents were in the atmosphere, and could be found intermixed in the solvent bottles. The solvents for air- and moisture-sensitive reactions were dried over sodium benzophenone ketyl, calcium hydride, or by the method of Grubbs.[15] All NMR solvents were purchased from Cambridge Isotopes Laboratories, Inc. Chlorobenzene-*d$_5$* (C_6D_5Cl) and dichloromethane-*d$_2$* (CD_2Cl_2) were freeze-pump-thaw degassed three times before being run through a small column of activated alumina. Tetrahydrofuran-*d$_8$* (THF-*d$_8$*) was purchased in a sealed ampoule, and

dried by passage through activated alumina. Unless noted, other materials were used as received. [**1**][BF_4][3b] and [$(PPh_3)_2Re(CO)_4$][BF_4][14] were prepared according to literature procedures; treatment with one equivalent $NaBAr^F{}_4$ in CH_2Cl_2 afforded anion exchange to yield [**1**][$BAr^F{}_4$] and [$(PPh_3)_2Re(CO)_4$][$BAr^F{}_4$] essentially quantitatively, after filtration and removal of solvents. [$Pt(dmpe)_2$][PF_6]$_2$,[16] [$HPt(dmpe)_2$][PF_6],[16] [$Ni(dmpe)_2$][BF_4]$_2$,[17] [$HNi(dmpe)_2$][PF_6],[16] ^{t}Bu(CH_2)$_2$B(C_8H_{14}),[18] and KOPh[4] were synthesized by literature methods. *tert*-Butylimino-tri(pyrrolidino)phosphorane (**P$_1$**) and *tert*-Octylimino-tris(dimethylamino)phosphorane (***t*Oct**P$_1$) were purchased from Sigma-Aldrich. All other materials were readily commercially available, and used as received. ^{1}H and ^{13}C NMR spectra were recorded on Varian Mercury 300 MHz, or Varian INOVA-500 or 600 MHz spectrometers at room temperature, unless indicated otherwise. Chemical shifts are reported with respect to residual internal protio solvent for ^{1}H and ^{13}C{^{1}H} spectra. Other nuclei were referenced to an external standard: H_3PO_4 (^{31}P), 15% BF_3•Et_2O/$CDCl_3$ (^{11}B), $CFCl_3$ (^{19}F), all at 0 ppm.

X-ray Crystallography Procedures

Colorless single crystals of [**1**•$(THF)_2$][BF_4] suitable for X-Ray diffraction were grown by vapor diffusion of pentane into a THF solution of [**1**][BF_4]. The crystals were mounted on a glass fiber with Paratone-N oil. Structures were determined using direct methods with standard Fourier techniques using the Bruker AXS software package. In some cases, Patterson maps were used in place of the direct methods procedure. There was some disorder in the BF_4 group, as discussed in the crystallographic details section, but

connectivity was unambiguously established as a bis-THF adduct. Full details are given in Appendix D.

Adduct formation between THF and [1][BF_4]

A J-Young Teflon-stoppered NMR tube was charged with 43.9 mg (0.0417 mmol) [**1**][BF_4] and ~0.6 mL CD_2Cl_2. Initial ^{1}H and ^{11}B NMR spectra were recorded. The tube was returned to the glovebox, and 3.4 μL (0.0417 mmol, 1 equiv) THF was added by syringe. After collecting ^{1}H and ^{11}B NMR spectra, the procedure was repeated, adding THF to give 3, 5, 9, 13, 17, 25, and 33 equivalents relative to [**1**]$^+$.

A Benesi-Hildebrand-type analysis[19] was performed according to a previously described derivation.[20] The THF dependence on chemical shift of the ^{11}B resonance and several ^{1}H resonances were recorded, and a Benesi-Hildebrand plot of 1/[THF] vs. 1/$\Delta\delta$ was obtained (Figure 4.5), where $\Delta\delta$ is the change in chemical shift between each addition of THF. The very broad ^{11}B resonance gave a satisfactory fit, but the CH_2 resonances in the ^{1}H NMR fit Benesi-Hildebrand relation better. The slope = $1/[(\Delta\delta)(K_{eq})]$, allowing K_{eq} for formation of the adduct with one of the pendent borane arms to be calculated. K_{eq} = 0.19(2) M^{-1}.

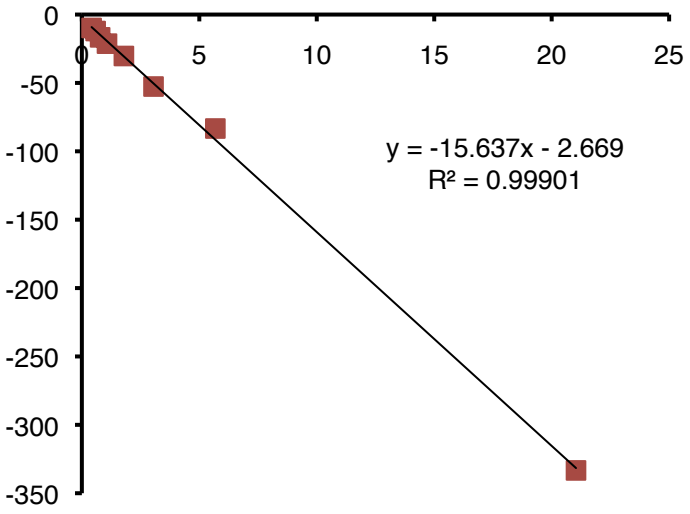

Figure 4.5. Benesi-Hildebrand plot ($1/[THF]$ vs. $1/\Delta\delta$) showing chemical shift dependence on added THF.

Synthetic Procedures and Reactions

Preparation of $[Pt(dmpe)_2][BAr^F{}_4]_2$. The procedure for the preparation of $[Pt(dmpe)_2][PF_6]_2$ was followed,[3] except that the intermediate $[Pt(dmpe)_2][Cl]_2$ was treated with $NaBAr^F{}_4$ rather than $[NH_4][PF_6]$. In a glovebox, a 100 mL round bottom flask was charged with 1 g (2.7 mmol) $Pt(COD)(Cl)_2$, 0.8 g (5.3 mmol) 1,2-bis(dimethylphosphino)ethane, and 30 mL acetonitrile. The reaction mixture was stirred overnight. After ~12 hours, the acetonitrile was removed *in vacuo*, and the solids were dissolved in 40 mL of water. To the colorless solution was added 4.7 g (5.3 mmol) $NaBAr^F{}_4$ as a solid, and the slurry was stirred for ~24 hours. The solids were collected by filtration through a sintered glass frit, and washed with 70 mL CH_2Cl_2, leaving behind white solids, which were collected and dried to afford 1.17 g (0.5 mmol, 25%) $[Pt(dmpe)_2][BAr^F{}_4]_2$. The product was spectroscopically very similar to $[Pt(dmpe)_2][PF_6]_2$. **^{1}H NMR** (THF-d_8, 300 MHz): δ 1.96 (m, $^3\mathcal{J}_{PtH}$ = 27.7 Hz, 24H, $Me_2PCH_2CH_2PMe_2$), 2.30 (m, 8H,

$Me_2PCH_2CH_2PMe_2$), 7.59 (8H, $BAr^F{}_4$), 7.80 (16H, $BAr^F{}_4$). **$^{31}P\{^1H\}$ NMR** (THF-d_8, 121 MHz): δ 33.6 (s, $^1\mathcal{J}_{PtP}$ = 2109 Hz).

Preparation of [HPt(dmpe)$_2$][BAr$^F{}_4$]. To a stirring 10 mL CH_2Cl_2 solution of 102.8 mg (0.16 mmol) $[HPt(dmpe)_2][PF_6]$ was added solid $NaBAr^F{}_4$ (142.1 mg, 0.16 mmol). The suspension was stirred for 6 hours, then filtered through celite, washing with 2 mL CH_2Cl_2. The filtrate was dried *in vacuo*, affording 194 mg (0.14 mmol, 89%) spectroscopically pure $[HPt(dmpe)_2][BAr^F{}_4]$. The product was spectroscopically very similar to $[HPt(dmpe)_2][PF_6]$. **^1H NMR** (C_6D_5Cl, 300 MHz): δ –11.94 (p, $^2\mathcal{J}_{PH}$ = 29.8 Hz, $^1\mathcal{J}_{PtH}$ = 700.9 Hz, 1H, *H*Pt), 1.16 (m, $^3\mathcal{J}_{PtH}$ = 22.7 Hz, 24H, $Me_2PCH_2CH_2PMe_2$), 1.22 (m, 8H, $Me_2PCH_2CH_2PMe_2$), 7.61 (4H, $BAr^F{}_4$), 8.23 (m, 8H, $BAr^F{}_4$). **$^{31}P\{^1H\}$ NMR** (C_6D_5Cl, 121 MHz): δ –8.0 (s, $\mathcal{J}_{PtP}$ = 2234 Hz). **^{19}F NMR** (C_6D_5Cl, 282 MHz): δ –62.3.

Preparation of [Ni(dmpe)$_2$][BAr$^F{}_4$]$_2$. A slurry of 358 mg (0.358 mmol) $[Ni(dmpe)_2][BF_4]_2$ in 10 mL CH_2Cl_2 was treated with 635 mg (0.717, 2 equiv) solid $NaBAr^F{}_4$. The mixture was stirred ~12 hours, then filtered, giving a yellow filtrate with plenty of light yellow solids remaining on the fritted funnel. The filtrate was dried under vacuum, giving a low (20%) yield of pure $[Ni(dmpe)_2][BAr^F{}_4]_2$, which was identified by comparison of NMR resonances to the previously reported [BF_4] salt. **^1H NMR** (THF-d_8, 300 MHz): δ 1.82 (m, 24 H, $Me_2PCH_2CH_2PMe_2$), 2.29 (m, 8H, $Me_2PCH_2CH_2PMe_2$), 7.58 (8H, $BAr^F{}_4$), 7.79 (m, 16H, $BAr^F{}_4$). **$^{31}P\{^1H\}$ NMR** (THF-d_8, 121 MHz): δ 45.3. **^{19}F NMR** (THF-d_8, 282 MHz): δ – 66.

NMR Scale Reaction of KOPh with [1][BF_4], and subsequent attempted reduction with [HPt]$^+$. A J-Young NMR tube was charged with 22.4 mg (0.021 mmol) [**1**][BF_4], 11.3 mg (0.085 mmol) KOPh, and ~0.6 mL THF-*d*$_8$. Some fine precipitates were visible, although the bulk of the KOPh (mostly insoluble in THF) seemed to dissolve. NMR analysis after 20 minutes revealed complete conversion to a new symmetric species (^{31}P δ 2.1). IR spectroscopy (THF solution) showed a single CO stretch at 1990 cm^{-1} (s), shifted slightly from 1998 cm^{-1} in [**1**][BF_4], consistent with a tetracarbonyl structure (PhO$^-$ stretches were observed at 1585 and 1490 cm^{-1}). ^{11}B NMR showed a broad resonance at δ –0.1, but neither a downfield resonances consistent with 3-coordinate boron, nor a [BF_4]$^-$ resonance was observed. Taken together, these data are consistent with phenoxide addition to the borane of [**1**]$^+$ to give a zwitterionic borate species, which would be anionic (accounting for the slight IR shift to lower energy). There is no IR or NMR evidence of attack at a carbonyl. Nonetheless, addition of 14 mg (0.022 mmol) [HPt][PF_6] to this mixture resulted in no detectable reaction, confirming that no Lewis acid-assisted reduction takes place.

NMR scale reaction of [1][BF_4] with [HPt][PF_6] in THF-*d*$_8$. A small vial was charged with 30 mg (0.029 mmol) [**1**][BF_4] and ~0.6 mL THF-*d*$_8$. With stirring, 18 mg (0.029 mmol) [**HPt**][PF_6] was added as a solid, portionwise. The mixture, containing some precipitates, was transferred to an NMR tube, and NMR spectra showed partial conversion (~50%) to a formyl species, which disproportionated overnight to give [**3**]$^-$ and [**1**]$^+$. The viability of THF as a solvent medium for Lewis acid-assisted reductions was thus established.

NMR scale reaction of [1][BF_4] with pyridine, and attempted reaction with [HPt][PF_6]. A J-Young NMR tube was charged with 27.7 mg (0.026 mmol) [**1**][BF_4] and ~0.6 mL C_6D_5Cl. Pyridine (4.2 μL, 0.052 mmol, 2 equiv) was added by syringe, and the tube was sealed. Multinuclear NMR spectroscopy was consistent with strong adduct formation: a new set of pyridine resonances, distinct from free pyridine, was observed by ^{1}H NMR; the CH_2 protons of [**1**]$^+$ shifted upfield by ~1 ppm; the ^{31}P resonance of [**1**]$^+$ shifted slightly (δ 2.1, vs. δ 1.3 for pure [**1**][BF_4] in C_6D_5Cl); and the ^{11}B resonance of [**1**]$^+$ shifted upfield. The resonance was far enough upfield to be obstructed by the large borosilicate signal due to glass construction in the probe. The tube was returned to the glovebox, and the reaction mixture was poured onto 16.6 mg (0.026 mmol, 1 equiv) solid [**HPt**][PF_6]. The solution was returned to the tube, and monitored by NMR. No reduction to **2** or [**3**]$^-$ was observed, nor was any consumption of [**HPt**][PF_6] seen after 24 hours. **^{1}H NMR** (C_6D_5Cl, 500 MHz) of pyridine adduct: δ 0.42 (br s, 2H), 0.84 (br s, 2H), 1.3 (m, 3H), 1.47 (m, 1H), 1,6 (m, 4H), 1.79 (m, 2H), 1.90 (m, 2H), 2.26 (br m, 2H), 7.17 (t, $\mathcal{J}$ = 7.3 Hz, 2H, pyridine), 7.25 (t, $\mathcal{J}$ = 7.46, 4H, $Ph_2PCH_2CH_2B(C_8H_{14})$), 7.38 (m, 6H, $Ph_2PCH_2CH_2B(C_8H_{14})$), 7.67 (t, $\mathcal{J}$ = 7.4 Hz, 1H, pyridine), 8.25 (d, $\mathcal{J}$ = 5.5 Hz, 2H, pyridine). **^{11}B NMR** (C_6D_5Cl, 500 MHz): δ 0.0 ([BF_4]$^-$). **^{31}P{^{1}H} NMR** (C_6D_5Cl, 121 MHz): δ 2.1.

Addition of NEt_3 to [1][BF_4]; Reduction of [1][BF_4] by [HPt][PF_6] in the presence of NEt_3. Two separate experiments were carried out. First, [**1**][BF_4] and NEt_3 were mixed to determine whether strong adduct formation would occur. A J-Young NMR tube was charged with 25.5 mg (0.024 mmol) [**1**][BF_4], 4.9 mg (0.048 mmol, 2 equiv) NEt_3,

and ~0.6 mL CD_2Cl_2. The tube was sealed and ^1H, ^{11}B, and $^{31}P\{^1H\}$ NMR were acquired, showing minimal interaction between NEt_3 and $[\mathbf{1}]^+$.

Next, reduction was attempted in the presence of NEt_3. A small vial was charged with 23.4 mg (0.022 mmol) $[\mathbf{1}][BF_4]$ and ~0.6 mL THF-d_8. NEt_3 (6.2 μL, 0.044 mmol, 2 equiv) was added by syringe, and the mixture was stirred for 1 minute, after which time solid $[\mathbf{HPt}][PF_6]$ (31 mg, 0.048 mmol, 2.2 equiv) was added. The colorless solution quickly turned bright yellow. The reaction mixture was transferred to an NMR tube, and ^1H and ^{31}P NMR spectra revealed complete conversion of $[\mathbf{1}]^+$ to $[\mathbf{3}]^-$, along with some unreacted $[\mathbf{HPt}]^+$ (as an excess was present).

Addition of P_1 to $[1][BF_4]$; Reduction of $[1][BF_4]$ by $[HPt][PF_6]$ in the presence of P_1. Two separate experiments were carried out. First, the stability of $[\mathbf{1}][BF_4]$ to $\mathbf{P_1}$ was established. In a glovebox, 20.2 mg (0.019 mmol) $[\mathbf{1}][BF_4]$, 6.0 mg (0.019 mmol) $\mathbf{P_1}$, and ~0.6 mL C_6D_5Cl were combined in a J-Young NMR tube. The tube was sealed, and the reaction monitored over a few days. Shifts were observed in some resonances of the ^1H NMR spectrum (Figure 4.6); a shift was also observed in the ^{11}B NMR spectrum, to δ 82.7 (from δ 87.7 in pure $[\mathbf{1}][BF_4]$, but still ~80 ppm from normal 4-coordinate region.); only a very minor shift was noted in the $^{31}P\{^1H\}$ NMR, to δ 1.7 (pure $[\mathbf{1}][BF_4]$, δ 1.3 in C_6D_5Cl). The lack of broadening indicates that any interaction is fast and reversible on the NMR timescale, and the minor shifts indicate that the equilibrium lies towards no interaction. Very minor (1-2%) degradation was observed over 2 days.

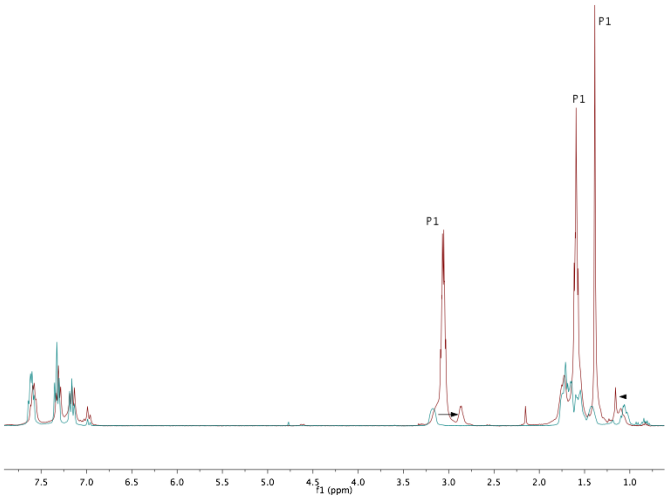

Figure 4.6. ^{1}H NMR of [**1**][BF_4] in the presence of **P$_1$** (red trace), overlaid with pure [**1**][BF_4] (blue).

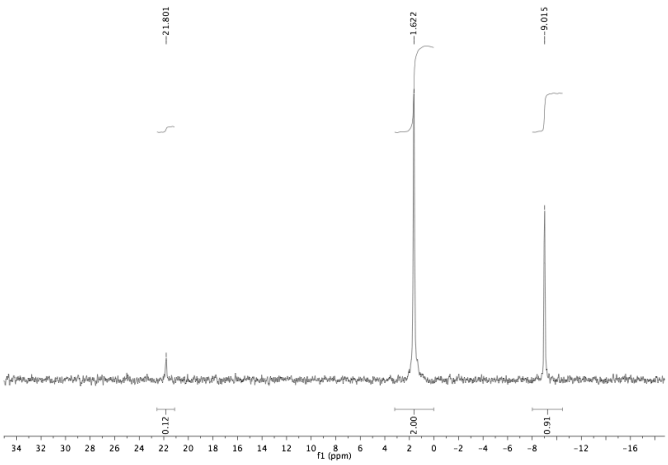

Figure 4.7. ^{31}P{^{1}H} NMR of [**1**][BF_4] in the presence of **P$_1$** (peak at 21.8 is small amount of [**HP$_1$**]$^{+}$).

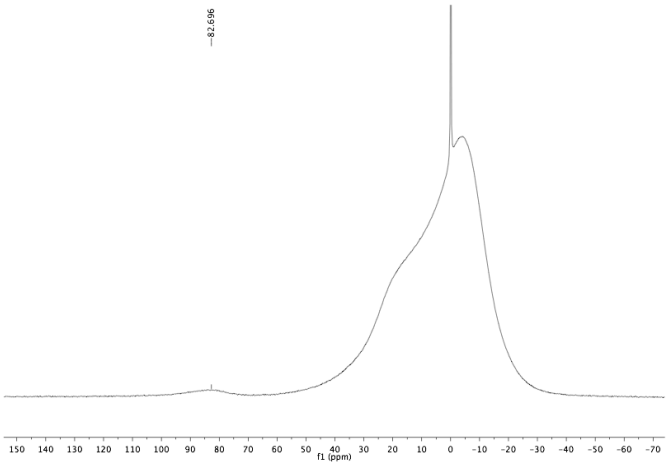

Figure 4.8. ^{11}B NMR of [**1**][BF_4] in the presence of $\mathbf{P_1}$ (sharp peak is $[BF_4]^-$).

To establish whether $[\mathbf{1}]^+$ could be reduced by $[\mathbf{HPt}]^+$ in the presence of $\mathbf{P_1}$, a J-Young NMR tube was charged with 27.3 mg (0.026 mmol) $[\mathbf{1}]^+$, 8.1 mg (0.026 mmol) $\mathbf{P_1}$, 16.6 mg (0.026 mmol) $[\mathbf{HPt}]^+$, and ~0.6 mL THF-*d*$_8$. The tube was sealed and shaken to mix. The solution turned yellow, and after 30 minutes, the major product was **2**, along with $[\mathbf{3}]^-$ and unreacted $[\mathbf{1}]^+$ ($[\mathbf{1}]^+$:**2**:$[\mathbf{3}]^-$ of 1.0:3.2:1.2). Essentially all $[\mathbf{HPt}]^+$ had reacted already. After 4 hours, **2** had mostly disproportionated to $[\mathbf{3}]^-$ and $[\mathbf{1}]^+$ ($[\mathbf{1}]^+$:**2**:$[\mathbf{3}]^-$ of 1.0:0.3:1.2).

Heterolytic cleavage of H_2 with $[Pt][BAr^F_4]_2$ and P_1. A J-Young Teflon-sealed NMR tube was charged with 16.4 mg (0.0074 mmol) $[Pt][BAr^F_4]_2$, 23.1 mg (0.074 mmol, 10 equiv) $\mathbf{P_1}$, and ~0.6 mL THF-*d*$_8$. The tube was degassed by two freeze-pump-thaw cycles, and ~3 atm H_2 (~0.2 mmol, ~30 equiv) was condensed into the tube at 77 K. The tube was sealed, carefully thawed, and monitored by ^{1}H and ^{31}P NMR. Clean first order transformation of $[\mathbf{Pt}][BAr^F_4]_2$ into $[\mathbf{HPt}][BAr^F_4]$ was observed, along with formation of $[\mathbf{HP_1}][BArF_4]$. The phosphazene ^{31}P NMR signal broadened during the course of the

reaction, presumably due to exchange with the generated $[\mathbf{HP_1}]^+$ (not observed). The half-life for the reaction was found to be 10.2 hours.

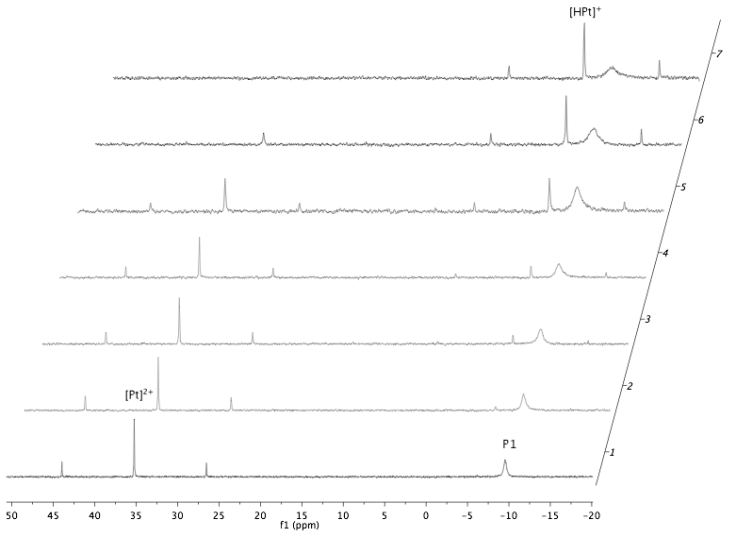

Figure 4.9. $^{31}P\{^1H\}$ NMR time course of H_2 splitting reaction.

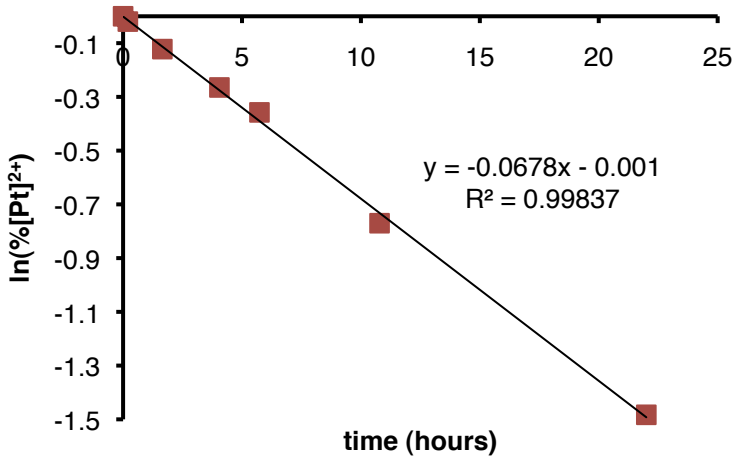

Figure 4.10. Log plot of consumption of $[\mathbf{Pt}]^{2+}$ during reaction with $\mathbf{P_1}$ and H_2.

General Procedure for Metal-Added H_2 Reductions. A J-Young Teflon-sealed NMR tube was charged with ~0.03 mmol [**1**][X] (X = BF_4 or $BAr^F{}_4$), ~0.06-0.60 mmol (2-20 equiv) $\mathbf{P_1}$, ~0.003-0.015 (0.1-0.5 equiv) $[M(dmpe)_2]^{2+}$ (M = Ni, Pt), and ~0.6 mL THF-

d8. The tube was sealed, and NMR spectra (^{1}H, ^{31}P{^{1}H}) were obtained. The tube was degassed by two freeze-pump-thaw cycles, and between 1 and 4 atm H_2 was added by introducing an atmosphere of H_2 at either 298 or 77 K. The tube was affixed to a slowly spinning motor to ensure good mixing, and the reaction was monitored periodically by ^{1}H and ^{31}P NMR. Precise yields were measured by integration to a solution of $P(Mes)_3$ (Mes = 2,4,6-trimethylphenyl) in THF-*d8* in the J-Young tube in a coaxial capillary, with a range from 85-95% depending on conditions.

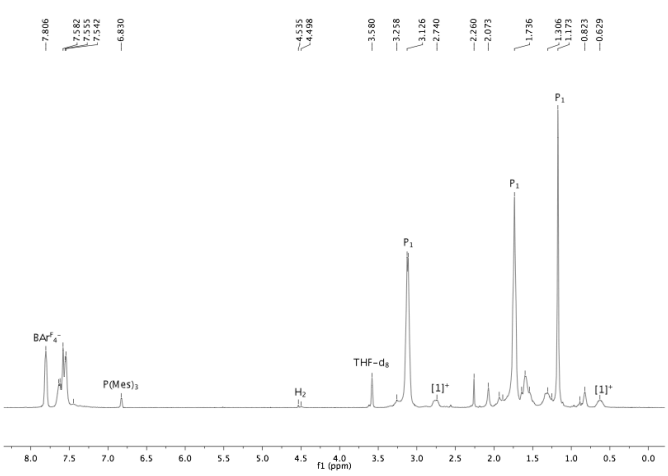

Figure 4.11. ^{1}H NMR of Pt-containing reductive coupling immediately after H_2 addition (15 mol% [**Pt**]$^{2+}$, 4 equiv **P1**).

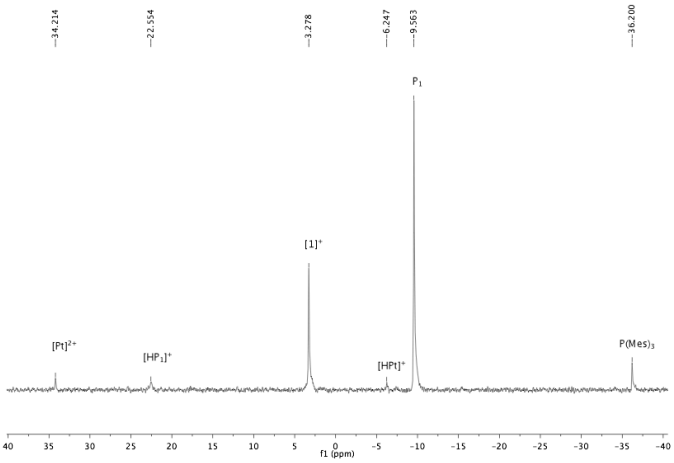

Figure 4.12. $^{31}P\{^{1}H\}$ NMR of Pt-containing reductive coupling immediately after H_2 addition.

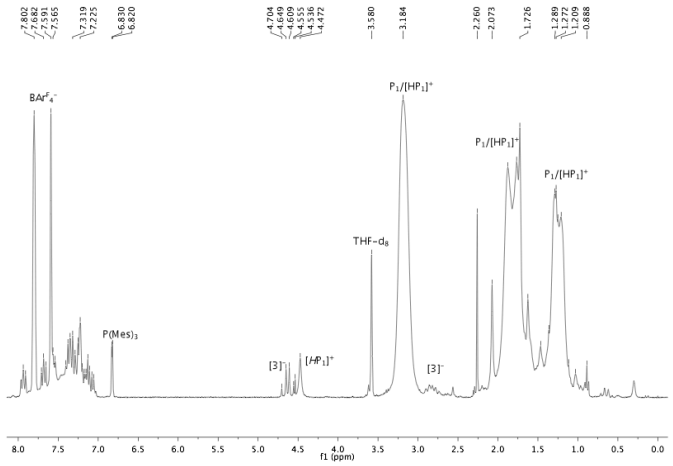

Figure 4.13. ^{1}H NMR of Pt-containing reductive coupling after 13 days (reaction complete, 85% yield by integration).

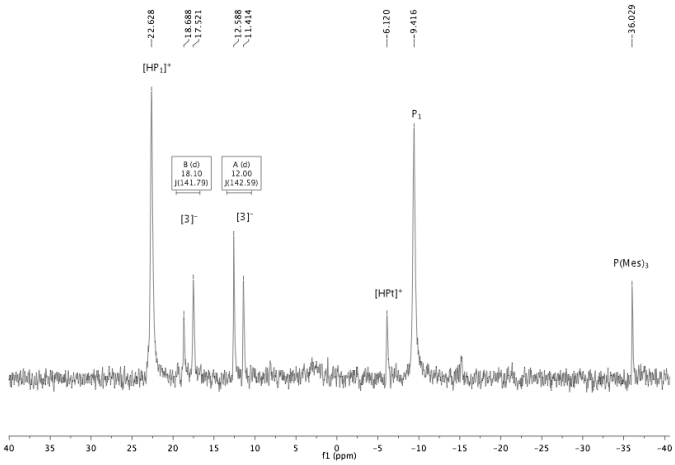

Figure 4.14. $^{31}P\{^{1}H\}$ NMR of Pt-containing reductive coupling after 13 days.

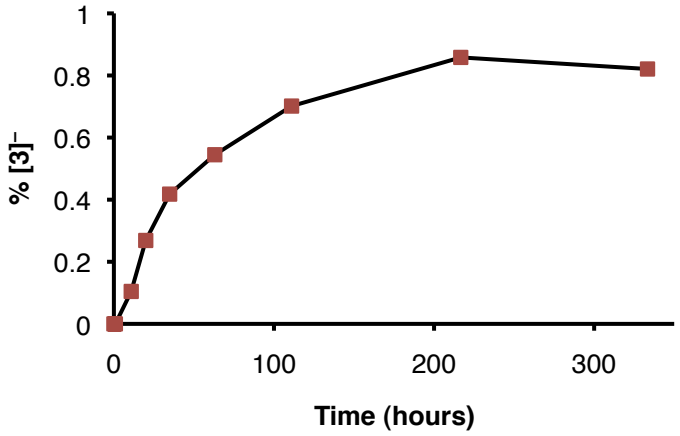

Figure 4.15. Formation of [**3**]$^{-}$ from [**1**][BAr^{F}_{4}], 15 mol% [**Pt**][BAr^{F}_{4}]$_2$, 4 equiv **P1**, 4 atm H_2.

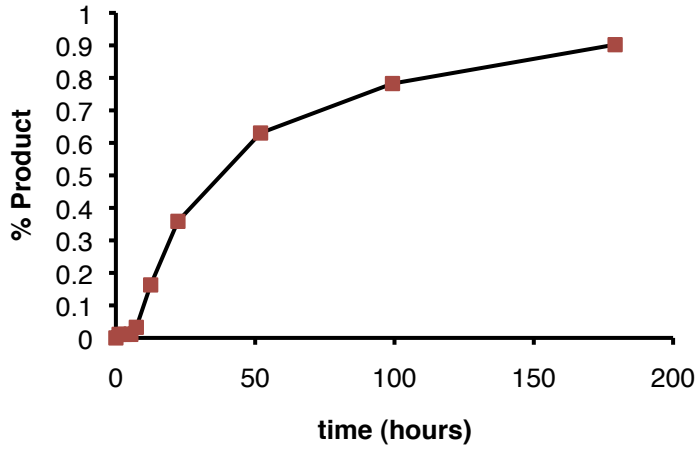

Figure 4.16. Time course of Pt-containing reductive coupling showing induction period (55% [**Pt**]$^{2+}$, 5.5 equiv $\mathbf{P_1}$, ~90% yield by integration to $BAr^F{}_4$ peaks).

Reaction of [1][BAr$^F{}_4$] with [HPt][BAr$^F{}_4$]. A vial was charged with [**1**][$BAr^F{}_4$] (36.3 mg, 0.020 mmol) and [**HPt**][$BAr^F{}_4$] (27.0 mg, 0.020 mmol). To the vial was added ~0.6 mL C_6D_5Cl, which dissolved the solids, and the reaction mixture was transferred to a J-Young NMR tube. Periodic NMR spectra were acquired, which showed no discernable reaction over more than 24 hours.

Reaction of [1][BF_4] with [HNi(dmpe)$_2$][PF_6]. A J-Young NMR tube was charged with 21.6 mg (0.021 mmol) [**1**][BF_4], 20.7 mg (0.041 mmol) [HNi(dmpe)$_2$][PF_6], and ~0.6 mL THF-*d*$_8$. Over 48 hours no discernable reaction took place, with only the starting materials visible by NMR spectroscopy.

Reaction of 2 with [Pt][BAr$^F{}_4$]$_2$. Carbene **2** was prepared in the usual manner by dropwise addition of $NaHBEt_3$ (24.9 μL of a 1.0 M in toluene solution) into a rapidly stirring C_6D_5Cl solution of [**1**][BF_4] (26.2 mg, 0.025 mmol). The mixture was transferred to an NMR tube, and NMR studies showed essentially quantitative formation of **2**. The tube

was returned to the glovebox and 85 mg (0.037 mmol) [**Pt**][BAr^F_4]$_2$ was added. The tube was sealed and shaken vigorously. Subsequent NMR studies showed complete conversion to [**1**][BAr^F_4] and [**HPt**][BAr^F_4].

General Procedure for Metal-Free H_2 Reductions. A J-Young NMR tube was charged with ~0.03 mmol [**1**][X] (X = BF_4 or BAr^F_4), ~0.06-0.60 mmol (2-20 equiv) $\mathbf{P_1}$, and ~0.6 mL THF-*d*$_8$. The tube was sealed, and NMR spectra (^{1}H, ^{31}P{^{1}H}) were obtained. The tube was degassed by two freeze-pump-thaw cycles, and between 1 and 4 atm H_2 was added by introducing H_2 at either 298 or 77 K. The tube was affixed to a slowly spinning motor to ensure good mixing, and the reaction was monitored periodically by ^{1}H and ^{31}P NMR. When D_2 was used instead of H_2, all ^{1}H and ^{31}P signals were observed *except for the CH_2 group* of [**3**]$^-$, verifying deuterium incorporation at that position and confirming that dihydrogen is the sole source of hydride. Precise yields were measured by integration to a solution of P(Mes)$_3$ (Mes = 2,4,6-trimethylphenyl) in THF-*d*$_8$ in the J-Young tube in a coaxial capillary. Conditions: ~4 mM [**1**][BF_4], 10 equiv. P_1, ~3 atm H_2 (or D_2), giving yields of 92% for both H_2 and D_2. Integration to the protons of [BAr^F_4] gave similar yields (85-90%), except when 20 equiv P1 was added, when a reduced (70%) yield was obtained. Preliminary experiments with D_2 suggested a small kinetic isotope effect.

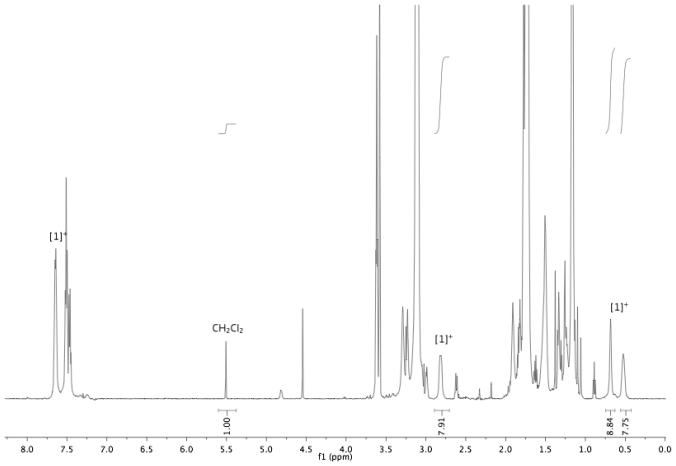

Figure 4.17. ^{1}H NMR of metal-free reductive coupling immediately after H_2 addition (10 equiv **P1**). Minor CH_2Cl_2 impurity remains unchanged throughout the reaction; **P1** is left off-scale to show the Re-containing species.

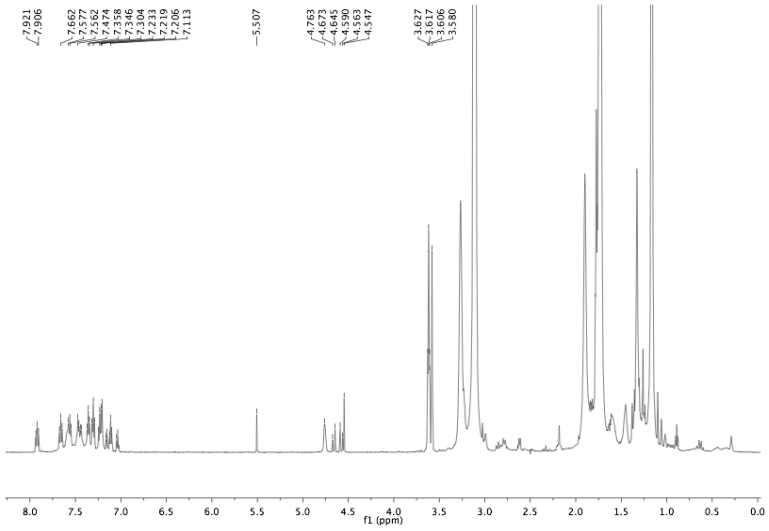

Figure 4.18. ^{1}H NMR of metal-free reductive coupling after ~5 days (~85% yield).

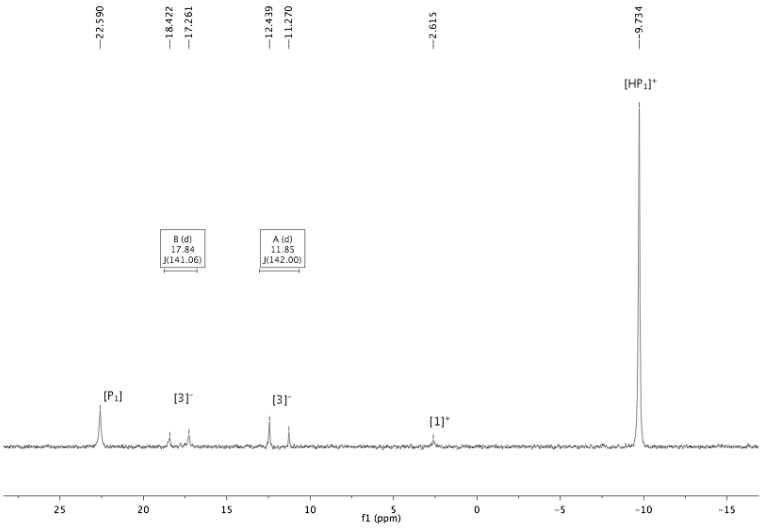

Figure 4.19. $^{31}P\{^{1}H\}$ NMR of metal-free reductive coupling after ~5 days.

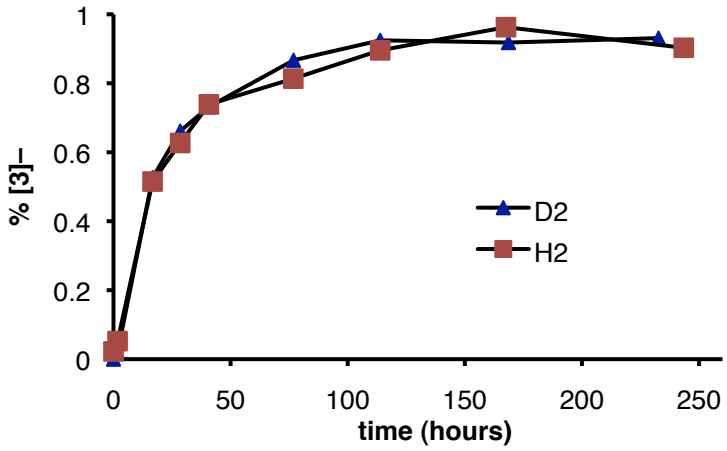

Figure 4.20. Time course of reaction of 1 equiv $[\mathbf{1}]^+$ and 10 equiv $\mathbf{P_1}$ with H_2 (red squares) or D_2 (blue triangles).

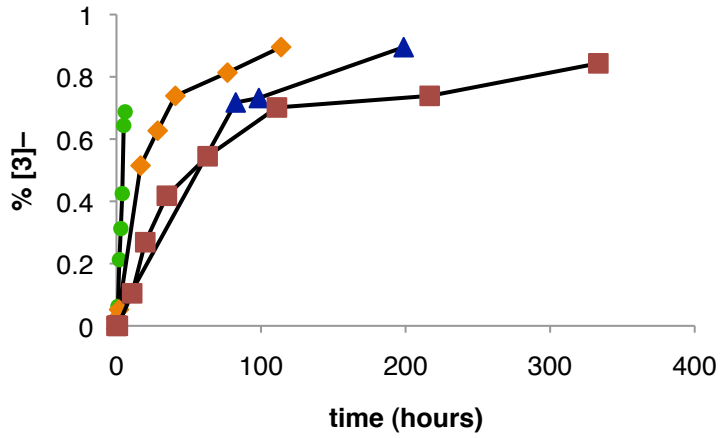

Figure 4.21. Crude comparison of rates of formation of $[\mathbf{3}]^-$ with and without $[\mathbf{Pt}]^{2+}$, and varying $\mathbf{P_1}$. Red squares, 4 equiv $\mathbf{P_1}$ (*and* 15 mol % $[\mathbf{Pt}]^{2+}$); blue triangles, 4 equiv $\mathbf{P_1}$; orange diamonds, 10 equiv $\mathbf{P_1}$; green circles, 20 equiv $\mathbf{P_1}$.

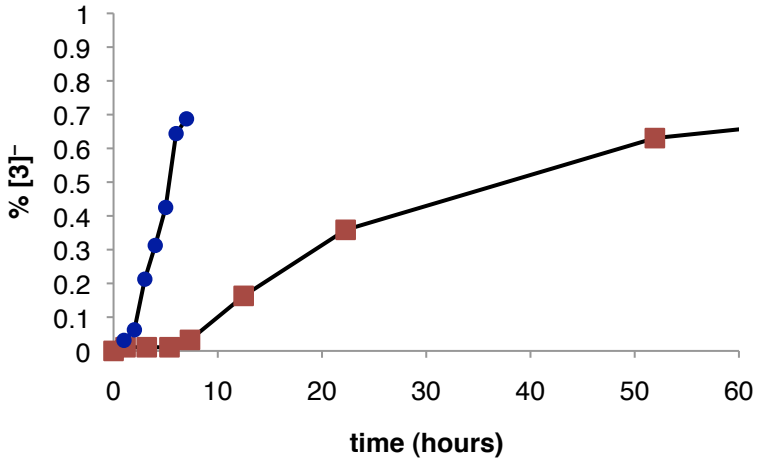

Figure 4.22. Time course showing the elimination of induction period when $[\mathbf{Pt}]^{2+}$ is omitted from the reaction.

NMR scale reaction of [1][BF$_4$] with H$_2$. A J-Young Teflon-sealed NMR tube was charged with 12.2 mg (0.012 mmol) [**1**][BF$_4$] and ~0.6 mL THF-d_8. The tube was submerged in liquid nitrogen, and the headspace was evacuated, and refilled with H$_2$, affording ~2-3 atm H$_2$. The tube was sealed and the reaction monitored by ^{1}H and ^{31}P NMR. No reaction was discernable over a number of days.

H_2/D_2 Equilibration Experiments. A J-Young Teflon-sealed NMR tube was charged with ~30 mg (0.1 mmol) **P_1** and 0.6 mL THF-*d*$_8$. After two freeze-pump-thaw cycles a 1:1 mixture of H_2:D_2, freshly mixed in a 500 mL bulb, was introduced while the tube was cooled to 77 K. The tube was sealed and the solution carefully thawed, and the reaction monitored by NMR. No HD peak was observed after 24 hours.

In a typical experiment, a J-Young NMR tube was charged with 31.2 mg (0.10 mmol) **P_1**, 20.6 mg (0.10 mmol) ^{t}Bu(CH$_2$)$_2$B(C$_8$H$_{14}$), and ~0.6 mL THF-*d*$_8$. The tube was sealed and moved from the glovebox to a vacuum line, where it was subjected to two freeze-pump-thaw cycles, at which point a 1:1 H_2:D_2 mixture (freshly mixed in a 500 mL bulb) was introduced at 77 K. After carefully thawing the reaction mixture, the reaction was monitored by ^{1}H NMR. After 30 minutes a significant amount of HD (HD:H_2 was observed, which slowly increased. After two days, the ratio of HD:H_2 was 0.46:1.00. Another spectrum was taken 10 days later, showing complete equilibration (HD:H_2, 1.98:1.00) occurred at some point between 2 and 12 days from the start of the reaction.

Reaction of [1][BF_4] with ^{tOct}P_1 under H_2. A J-Young NMR tube was charged with 24.2 mg (0.0230 mmol) [**1**][BF4]. A ~0.6 mL THF-*d*$_8$ solution of 33.4 mg (0.114 mmol, 5 equiv) *tert*-Octylimino-tris(dimethylamino)phosphorane (**$^{tOct}P_1$**) was added to the tube, which was sealed and monitored by multinuclear NMR spectroscopy. Initial spectra showed no reaction. The reaction was put under ~3 atm H_2, and after 6 hours no reaction was observed. The tube was heated to 70 °C, and after 24 hours, the major product was a ligand activated species formed from **2**.

Reaction of $[(PPh_3)_2Re(CO)_4][BAr^F_4]$ with P_1 under H_2. A J-Young NMR tube was charged with 40.6 mg (0.024 mmol) $[(PPh_3)_2Re(CO)_4][BAr^F_4]$, and a ~0.6 mL THF-$d_8$ solution of 75 mg (0.24 mmol, 10 equiv) **P_1**. Before addition of H_2, initial NMR spectra were acquired, which showed a small amount of Re–H species (~7%), attributed to adventitious water (which could lead to hydroxide attack at Re–CO and elimination of CO_2 to give Re–H). The tube was freeze-pump-thawed twice, and H_2 was introduced at 77K (2-4 atm). The tube was affixed to a slowly spinning motor to ensure good mixing, and the reaction monitored periodically by NMR spectroscopy. The amount of Re–H species remained essentially constant over more than 48 hours.

Reaction of $[(PPh_3)_2Re(CO)_4][BAr^F_4]$ with the frustrated Lewis pair P_1 / ^{t}Bu$(CH_2)_2$B(C_8H_{14}) under H_2. A J-Young NMR tube was charged with 41.8 mg (0.025 mmol) $[(PPh_3)_2Re(CO)_4][BAr^F_4]$, and a ~0.6 mL THF-$d_8$ solution of 78 mg (0.25 mmol, 10 equiv) **P_1** and 5.1 mg (0.025 mmol, 1 equiv) ^{t}Bu$(CH_2)_2$B(C_8H_{14}). As in the absence of Lewis acid, a small amount (~2%) of Re–H species was initially formed, as above. The tube was freeze-pump-thawed twice, and H_2 was introduced at 77 K (2-4 atm). After careful thawing, the tube was slowly rotated on a motor to mix, and was monitored by NMR spectroscopy. After a few hours, ~8% formyl was present; after 24 hours ~70% conversion to a mixture of Re formyl and hydride species was observed (formyl:hydride, 1.0:0.67), and after 48 hours ~80% conversion to the mixture of $(PPh_3)_2Re(CO)_3(CHO)$, $(PPh_3)_2Re(CO)_3H$, and $(PPh_3)Re(CO)_4H$ was observed (formyl: hydride, 1.0:1.37). After 48 hours all Re starting material had been consumed, and the other 20% Re comprised a few minor uncharacterized products.

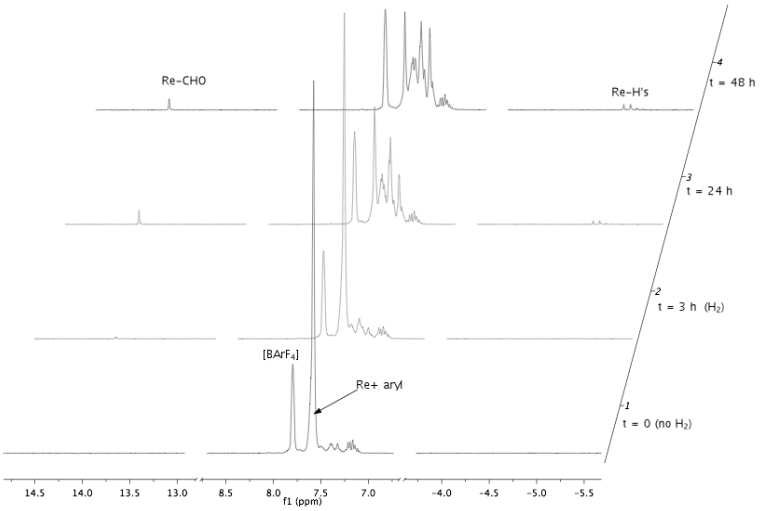

Figure 4.23. Time course (^{1}H NMR) of reduction facilitated by external Lewis acid.

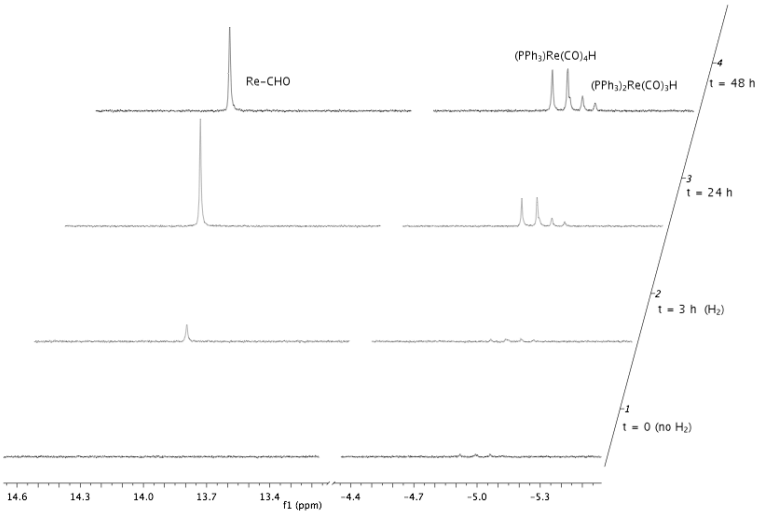

Figure 4.24. Time course (^{1}H NMR) of reduction facilitated by external Lewis acid (formyl and hydride region).

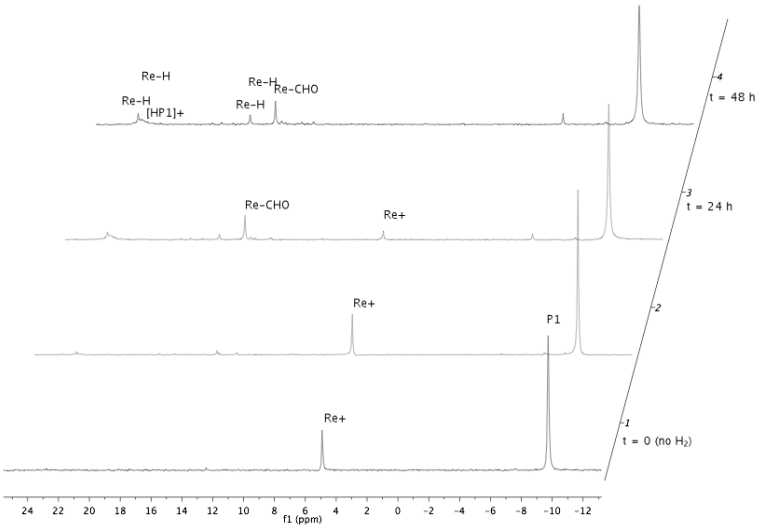

Figure 4.25. Time course (^{31}P NMR) of reduction facilitated by external Lewis acid.

Catalytic reduction of $[(PPh_3)_2Re(CO)_4][BAr^F_4]$ with P_1 / ^{t}Bu$(CH_2)_2$B(C_8H_{14}) under H_2. A J-Young NMR tube was charged with 104.2 mg (0.0618 mmol) $[(PPh_3)_2Re(CO)_4][BAr^F_4]$, 96.5 mg (0.309 mmol, 5 equiv) **P_1**, 12.4 μL (0.012 mmol, 0.2 equiv) ^{t}Bu$(CH_2)_2$B(C_8H_{14}), and 0.6 mL THF-*d*$_8$. The tube was placed under ~4 atm H_2 and monitored by NMR. Integration against the BAr^F_4 protons established that 6% $(PPh_3)_2Re(CO)_3(CHO)$ formed over the first 18 hours, and that level was roughly maintained through the reaction, while the amount of hydride steadily increased to 54% yield over 8 days. The total amount of hydride transferred from H_2 to Re represents 2.6 turnovers in borane.

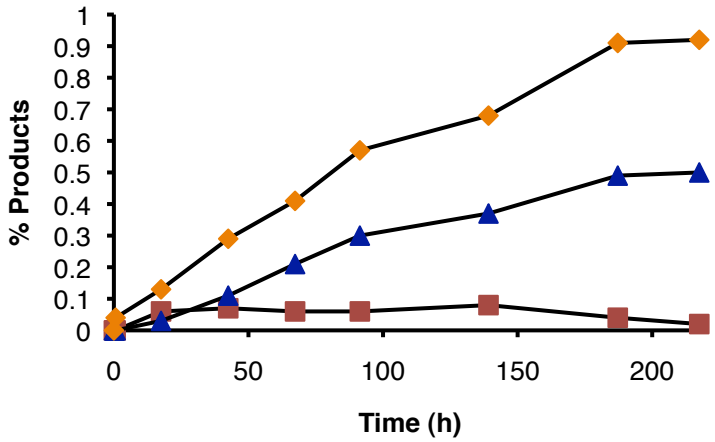

Figure 4.26. Time course of catalytic reduction of $[(PPh_3)_2Re(CO)_4]^+$, monitored by NMR. Red squares, $(PPh_3)_2Re(CO)_3(CHO)$; blue triangles, sum of $(PPh_3)_2Re(CO)_3H$ and $(PPh_3)Re(CO)_4H$; orange diamonds, $[\mathbf{HP_1}]^+$.

References

1. (a) Dombek, B. D. *Adv. Catal.* **1983**, *32*, 325; (b) Maitlis, P. M.; Zanotti, V. *Chem. Commun.* **2009**, 1619.
2. DuBois, M. R.; DuBois, D. L. *Chem. Soc. Rev.* **2009**, *38*, 62.
3. (a) Elowe, P. R.; West, N. M.; Labinger, J. A.; Bercaw, J. E. *Organometallics* **2009**, *28*, 6218; (b) Miller, A. J. M.; Labinger, J. A.; Bercaw, J. E. *J. Am. Chem. Soc.* **2008**, *130*, 11874; (c) Miller, A. J. M.; Labinger, J. A.; Bercaw, J. E. *Organometallics* **2010**, *29*, 4499.
4. Curtis, C. J.; Miedaner, A.; Ellis, W. W.; DuBois, D. L. *J. Am. Chem. Soc.* **2002**, *124*, 1918.
5. Ellis, W. W.; Miedaner, A.; Curtis, C. J.; Gibson, D. H.; DuBois, D. L. *J. Am. Chem. Soc.* **2002**, *124*, 1926.
6. (a) Schwesinger, R.; Schlemper, H. *Angew. Chem. Int. Ed.* **1987**, *26*, 1167; (b) Schwesinger, R.; Willaredt, J.; Schlemper, H.; Keller, M.; Schmitt, D.; Fritz, H. *Chem. Ber.* **1994**, *127*, 2435.
7. Kaljurand, I.; Kutt, A.; Soovali, L.; Rodima, T.; Maemets, V.; Leito, I.; Koppel, I. A. *J. Org. Chem.* **2005**, *70*, 1019.
8. Izutsu, K., *Acid-Base Dissociation Constants in Dipolar Aprotic Solvents*. Blackwell Scientific Publications: Boston, 1990; p 166.
9. Brown, H. C.; Schlesinger, H. I.; Cardon, S. Z. *J. Am. Chem. Soc.* **1942**, *64*, 325.

10. (a) Stephan, D. W. *Org. & Biomol. Chem.* **2008**, *6*, 1535; (b) Stephan, D. W. *Dalton Trans.* **2009**, 3129; (c) Stephan, D. W.; Erker, G. *Angew. Chem. Int. Ed.* **2010**, *49*, 46.
11. (a) Welch, G. C.; Juan, R. R. S.; Masuda, J. D.; Stephan, D. W. *Science* **2006**, *314*, 1124; (b) Welch, G. C.; Stephan, D. W. *J. Am. Chem. Soc.* **2007**, *129*, 1880; (c) Geier, S. J.; Gille, A. L.; Gilbert, T. M.; Stephan, D. W. *Inorg. Chem.* **2009**, *48*, 10466.
12. (a) Chase, P. A.; Welch, G. C.; Jurca, T.; Stephan, D. W. *Angew. Chem. Int. Edit.* **2007**, *46*, 8050; (b) Chase, P. A.; Jurca, T.; Stephan, D. W. *Chem. Commun.* **2008**, 1701.
13. Rokob, T. A.; Hamza, A.; Papai, I. *J. Am. Chem. Soc.* **2009**, *131*, 10701.
14. Gibson, D. H.; Owens, K.; Mandal, S. K.; Sattich, W. E.; Franco, J. O. *Organometallics* **1989**, *8*, 498.
15. Pangborn, A. B.; Giardello, M. A.; Grubbs, R. H.; Rosen, R. K.; Timmers, F. J. *Organometallics* **1996**, *15*, 1518.
16. Miedaner, A.; DuBois, D. L.; Curtis, C. J.; Haltiwanger, R. C. *Organometallics* **1993**, *12*, 299.
17. Berning, D. E.; Noll, B. C.; DuBois, D. L. *J. Am. Chem. Soc.* **1999**, *121*, 11432.
18. Hirano, K.; Yorimitsu, H.; Oshima, K. *Org. Lett.* **2005**, *7*, 4689.
19. (a) Benesi, H. A.; Hildebrand, J. H. *J. Am. Chem. Soc.* **1949**, *71*, 2703; (b) Rose, N. J.; Drago, R. S. *J. Am. Chem. Soc.* **1959**, *81*, 6138.
20. Baldwin, S. M.; Bercaw, J. E.; Brintzinger, H. H. *J. Am. Chem. Soc.* **2008**, *130*, 17423.

Chapter 5

Lewis Acid-Assisted CO_2 Reduction

Chapter 5

Introduction

Combustion of fossil fuels generates some of the vast abundance of atmospheric CO_2; carbon neutrality could be achieved by recycling the produced CO_2 through catalytic conversion to fuels and chemicals.[1] The two main approaches to CO_2 reduction are electrocatalysis,[1a] in which protons and electrons are sequentially (and/or concertedly) added, and hydrogenation,[1b] in which H_2 is the source of protons and electrons (Scheme 5.1). While in principle the products could be the same, most of the electrocatalytic systems generate CO and H_2O (at quite reducing potentials), while the hydrogenation systems generally produce formic acid (under forcing pressures), as depicted in Scheme 5.1. Lewis and Brønsted acid additives, particularly from the alkali and alkaline earth metals, have shown promise in improving electrocatalytic CO_2 reduction, notably in low-valent Fe porphyrins.[2] Bimetallic catalysts, including biological [NiFe] CO dehydrogenase, feature one metal bound to C while another metal binds O, acting as a Lewis acid.[3] Similar Lewis acid (e.g., AlO_x, TiO_x) enhancements have been noted in heterogeneous systems that convert CO_2 and CO to CH_4.[4] Stoichiometric boron additives in homogeneous Cu[5] and Ni[6] systems have also been reported, wherein a diborane B–B[5] or secondary borane B–H[6] bond is replaced with a B–O bond to help drive a reaction. These homogeneous catalytic reactions effectively replace H_2 with borane reductants. "Frustrated Lewis pairs"[7] have also utilized the strength of B–O bonds to stabilize reduced CO_2 products, including methanol

upon hydrolysis.[8] Catalytic B–O bond cleavage in all of these cases is difficult, if not impossible; presently, stoichiometric boranes are required.

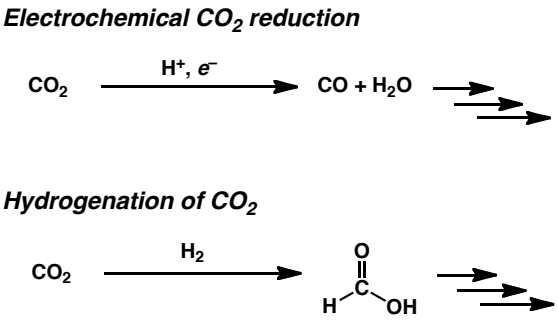

Scheme 5.1

Chemical industry generates concentrated CO_2 streams as a flue gas, the utilization of which would be convenient relative to collection of CO_2 dispersed in the atmosphere. CO_2 is also an impurity in key pipeline feedstocks such as synthesis gas (CO + H_2). An ideal syngas conversion catalyst would either be tolerant to CO_2, or would react equally well with CO_2 to form reduced products. The widely implemented $CuO/ZnO/Al_2O_3$ catalyst that converts syngas to methanol meets this requirement, converting a mixture of CO_2 and CO to methanol.[9] Our interest in syngas conversion to higher organics[10] initially prompted us to examine the reactivity of CO_2 with partially reduced M–CO species and the late transition metal hydride species employed in CO reduction. Further, a CO_2-tolerant catalyst could hypothetically utilize the CO produced by electrocatalytic CO_2 reduction to generate further reduced products.

We report here that the late transition metal hydrides and reduced metal carbonyl components of our CO reductive coupling system both reduce CO_2 to $[HCO_2]^-$. The

Lewis acidic trialkylboranes — which promote CO reductive coupling — also play a key role in facilitating CO_2 reduction. The resulting formate-borane adduct is quite weakly bound relative to the strong covalent bonds to boron discussed above, signifying a promising new approach to promoting CO_2 reduction by H_2 with Ni/BR_3 cooperation.

Results and Discussion

Reactivity of rhenium species with CO_2.

We have previously reported that the Re carbonyl cation $[(Ph_2P(CH_2)_2B(C_8H_{14})_2Re(CO)_4][BF_4]$ ([**1**][BF_4]), bearing pendent alkylboranes in the secondary coordination sphere of the metal, is readily reduced by $NaHBEt_3$ or $[HPt(dmpe)_2][PF_6]$, initially forming boroxycarbene **2** before a second reduction initiates C–C coupling (Scheme 5.2).[10a] Further studies of **2** showed that it reacts as a relatively potent hydride source, releasing H_2 upon treatment with water or weak acids (Chapter 3).[10d]

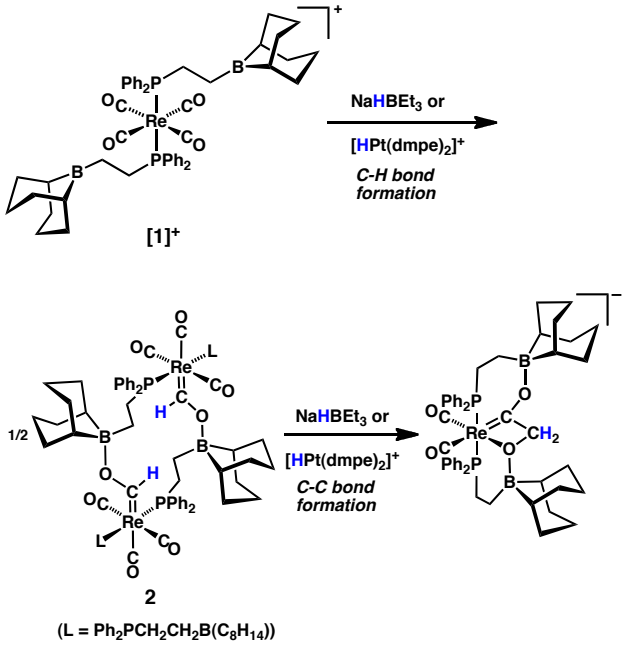

Scheme 5.2

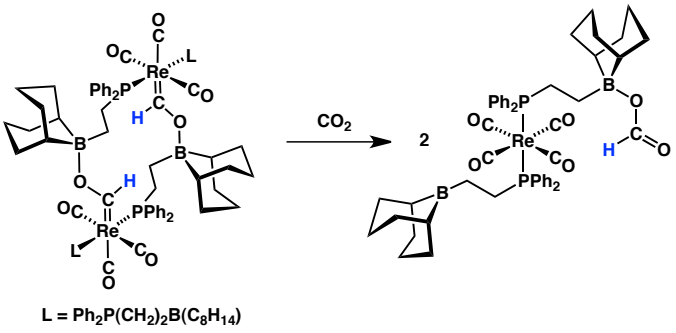

Scheme 5.3

A solution of **2**, formed *in situ* from [**1**][BF_4] and $NaHBEt_3$ in C_6D_5Cl,[10a] was degassed by three freeze—pump—thaw cycles before admission of 1 atm CO_2. A few minutes later a new ^1H NMR resonance was observed at δ 8.44. ^{31}P NMR showed complete consumption of **2** and formation of a symmetric Re product with a chemical shift similar to [**1**]$^+$. Infrared spectroscopy confirmed the presence of a $Re(CO)_4^+$ core (single strong stretch at 1993 cm^{-1}) and a C=O functionality (1620 cm^{-1}). The spectroscopic data point to hydride transfer

from **2** to CO_2 to form [**1**]$^+$ and $[HCO_2]^-$, which form an adduct, **1**•(HCO_2) (Scheme 5.3). The NMR spectra are consistent with a high symmetry species, presumably through fluxional processes such as exchange of formate between boranes or additional adduct formation.

After about an hour, large amounts of precipitate formed, and the signals corresponding to **1**•(HCO_2) dissipated; we speculate that this is due to oligomerization of **1**•(HCO_2) through the two oxygens of formate (i.e., R_3B–OC(H)O–BR_3). Similar oligomerization was observed for the series $(Ph_2P(CH_2)_nB(C_8H_{14}))_2Re(CO)_3(CHO)$ (n = 2, 3): **2** (n = 2) undergoes monomer-dimer equilibrium in solution but crystallizes spontaneously from CH_2Cl_2 as a dimer;[10a] for n = 3, intermolecular B–O interactions appear to dominate, and the higher aggregates precipitate from solution.[10d] The presence of formate in **1**•(HCO_2) was further confirmed by addition of $[Bu_4N][HCO_2]$ to [**1**][BF_4] in C_6D_5Cl, which gave **1**•(HCO_2) as judged by ^{1}H, ^{31}P{^{1}H} NMR, and IR spectroscopy. **1**•(HCO_2) produced in this fashion also precipitated from C_6D_5Cl over the course of a few hours.

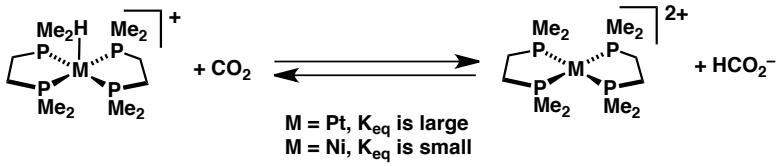

Scheme 5.4

We have used the platinum hydride $[HPt(dmpe)_2][PF_6]$, originally reported by DuBois,[11] extensively in CO reduction chemistry.[10a-d] This reagent is not compatible with CO_2: DuBois reported that $[HPt(dmpe)_2][PF_6]$ (ΔG_{H^-} = 42.5 kcal mol^{-1}) reduces CO_2 to HCO_2^- according to the equilibrium in Scheme 5.4. The hydride donor strength, ΔG_{H^-}, is known

for a large number of late transition metal bis(diphosphine) complexes;[12] smaller values indicate more facile dissociation of H^- and therefore more potent reductants. DuBois estimated that $[HCO_2]^-$ is a hydride donor of similar potency to $[HPt(depe)_2]^+$, ΔG_{H^-} = 44.2 kcal mol^{-1} (recalculated from the originally published value[12a] using DuBois' more recent pKa value[12d]). Weaker hydride donors, such as $[HNi(dmpe)_2][PF_6]$ (ΔG_{H^-} = 50.9 kcal mol^{-1}), do not reduce CO_2;[13] in fact the reverse reaction is observed, as $[Bu_4N][HCO_2]$ transfers hydride to $[Ni(dmpe)_2]^{2+}$ to yield $[HNi(dmpe)_2]^+$ (Scheme 5.4). Boroxycarbene **2** is intermediate in hydride strength between $[HNi(dmpe)_2][PF_6]$ and $[HPt(dmpe)_2][PF_6]$; it is readily formed from $[\mathbf{1}][BF_4]$ and $[HPt(dmpe)_2][PF_6]$, but mixtures of $[\mathbf{1}][BF_4]$ and $[HNi(dmpe)_2][PF_6]$ show no discernible reaction.

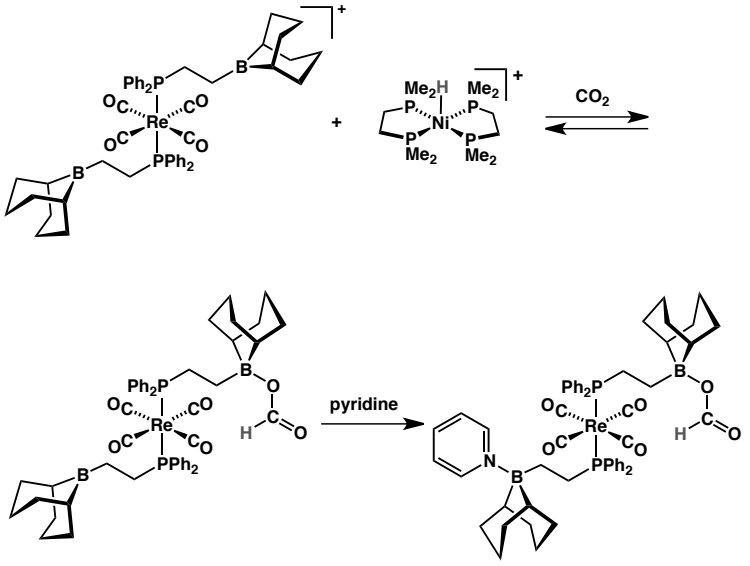

Scheme 5.5

Given the above observations, we were surprised to find that addition of CO_2 to a mixture of $[HNi(dmpe)_2][PF_6]$ and $[\mathbf{1}][BF_4]$ produced significant amounts of formate (δ 8.43) over 24 hours at room temperature (Scheme 5.5). The reaction did not proceed to completion,

as evidenced by the presence of unreacted $[HNi(dmpe)_2]^+$ and chemical shifts for the sole visible Re-containing species being intermediate between $[\mathbf{1}]^+$ and **1**•(HCO_2) (suggesting an equilibrium between these species). As in the reaction of **2** with CO_2, precipitates formed over time; boroxycarbene **2** was not observed before precipitation. The isolated precipitates partially dissolved upon treatment with pyridine, and signals from both the formate (δ 8.88) and phosphinoborane ligands (now in an asymmetric environment) were present (^{31}P NMR δ 1.95 d, 2.98 d, $\mathcal{J}_{PP}$ = 77 Hz). This species is assigned to zwittterionic **1**•$(HCO_2)(C_5H_5N)$, with one borane bound by pyridine and the other by formate; pyridine adduct formation would prevent oligomerization by binding the boranes to give soluble monomers.

Reactivity of group 9 and 10 hydrides with CO_2

Based on thermodynamic hydride donor strength, it is surprising that mixtures of $[HNi(dmpe)_2]^+$ and $[\mathbf{1}]^+$ reduce CO_2: the ultimate reaction is a transfer of hydride from $[HNi(dmpe)_2]^+$ to CO_2, which is apparently uphill by ~7 kcal mol^{-1} (Scheme 5.4).[13] Suspecting the central involvement of the Lewis acidic functionality of $[\mathbf{1}]^+$, $[HNi(dmpe)_2][PF_6]$ was allowed to react with 1 atm CO_2 in the presence of trialkylborane ^{t}Bu$(CH_2)_2$B(C_8H_{14}) in C_6D_5Cl (Scheme 5.7). Over a few hours, a ^{1}H NMR resonance at δ 8.73 grew in as the hydride resonance of $[HNi(dmpe)_2]^+$ diminished and $[Ni(dmpe)_2]^{2+}$ precipitated. The reaction did not go to completion, but NMR yields (~50% formate) were greatly increased relative to acid-free conditions (~5% formate). As the reaction proceeded, ^{1}H NMR resonances for formate shifted upfield ($[HCO_2]^-$ δ 8.73 at 2 h, 8.66 at 18 h) while the *tert*-butyl group of ^{t}Bu$(CH_2)_2$B(C_8H_{14}) shifted downfield (^{t}*Bu*$(CH_2)_2$B(C_8H_{14}), δ 0.89

initially, 0.95 at 2 h, 0.97 at 18 h). Monitoring the reaction by ^{11}B NMR spectroscopy showed significant peak broadening along with an upfield shift as the reaction proceeded (Figure 5.1; δ 88.2 initially, 65 at 2 h, 51 at 18 h).

The CO_2 reduction product is conclusively assigned to formate based on separate experiments adding authentic sources of formate and reducing $^{13}CO_2$ (*vide infra*). As in **1**•(HCO_2), the [*H*CO_2]$^-$ ^{1}H NMR resonance does not match that of "free" [Bu_4N][HCO_2]. The dynamic spectral shifts and broadening are ascribed to adduct formation between formate and the trialkylborane;[10c] addition of ^{t}Bu(CH_2)$_2$B(C_8H_{14}) to [Bu_4N][HCO_2] in C_6D_5Cl prompted an upfield shift in the *H*CO_2 ^{1}H NMR resonance from δ 9.58 (no borane) to δ 8.89 (one equivalent of borane). The latter value compares well to the reaction of [HNi(dmpe)$_2$][PF_6] with ^{t}Bu(CH_2)$_2$B(C_8H_{14}) and CO_2 after addition of hept$_4$NBr (δ 8.79).

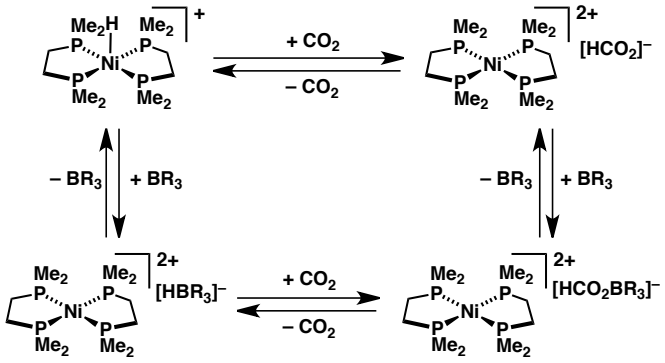

Scheme 5.6

The presence of a borane-formate adduct is also likely responsible for the enhanced CO_2 reduction chemistry of [HNi(dmpe)$_2$]$^+$. The mechanism of acid promotion (Scheme 5.6) could be thermodynamic in nature, if formate is stabilized by adduct formation by more

than 7 kcal mol^{-1} (the amount by which the reaction without borane is uphill, *vide supra*). The borane could play a kinetic role as well, such as through a "hydride shuttle" mechanism,[10d] but kinetic studies have not been undertaken as of yet. The reversible binding process exhibited by the borane-formate adduct could be extremely beneficial in a catalytic process, as compared to irreversible B–O formation in other catalytic transformations.

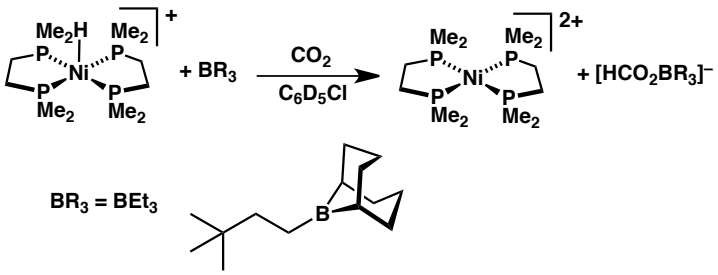

Scheme 5.7

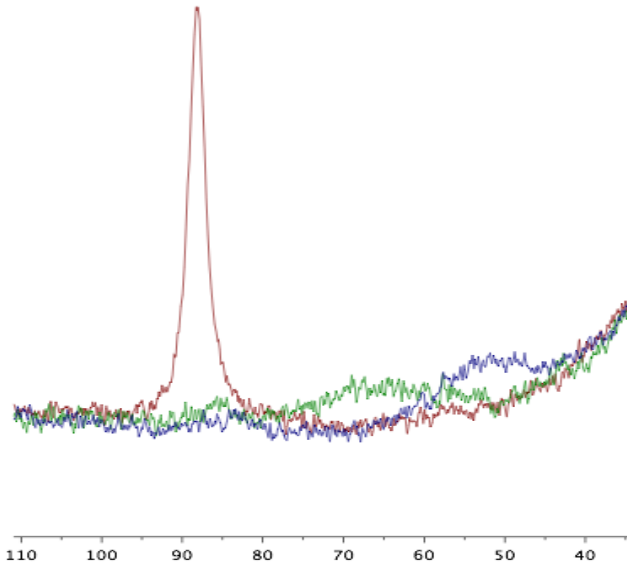

Figure 5.1. ^{11}B NMR spectra before CO_2 addition (red), after 2 hours (green), and after 18 hours (blue).

The reaction may stop at 50% conversion because of a natural equilibrium, or because of complications relating to precipitation of $[Ni(dmpe)_2]^{2+}$ from C_6D_5Cl. The slight shifts of the hydride signal of $[HNi(dmpe)_2]^+$ over the course of the reaction could be indicative of a change in counterion. Perhaps $[HNi(dmpe)_2][HCO_2]$ is stable relative to other species. The reaction was driven to completion upon addition of $hept_4NBr$ (and readmission of 1 atm CO_2). The tetraheptylammonium salt coaxes precipitation of $[Ni(dmpe)_2][Br]_2$ and provides a counter cation for $[HCO_2]^-$ other than either of the Ni species.

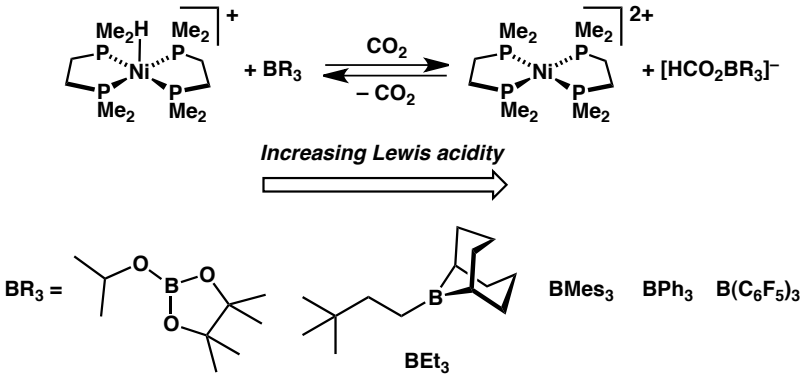

Scheme 5.8

A variety of boranes of varying Lewis acidity were employed in the reaction to assess the limits of Lewis acid assistance (Scheme 5.8). Isopropyl pinacol borate did not have any noticeable effect on the amount of formate produced. The small amount of formate that was produced resonated upfield of the formate produced in the absence of any Lewis acid (δ 8.84 vs. 8.74). Trimesitylborane also did not effect significant CO_2 reduction, perhaps due to steric constraints, but had a more pronounced upfield shift in the small amount of formate generated (δ 8.63), quite similar to the chemical shift in the trialkylborane

reactions. The upfield chemical shifts are consistent with some adduct formation, but the adduct appears to be disfavored by the less acidic and more bulky Lewis acids.

Addition of triphenylborane did impact the reduction, however: NMR monitoring showed formation of formate, along with some side products. The strong acid $B(C_6F_5)_3$ was also screened, but hydride transfer from Ni to B was observed before any CO_2 reduction could occur. A "frustrated Lewis pair" consisting of TMP (TMP = 2,2,6,6-tetramethylpiperidine) and $B(C_6F_5)_3$ have recently been shown to cleave H_2 to generate $[TMPH][HB(C_6F_5)_3]$, which reduces CO_2 to $HCO_2B(C_6F_5)_3$ at 100 °C.[8] We did not pursue this chemistry further, as we wished to avoid the strong B–O bonds of $HCO_2B(C_6F_5)_3$ and focus on Ni-based reactivity.

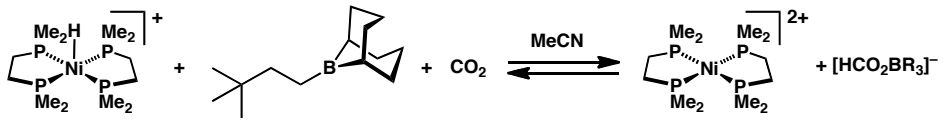

Scheme 5.9

All of the constituents are soluble in MeCN, which could allow observation of a true equilibrium process. Despite fears that MeCN would bind the borane too tightly to observe any acid assistance, treatment of $[HNi(dmpe)_2][PF_6]$ with 0-10 equiv $^tBu(CH_2)_2B(C_8H_{14})$ in CD_3CN did exhibit equilibrium behavior. With no added borane, ~5% conversion to $[Ni(dmpe)_2]^{2+}$ and $[HCO_2]^-$ (δ 8.40) was observed. Addition of just a single equivalent of borane promoted 60% conversion to $[HCO_2]^-$ (δ 8.29), consistent with a much larger K_{eq} (in different units). Addition of 10 equiv borane led to essentially complete conversion to

$[Ni(dmpe)_2]^{2+}$ and $[HCO_2]^-$ (δ 8.22). Accurate values for the equilbrium constants have not yet been measured.

Addition of one equivalent of $[Bu_4N][HCO_2]$ to the mixture at the end of the reaction led to an essentially negligible (0.003 ppm) shift in the $[HCO_2]^-$ resonance while the peak intensity and integration roughly doubled, indicating that the resonance between δ 8.2 and 8.4 was indeed formate. The origin of the formate was conclusively shown to be CO_2 by reaction of $[HNi(dmpe)_2][PF_6]$ with one equiv $^{13}CO_2$, which produced a 202 Hz doublet, δ 8.21, in the ^1H NMR spectrum, along with an intense resonance, δ 174.16, in the $^{13}C\{^1H\}$ NMR spectrum. The ^{11}B NMR resonance of the borane in CD_3CN is far upfield of the resonance in C_6D_5Cl, consistent with CD_3CN adduct formation. This must be reversible, however, as the ^{11}B NMR resonance shifts further upfield by ~3 ppm as formate is produced. A formate-borane adduct is also evidenced by shifts in ^1H NMR resonances of the borane and formate as the reaction proceeds. Borane adduct formation with formate must be significantly stronger than adduct formation with CD_3CN. The ready availability of $[HNi(dmpe)_2][PF_6]$ from H_2 with a suitable base such as NEt_3 suggests a net transformation of H_2 and CO_2 to $[HNEt_3][HCO_2]$ using a Ni species and Lewis acid assistance.

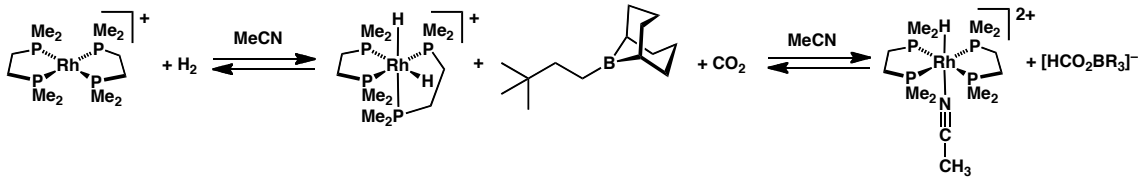

Scheme 5.10

Hydrogen could be used directly for CO_2 reduction by employing the rhodium cation $[Rh(dmpe)_2][OTf]$. Treatment of $[Rh(dmpe)_2][OTf]$ with a mixture of H_2 and CO_2 (1 atm total) in CD_3CN led to formation of some $[H_2Rh(dmpe)_2][OTf]$ (ΔG_{H^-} = 50.4 kcal mol^{-1}),[14] but no formate production over 4 days. Inclusion of ^{t}Bu$(CH_2)_2$B(C_8H_{14}) in the reaction led to the observation of formate over a few hours (δ 8.24) in addition to the Rh product of hydride transfer, $[HRh(dmpe)_2(MeCN)]^{2+}$ (Scheme 5.10). With one equivalent of borane, the reaction yielded ~25% formate. Some $[Rh(dmpe)_2]^+$ remained during the course of the reaction, consistent with H_2 oxidative addition being uphill by 0.44 kcal mol^{-1}.[14] Under 1 atm H_2 complete conversion is observed, but only ~0.5 atm H_2 is present at the start of these reactions. The similarity of the borane/formate chemical shifts in the Ni and Rh reactions suggests that adduct formation does not involve the metal center.

With the help of even small amounts of the appropriate borane Lewis acid, the Rh dihydride (with similar hydride strength to $[HNi(dmpe)_2]^+$) can utilize H_2 directly to reduce CO_2 under very mild conditions of pressure and temperature, and without the need for external base additives. The resulting Rh dication, $[HRh(dmpe)_2(MeCN)]^{2+}$, has a pK_a almost identical to $[HNEt_3]^+$ in MeCN (18.9[14] and 18.8,[15] respectively).

Attempted catalysis and dihydrogen cleavage solvent dependence

In order to achieve a catalytic reaction in nickel, a suitable base such as NEt_3[12d] must cleave H_2 in concert with $[Ni(dmpe)_2]^{2+}$, followed by hydride delivery to CO_2. All of the reagents are compatible with each other; sufficient steric bulk is required to avoid stable Lewis adduct formation. A mixture of $[Ni]^{2+}$, 4 equiv NEt_3, and 4 equiv BEt_3 were subjected to a

1:1 mixture of H_2/CO_2 (1 atm) in CD_3CN, and slow conversion to small amounts of formate was observed. Only ~8% formate relative to Ni was observed over 3 days; but this non-catalytic reaction confirmed that even $[Ni(dmpe)_2]^{2+}$ can moderate CO_2 reduction using H_2 (and NEt_3) directly. Formation of $[HNi(dmpe)_2]^+$ is extremely slow in these conditions, perhaps accounting for the problems; a mixture of $[Ni(dmpe)_2][PF_6]_2$ and NEt_3 (4 equiv) was only 30% converted to $[HNi(dmpe)_2][PF_6]$ after 3 days under 1 atm H_2.

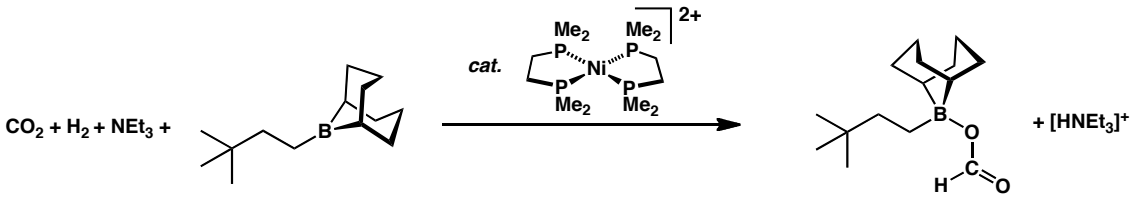

Scheme 5.11

Frustrated by the sluggish H_2 cleavage reactivity of $[Ni(dmpe)_2][PF_6]_2$ in CD_3CN, we generated $[Ni(dmpe)_2][BAr^F{}_4]_2$ and tested the reactivity in C_6D_5Cl. Surprisingly, the reaction of $[Ni(dmpe)_2][BAr^F{}_4]_2$ and NEt_3 with H_2 proceeded far faster in C_6D_5Cl, with high conversion to $[HNi(dmpe)_2]^+$ in 3 hours, and full conversion after 18 hours.

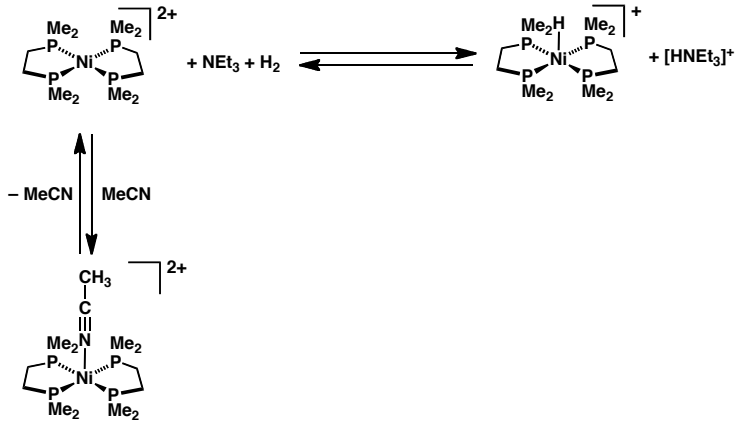

Scheme 5.12

It is exciting that the slow kinetics of H_2 cleavage are not a result of any implicit characteristic of $[Ni(dmpe)_2]^{2+}$, but rather appear to be a problem unique to acetonitrile solutions. Waiting days for hydride formation would preclude the use of bis(diphosphine)nickel complexes in any practical applications; the use of non-coordinating solvents makes these nickel hydride delivery reagents more relevant (and able to compete with more expensive Pt analogues in terms of rates). Anion effects were discounted by placing $[Ni(dmpe)_2][BAr^F{}_4]_2$ and NEt_3 under H_2 in CD_3CN, which proceeded at roughly the same rate as heterolytic cleavage by $[Ni(dmpe)_2][PF_6]_2$. We ascribe the slow heterolytic cleavage of H_2 in CD_3CN to solvent inhibition, as shown in Scheme 5.12: the 5-coordinate 18 e^- MeCN adduct $[Ni(dmpe)_2(MeCN)]^{2+}$ has been structurally characterized,[12a] and dissociation of MeCN would be inhibited by the solvent. DuBois estimated $K_{eq} = 0.3$ for adduct formation using electrochemical techniques. While this equilibrium must be dealt with in MeCN solutions, in chlorobenzene no donor binds the axial position of the square planar Ni (a structure of 4-coordinate $[Ni(dmpe)_2]^{2+}$ is also known)[12a]. Bis(diphosphine)platinum dications do not form 5-coordinate species in acetonitrile, accounting for the difference in reactivity between Ni and Pt in that solvent.

Catalytic conditions similar to those in acetonitrile were employed, and despite the steady growth of $[HNi(dmpe)_2]^+$ over a few days, the reaction did not produce any detectable formate. Reactions in the more commonly used solvent CD_2Cl_2 were also briefly explored, but formation of CD_2HCl was observed, indicating a hydride transfer side reaction. It is unclear why no formate is observed in chlorobenzene, especially in light of the partial conversion in CD_3CN. One possibility is that while the H_2 cleavage reaction is enhanced by

the BAr^{F}_{4} counterions, the hydride transfer reaction is slowed, as observed for CO reduction.[10d]

Conclusions

Partially reduced rhenium carbonyl species and late transition metal bis(diphosphine) hydrides both reduce carbon dioxide to formate. The trialkylborane groups that promote key steps in CO reduction are also crucial to the observed CO_2 reduction reactivity. Borane-formate adduct formation is likely responsible for the favorable shift in equilibrium towards formate products. Encouragingly, the borane-formate adduct is relatively weakly bound (as judged by NMR spectroscopy), which raises the promise of such additives being useful in catalytic systems. While catalysis has so far eluded us, we have also shown that H_2 and CO_2 can be used directly in Ni and Rh systems to produce the borane-formate adduct; notably, these systems are unable to reduce more than a trace amount of CO_2 in the absence of an appropriate Lewis acid. The dihydrogen cleavage step required for catalysis was also briefly explored, and the judicious choice of anion and solvent can greatly accelerate the heterolytic cleavage of dihydrogen by bis(diphosphine)nickel dications. The reported improvements in dihydrogen cleavage, coupled with a new gentle strategy for promoting CO_2 reduction by hydride transfer, point towards a practical catalytic CO_2 hydrogenation system based on a nickel.

Experimental Section

General Considerations

All air- and moisture-sensitive compounds were manipulated using standard vacuum line or Schlenk techniques, or in a glovebox under a nitrogen atmosphere. Under standard glovebox conditions, petroleum ether, diethyl ether, benzene, toluene, and tetrahydrofuran were used without purging, such that traces of those solvents were in the atmosphere, and could be found intermixed in the solvent bottles. The solvents for air- and moisture-sensitive reactions were dried over sodium benzophenone ketyl, calcium hydride, or by the method of Grubbs.[16] All NMR solvents were purchased from Cambridge Isotopes Laboratories, Inc. Chlorobenzene-d_5 (C_6D_5Cl) and dichloromethane-d_2 (CD_2Cl_2) were freeze–pump–thaw degassed three times before being run through a small column of activated alumina. Tetrahydrofuran-d_8 (THF-d_8) was purchased in a sealed ampoule, and dried by passage through activated alumina. Unless noted, other materials were used as received. [**1**][BF_4][10a] **2**, [Pt(dmpe)$_2$][PF_6]$_2$,[11] [HPt(dmpe)$_2$][PF_6],[11] [Ni(dmpe)$_2$][BF_4]$_2$,[12a] [HNi(dmpe)$_2$][PF_6],[11] ^{t}Bu(CH_2)$_2$B(C_8H_{14}),[17] [Bu_4N][HCO_2],[18] [Ni(dmpe)$_2$][$BAr^F{}_4$]$_2$,[10c] and [Rh(dmpe)$_2$][OTf][12h,14] were synthesized by literature methods. All other materials were readily commercially available, and used as received. ^{1}H and ^{13}C NMR spectra were recorded on Varian Mercury 300 MHz, or Varian INOVA-500 or 600 MHz spectrometers at room temperature, unless indicated otherwise. Chemical shifts are reported with respect to residual internal protio solvent for ^{1}H and ^{13}C{^{1}H} spectra. Other nuclei were referenced to an external standard: H_3PO_4 (^{31}P), 15% BF_3•Et_2O/$CDCl_3$ (^{11}B), $CFCl_3$ (^{19}F), all at 0 ppm.

Experimental Procedures

Reaction of 2 with CO_2. A 10 mL vial was charged with 26.4 mg (0.0251 mmol) [**1**][BF_4] and ~0.6 mL C_6D_5Cl. With stirring, 25.1 μL (0.0251 mmol) $NaHBEt_3$ (1.0 M in toluene) was added dropwise to provide a pale yellow solution. The reaction mixture was transferred to a J-Young NMR tube and initial spectroscopic measurements showed clean conversion to boroxycarbene **2**. The tube was placed under vacuum for 1 minute with gentle shaking to degas, and one atmosphere of CO_2 was then admitted to the tube. NMR spectroscopy after 5 minutes showed complete conversion to a new product, most of which precipitated overnight. **^{1}H NMR** (C_6D_5Cl, 500 MHz): toluene and BEt_3 are omitted, but overlap with some aliphatic peaks, preventing good integration. δ 0.69 (br s, 4H), 1.59 (br s, overlapping), 1.84 (br, overlapping), 2.05 (br m, overlapping), 2.73 (br, 4H), 7.41 (br, 12H), 8.45 (s, 1H, *H*CO_2^-). **^{31}P{^{1}H} NMR** (C_6D_5Cl, 121 MHz): δ 2.2. **IR** (C_6D_5Cl): ν_{CO}1993, 1620 cm^{-1}.

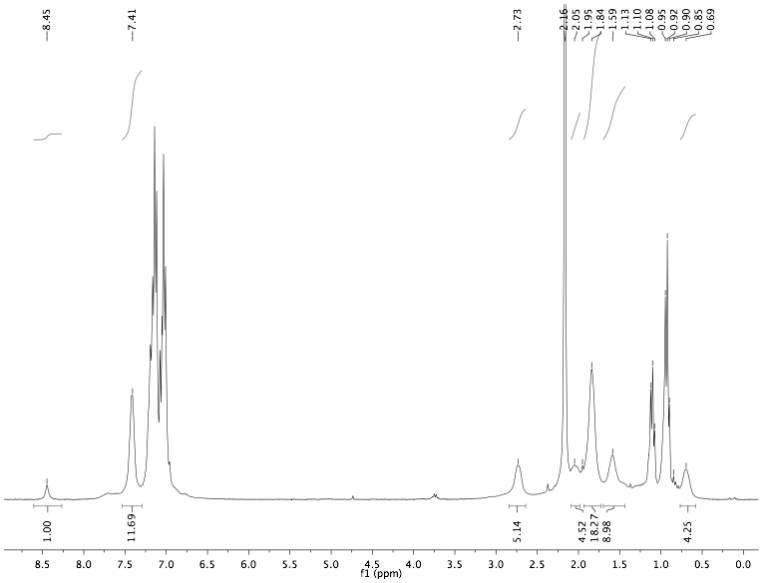

Figure 5.2. ^{1}H NMR of **1**•(HCO_2).

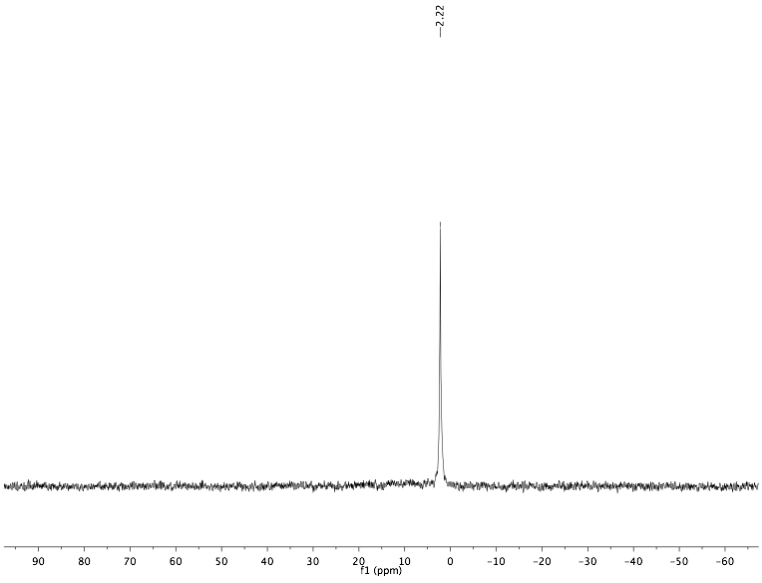

Figure 5.3. $^{31}P\{^{1}H\}$ NMR of **1**•(HCO_2).

Reaction of [1][BF_4] with [Bu_4N][HCO_2]. A J-Young NMR tube was charged with 29.1 mg (0.0276 mmol) [**1**][BF_4], 7.9 mg (0.0276 mmol) [Bu_4N][HCO_2], and ~0.6 mL C_6D_5Cl. After 15 minutes, ^{1}H and $^{31}P\{^{1}H\}$ NMR spectroscopy showed essentially complete conversion to **1**•(HCO_2). After about 30 minutes, some precipitates were

observed, and precipitation of white solids continued over the next 3 hours. At this time, the solution was decanted, and IR spectroscopy showed resonances that matched the preparation of **1**•(HCO_2) from CO_2; an additional peak at 1660 cm^{-1} is unidentified, however. **^{1}H NMR** (C_6D_5Cl, 400 MHz): $[Bu_4N]^+$ peaks omitted. δ 0.68 (br, 4H), 0.95 (br, 4H), 1.58 (br, 4H), 1.83 (br, 16H), 2.03 (br, 4H), 2.75 (br, 4H), 7.1-7.2 (m, 12H), 7.4 (m, 8H), 8.49 (s, 1H, $[HCO_2]^-$). **^{31}P{^{1}H} NMR** (C_6D_5Cl, 162 MHz): δ 2.4. IR (C_6D_5Cl): 1993, 1660, 1621 cm^{-1}.

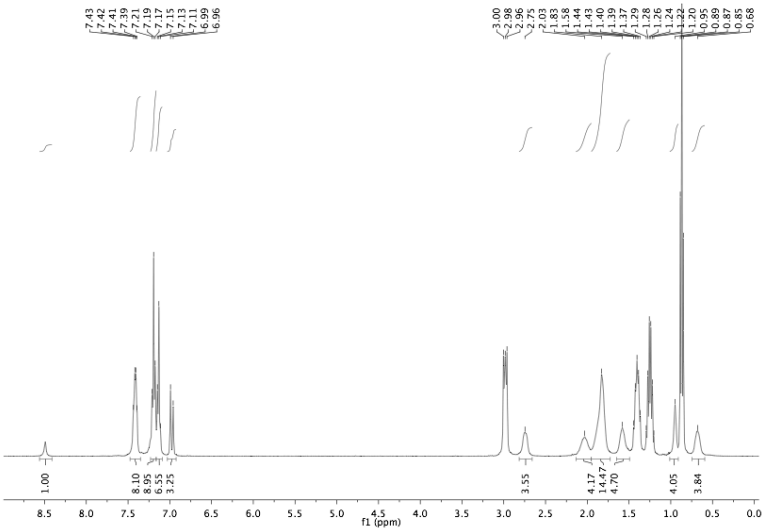

Figure 5.4. ^{1}H NMR of **1**•(HCO_2) (from $[Bu_4N][HCO_2]$).

Reaction of [1][BF_4] and [HNi(dmpe)$_2$][PF_6] with CO_2 in C_6D_5Cl. A J-Young NMR tube was charged with 24.3 mg (0.0231 mmol) [**1**][BF_4], 11.6 mg (0.0231 mmol) [HNi(dmpe)$_2$][PF_6], and ~0.6 mL C_6D_5Cl. The tube was sealed and initial NMR spectroscopic measurements were made which showed no reaction, at which point 1 atm CO_2 was added. After ~20 minutes some formate was observed, which grew in over a few hours. During this time precipitates formed, and after about 12 hours there was essentially

no formate-containing products in solution. The solids were collected, and washed with CD_3CN (which extracted $[Ni(dmpe)_2][PF_6]_2$) and C_6D_5Cl. Then the solids were treated with C_6D_5Cl and 3.8 μL (0.0462 mmol, 2 equiv) pyridine, which prompted the majority of the solids to dissolve. An asymmetric product was observed by NMR which was assigned as **1**•(HCO_2)(pyridine).

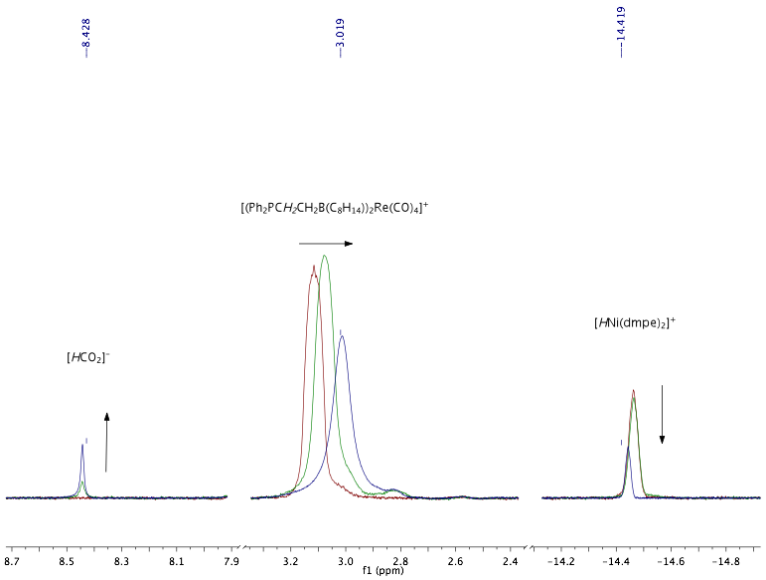

Figure 5.5. Time course (^{1}H NMR excerpts) of reaction of [**1**]$^+$ with $[HNi(dmpe)_2]^+$ and CO_2.

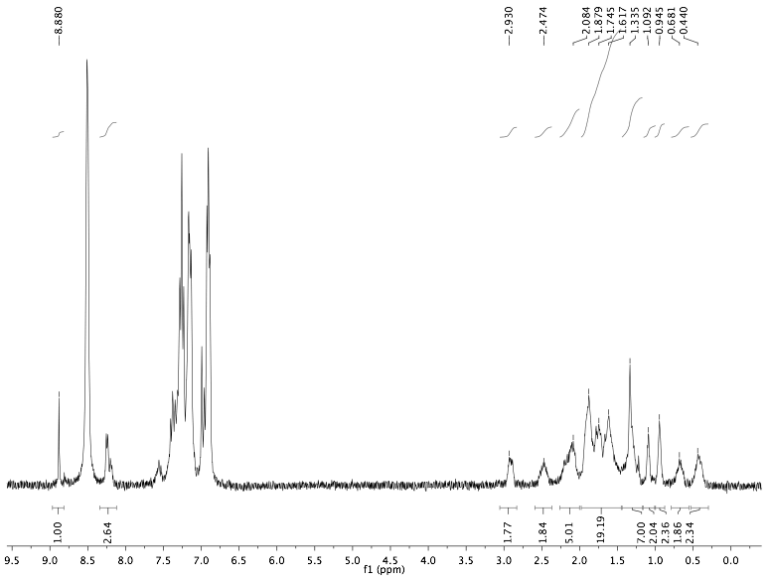

Figure 5.6. ^{1}H NMR of **1**•(HCO_2)(pyridine).

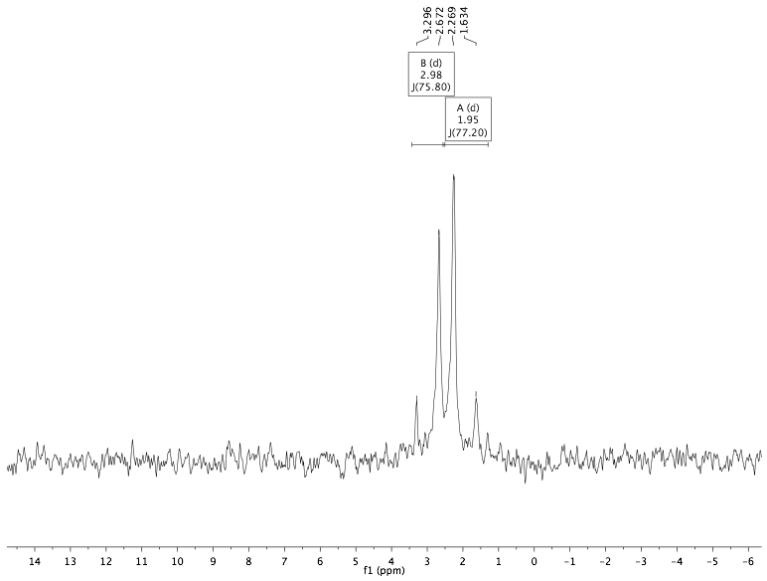

Figure 5.7. $^{31}P\{^{1}H\}$ NMR of **1**•(HCO_2)(pyridine).

Reactions in chlorobenzene

Reaction of [HNi(dmpe)$_2$][PF$_6$] with ^{t}Bu(CH$_2$)$_2$B(C$_8$H$_{14}$) and CO$_2$. A ~0.6 mL C_6D_5Cl solution of 6.7 mg (0.0327 mmol) ^{t}Bu(CH_2)$_2$B(C_8H_{14}) was added to 16.5 mg (0.0327

mmol) solid $[HNi(dmpe)_2][PF_6]$. The reaction mixture was transferred to a J-Young NMR tube, and initial spectroscopic measurements were made. After two freeze–pump–thaw cycles, 1 atm CO_2 was admitted to the tube, and the reaction was monitored by NMR spectroscopy. After 24 hours the reaction had reached partial conversion, which did not change over 4 days. Addition of 16.0 mg (0.0327 mmol) $[hept_4N][Br]$ led to essentially complete conversion to $[hept_4N][HCO_2BR_3]$.

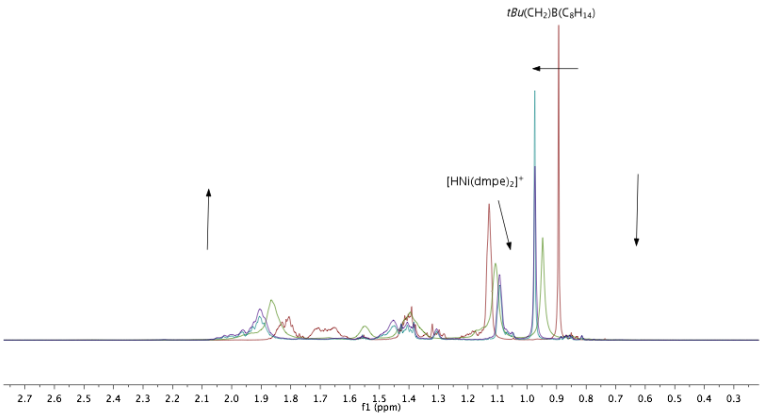

Figure 5.8. Time course (^{1}H NMR alkyl region) of reaction of $[HNi(dmpe)_2]^+$ with ^{t}Bu$(CH_2)_2B(C_8H_{14})$ and CO_2.

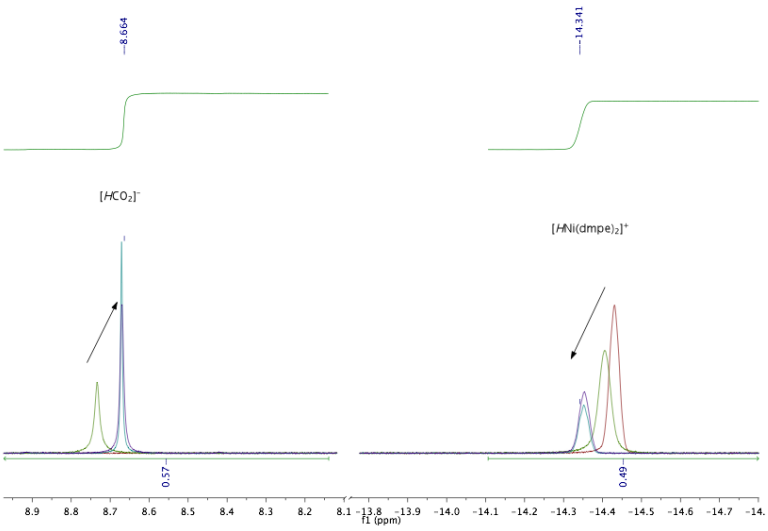

Figure 5.9. Time course (^{1}H NMR formate and hydride region) of reaction of $[HNi(dmpe)_2]^+$ with ^{t}Bu$(CH_2)_2$B(C_8H_{14}) and CO_2.

General procedure for reactions of [HNi(dmpe)$_2$][PF$_6$] with other boranes. A ~0.6 mL C_6D_5Cl solution of borane (~0.03 mmol) was added to an equimolar amount of solid $[HNi(dmpe)_2][PF_6]$. The reaction mixture was transferred to a J-Young NMR tube, and initial spectroscopic measurements were made. After two freeze–pump–thaw cycles, 1 atm CO_2 was admitted to the tube, and the reaction was monitored by NMR spectroscopy.

Isopropyl pinacol borate. The reaction proceeded essentially the same as that with no borane added. The formate resonance appears between δ 8.70 and 8.74 during the reaction, significantly upfield of $[Bu_4N][HCO_2]$ (δ 9.58) and the trace formate produced in acid-free reaction (δ 8.84), but downfield of the reaction with ^{t}Bu$(CH_2)_2$B(C_8H_{14}) (δ 8.66); this could be due to a weak B–O interaction or effects related to the identity of the counter cation.

Triphenylborane. A presumed formate resonance is visible at 8.8 ppm by ^{1}H NMR, along with some unidentified peaks between 5 and 6 ppm. The phenyl region of BPh_3 suggests formation of multiple products, and essentially complete transfer of $[HNi(dmpe)_2]^+$ is observed.

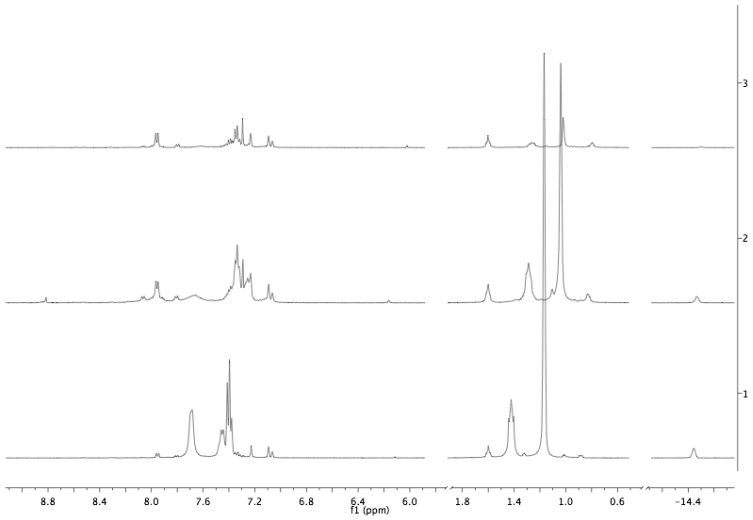

Figure 5.10. Reaction of $[HNi(dmpe)_2]^+$ and BPh_3 before CO_2 addition (bottom); 5 hours after addition (middle); 2 days after addition (top).

Trimesitylborane. No change in reactivity was observed as compared to the reaction without borane. Formate chemical shift (δ 8.63) was, however, similar to the reaction with ^{t}Bu$(CH_2)_2$B(C_8H_{14}) (δ 8.66).

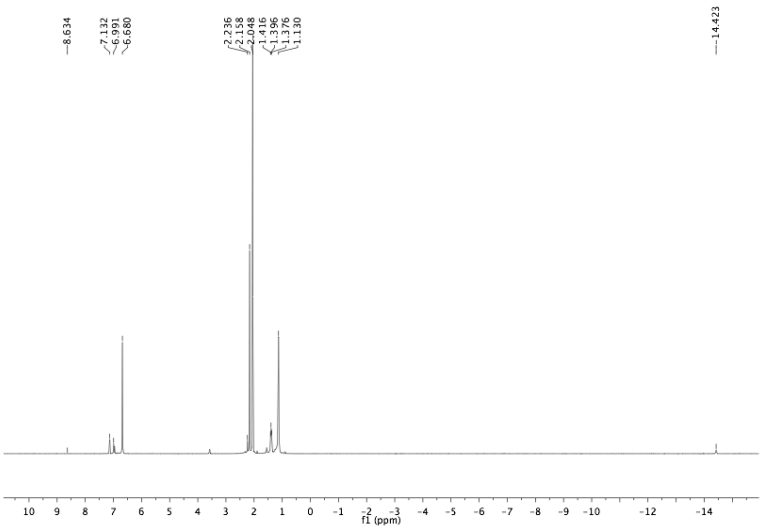

Figure 5.11. ^{1}H NMR of mixture of $[HNi(dmpe)_2]^+$, $BMes_3$, and CO_2.

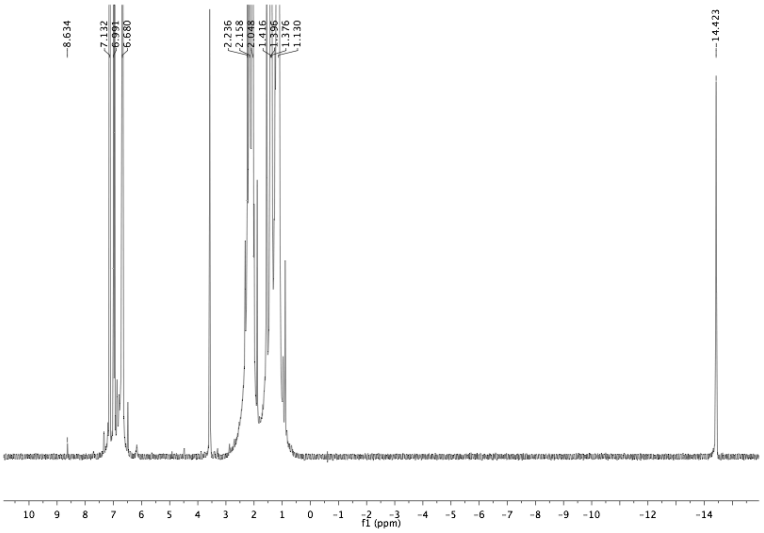

Figure 5.12. ^{1}H NMR (blow-up) of mixture of $[HNi(dmpe)_2]^+$, $BMes_3$, and CO_2.

$B(C_6F_5)_3$. This reaction appears to result in hydride abstraction to form $[HB(C_6F_5)_3]^-$. The ^{19}F NMR is consistent with a 4-coordinate borate environment, and complete comsumption of $B(C_6F_5)_3$ (some $[HNi(dmpe)_2]^+$ was left over due to poor stoichiometry); ^{11}B NMR is also consistent, although the resonance is slightly downfield from the expected chemical shift of $[HB(C_6F_5)_3]^-$, and the resonance is broadened beyond being able to

observe coupling. This could be due to exchange with some free borane or with the Ni if the reaction is reversible. Even if CO_2 is added after this point, no formate was observed overnight at room temperature. Heating to 100 °C resulted in a small amount of formate, consistent with hydride transfer from either the small amount of remaining $[HNi(dmpe)_2]^+$ or from $[HB(C_6F_5)_3]^-$ as reported by Ashley et al.[8]

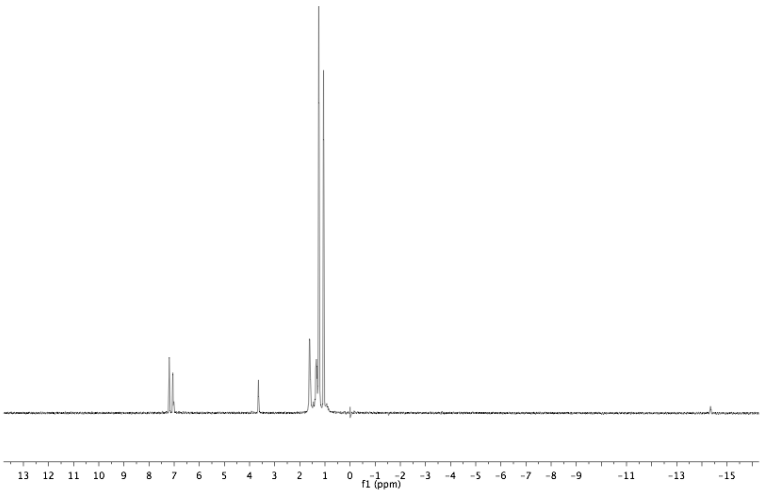

Figure 5.13. ^1H NMR of reaction of $[HNi(dmpe)_2]^+$ with $B(C_6F_5)_3$ and CO_2.

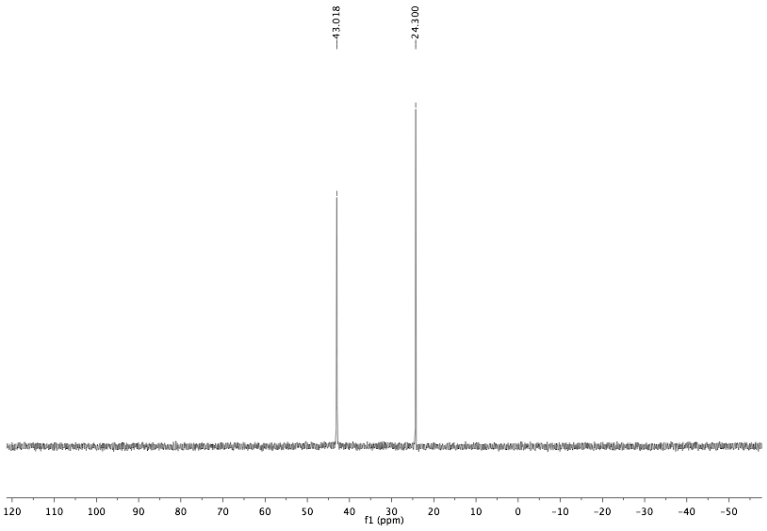

Figure 5.14. $^{31}P\{^{1}H\}$ NMR of reaction of $[HNi(dmpe)_2]^+$ with $B(C_6F_5)_3$ and CO_2.

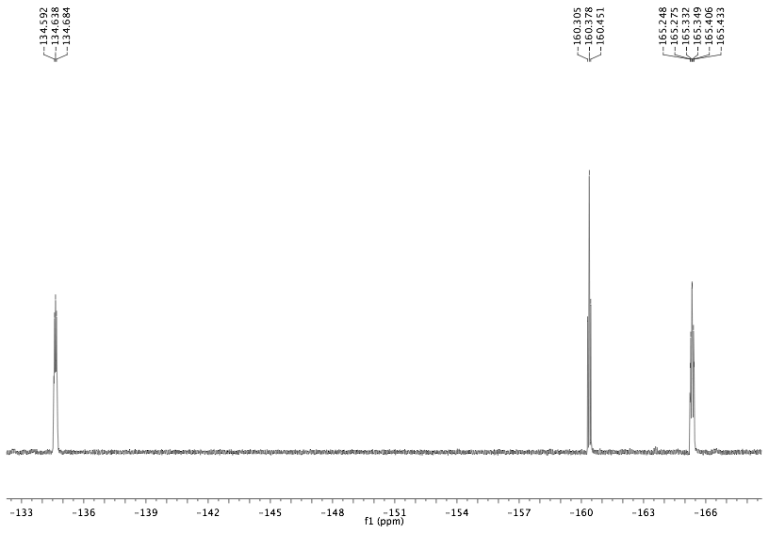

Figure 5.15. ^{19}F NMR of reaction of $[HNi(dmpe)_2]^+$ with $B(C_6F_5)_3$ and CO_2.

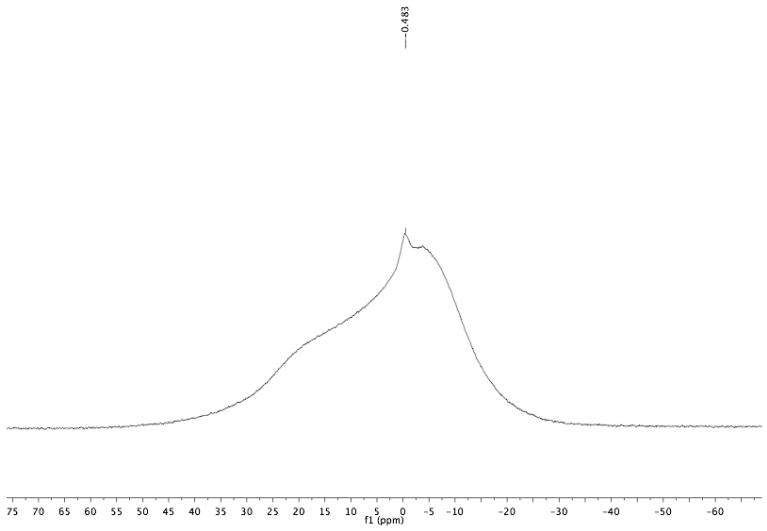

Figure 5.16. ^{11}B NMR of reaction of $[HNi(dmpe)_2]^+$ with $B(C_6F_5)_3$ and CO_2.

Reaction of $[Bu_4N][HCO_2]$ with ^{t}Bu$(CH_2)_2$B(C_8H_{14}) in C_6D_5Cl. A J-Young NMR tube was charged with 15.8 mg (0.0549 mmol) $[Bu_4N][HCO_2]$, 11.3 mg (0.0549 mmol) ^{t}Bu$(CH_2)_2$B(C_8H_{14}), and ~0.6 mL C_6D_5Cl. NMR spectroscopy revealed a formate resonance at δ 8.89, well upfield of $[Bu_4N][HCO_2]$ in the absence of borane (δ 9.58). The broad ^{11}B signal appears to be around δ 2.7. **^{1}H NMR** (C_6D_5Cl, 500 MHz): δ 0.76 (m, ^{t}BuCH$_2$C*H$_2$*B(C_8H_{14}), 2H), 0.86 (t, J = 7.3 Hz, N$(CH_2CH_2CH_2CH_3)_4$, 12H), 1.04 (s, ^{t}*Bu*CH$_2$CH$_2$B(C_8H_{14}), 9H), 1.25 (q, J = 7.2 Hz, N$(CH_2CH_2CH_2CH_3)_4$, 8H), 1.4 (m, 10H, N$(CH_2CH_2CH_2CH_3)_4$ and ^{t}BuC*H$_2$*CH$_2$B(C_8H_{14}) overlapping), 1.83 (br, ^{t}BuCH$_2$CH$_2$B(C_8H_{14}), 2H), 1.97 (br, ^{t}BuCH$_2$CH$_2$B(C_8H_{14}), 4H), 2.28 (br, ^{t}BuCH$_2$CH$_2$B(C_8H_{14}), 6H), 3.00 (m, N$(CH_2CH_2CH_2CH_3)_4$), 8.89 (s, HCO_2^-, 1H). **^{13}C{^{1}H} NMR** (C_6D_5Cl, 126 MHz): δ 13.66, 19.87, 23.91, 26.80, 30.05, 31.35, 33.0 (br), 40.75, 58.66, 168.48. **^{11}B NMR** (C_6D_5Cl, 160 MHz): δ 2.7.

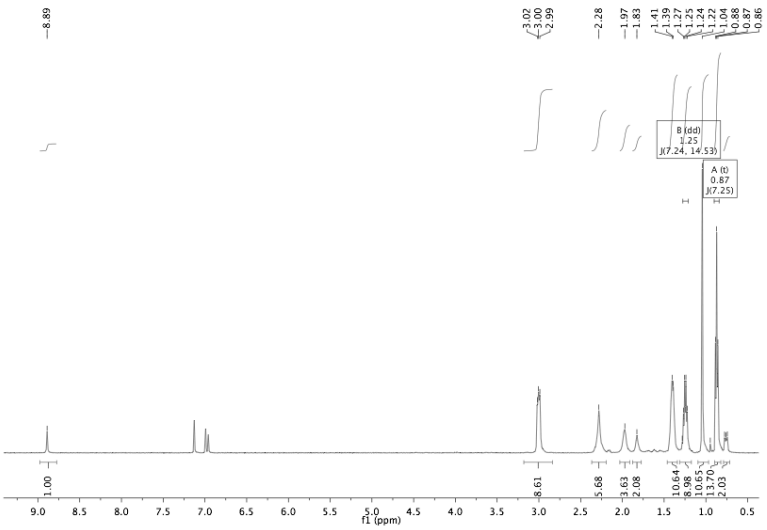

Figure 5.17. ^{1}H NMR of $[Bu_4N][HCO_2BR_3]$.

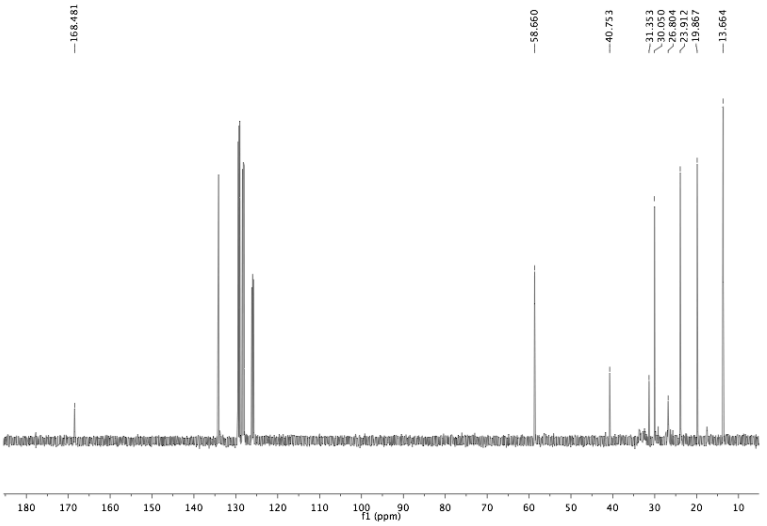

Figure 5.18. $^{13}C\{^{1}H\}$ NMR of $[Bu_4N][HCO_2BR_3]$.

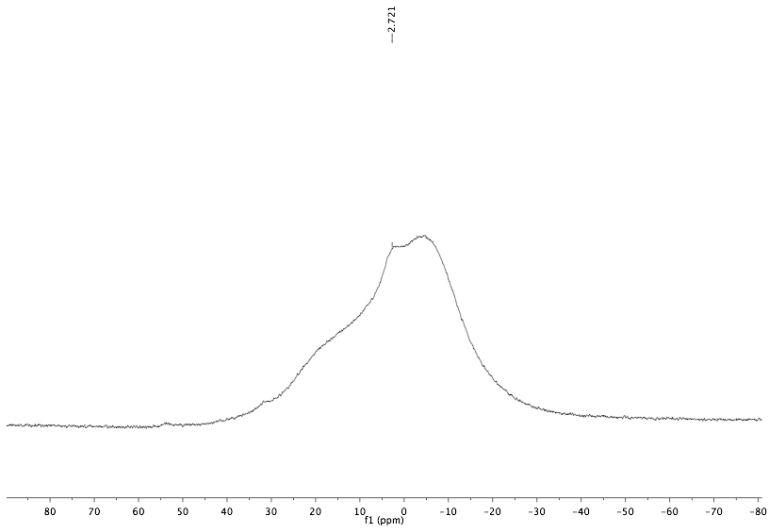

Figure 5.19. ^{11}B NMR of $[Bu_4N][HCO_2BR_3]$.

General procedure for reactions of $[HNi(dmpe)_2][PF_6]$ in acetonitrile. A J-Young NMR tube was charged with $[HNi(dmpe)_2][PF_6]$ (~0.03 mmol), the appropriate amount of $^tBu(CH_2)_2B(C_8H_{14})$ (0, 1, 10 equiv), and ~0.6 mL C_6D_5Cl. The tube was sealed, initial NMR measurements were taken, and the atmosphere replaced with 1 atm CO_2 (after freeze–pump–thaw degassing twice). The reactions were monitored periodically by multinuclear NMR until equilibrium was reached (under 24 hours). The spectra at equilibrium are overlaid below.

CO_2. About 5% hydride transfer was observed.

1 equiv $^tBu(CH_2)_2B(C_8H_{14})$ and CO_2. About 65% hydride transfer was observed.

10 equiv $^tBu(CH_2)_2B(C_8H_{14})$ and CO_2. Nearly quantitative hydride transfer was observed.

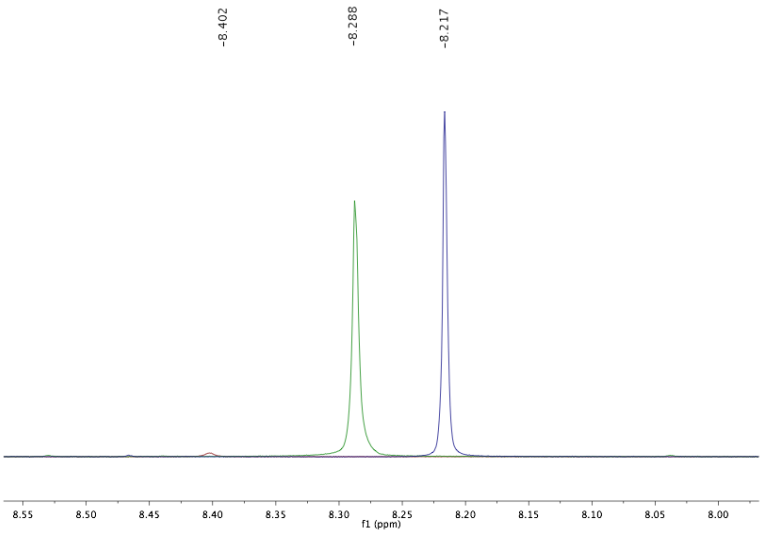

Figure 5.20. Overlay (^{1}H NMR, formate region) of equilibrated reactions of $[HNi(dmpe)_2]^+$ with CO_2 and 0 (red), 1 (green) and 10 (blue) equiv ^{t}Bu$(CH_2)_2$B(C_8H_{14}).

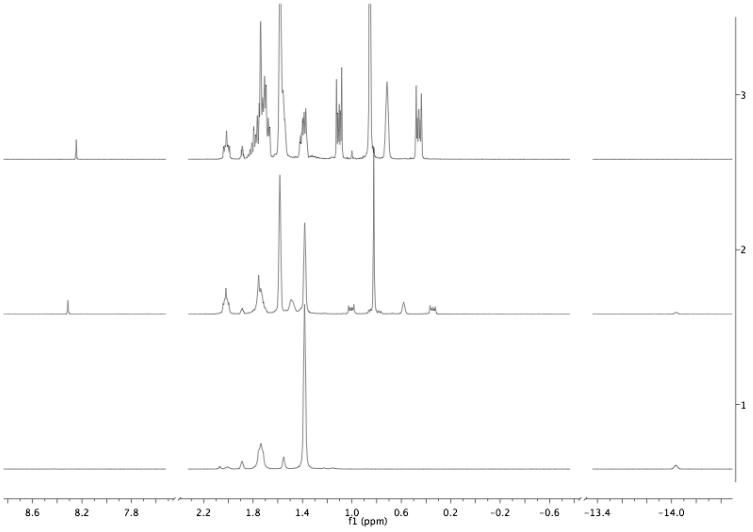

Figure 5.21. Comparison (^{1}H NMR) of equilibrated reactions of $[HNi(dmpe)_2]^+$ with CO_2 and 0 (bottom), 1 (middle) and 10 (top) equiv ^{t}Bu$(CH_2)_2$B(C_8H_{14}).

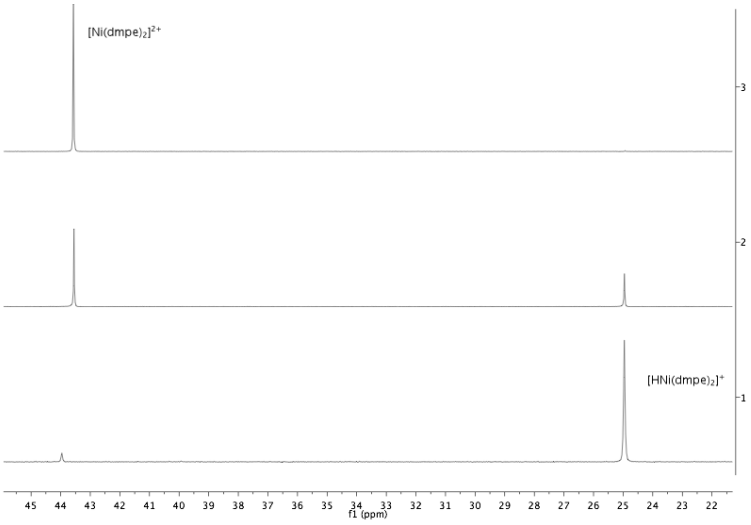

Figure 5.22. Comparison ($^{31}P\{^{1}H\}$ NMR) of equilibrated reactions of $[HNi(dmpe)_2]^+$ with CO_2 and 0 (bottom), 1 (middle) and 10 (top) equiv $^{t}Bu(CH_2)_2B(C_8H_{14})$.

Addition of $[Bu_4N][HCO_2]$. A 1:10 mixture of $[HNi(dmpe)_2][PF_6]$ and $^{t}Bu(CH_2)_2B(C_8H_{14})$ was treated with CO_2 according to the general procedure. After reaction was complete, the tube was brought into a glovebox and 1 equiv $[Bu_4N][HCO_2]$ was added to the tube. The spectra showed a tiny (0.003 ppm) shift in the formate peak, while it grew in intensity, thereby confirming its identity.

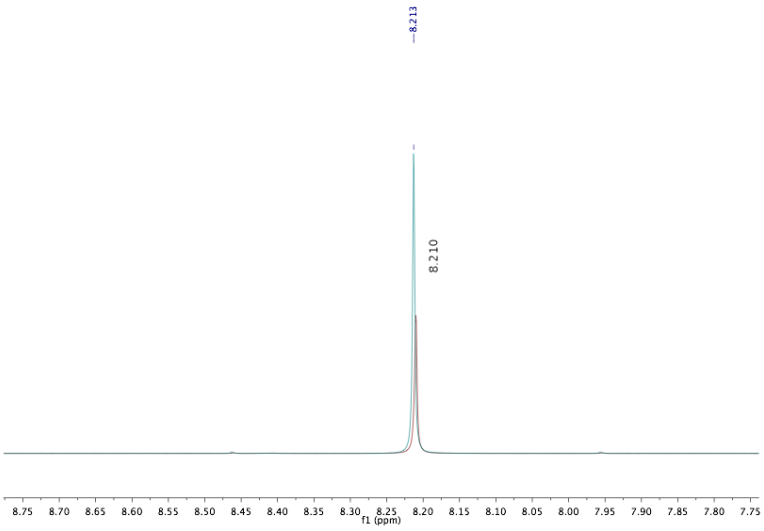

Figure 5.23. ^{1}H NMR (formate region) after reaction of $[HNi(dmpe)_2]^+$ with $^{t}Bu(CH_2)_2B(C_8H_{14})$ and CO_2 (red); after addition of $[Bu_4N][HCO_2]$ (blue).

Reaction with $^{13}CO_2$. A J-Young NMR tube was charged with 18.9 mg (0.0374 mmol) $[HNi(dmpe)_2][PF_6]$, 38.6 mg (0.187 mmol, 5 equiv) $^{t}Bu(CH_2)_2B(C_8H_{14})$, and ~0.6 mL CD_3CN. After initial NMR spectroscopic measurements, the tube was subjected to two freeze–pump–thaw cycles, and 0.0187 mmol (0.5 equiv) $^{13}CO_2$ was condensed from a 2.87 mL calibrated gas bulb (11.8 mmHg). About 5% conversion to $[Ni(dmpe)_2][PF_6]_2$ had occurred after 30 minutes, and a small doublet could be seen by ^{1}H NMR. After 12 hours, a large doublet at δ 8.21 (202 Hz) was visible, consistent with formation of $[H^{13}CO_2]^-$.

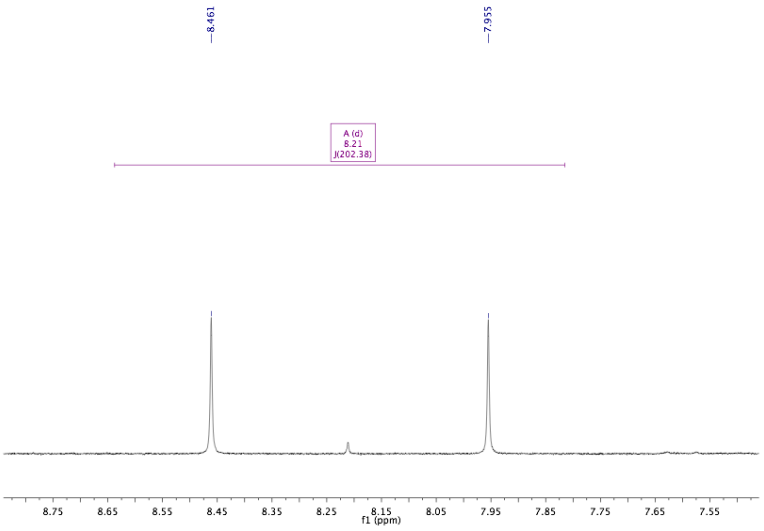

Figure 5.24. 1H NMR (formate region) of reaction of $[HNi(dmpe)_2]^+$ with $^tBu(CH_2)_2B(C_8H_{14})$ and $^{13}CO_2$ (12 hours).

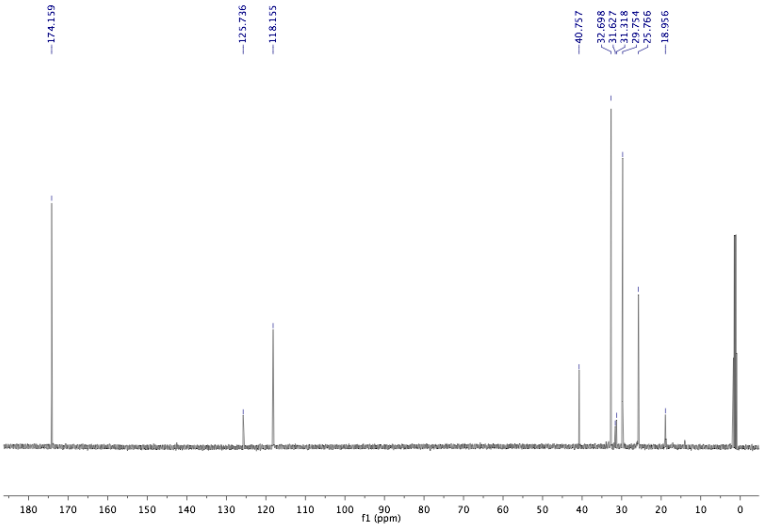

Figure 5.25. $^{13}C\{^1H\}$ NMR of reaction of $[HNi(dmpe)_2]^+$ with $^tBu(CH_2)_2B(C_8H_{14})$ and $^{13}CO_2$ (12 hours).

Reaction of $[Ni(dmpe)_2][PF_6]_2$ with $[Bu_4N][HCO_2]$. A small vial was charged with 19.7 mg (0.0359 mmol) $[Ni(dmpe)_2][PF_6]_2$ and 10.3 mg (0.0359 mmol), and ~0.6 mL CD_3CN. As the mixture was stirred a color change from yellow to dark orange was observed. The mixture was transferred to a J-Young NMR tube, and monitored. The color

faded to a lighter orange over a few minutes. After 15 minutes, almost complete conversion (~95%) to $[HNi(dmpe)_2][PF_6]$ was observed, although a slight excess of $[HCO_2]^-$ was still present.

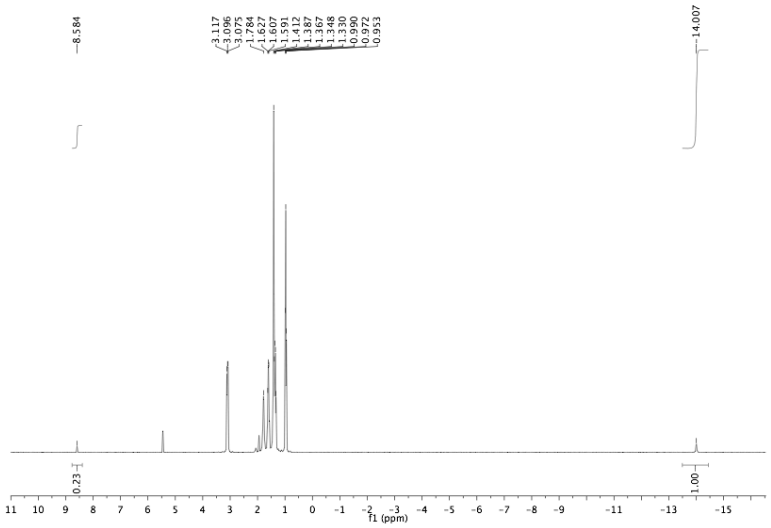

Figure 5.26. ^1H NMR after mixing $[Ni(dmpe)_2][PF_6]_2$ with $[Bu_4N][HCO_2]$.

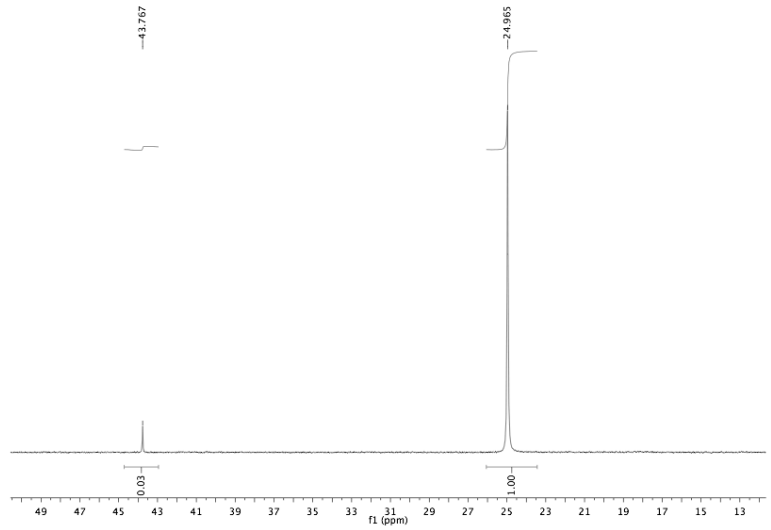

Figure 5.27. $^{31}P\{^1H\}$ NMR after mixing $[Ni(dmpe)_2][PF_6]_2$ with $[Bu_4N][HCO_2]$.

Reaction of $[Rh(dmpe)_2][OTf]$ with H_2 and CO_2. A J-Young NMR tube was charged with 19 mg (0.0344 mmol) $[Rh(dmpe)_2][OTf]$ and ~0.6 mL CD_3CN. The tube

was placed under 1 atm of a 1:1 mixture of H_2 and CO_2, mixed by diffusion in a large round bulb on a vacuum manifold. The reaction was monitored by multinuclear NMR, which showed formation of $[H_2Rh(dmpe)_2][OTf]$, but no more than a trace of formate was observed.

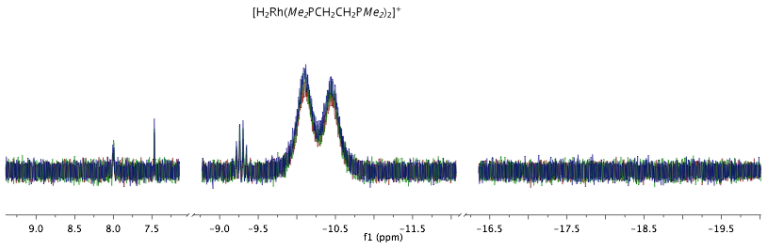

Figure 5.28. ^1H NMR overlay (formate and hydride regions) of reaction of $[Rh(dmpe)_2]^+$ with CO_2 and H_2. After 3 hours (red), 24 hours (green), 4 days (blue).

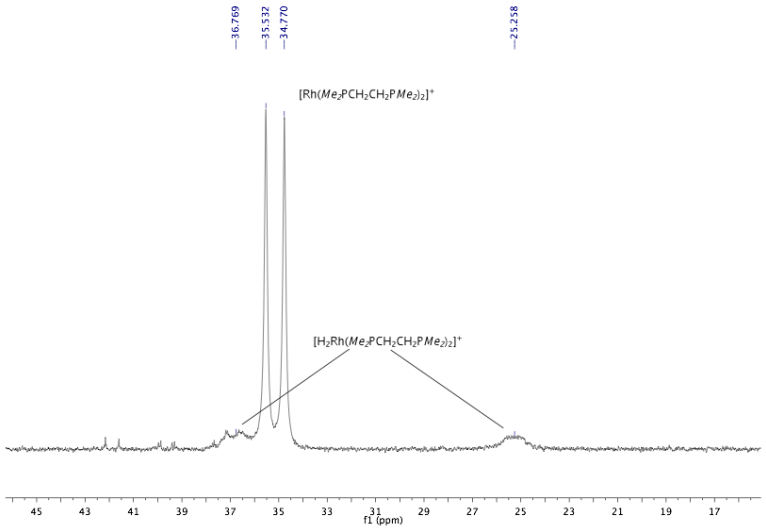

Figure 5.29. $^{31}P\{^1H\}$ NMR of reaction of $[Rh(dmpe)_2]^+$ with CO_2 and H_2 after 24 hours.

Reaction of $[Rh(dmpe)_2][OTf]$ with ^{t}Bu$(CH_2)_2$B(C_8H_{14}) and H_2/CO_2. A J-Young NMR tube was charged with 15.9 mg (0.0288 mmol) $[Rh(dmpe)_2][OTf]$, 5.9 mg (0.0288 mmol) ^{t}Bu$(CH_2)_2$B(C_8H_{14}), and ~0.6 mL CD_3CN. The tube was placed under 1 atm of a

1:1 mixture of H_2 and CO_2, mixed by diffusion in a large round bulb on a vacuum manifold. The reaction was monitored by NMR spectroscopy, which showed growth of signals attributable to $[H_2Rh(dmpe)_2]^+$, and eventually $[HCO_2]^-$ and $[HRh(dmpe)_2(MeCN)]^{2+}$.

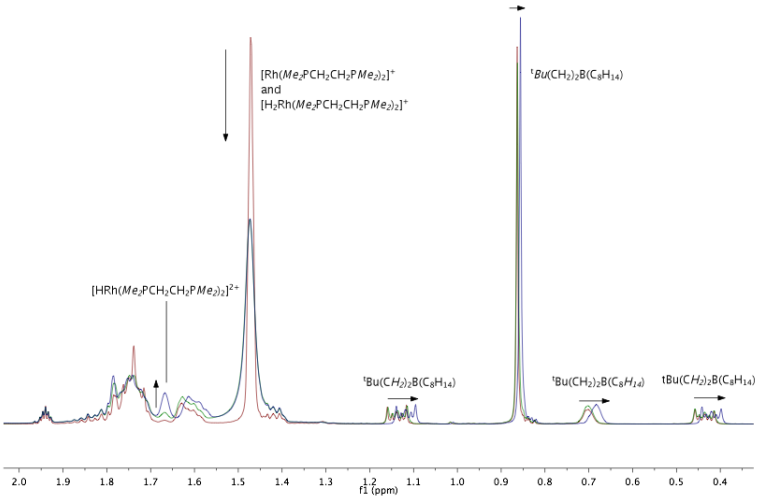

Figure 5.30. ^{1}H NMR time course (aliphatic region) of reaction of $[Rh(dmpe)_2]^+$ with ^{t}Bu$(CH_2)_2$B(C_8H_{14}), CO_2 and H_2. Red: before H_2/CO_2 addition. green, 1.5 hrs after H_2/CO_2 addition. yellow, 18 hrs after H_2/CO_2 addition.

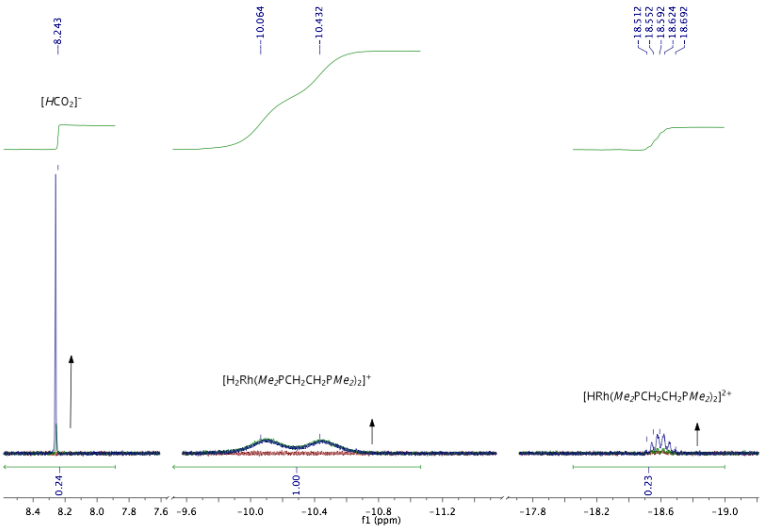

Figure 5.31. ^{1}H NMR time course (formate and hydride regions) of reaction of $[Rh(dmpe)_2]^+$ with ^{t}Bu$(CH_2)_2$B(C_8H_{14}), CO_2 and H_2. Red: before H_2/CO_2 addition. green, 1.5 hrs after H_2/CO_2 addition. yellow, 18 hrs after H_2/CO_2 addition.

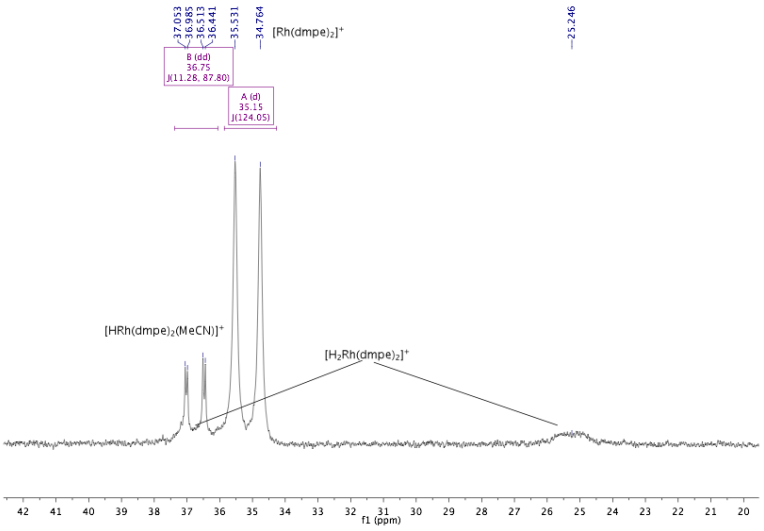

Figure 5.32. ^{31}P NMR (partially decoupled) 18 hours after reaction of $[Rh(dmpe)_2]^+$ with ^{t}Bu$(CH_2)_2$B(C_8H_{14}), CO_2 and H_2.

Attempted catalytic reactions

Acetonitrile. A J-Young NMR tube was charged with 5.0 mg (0.0102 mmol, 1 equiv) $[Ni(dmpe)_2][BF_4]_2$, 7.1 μL (0.0511 mmol, 5 equiv) NEt_3, 10.5 mg (0.0511 mmol, 5 equiv)

^{t}Bu(CH$_2$)$_2$B(C$_8$H$_{14}$), and ~0.6 mL CD$_3$CN. The tube was subjected to two freeze–pump–thaw cycles, and 1 atm of a 1:1 H_2:CO_2 mixture (mixed in a large round bulb on a vacuum line) was admitted. The reaction was monitored by NMR spectroscopy, and a small formate peak gradually grew in over 3 days, along with another product, δ ~6.8. Heating the tube to 60 °C for ~24 hours generated visible amounts of [HNi(dmpe)$_2$]$^+$, but also several unidentified products.

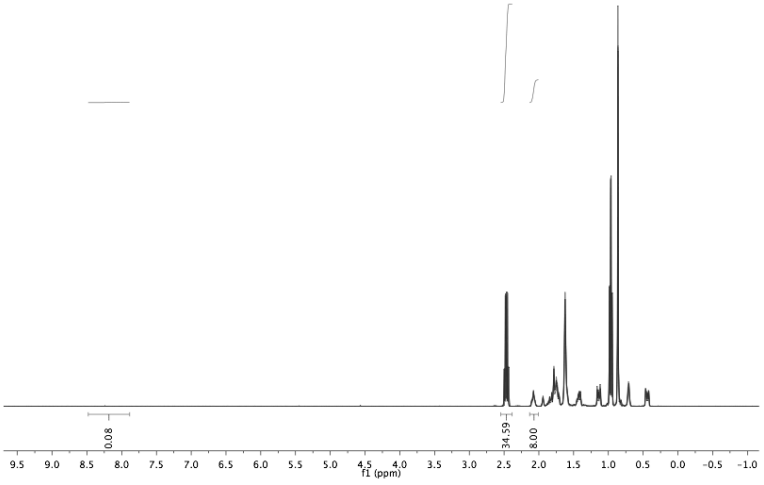

Figure 5.33. ^{1}H NMR time course of attempted catalysis in CD$_3$CN.

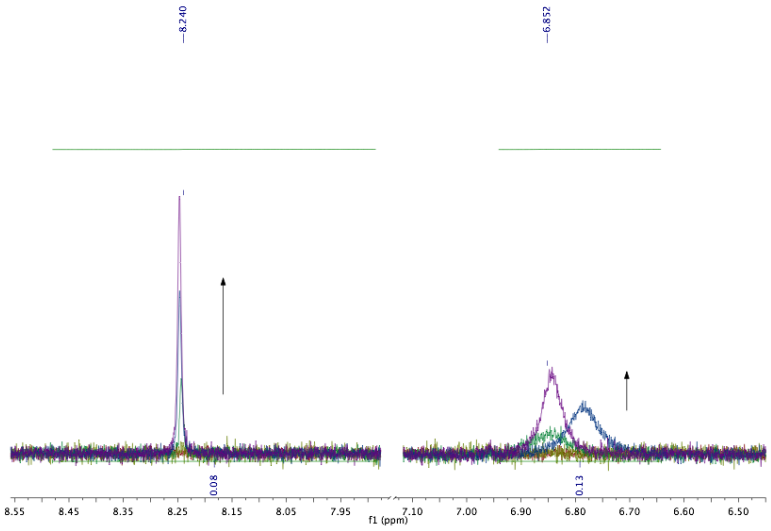

Figure 5.34. ^{1}H NMR time course (over 3 days) of attempted catalysis in CD_3CN.

Chlorobenzene. A J-Young NMR tube was charged with 35.5 mg (0.0174 mmol, 1 equiv) $[Ni(dmpe)_2][BAr^F{}_4]_2$, 10.0 μL (0.0695 mmol, 4 equiv) NEt_3, 3.6 mg (0.0174, 1 equiv) ^{t}Bu$(CH_2)_2$B(C_8H_{14}), and ~0.6 mL C_6D_5Cl. The Ni dication formed a yellow oil at the bottom of the tube if it was allowed to settle. The tube was subjected to two freeze–pump–thaw cycles, and 1 atm of a 1:1 mixture of H_2:CO_2 (mixed in a large round bulb on a vacuum line) was admitted to the tube. NMR spectroscopic monitoring showed steady generation of $[HNi(dmpe)_2][BAr^F{}_4]$, but no evidence of formate was observed. The $BAr^F{}_4$ signal grows in as the mostly insoluble oil $[Ni(dmpe)_2][BAr^F{}_4]_2$ reacts.

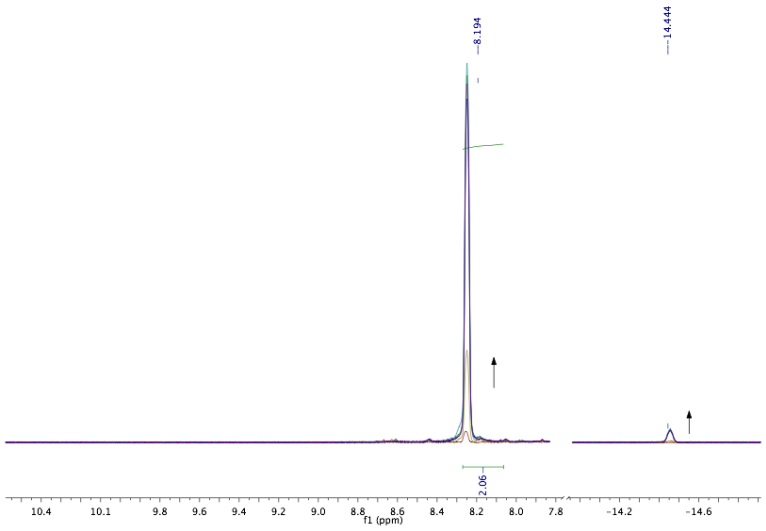

Figure 5.35. ^{1}H NMR time course of attempted catalysis in C_6D_5Cl.

Hydrogen cleavage reactions

Acetonitrile. A J-Young NMR tube was charged with 32.6 mg (0.0159 mmol) $[Ni(dmpe)_2][BAr^F{}_4]_2$, 8.9 μL (0.0639 mmol, 4 equiv) NEt_3, and ~0.6 mL CD_3CN. The tube was subjected to two freeze–pump–thaw cycles and 1 atm of H_2 was admitted. The reaction was monitored, revealing about 30% conversion to $[HNi(dmpe)_2]^+$ over 3 days.

Chlorobenzene. A J-Young NMR tube was charged with 29.0 mg (0.0140 mmol) $[Ni(dmpe)_2][BAr^F{}_4]_2$, 7.9 μL (0.0568 mmol, 4 equiv) NEt_3, and ~0.6 mL C_6D_5Cl. The Ni dication was insoluble, and formed an oil at the bottom of the tube. Initial NMR measurements detected no Ni species. The tube was subjected to two freeze–pump–thaw cycles and 1 atm H_2 was admitted. The tube was sealed and monitored by NMR, which revealed relatively rapid growth of $[HNi(dmpe)_2][BAr^F{}_4]$. After 18 hours, no insolubles were visible, and a large amount of Ni hydride was present. The two phase reaction prevented precise yields or equilibrium measurements.

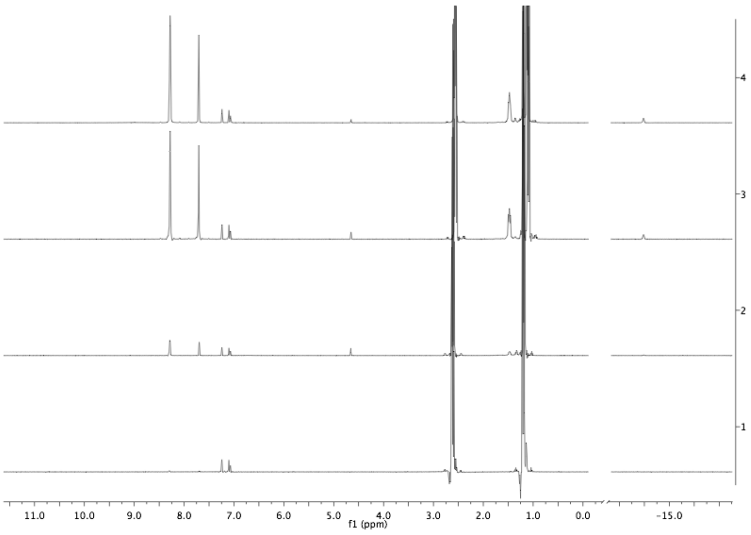

Figure 5.36. ^{1}H NMR time course of H_2 cleavage by $[Ni(dmpe)_2][BAr^F{}_4]_2$ (excess NEt_3 cut off).

References

1. (a) Benson, E. E.; Kubiak, C. P.; Sathrum, A. J.; Smieja, J. M. *Chem. Soc. Rev.* **2009**, *38*, 89; (b) Leitner, W. *Angew. Chem. Int. Edit.* **1995**, *34*, 2207.
2. (a) Saveant, J.-M. *Chem. Rev.* **2008**, *108*, 2348; (b) Hammouche, M.; Lexa, D.; Momenteau, M.; Saveant, J. M. *J. Am. Chem. Soc.* **1991**, *113*, 8455; (c) Bhugun, I.; Lexa, D.; Saveant, J.-M. *J. Am. Chem. Soc.* **1994**, *116*, 5015; (d) Bhugun, I.; Lexa, D.; Saveant, J.-M. *J. Am. Chem. Soc.* **1996**, *118*, 1769; (e) Bhugun, I.; Lexa, D.; Saveant, J.-M. *J. Phys. Chem.* **1996**, *100*, 19981; (f) Gennaro, A.; Isse, A. A.; Severin, M.-G.; Vianello, E.; Bhugun, I.; Saveant, J.-M. *J. Chem. Soc., Faraday Trans.* **1996**, *92*, 3963; (g) Wong, K.-Y.; Chung, W.-H.; Lau, C.-P. *J. Electroanal. Chem.* **1998**, *453*, 161.
3. (a) Dubois, M. R.; Dubois, D. L. *Acc. Chem. Res.* **2009**, *42*, 1974; (b) Steffey, B. D.; Curtis, C. J.; DuBois, D. L. *Organometallics* **1995**, *14*, 4937; (c) Jeoung, J.-H.; Dobbek, H. *Science* **2007**, *318*, 1461.
4. Boffa, A.; Lin, C.; Bell, A. T.; Somorjai, G. A. *J. Catal.* **1994**, *149*, 149.
5. Laitar, D. S.; Muller, P.; Sadighi, J. P. *J. Am. Chem. Soc.* **2005**, *127*, 17196.
6. Chakraborty, S.; Zhang, J.; Krause, J. A.; Guan, H. R. *J. Am. Chem. Soc.* **2010**, *132*, 8872.
7. Stephan, D. W.; Erker, G. *Angew. Chem. Int. Ed.* **2010**, *49*, 46.
8. Ashley, A. E.; Thompson, A. L.; O'Hare, D. *Angew. Chem. Int. Edit.* **2009**, *48*, 9839.

9. Rozovskii, A. Y.; Lin, G. I. *Top. Catal.* **2003**, *22*, 137.
10. (a) Miller, A. J. M.; Labinger, J. A.; Bercaw, J. E. *J. Am. Chem. Soc.* **2008**, *130*, 11874; (b) Elowe, P. R.; West, N. M.; Labinger, J. A.; Bercaw, J. E. *Organometallics* **2009**, *28*, 6218; (c) Miller, A. J. M.; Labinger, J. A.; Bercaw, J. E. *J. Am. Chem. Soc.* **2010**, *132*, 3301; (d) Miller, A. J. M.; Labinger, J. A.; Bercaw, J. E. *Organometallics* **2010**, *29*, 4499; (e) West, N. M.; Miller, A., J. M.; Labinger, J. A.; Bercaw, J. E. *Coord. Chem. Rev.* **2010**, *In Press*.
11. Miedaner, A.; DuBois, D. L.; Curtis, C. J.; Haltiwanger, R. C. *Organometallics* **1993**, *12*, 299.
12. (a) Berning, D. E.; Noll, B. C.; DuBois, D. L. *J. Am. Chem. Soc.* **1999**, *121*, 11432; (b) Berning, D. E.; Miedaner, A.; Curtis, C. J.; Noll, B. C.; Rakowski DuBois, M. C.; DuBois, D. L. *Organometallics* **2001**, *20*, 1832; (c) Ciancanelli, R.; Noll, B. C.; DuBois, D. L.; DuBois, M. R. *J. Am. Chem. Soc.* **2002**, *124*, 2984; (d) Curtis, C. J.; Miedaner, A.; Ellis, W. W.; DuBois, D. L. *J. Am. Chem. Soc.* **2002**, *124*, 1918; (e) Price, A. J.; Ciancanelli, R.; Noll, B. C.; Curtis, C. J.; DuBois, D. L.; DuBois, M. R. *Organometallics* **2002**, *21*, 4833; (f) Miedaner, A.; Raebiger, J. W.; Curtis, C. J.; Miller, S. M.; DuBois, D. L. *Organometallics* **2004**, *23*, 2670; (g) Raebiger, J. W.; DuBois, D. L. *Organometallics* **2005**, *24*, 110; (h) DuBois, D. L.; Blake, D. M.; Miedaner, A.; Curtis, C. J.; DuBois, M. R.; Franz, J. A.; Linehan, J. C. *Organometallics* **2006**, *25*, 4414; (i) Nimlos, M. R.; Chang, C. H.; Curtis, C. J.; Miedaner, A.; Pilath, H. M.; DuBois, D. L. *Organometallics* **2008**, *27*, 2715.
13. DuBois, D. L.; Berning, D. E. *Appl. Organomet. Chem.* **2000**, *14*, 860.
14. Wilson, A. D.; Miller, A. J. M.; DuBois, D. L.; Labinger, J. A.; Bercaw, J. E. *Inorg. Chem.* **2010**, *49*, 3918.
15. Kaljurand, I.; Kutt, A.; Soovali, L.; Rodima, T.; Maemets, V.; Leito, I.; Koppel, I. A. *J. Org. Chem.* **2005**, *70*, 1019.
16. Pangborn, A. B.; Giardello, M. A.; Grubbs, R. H.; Rosen, R. K.; Timmers, F. J. *Organometallics* **1996**, *15*, 1518.
17. Hirano, K.; Yorimitsu, H.; Oshima, K. *Org. Lett.* **2005**, *7*, 4689.
18. Silavwe, N. D.; Goldman, A. S.; Ritter, R.; Tyler, D. R. *Inorg. Chem.* **1989**, *28*, 1231.

Chapter 6

Dehydrogenation of Amine-Boranes with a Frustrated Lewis Pair

Adapted in part from:
Miller, A. J. M.; Bercaw, J. E. *Chem. Commun.* **2010**, *46*, 1709.

Chapter 6

Introduction

Amine-boranes are the subject of intense interest due to their potential application in hydrogen storage schemes.[1] A number of fast and efficient transition metal dehydrocoupling catalysts have been discovered,[2] and various coordination compounds relevant to the catalytic pathways have been isolated.[3] Progress has also been made in the challenging area of regeneration of spent ammonia-borane fuel.[4] Theoretical studies[5] of one amine-borane dehydrocoupling system employing N-heterocyclic carbenes (NHCs) as ligands[2a] suggested that the free NHC could heterolytically dehydrogenate NH_3•BH_3, yielding $(NH_2BH_2)_n$ and NHC–H_2, similar to the H_2 addition reactivity of Bertrand's carbenes.[6] Because the reactivity of these NHC species has been compared to that of bulky phosphine-borane "frustrated Lewis pairs" (FLPs), it occurred to us that FLPs might also be able to dehydrogenate amine-boranes.

FLPs — combinations of bulky Lewis acids and bases that are unable to form traditional Lewis acid-base pairs[7] — exhibit a number of unusual reactions,[8] including amine activation[9] and in particular the heterolytic cleavage of H_2,[10] which has been utilized for metal-free catalytic hydrogenation of bulky imines.[11] *De*hydrogenation reactions have only very recently been realized using FLPs; examples include self-dehydrogenation of an

NHC/$B(C_6F_5)_3$ FLP,[12] and unusual dehydrogenations of Ge species.[13] Mention of a phosphinoborane-catalyzed transfer hydrogenation from ammonia-borane to bulky imines[8a] was likely premature, as the reaction proceeds without any FLP participation.[14] Calculations suggested that FLP dehydrogenation of polarized substrates such as alcohols to aldehydes should be possible.[15] During this rapidly evolving period, we reported that the simple frustrated Lewis pair $P^tBu_3/B(C_6F_5)_3$ rapidly and cleanly dehydrogenates amine-boranes at room temperature, with concomitant formation of the phosphonium borohydride salt $[^tBu_3PH][HB(C_6F_5)_3]$ (Scheme 6.1). Closely following our publication, a theoretical treatment "predicted" that dehydrogenations of amine-boranes could be carred out by FLPs,[16] consistent with our findings.

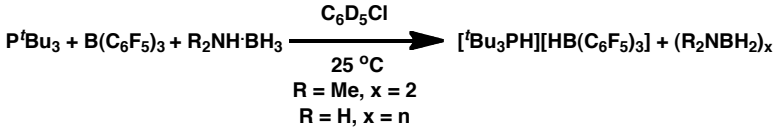

Scheme 6.1

Results and Discussion

Initial experiments were carried out with $Me_2NH{\bullet}BH_3$, a common model for $NH_3{\bullet}BH_3$ which has desirable solubility properties and generally releases only a single equivalent of H_2. The frustrated Lewis pair $P^tBu_3/B(C_6F_5)_3$ was formed according to literature procedures in C_6D_5Cl,[10b] and no discernable reaction was observed by NMR. The preformed FLP (which was yellow in our hands; see Experimental Section) was added to a C_6D_5Cl solution of $Me_2NH{\bullet}BH_3$ at 25 °C, and the yellow color bleached to a clear colorless solution. ^1H, ^{31}P (Figure 6.1), ^{19}F, and ^{11}B (Figure 6.2) NMR experiments

confirmed that > 95% of the FLP-derived product was $[^tBu_3PH][HB(C_6F_5)_3]$.[10b] The major dehydrocoupling product was dimeric $(Me_2NBH_2)_2$, assigned by a diagnostic ^{11}B NMR resonance at δ 5.2 (t, $\mathcal{J}_{BH}$ = 112 Hz), and by signals in the ^1H NMR spectrum at δ 2.28 (s, Me_2N) and δ 2.83 (1:1:1:1 q, $\mathcal{J}_{BH}$ = 112 Hz, BH_2). Minor side products, including monomeric $Me_2N{=}BH_2$ (^{11}B NMR δ 37.6, t, $\mathcal{J}_{HB}$ = 127 Hz) and $HB(NMe_2)_2$ (^{11}B NMR δ 28.5, d, $\mathcal{J}_{HB}$ = 124 Hz), dissipated over time, leaving ~97% dimeric $(Me_2NBH_2)_2$ along with traces of $(BH_2)_2NMe_2(\mu\text{–}H)$ (**A**) and $H_3B{\bullet}NMe_2BH_2{\bullet}NHMe_2$ (**B**). The two boron resonances of $H_3B{\bullet}NMe_2BH_2{\bullet}NHMe_2$ are similar to $Me_2NH{\bullet}BH_3$ and the cyclic trimer $(Me_2NHBH_2)_3$. The latter species is unstable; the persistence of the resonances rule out the trimer. ^1H NMR data and the observed 1:1 ratio of ^{11}B NMR resonances both point to the double-adduct assignment. This product distribution is similar to that observed in metal-catalyzed dehydrocoupling of $Me_2NH{\bullet}BH_3$;[17] thermolysis of a $Me_2NH{\bullet}BH_3$ melt at 150 °C also affords $(Me_2NBH_2)_2$, along with trace impurities including $HB(NMe_2)_2$.[17b,18]

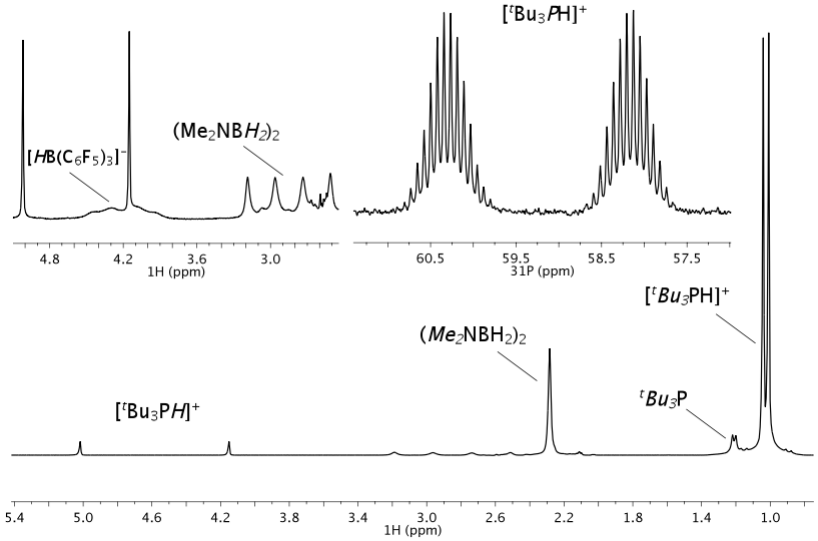

Figure 6.1. ^{1}H NMR spectrum after FLP-mediated dehydrocoupling of $Me_2NH{\bullet}BH_3$. Left inset is a blow-up of the borohydride ^{1}H NMR resonances; right inset is the ^{31}P NMR spectrum of $[^{t}Bu_3PH][HB(C_6F_5)_3]$.

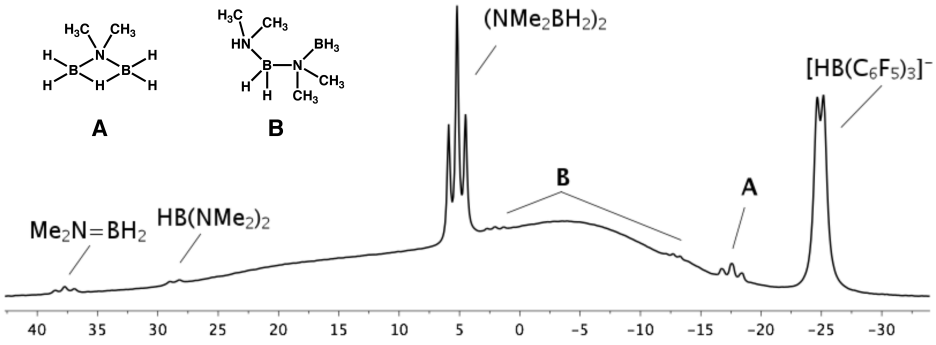

Figure 6.2. ^{11}B NMR spectrum shortly after FLP-mediated dehydrocoupling of $Me_2NH{\bullet}BH_3$. The underlying broad feature arises from borosilicate glass in the probe construction.

The order of reagent addition is important in the dehydrocoupling reaction. If $B(C_6F_5)_3$ and $Me_2NH{\bullet}BH_3$ are dissolved in C_6D_5Cl a few minutes prior to addition of $P^{t}Bu_3$, several products including only ~50% $(Me_2NBH_2)_2$ are produced. On the other hand, combining $P^{t}Bu_3$ and $Me_2NH{\bullet}BH_3$ in C_6D_5Cl, followed by addition of $B(C_6F_5)_3$ led to near-quantitive

formation of [^{t}Bu$_3$PH][HB(C$_6$F$_5$)$_3$] and (Me$_2$NBH$_2$)$_2$, in essentially the same distribution as with prior formation of the FLP.

To explore the possibility of H_2 release and amine-borane regeneration, the mixture of [^{t}Bu$_3$PH][HB(C$_6$F$_5$)$_3$] and (Me$_2$NBH$_2$)$_2$ was heated between 90 and 130 °C. We hoped that regeneration might be driven by formation of more stable Lewis adducts P^{t}Bu$_3$•BH$_3$ and NH$_3$•B(C$_6$F$_5$)$_3$. Complete decomposition of the dimer to a variety of species was observed; only P^{t}Bu$_3$•BH$_3$ and [HB(C$_6$F$_5$)$_3$]$^-$ were readily identified by ^{11}B NMR,[19] leaving this experiment inconclusive. In isolation, (Me$_2$NBH$_2$)$_2$ is stable up to 450 °C in the gas phase[17b] and 130 °C in a melt.[18] Similarly, it has been reported that [^{t}Bu$_3$PH][HB(C$_6$F$_5$)$_3$] is stable to H_2 loss up to 150 °C.[10b]

The FLP system can dehydrogenate NH$_3$•BH$_3$ as well. Treatment of NH$_3$•BH$_3$ with P^{t}Bu$_3$/B(C$_6$F$_5$)$_3$ afforded once again [^{t}Bu$_3$PH][HB(C$_6$F$_5$)$_3$] as a principal product (85%, ^{31}P NMR; ~80%, ^{19}F NMR). The major dehydrocoupling product is consistent with branched-chain polyaminoborane ((NH$_2$BH$_2$)$_n$, broad ^{11}B NMR, δ –7.7, –14.4, –27.2) as observed upon thermolysis of NH$_3$•BH$_3$ in ionic liquids.[20] The other ^{11}B NMR signals correspond to [HB(C$_6$F$_5$)$_3$]$^-$ and two smaller peaks which could be Lewis adducts between P^{t}Bu$_3$ and boranes; two broad resonances in the ^{31}P NMR spectrum are consistent with this formulation. Apparently dehydrocoupling is more favorable than forming stable Lewis pairs, although in this case some of that competing pathway is observed. Lewis adduct formation has been observed when Me$_2$NH•BH$_3$ and P^{i}Pr$_3$ were heated to 85 °C for 1 hour (giving ^{i}Pr$_3$P•BH$_3$).[2c] Some insoluble colorless material was extracted with pyridine and shown to be unreacted NH$_3$•BH$_3$, consistent with some amount of deactivation of the FLP

(by strong Lewis adduct formation) before quantitative dehydrocoupling could take place. Neither the insoluble cyclic pentamer $(NH_2BH_2)_5$[2b,3d] nor long linear polymers[21] were detected, in contrast to a number of metal-catalyzed reactions. Treatment of NH_3•BH_3 with excess FLP did not lead to detectable amounts of borazine, suggesting that only one equivalent of H_2 could be released using this method.

$B(C_6F_5)_3$ by itself can *catalytically* dehydrogenate NH_3•BH_3,[22] but only at elevated temperatures; no significant amounts of product are observed under the present conditions without P^tBu_3. Importantly, $B(C_6F_5)_3$ by itself is unable to dehydrocouple Me_2NH•BH_3,[17b] leading us to conclude that the FLP is essential for rapid, ambient-condition dehydrocoupling. Initial attempts at catalytic H_2 release from Me_2NH•BH_3 under mild conditions using an FLP were met with disappointment. The FLP $B(p\text{-}C_6F_4H)_3/P(o\text{-tolyl})_3$ — which releases H_2 from $[(o\text{-tolyl})_3PH][HB(p\text{-}C_6F_4H)_3]$ under vacuum[10c] — did not give clean dehydrocoupling chemistry when allowed to react with Me_2NH•BH_3, precluding attempts to release H_2 from the phosphonium borohydride and turn over a cycle.

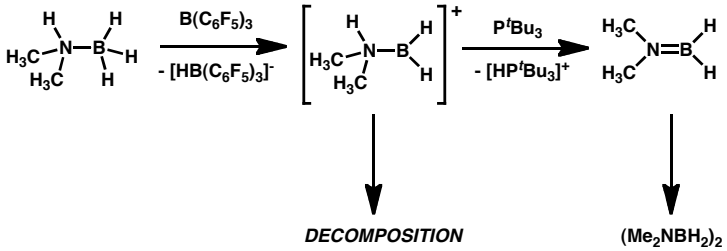

Scheme 6.2

The mechanism of heterolytic cleavage of H_2 by FLP's has not been fully elucidated, although a number of theoretical studies have been performed.[8a,23] DFT calculations suggest that a weak interaction holds the borane and phosphine in proximity; a molecule of

H_2 approaches the pair and is cleaved in a concerted fashion. Since the heterolytic dehydrogenation of amine-boranes constitutes a net transfer of H_2 and gives a similar product, one could invoke a similar mechanism. We prefer an alternative, stepwise mechanism in which $B(C_6F_5)_3$ first abstracts a hydride from $Me_2NH•BH_3$, followed by fast deprotonation of the resulting $[Me_2NHBH_2]^+$, affording the $Me_2N=BH_2$ unit that dimerizes to the final product (Scheme 6.2). In the absence of P^tBu_3, oligomerization of the cationic intermediate might take place (as suggested by Baker for the reaction of acid with $NH_3•BH_3$[22]) accounting for the multiple side products observed when $B(C_6F_5)_3$ is added first.

We have shown that frustrated Lewis pairs consisting of bulky tertiary phosphines and $B(C_6F_5)_3$ are capable of rapidly dehydrocoupling $Me_2NH•BH_3$ and $NH_3•BH_3$. While the current FLP systems could serve as H_2 storage compounds themselves,[10a] their weight % capacity is far from ideal. Using FLPs as a H_2 shuttle with lighter, non-frustrated amine-boranes as the terminal H_2 storage medium is perhaps more attractive. Recent advances in H_2 release from FLPs[10c,24] may open the door to catalytic dehydrocoupling, and indeed perhaps dehydrogenation of a wider variety of substrates.

Experimental Section

General Considerations

All air- and moisture-sensitive compounds were manipulated using standard vacuum line or Schlenk techniques, or in a glovebox under a nitrogen atmosphere. Under standard glovebox conditions, petroleum ether, diethyl ether, benzene, toluene, and tetrahydrofuran were used without purging, such that traces of those solvents were in the atmosphere, and could be found intermixed in the solvent bottles. The solvents for air- and moisture-sensitive reactions were dried over sodium benzophenone ketyl, calcium hydride, or by the method of Grubbs.[25] NMR solvents were purchased from Cambridge Isotopes Laboratories, Inc. Chlorobenzene-d_5 was degassed by three freeze-pump-thaw cycles and dried by passage through a small column of activated alumina. Unless noted, other materials were used as received. P^tBu_3 and $B(C_6F_5)_3$ were purchased from Strem Chemicals, Inc., and $B(C_6F_5)_3$ was sublimed before use. $NH_3{\bullet}BH_3$, and $Me_2NH{\bullet}BH_3$ were purchased from Aldrich. ^1H, ^{31}P, ^{19}F, ^{11}B, and ^{13}C NMR spectra were recorded on Varian Mercury 300 MHz, or Varian INOVA 500 MHz spectrometers at room temperature, unless indicated otherwise. Chemical shifts are reported with respect to residual internal protio solvent for ^1H and ^{13}C spectra. Other nuclei were referenced to an external standard: 85% H_3PO_4 (^{31}P), 15% $BF_3{\bullet}Et_2O/CDCl_3$ (^{11}B), $CFCl_3$ (^{19}F), all at 0 ppm.

Experimental Procedures

Dehydrocoupling of $Me_2NH{\bullet}BH_3$ by $P^tBu_3/B(C_6F_5)_3$ Pair. A 10 mL vial was charged with 97 mg (0.19 mmol) $B(C_6F_5)_3$ 39 mg (0.19 mmol) P^tBu_3, and ~0.3 mL C_6D_5Cl.

Upon dissolution, the solution turned yellow. In a separate 10 mL vial, 11 mg (0.19 mmol) $Me_2NH•BH_3$ was dissolved in ~0.3 mL C_6D_5Cl with stirring. The yellow borane/phosphine solution was added to the stirring $Me_2NH•BH_3$ solution, and the mixture immediately lost the yellow color, giving a clear colorless solution. The reaction mixture was transferred to a J-Young Teflon-stoppered NMR tube, and multinuclear NMR experiments showed high conversion to $(Me_2NBH_2)_2$. After 24 hours the spectra were reacquired, showing the disappearance of some minor side products, giving ~97% pure $(Me_2NBH_2)_2$. **^{1}H NMR** (C_6D_5Cl, 500 MHz): δ 1.03 (d, $\mathcal{J}_{PH}$ = 15.7 Hz, 27H, $[HP^tBu_3]^+$), 1.14 (d, $\mathcal{J}_{PH}$ = 9.4 Hz, ~5% P^tBu_3 impurity), 2.28 (s, 6H, $(Me_2NBH_2)_2$), 2.85 (1:1:1:1 q, $\mathcal{J}_{BH}$ = 112.4 Hz, 2H, $(Me_2NBH_2)_2$), 4.2 (br 1:1:1:1 q, $\mathcal{J}_{BH}$ ~ 84 Hz, 1H, $[HB(C_6F_5)_3]^-$), 4.58 (d, $\mathcal{J}_{PH}$ = 433.1 Hz, 1H, $[HP^tBu_3]^+$). **^{31}P{^{1}H} NMR** (C_6D_5Cl, 202 MHz): δ 59.2 (s, 1P, $[HP^tBu_3]^+$), 62.4 (s, ~5% P^tBu_3 impurity). **^{31}P NMR** (C_6D_5Cl, 202 MHz): δ 59.2 (doublet of 14-line (*observed*, 28-line hypothetical) patterns, $\mathcal{J}_{PH}$ = 432.6, 15.7 Hz, 1P, $[HP^tBu_3]^+$), 62.4 (br s, ~5% P^tBu_3 impurity), **^{19}F NMR** (C_6D_5Cl, 282 MHz): δ –132.63 (br d, $\mathcal{J}_{FF}$ = 20.0 Hz, 6F, *o*-C_6F_5), –163.61 (br t, $\mathcal{J}_{FF}$ = 20.0 Hz, 3F, *p*-C_6F_5), –166.53 (br d, $\mathcal{J}_{FF}$ = 15.77 Hz, *m*-C_6F_5). **^{11}B NMR** (C_6D_5Cl, 160 MHz): δ –25.0 (d, $\mathcal{J}_{BH}$ = 84.3 Hz, $[HB(C_6F_5)_3]^-$), –17.6 (minor, dt, $\mathcal{J}_{BH}$ = 129 Hz, 31 Hz, $(BH_2)_2NMe_2(\mu–H)$), –12.85 (minor, q, $\mathcal{J}_{BH}$ = 92 Hz, $H_3B•NMe_2BH_2•NHMe_2$), 2.00 (minor, 116 MHz, $H_3B•NMe_2BH_2•NHMe_2$), –5.2 (t, $\mathcal{J}_{BH}$ = 112.7 Hz, $(Me_2NBH_2)_2$). **^{13}C{^{1}H} NMR** (C_6D_5Cl, 126 MHz): δ 29.11 (s, $P(C(CH_3)_3)_3$), 36.79 (d, $\mathcal{J}_{PC}$ = 27.0 Hz, $P(C(CH_3)_3)$), 51.54 (s, $(Me_2NBH_2)_2$), 136.83 (dm, $^1\mathcal{J}_{FC}$ = 245.4 Hz, $[HB(m\text{-}C_6F_5)_3]^-$), 138.12 (dm, $^1\mathcal{J}_{FC}$ = 244 Hz, $[HB(p\text{-}C_6F_5)_3]^-$), 148.71 (dm, $^1\mathcal{J}_{FC}$ = 236 Hz, $[HB(o\text{-}C_6F_5)_3]^-$).

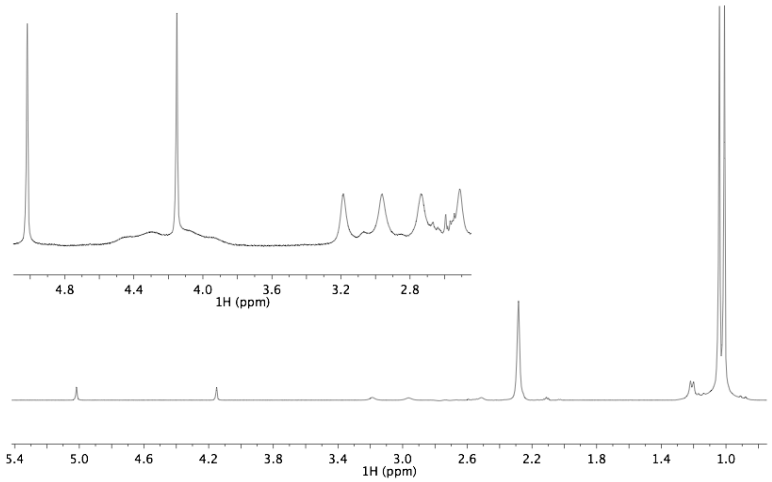

Figure 6.3. ^{1}H NMR of $(Me_2NBH_2)_2$ and $[^{t}Bu_3PH][HB(C_6F_5)_3]$ (with enlargement inset).

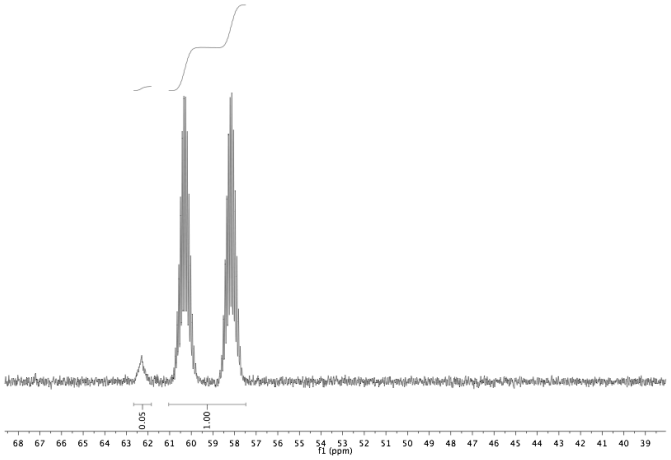

Figure 6.4. ^{31}P NMR of $(Me_2NBH_2)_2$ and $[^{t}Bu_3PH][HB(C_6F_5)_3]$.

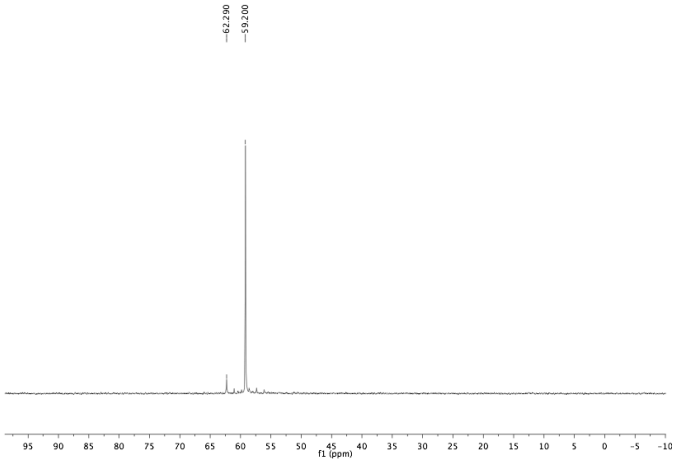

Figure 6.5. $^{31}P\{^{1}H\}$ NMR of $(Me_2NBH_2)_2$ and $[^tBu_3PH][HB(C_6F_5)_3]$.

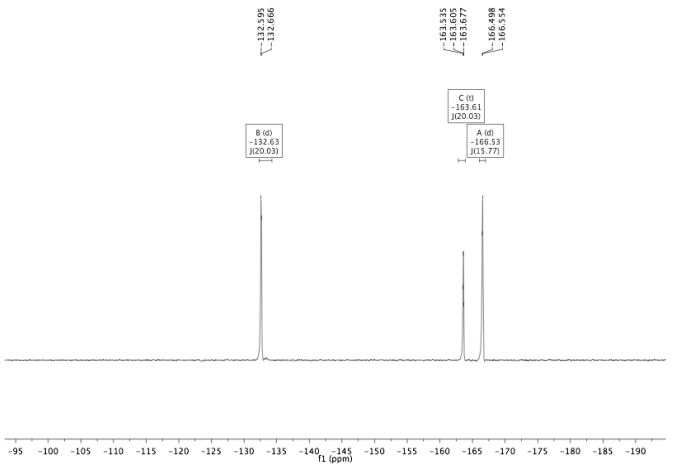

Figure 6.6. ^{19}F NMR of $(Me_2NBH_2)_2$ and $[^tBu_3PH][HB(C_6F_5)_3]$.

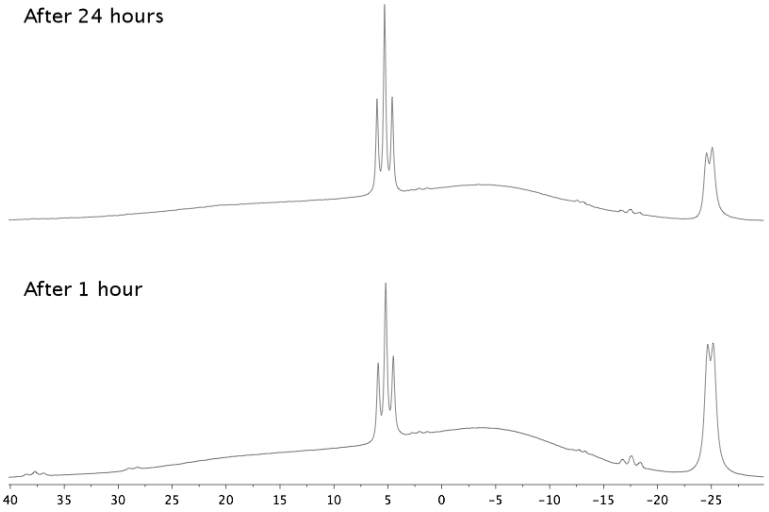

Figure 6.7. ^{11}B NMR of $(Me_2NBH_2)_2$ and $[^tBu_3PH][HB(C_6F_5)_3]$, at 1 and 24 hours.

Reaction of $Me_2NH•BH_3$ with $B(C_6F_5)_3$, followed by P^tBu_3. In a 10 mL vial, 6.7 mg (0.114 mmol) $Me_2NH•BH_3$ was dissolved in ~0.2 mL C_6D_5Cl. To the solution was added 58.2 mg (0.114 mmol) $B(C_6F_5)_3$ in ~0.4 mL C_6D_5Cl, and the mixture was mixed well and added to a J-Young Teflon-sealed NMR tube. Multinuclear NMR experiments showed a mixture of products, including a number of broad features in the ^{19}F and ^{11}B NMR spectra. A short while later, the tube was returned to the glovebox, and the contents poured into a vial containing 23.0 mg (0.114 mmol) P^tBu_3. The reaction mixture was returned to the NMR tube and shaken well, and further NMR experiments were undertaken. Multiple species were observed by NMR, including ~80% $[^tBu_3PH][HB(C_6F_5)_3]$, and only ~50% dimeric $(Me_2NBH_2)_2$.

Reaction of $Me_2NH•BH_3$with P^tBu_3, followed by $B(C_6F_5)_3$. A 10 mL vial was charged with 6.3 mg (0.107 mmol) $Me_2NH•BH_3$, 21.6 mg (0.107 mmol) P^tBu_3, and ~0.6 mL C_6D_5Cl. The colorless solution was mixed well, and then added to another vial charged

with solid 54.8 (0.107 mmol) $B(C_6F_5)_3$. The clear, colorless reaction mixture was transferred to a J-Young Teflon-sealed NMR tube, sealed, and assessed by multinuclear NMR. After 30 minutes, clean conversion to a product distribution similar to that of the preformed FLP was observed.

Dehydrocoupling of NH_3•BH_3 by $P^tBu_3/B(C_6F_5)_3$ Pair. A small vial was charged with 30 mg (0.15 mmol) P^tBu_3 and 76 mg (0.15 mmol) $B(C_6F_5)_3$ and ~0.6 mL C_6D_5Cl to give a yellow solution. A J-Young Teflon-sealed NMR tube was charged with 2.3 mg (0.075 mmol) NH_3•BH_3, and the phosphine/borane mixture was added to the tube. The NH_3•BH_3 slowly dissolved, and the yellow color slowly bleached to give a clear colorless solution, which was examined by multinuclear NMR spectroscopy. **^{1}H NMR** (C_6D_5Cl, 500 MHz): δ 1.03 (d, $\mathcal{J}_{PH}$ = 15.7 Hz), 1.15 (minor, d, $\mathcal{J}_{PH}$ = 12.2 Hz), 1.23 (minor, d, $\mathcal{J}_{PH}$ = 11.6 Hz), 4.1 (br, q $[HB(C_6F_5)_3]^-$). A number of additional broad peaks were observed, assigned to various polyaminoborane BH and NH resonances. **^{31}P NMR** (C_6D_5Cl, 121 MHz): δ 33.5 (minor, br), 35.9 (minor, br), 58.6 (doublet of multiplets, $\mathcal{J}_{PH}$ = 434.5 Hz, $[HP^tBu_3]^+$). **^{19}F NMR** (C_6D_5Cl, 282 MHz): δ –132.61 (br d, $\mathcal{J}_{FF}$ = 21.4 Hz, 6F, *o*-C_6F_5), –163.64 (br t, $\mathcal{J}_{FF}$ = 20.4 Hz, 3F, *p*-C_6F_5), –166.57 (br d, $\mathcal{J}_{FF}$ = 18.4 Hz, 6F, *m*-C_6F_5). A number of unidentified peaks were observed as well. **^{11}B NMR** (C_6D_5Cl, 160 MHz): δ –34.3 (br m, $^tBu_3P$•BH_3), –29.6 (t, $\mathcal{J}_{BH}$ = 78 Hz, unknown), –27.2 (br sh, $(NH_2BH_2)_n$), –25.1 (d, $\mathcal{J}_{BH}$ = 82.3, $[HB(C_6F_5)_3]^-$), -14.5 (br, $(NH_2BH_2)_n$), -7.7 (br, $(NH_2BH_2)_n$).

Thermolysis of $(Me_2NBH_2)_2$ / $[^tBu_3PH][HB(C_6F_5)_3]$ Mixture. A mixture of $(Me_2NBH_2)_2$ and $[^tBu_3PH][HB(C_6F_5)_3]$ in C_6D_5Cl, formed (including trace impurities) as

described above, was heated to either 90 °C or 130 °C in separate experiments. Both temperatures led to similar product mixtures, although at 90 °C the products grew in more slowly. Heating at 130 °C led to complete consumption of $(Me_2NBH_2)_2$ in a few hours. Along with $[HB(C_6F_5)_3]^-$, a number of other B–containing species are present, including $^tBu_3P{\bullet}BH_3$.

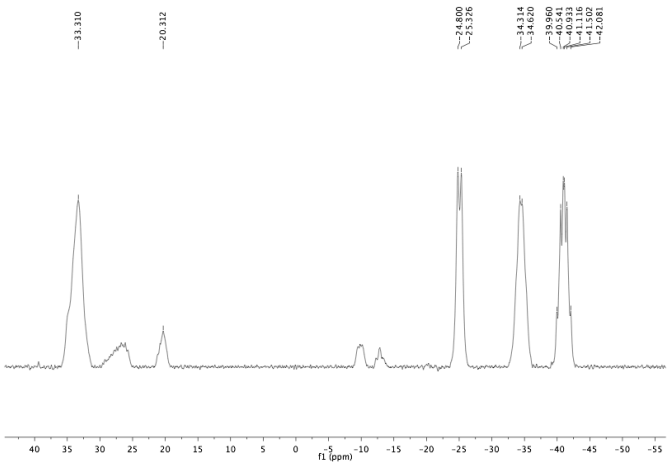

Figure 6.8. ^{11}B NMR after thermolysis of $(Me_2NBH_2)_2$ and $[^tBu_3PH][HB(C_6F_5)_3]$ (with linear prediction subtraction of borosilicate signals).

References

1. (a) Stephens, F. H.; Pons, V.; Baker, R. T. *Dalton Trans.* **2007**, 2613; (b) Hamilton, C. W.; Baker, R. T.; Staubitz, A.; Manners, I. *Chem. Soc. Rev.* **2009**, *38*, 279; (c) Staubitz, A.; Robertson, A. P. M.; Manners, I. *Chem. Rev.* **2010**, *110*, 4079.
2. (a) Keaton, R. J.; Blacquiere, J. M.; Baker, R. T. *J. Am. Chem. Soc.* **2007**, *129*, 1844; (b) Denney, M. C.; Pons, V.; Hebden, T. J.; Heinekey, D. M.; Goldberg, K. I. *J. Am. Chem. Soc.* **2006**, *128*, 12048; (c) Blaquiere, N.; Diallo-Garcia, S.; Gorelsky, S. I.; Black, D. A.; Fagnou, K. *J. Am. Chem. Soc.* **2008**, *130*, 14034; (d) Clark, T. J.; Russell, C. A.; Manners, I. *J. Am. Chem. Soc.* **2006**, *128*, 9582; (e) Jiang, Y.; Berke, H. *Chem. Commun.* **2007**, 3571; (f) Sloan, M. E.; Staubitz, A.; Clark, T. J.; Russell, C. A.; Lloyd-Jones, G. C.; Manners, I. *J. Am. Chem. Soc.* **2010**, *132*, 3831; (g) Conley, B. L.; Williams, T. J. *Chem. Commun.* **2010**, *46*, 4815; (h) Kim, S.-K.; Han,

W.-S.; Kim, T.-J.; Kim, T.-Y.; Nam, S. W.; Mitoraj, M.; PiekosÃÅ, Å.; Michalak, A.; Hwang, S.-J.; Kang, S. O. *J. Am. Chem. Soc.* **2010**, *132*, 9954.

3. (a) Alcaraz, G.; Sabo-Etienne, S. *Angew. Chem. Int. Ed.* **2010**, *49*, 7170; (b) Douglas, T. M.; Chaplin, A. B.; Weller, A. S. *J. Am. Chem. Soc.* **2008**, *130*, 14432; (c) Dallanegra, R.; Chaplin, A. B.; Weller, A. S. *Angew. Chem., Int. Ed.* **2009**, *48*, 6875; (d) Pons, V.; Baker, R. T.; Szymczak, N. K.; Heldebrant, D. J.; Linehan, J. C.; Matus, M. H.; Grant, D. J.; Dixon, D. A. *Chem. Commun.* **2008**, 6597.
4. (a) Ramachandran, P. V.; Gagare, P. D. *Inorg. Chem.* **2007**, *46*, 7810; (b) Davis, B. L.; Dixon, D. A.; Garner, E. B.; Gordon, J. C.; Matus, M. H.; Scott, B.; Stephens, F. H. *Angew. Chem. Int. Edit.* **2009**, *48*, 6812; (c) Mock, M. T.; Potter, R. G.; Camaioni, D. M.; Li, J.; Dougherty, W. G.; Kassel, W. S.; Twamley, B.; DuBois, D. L. *J. Am. Chem. Soc.* **2009**, *131*, 14454.
5. (a) Zimmerman, P. M.; Paul, A.; Zhang, Z. Y.; Musgrave, C. B. *Angew. Chem. Int. Edit.* **2009**, *48*, 2201; (b) Zimmerman, P. M.; Paul, A.; Musgrave, C. B. *Inorg. Chem.* **2009**, *48*, 5418.
6. Frey, G. D.; Lavallo, V.; Donnadieu, B.; Schoeller, W. W.; Bertrand, G. *Science* **2007**, *316*, 439.
7. Brown, H. C.; Schlesinger, H. I.; Cardon, S. Z. *J. Am. Chem. Soc.* **1942**, *64*, 325.
8. (a) Stephan, D. W.; Erker, G. *Angew. Chem. Int. Ed.* **2010**, *49*, 46; (b) Stephan, D. W. *Dalton Trans.* **2009**, 3129; (c) Stephan, D. W. *Org. & Biomol. Chem.* **2008**, *6*, 1535.
9. (a) Chase, P. A.; Stephan, D. W. *Angew. Chem. Int. Edit.* **2008**, *47*, 7433; (b) Sumerin, V.; Schulz, F.; Nieger, M.; Leskelä, M.; Repo, T.; Rieger, B. *Angew. Chem. Int. Ed.* **2008**, *47*, 6001.
10. (a) Welch, G. C.; Juan, R. R. S.; Masuda, J. D.; Stephan, D. W. *Science* **2006**, *314*, 1124; (b) Welch, G. C.; Stephan, D. W. *J. Am. Chem. Soc.* **2007**, *129*, 1880; (c) Ullrich, M.; Lough, A. J.; Stephan, D. W. *J. Am. Chem. Soc.* **2009**, *131*, 52.
11. (a) Chase, P. A.; Welch, G. C.; Jurca, T.; Stephan, D. W. *Angew. Chem. Int. Edit.* **2007**, *46*, 8050; (b) Chase, P. A.; Jurca, T.; Stephan, D. W. *Chem. Commun.* **2008**, 1701.
12. Holschumacher, D.; Taouss, C.; Bannenberg, T.; Hrib, C. G.; Daniliuc, C. G.; Jones, P. G.; Tamm, M. *Dalton Trans.* **2009**, 6927.
13. (a) Jana, A.; Objartel, I.; Roesky, H. W.; Stalke, D. *Inorg. Chem.* **2009**, *48*, 7645; (b) Jana, A.; Tavcar, G.; Roesky, H. W.; Schulzke, C. *Dalton Trans.* **2010**, *39*, 6217.
14. Yang, X.; Zhao, L.; Fox, T.; Wang, Z. X.; Berke, H. *Angew. Chem. Int. Ed.* **2010**, *49*, 2058.
15. Privalov, T. *Chemistry-a European Journal* **2009**, *15*, 1825.
16. Guo, Y.; He, X.; Li, Z.; Zou, Z. *Inorg. Chem.* **2010**, *49*, 3419.
17. (a) Douglas, T. M.; Chaplin, A. B.; Weller, A. S.; Yang, X.; Hall, M. B. *J. Am. Chem. Soc.* **2009**, *141*, 15440; (b) Jaska, C. A.; Temple, K.; Lough, A. J.; Manners, I. *J. Am. Chem. Soc.* **2003**, *125*, 9424.
18. Burg, A. B.; Randolph, C. L. *J. Am. Chem. Soc.* **1949**, *71*, 3451.
19. Baban, J. A.; Roberts, B. P. *J. Chem. Soc., Perkin Trans. 2* **1984**, 1717.
20. (a) Bluhm, M. E.; Bradley, M. G.; Butterick, R.; Kusari, U.; Sneddon, L. G. *J. Am. Chem. Soc.* **2006**, *128*, 7748; (b) Himmelberger, D. W.; Alden, L. R.; Bluhm, M. E.; Sneddon, L. G. *Inorg. Chem.* **2009**, *48*, 9883.

21. Staubitz, A.; Presa Soto, A.; Manners, I. *Angew. Chem. Int. Ed.* **2008**, *47*, 6212.
22. Stephens, F. H.; Baker, R. T.; Matus, M. H.; Grant, D. J.; Dixon, D. A. *Angew. Chem. Int. Edit.* **2007**, *46*, 746.
23. (a) Rokob, T. A.; Hamza, A.; Stirling, A.; Soos, T.; Papai, I. *Angew. Chem. Int. Edit.* **2008**, *47*, 2435; (b) Hamza, A.; Stirling, A.; Rokob, T. A.; Papai, I. *Int. J. Quant. Chem.* **2009**, *109*, 2416; (c) Rokob, T. A.; Hamza, A.; Papai, I. *J. Am. Chem. Soc.* **2009**, *131*, 10701.
24. Wang, H.; Frohlich, R.; Kehr, G.; Erker, G. *Chem. Commun.* **2008**, 5966.
25. Pangborn, A. B.; Giardello, M. A.; Grubbs, R. H.; Rosen, R. K.; Timmers, F. J. *Organometallics* **1996**, *15*, 1518.

Appendix A

Investigations into Brønsted Acid-Assisted CO Reduction

Appendix A

Introduction

Chapters 3 and 4 detailed the role that Lewis acids can play in CO reduction chemistry. In theory, Brønsted acids could also aid in C–H or C–C bond formation; Shriver indeed reported that a slight excess of proton acid (of appropriate pK_a) accelerated migratory insertion by up to a factor of 10.[1] Other potential benefits include a) the ability of the acid to transfer protons to reduced CO species; or b) the ability of the conjugate base to help cleave dihydrogen in concert with a late transition metal.[2] Our initial studies, focused on ammonium-substituted cyclopentadienyl (Cp) ligands, are described here.

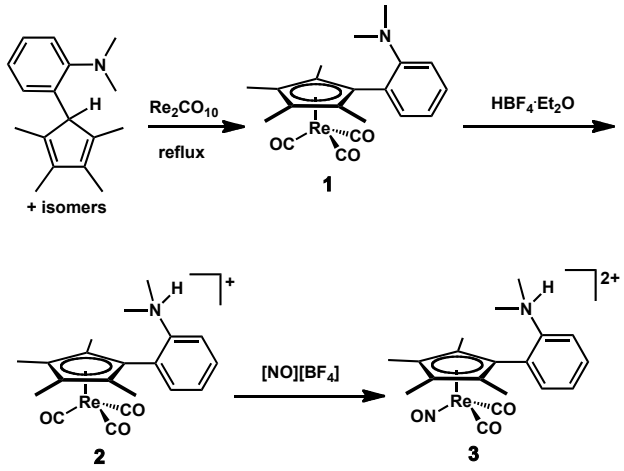

Scheme A.1

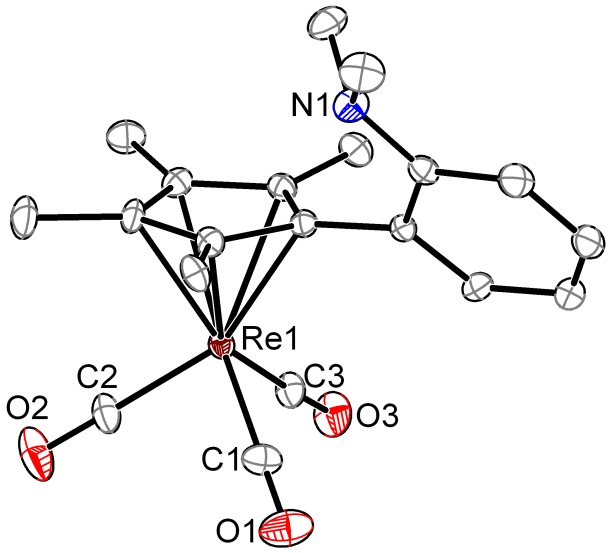

Figure A.1. Structural representation of **1**, ellipsoids at 50% probability. Hydrogen atoms omitted for clarity. Selected bond distances (Å) and angles (°): Re1–C1 1.911(4), Re1–C3 1.917(3), Re1–C2 1.918(3), C1–Re1–C3 89.82(16), C1–Re1–C2 89.27(18), C3–Re1–C2 88.96(14).

Results and Discussion

Aniline-based Cp ligands were explored first; the ligand was synthesized according to literature procedures,[3] and metallated with Re_2CO_{10} under thermally forcing conditions to form ^{NAr}Cp*Re(CO)$_3$ (**1**, Scheme A.1). Crystals of **1** suitable for XRD were grown from cold hexanes, allowing structural characterization (Figure A.1). Protonation by HBF_4 provided cationic **2** (also structurally characterized, Figure A.2), which was treated with [NO][BF_4] to effect ligand exchange, yielding the desired dicationic nitrosyl complex, [^{HNAr}Cp*Re(CO)$_2$(NO)][BF_4]$_2$ (**3**). Despite being doubly charged, the CO stretching frequencies of **3** are essentially identical to that of [Cp*Re(CO)$_2$NO]$^+$.

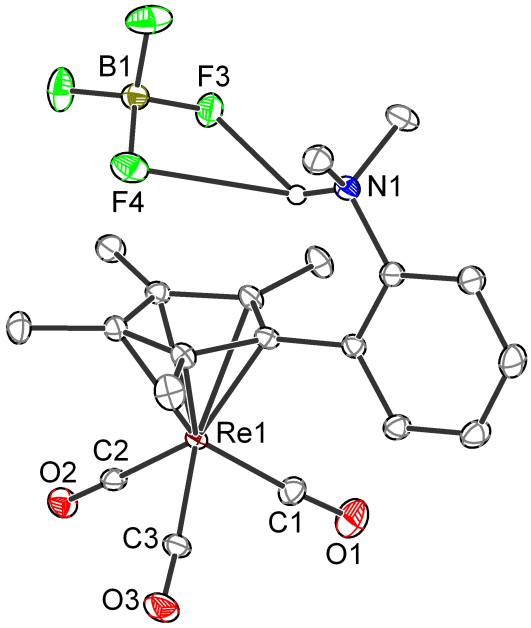

Figure A.2. Structural representation of **2**, ellipoids at 50% probability. Most hydrogen atoms omitted for clarity. Selected bond distances (Å) and angles (°): Re1–C3 1.918(2) Re1–C2 1.923(2), Re1–C1 1.927(3), N1–F3 2.791(3), C3–Re1–C2 88.34(10), C3–Re1–C1 91.37(11), C2–Re1–C1 90.77(11).

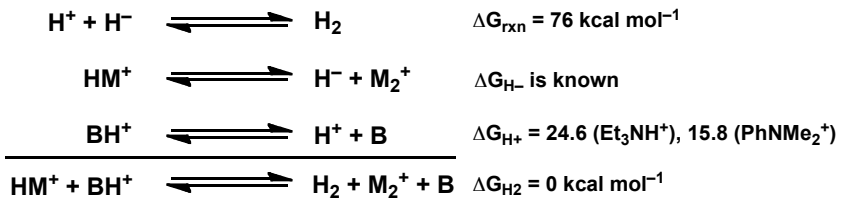

Scheme A.2

Treatment of **3** with the weak hydride $[HNi(depe)_2]^+$ (depe = bis(diethylphosphino)ethane.) resulted only in deprotonation of the pendent ammonium, evidenced by H_2 evolution and the formation of $[Ni(depe)_2]^{2+}$. Presumably, the anilinium group is too acidic to be used with late transition metal hydrides. Thermodynamic analysis according to Scheme A.2 (using pK_a of *N*,*N*-dimethylanilinium and triethylammonium) can put a lower bound on the hydricity required to avoid forming H_2. These calculations suggest that a hydride donor

with $\Delta G_{H^-} > 60$ kcal mol^{-1} will be required to avoid reaction with anilinium acids, while a hydride donor with $\Delta G_{H^-} > 51$ kcal mol^{-1} will be required to avoid reaction with trialkylammonium acids. Cp*Re(CO)(NO)(CHO) has $\Delta G_{H^-} = 52.6$ kcal mol^{-1}; a hydride with $\Delta G_{H^-} < 52.6$ kcal mol^{-1} is required to reduce it. If there is *no Brønsted acid assitance*, there is no hydride that can satisfy both requirements for a pendent anilinium group (ΔG_{H^-} larger than 60 kcal mol^{-1} but also smaller than 52.6 kcal mol^{-1}), consistent with the observed reactivity; a very small window, between 51 and 52.6 kcal mol^{-1} exists for trialkylammonium groups. This narrow window of opportunity might be widened if a large Brønsted acid assistance was engendered by the ammonium salts.

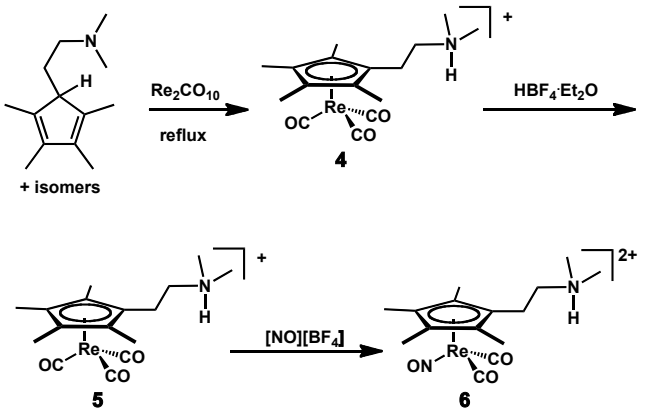

Scheme A.3

Based on the thermodynamic calculations, a new ligand containing an alkyl linker between the amine and cyclopentadienyl was targeted.[4] DuBois has observed that $[HNi(dmpe)_2]^+$ is able to reduce $[Cp^*Re(CO)_2(NO)]^+$ as well as remain stable in the presence of the $HNEt_3^+$ under H_2.[2a] We hoped that the less acidic protons of complex **6** (Scheme A.3), formed by the same route as the anilinium analogue, would be less susceptible to H_2 formation.

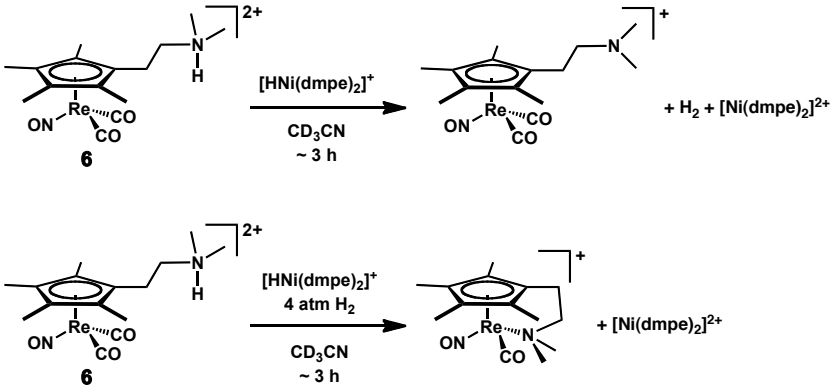

Scheme A.4

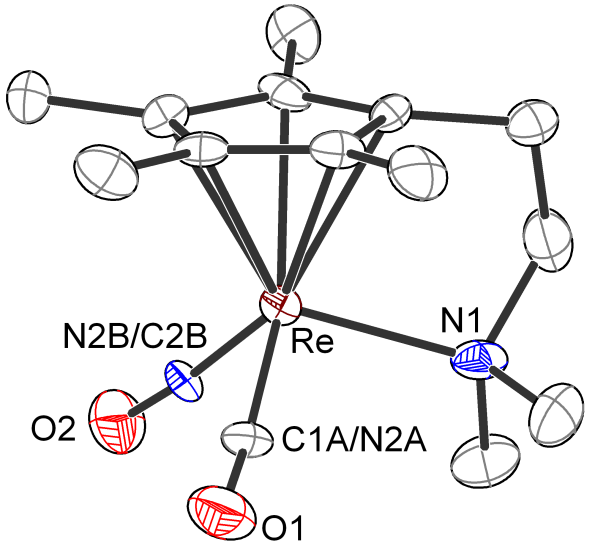

Figure A.3. Structural representation of **7**, ellipsoids at 50% probability. Hydrogen atoms and PF_6 counterion omitted for clarity. Selected bond distances (Å) and angles (°): Re–C1A/N2A 1.855(8), Re–N2B/C2B 1.838(8), Re–N1 2.186(7), C1A/N2A–Re–N2B/C2B 93.6(3), C1A/N2A–Re–N1 99.5(3), N2B/C2B–Re–N1 100.9(3).

Reaction of $[^{HNEt}Cp^*Re(CO)_2(NO)][BF_4]_2$ (**6**) in acetonitrile with $[HNi(dmpe)_2][PF_6]$ leads to clean deprotonation under N_2, as shown in Scheme A.4. The same reaction was carried out under 4 atm of H_2, which might disfavor H_2 formation. Indeed, treatment of **6** with $[HNi(dmpe)_2][PF_6]$ under 4 atm H_2 led to different reactivity (Scheme A.4), with the major product being a new Re-containing species, identified by ^1H NMR, IR, and XRD as **7**

(Figure A.3). Spectroscopic data are similar to a related complex.[5] It is not entirely clear how **7** is formed. No deprotonation is observed, although such a reaction cannot be ruled out. Additionally, compound **6** is stable in CD_3CN solutions for 48 hours, and does not spontaneously lose CO to form **7**. No sign of common reduced species, such as methane, methanol, or two-carbon species are visible by NMR spectroscopy.

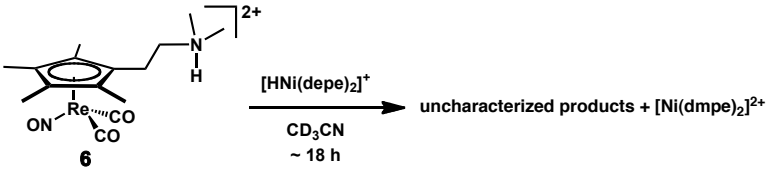

Scheme A.5

Treatment of **6** with the weaker hydride donor $[HNi(depe)_2][PF_6]$ under N_2 does not result in any deprotonation; unknown products grew in over 18 hours. These products remain unidentified, but do not contain the signature downfield shifts of Re formyl or carbene species, nor the upfield shifts of Re hydrides. $[HNi(depe)_2][PF_6]$ and $[Cp^*Re(CO)_2(NO)][BF_4]$ do not obviously react over 48 hours.

Conclusions

Few encouraging signs of productive CO reduction were observed in these reactions, even when a relatively weak acid was employed. In cases where deprotonation was not observed, very little effect on reactivity could be ascribed to the Brønsted acid; in fact, this may be due in part to the necessity to use such weak acids. In light of these problems, this approach was abandoned in favor of Lewis acidic pendent groups, which retain their acidity without problematic elimination of H_2.

Experimental Section

General Considerations

All air- and moisture-sensitive compounds were manipulated using standard vacuum line or Schlenk techniques, or in a glovebox under a nitrogen atmosphere. The solvents for air- and moisture-sensitive reactions were dried over sodium benzophenone ketyl, calcium hydride, or by the method of Grubbs.[6] All NMR solvents were purchased from Cambridge Isotopes Laboratories, Inc. Dichloromethane-*d*$_2$ (CD_2Cl_2) was freeze-pump-thaw degassed three times before being run through a small column of activated alumina. Acetonitrile-*d*$_3$ (CD_3CN) was degassed and vacuum transferred from CaH_2 prior to use. Unless noted, other materials were used as received. 1-(2-*N*,*N*-Dimethylaminophenyl)-2,3,4,5-tetramethylcyclopentadiene,[3] [2-(*N*,*N*-Dimethylamino)ethyl]tetramethylcyclopentadiene,[4] $[HNi(dmpe)_2][PF_6]$[7] and $[HNi(depe)_2][PF_6]$[8] were synthesized by literature methods. ^1H and ^{13}C NMR spectra were recorded on Varian Mercury 300 MHz, or Varian INOVA-500 or 600 MHz spectrometers at room temperature, unless indicated otherwise. Chemical shifts are reported with respect to residual internal protio solvent for ^1H and $^{13}C\{^1H\}$ spectra. Other nuclei were referenced to an external standard: H_3PO_4 (^{31}P), 15% BF_3•Et_2O/$CDCl_3$ (^{11}B), $CFCl_3$ (^{19}F), all at 0 ppm.

Synthetic Procedures

Preparation of 1. In air, a 10 mL Schlenk tube was charged with 1.41 g (5.83 mmol) of oily solid 1-(2-*N*,*N*-Dimethylaminophenyl)-2,3,4,5-tetramethylcyclopentadiene (as a mixture

of double bond isomers). The vessel was degassed by evacuation, and 1.0 g (1.53 mmol) solid Re_2CO_{10} was added under Ar counterflow. The tube was equipped with a reflux condenser, and the semisolid mixture was heated neat to 170 ºC. As it was heated the Re_2CO_{10} dissolved in the ligand to give an orange solution that bubbled vigorously during the reaction. The temperature was raised over 3 hours to 210 ºC, and heated overnight at 195 ºC. The reaction mixture was allowed to cool to room temperature, and ~15 mL cold hexanes was added, causing a white precipitate to form. The solids were collected on a frit, and washed with more cold hexanes. The solids gave 285 mg clean product; the filtrate was placed in a –25 ºC freezer, and white crystals grew. The crystals were collected on a frit and washed with cold hexanes to provide another 458 mg **1** (total, 743 mg, 95%). **^{1}H NMR** ($CDCl_3$, 300 MHz): δ 2.04 (s, 6H, C_5Me_4R), 2.36 (s, 6H, C_5Me_4R), 2.52 (s, 6H, NMe_2), 6.9 (m, 2H, *Ar*NMe_2), 7.2 (m, 2H, *Ar*NMe_2). **IR** (CH_2Cl_2): ν_{CO}, 2008, 1910.

Preparation of 2. In air, a 20 mL scintillation vial was charged with 285.0 mg (0.558 mmol) **1**, and 10 mL untreated ("wet") Et_2O. To the stirring solution was added 85 μL (0.614 mmol) HBF_4•Et_2O by syringe dropwise. As the acid is added, fluffy white precipitates formed. The mixture was stirred 15 minutes after addition, at which point the white solids were collected on a frit, washed with additional Et_2O, and dried under vacuum to afford 281.6 (84%) **2**. **^{1}H NMR** (CD_2Cl_2, 300 MHz): δ 2.02 (s, 6H, C_5Me_4R), 2.28 (s, 6H, C_5Me_4R), 3.32 (d, $\mathcal{J}$ = 5.1 Hz, $HNMe_2Ar$), 7.5 (m, 3H, $HNMe_2Ar$), 7.7 (m, 1H, $HNMe_2Ar$), 8.5 (br, 1H, *H*NMe_2Ar). **^{19}F NMR** (282 MHz): –152.4. **IR** (CH_2Cl_2): ν_{CO}, 2014, 1921 cm^{-1}.

Preparation of 3. An oven-heated Schlenk flask was cooled under vacuum, and then charged with 183.0 mg (0.306 mmol) **2** and a magnetic stir bar under Ar counterflow. At 0 °C, ~10 mL CH_2Cl_2 was added by cannula, and 53.6 mg (0.459 mmol) $[NO][BF_4]$ (previously washed with CH_2Cl_2 and dried under vacuum) was added as a solid under counterflow. The reaction was allowed to stir overnight while the ice bath slowly warmed. Brown solids precipitated during this time. After ~10 hours, the solids were collected on a frit, and washed with THF (to quench and extract excess NO^+) until the filtrate ran colorless, leaving a yellow powder which was dried in vacuo to afford 138.4 mg (65%) **3**. **^{1}H NMR** (CD_3CN, 300 MHz): 2.16 (s, 6H, C5Me4R), 2.42 (s, 6H, C5Me4R), 3.29 (s, 6H, HNMe2Ar), 7.24 (dd, $\mathcal{J}$ = 1.3, 7.6 Hz, 1H, Ar), 7.68 (t, $\mathcal{J}$ = 7.7 Hz, 1H, Ar), 7.85-7.95 (m, 2H, Ar). **IR** (CH_3CN): ν_{CO}, 2100, 2050; ν_{NO}, 1811 cm^{-1}.

Preparation of 4. A Teflon-sealed pressure vessel was charged with 860 mg (4.45 mmol) ligand, and degassed under vacuum. Under counterflow, 829 mg (1.27 mmol) of Re_2CO_{10} was added as a solid. The vessel was sealed, and the components were heated neat to 200 °C, which prompted dissolution to a pale yellow solution, and vigorous bubbling. After 20 hours, the mixture was allowed to cool to room temperature. Both the product and the excess ligand were very soluble in hexanes, preventing facile separation. Crude **4**, containing a small amount of free ligand, was used in subsequent steps. **^{1}H NMR** (CD_2Cl_2, 300 MHz): δ 2.16 (s, 6H, C_5Me_4R), 2.17 (s, 6H, C_5Me_4R), 2.23 (s, 6H, $CpCH_2CH_2NMe_2$), 2.23-2.27 (m, 2H, $CpCH_2CH_2NMe_2$), 2.53-2.59 (m, 2H, $CpCH_2CH_2NMe_2$). **IR** (CH_2Cl_2): ν_{CO}, 2006, 1907 cm^{-1}.

Preparation of 5. In air, a Et_2O solution of 1.1 g (2.45 mmol) crude **4** was treated with 673 *m*L (4.9 mmol) HBF_4.Et_2O (added dropwise by syringe with stirring). Beige precipitates formed, which were collected and crystallized from CH_2Cl_2/Et_2O at –30 ºC, affording ~800 mg pure white crystalline **5**. **^{1}H NMR** (CD_2Cl_2, 300 MHz): δ 2.16 (s, 6H, C_5Me_4R), 2.21 (s, 6H, C_5Me_4R), 2.5 (m, 2H, $CpCH_2CH_2NHMe_2$), 3.01 (d, $\mathcal{J}$ = 5.1 Hz, 6H, $CpCH_2CH_2NHMe_2$), 3.04 (m, 2H, $CpCH_2CH_2NHMe_2$) 7.7 (br, 1H, $CpCH_2CH_2NHMe_2$). **^{19}F NMR** (CD_2Cl_2, 282 MHz): δ –151.6.

Preparation of 6. A Schlenk flask was charged with 224.3 mg (0.408 mmol) **5** and a stir bar. After degassing under vacuum, 30 mL CH_2Cl_2 was added by cannula. At 0 ºC, 110 mg (0.941 mmol) $[NO][BF_4]$ was added as a solid under counterflow. The mixture was stirred overnight, with the ice bath slowly warming to room temperature during this time. The solids were collected on a frit, and washed copiously with THF (to quench and extract excess NO^+) to provide a 118 mg (45%) yellow powder **6**. **^{1}H NMR** (CD_3CN, 300 MHz): δ 2.30 (s, 6H, C_5Me_4R), 2.36 (s, 6H, C_5Me_4R), 2.91 (d, J = 5.1 Hz, 6H, $CpCH_2CH_2NHMe_2$), 2.91-2.96 (m, 2H, $CpCH_2CH_2NHMe_2$), 3.09-3.14 (m, 2H, $CpCH_2CH_2NHMe_2$). **IR** (CH_3CN): ν_{CO}, 2098, 2041, ν_{NO}, 1798 cm^{-1}.

Treatment of 3 with $[HNi(depe)_2]^+$. A J-Young NMR tube was charged with 10.3 mg (0.015 mmol) **3**, 10.2 mg (0.0165 mmol) $[HNi(depe)_2][PF_6]$, and ~0.6 mL CD_3CN. Monitoring by NMR showed steady evolution of H_2 and formation of $[Ni(depe)_2]^{2+}$ and deprotonated **3** over 7 hours.

Treatment of 6 with $[HNi(dmpe)_2]^+$. A J-Young NMR tube was charged with 19.9 mg (0.0311 mmol) **6**, 15.7 mg (0.0311 mmol) $[HNi(dmpe)_2][PF_6]$, and ~0.6 mL CD_3CN. After 10 minutes, a ~ 1:1 mixture of $[Ni]^{2+}$:$[HNi]^+$ was observed, along with H_2 and deprotonated **6**. After 1 hour almost no Ni–H remained, and conversion was complete after ~8 hours.

Treatment of 6 with $[HNi(dmpe)_2]^+$ under H_2. A J-Young NMR tube was charged with a 200 μL solution of 10.2 mg (0.015 mmol) **6**, and frozen in an LN_2 cooled cold well in the glovebox. A layer of 200 μL CD_3CN was added, and frozen again. A final 200 μL CD_3CN solution of 8.9 mg (0.0176 mmol) $[HNi(dmpe)_2][PF_6]$ was added, and the tube frozen. The tube was removed from the glovebox and 4 atm H_2 were added (condensed at LN_2 temperature). The tube was thawed and shaken well just before insertion into the NMR probe. The first NMR showed minimal consumption of Re, but over 18 hours a new major Re product formed. No formyl or other discernible reduced CO products were observed. Crystals grown from THF/Et_2O vapor diffusion were suitable for XRD, and assigned the intramolecularly coordinated product **7**. **^{1}H NMR** (THF-d_8, 300 MHz): δ 1.98 (s, 3H), 2.52 (s, 3H), 2.45 (s, 3H), 2.55 (s, 3H), 2.7 (m, 1H), 2.9 (m, 1H) 3.31 (s, 3H), 3.55 (s, 3H), 3.91 (t, $\mathcal{J}$ = 6.3 Hz).

Treatment of 6 with $[HNi(depe)_2]^+$. A J-Young NMR tube was charged with 14.6 mg (0.0228 mmol) **6**, 14.1 mg (0.0228 mmol) $[HNi(depe)_2][PF_6]$, and ~0.6 mL CD_3CN. Monitoring over the first 2 hours showed no observable reaction, while over 10 hours new

asymmetric products grew in by NMR, with **7** appearing to be the major product. No formyl or other discernible reduced CO species were observed.

References

1. Butts, S. B.; Richmond, T. G.; Shriver, D. F. *Inorg. Chem.* **1981**, *20*, 278.
2. (a) Curtis, C. J.; Miedaner, A.; Ellis, W. W.; DuBois, D. L. *J. Am. Chem. Soc.* **2002**, *124*, 1918; (b) Ellis, W. W.; Miedaner, A.; Curtis, C. J.; Gibson, D. H.; DuBois, D. L. *J. Am. Chem. Soc.* **2002**, *124*, 1926.
3. Enders, M.; Ludwig, G.; Pritzkow, H. *Organometallics* **2001**, *20*, 827.
4. Jutzi, P.; Dahlhaus, J. *Synthesis* **1993**, 684.
5. Wang, T. F.; Lai, C. Y.; Wen, Y. S. *J. Organomet. Chem.* **1996**, *523*, 187.
6. Pangborn, A. B.; Giardello, M. A.; Grubbs, R. H.; Rosen, R. K.; Timmers, F. J. *Organometallics* **1996**, *15*, 1518.
7. Miedaner, A.; DuBois, D. L.; Curtis, C. J.; Haltiwanger, R. C. *Organometallics* **1993**, *12*, 299.
8. Berning, D. E.; Noll, B. C.; DuBois, D. L. *J. Am. Chem. Soc.* **1999**, *121*, 11432.

Appendix B

Crown Ether Alteration of Triethylborohydride Speciation

Appendix B

Introduction

Triethylborohydride reagents, often termed "Super-hydrides", are versatile main group reductants, used in a variety of organic and inorganic transformations.[1] In the course of our studies on metal carbonyl reduction (Chapter 3), we noticed subtle differences in reactivity between the Li, Na, and K salts of $[HBEt_3]^-$. Such variability could be due to different solvation or solubility effects, or the speciation of the borohydride in solution. To probe the role of speciation in reduction chemistry, reductions were performed with two discrete reagents: $KHBEt_3$ and the corresponding 18-crown-6 adduct, 18c6/$KHBEt_3$. Here we briefly compare the structure and reactivity of these reagents.

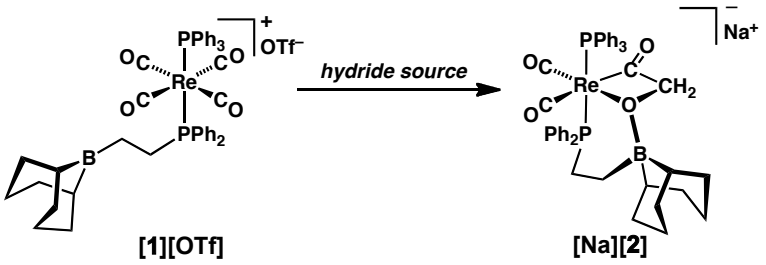

Scheme B.1

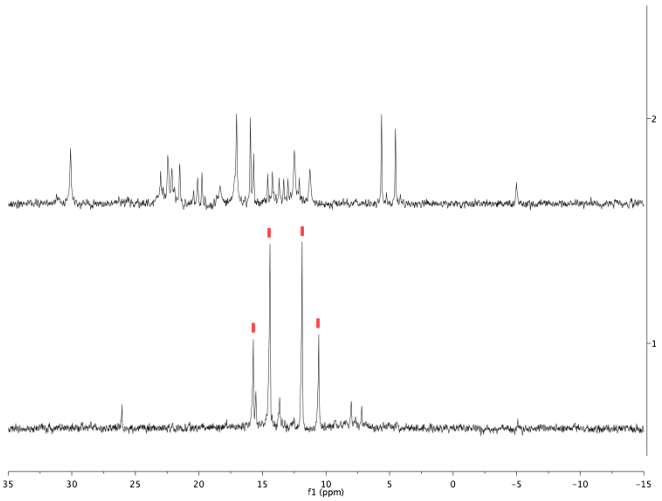

Figure B.1. $^{31}P\{^{1}H\}$ NMR spectra after reduction of [**1**][OTf] with $KHBEt_3$ (top) and 18c6/$KHBEt_3$ (bottom). Red squares indicate $[\mathbf{2}]^-$.

Results and Discussion

Reduction of *trans*-$[(Ph_2P(CH_2)_2B(C_8H_{14}))(PPh_3)Re(CO)_4][OTf]$ ([**1**][OTf]) with two equivalents $KHBEt_3$ (prepared from KH and BEt_3 following a literature procedure[2]) in C_6D_5Cl produced an intractable mixture of products. As an alternative to $KHBEt_3$, which is only sparingly soluble in C_6D_5Cl, 18c6/$KHBEt_3$ was prepared. Addition of the crown ether to a chlorobenzene suspension of $KHBEt_3$ led to incorporation of all solids into solution, and provided microcrystalline 18c6/$KHBEt_3$ upon removal of solvents *in vacuo*. Two equivalents of 18c6/$KHBEt_3$ was added as a solid to a stirring C_6D_5Cl solution of [**1**][OTf], and surprisingly afforded just one major product, containing a new C–C bond (Scheme B.1). Full details of characterization (including structural analysis) are provided in Chapter 3. The change in reactivity might be ascribed to changes in speciation, either in the hydride source itself, or in the K^+ salts of a product. Addition of 18c6 also increases the solubility of $KHBEt_3$ in C_6D_5Cl, which could play a role.

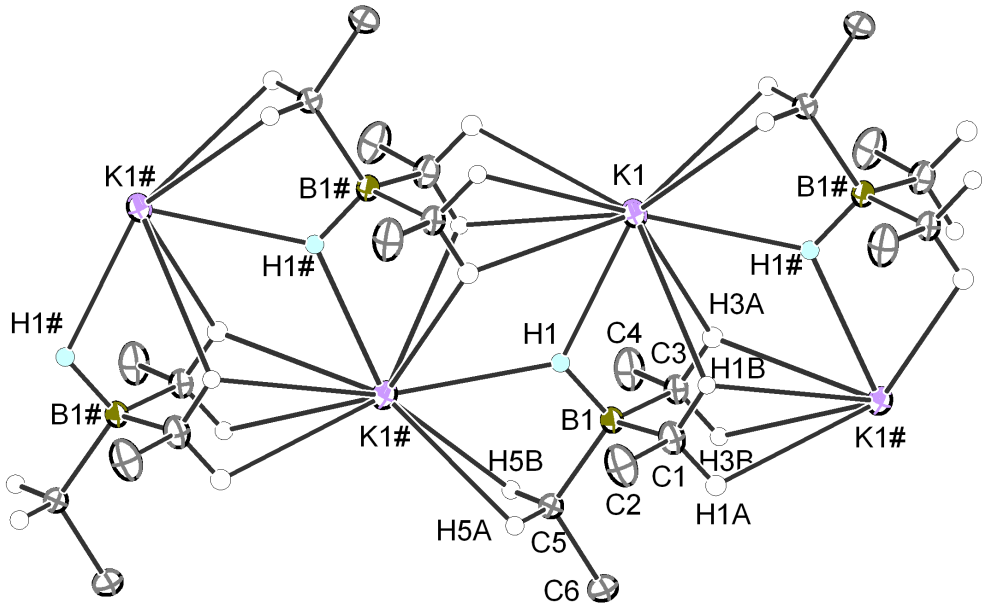

Figure B.2. Structural representation of $KHBEt_3$, ellipsoids at 50% probability.

Table B.1. Selected interatomic distances of $KHBEt_3$.

Atoms	Distance
K1–H1	2.544(9)
K1–H1#	2.70(1)
K1#–H1A	2.93(1)
K1–H1B	2.975(9)
K1#–H1B	2.966(9)
K1–H3A	2.74(1)
K1#–H3A	2.95(1)
K1#–H3B	2.959(9)
K1#–H5A	2.782(9)
K1#–H5B	2.758(9)
B1–H1	1.196(9)
B1–C1	1.642(1)
B1–C3	1.643(1)
B1–C5	1.640(1)
K1#–C1	3.5164(8)
K1–C1	3.3808(9)
K1–C3	3.3086(8)
K1#–C3	3.3896(8)
K1#–C5	3.0976(8)
K1#–B1	3.4627(9)
K1–B1	3.2038(8)

Differences in speciation of the borohydride reagents were investigated in the *solid state* by single crystal X-Ray diffraction. Structural characterization of polyhydridoborates is quite common, but this is not the case for trialkylmonohydridoborates. A few salts, all with solvent or ligand supporting the alkali cation, have been characterized in a variety of nuclearity and binding modes.[3] There are also a number of cases where $[HBR_3]^-$ interacts with transition metals in some fashion.[4] Crystals of $KHBEt_3$ were grown from concentrated toluene solutions at –35 °C. The crystals were packed in the space group P $2_12_12_1$ and all hydrogen atoms were located in the difference map and refined without constraint. The solid-state structure (Figure B.2) is firstly remarkable for containing only $KHBEt_3$ and no solvents or other ligands to bind K^+. Perhaps as a result, the crystal lattice is made up of a dense polymeric network with a number of unusual K^+ supporting interactions (Figure B.4). The core is built from an asymmetric bridging K_2–μ–H–BEt_3 moiety. Two different interactions between K and C–H bonds are present: two of the ethyl groups arrange themselves to donate 4 C–H bonds to K^+, while the other donates 2 C–H bonds to a different K^+. This unusual stabilization has been observed before for tetraalkylborate species interacting with alkali metal cations.[2,5] These cores string together into repeating units, forming long chains in the lattice. Interatomic distances and angles are summarized in Table B.1.

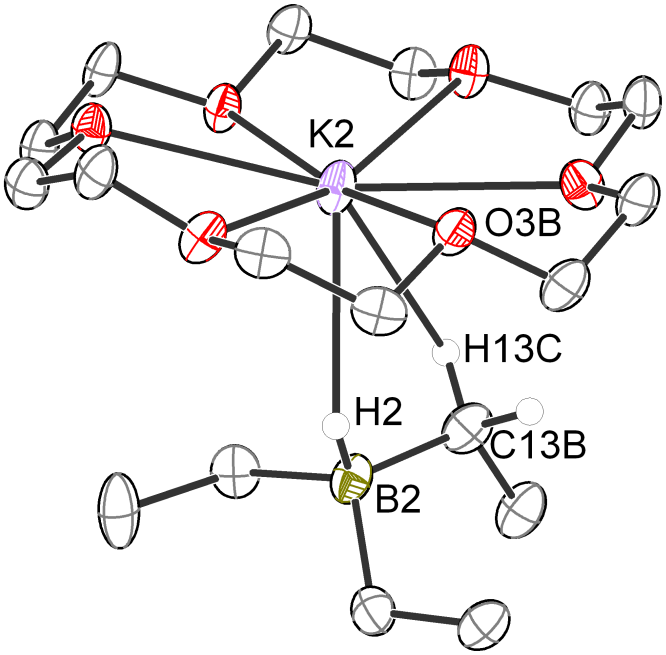

Figure B.3. Structural representation of 18c6/KHBEt$_3$, ellipsoids at 50% probability.

Table B.2. Selected interatomic distances of 18c6/KHBEt$_3$.

Atoms	Distance
K1–B1	3.568(3)
K1–C13A	3.254(3)
K2–B2	3.395(3)
K2–C13B	3.469(3)
K3–B3	3.494(3)
K3–C13C	3.378(3)
K4–B4	3.558(3)
K4–C13D	3.268(3)
B1–C13A	1.640(5)
B1–C15A	1.636(4)
B1–C17A	1.643(4)
K1–O1A	2.779(2)
K1–O2A	2.826(2)
K1–O3A	2.859(2)
K1–O4A	2.801(2)
K1–O5A	2.947(2)
K1–O6A	2.831(2)

Crystals of 18c6/KHBEt$_3$ were grown from concentrated chlorobenzene at −35 °C. The crystals were twinned, and as such the hydrogen atom positions were calculated. Nonetheless, the overall structure (Figure B.3) contrasts starkly with that of the crown-free borohydride: the solid state structure (space group P $2_1/c$) features a strictly monomeric core, with no bridging interactions between multiple K^+ ions (Figure B.4). The K^+ ion is sequestered in the crown ether, and is additionally stabilized by interaction with the $[HBEt_3]^-$ fragment, which is positioned to donate electron density from the B–H bond and a C–H bond of a methylene unit. The C–K and B–K distances differ significantly between the different molecules in the asymmetric unit, consistent with differing amounts of C–H or B–H donation in the independent molecules. Details of bond lengths and angles are provided in Table B.2.

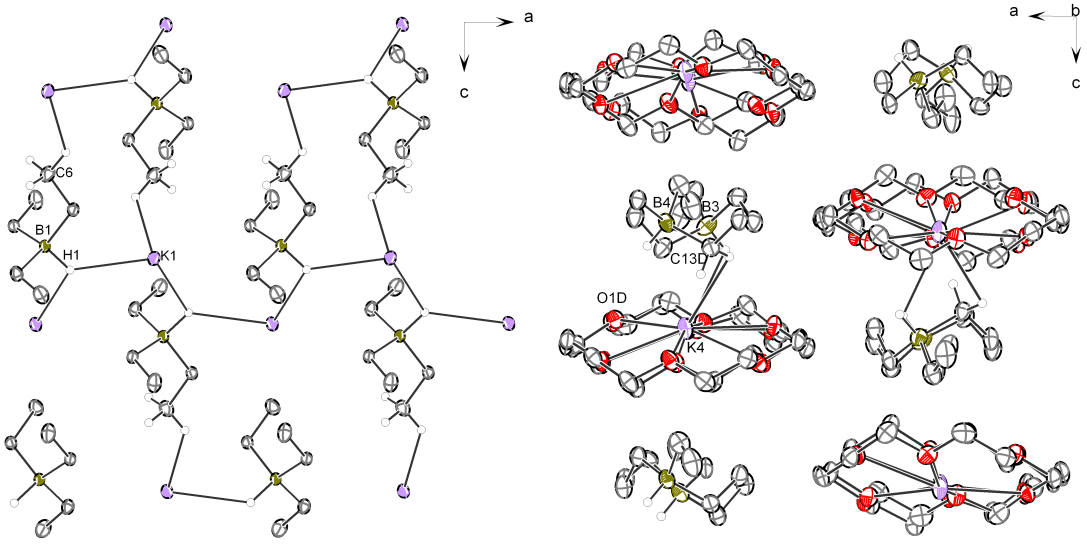

Figure B.4. Packing diagrams of KHBEt$_3$ (left) and 18c6/KHBEt$_3$ (right), both looking down the b axis. For clarity, hydrogen atoms are drawn isotropically, and only certain K–H interactions are drawn. The closest K–H interaction was drawn for each independent molecule in 18c6/KHBEt$_3$, showing the different binding modes.

Conclusions

While it would be foolhardy to suggest that the disparate solid state structures of $KHBEt_3$ and 18c6/$KHBEt_3$ are indicators of solution reactivity without a much more detailed study, the two different structures are interesting in their own right. Further, it seems plausible that monomeric 18c6/$KHBEt_3$ would be more easily dissolved than the dense polymer network of $KHBEt_3$ itself. Whether or not the origin lies in solubility or speciation differences, the crown ether adduct of 18c6/$KHBEt_3$ shows promising reactivity in one case relative to $KHBEt_3$, and may be of general interest as an alternative hydride source.

Experimental Section

General Considerations

All air- and moisture-sensitive compounds were manipulated using standard vacuum line or Schlenk techniques, or in a glovebox under a nitrogen atmosphere. The solvents for air- and moisture-sensitive reactions were dried over sodium benzophenone ketyl, calcium hydride, or by the method of Grubbs.[6] All NMR solvents were purchased from Cambridge Isotopes Laboratories, Inc. Chlorobenzene-d_5 (C_6D_5Cl) was freeze-pump-thaw degassed three times before being run through a small column of activated alumina. Unless noted, other materials were used as received. ^1H and ^{13}C NMR spectra were recorded on Varian Mercury 300 MHz, or Varian INOVA-500 or 600 MHz spectrometers at room temperature, unless indicated otherwise. Chemical shifts are reported with respect to

residual internal protio solvent for ^{1}H and $^{13}C\{^{1}H\}$ spectra. Other nuclei were referenced to an external standard: 85% H_3PO_4 (^{31}P), 15% BF_3•Et_2O/$CDCl_3$ (^{11}B), $CFCl_3$ (^{19}F), all at 0 ppm.

Preparation of $KHBEt_3$. Following a literature procedure,[2] a scintillation vial was charged with 238.8 mg (5.95 mmol) KH and 7 mL toluene. To the stirring suspension was added 5.9 mL (5.9 mmol) BEt_3 (1.0 M in hexanes) slowly by syringe. The reaction mixture, which warmed slightly during the addition, was allowed to stir for 3 hours before filtration through a frit. Some solids remaining on the frit were extracted with 5 mL toluene, and the mixture was concentrated to about 4 mL before storage at –35 °C. Large colorless single crystals formed overnight; a few were retained for X-Ray structural analysis, while the bulk of the material was collected and dried under vacuum, yielding 480 mg (59%) $KHBEt_3$. **^{1}H NMR** (C_6D_5Cl, 300 Mhz): δ 0.17 (br, 6H, BCH_2CH_3), 0.97 (t, $\mathcal{J}$ = 7.5 Hz, 9H, BCH_2CH_3).

Preparation of 18-crown-6/$KHBEt_3$. To a stirring slurry of 204.7 mg (1.48 mmol) $KHBEt_3$ in 5 mL chlorobenzene was added 391.5 mg (1.48 mmol) of solid 18-crown-6. After stirring for 24 hours, there were still some undissolved solids, which went into solution upon addition of another 5 mL chlorobenzene. The mixture was filtered; 1 mL of filtrate was reserved for single crystal growth (at –35 °C), while the rest was placed under vacuum to remove the solvent to dryness, yielding 548 mg (92%) 18c6/$KHBEt_3$. **^{1}H NMR** (C_6D_5Cl, 300 MHz): δ 0.69 (br q, 6H, $HBCH_2CH_3$), 1.00 (br, 1H, $HBCH_2CH_3$), 1.37 (br t, 9H, $HBCH_2CH_3$), 3.26 (s, 24H, $–OCH_2CH_2O–$).

Reduction of *trans*-[($Ph_2P(CH_2)_2B(C_8H_{14})$)($PPh_3$)$Re(CO)_4$][OTf] with $KHBEt_3$. A small vial was charged with 13.5 mg (0.098 mmol) $KHBEt_3$, 51.0 mg (0.049 mmol) *trans*-[($Ph_2P(CH_2)_2B(C_8H_{14})$)($PPh_3$)$Re(CO)_4$][OTf], and a stir bar. With stirring, ~1 mL C_6D_5Cl was added, and the mixture was stirred overnight before being filtered into a J-Young NMR tube. A large number of resonances were observed by ^1H and ^{31}P NMR spectra.

Reduction of *trans*-[($Ph_2P(CH_2)_2B(C_8H_{14})$)($PPh_3$)$Re(CO)_4$][OTf] with 18c6/$KHBEt_3$. A J-Young NMR tube was charged with 34.7 mg (0.033 mmol) *trans*-[($Ph_2P(CH_2)_2B(C_8H_{14})$)($PPh_3$)$Re(CO)_4$][OTf], 26.7 mg (0.067 mmol) solid 18-crown-6/$KHBEt_3$, and ~0.6 mL C_6D_5Cl. The tube was shaken well, and darkened considerably. NMR spectroscopy revealed quite clean conversion to an asymmetric Re compound, which was identified (see Chapter 3) as a C–C coupled acyl anion.

References

1. *Encyclopedia of Reagents for Organic Synthesis*. Wiley: New York, 1995.
2. Fryzuk, M. D.; Lloyd, B. R.; Clentsmith, G. K. B.; Rettig, S. J. *J. Am. Chem. Soc.* **1994**, *116*, 3804.
3. (a) Boss, S. R.; Coles, M. P.; Eyre-Brook, V.; Garcia, F.; Haigh, R.; Hitchcock, P. B.; McPartlin, M.; Morey, J. V.; Naka, H.; Raithby, P. R.; Sparkes, H. A.; Tate, C. W.; Wheatley, A. E. H. *Dalton Trans.* **2006**, 5574; (b) Haywood, J.; Wheatley, A. E. H. *Eur. J. Inorg. Chem.* **2009**, 5010; (c) Koster, R.; Schussler, W.; Boese, R.; Blaser, D. *Chem. Ber.* **1991**, *124*, 2259; (d) Bell, N. A.; Shearer, H. M. M.; Spencer, S. B. *Acta Crystallogr., Sect. C: Cryst. Struct. Commun.* **1983**, *39*, 694; (e) Bell, N. A.; Shearer, H. M. M.; Spencer, C. B. *J. Chem. Soc., Chem. Commun.* **1980**, 711.
4. (a) Boro, B. J.; Duesler, E. N.; Goldberg, K. I.; Kemp, R. A. *Inorg. Chem. Commun.* **2008**, *11*, 1426; (b) Dawson, D. M.; Meetsma, A.; Roedelof, J. B.; Teuben, J. H. *Inorg. Chim. Acta* **1997**, *259*, 237; (c) Liang, F.; Schmalle, H. W.; Berke, H. *Eur. J. Inorg. Chem.* **2006**, *2006*, 5081; (d) Cotton, F. A.; Matonic, J. H.; Murillo, C. A. *J. Am.*

Chem. Soc. **1998**, *120*, 6047; (e) Drouin, S. D.; Amoroso, D.; Yap, G. P. A.; Fogg, D. E. *Organometallics* **2002**, *21*, 1042; (f) Dawson, D. M.; Meetsma, A.; Roedelof, J. B.; Teuben, J. H. *Inorg. Chim. Acta* **1997**, *259*, 237.

5. Rhine, W. E.; Stucky, G.; Peterson, S. W. *J. Am. Chem. Soc.* **1975**, *97*, 6401.
6. Pangborn, A. B.; Giardello, M. A.; Grubbs, R. H.; Rosen, R. K.; Timmers, F. J. *Organometallics* **1996**, *15*, 1518.

Appendix C

NMR Chemical Shifts of Trace Impurities: Common Laboratory Solvents, Organics, and Gases in Deuterated Solvents Relevant to the Organometallic Chemist

Adapted in part from:
Fulmer, G. R.; Miller, A. J. M.; Sherden, N. H.; Gottlieb, H. E.; Nudelman, A.; Stoltz, B. M.; Bercaw, J. E.; Goldberg, K. I. *Organometallics* **2010**, *29*, 2176.
http://dx.doi.org/10.1021/om100106e

Appendix C

Introduction

Synthetic chemists rely heavily on NMR spectroscopy as a tool for product characterization and reaction monitoring. An essential reference tool was published in 1997 by Gottlieb, Kotlyar, and Nudelman: "NMR Chemical Shifts of Common Laboratory Solvents as Trace Impurities"[1] compiles the chemical shifts of a large number of contaminants commonly encountered in synthetic chemistry, allowing for easy identification of known impurities as well as providing a quick means of estimating the functionality and structure of unknown compounds in a variety of deuterated organic solvents. However, despite the utility of Gottlieb et al.'s work, the chemical shifts of impurities in a number of NMR solvents often used by organometallic chemists were not included. Tetrahydrofuran-d_8 (THF-d_8), toluene-d_8, dichloromethane-d_2 (CD_2Cl_2), chlorobenzene-d_5 (C_6D_5Cl), and 2,2,2-trifluoroethanol-d_3 (TFE-d_3) are commonplace in laboratories practicing inorganic syntheses. Therefore, we have expanded the spectral data compilation with the inclusion of chemical shifts of common impurities recorded in the deuterated solvents heavily employed in our organometallic laboratories. The chemical shifts of various gases (hydrogen, methane, ethane, propane, ethylene, propylene, and carbon dioxide), often encountered as reagents or products in organometallic reactions, along with organic compounds relevant to organometallic chemists (allyl acetate, benzaldehyde, carbon disulfide, carbon tetrachloride, 18-crown-6, cyclohexanone, diallyl carbonate, dimethyl carbonate, dimethyl malonate,

furan, Apiezon H grease, hexamethylbenzene, hexamethyldisiloxane, imidazole, pyrrole, and pyrrolidine) have also been added to this expanded list.

Results and Discussion

Chemical shifts for each of the impurities are reported in the tables below: ^{1}H and ^{13}C NMR spectral data of all substrates are presented in Tables C.1 and C.2, respectively. Notably, physically larger tables with bigger font sizes, containing all the data from Tables C.1–C.2 as well as the chemical shifts of additional organic compounds are provided in the Supporting Information. Unless noted otherwise, coupling constants (reported in Hz) and resonance multiplicities (abbreviated with the following: s = singlet, d = doublet, t = triplet, q = quartet, sept = septet, m = multiplet, br = broad) were observed to be solvent-independent.

It was noted that the amount of gas dissolved in solution gave ^{1}H NMR signal integrations that were qualitatively comparable to the solutions made with the 3 μL additions of the liquid or solid contaminants. However, typically in order to observe signals for the gas samples by ^{13}C NMR spectroscopy, additional time for data collection was required. The solubility of each gas in D_2O was extremely limited, making ^{13}C detection impractical. Of all the gases, methane required the most number of transients in order to obtain an observable signal by ^{13}C NMR spectroscopy. In most cases, the ^{13}C chemical shift of methane was acquired through the use of gs-HMQC NMR spectroscopy to provide enhanced sensitivity. In order to reflect what would be observed in typical NMR-scale

experiments, ^{13}C detection was not pursued with isotopically enriched gases. A number of misreported values were discovered in the years since the original publication and in the preparation of this manuscript. These are detailed in the Supporting Information, and the values are now correctly listed in Tables C.1 and C.2.

Table C.1. ^{1}H NMR data[a]

	proton	mult	THF-d_8	CD_2Cl_2	$CDCl_3$	toluene-d_8	C_6D_6	C_6D_5Cl	$(CD_3)_2CO$	$(CD_3)_2SO$	CD_3CN	TFE-d_3	CD_3OD	D_2O
solvent residual signals			1.72 3.58	5.32	7.26	2.08 6.97 7.01 7.09	7.16	6.96 6.99 7.14	2.05	2.50	1.94	5.02 3.88	3.31	4.79
water	OH	s	2.46	1.52	1.56	0.43	0.40	1.03	2.84[b]	3.33[b]	2.13	3.66	4.87	-
acetic acid	CH_3	s	1.89	2.06	2.10	1.57	1.52	1.76	1.96	1.91	1.96	2.06	1.99	2.08
acetone	CH_3	s	2.05	2.12	2.17	1.57	1.55	1.77	2.09	2.09	2.08	2.19	2.15	2.22
acetonitrile	CH_3	s	1.95	1.97	2.10	0.69	0.58	1.21	2.05	2.07	1.96	1.95	2.03	2.06
benzene	CH	s	7.31	7.35	7.36	7.12	7.15	7.20	7.36	7.37	7.37	7.36	7.33	-
tert-butyl alcohol	CH_3	s	1.15	1.24	1.28	1.03	1.05	1.12	1.18	1.11	1.16	1.28	1.40	1.24
	OH	s	3.16	-	-	0.58	0.63	1.30	-	4.19	2.18	2.20	-	-
chloroform	CH	s	7.89	7.32	7.26	6.10	6.15	6.74	8.02	8.32	7.58	7.33	7.90	-
18-crown-6	CH_2	s	3.57	3.59	3.67	3.36	3.39	3.41	3.59	3.51	3.51	3.64	3.64	3.80
cyclohexane	CH_2	s	1.44	1.44	1.43	1.40	1.40	1.37	1.43	1.40	1.44	1.47	1.45	-
1,2-dichloroethane	CH_2	s	3.77	3.76	3.73	2.91	2.90	3.26	3.87	3.90	3.81	3.71	3.78	-
dichloromethane	CH_2	s	5.51	5.33	5.30	4.32	4.27	4.77	5.63	5.76	5.44	5.24	5.49	-
diethyl ether	CH_3	t, 7	1.12	1.15	1.21	1.10	1.11	1.10	1.11	1.09	1.12	1.20	1.18	1.17
	CH_2	q, 7	3.38	3.43	3.48	3.25	3.26	3.31	3.41	3.38	3.42	3.58	3.49	3.56
diglyme	CH_2	m	3.43	3.57	3.65	3.43	3.46	3.49	3.56	3.51	3.53	3.67	3.61	3.67
	CH_2	m	3.53	3.50	3.57	3.31	3.34	3.37	3.47	3.38	3.45	3.62	3.58	3.61
	OCH_3	s	3.28	3.33	3.39	3.12	3.11	3.16	3.28	3.24	3.29	3.41	3.35	3.37
1,2-dimethoxyethane	CH_3	s	3.28	3.34	3.40	3.12	3.12	3.17	3.28	3.24	3.28	3.40	3.35	3.37
	CH_2	s	3.43	3.49	3.55	3.31	3.33	3.37	3.46	3.43	3.45	3.61	3.52	3.60
dimethylformamide	CH	s	7.91	7.96	8.02	7.57	7.63	7.73	7.96	7.95	7.92	7.86	7.97	7.92
	CH_3	s	2.88	2.91	2.96	2.37	2.36	2.51	2.94	2.89	2.89	2.98	2.99	3.01
	CH_3	s	2.76	2.82	2.88	1.96	1.86	2.30	2.78	2.73	2.77	2.88	2.86	2.85
1,4-dioxane	CH_2	s	3.56	3.65	3.71	3.33	3.35	3.45	3.59	3.57	3.60	3.76	3.66	3.75
ethane	CH_3	s	0.85	0.85	0.87	0.81	0.80	0.79	0.83	0.82	0.85	0.85	0.85	0.82
ethanol	CH_3	t, 7	1.10	1.19	1.25	0.97	0.96	1.06	1.12	1.06	1.12	1.22	1.19	1.17
	CH_2	q, 7[c]	3.51	3.66	3.72	3.36	3.34	3.51	3.57	3.44	3.54	3.71	3.60	3.65
	OH	s[c,d]	3.30	1.33	1.32	0.83	0.50	1.39	3.39	4.63	2.47	-	-	-
ethyl acetate	CH_3CO	s	1.94	2.00	2.05	1.69	1.65	1.78	1.97	1.99	1.97	2.03	2.01	2.07
	CH_2CH_3	q, 7	4.04	4.08	4.12	3.87	3.89	3.96	4.05	4.03	4.06	4.14	4.09	4.14
	CH_2CH_3	t, 7	1.19	1.23	1.26	0.94	0.92	1.04	1.20	1.17	1.20	1.26	1.24	1.24
ethylene	CH_2	s	5.36	5.40	5.40	5.25	5.25	5.29	5.38	5.41	5.41	5.40	5.39	5.44
ethylene glycol	CH_2	s[e]	3.48	3.66	3.76	3.36	3.41	3.58	3.28	3.34	3.51	3.72	3.59	3.65
H grease	CH_3	m	0.85–0.91	0.84–0.90	0.84–0.87	0.89–0.96	0.90–0.98	0.86–0.92	0.90	0.82–0.88	-	0.88–0.94	0.86–0.93	-
	CH_2	br s	1.29	1.27	1.25	1.33	1.32	1.30	1.29	1.24	-	1.33	1.29	-
hexamethylbenzene	CH_3	s	2.18	2.20	2.24	2.10	2.13	2.10	2.17	2.14	2.19	2.24	2.19	-
hexamethyldisoloxane	CH_3	s	0.07	0.07	0.07	0.10	0.12	0.10	0.07	0.06	0.07	0.08	0.07	0.28
n-hexane	CH_3	t, 7	0.89	0.89	0.88	0.88	0.89	0.85	0.88	0.86	0.89	0.91	0.90	-
	CH_2	m	1.29	1.27	1.26	1.22	1.24	1.19	1.28	1.25	1.28	1.31	1.29	-
HMPA	CH_3	d, 9.5	2.58	2.60	2.65	2.42	2.40	2.47	2.59	2.53	2.57	2.63	2.64	2.61
hydrogen	H_2	s	4.55	4.59	4.62	4.50	4.47	4.49	4.54	4.61	4.57	4.53	4.56	-
imidazole	CH(2)	s	7.48	7.63	7.67	7.30	7.33	7.53	7.62	7.63	7.57	7.61	7.67	7.78
	CH(4,5)	s	6.94	7.07	7.10	6.86	6.90	7.01	7.04	7.01	7.01	7.03	7.05	7.14
methane	CH_4	s	0.19	0.21	0.22	0.17	0.16	0.15	0.17	0.20	0.20	0.18	0.20	0.18
methanol	CH_3	s[f]	3.27	3.42	3.49	3.03	3.07	3.25	3.31	3.16	3.28	3.44	3.34	3.34
	OH	s[d,f]	3.02	1.09	1.09	-	-	1.30	3.12	4.01	2.16	-	-	-
nitromethane	CH_3	s	4.31	4.31	4.33	3.01	2.94	3.59	4.43	4.42	4.31	4.28	4.34	4.40
n-pentane	CH_3	t, 7	0.89	0.89	0.88	0.87	0.87	0.84	0.88	0.86	0.89	0.90	0.90	-
	CH_2	m	1.31	1.30	1.27	1.25	1.23	1.23	1.27	1.27	1.29	1.33	1.29	-
propane	CH_3	t, 7.3	0.90	0.90	0.90	0.89	0.86	0.84	0.88	0.87	0.90	0.90	0.91	0.88
	CH_2	sept, 7.3	1.33	1.32	1.32	1.32	1.26	1.26	1.31	1.29	1.33	1.33	1.34	1.30
2-propanol	CH_3	d, 6	1.08	1.17	1.22	0.95	0.95	1.04	1.10	1.04	1.09	1.20	1.50	1.17
	CH	sept, 6	3.82	3.97	4.04	3.65	3.67	3.82	3.90	3.78	3.87	4.05	3.92	4.02
propylene	CH_3	dt, 6.4, 1.5	1.69	1.71	1.73	1.55	1.55	1.58	1.68	1.68	1.70	1.70	1.70	1.70
	CH_2(1)	dm, 10	4.89	4.93	4.94	4.92	4.95	4.91	4.90	4.94	4.93	4.93	4.91	4.95
	CH_2(2)	dm, 17	4.99	5.03	5.03	4.98	5.01	4.98	5.00	5.03	5.04	5.03	5.01	5.06
	CH	m	5.79	5.84	5.83	5.70	5.72	5.72	5.81	5.80	5.85	5.87	5.82	5.90
pyridine	CH(2,6)	m	8.54	8.59	8.62	8.47	8.53	8.51	8.58	8.58	8.57	8.45	8.53	8.52
	CH(3,5)	m	7.25	7.28	7.29	6.67	6.66	6.90	7.35	7.39	7.33	7.40	7.44	7.45
	CH(4)	m	7.65	7.68	7.68	6.99	6.98	7.25	7.76	7.79	7.73	7.82	7.85	7.87
pyrrole	NH	br t	9.96	8.69	8.40	7.71	7.80	8.61	10.02	10.75	9.27	-	-	-
	CH(2,5)	m	6.66	6.79	6.83	6.43	6.48	6.62	6.77	6.73	6.75	6.84	6.72	6.93
	CH(3,4)	m	6.02	6.19	6.26	6.27	6.37	6.27	6.07	6.01	6.10	6.24	6.08	6.26
pyrrolidine[g]	CH_2(2,5)	m	2.75	2.82	2.87	2.54	2.54	2.64	-	2.67	2.75	3.11	2.80	3.07
	CH_2(3,4)	m	1.59	1.67	1.68	1.36	1.33	1.43	-	1.55	1.61	1.93	1.72	1.87
silicone grease	CH_3	s	0.11	0.09	0.07	0.26	0.29	0.14	0.13	–0.06	0.08	0.16	0.10	-
tetrahydrofuran	CH_2(2,5)	m	3.62	3.69	3.76	3.54	3.57	3.59	3.63	3.60	3.64	3.78	3.71	3.74
	CH_2(3,4)	m	1.79	1.82	1.85	1.43	1.40	1.55	1.79	1.76	1.80	1.91	1.87	1.88
toluene	CH_3	s	2.31	2.34	2.36	2.11	2.11	2.16	2.32	2.30	2.33	2.33	2.32	-
	CH(2,4,6)	m	7.10	7.15	7.17	6.96–7.01	7.02	7.01–7.08	7.10–7.20	7.18	7.10–7.30	7.10–7.30	7.16	-
	CH(3,5)	m	7.19	7.24	7.25	7.09	7.13	7.10–7.17	7.10–7.20	7.25	7.10–7.30	7.10–7.30	7.16	-
triethylamine	CH_3	t, 7	0.97	0.99	1.03	0.95	0.96	0.93	0.96	0.93	0.96	1.31	1.05	0.99
	CH_2	q, 7	2.46	2.48	2.53	2.39	2.40	2.39	2.45	2.43	2.45	3.12	2.58	2.57

a) Except for the compounds in solutions 8–10, as well as the gas samples, hexamethylbenzene, and the corrected values mentioned in the Supporting Information, all data for the solvents $CDCl_3$, C_6D_6, $(CD_3)_2CO$, $(CD_3)_2SO$, CD_3CN, CD_3OD, and D_2O were previously reported[1]. b) A signal for HDO is also observed in $(CD_3)_2SO$ (3.30 ppm) and $(CD_3)_2CO$ (2.81 ppm), often seen as a 1:1:1 triplet ($^2\mathcal{J}_{H,D}$ = 1 Hz). c) In some solvents, the coupling interaction between the CH_3 and the OH protons may be observed ($\mathcal{J}$ = 5 Hz) d) Not all OH signals were observable. e) In CD_3CN, the OH proton was seen as a multiplet at 2.69 ppm, as well as extra coupling to the CH_2 resonance. f) In some solvents, the coupling interaction between the CH_3 and the OH protons may be observed ($\mathcal{J}$ = 5.5 Hz). g) Pyrrolidine was observed to react with $(CD_3)_2CO$.

Table C.2. ^{13}C NMR data[a]

	carbon	THF-d_8	CD_2Cl_2	$CDCl_3$	toluene-d_8	C_6D_6	C_6D_5Cl	$(CD_3)_2CO$	$(CD_3)_2SO$	CD_3CN	TFE-d_3	CD_3OD	D_2O
solvent signals		67.21	53.84	77.16	137.48	128.06	134.19	29.84	39.52	1.32	61.50	49.00	-
		25.31			128.87		129.26	206.26		118.26	126.28		
					127.96		128.25						
					125.13		125.96						
					20.43								
acetic acid	CO	171.69	175.85	175.99	175.30	175.82	175.67	172.31	171.93	173.21	177.96	175.11	177.21
	CH_3	20.13	20.91	20.81	20.27	20.37	20.40	20.51	20.95	20.73	20.91	20.56	21.03
acetone	CO	204.19	206.78	207.07	204.00	204.43	204.83	205.87	206.31	207.43	32.35	209.67	215.94
	CH_3	30.17	31.00	30.92	30.03	30.14	30.12	30.60	30.56	30.91	214.98	30.67	30.89
acetonitrile	CN	116.79	116.92	116.43	115.76	116.02	115.93	117.60	117.91	118.26	118.95	118.06	119.68
	CH_3	0.45	2.03	1.89	0.03	0.20	0.63	1.12	1.03	1.79	1.00	0.85	1.47
benzene	CH	128.84	128.68	128.37	128.57	128.62	128.38	129.15	128.30	129.32	129.84	129.34	-
tert-butyl alcohol	$(CH_3)_3\boldsymbol{C}$	67.50	69.11	69.15	68.12	68.19	68.19	68.13	66.88	68.74	72.35	69.40	70.36
	$(\boldsymbol{C}H_3)_3C$	30.57	31.46	31.25	30.49	30.47	31.13	30.72	30.38	30.68	31.07	30.91	30.29
carbon dioxide	CO_2	125.69	125.26	124.99	124.86	124.76	126.08	125.81	124.21	125.89	126.92	126.31	-
carbon disulfide	CS_2	193.37	192.95	192.83	192.71	192.69	192.49	193.58	192.63	193.60	196.26	193.82	197.25
carbon tetrachloride	CCl_4	96.89	96.52	96.34	96.57	96.44	96.38	96.65	95.44	96.68	97.74	97.21	96.73
chloroform	CH	79.24	77.99	77.36	77.89	77.79	77.67	79.19	79.16	79.17	78.83	79.44	-
18-crown-6	CH_2	71.34	70.47	70.55	70.86	70.59	70.55	71.25	69.85	71.22	70.80	71.47	70.14
cyclohexane	CH_2	27.58	27.38	26.94	27.31	27.23	26.99	27.51	26.33	27.63	28.34	27.96	-
1,2-dichloroethane	CH_2	44.64	44.35	43.50	43.40	43.59	43.60	45.25	45.02	45.54	45.28	45.11	-
dichloromethane	CH_2	54.67	54.24	53.52	53.47	53.46	53.54	54.95	54.84	55.32	54.46	54.78	-
diethyl ether	CH_3	15.49	15.44	15.20	15.47	15.46	15.35	15.78	15.12	15.63	15.33	15.46	14.77
	CH_2	66.14	64.67	65.91	65.94	65.94	65.79	66.12	62.05	66.32	67.55	66.88	66.42
diglyme	CH_3	58.72	58.95	59.01	58.62	58.66	58.42	58.77	57.98	58.90	59.40	59.06	58.67
	CH_2	71.17	70.70	70.51	70.92	70.87	70.56	71.03	69.54	70.99	73.05	71.33	70.05
	CH_2	72.72	72.25	71.90	72.39	72.35	72.07	72.63	71.25	72.63	71.33	72.92	71.63
1,2-dimethoxyethane	CH_3	58.72	59.02	59.08	58.63	58.68	58.31	58.45	58.03	58.89	59.52	59.06	58.67
	CH_2	72.58	72.24	71.84	72.25	72.21	71.81	72.47	71.17	72.47	72.87	72.72	71.49
dimethylformamide	CH	161.96	162.57	162.62	161.93	162.13	162.01	162.79	162.29	163.31	166.01	164.73	165.53
	CH_3	35.65	36.56	36.50	35.22	35.25	35.45	36.15	35.73	36.57	37.76	36.89	37.54
	CH_3	30.70	31.39	31.45	30.64	30.72	30.71	31.03	30.73	31.32	30.96	31.61	32.03
1,4-dioxane	CH_2	67.65	67.47	67.14	67.17	67.16	66.95	67.60	66.36	67.72	68.52	68.11	67.19
ethane	CH_3	6.79	6.91	6.89	6.94	6.96	6.91	6.88	6.61	6.99	7.01	6.98	-
ethanol	CH_3	18.90	18.69	18.41	18.78	18.72	18.55	18.89	18.51	18.80	18.11	18.40	17.47
	CH_2	57.60	58.57	58.28	57.81	57.86	57.63	57.72	56.07	57.96	59.68	58.26	58.05
ethyl acetate	$\boldsymbol{C}H_3CO$	20.45	21.15	21.04	20.46	20.56	20.50	20.83	20.68	21.16	21.18	20.88	21.15
	CO	170.32	171.24	171.36	170.02	170.44	170.20	170.96	170.31	171.68	175.55	172.89	175.26
	CH_2	60.30	60.63	60.49	60.08	60.21	60.06	60.56	59.74	60.98	62.70	61.50	62.32
	CH_3	14.37	14.37	14.19	14.23	14.19	14.07	14.50	14.40	14.54	14.36	14.49	13.92
ethylene	CH_2	123.09	123.20	123.13	122.92	122.96	122.95	123.47	123.52	123.69	124.08	123.46	-
ethylene glycol	CH_2	64.35	64.08	63.79	64.29	64.34	64.03	64.26	62.76	64.22	64.87	64.30	63.17
H grease	CH_2	30.45	30.14	29.71	30.31	30.22	30.11	-	-	-	-	-	-
hexamethylbenzene	C	131.88	132.09	132.21	131.72	131.79	131.54	132.22	131.10	132.61	134.04	132.53	-
	CH_3	16.71	16.93	16.98	16.84	16.95	16.68	16.86	16.60	16.94	17.04	16.90	-
hexamethyldisiloxane	CH_3	1.83	1.96	1.97	1.99	2.05	1.92	2.01	1.96	2.07	2.09	1.99	2.31
n-hexane	CH_3	14.22	14.28	14.14	14.34	14.32	14.18	14.34	13.88	14.43	14.63	14.45	-
	CH_2(2,5)	23.33	23.07	22.70	23.12	23.04	22.86	23.28	22.05	23.40	24.06	23.68	-
	CH_2(3,4)	32.34	32.01	31.64	32.06	31.96	31.77	32.30	30.95	32.36	33.17	32.73	-
HMPA[b]	CH_3	36.89	36.99	36.87	36.80	36.88	36.64	37.04	36.42	37.10	37.21	37.00	36.46
imidazole	CH(2)	135.72	135.76	135.38	135.57	135.76	135.50	135.89	135.15	136.33	136.58	136.31	136.65
	CH(4,5)	122.20	122.16	122.00	122.13	122.16	121.96	122.31	121.55	122.78	122.93	122.60	122.43
methane	CH_4	–4.90	–4.33	–4.63	–4.34	–4.29	–4.33	–5.33	–4.01	–4.61	–5.88	–4.90	-
methanol	CH_3	49.64	50.45	50.41	49.90	49.97	49.66	49.77	48.59	49.90	50.67	49.86	49.50[c]
nitromethane	CH_3	62.49	63.03	62.50	61.14	61.16	61.68	63.21	63.28	63.66	63.17	63.08	63.22
n-pentane	CH_3	14.18	14.24	14.08	14.27	14.25	14.10	14.29	13.28	14.37	14.54	14.39	-
	CH_2(2,4)	23.00	22.77	22.38	22.79	22.72	22.54	22.98	21.70	23.08	23.75	23.38	-
	CH_2(3)	34.87	34.57	34.16	34.54	34.45	34.26	34.83	33.48	34.89	35.76	35.30	-
propane	CH_3	16.60	16.63	16.63	16.65	16.66	16.56	16.68	16.34	16.73	16.93	16.80	-
	CH_2	16.82	16.63	16.37	16.63	16.60	16.48	16.78	15.67	16.91	17.46	17.19	-
2-propanol	CH_3	25.70	25.43	25.14	25.24	25.18	25.14	25.67	25.43	25.55	25.21	25.27	24.38
	CH	66.14	64.67	64.50	64.12	64.23	64.18	63.85	64.92	64.30	66.69	64.71	64.88
propylene	CH_3	19.27	19.47	19.50	19.32	19.38	19.32	19.42	19.20	19.48	19.63	19.50	-
	CH_2	115.74	115.70	115.74	115.89	115.92	115.86	116.03	116.07	116.12	116.38	116.04	-
	CH	134.02	134.21	133.91	133.61	133.69	133.57	134.34	133.55	134.78	136.00	134.61	-
pyridine	CH(2,6)	150.57	150.27	149.90	150.25	150.27	149.93	150.67	149.58	150.76	149.76	150.07	149.18
	CH(3,5)	124.08	124.06	123.75	123.46	123.58	123.49	124.57	123.84	127.76	126.27	125.53	125.12
	CH(4)	135.99	136.16	135.96	135.17	135.28	135.32	136.56	136.05	136.89	139.62	138.35	138.27
pyrrole	CH(2,5)	118.03	117.93	117.77	117.61	117.78	117.65	117.98	117.32	118.47	119.61	118.28	119.06
	CH(3,4)	107.74	108.02	107.98	108.15	108.21	108.03	108.04	107.07	108.31	108.85	108.11	107.83
pyrrolidine[d]	CH(2,5)	45.82	47.02	46.93	47.12	46.86	46.75	-	46.51	47.57	47.43	47.23	46.83
	CH(3,4)	26.17	25.83	25.56	25.75	25.65	25.59	-	25.26	26.34	25.73	26.29	25.86
silicone grease	CH_3	1.20	1.22	1.19	1.37	1.38	1.09	1.40	-	-	2.87	2.10	-
tetrahydrofuran	CH_2(2,5)	68.03	68.16	67.97	67.75	67.80	67.64	68.07	67.03	68.33	69.53	68.83	68.68
	CH_2(3,4)	26.19	25.98	25.62	25.79	25.72	25.68	26.15	25.14	26.27	26.69	26.48	25.67
toluene	CH_3	21.29	21.53	21.46	21.37	21.10	21.23	21.46	20.99	21.50	21.62	21.50	-
	C(1)	138.24	138.36	137.89	137.84	137.91	137.65	138.48	137.35	138.90	139.92	138.85	-
	CH(2,6)	129.47	129.35	129.07	129.33	129.33	129.12	129.76	128.88	129.94	130.58	129.91	-
	CH(3,5)	128.71	128.54	128.26	128.51	128.56	128.31	129.03	128.18	129.23	129.79	129.20	-
	CH(4)	125.84	125.62	125.33	125.66	125.68	125.43	126.12	125.29	126.28	126.82	126.29	-
triethylamine	CH_3	12.51	12.12	11.61	12.39	12.35	11.87	12.49	11.74	12.38	9.51	11.09	9.07
	CH_2	47.18	46.75	46.25	46.82	46.77	46.36	47.07	45.74	47.10	48.45	46.96	47.19

a) Except for the compounds in solutions 8–10, as well as the gas samples, hexamethylbenzene, and the corrected values mentioned in the Supporting Information, all data for the solvents $CDCl_3$, C_6D_6, $(CD_3)_2CO$, $(CD_3)_2SO$, CD_3CN, CD_3OD, and D_2O were previously reported[1]. b) Phosphorus coupling was observed ($^2J_{PC}$ = 3 Hz). c) Internal reference; see text. d) Pyrrolidine was observed to react with $(CD_3)_2CO$.

Experimental Section

All deuterated solvents were obtained commercially through Cambridge Isotope Laboratories, Inc. NMR spectra were recorded at 298 K using 300, 500, or 600 MHz spectrometers (^{13}C frequencies of 75.5, 126, or 151 MHz, respectively). Adopting the previously reported strategy,[1] standard solutions of mixtures of specific impurities were used to reduce the number of necessary individual NMR experiments. The combinations of organic compounds were chosen in a way in which intermolecular interactions and resonance convolution would be minimized. Unless otherwise stated, the standard solutions were prepared with qualitatively equal molar amounts of the following compounds: solution 1 – acetone, dimethylformamide, ethanol, toluene; solution 2 – benzene, dimethylsulfoxide, ethyl acetate, methanol; solution 3 – acetic acid, chloroform, diethyl ether, 2-propanol, tetrahydrofuran; solution 4 – acetonitrile, dichloromethane, 1,4-dioxane, *n*-hexane, hexamethylphosphoramide (HMPA); solution 5 – 1,2-dichloroethane, *n*-pentane, pyridine, hexamethylbenzene; solution 6 – *tert*-butyl alcohol, 2,6-di-*tert*-butyl-4-methylphenol (BHT), cyclohexane, 1,2-dimethoxyethane, nitromethane, poly(dimethylsiloxane) (silicone grease), triethylamine; solution 7 – diglyme, dimethylacetamide, ethylene glycol, ethyl methyl ketone; solution 8 – allyl acetate, 2,6-di-*tert*-butyl-4-methoxyphenol (BHA), and long-chain, linear aliphatic hydrocarbons from pump oil (VWR brand vacuum pump oil #19); solution 9 – benzaldehyde, carbon disulfide, carbon tetrachloride, cyclohexanone, dimethyl malonate, furan, Apiezon H grease (H grease); solution 10 – 18-crown-6, diallyl carbonate, dimethyl carbonate, hexamethyldisoloxane, imidazole, pyrrole, pyrrolidine. The components of solution 10 were stable together in dilute solution but unstable when neat

mixtures were prepared. In general it was observed that the nitrogen containing compounds and possibly 18-crown-6 either catalyzed the hydrolysis of the carbonates, reacted directly with them, or both. Therefore, for the purpose of storage, the solution was partitioned into two sub-solutions: 10A – 18-crown-6, imidazole, pyrrole, and pyrrolidine; 10B – diallyl carbonate, dimethyl carbonate, and hexamethyldisiloxane. These sub-solutions were stable for long periods as neat mixtures and were combined to form solution 10 by adding equal portions to an NMR tube containing the desired deuterated solvent. In the case of TFE-d_3, nitromethane was omitted from standard 6 and run separately since the protons of CH_3NO_2 exchange with deuterium from TFE-d_3 in the presence of triethylamine. In the case of $(CD_3)_2CO$, pyrrolidine was omitted from solution 10 since the two compounds were observed to react with each other. The gases used in this study included hydrogen, methane, ethane, propane, ethylene, propylene, and carbon dioxide.

Before examining the various standard contaminant solutions by ^{1}H NMR spectroscopy, solvent signals from residual proteo impurity and chemical shifts for H_2O for each NMR solvent were referenced against tetramethylsilane (TMS, δ = 0 ppm) and reported. Note that the chemical shift of H_2O can shift widely based on a number of factors such as temperature and concentration.[1] Before collecting ^{13}C NMR spectral data, solvent signals were recorded with reference to the signal of a TMS internal standard. For D_2O, ^{1}H NMR spectra were referenced to the methyl signal (δ = 0 ppm) of sodium-3-(trimethylsilyl) propanesulfonate,[2] and ^{13}C NMR spectra were referenced to the signal for the methyl group of methanol (one drop, added as an internal standard) which was set to 49.50 ppm.[1]

In a typical experiment for collecting ^{1}H NMR spectral data, a 3 μL sample of a standard contaminant solution was added to a NMR tube containing approximately 0.4 mL of a deuterated solvent. For ^{13}C NMR spectral data collection, an approximately 50 μL sample of the standard contaminant solution was added. When there was any uncertainty on the assignment of a resonance, the solution was spiked with an additional 1–2 μL of the impurity in question to accurately identify its chemical shift. In cases where the chemical shifts of resonances were highly dependent on the concentration of the impurities present, ambiguous resonances were instead resolved via gradient-selected heteronuclear single-quantum coherence (gs-HSQC) and gradient-selected heteronuclear multiple-quantum coherence (gs-HMQC) NMR spectroscopies. For the experiments involving gases, a J. Young NMR tube containing approximately 0.4 mL of NMR solvent was first degassed with three freeze-pump-thaw cycles. Using a vacuum line equipped with a gas manifold, 1 atm of the desired gas was added to the tube. Each gas was run separately, degassing between each set of gas sample.

References

1. Gottlieb, H. E.; Kotlyar, V.; Nudelman, A. *J. Org. Chem.* **1997**, *62*, 7512.
2. Harris, R. K.; Becker, E. D.; De Menezes, S. M. C.; Granger, P.; Hoffman, R. E.; Zilm, K. W. *Pure Appl. Chem.* **2008**, *80*, 59.

Appendix D

Crystallographic Tables

Appendix D

Special Refinement Details for All Structures

Crystals were mounted on a glass fiber using Paratone oil then placed on the diffractometer under a nitrogen stream at 100K. Refinement of F^2 against ALL reflections. The weighted R-factor (*w*R) and goodness of fit (S) are based on F^2, conventional R-factors (R) are based on F, with F set to zero for negative F^2. The threshold expression of $F^2 > 2\sigma(F^2)$ is used only for calculating R-factors(gt) etc. and is not relevant to the choice of reflections for refinement. R-factors based on F^2 are statistically about twice as large as those based on F, and R-factors based on ALL data will be even larger.

All esds (except the esd in the dihedral angle between two l.s. planes) are estimated using the full covariance matrix. The cell esds are taken into account individually in the estimation of esds in distances, angles and torsion angles; correlations between esds in cell parameters are only used when they are defined by crystal symmetry. An approximate (isotropic) treatment of cell esds is used for estimating esds involving l.s. planes.

Additional details are provided at the end of the crystal data and structure refinement tables for each structure.

Chapter 2 Crystallographic Tables

[PN]Cu(PPh$_3$)$_2$ (2, ajmm03).

Table 1. Crystal data and structure refinement for ajmm03.

Empirical formula	C54 H53 Cu N P3	
Formula weight	872.42	
Temperature	100(2) K	
Wavelength	0.71073 α	
Crystal system	Monoclinic	
Space group	P2(1)/c	
Unit cell dimensions	a = 10.764(2) Å	a= 90°.
	b = 18.894(4) Å	b= 98.135(13)°.
	c = 22.199(4) Å	g = 90°.
Volume	4469.0(14) Å^3	
Z	4	
Density (calculated)	1.297 Mg/m^3	
Absorption coefficient	0.634 mm^{-1}	
Crystal size	0.407 x 0.241 x 0.222 mm^3	
Theta range for data collection	1.85 to 36.01°.	
Index ranges	-16<=h<=17, -30<=k<=24, -36<=l<=32	
Completeness to theta = 36.01°	86.2 %	
Absorption correction	None	
Refinement method	Full-matrix least-squares on F^2	
Data / restraints / parameters	18249 / 0 / 536	
Goodness-of-fit on F^2	1.309	
Final R indices [I>2sigma(I)]	R1 = 0.0469, wR2 = 0.0704	
R indices (all data)	R1 = 0.0878, wR2 = 0.0757	

Table 2. Atomic coordinates (x 10^4) and equivalent isotropic displacement parameters (Å^{2}x 10^3) for ajmm03. U(eq) is defined as one third of the trace of the orthogonalized U^{ij} tensor.

	x	y	z	U(eq)
Cu(1)	6584(1)	2629(1)	5930(1)	12(1)
P(2)	7325(1)	1788(1)	6662(1)	13(1)
P(1)	8081(1)	3309(1)	5545(1)	13(1)
P(3)	4995(1)	2201(1)	5202(1)	13(1)
C(22)	10822(2)	2672(1)	7885(1)	23(1)
C(32)	6515(2)	1691(1)	7830(1)	21(1)
N(1)	6311(1)	3545(1)	6417(1)	13(1)
C(1)	9725(1)	3082(1)	5460(1)	16(1)
C(44)	3364(2)	2993(1)	4302(1)	20(1)
C(21)	9718(2)	3059(1)	7771(1)	20(1)
C(19)	8725(1)	2100(1)	7158(1)	15(1)
C(3)	10384(1)	2762(1)	6053(1)	20(1)
C(39)	7096(2)	1702(1)	3858(1)	25(1)
C(7)	7279(1)	4029(1)	6502(1)	13(1)
C(18)	4542(1)	3123(1)	6884(1)	15(1)
C(45)	2517(2)	3539(1)	4137(1)	22(1)

C(50)	4423(2)	778(1)	5418(1)	21(1)
C(31)	6297(1)	1516(1)	7214(1)	14(1)
C(13)	5201(1)	3687(1)	6657(1)	13(1)
C(48)	3420(1)	3325(1)	5347(1)	16(1)
C(14)	4620(1)	4355(1)	6635(1)	17(1)
C(37)	5473(2)	1836(1)	4505(1)	16(1)
C(43)	3830(1)	2875(1)	4913(1)	15(1)
C(25)	7828(1)	937(1)	6381(1)	16(1)
C(30)	7839(2)	306(1)	6709(1)	23(1)
C(10)	9445(2)	4918(1)	6722(1)	20(1)
C(2)	9830(2)	2595(1)	4918(1)	20(1)
C(6)	6317(2)	4221(1)	4913(1)	22(1)
C(26)	8252(2)	928(1)	5817(1)	20(1)
C(38)	6706(2)	1929(1)	4398(1)	18(1)
C(17)	3366(2)	3223(1)	7061(1)	20(1)
C(15)	3453(2)	4452(1)	6820(1)	20(1)
C(46)	2133(2)	3981(1)	4570(1)	19(1)
C(27)	8694(2)	308(1)	5588(1)	28(1)
C(51)	3728(2)	233(1)	5632(1)	27(1)
C(47)	2583(2)	3870(1)	5177(1)	19(1)
C(8)	8264(1)	3986(1)	6133(1)	14(1)
C(16)	2805(2)	3884(1)	7032(1)	22(1)
C(33)	5640(2)	1511(1)	8212(1)	25(1)
C(12)	7430(1)	4543(1)	6975(1)	16(1)
C(34)	4563(2)	1145(1)	7988(1)	22(1)
C(9)	9316(2)	4430(1)	6254(1)	17(1)
C(20)	8684(2)	2779(1)	7408(1)	16(1)
C(41)	5019(2)	1267(1)	3522(1)	28(1)
C(5)	8478(2)	4286(1)	4596(1)	22(1)
C(53)	2207(2)	1068(1)	5866(1)	31(1)
C(54)	2892(2)	1612(1)	5651(1)	26(1)
C(24)	9837(2)	1712(1)	7279(1)	18(1)
C(29)	8269(2)	-316(1)	6473(1)	31(1)
C(49)	4011(1)	1477(1)	5425(1)	15(1)
C(42)	4635(2)	1487(1)	4061(1)	22(1)
C(35)	4342(2)	968(1)	7379(1)	24(1)
C(11)	8483(2)	4967(1)	7082(1)	19(1)
C(36)	5198(2)	1155(1)	6995(1)	22(1)
C(23)	10882(2)	2001(1)	7635(1)	23(1)
C(4)	7505(2)	3803(1)	4832(1)	17(1)
C(40)	6245(2)	1381(1)	3418(1)	28(1)
C(28)	8695(2)	-315(1)	5916(1)	31(1)
C(52)	2625(2)	378(1)	5858(1)	26(1)

[PN]Cu(PMe$_3$)$_2$ (3, ajmm08).

Table 1. Crystal data and structure refinement for ajmm08.

Empirical formula	$C_{24}H_{41}CuNP_3$	
Formula weight	500.03	
Temperature	100(2) K	
Wavelength	0.71073 α	
Crystal system	Orthorhombic	
Space group	P2(1)2(1)2(1)	
Unit cell dimensions	a = 9.9195(4) Å	a= 90°.
	b = 16.3588(7) Å	b= 90°.
	c = 16.5646(7) A	g = 90°.
Volume	2687.96(19) Å^3	
Z	4	
Density (calculated)	1.236 Mg/m^3	
Absorption coefficient	1.002 mm^{-1}	
Crystal size	0.444 x 0.148 x 0.130 mm^3	
Theta range for data collection	1.75 to 38.21°.	
Index ranges	-14<=h<=17, -27<=k<=27, -20<=l<=28	
Completeness to theta = 38.21°	91.1 %	
Absorption correction	None	
Refinement method	Full-matrix least-squares on F^2	
Data / restraints / parameters	12091 / 0 / 272	
Goodness-of-fit on F^2	1.070	
Final R indices [I>2sigma(I)]	R1 = 0.0424, wR2 = 0.0615	
R indices (all data)	R1 = 0.0734, wR2 = 0.0660	
Absolute structure parameter	-0.025(7)	

Table 2. Atomic coordinates (x 10^4) and equivalent isotropic displacement parameters (Å^{2}x 10^3) for ajmm08. U(eq) is defined as one third of the trace of the orthogonalized U^{ij} tensor.

	x	y	z	U(eq)
C(1)	5897(2)	5983(1)	8325(1)	14(1)
C(2)	5086(2)	6749(1)	8545(1)	20(1)
C(3)	5428(2)	5648(1)	7508(1)	21(1)
C(4)	6906(2)	4379(1)	8818(1)	15(1)
C(5)	8337(2)	4694(1)	8662(1)	20(1)
C(6)	6941(2)	3707(1)	9465(1)	20(1)
C(7)	5923(2)	5272(1)	10757(1)	12(1)
C(8)	6423(2)	5611(1)	10024(1)	12(1)
C(9)	7399(2)	6232(1)	10038(1)	14(1)
C(10)	7886(2)	6537(1)	10761(1)	17(1)
C(11)	7386(2)	6225(1)	11482(1)	17(1)
C(12)	6431(2)	5611(1)	11484(1)	15(1)
C(13)	4795(2)	4091(1)	11304(1)	14(1)
C(14)	5854(2)	3817(1)	11808(1)	15(1)
C(15)	5663(2)	3192(1)	12360(1)	18(1)
C(16)	4432(2)	2803(1)	12441(1)	21(1)
C(17)	3375(2)	3058(1)	11948(1)	20(1)
C(18)	3554(2)	3682(1)	11391(1)	18(1)
C(19)	3176(2)	6591(1)	10694(1)	24(1)

C(20)	1240(2)	6370(1)	9444(1)	23(1)
C(21)	1124(2)	5426(1)	10879(1)	29(1)
C(22)	2075(2)	4013(1)	8083(1)	29(1)
C(23)	1129(2)	3307(1)	9541(1)	22(1)
C(24)	3594(2)	2793(1)	8885(1)	32(1)
Cu	3714(1)	4775(1)	9688(1)	13(1)
N	4924(1)	4683(1)	10714(1)	13(1)
P(1)	5679(1)	5191(1)	9112(1)	11(1)
P(2)	2660(1)	3730(1)	9093(1)	17(1)
P(3)	2325(1)	5785(1)	10123(1)	16(1)

$[^{Me}PN]Cu(PPh_3)_2$ (7, ajmm15).

Table 1. Crystal data and structure refinement for ajmm15.

Empirical formula	$C_{59}H_{65}CuNOP_3$	
Formula weight	960.57	
Temperature	100(2) K	
Wavelength	0.71073 α	
Crystal system	Monoclinic	
Space group	P2(1)/n	
Unit cell dimensions	a = 11.099(4) Å	a= 90°.
	b = 21.513(7) Å	b= 103.72(3)°.
	c = 21.933(6) Å	g = 90°.
Volume	5088(3) $Å^3$	
Z	4	
Density (calculated)	1.254 Mg/m^3	
Absorption coefficient	0.565 mm^{-1}	
Crystal size	0.407 x 0.1184 x 0.111 mm^3	
Theta range for data collection	1.89 to 28.31∞.	
Index ranges	-14<=h<=13, -27<=k<=28, -25<=l<=28	
Completeness to theta = 28.31°	87.7 %	
Absorption correction	None	
Refinement method	Full-matrix least-squares on F^2	
Data / restraints / parameters	11108 / 0 / 593	
Goodness-of-fit on F^2	1.589	
Final R indices [I>2sigma(I)]	R1 = 0.0497, wR2 = 0.0938	
R indices (all data)	R1 = 0.0732, wR2 = 0.0974	

Special Refinement Details

A diethyl ether molecule of crystallization was present in the lattice.

Table 2. Atomic coordinates (x 10^4) and equivalent isotropic displacement parameters ($Å^2$x 10^3) for ajmm15. U(eq) is defined as one third of the trace of the orthogonalized U^{ij} tensor.

	x	y	z	U(eq)
Cu	2313(1)	4290(1)	2852(1)	13(1)
P(1)	1103(1)	4639(1)	3515(1)	12(1)
P(2)	1318(1)	3637(1)	2031(1)	13(1)
P(3)	3479(1)	5035(1)	2486(1)	12(1)
C(1)	2644(2)	5733(1)	2130(1)	14(1)
C(2)	1663(3)	5944(1)	2361(1)	22(1)
C(3)	475(3)	2850(1)	2836(1)	20(1)
C(4)	2117(2)	3027(1)	1681(1)	14(1)
C(5)	2378(2)	3600(1)	4039(1)	13(1)
C(6)	695(2)	3268(1)	4775(1)	19(1)
C(7)	6032(3)	6242(1)	3567(1)	25(1)
C(8)	5571(2)	4981(1)	3484(1)	16(1)
C(9)	-1114(2)	3127(1)	1924(1)	20(1)
N	3084(2)	3737(1)	3621(1)	12(1)
C(10)	-579(2)	4823(1)	3366(1)	17(1)
C(11)	1761(3)	2915(1)	4811(1)	18(1)
C(12)	6550(2)	5213(1)	3941(1)	19(1)

C(13)	-889(3)	5455(1)	3054(1)	24(1)
C(14)	4164(2)	4752(1)	1854(1)	13(1)
C(15)	4821(2)	3395(1)	3220(1)	16(1)
C(16)	5148(3)	4236(1)	901(1)	29(1)
C(17)	3294(2)	3137(1)	1589(1)	17(1)
C(18)	5058(2)	6015(1)	3101(1)	20(1)
C(19)	2377(3)	6620(1)	1437(1)	25(1)
C(20)	6402(2)	3413(1)	4394(1)	22(1)
C(21)	5155(2)	3542(1)	4330(1)	17(1)
C(22)	5854(3)	4261(1)	1510(1)	27(1)
C(23)	4809(2)	5379(1)	3058(1)	13(1)
C(24)	6773(2)	5842(1)	3989(1)	22(1)
C(25)	121(2)	3171(1)	2267(1)	16(1)
C(26)	-370(3)	2499(1)	3053(2)	27(1)
C(28)	5370(2)	4518(1)	1985(1)	21(1)
C(29)	-1599(3)	2461(1)	2711(2)	29(1)
C(30)	3950(3)	4463(1)	769(1)	24(1)
C(31)	1391(3)	6825(1)	1666(2)	31(1)
C(32)	1134(2)	5415(1)	4576(1)	19(1)
C(33)	-1951(3)	2775(1)	2148(1)	24(1)
C(34)	4327(2)	3544(1)	3735(1)	13(1)
C(35)	6874(3)	3276(1)	3880(2)	25(1)
C(36)	2184(3)	2001(1)	1234(1)	25(1)
C(37)	486(2)	3789(1)	4389(1)	16(1)
C(38)	-1343(2)	4309(1)	2971(1)	22(1)
C(39)	1563(3)	2447(1)	1503(1)	20(1)
C(40)	1821(2)	5277(1)	4063(1)	16(1)
C(41)	2996(2)	6081(1)	1662(1)	19(1)
C(42)	1297(2)	3962(1)	4028(1)	13(1)
C(43)	1037(3)	6491(1)	2136(2)	31(1)
O	3095(2)	3882(1)	9373(1)	51(1)
C(45)	10(3)	3798(1)	754(1)	25(1)
C(46)	2585(2)	3082(1)	4453(1)	14(1)
C(47)	406(2)	4056(1)	1345(1)	17(1)
C(48)	3187(2)	5132(1)	4351(1)	19(1)
C(49)	28(3)	4657(1)	1444(1)	24(1)
C(50)	3461(2)	4712(1)	1242(1)	18(1)
C(51)	3348(3)	2119(1)	1145(1)	24(1)
C(52)	-717(3)	4997(2)	969(2)	37(1)
C(53)	3904(3)	2689(1)	1318(1)	21(1)
C(54)	6064(2)	3269(1)	3291(1)	21(1)
C(59)	2015(3)	2346(1)	5235(2)	28(1)
C(55)	3907(3)	3999(2)	8960(2)	44(1)
C(57)	1749(4)	3247(2)	9743(2)	56(1)
C(58)	2620(4)	3278(2)	9330(2)	60(1)
C(56)	3193(3)	4130(2)	8313(2)	50(1)
C(60)	-1103(3)	4732(2)	384(2)	43(1)
C(61)	-740(3)	4141(2)	271(2)	40(1)

$[^{CF3}PN]Cu(PPh_3)_2$ (8, ajmm12).

Table 1. Crystal data and structure refinement for ajmm12.

Empirical formula	$C_{59}H_{62}CuF_3NOP_3$	
Formula weight	1014.55	
Temperature	100(2) K	
Wavelength	0.71073 α	
Crystal system	Monoclinic	
Space group	P2(1)/n	
Unit cell dimensions	a = 11.101(16) Å	a= 90°.
	b = 21.70(5) Å	b= 103.11(7)°.
	c = 22.30(4) Å	g = 90°.
Volume	5231(17) Å^3	
Z	4	
Density (calculated)	1.288 Mg/m^3	
Absorption coefficient	0.561 mm^{-1}	
Crystal size	0.296 x 0.0518 x 0.037 mm^3	
Theta range for data collection	1.88 to 28.30°.	
Index ranges	-14<=h<=14, -28<=k<=28, -29<=l<=28	
Completeness to theta = 28.30°	91.5 %	
Absorption correction	None	
Refinement method	Full-matrix least-squares on F^2	
Data / restraints / parameters	11900 / 0 / 619	
Goodness-of-fit on F^2	1.320	
Final R indices [I>2sigma(I)]	R1 = 0.0617, wR2 = 0.1007	
R indices (all data)	R1 = 0.1176, wR2 = 0.1078	

Special Refinement Details

A highly disordered molecule of diethyl ether was cocrystallized with **8**.

Table 2. Atomic coordinates (x 10^4) and equivalent isotropic displacement parameters (Å^{2}x 10^3) for ajmm12. U(eq) is defined as one third of the trace of the orthogonalized U^{ij} tensor.

	x	y	z	U(eq)
Cu(1)	7353(1)	4340(1)	2853(1)	14(1)
P(2)	8523(1)	5077(1)	2481(1)	13(1)
P(3)	6334(1)	3682(1)	2053(1)	15(1)
P(1)	6114(1)	4696(1)	3505(1)	13(1)
N(1)	8107(3)	3795(1)	3621(1)	15(1)
C(50)	7696(3)	5779(2)	2137(2)	17(1)
F(3)	6316(3)	1918(1)	4906(1)	63(1)
F(2)	8102(2)	2258(1)	5355(1)	58(1)
C(14)	9339(3)	3583(1)	3729(2)	12(1)
F(1)	6532(2)	2490(1)	5704(1)	46(1)
C(15)	10165(3)	3574(2)	4316(2)	18(1)
C(55)	6776(3)	6014(2)	2406(2)	22(1)
C(33)	4966(3)	3874(2)	809(2)	24(1)
C(10)	6715(3)	2984(2)	4776(2)	16(1)
C(13)	6916(4)	2422(2)	5175(2)	26(1)
C(31)	8310(3)	3177(2)	1607(2)	17(1)
C(21)	5525(3)	2879(2)	2845(2)	20(1)

C(38)	9218(3)	4791(2)	1856(2)	16(1)
C(26)	7114(3)	3076(2)	1688(2)	15(1)
C(20)	5155(3)	3207(2)	2293(2)	17(1)
C(19)	9832(3)	3425(2)	3222(2)	17(1)
C(3)	3686(3)	4370(2)	2957(2)	25(1)
C(22)	4703(4)	2508(2)	3064(2)	28(1)
C(11)	7569(3)	3139(2)	4436(1)	14(1)
C(1)	4439(3)	4879(2)	3349(2)	19(1)
C(51)	7983(4)	6099(2)	1648(2)	26(1)
C(52)	7346(4)	6636(2)	1429(2)	34(1)
C(7)	6287(3)	4015(2)	4004(1)	14(1)
C(16)	11403(3)	3421(2)	4378(2)	22(1)
C(36)	4408(4)	5093(2)	1047(2)	30(1)
C(8)	5430(3)	3838(2)	4351(2)	16(1)
C(23)	3474(4)	2468(2)	2736(2)	28(1)
C(32)	5422(3)	4122(2)	1398(2)	17(1)
C(24)	3098(3)	2789(2)	2188(2)	23(1)
C(34)	4227(4)	4237(2)	347(2)	33(1)
C(25)	3926(3)	3161(2)	1965(2)	18(1)
C(37)	5139(3)	4739(2)	1505(2)	23(1)
C(45)	10582(3)	5015(2)	3472(2)	18(1)
C(28)	7155(4)	2066(2)	1215(2)	27(1)
C(44)	9846(3)	5410(2)	3042(2)	14(1)
C(41)	10206(4)	4263(2)	914(2)	29(1)
C(54)	6154(4)	6559(2)	2187(2)	36(1)
C(42)	10912(3)	4307(2)	1505(2)	30(1)
C(39)	8491(3)	4734(2)	1252(2)	20(1)
C(49)	10116(3)	6044(2)	3084(2)	22(1)
C(40)	8988(3)	4479(2)	785(2)	26(1)
C(43)	10422(3)	4567(2)	1976(2)	24(1)
C(12)	7377(3)	3657(2)	4022(1)	13(1)
C(18)	11066(3)	3279(2)	3289(2)	21(1)
C(30)	8919(3)	2728(2)	1336(2)	23(1)
C(2)	4142(3)	5510(2)	3042(2)	23(1)
C(9)	5626(3)	3323(2)	4734(2)	19(1)
C(29)	8348(4)	2178(2)	1138(2)	26(1)
C(27)	6543(3)	2514(2)	1491(2)	22(1)
C(53)	6437(4)	6868(2)	1702(2)	38(1)
C(35)	3955(4)	4840(2)	469(2)	34(1)
C(17)	11871(3)	3281(2)	3866(2)	25(1)
C(5)	6124(3)	5444(2)	4572(2)	19(1)
C(4)	6819(3)	5320(2)	4059(2)	16(1)
C(6)	8191(3)	5171(2)	4345(2)	21(1)
C(47)	11800(4)	5870(2)	3968(2)	26(1)
C(48)	11083(3)	6273(2)	3541(2)	26(1)
C(46)	11558(3)	5242(2)	3930(2)	20(1)
O(1)	7864(4)	3820(2)	9440(2)	87(1)
C(56)	6505(9)	3217(3)	9751(3)	160(5)
C(58)	8785(6)	3964(3)	8951(3)	80(2)
C(57)	7548(8)	3295(3)	9352(5)	228(8)
C(59)	8178(6)	4097(3)	8370(4)	110(3)

[PN]Ag(PPh$_3$)$_2$ (9, ajmm05).

Table 1. Crystal data and structure refinement for ajmm05.

Empirical formula	C54 H53 Ag N P3	
Formula weight	916.75	
Temperature	100(2) K	
Wavelength	0.71073 α	
Crystal system	Monoclinic	
Space group	P2(1)/c	
Unit cell dimensions	a = 10.8189(5) Å	a= 90°.
	b = 19.1162(8) Å	b= 97.2540(10)°.
	c = 22.2135(9) Å	g = 90°.
Volume	4557.3(3) Å^3	
Z	4	
Density (calculated)	1.336 Mg/m^3	
Absorption coefficient	0.585 mm^{-1}	
Crystal size	0.370 x 0.222 x 0.185 mm^3	
Theta range for data collection	1.41 to 35.99°.	
Index ranges	-16<=h<=17, -31<=k<=31, -35<=l<=30	
Completeness to theta = 35.99°	90.7 %	
Absorption correction	None	
Refinement method	Full-matrix least-squares on F^2	
Data / restraints / parameters	19574 / 0 / 536	
Goodness-of-fit on F^2	1.446	
Final R indices [I>2sigma(I)]	R1 = 0.0378, wR2 = 0.0629	
R indices (all data)	R1 = 0.0585, wR2 = 0.0662	

Table 2. Atomic coordinates (x 10^4) and equivalent isotropic displacement parameters (Å^{2}x 10^3) for ajmm05. U(eq) is defined as one third of the trace of the orthogonalized U^{ij} tensor.

	x	y	z	U(eq)
Ag(1)	1581(1)	7437(1)	858(1)	12(1)
C(1)	2604(1)	6150(1)	-209(1)	16(1)
C(2)	3553(1)	5639(1)	-417(1)	21(1)
C(3)	1368(1)	5784(1)	-141(1)	21(1)
C(4)	4775(1)	6879(1)	419(1)	15(1)
C(5)	5384(1)	7215(1)	1008(1)	21(1)
C(6)	4821(1)	7371(1)	-124(1)	20(1)
C(7)	2308(1)	5924(1)	1470(1)	13(1)
C(8)	3296(1)	5978(1)	1101(1)	13(1)
C(9)	4357(1)	5552(1)	1219(1)	16(1)
C(10)	4492(1)	5067(1)	1687(1)	19(1)
C(11)	3528(1)	5003(1)	2047(1)	18(1)
C(12)	2468(1)	5412(1)	1943(1)	15(1)
C(13)	224(1)	6250(1)	1628(1)	13(1)
C(14)	-354(1)	5587(1)	1616(1)	16(1)
C(15)	-1536(1)	5501(1)	1785(1)	21(1)
C(16)	-2206(1)	6071(1)	1969(1)	23(1)
C(17)	-1645(1)	6723(1)	1991(1)	20(1)
C(18)	-457(1)	6815(1)	1831(1)	16(1)
C(19)	3702(1)	7936(1)	2151(1)	14(1)
C(20)	3624(1)	7249(1)	2360(1)	16(1)

C(21)	4651(1)	6931(1)	2691(1)	19(1)
C(22)	5773(1)	7289(1)	2804(1)	21(1)
C(23)	5865(1)	7968(1)	2587(1)	21(1)
C(24)	4836(1)	8293(1)	2268(1)	18(1)
C(25)	1268(1)	8515(1)	2222(1)	14(1)
C(26)	1460(1)	8346(1)	2836(1)	20(1)
C(27)	553(2)	8494(1)	3210(1)	25(1)
C(28)	-546(1)	8822(1)	2977(1)	22(1)
C(29)	-745(2)	8995(1)	2365(1)	25(1)
C(30)	147(1)	8836(1)	1991(1)	22(1)
C(31)	2866(1)	9134(1)	1427(1)	16(1)
C(32)	2898(2)	9739(1)	1783(1)	24(1)
C(33)	3344(2)	10361(1)	1569(1)	32(1)
C(34)	3760(2)	10388(1)	1005(1)	33(1)
C(35)	3729(2)	9794(1)	648(1)	30(1)
C(36)	3268(1)	9170(1)	857(1)	22(1)
C(37)	-1124(1)	8581(1)	346(1)	14(1)
C(38)	-2251(1)	8431(1)	556(1)	24(1)
C(39)	-2932(2)	8951(1)	807(1)	30(1)
C(40)	-2492(2)	9630(1)	842(1)	26(1)
C(41)	-1381(2)	9788(1)	629(1)	24(1)
C(42)	-692(1)	9271(1)	387(1)	20(1)
C(43)	373(1)	8229(1)	-592(1)	16(1)
C(44)	1591(1)	8089(1)	-698(1)	19(1)
C(45)	2019(2)	8302(1)	-1235(1)	26(1)
C(46)	1227(2)	8651(1)	-1670(1)	29(1)
C(47)	16(2)	8808(1)	-1568(1)	28(1)
C(48)	-411(2)	8603(1)	-1030(1)	22(1)
C(49)	-1245(1)	7189(1)	-158(1)	13(1)
C(50)	-1474(1)	6694(1)	275(1)	17(1)
C(51)	-2254(1)	6128(1)	123(1)	20(1)
C(52)	-2819(1)	6050(1)	-470(1)	19(1)
C(53)	-2620(1)	6543(1)	-900(1)	22(1)
C(54)	-1831(1)	7113(1)	-750(1)	20(1)
N(1)	1333(1)	6388(1)	1397(1)	13(1)
P(1)	3152(1)	6636(1)	503(1)	12(1)
P(2)	-137(1)	7882(1)	102(1)	13(1)
P(3)	2339(1)	8287(1)	1680(1)	13(1)

$[PN]_2Zn$ (10, ajmm06).

Table 1. Crystal data and structure refinement for ajmm06.

Empirical formula	$C_{36}H_{46}N_2P_2Zn$	
Formula weight	634.06	
Temperature	100(2) K	
Wavelength	0.71073 α	
Crystal system	Monoclinic	
Space group	C2/c	
Unit cell dimensions	a = 21.074(14) Å	a= 90°.
	b = 8.729(6) Å	b= 110.905(14)°.
	c = 19.086(13) Å	g = 90°.
Volume	3280(4) $Å^3$	
Z	4	
Density (calculated)	1.284 Mg/m^3	
Absorption coefficient	0.873 mm^{-1}	
Crystal size	0.259 x 0.244 x 0.152 mm^3	
Theta range for data collection	2.07 to 38.26°.	
Index ranges	-27<=h<=36, -15<=k<=14, -31<=l<=30	
Completeness to theta = 38.26°	88.9 %	
Absorption correction	None	
Refinement method	Full-matrix least-squares on F^2	
Data / restraints / parameters	8084 / 0 / 190	
Goodness-of-fit on F^2	1.390	
Final R indices [I>2sigma(I)]	R1 = 0.0451, wR2 = 0.0713	
R indices (all data)	R1 = 0.0791, wR2 = 0.0752	

Table 2. Atomic coordinates (x 10^4) and equivalent isotropic displacement parameters ($Å^2$x 10^3) for ajmm06. U(eq) is defined as one third of the trace of the orthogonalized U^{ij} tensor.

	x	y	z	U(eq)
Zn	0	206(1)	2500	11(1)
P	968(1)	-1117(1)	2455(1)	12(1)
N	22(1)	1322(1)	1613(1)	13(1)
C(8)	1072(1)	29(1)	1719(1)	13(1)
C(7)	566(1)	1162(1)	1377(1)	12(1)
C(5)	1706(1)	-1854(2)	3928(1)	21(1)
C(1)	770(1)	-3103(1)	2100(1)	16(1)
C(18)	-836(1)	3175(1)	1591(1)	16(1)
C(9)	1647(1)	-86(2)	1510(1)	16(1)
C(13)	-548(1)	2204(1)	1202(1)	13(1)
C(4)	1799(1)	-1180(1)	3232(1)	16(1)
C(10)	1738(1)	876(2)	980(1)	19(1)
C(17)	-1438(1)	3952(2)	1217(1)	19(1)
C(15)	-1486(1)	2822(2)	65(1)	20(1)
C(11)	1252(1)	1982(2)	650(1)	18(1)
C(6)	2119(1)	402(2)	3414(1)	22(1)
C(16)	-1764(1)	3791(2)	453(1)	20(1)
C(2)	146(1)	-3078(2)	1375(1)	23(1)
C(14)	-890(1)	2032(2)	428(1)	17(1)
C(12)	678(1)	2128(1)	838(1)	16(1)
C(3)	1353(1)	-3965(2)	1979(1)	23(1)

Chapter 3 Crystallographic Tables

[($Ph_2P(CH_2)_2B(C_8H_{14})_2Re(CO)_4$][$BF_4$] ([1-$E_2$][$BF_4$], ajmm22).

Table 1. Crystal data and structure refinement for AJMM22 (CCDC 677279).

Empirical formula	$[C_{48}H_{56}B_2O_4P_2Re]^+ BF_4^- \bullet 2(CH_2Cl_2)$	
Formula weight	1223.35	
Crystallization Solvent	Dichloromethane	
Crystal Habit	Plate	
Crystal size	0.36 x 0.34 x 0.01 mm^3	
Crystal color	Colorless	
Data Collection Temperature	100(2) K	
Unit cell dimensions	a = 13.5643(10) Å	a= 71.725(4)°
	b = 14.4026(10) Å	b= 70.883(4)°
	c = 14.6998(11) Å	g = 89.203(5)°
Volume	2563.9(3) $Å^3$	
Z	2	
Crystal system	Triclinic	
Space group	P-1	
Density (calculated)	1.585 Mg/m^3	
q range for data collection	1.77 to 41.25°	
Completeness to θ = 41.25°	89.6 %	
Index ranges	$-24 \le h \le 23$, $-25 \le k \le 26$, $-25 \le l \le 26$	
Absorption coefficient	2.699 mm^{-1}	
Absorption correction	Semi-empirical from equivalents	
Refinement method	Full matrix least-squares on F^2	
Data / restraints / parameters	30749 / 0 / 616	
Treatment of hydrogen atoms	Riding	
Goodness-of-fit on F^2	2.971	
Final R indices [I>2s(I), 18556 reflections]	R1 = 0.0515, *w*R2 = 0.0876	
R indices (all data)	R1 = 0.1091, *w*R2 = 0.0895	

Special Refinement Details

The asymmetric unit is composed of two half-molecules each sitting on inequivalent centers of symmetry with the net effect of one molecule per asymmetric unit..

Table 2. Atomic coordinates (x 10^4) and equivalent isotropic displacement parameters ($Å^2$x 10^3) for AJMM22 (CCDC 677279). U(eq) is defined a the trace of the orthogonalized U^{ij} tensor.

	x	y	z	U_{eq}
Re(1)	10000	10000	0	13(1)
P(1A)	9410(1)	8612(1)	-369(1)	16(1)
O(1A)	7658(2)	10358(2)	891(2)	29(1)
O(2A)	9660(2)	8687(2)	2246(2)	25(1)
B(1A)	6923(4)	6673(3)	2056(4)	35(1)
C(1A)	8513(3)	10252(2)	535(2)	19(1)
C(2A)	9815(3)	9148(2)	1425(2)	18(1)
C(3A)	9362(2)	9000(2)	-1651(2)	17(1)
C(4A)	8524(3)	9484(2)	-1838(3)	24(1)

C(5A)	8497(3)	9851(2)	-2819(3)	29(1)
C(6A)	9294(3)	9732(2)	-3615(3)	27(1)
C(7A)	10131(3)	9266(2)	-3446(3)	23(1)
C(8A)	10186(3)	8901(2)	-2472(2)	18(1)
C(9A)	10175(2)	7560(2)	-270(2)	16(1)
C(10A)	10087(2)	6887(2)	-755(2)	19(1)
C(11A)	10641(3)	6063(2)	-639(3)	24(1)
C(12A)	11252(3)	5889(2)	-25(3)	27(1)
C(13A)	11315(3)	6532(2)	486(3)	25(1)
C(14A)	10782(3)	7379(2)	344(3)	21(1)
C(15A)	8088(3)	8019(2)	378(3)	28(1)
C(16A)	7882(3)	7491(3)	1484(3)	36(1)
C(17A)	6697(3)	5862(3)	1625(3)	41(1)
C(18A)	5558(3)	5849(3)	1638(3)	52(1)
C(19A)	4721(3)	5798(3)	2679(3)	49(1)
C(20A)	5030(3)	6474(3)	3165(3)	39(1)
C(21A)	6174(3)	6495(2)	3140(3)	34(1)
C(22A)	6448(4)	5549(3)	3786(4)	50(1)
C(23A)	6399(3)	4678(3)	3455(3)	41(1)
C(24A)	6902(3)	4857(3)	2321(3)	45(1)
Re(2)	0	5000	5000	10(1)
P(1B)	455(1)	3608(1)	4386(1)	12(1)
O(1B)	2363(2)	5777(2)	4294(2)	24(1)
O(2B)	363(2)	3913(2)	7056(2)	25(1)
B(1B)	2833(3)	2080(2)	5251(3)	19(1)
C(1B)	1509(3)	5514(2)	4519(2)	16(1)
C(2B)	187(2)	4279(2)	6329(3)	17(1)
C(3B)	1444(2)	3820(2)	3132(2)	14(1)
C(4B)	1663(2)	3029(2)	2755(2)	19(1)
C(5B)	2445(3)	3140(2)	1848(3)	23(1)
C(6B)	3038(3)	4033(2)	1291(3)	24(1)
C(7B)	2827(2)	4823(2)	1642(2)	21(1)
C(8B)	2035(2)	4720(2)	2550(2)	17(1)
C(9B)	-677(2)	3011(2)	4307(2)	13(1)
C(10B)	-878(2)	3258(2)	3400(2)	17(1)
C(11B)	-1778(2)	2842(2)	3370(3)	21(1)
C(12B)	-2482(3)	2193(2)	4242(3)	22(1)
C(13B)	-2295(2)	1960(2)	5149(3)	21(1)
C(14B)	-1400(2)	2356(2)	5186(2)	17(1)
C(15B)	969(2)	2611(2)	5180(2)	16(1)
C(16B)	2057(2)	2905(2)	5154(2)	20(1)
C(17B)	2524(3)	970(2)	5480(3)	26(1)
C(18B)	3062(3)	279(2)	6164(3)	34(1)
C(19B)	3753(3)	829(2)	6492(3)	33(1)
C(20B)	4559(3)	1596(2)	5587(3)	32(1)
C(21B)	4036(3)	2327(2)	4915(3)	25(1)
C(22B)	4373(3)	2267(3)	3808(3)	38(1)
C(23B)	4064(3)	1234(3)	3820(3)	46(1)
C(24B)	2914(3)	903(3)	4380(3)	37(1)
B(1)	7655(3)	2185(3)	8024(3)	23(1)
F(1)	7060(2)	2850(2)	8432(2)	42(1)
F(2)	7838(2)	1458(1)	8807(2)	36(1)
F(3)	7110(2)	1765(1)	7578(2)	33(1)
F(4)	8595(2)	2676(2)	7315(2)	43(1)

C(31)	5116(4)	1279(5)	9345(4)	82(2)
Cl(1)	4201(1)	1321(1)	10528(1)	89(1)
Cl(2)	4463(1)	881(1)	8654(1)	71(1)
C(32)	6273(3)	2170(3)	1048(3)	46(1)
Cl(3)	6928(1)	2019(1)	1956(1)	43(1)
Cl(4)	5642(1)	3196(1)	921(1)	64(1)

$(Ph_2P(CH_2)_2B(C_8H_{14}))_2Re(CO)_3(CHO)$ (2-E$_2$, ajmm24).

Table 1. Crystal data and structure refinement for AJMM24 (CCDC 681294).

Empirical formula	$C_{96}H_{114}B_4O_8P_4Re_2 \bullet 2(CH_2Cl_2)$	
Formula weight	2105.24	
Crystallization Solvent	Dichloromethane/toluene	
Crystal Habit	Fragment	
Crystal size	0.20 x 0.20 x 0.14 mm^3	
Crystal color	Colorless	
Data Collection Temperature	100(2) K	
Unit cell dimensions	a = 11.2518(5) Å	a= 88.406(3)°
	b = 13.3609(6) Å	b= 74.156(3)°
	c = 16.3588(7) Å	g = 80.300(3)°
Volume	2331.60(18) Å^3	
Z	1	
Crystal system	Triclinic	
Space group	P-1	
Density (calculated)	1.499 Mg/m^3	
q range for data collection	1.91 to 54.57°	
Completeness to θ = 54.57°	94.9 %	
Index ranges	$-25 \le h \le 25$, $-26 \le k \le 30$, $-37 \le l \le 35$	
Absorption coefficient	2.832 mm^{-1}	
Absorption correction	None	
Refinement method	Full matrix least-squares on F^2	
Data / restraints / parameters	55878 / 0 / 541	
Treatment of hydrogen atoms	Riding	
Goodness-of-fit on F^2	1.248	
Final R indices [I>2s(I), 43261 reflections]	R1 = 0.0351, *w*R2 = 0.0668	
R indices (all data)	R1 = 0.0521, *w*R2 = 0.0681	

Table 2. Atomic coordinates (x 10^4) and equivalent isotropic displacement parameters (Å^{2}x 10^3) for AJMM24 (CCDC 681294). U(eq) is defined a the trace of the orthogonalized U^{ij} tensor.

	x	y	z	U_{eq}
Re(1)	6790(1)	2417(1)	3610(1)	8(1)
P(1)	7415(1)	2189(1)	2080(1)	10(1)
P(2)	6137(1)	2705(1)	5142(1)	9(1)
O(1)	4568(1)	1241(1)	3682(1)	25(1)
O(2)	8618(1)	425(1)	3732(1)	22(1)
O(3)	8738(1)	3848(1)	3524(1)	20(1)
O(4)	4334(1)	3805(1)	3688(1)	14(1)
B(1)	7675(2)	5155(1)	1063(1)	23(1)
B(2)	6634(1)	5262(1)	6530(1)	11(1)
C(1)	5373(1)	1664(1)	3670(1)	15(1)
C(2)	7950(1)	1163(1)	3691(1)	13(1)
C(3)	8046(1)	3298(1)	3544(1)	12(1)
C(4)	5498(1)	3744(1)	3535(1)	11(1)
C(5)	7114(1)	3317(1)	1454(1)	15(1)
C(6)	7749(1)	4188(1)	1630(1)	19(1)
C(7)	7326(2)	6265(1)	1415(1)	42(1)
C(8)	8218(3)	6959(2)	843(1)	54(1)

C(9)	9118(2)	6407(1)	50(1)	28(1)
C(10)	8483(2)	5860(2)	-445(1)	36(1)
C(11)	7673(2)	5112(1)	93(1)	31(1)
C(12)	6292(2)	5416(2)	118(1)	39(1)
C(13)	5725(2)	6461(2)	526(2)	43(1)
C(14)	5916(2)	6573(2)	1395(1)	44(1)
C(15)	6374(1)	3954(1)	5441(1)	12(1)
C(16)	6202(1)	4194(1)	6379(1)	12(1)
C(17)	6631(1)	5481(1)	7502(1)	14(1)
C(18)	7620(1)	4669(1)	7735(1)	16(1)
C(19)	8948(1)	4584(1)	7122(1)	18(1)
C(20)	8990(1)	4606(1)	6174(1)	17(1)
C(21)	8002(1)	5422(1)	5944(1)	13(1)
C(22)	8218(1)	6518(1)	6044(1)	17(1)
C(23)	7988(1)	6893(1)	6963(1)	20(1)
C(24)	6826(1)	6583(1)	7601(1)	17(1)
C(25)	6650(1)	1251(1)	1715(1)	15(1)
C(26)	6901(1)	245(1)	1968(1)	22(1)
C(27)	6322(2)	-499(1)	1744(1)	32(1)
C(28)	5475(2)	-249(2)	1260(1)	40(1)
C(29)	5217(2)	742(2)	1007(1)	34(1)
C(30)	5805(1)	1498(1)	1232(1)	23(1)
C(31)	9071(1)	1708(1)	1569(1)	11(1)
C(32)	10007(1)	1752(1)	1969(1)	14(1)
C(33)	11264(1)	1405(1)	1549(1)	17(1)
C(34)	11587(1)	1007(1)	728(1)	16(1)
C(35)	10666(1)	966(1)	324(1)	16(1)
C(36)	9413(1)	1316(1)	736(1)	13(1)
C(37)	4496(1)	2631(1)	5628(1)	12(1)
C(38)	4084(1)	1695(1)	5668(1)	20(1)
C(39)	2816(1)	1636(1)	5979(1)	27(1)
C(40)	1945(1)	2508(1)	6236(1)	26(1)
C(41)	2334(1)	3446(1)	6194(1)	21(1)
C(42)	3605(1)	3504(1)	5889(1)	16(1)
C(43)	7010(1)	1846(1)	5741(1)	13(1)
C(44)	6449(1)	1325(1)	6454(1)	23(1)
C(45)	7183(2)	662(2)	6869(1)	32(1)
C(46)	8484(1)	532(1)	6583(1)	28(1)
C(47)	9052(1)	1068(1)	5883(1)	22(1)
C(48)	8319(1)	1719(1)	5467(1)	17(1)
C(51)	1371(2)	7903(2)	1742(1)	38(1)
Cl(1)	8(1)	8813(1)	1843(1)	33(1)
Cl(2)	2624(1)	8196(1)	905(1)	48(1)

[Na][($Ph_2P(CH_2)_2B(C8H_{14})2Re(CO)_2(=C(O–)CH_2O–)$] ([Na][3-$E_2$], ajmm29).

Table 1. Crystal data and structure refinement for AJMM29 (CCDC 687691).

Empirical formula	$C_{48}H_{58}B_2O_4P_2Re \bullet Na3.52(C_4H_8O)0.48(C_4H_{10}O)$	
Formula weight	1281.12	
Crystallization Solvent	THF/diethylether	
Crystal Habit	Plate	
Crystal size	0.33 x 0.31 x 0.09 mm^3	
Crystal color	Pale yellow	
Data Collection Temperature	100(2) K	
Unit cell dimensions	a = 11.5211(5) Å	a= 81.125(2)°
	b = 12.3378(5) Å	b= 81.140(2)°
	c = 23.1407(8) Å	g = 67.210(2)°
Volume	2980.1(2) $Å^3$	
Z	2	
Crystal system	Triclinic	
Space group	P-1	
Density (calculated)	1.428 Mg/m^3	
q range for data collection	1.93 to 52.54°	
Completeness to θ = 52.54°	89.3 %	
Index ranges	$-23 \le h \le 24$, $-26 \le k \le 26$, $-48 \le l \le 49$	
Absorption coefficient	2.154 mm^{-1}	
Absorption correction	Semi-empirical from equivalents	
Refinement method	Full matrix least-squares on F^2	
Data / restraints / parameters	62112 / 15 / 833	
Treatment of hydrogen atoms	Riding	
Goodness-of-fit on F^2	1.696	
Final R indices [I>2s(I), 47581 reflections]	R1 = 0.0440, *w*R2 = 0.0574	
R indices (all data)	R1 = 0.0691, *w*R2 = 0.0590	

Special Refinement Details

Ligands to Na are disordered. The three equatorial ligands are disordered THF with each exhibiting different types of disorder, refined without restraints. The axial ligand is a mixture of THF and diethylethher, distances and angle in the diethylether were restrained.

Table 2. Atomic coordinates (x 10^4) and equivalent isotropic displacement parameters ($Å^2$x 10^3) for AJMM29 (CCDC 687691). U(eq) is defined as the trace of the orthogonalized U^{ij} tensor.

	x	y	z	U_{eq}	Occ
Re(1)	6928(1)	4885(1)	6946(1)	13(1)	1
P(1)	8846(1)	5303(1)	6769(1)	14(1)	1
P(2)	5094(1)	4335(1)	7119(1)	15(1)	1
O(1)	7765(1)	3353(1)	5896(1)	26(1)	1
O(2)	8312(1)	2796(1)	7793(1)	27(1)	1
O(3)	6370(1)	6749(1)	7894(1)	19(1)	1
O(4)	5632(1)	6594(1)	6529(1)	15(1)	1
B(1)	7422(1)	6220(1)	8342(1)	18(1)	1
B(2)	4525(1)	6892(1)	6133(1)	15(1)	1
C(1)	7444(1)	3927(1)	6280(1)	18(1)	1
C(2)	7795(1)	3598(1)	7454(1)	19(1)	1
C(3)	5314(1)	7177(1)	7049(1)	18(1)	1

C(4)	6238(1)	6309(1)	7458(1)	16(1)	1
C(5)	6190(1)	8197(1)	8808(1)	23(1)	1
C(6)	5543(1)	7602(1)	9313(1)	28(1)	1
C(7)	5612(1)	6385(1)	9197(1)	26(1)	1
C(8)	6911(1)	5571(1)	8929(1)	22(1)	1
C(9)	7934(1)	5127(1)	9361(1)	29(1)	1
C(10)	8332(1)	6099(1)	9517(1)	32(1)	1
C(11)	8493(1)	6994(1)	8998(1)	26(1)	1
C(12)	7502(1)	7391(1)	8553(1)	20(1)	1
C(13)	8740(1)	5373(1)	8008(1)	20(1)	1
C(14)	9130(1)	5894(1)	7393(1)	19(1)	1
C(15)	10237(1)	3959(1)	6650(1)	19(1)	1
C(16)	11074(1)	3396(1)	7073(1)	31(1)	1
C(17)	12121(2)	2362(1)	6962(1)	48(1)	1
C(18)	12320(2)	1884(1)	6440(1)	46(1)	1
C(19)	11491(1)	2433(1)	6018(1)	37(1)	1
C(20)	10452(1)	3466(1)	6120(1)	28(1)	1
C(21)	9138(1)	6361(1)	6176(1)	18(1)	1
C(22)	8171(1)	7464(1)	6093(1)	23(1)	1
C(23)	8367(1)	8355(1)	5690(1)	28(1)	1
C(24)	9528(1)	8139(1)	5357(1)	31(1)	1
C(25)	10489(1)	7044(1)	5430(1)	32(1)	1
C(26)	10304(1)	6159(1)	5842(1)	26(1)	1
C(27)	6213(1)	6822(1)	5238(1)	21(1)	1
C(28)	5785(1)	8176(1)	5159(1)	22(1)	1
C(29)	4940(1)	8799(1)	5686(1)	21(1)	1
C(30)	3908(1)	8320(1)	5969(1)	18(1)	1
C(31)	2860(1)	8613(1)	5561(1)	20(1)	1
C(32)	3272(1)	7958(1)	5006(1)	21(1)	1
C(33)	4121(1)	6640(1)	5107(1)	20(1)	1
C(34)	5171(1)	6356(1)	5513(1)	16(1)	1
C(35)	3498(1)	6336(1)	6486(1)	17(1)	1
C(36)	3990(1)	4979(1)	6560(1)	18(1)	1
C(37)	4092(1)	4632(1)	7814(1)	21(1)	1
C(38)	2822(1)	4783(2)	7872(1)	39(1)	1
C(39)	2112(1)	4928(2)	8413(1)	56(1)	1
C(40)	2647(2)	4921(2)	8906(1)	45(1)	1
C(41)	3902(2)	4776(2)	8856(1)	44(1)	1
C(42)	4623(1)	4644(2)	8312(1)	34(1)	1
C(43)	5460(1)	2743(1)	7137(1)	18(1)	1
C(44)	5530(1)	2233(1)	6631(1)	27(1)	1
C(45)	5810(1)	1027(1)	6651(1)	32(1)	1
C(46)	6021(1)	312(1)	7173(1)	28(1)	1
C(47)	5968(2)	804(1)	7679(1)	36(1)	1
C(48)	5687(1)	2010(1)	7660(1)	31(1)	1
Na(1)	10115(1)	1207(1)	8119(1)	49(1)	1
O(5A)	8748(1)	1072(1)	8978(1)	44(1)	1
C(51A)	8097(2)	2137(2)	9251(1)	70(1)	1
C(52A)	7024(5)	2081(5)	9577(3)	53(2)	0.412(9)
C(52B)	6702(3)	2371(3)	9267(2)	51(1)	0.588(9)
C(53A)	6623(2)	1261(2)	9263(1)	62(1)	1
C(54A)	7851(2)	563(2)	8936(1)	64(1)	1
O(6A)	9848(1)	323(1)	7362(1)	46(1)	1
C(55A)	9232(1)	1009(1)	6855(1)	30(1)	1

C(56A)	9443(10)	198(8)	6393(5)	36(2)	0.355(6)
C(57A)	9645(7)	-971(9)	6769(4)	33(2)	0.355(6)
C(58A)	9625(5)	-709(3)	7434(2)	31(1)	0.355(6)
C(56B)	9669(7)	145(5)	6399(2)	45(1)	0.645(6)
C(57B)	9945(6)	-1055(5)	6757(3)	56(2)	0.645(6)
C(58B)	10438(4)	-952(2)	7208(2)	51(1)	0.645(6)
O(7A)	11431(2)	2058(2)	8590(1)	45(1)	0.510(3)
C(59A)	12796(3)	1614(3)	8451(2)	48(1)	0.510(3)
C(60A)	13317(5)	1454(6)	9042(3)	70(2)	0.510(3)
C(61A)	12264(6)	1439(5)	9494(2)	68(2)	0.510(3)
C(62A)	11149(4)	2231(4)	9201(2)	61(1)	0.510(3)
O(7B)	11194(2)	1624(2)	8788(1)	35(1)	0.490(3)
C(59B)	11667(3)	2568(3)	8728(2)	42(1)	0.490(3)
C(60B)	12967(4)	1995(4)	8933(2)	46(1)	0.490(3)
C(61B)	12889(6)	1040(4)	9374(4)	62(2)	0.490(3)
C(62B)	11702(4)	864(4)	9297(2)	54(1)	0.490(3)
O(8A)	11421(2)	-939(2)	8409(1)	30(1)	0.518(3)
C(64A)	13159(3)	-537(3)	7869(1)	39(1)	0.518(3)
C(65A)	12764(3)	-1443(3)	8263(2)	36(1)	0.518(3)
C(66A)	10893(3)	-1775(2)	8690(1)	34(1)	0.518(3)
C(67A)	11075(3)	-2070(3)	9338(1)	44(1)	0.518(3)
O(8B)	11616(3)	-412(3)	8376(2)	53(1)	0.482(3)
C(64B)	11700(5)	-989(3)	8935(2)	66(1)	0.482(3)
C(65B)	11960(4)	-2256(4)	8884(2)	59(1)	0.482(3)
C(66B)	12596(4)	-2435(3)	8258(2)	53(1)	0.482(3)
C(67B)	12599(4)	-1208(4)	7988(3)	55(1)	0.482(3)

[Na][($Ph_2P(CH_2)_2B(C8H_{14})2Re(CO)_2(=C(O–)CH_2O–)$] ([Na][3-$E_2$], ajmm29).

Table 1. Crystal data and structure refinement for AJMM23 (CCDC 687834).

Empirical formula	$C_{48}H_{58}B_2O_4P_2Re \bullet Na(C_4H_{10}O)_3$	
Formula weight	1214.05	
Crystallization Solvent	Diethylether	
Crystal Habit	Plate	
Crystal size	0.21 x 0.15 x 0.04 mm^3	
Crystal color	Colorless	
Data Collection Temperature	100(2) K	
Unit cell dimensions	a = 11.5493(10) Å	a= 90.795(5)°
	b = 12.2399(10) Å	b= 100.549(5)°
	c = 22.961(2) Å	g = 113.895(5)°
Volume	2903.4(4) $Å^3$	
Z	2	
Crystal system	Triclinic	
Space group	P-1	
Density (calculated)	1.389 Mg/m^3	
q range for data collection	1.81 to 32.08°	
Completeness to θ = 32.08°	98.0 %	
Index ranges	$-17 \le h \le 17, -18 \le k \le 18, -34 \le l \le 34$	
Absorption coefficient	2.206 mm^{-1}	
Absorption correction	None	
Refinement method	Full matrix least-squares on F^2	
Data / restraints / parameters	19892 / 0 / 664	
Treatment of hydrogen atoms	Riding	
Goodness-of-fit on F^2	2.715	
Final R indices [I>2s(I), 16074 reflections]	R1 = 0.0756, *w*R2 = 0.1263	
R indices (all data)	R1 = 0.0950, *w*R2 = 0.1273	

Table 2. Atomic coordinates (x 10^4) and equivalent isotropic displacement parameters ($Å^2$x 10^3) for AJMM23 (CCDC 687834). U(eq) is defined as the trace of the orthogonalized U^{ij} tensor.

	x	y	z	U_{eq}
Re(1)	1459(1)	9357(1)	8040(1)	12(1)
P(1)	3392(1)	8986(1)	8216(1)	16(1)
P(2)	-381(1)	9865(1)	7864(1)	14(1)
O(1)	2529(4)	11181(4)	9174(2)	30(1)
O(2)	2788(4)	11247(3)	7262(2)	26(1)
O(3)	671(3)	7100(3)	7071(2)	19(1)
O(4)	203(3)	7775(3)	8441(2)	15(1)
B(1)	1614(6)	7498(5)	6608(3)	20(1)
B(2)	-824(6)	7631(5)	8842(3)	17(1)
C(1)	2106(5)	10498(5)	8751(2)	19(1)
C(2)	2291(5)	10519(4)	7566(2)	17(1)
C(3)	-249(5)	6987(4)	7906(2)	17(1)
C(4)	625(5)	7711(4)	7507(2)	16(1)
C(5)	218(5)	5282(5)	6116(3)	26(1)
C(6)	-572(6)	5715(5)	5640(3)	31(2)
C(7)	-457(6)	6989(5)	5792(3)	32(2)
C(8)	922(6)	7927(5)	6041(3)	26(1)
C(9)	1826(7)	8236(6)	5586(3)	39(2)
C(10)	2153(7)	7208(6)	5389(3)	39(2)
C(11)	2472(6)	6503(5)	5896(3)	31(2)

C(12)	1633(5)	6235(4)	6362(2)	21(1)
C(13)	3034(6)	8463(5)	6955(3)	25(1)
C(14)	3517(5)	8153(5)	7568(2)	21(1)
C(15)	4855(5)	10376(4)	8365(2)	20(1)
C(16)	5647(5)	10762(5)	7953(3)	27(1)
C(17)	6789(6)	11820(5)	8092(3)	38(2)
C(18)	7115(6)	12469(5)	8634(3)	39(2)
C(19)	6330(6)	12090(5)	9040(3)	37(2)
C(20)	5204(5)	11064(5)	8910(3)	29(1)
C(21)	3780(5)	8115(5)	8795(2)	21(1)
C(22)	2824(6)	7013(5)	8866(3)	28(1)
C(23)	3078(6)	6237(5)	9258(3)	30(1)
C(24)	4313(6)	6562(5)	9577(3)	32(1)
C(25)	5275(6)	7637(6)	9528(3)	33(2)
C(26)	5025(6)	8418(5)	9128(3)	29(1)
C(27)	1077(6)	8032(5)	9744(3)	25(1)
C(28)	619(6)	6692(5)	9808(3)	26(1)
C(29)	-373(6)	5850(4)	9264(2)	25(1)
C(30)	-1447(6)	6249(4)	8987(2)	23(1)
C(31)	-2421(5)	6093(4)	9401(2)	22(1)
C(32)	-1853(6)	6958(4)	9975(2)	25(1)
C(33)	-970(6)	8259(4)	9890(2)	23(1)
C(34)	-16(5)	8407(4)	9479(2)	20(1)
C(35)	-1892(5)	8079(4)	8492(2)	18(1)
C(36)	-1361(5)	9441(4)	8428(2)	17(1)
C(37)	-1562(5)	9293(4)	7155(2)	18(1)
C(38)	-2821(6)	9100(7)	7085(3)	49(2)
C(39)	-3658(7)	8750(7)	6528(4)	55(2)
C(40)	-3248(8)	8578(7)	6047(4)	50(2)
C(41)	-1948(9)	8788(8)	6105(3)	65(3)
C(42)	-1130(8)	9122(7)	6647(3)	49(2)
C(43)	25(5)	11474(4)	7842(2)	19(1)
C(44)	108(5)	12183(4)	8341(3)	21(1)
C(45)	425(5)	13409(5)	8319(3)	27(1)
C(46)	672(6)	13929(5)	7805(3)	31(2)
C(47)	637(7)	13245(5)	7310(3)	37(2)
C(48)	308(6)	12028(5)	7329(3)	28(1)
Na(1)	4314(3)	12807(2)	6918(1)	51(1)
O(5)	3270(6)	13093(5)	6011(2)	64(2)
C(51)	1252(9)	11370(8)	5738(4)	84(3)
C(52)	1946(8)	12645(8)	5994(4)	63(2)
C(53)	3603(9)	13430(10)	5445(4)	85(4)
C(54)	5083(10)	14067(12)	5552(6)	142(6)
O(6)	4629(4)	14189(4)	7665(2)	39(1)
C(55)	3887(8)	13719(7)	8596(4)	64(2)
C(56)	4830(7)	13762(6)	8244(3)	46(2)
C(57)	4725(8)	15375(6)	7708(4)	64(3)
C(58)	4849(9)	15826(7)	7122(4)	73(3)
O(7)	5918(5)	12434(5)	6604(3)	64(2)
C(59)	7436(8)	14348(7)	7012(4)	64(3)
C(60)	7220(8)	13215(7)	6656(4)	62(2)
C(61)	5575(12)	11190(7)	6356(5)	106(5)
C(62)	5316(9)	11160(7)	5763(4)	101(5)

$(PPh_3)_2Re(CO)_3(CHOBEt_3)$ (2-Ph_2•BEt_3, ajmm59).

Table 1. Crystal data and structure refinement for AJMM59 (CCDC 770577).

Empirical formula	$C_{46}H_{46}BO_4P_2Re \bullet C_7H_8$	
Formula weight	1013.91	
Crystallization Solvent	Toluene	
Crystal Habit	Fragment	
Crystal size	0.19 x 0.19 x 0.06 mm^3	
Crystal color	Colorless	
Data Collection Temperature	100(2) K	
Unit cell dimensions	a = 14.9591(6) Å	
	b = 25.5104(9) Å	b= 105.268(2)°
	c = 25.5702(10) Å	
Volume	9413.5(6) $Å^3$	
Z	8	
Crystal system	Monoclinic	
Space group	P $2_1/n$	
Density (calculated)	1.431 Mg/m^3	
q range for data collection	1.43 to 28.89°	
Completeness to θ = 28.89°	99.7 %	
Index ranges	$-20 \le h \le 19$, $-34 \le k \le 34$, $-34 \le l \le 34$	
Absorption coefficient	2.694 mm^{-1}	
Absorption correction	Semi-empirical from equivalents	
Refinement method	Full matrix least-squares on F^2	
Data / restraints / parameters	24722 / 0 / 1107	
Treatment of hydrogen atoms	Riding	
Goodness-of-fit on F^2	1.689	
Final R indices [I>2s(I), 19590 reflections]	R1 = 0.0325, *w*R2 = 0.0499	
R indices (all data)	R1 = 0.0491, *w*R2 = 0.0515	

Special Refinement Details

The crystal contains two molecules per asymmetric unit with each molecule accompanied by a toluene solvent of crystallization.

Table 2. Atomic coordinates (x 10^4) and equivalent isotropic displacement parameters ($Å^2$x 10^3) for AJMM59 (CCDC 770577). U(eq) is defined as the trace of the orthogonalized U^{ij} tensor.

	x	y	z	U_{eq}
Re(1)	7124(1)	3019(1)	6560(1)	11(1)
P(1A)	6635(1)	3000(1)	5580(1)	12(1)
P(2A)	7612(1)	3088(1)	7539(1)	12(1)
O(1A)	5428(1)	3758(1)	6516(1)	27(1)
O(2A)	5743(1)	2118(1)	6612(1)	27(1)
O(3A)	8837(1)	2319(1)	6568(1)	25(1)
O(4A)	7461(1)	4169(1)	6408(1)	22(1)
B(1A)	7928(2)	4762(1)	6421(1)	24(1)
C(1A)	6040(2)	3494(1)	6536(1)	17(1)
C(2A)	6289(2)	2433(1)	6597(1)	17(1)
C(3A)	8206(2)	2577(1)	6566(1)	16(1)
C(4A)	7863(2)	3735(1)	6522(1)	16(1)
C(5A)	5554(2)	3360(1)	5322(1)	14(1)
C(6A)	4727(2)	3120(1)	5339(1)	17(1)

C(7A)	3900(2)	3399(1)	5209(1)	22(1)
C(8A)	3892(2)	3918(1)	5060(1)	24(1)
C(9A)	4711(2)	4163(1)	5041(1)	26(1)
C(10A)	5543(2)	3887(1)	5177(1)	21(1)
C(11A)	6350(2)	2354(1)	5256(1)	13(1)
C(12A)	6665(2)	1891(1)	5538(1)	18(1)
C(13A)	6488(2)	1409(1)	5274(1)	21(1)
C(14A)	6011(2)	1387(1)	4735(1)	21(1)
C(15A)	5689(2)	1842(1)	4454(1)	21(1)
C(16A)	5849(2)	2324(1)	4713(1)	18(1)
C(17A)	7415(2)	3268(1)	5199(1)	15(1)
C(18A)	7090(2)	3396(1)	4652(1)	20(1)
C(19A)	7684(2)	3579(1)	4362(1)	23(1)
C(20A)	8621(2)	3634(1)	4611(1)	24(1)
C(21A)	8958(2)	3507(1)	5155(1)	22(1)
C(22A)	8357(2)	3324(1)	5446(1)	19(1)
C(23A)	6733(2)	3411(1)	7803(1)	14(1)
C(24A)	6128(2)	3119(1)	8023(1)	21(1)
C(25A)	5396(2)	3365(1)	8166(1)	27(1)
C(26A)	5272(2)	3900(1)	8100(1)	27(1)
C(27A)	5860(2)	4192(1)	7879(1)	23(1)
C(28A)	6581(2)	3948(1)	7725(1)	18(1)
C(29A)	7845(2)	2483(1)	7938(1)	14(1)
C(30A)	7750(2)	1987(1)	7706(1)	19(1)
C(31A)	7897(2)	1539(1)	8031(1)	23(1)
C(32A)	8146(2)	1584(1)	8587(1)	26(1)
C(33A)	8261(2)	2079(1)	8824(1)	28(1)
C(34A)	8118(2)	2522(1)	8500(1)	21(1)
C(35A)	8698(2)	3442(1)	7831(1)	13(1)
C(36A)	9491(2)	3258(1)	7696(1)	19(1)
C(37A)	10345(2)	3490(1)	7911(1)	20(1)
C(38A)	10427(2)	3911(1)	8259(1)	19(1)
C(39A)	9655(2)	4098(1)	8399(1)	18(1)
C(40A)	8795(2)	3862(1)	8191(1)	17(1)
C(41A)	7402(2)	5005(1)	5840(1)	32(1)
C(42A)	7752(2)	4829(1)	5355(1)	40(1)
C(43A)	9032(2)	4718(1)	6505(1)	26(1)
C(44A)	9641(2)	4657(1)	7089(1)	32(1)
C(45A)	7626(2)	5029(1)	6922(1)	25(1)
C(46A)	6579(2)	5109(1)	6839(1)	35(1)
Re(2)	2064(1)	2200(1)	6557(1)	11(1)
P(1B)	2583(1)	2086(1)	7530(1)	13(1)
P(2B)	1582(1)	2198(1)	5576(1)	13(1)
O(1B)	353(1)	1475(1)	6524(1)	21(1)
O(2B)	699(1)	3115(1)	6601(1)	27(1)
O(3B)	3781(1)	2906(1)	6575(1)	26(1)
O(4B)	2468(1)	1055(1)	6413(1)	17(1)
B(1B)	2982(2)	491(1)	6395(1)	19(1)
C(1B)	983(2)	1729(1)	6539(1)	16(1)
C(2B)	1235(2)	2791(1)	6591(1)	16(1)
C(3B)	3151(2)	2649(1)	6569(1)	16(1)
C(4B)	2818(2)	1501(1)	6518(1)	14(1)
C(5B)	1712(2)	1755(1)	7800(1)	15(1)
C(6B)	1178(2)	2033(1)	8079(1)	20(1)

C(7B)	450(2)	1789(1)	8224(1)	28(1)
C(8B)	255(2)	1266(1)	8102(1)	29(1)
C(9B)	785(2)	985(1)	7826(1)	25(1)
C(10B)	1497(2)	1231(1)	7669(1)	19(1)
C(11B)	2885(2)	2662(1)	7965(1)	16(1)
C(12B)	2711(2)	3168(1)	7758(1)	17(1)
C(13B)	2912(2)	3601(1)	8107(1)	22(1)
C(14B)	3294(2)	3526(1)	8654(1)	28(1)
C(15B)	3486(2)	3024(1)	8860(1)	31(1)
C(16B)	3283(2)	2596(1)	8518(1)	24(1)
C(17B)	3649(2)	1694(1)	7764(1)	14(1)
C(18B)	4433(2)	1880(1)	7627(1)	18(1)
C(19B)	5262(2)	1604(1)	7778(1)	20(1)
C(20B)	5314(2)	1139(1)	8060(1)	20(1)
C(21B)	4536(2)	952(1)	8200(1)	20(1)
C(22B)	3711(2)	1233(1)	8059(1)	16(1)
C(23B)	492(2)	1844(1)	5344(1)	14(1)
C(24B)	-330(2)	2104(1)	5342(1)	18(1)
C(25B)	-1158(2)	1829(1)	5249(1)	22(1)
C(26B)	-1172(2)	1295(1)	5158(1)	25(1)
C(27B)	-357(2)	1033(1)	5159(1)	24(1)
C(28B)	471(2)	1305(1)	5259(1)	19(1)
C(29B)	1349(2)	2829(1)	5221(1)	18(1)
C(30B)	1647(2)	3300(1)	5486(1)	19(1)
C(31B)	1530(2)	3772(1)	5197(1)	25(1)
C(32B)	1123(2)	3771(1)	4645(1)	29(1)
C(33B)	816(2)	3305(1)	4378(1)	31(1)
C(34B)	924(2)	2838(1)	4667(1)	25(1)
C(35B)	2340(2)	1892(1)	5204(1)	14(1)
C(36B)	3297(2)	1898(1)	5424(1)	18(1)
C(37B)	3886(2)	1691(1)	5138(1)	21(1)
C(38B)	3529(2)	1470(1)	4634(1)	20(1)
C(39B)	2576(2)	1465(1)	4408(1)	18(1)
C(40B)	1994(2)	1676(1)	4692(1)	17(1)
C(41B)	2552(2)	133(1)	6793(1)	30(1)
C(42B)	1498(2)	61(1)	6637(2)	48(1)
C(43B)	4092(2)	552(1)	6633(1)	22(1)
C(44B)	4659(2)	798(1)	6281(1)	35(1)
C(45B)	2637(2)	345(1)	5760(1)	26(1)
C(46B)	2988(2)	-192(1)	5623(1)	32(1)
C(51C)	3286(3)	4895(1)	6250(1)	40(1)
C(52C)	3653(3)	4505(2)	6610(2)	57(1)
C(53C)	3078(3)	4230(2)	6838(2)	66(1)
C(54C)	2135(3)	4323(1)	6713(2)	51(1)
C(55C)	1764(3)	4725(2)	6363(2)	63(1)
C(56C)	2353(2)	5017(1)	6116(2)	36(1)
C(57C)	3948(3)	5197(2)	5981(2)	58(1)
C(51D)	8396(2)	91(1)	6036(1)	30(1)
C(52D)	8814(2)	506(1)	6354(1)	34(1)
C(53D)	8349(2)	795(1)	6659(1)	41(1)
C(54D)	7460(2)	671(1)	6657(2)	41(1)
C(55D)	7024(2)	254(1)	6335(2)	47(1)
C(56D)	7494(2)	-28(1)	6033(2)	41(1)
C(57D)	8903(2)	-226(1)	5708(1)	38(1)

$[(Ph_2PCH_2B(C_8H_{14}))_2Re(CO)_4][B(C_6F_5)_4]$ ($[1\text{-}M_2][B(C_6F_5)_4]$, ajmm43).

Table 1. Crystal data and structure refinement for AJMM43 (CCDC 768445).

Empirical formula	$[C_{46}H_{52}B_2O_4P_2Re]^+ [C_{24}BF_{20}]^- \bullet C_2H_4Cl_2$
Formula weight	1716.64
Crystallization Solvent	Dichloroethane
Crystal Habit	Block
Crystal size	0.26 x 0.21 x 0.14 mm^3
Crystal color	Colorless
Data Collection Temperature	100(2) K
Unit cell dimensions	a = 16.0785(8) Å
	b = 19.3393(9) Å b= 90.578(2)°
	c = 22.2924(10) Å
Volume	6931.4(6) $Å^3$
Z	4
Crystal system	Monoclinic
Space group	P $2_1/n$
Density (calculated)	1.645 Mg/m^3
q range for data collection	1.88 to 36.56°
Completeness to θ = 36.56°	86.5 %
Index ranges	$-23 \le h \le 25$, $-28 \le k \le 31$, $-36 \le l \le 36$
Absorption coefficient	1.980 mm^{-1}
Absorption correction	Semi-empirical from equivalents
Refinement method	Full matrix least-squares on F^2
Data / restraints / parameters	29574 / 117 / 983
Treatment of hydrogen atoms	Riding
Goodness-of-fit on F^2	2.971
Final R indices [I>2s(I), 24164 reflections]	R1 = 0.0371, *w*R2 = 0.0708
R indices (all data)	R1 = 0.0515, *w*R2 = 0.0713

Special Refinement Details

One of the borabicylcononane ligands is disordered by a rotation around the B-C bond. Both the minor (34%) and major (66%) components were restrained to the same geometry as the ordered ligand. The minor component was refined as isotropic and the major component was refined as anisotropic but was restrained to simulate isotropic behavior. The dichloroethane solvent of crystallization was also disordered with both orientations apparently sharing one common Cl site and the ethyl portion flipped about the approximated Cl-Cl vector. The minor component (34%) was refined isotropically and the major component (66%) anisotropically; no geometry restraints were imposed.

Table 2. Atomic coordinates (x 10^4) and equivalent isotropic displacement parameters ($Å^2$x 10^3) for AJMM43 (CCDC 768445). U(eq) is defined as the trace of the orthogonalized U^{ij} tensor.

	x	y	z	U_{eq}	Occ
Re(1)	2798(1)	8597(1)	5895(1)	13(1)	1
P(1)	3164(1)	7812(1)	5075(1)	14(1)	1
P(2)	2388(1)	9494(1)	6610(1)	15(1)	1
O(1)	1562(1)	7577(1)	6497(1)	32(1)	1
O(2)	4156(1)	7916(1)	6715(1)	32(1)	1
O(3)	4159(1)	9649(1)	5463(1)	24(1)	1
O(4)	1352(1)	9123(1)	5055(1)	26(1)	1
C(1)	2001(2)	7949(1)	6260(1)	20(1)	1
C(2)	3671(2)	8176(1)	6416(1)	20(1)	1

C(3)	3657(1)	9272(1)	5597(1)	18(1)	1
C(4)	1890(2)	8953(1)	5354(1)	18(1)	1
C(5)	3959(1)	8200(1)	4603(1)	16(1)	1
C(6)	4795(2)	8171(1)	4779(1)	21(1)	1
C(7)	5397(2)	8484(1)	4428(1)	25(1)	1
C(8)	5168(2)	8832(1)	3905(1)	23(1)	1
C(9)	4346(2)	8871(1)	3735(1)	21(1)	1
C(10)	3740(1)	8558(1)	4082(1)	18(1)	1
C(11)	3604(1)	6976(1)	5276(1)	17(1)	1
C(12)	4053(2)	6603(1)	4856(1)	23(1)	1
C(13)	4347(2)	5948(1)	4994(1)	30(1)	1
C(14)	4203(2)	5660(1)	5547(1)	30(1)	1
C(15)	3752(2)	6020(1)	5970(1)	27(1)	1
C(16)	3452(2)	6676(1)	5835(1)	21(1)	1
C(17)	2338(1)	7574(1)	4547(1)	17(1)	1
B(1)	1715(2)	6994(1)	4782(1)	20(1)	1
C(18)	1820(2)	6227(1)	4641(1)	22(1)	1
C(19)	1479(2)	5736(1)	5122(1)	28(1)	1
C(20)	1114(2)	6114(1)	5649(1)	36(1)	1
C(21)	493(2)	6662(1)	5487(1)	35(1)	1
C(22)	802(2)	7180(1)	5011(1)	27(1)	1
C(23)	325(2)	7122(1)	4421(1)	32(1)	1
C(24)	400(2)	6407(1)	4123(1)	31(1)	1
C(25)	1282(2)	6187(1)	4040(1)	26(1)	1
C(26)	1853(2)	10193(1)	6209(1)	19(1)	1
C(27)	2319(2)	10675(1)	5892(1)	29(1)	1
C(28)	1918(2)	11175(1)	5544(1)	44(1)	1
C(29)	1061(2)	11200(2)	5516(1)	48(1)	1
C(30)	597(2)	10723(1)	5832(1)	41(1)	1
C(31)	998(2)	10221(1)	6176(1)	30(1)	1
C(32)	3189(1)	9960(1)	7028(1)	17(1)	1
C(33)	3993(1)	9706(1)	7101(1)	19(1)	1
C(34)	4576(2)	10061(1)	7449(1)	24(1)	1
C(35)	4362(2)	10676(1)	7724(1)	26(1)	1
C(36)	3564(2)	10934(1)	7651(1)	30(1)	1
C(37)	2977(2)	10583(1)	7308(1)	25(1)	1
C(38)	1655(1)	9232(1)	7183(1)	21(1)	1
B(2A)	1942(2)	8780(1)	7730(1)	33(1)	0.343(3)
C(39A)	1781(4)	8026(2)	7893(3)	49(2)	0.343(3)
C(40A)	2547(6)	7591(4)	8063(5)	206(13)	0.343(3)
C(41A)	3094(7)	7905(5)	8543(5)	94(4)	0.343(3)
C(42A)	3304(5)	8645(5)	8422(6)	138(8)	0.343(3)
C(43A)	2553(4)	9095(3)	8233(3)	70(4)	0.343(3)
C(44A)	1947(6)	9212(4)	8740(4)	79(5)	0.343(3)
C(45A)	1432(6)	8581(4)	8935(3)	57(3)	0.343(3)
C(46A)	1167(5)	8106(5)	8443(3)	62(4)	0.343(3)
B(2B)	1942(2)	8780(1)	7730(1)	33(1)	0.657(3)
C(39B)	2744(2)	8403(2)	7893(1)	40(1)	0.657(3)
C(40B)	2638(3)	7641(2)	8069(2)	49(2)	0.657(3)
C(41B)	1926(3)	7481(3)	8478(3)	78(2)	0.657(3)
C(42B)	1118(3)	7809(2)	8301(3)	106(3)	0.657(3)
C(43B)	1169(2)	8586(2)	8145(2)	67(2)	0.657(3)
C(44B)	1400(3)	9042(3)	8674(2)	86(2)	0.657(3)
C(45B)	2319(3)	9066(4)	8871(2)	87(2)	0.657(3)

C(46B)	2998(4)	8869(3)	8453(2)	119(3)	0.657(3)
B(3)	1787(2)	9973(1)	2479(1)	15(1)	1
F(1)	3560(1)	9472(1)	2231(1)	24(1)	1
F(2)	4116(1)	9041(1)	1195(1)	37(1)	1
F(3)	3114(1)	9010(1)	203(1)	34(1)	1
F(4)	1507(1)	9459(1)	289(1)	30(1)	1
F(5)	930(1)	9927(1)	1332(1)	23(1)	1
F(6)	1818(1)	11156(1)	1547(1)	28(1)	1
F(7)	1180(1)	12389(1)	1707(1)	52(1)	1
F(8)	301(1)	12706(1)	2710(1)	60(1)	1
F(9)	53(1)	11699(1)	3553(1)	38(1)	1
F(10)	712(1)	10455(1)	3413(1)	23(1)	1
F(11)	2398(1)	8626(1)	2828(1)	25(1)	1
F(12)	1543(1)	7470(1)	2988(1)	37(1)	1
F(13)	-151(1)	7466(1)	2871(1)	39(1)	1
F(14)	-951(1)	8658(1)	2550(1)	34(1)	1
F(15)	-109(1)	9815(1)	2374(1)	23(1)	1
F(16)	3208(1)	10879(1)	2361(1)	23(1)	1
F(17)	4266(1)	11296(1)	3213(1)	32(1)	1
F(18)	4083(1)	10859(1)	4366(1)	38(1)	1
F(19)	2839(1)	9957(1)	4632(1)	33(1)	1
F(20)	1838(1)	9474(1)	3793(1)	24(1)	1
C(51)	2216(1)	9753(1)	1837(1)	15(1)	1
C(52)	3014(1)	9500(1)	1766(1)	18(1)	1
C(53)	3326(2)	9261(1)	1227(1)	23(1)	1
C(54)	2824(2)	9256(1)	727(1)	24(1)	1
C(55)	2016(2)	9484(1)	769(1)	21(1)	1
C(56)	1729(1)	9723(1)	1317(1)	18(1)	1
C(57)	1287(1)	10718(1)	2465(1)	16(1)	1
C(58)	1379(2)	11250(1)	2054(1)	22(1)	1
C(59)	1058(2)	11906(1)	2127(1)	33(1)	1
C(60)	615(2)	12066(1)	2631(1)	36(1)	1
C(61)	490(2)	11560(1)	3053(1)	27(1)	1
C(62)	827(1)	10915(1)	2965(1)	19(1)	1
C(63)	1189(1)	9295(1)	2616(1)	16(1)	1
C(64)	1562(2)	8663(1)	2763(1)	19(1)	1
C(65)	1129(2)	8057(1)	2849(1)	26(1)	1
C(66)	282(2)	8050(1)	2787(1)	27(1)	1
C(67)	-122(2)	8653(1)	2627(1)	24(1)	1
C(68)	340(1)	9252(1)	2541(1)	19(1)	1
C(69)	2470(1)	10140(1)	3019(1)	15(1)	1
C(70)	3104(1)	10614(1)	2918(1)	18(1)	1
C(71)	3652(2)	10848(1)	3352(1)	22(1)	1
C(72)	3566(2)	10626(1)	3934(1)	25(1)	1
C(73)	2940(2)	10175(1)	4062(1)	22(1)	1
C(74)	2421(1)	9936(1)	3614(1)	18(1)	1
Cl(2)	4306(1)	3070(1)	3839(1)	69(1)	1
Cl(1C)	1876(1)	2234(1)	4081(1)	79(1)	0.661(6)
C(81C)	3264(3)	2757(2)	3663(2)	40(1)	0.661(6)
C(82C)	2941(3)	2492(3)	4239(2)	51(2)	0.661(6)
Cl(1D)	1869(11)	2162(9)	4066(7)	371(11)	0.339(6)
C(81D)	2810(6)	2554(4)	3677(3)	28(2)	0.339(6)
C(82D)	3473(5)	2678(3)	4170(3)	17(2)	0.339(6)

[(Ph$_2$PCH$_2$B(C$_8$H$_{14}$))Re(CO)$_5$][OTf] ([1-M$_1$][OTf] ajmm45).

Table 1. Crystal data and structure refinement for AJMM45 (CCDC 779779).

Empirical formula	$[C_{26}H_{26}BO_5PRe]^+ [CF_3O_3S]^-$	
Formula weight	795.52	
Crystallization Solvent	Dichloromethane/pentane	
Crystal Habit	Block	
Crystal size	0.25 x 0.21 x 0.09 mm^3	
Crystal color	Colorless	
Data Collection Temperature	100(2) K	
Unit cell dimensions	a = 17.3374(4) Å	a= 85.9010(10)°
	b = 17.3374(4) Å	b= 85.9010(10)°
	c = 17.3374(4) Å	g = 85.9010(10)°
Volume	5173.2(2) Å^3	
Z	6	
Crystal system	Rhombohedral	
Space group	R -3	
Density (calculated)	1.532 Mg/m^3	
Completeness to θ = 37.73°	94.6 %	
Index ranges	-26 ≤ h ≤ 29, -26 ≤ k ≤ 29, -29 ≤ l ≤ 28	
Absorption coefficient	3.687 mm^{-1}	
Absorption correction	Semi-empirical from equivalents	
Refinement method	Full matrix least-squares on F^2	
Data / restraints / parameters	17454 / 0 / 440	
Treatment of hydrogen atoms	Riding	
Goodness-of-fit on F^2	2.593	
Final R indices [I>2s(I), 14238 reflections]	R1 = 0.0328, *w*R2 = 0.0541	
R indices (all data)	R1 = 0.0432, *w*R2 = 0.0547	

Special Refinement Details

SQUEEZE[1] was used to model disordered solvent. A void near the origin, volume = 867 Å^3, presumably filled with dichloromethane and pentane, was accounted for by 309e$^-$. The two phenyl rings are disordered by rotation around the P-C bond. Each was constrained to a regular hexagon.

Table 2. Atomic coordinates (x 10^4) and equivalent isotropic displacement parameters (Å^{2}x 10^3) for AJMM45 (CCDC 779779). U(eq) is defined as the trace of the orthogonalized U^{ij} tensor.

	x	y	z	U_{eq}	Occ
Re(1)	3232(1)	6057(1)	3009(1)	17(1)	1
P(1)	2116(1)	7035(1)	2933(1)	21(1)	1
O(1)	4341(1)	7337(1)	2316(1)	30(1)	1
O(2)	3122(1)	5574(1)	1315(1)	54(1)	1
O(3)	2062(1)	4807(1)	3598(1)	36(1)	1
O(4)	3517(1)	6401(1)	4718(1)	25(1)	1
O(5)	4600(1)	4831(1)	3254(1)	32(1)	1
B(1)	1369(1)	8316(1)	3775(1)	26(1)	1
C(1)	3949(1)	6880(1)	2576(1)	23(1)	1
C(2)	3150(1)	5762(1)	1925(1)	33(1)	1
C(3)	2478(1)	5264(1)	3401(1)	25(1)	1
C(4)	3381(1)	6309(1)	4107(1)	19(1)	1
C(5)	4110(1)	5280(1)	3138(1)	23(1)	1

C(6)	1948(1)	7581(1)	3792(1)	21(1)	1
C(7)	565(1)	8436(1)	3415(2)	42(1)	1
C(8)	-15(1)	8347(2)	4147(2)	65(1)	1
C(9)	112(2)	8870(2)	4812(2)	58(1)	1
C(10)	952(2)	8899(1)	4976(2)	47(1)	1
C(11)	1511(1)	9008(1)	4265(2)	40(1)	1
C(12)	1401(2)	9784(2)	3810(2)	66(1)	1
C(13)	705(3)	9912(2)	3372(2)	92(1)	1
C(14)	487(2)	9224(2)	2974(2)	82(1)	1
C(15A)	2407(2)	7761(3)	2119(2)	18(1)	0.358(2)
C(16A)	2512(2)	7539(2)	1362(2)	23(1)	0.358(2)
C(17A)	2777(3)	8059(2)	772(2)	33(1)	0.358(2)
C(18A)	2938(3)	8801(2)	939(3)	42(2)	0.358(2)
C(19A)	2834(3)	9023(2)	1696(3)	50(3)	0.358(2)
C(20A)	2569(3)	8503(3)	2286(2)	22(2)	0.358(2)
C(15B)	2139(2)	7789(2)	2172(2)	44(1)	0.642(2)
C(16B)	1668(2)	7839(2)	1552(2)	91(2)	0.642(2)
C(17B)	1739(2)	8435(3)	976(2)	150(4)	0.642(2)
C(18B)	2281(3)	8981(3)	1020(3)	197(6)	0.642(2)
C(19B)	2752(2)	8931(2)	1640(3)	110(4)	0.642(2)
C(20B)	2681(2)	8335(3)	2216(2)	56(2)	0.642(2)
C(21A)	1213(2)	6700(2)	2709(2)	13(1)	0.358(2)
C(22A)	860(3)	6242(3)	3304(2)	22(1)	0.358(2)
C(23A)	154(3)	5941(3)	3204(2)	30(2)	0.358(2)
C(24A)	-197(2)	6098(3)	2509(3)	33(2)	0.358(2)
C(25A)	156(2)	6556(3)	1914(2)	38(2)	0.358(2)
C(26A)	862(2)	6857(2)	2014(2)	29(1)	0.358(2)
C(21B)	1232(1)	6507(2)	2854(1)	23(1)	0.642(2)
C(22B)	663(2)	6437(2)	3457(1)	23(1)	0.642(2)
C(23B)	44(1)	5985(2)	3390(1)	30(1)	0.642(2)
C(24B)	-7(1)	5603(2)	2719(2)	57(2)	0.642(2)
C(25B)	562(1)	5673(2)	2115(2)	73(2)	0.642(2)
C(26B)	1181(1)	6125(2)	2183(1)	57(2)	0.642(2)
C(41)	5806(1)	618(2)	6182(1)	39(1)	1
F(1)	5360(1)	140(1)	5898(1)	56(1)	1
F(2)	6539(1)	330(1)	6074(1)	63(1)	1
F(3)	5645(1)	607(1)	6949(1)	74(1)	1
O(6)	4878(1)	1820(1)	5966(1)	30(1)	1
O(7)	6232(1)	2010(1)	6106(1)	41(1)	1
O(8)	5849(1)	1512(1)	4933(1)	35(1)	1
S(1)	5677(1)	1604(1)	5746(1)	23(1)	1

$[(Ph_2P(CH_2)_2B(C_8H_{14}))_2Re(CO)_4]_2$-*m*-$(OH)_2$ (8, ajmm42).

Table 1. Crystal data and structure refinement for AJMM42 (CCDC 768183).

Empirical formula	$C_{96}H_{112}B_4O_{10}P_4Re_2 \bullet 0.42(C_5H_{12}) \bullet 2.58(C_6H_6)$
Formula weight	2197.16
Crystallization Solvent	Benzene/pentane/heptane
Crystal Habit	Fragment
Crystal size	0.21 x 0.15 x 0.11 mm^3
Crystal color	Colorless
Data Collection Temperature	100(2) K
Unit cell dimensions	a = 15.2592(6) Å
	b = 27.8836(12) Å b= 98.936(2)°
	c = 25.0134(11) Å
Volume	10513.6(8) $Å^3$
Z	4
Crystal system	Monoclinic
Space group	P $2_1/n$
Density (calculated)	1.388 Mg/m^3
Completeness to θ = 29.89°	90.2 %
Index ranges	$-20 \le h \le 21$, $-38 \le k \le 33$, $-35 \le l \le 33$
Absorption coefficient	2.419 mm^{-1}
Absorption correction	Semi-empirical from equivalents
Refinement method	Full matrix least-squares on F^2
Data / restraints / parameters	27378 / 0 / 1186
Treatment of hydrogen atoms	Riding
Goodness-of-fit on F^2	2.100
Final R indices [I>2s(I), 22663 reflections]	R1 = 0.0332, *w*R2 = 0.0504
R indices (all data)	R1 = 0.0463, *w*R2 = 0.0510

Special Refinement Details

There are three sites containing solvent, two contain benzene only. The third site is a mixture of benzene and pentane. The benzene in this site was restrained to an ideal hexagon and the pentane had no restraints applied.

Table 2. Atomic coordinates (x 10^4) and equivalent isotropic displacement parameters ($Å^2$x 10^3) for AJMM42 (CCDC 768183). U(eq) is defined at he trace of the orthogonalized U^{ij} tensor.

	x	y	z	U_{eq}	Occ
Re(1)	3351(1)	6419(1)	3945(1)	18(1)	1
Re(2)	1546(1)	9026(1)	3821(1)	18(1)	1
P(1)	2306(1)	6227(1)	4561(1)	22(1)	1
P(2)	4392(1)	6613(1)	3323(1)	17(1)	1
P(3)	2982(1)	9387(1)	4179(1)	17(1)	1
P(4)	35(1)	8764(1)	3472(1)	19(1)	1
O(1)	2618(1)	7471(1)	3852(1)	27(1)	1
O(2)	1979(1)	5996(1)	3004(1)	36(1)	1
O(3)	4127(2)	5380(1)	4058(1)	53(1)	1
O(4)	4834(1)	6591(1)	4936(1)	38(1)	1
O(5)	2442(1)	8370(1)	3043(1)	34(1)	1
O(6)	1234(1)	9841(1)	2955(1)	43(1)	1
O(7)	768(1)	9657(1)	4675(1)	34(1)	1
O(8)	1735(1)	8140(1)	4603(1)	29(1)	1

O(9)	5530(1)	8237(1)	4024(1)	21(1)	1
O(10)	-578(1)	7075(1)	3694(1)	25(1)	1
B(1)	-251(2)	6957(1)	4324(1)	32(1)	1
B(2)	5355(2)	8071(1)	3406(1)	21(1)	1
B(3)	5026(2)	8335(1)	4530(1)	18(1)	1
B(4)	-247(2)	7267(1)	3158(1)	26(1)	1
C(1)	2868(2)	7081(1)	3875(1)	21(1)	1
C(2)	2462(2)	6173(1)	3340(1)	23(1)	1
C(3)	3836(2)	5755(1)	4014(1)	32(1)	1
C(4)	4286(2)	6560(1)	4572(1)	25(1)	1
C(5)	2110(2)	8611(1)	3318(1)	24(1)	1
C(6)	1354(2)	9549(1)	3272(1)	27(1)	1
C(7)	1039(2)	9426(1)	4362(1)	23(1)	1
C(8)	1682(2)	8468(1)	4329(1)	22(1)	1
C(9)	1124(2)	6332(1)	4312(1)	26(1)	1
C(10)	821(2)	6857(1)	4386(1)	32(1)	1
C(11)	-506(2)	7402(1)	4694(1)	36(1)	1
C(12)	-1501(2)	7532(1)	4516(1)	41(1)	1
C(13)	-2151(2)	7112(1)	4532(1)	45(1)	1
C(14)	-1849(2)	6638(1)	4332(1)	41(1)	1
C(15)	-852(2)	6522(1)	4487(1)	34(1)	1
C(16)	-604(2)	6407(1)	5091(1)	42(1)	1
C(17)	-695(2)	6825(1)	5487(1)	46(1)	1
C(18)	-293(2)	7291(1)	5299(1)	42(1)	1
C(19)	2415(2)	6521(1)	5216(1)	22(1)	1
C(20)	2811(2)	6963(1)	5322(1)	27(1)	1
C(21)	2725(2)	7211(1)	5793(1)	36(1)	1
C(22)	2228(2)	7021(1)	6156(1)	37(1)	1
C(23)	1836(2)	6581(1)	6056(1)	36(1)	1
C(24)	1932(2)	6325(1)	5598(1)	29(1)	1
C(25)	2413(2)	5596(1)	4742(1)	29(1)	1
C(26)	1850(2)	5254(1)	4466(1)	43(1)	1
C(27)	1991(3)	4771(1)	4583(2)	62(1)	1
C(28)	2685(3)	4629(1)	4970(2)	68(1)	1
C(29)	3245(3)	4966(1)	5251(1)	59(1)	1
C(30)	3105(2)	5448(1)	5131(1)	40(1)	1
C(31)	5154(2)	6118(1)	3261(1)	18(1)	1
C(32)	4868(2)	5716(1)	2951(1)	26(1)	1
C(33)	5433(2)	5328(1)	2928(1)	32(1)	1
C(34)	6283(2)	5342(1)	3204(1)	36(1)	1
C(35)	6571(2)	5735(1)	3508(1)	36(1)	1
C(36)	6011(2)	6121(1)	3539(1)	26(1)	1
C(37)	3940(2)	6757(1)	2623(1)	17(1)	1
C(38)	4509(2)	6746(1)	2235(1)	23(1)	1
C(39)	4234(2)	6919(1)	1719(1)	28(1)	1
C(40)	3396(2)	7106(1)	1578(1)	28(1)	1
C(41)	2820(2)	7115(1)	1956(1)	28(1)	1
C(42)	3099(2)	6944(1)	2476(1)	21(1)	1
C(43)	5113(2)	7129(1)	3512(1)	19(1)	1
C(44)	4678(2)	7618(1)	3362(1)	20(1)	1
C(45)	6330(2)	7968(1)	3242(1)	21(1)	1
C(46)	6211(2)	7810(1)	2646(1)	26(1)	1
C(47)	5720(2)	8169(1)	2249(1)	32(1)	1
C(48)	4889(2)	8380(1)	2423(1)	28(1)	1

C(49)	4982(2)	8525(1)	3026(1)	23(1)	1
C(50)	5575(2)	8966(1)	3173(1)	28(1)	1
C(51)	6558(2)	8886(1)	3130(1)	32(1)	1
C(52)	6937(2)	8406(1)	3356(1)	28(1)	1
C(53)	3067(2)	9976(1)	3872(1)	20(1)	1
C(54)	3631(2)	10061(1)	3496(1)	28(1)	1
C(55)	3607(2)	10497(1)	3228(1)	41(1)	1
C(56)	3026(2)	10849(1)	3328(1)	41(1)	1
C(57)	2467(2)	10776(1)	3704(1)	32(1)	1
C(58)	2499(2)	10344(1)	3977(1)	26(1)	1
C(59)	3198(2)	9512(1)	4904(1)	17(1)	1
C(60)	3782(2)	9876(1)	5104(1)	21(1)	1
C(61)	4029(2)	9939(1)	5653(1)	25(1)	1
C(62)	3706(2)	9638(1)	6018(1)	27(1)	1
C(63)	3117(2)	9282(1)	5828(1)	25(1)	1
C(64)	2859(2)	9220(1)	5275(1)	21(1)	1
C(65)	3979(2)	9061(1)	4085(1)	19(1)	1
C(66)	4042(2)	8552(1)	4317(1)	18(1)	1
C(67)	5689(2)	8682(1)	4923(1)	20(1)	1
C(68)	6612(2)	8449(1)	5084(1)	25(1)	1
C(69)	6605(2)	7945(1)	5321(1)	29(1)	1
C(70)	5897(2)	7615(1)	5015(1)	30(1)	1
C(71)	4974(2)	7845(1)	4875(1)	24(1)	1
C(72)	4563(2)	7957(1)	5388(1)	34(1)	1
C(73)	4978(2)	8381(1)	5732(1)	34(1)	1
C(74)	5250(2)	8808(1)	5417(1)	26(1)	1
C(75)	-745(2)	9096(1)	3815(1)	20(1)	1
C(76)	-939(2)	9570(1)	3684(1)	27(1)	1
C(77)	-1470(2)	9839(1)	3972(1)	32(1)	1
C(78)	-1807(2)	9631(1)	4396(1)	32(1)	1
C(79)	-1629(2)	9166(1)	4531(1)	30(1)	1
C(80)	-1098(2)	8890(1)	4242(1)	25(1)	1
C(81)	-370(2)	8867(1)	2757(1)	21(1)	1
C(82)	193(2)	8834(1)	2367(1)	34(1)	1
C(83)	-151(2)	8851(1)	1821(1)	49(1)	1
C(84)	-1041(2)	8921(1)	1657(1)	43(1)	1
C(85)	-1600(2)	8966(1)	2034(1)	35(1)	1
C(86)	-1268(2)	8935(1)	2579(1)	26(1)	1
C(87)	-246(2)	8140(1)	3558(1)	23(1)	1
C(88)	288(2)	7771(1)	3293(1)	24(1)	1
C(89)	332(2)	6858(1)	2912(1)	32(1)	1
C(90)	600(2)	7049(1)	2387(1)	48(1)	1
C(91)	-165(2)	7237(1)	1969(1)	58(1)	1
C(92)	-899(2)	7522(1)	2196(1)	50(1)	1
C(93)	-1144(2)	7323(1)	2721(1)	34(1)	1
C(94)	-1661(2)	6851(1)	2642(1)	44(1)	1
C(95)	-1115(2)	6417(1)	2495(1)	51(1)	1
C(96)	-186(2)	6381(1)	2836(1)	40(1)	1
C(1A)	4461(4)	4097(1)	8574(2)	79(2)	1
C(2A)	4850(3)	4023(1)	9124(2)	68(1)	1
C(3A)	4537(2)	3656(1)	9404(1)	47(1)	1
C(4A)	3877(2)	3369(1)	9159(1)	50(1)	1
C(5A)	3503(2)	3437(2)	8637(2)	67(1)	1
C(6A)	3777(3)	3795(2)	8348(2)	76(2)	1

C(1B)	5504(4)	9619(2)	1710(2)	112(2)	1
C(2B)	5879(4)	10047(2)	1840(2)	118(2)	1
C(3B)	6038(3)	10324(2)	1417(2)	85(1)	1
C(4B)	5860(3)	10161(2)	878(2)	70(1)	1
C(5B)	5489(3)	9742(2)	774(2)	70(1)	1
C(6B)	5311(3)	9460(2)	1188(2)	80(1)	1
C(1D)	2608(3)	9009(2)	1920(2)	80(2)	0.576(4)
C(2D)	2073(3)	9345(2)	1616(2)	91(3)	0.576(4)
C(3D)	1598(3)	9217(2)	1116(2)	77(2)	0.576(4)
C(4D)	1659(3)	8754(2)	921(2)	84(3)	0.576(4)
C(5D)	2195(4)	8418(2)	1226(3)	122(4)	0.576(4)
C(6D)	2670(4)	8545(2)	1725(3)	224(9)	0.576(4)
C(1E)	2819(7)	9773(4)	2014(4)	100(4)	0.424(4)
C(2E)	2863(9)	9309(5)	2064(5)	134(5)	0.424(4)
C(3E)	2415(7)	8966(3)	1574(4)	72(3)	0.424(4)
C(4E)	2387(8)	8491(3)	1677(3)	63(3)	0.424(4)
C(5E)	1818(7)	8244(4)	1151(4)	78(3)	0.424(4)

Dinuclear alkyl-dioxycarbene Compound 11 (ajmm55).

Table 1. Crystal data and structure refinement for AJMM55 (CCDC 776949).

Empirical formula	$C_{44}H_{39}BO_{10}P_2Re_2$	
Formula weight	1172.90	
Crystallization Solvent	Dichloromethane/Toluene	
Crystal Habit	Fragment	
Crystal size	0.10 x 0.09 x 0.03 mm^3	
Crystal color	Colorless	
Data Collection Temperature	100(2) K	
Unit cell dimensions	a = 15.776(2) Å	a= 90°
	b = 16.5631(19) Å	b= 90.322(5)°
	c = 16.523(2) Å	g = 90°
Volume	4317.5(9) $Å^3$	
Z	4	
Crystal system	Monoclinic	
Space group	P $2_1/n$	
Density (calculated)	1.804 Mg/m^3	
q range for data collection	1.74 to 26.41°	
Completeness to θ = 26.41°	98.1 %	
Absorption coefficient	5.733 mm^{-1}	
Absorption correction	Semi-empirical from equivalents	
Refinement method	Full matrix least-squares on F^2	
Data / restraints / parameters	8714 / 12 / 532	
Treatment of hydrogen atoms	Riding	
Goodness-of-fit on F^2	1.229	
Final R indices [I>2s(I), 4950 reflections]	R1 = 0.0658, *w*R2 = 0.0941	
R indices (all data)	R1 = 0.1423, *w*R2 = 0.1068	

Special Refinement Details

This is a small and weakly diffracting crystal. Restraints were placed on the ADP's of atoms C19 and C25 keep them fro going non-positive definite during refinement.

Table 2. Atomic coordinates (x 10^4) and equivalent isotropic displacement parameters ($Å^2$x 10^3) for AJMM55 (CCDC 776949). U(eq) is defined as the trace of the orthogonalized U^{ij} tensor.

	x	y	z	U_{eq}
Re(1)	6728(1)	10615(1)	6770(1)	21(1)
Re(2)	8595(1)	8846(1)	4369(1)	28(1)
P(1)	6569(2)	9536(2)	7797(2)	20(1)
P(2)	7988(2)	9338(2)	3095(2)	29(1)
O(1)	6538(6)	12008(5)	8023(6)	62(3)
O(2)	7207(6)	11874(5)	5452(6)	46(3)
O(3)	4811(5)	10761(4)	6286(5)	36(2)
O(4)	8691(5)	10374(5)	6954(6)	45(3)
O(5)	10382(6)	8206(5)	3971(6)	53(3)
O(6)	7907(7)	7114(6)	4256(9)	127(7)
O(7)	9235(6)	10617(5)	4576(6)	52(3)
O(8)	8780(6)	8647(5)	6239(6)	61(3)
O(9)	7154(5)	9938(5)	5168(5)	34(2)
O(10)	6547(5)	8952(4)	5845(4)	26(2)
B(1)	6062(9)	8448(7)	6519(7)	19(3)

C(1)	6614(8)	11473(6)	7575(7)	27(3)
C(2)	7002(7)	11407(6)	5905(8)	27(3)
C(3)	5511(9)	10700(6)	6504(7)	27(3)
C(4)	7953(8)	10470(5)	6924(7)	25(3)
C(5)	9707(9)	8442(7)	4122(9)	45(4)
C(6)	8134(9)	7765(8)	4258(11)	65(5)
C(7)	9012(7)	9962(7)	4505(7)	28(3)
C(8)	8731(9)	8691(8)	5502(10)	54(5)
C(9)	6805(8)	9664(6)	5844(8)	28(3)
C(10)	6109(8)	7521(6)	6157(7)	33(4)
C(11)	5660(8)	6965(6)	6777(8)	35(4)
C(12)	4756(8)	7167(6)	6937(8)	41(4)
C(13)	4603(8)	8095(6)	7114(7)	31(3)
C(14)	5080(7)	8665(6)	6546(7)	24(3)
C(15)	4727(7)	8673(6)	5681(7)	33(3)
C(16)	4828(8)	7863(6)	5212(7)	34(4)
C(17)	5723(8)	7487(6)	5325(7)	33(4)
C(18)	6616(7)	8539(5)	7342(6)	25(3)
C(19)	7416(7)	9570(5)	8567(6)	14(3)
C(20)	7834(7)	8879(6)	8815(7)	33(3)
C(21)	8437(8)	8908(6)	9417(7)	39(4)
C(22)	8617(8)	9630(7)	9789(7)	41(4)
C(23)	8202(8)	10301(7)	9565(8)	38(4)
C(24)	7588(7)	10304(6)	8970(7)	29(3)
C(25)	5636(8)	9544(6)	8428(7)	26(3)
C(26)	5538(8)	8953(7)	9006(8)	34(3)
C(27)	4833(10)	8904(8)	9496(8)	50(4)
C(28)	4180(8)	9472(8)	9400(8)	42(4)
C(29)	4266(9)	10083(8)	8839(8)	45(4)
C(30)	5009(7)	10135(6)	8354(7)	26(3)
C(31)	7207(8)	9927(6)	3665(7)	33(3)
C(32)	7266(9)	9368(8)	4477(8)	46(4)
C(33)	7386(8)	8673(7)	2419(8)	33(3)
C(34)	6677(8)	8288(6)	2681(8)	38(4)
C(35)	6200(9)	7779(7)	2177(9)	43(4)
C(36)	6494(10)	7686(7)	1391(9)	52(5)
C(37)	7190(9)	8081(8)	1094(9)	52(4)
C(38)	7642(8)	8576(7)	1608(8)	45(4)
C(39)	8573(8)	10016(6)	2455(7)	27(3)
C(40)	8175(8)	10578(7)	1988(7)	38(4)
C(41)	8648(9)	11142(7)	1534(9)	44(4)
C(42)	9510(10)	11073(7)	1523(8)	54(4)
C(43)	9907(9)	10476(7)	1954(8)	46(4)
C(44)	9439(8)	9965(7)	2429(7)	32(3)

[Na][($Ph_2PCH_2B(C_8H_{14})$)$Re(CO)_3(C(O)CH_2O–)$] ([Na][3-M_1], ajmm64).

Table 1. Crystal data and structure refinement for AJMM64 (CCDC 781654).

Empirical formula	$[C_{26}H_{28}BO_5PRe]^+ [Na]^- \bullet 3(C_4H_8O)$	
Formula weight	887.77	
Crystallization Solvent	Pentane/deuterobenzene	
Crystal Habit	Fragment	
Crystal size	0.17 x 0.11 x 0.02 mm^3	
Crystal color	Colorless	
Data Collection Temperature	100(2) K	
q range for 9975 reflections used in lattice determination	2.24 to 25.40°	
Unit cell dimensions	a = 11.6537(4) Å	a= 90°
	b = 27.6665(9) Å	b= 96.479(2)°
	c = 12.1243(4) Å	g = 90°
Volume	3884.1(2) $Å^3$	
Z	4	
Crystal system	Monoclinic	
Space group	P $2_1/n$	
Density (calculated)	1.518 Mg/m^3	
q range for data collection	1.84 to 27.72°	
Completeness to θ = 27.72°	89.9 %	
Index ranges	$-14 \le h \le 14$, $-35 \le k \le 34$, $-14 \le l \le 15$	
Absorption coefficient	3.230 mm^{-1}	
Absorption correction	Gaussian	
Refinement method	Full matrix least-squares on F^2	
Data / restraints / parameters	8198 / 0 / 451	
Treatment of hydrogen atoms	Riding	
Goodness-of-fit on F^2	1.487	
Final R indices [I>2s(I), 6185 reflections]	R1 = 0.0401, *w*R2 = 0.0514	
R indices (all data)	R1 = 0.0624, *w*R2 = 0.0528	

Table 2. Atomic coordinates (x 10^4) and equivalent isotropic displacement parameters ($Å^2$x 10^3) for AJMM64 (CCDC 781654). U(eq) is defined as the trace of the orthogonalized U^{ij} tensor.

	x	y	z	U_{eq}
Re(1)	2791(1)	3559(1)	2115(1)	16(1)
P(1)	3896(1)	4127(1)	1068(1)	14(1)
Na(1)	6474(2)	2740(1)	4390(1)	28(1)
O(1)	1769(3)	2847(1)	3710(3)	39(1)
O(2)	2932(3)	2714(1)	519(3)	32(1)
O(3)	356(3)	3808(1)	909(3)	31(1)
O(4)	3087(2)	4161(1)	3308(2)	16(1)
O(5)	5107(3)	3232(1)	3579(3)	29(1)
O(6)	7883(3)	3244(1)	3973(3)	35(1)
O(7)	5498(3)	2672(1)	5948(3)	39(1)
O(8)	6166(3)	2145(1)	3094(3)	66(1)
B(1)	3159(4)	4696(2)	2878(4)	15(1)
C(1)	2111(4)	3126(2)	3114(4)	28(1)
C(2)	2868(4)	3046(2)	1151(4)	25(1)
C(3)	1287(4)	3731(1)	1342(4)	21(1)
C(4)	4114(4)	3962(2)	3914(3)	22(1)

C(5)	4310(3)	3501(2)	3262(3)	19(1)
C(6)	3635(4)	5059(1)	3874(3)	16(1)
C(7)	2884(4)	5004(2)	4840(3)	20(1)
C(8)	1586(4)	5083(2)	4518(3)	23(1)
C(9)	1113(3)	4826(2)	3438(3)	18(1)
C(10)	1866(3)	4871(1)	2473(3)	14(1)
C(11)	1898(4)	5386(1)	1999(3)	19(1)
C(12)	2526(3)	5761(1)	2784(3)	20(1)
C(13)	3662(4)	5577(1)	3419(3)	20(1)
C(14)	4076(3)	4670(1)	1916(3)	15(1)
C(15)	3261(3)	4327(1)	-311(3)	13(1)
C(16)	2177(4)	4546(1)	-425(3)	16(1)
C(17)	1664(4)	4705(1)	-1441(3)	19(1)
C(18)	2232(4)	4646(2)	-2375(4)	22(1)
C(19)	3298(4)	4432(2)	-2281(4)	23(1)
C(20)	3820(4)	4275(1)	-1255(3)	17(1)
C(21)	5324(4)	3922(1)	788(3)	14(1)
C(22)	5499(4)	3443(1)	507(3)	21(1)
C(23)	6553(4)	3286(2)	234(4)	27(1)
C(24)	7467(4)	3602(2)	256(3)	23(1)
C(25)	7316(4)	4077(2)	540(3)	19(1)
C(26)	6256(4)	4236(2)	794(3)	16(1)
C(27)	7608(4)	3720(2)	3542(4)	35(1)
C(28)	8725(4)	3963(2)	3369(4)	30(1)
C(29)	9603(4)	3680(2)	4144(4)	37(1)
C(30)	9110(4)	3180(2)	4022(4)	40(2)
C(31)	5637(5)	3052(2)	6746(5)	58(2)
C(32)	4576(5)	3049(2)	7340(5)	62(2)
C(33)	3673(5)	2842(2)	6483(5)	64(2)
C(34)	4357(4)	2492(2)	5885(4)	41(2)
C(35)	5277(5)	2215(2)	2158(5)	71(2)
C(36)	4400(4)	1870(2)	2359(5)	62(2)
C(37)	5149(5)	1438(2)	2794(5)	81(2)
C(38)	6281(5)	1633(2)	3192(4)	46(2)

[Na][(PPh$_3$)(Ph$_2$P(CH$_2$)$_2$B(C$_8$H$_{14}$))Re(CO)$_2$(C(O)CH$_2$O–)] ([Na][3-E$_1$Ph$_1$], ajmm48).

Table 1. Crystal data and structure refinement for AJMM48 (CCDC 770346).

Empirical formula	$C_{56}H_{69}BNaO_7P_2Re$	
Formula weight	1136.05	
Crystallization Solvent	THF	
Crystal Habit	Block	
Crystal size	0.21 x 0.21 x 0.19 mm^3	
Crystal color	Colorless	
Data Collection Temperature	100(2) K	
Unit cell dimensions	a = 10.8404(4) Å	a= 80.396(2)°
	b = 12.8132(5) Å	b= 81.298(2)°
	c = 20.4220(7) Å	g = 65.477(2)°
Volume	2533.91(16) Å^3	
Z	2	
Crystal system	Triclinic	
Space group	P-1	
Density (calculated)	1.489 Mg/m^3	
q range for data collection	1.76 to 49.89°	
Completeness to θ = 49.89°	99.1 %	
Index ranges	-22 ≤ h ≤ 23, -27 ≤ k ≤ 27, -43 ≤ l ≤ 43	
Absorption coefficient	2.522 mm^{-1}	
Absorption correction	Semi-empirical from equivalents	
Refinement method	Full matrix least-squares on F^2	
Data / restraints / parameters	52421 / 0 / 613	
Treatment of hydrogen atoms	Riding	
Goodness-of-fit on F^2	1.289	
Final R indices [I>2s(I), 46790 reflections]	R1 = 0.0233, *w*R2 = 0.0399	
R indices (all data)	R1 = 0.0299, *w*R2 = 0.0407	

Table 2. Atomic coordinates (x 10^4) and equivalent isotropic displacement parameters (Å^{2}x 10^3) for AJMM48 (CCDC 770346). U(eq) is defined as the trace of the orthogonalized U^{ij} tensor.

	x	y	z	U_{eq}
Re(1)	8307(1)	6674(1)	7744(1)	7(1)
P(1)	7623(1)	8394(1)	8269(1)	8(1)
P(2)	9031(1)	4829(1)	7327(1)	9(1)
Na(1)	3113(1)	7110(1)	7741(1)	13(1)
O(1)	11150(1)	6783(1)	7445(1)	18(1)
O(2)	9054(1)	5179(1)	9071(1)	18(1)
O(3)	5224(1)	6857(1)	7982(1)	13(1)
O(4)	7378(1)	7816(1)	6833(1)	9(1)
O(5)	3119(1)	5810(1)	8669(1)	18(1)
O(6)	2139(1)	9100(1)	7554(1)	19(1)
O(7)	3896(1)	6686(1)	6674(1)	19(1)
B(1)	7315(1)	9051(1)	6539(1)	9(1)
C(1)	10099(1)	6714(1)	7553(1)	10(1)
C(2)	8763(1)	5760(1)	8564(1)	11(1)
C(3)	6222(1)	7019(1)	7677(1)	10(1)
C(4)	6080(1)	7737(1)	7000(1)	11(1)

C(5)	8843(1)	8917(1)	6232(1)	10(1)
C(6)	9418(1)	8040(1)	5717(1)	13(1)
C(7)	8496(1)	8255(1)	5161(1)	16(1)
C(8)	6963(1)	8648(1)	5384(1)	14(1)
C(9)	6403(1)	9529(1)	5898(1)	11(1)
C(10)	6374(1)	10723(1)	5594(1)	15(1)
C(11)	7782(1)	10771(1)	5416(1)	16(1)
C(12)	8802(1)	10121(1)	5942(1)	14(1)
C(13)	8738(1)	8276(1)	8895(1)	10(1)
C(14)	9801(1)	8649(1)	8728(1)	16(1)
C(15)	10657(1)	8537(1)	9204(1)	21(1)
C(16)	10472(1)	8040(1)	9850(1)	21(1)
C(17)	9435(1)	7646(1)	10018(1)	20(1)
C(18)	8570(1)	7771(1)	9546(1)	15(1)
C(19)	5961(1)	8921(1)	8758(1)	11(1)
C(20)	5198(1)	10097(1)	8810(1)	16(1)
C(21)	3978(1)	10465(1)	9217(1)	20(1)
C(22)	3508(1)	9664(1)	9583(1)	19(1)
C(23)	4251(1)	8495(1)	9531(1)	17(1)
C(24)	5466(1)	8123(1)	9115(1)	13(1)
C(25)	7630(1)	9636(1)	7691(1)	11(1)
C(26)	6693(1)	9905(1)	7134(1)	12(1)
C(27)	8493(1)	3781(1)	7891(1)	12(1)
C(28)	7111(1)	4128(1)	8108(1)	23(1)
C(29)	6616(1)	3343(1)	8480(1)	27(1)
C(30)	7496(1)	2210(1)	8652(1)	20(1)
C(31)	8873(1)	1863(1)	8452(1)	21(1)
C(32)	9369(1)	2643(1)	8071(1)	18(1)
C(33)	10893(1)	4065(1)	7220(1)	12(1)
C(34)	11640(1)	3749(1)	7775(1)	16(1)
C(35)	13057(1)	3230(1)	7701(1)	21(1)
C(36)	13752(1)	3021(1)	7072(1)	22(1)
C(37)	13021(1)	3328(1)	6520(1)	21(1)
C(38)	11603(1)	3848(1)	6589(1)	17(1)
C(39)	8597(1)	4655(1)	6532(1)	12(1)
C(40)	8334(1)	5571(1)	6025(1)	14(1)
C(41)	8168(1)	5424(1)	5385(1)	19(1)
C(42)	8268(1)	4361(1)	5254(1)	21(1)
C(43)	8502(1)	3453(1)	5761(1)	21(1)
C(44)	8661(1)	3594(1)	6400(1)	17(1)
C(45)	2028(1)	5445(1)	8908(1)	16(1)
C(46)	2625(1)	4435(1)	9432(1)	20(1)
C(47)	3577(1)	4779(1)	9749(1)	25(1)
C(48)	3777(1)	5741(1)	9244(1)	19(1)
C(49)	2669(1)	9827(1)	7775(1)	17(1)
C(50)	2770(1)	10683(1)	7168(1)	17(1)
C(51)	2026(1)	10499(1)	6643(1)	22(1)
C(52)	1276(1)	9796(1)	7044(1)	19(1)
C(53)	3458(1)	7300(1)	6042(1)	25(1)
C(54)	4344(1)	6510(1)	5526(1)	26(1)
C(55)	4605(1)	5322(1)	5901(1)	29(1)
C(56)	4708(1)	5485(1)	6603(1)	30(1)

$(PPh_3)(Ph_2P(CH_2)_2B(C_8H_{14}))Re(CO)_2(C(OCH_3)CH_2O–)$ (13, ajmm50).

Table 1. Crystal data and structure refinement for AJMM50 (CCDC 738920).

Empirical formula	$C_{45}H_{48}BO_4P_2Re \bullet ½ (C_6H_5Cl)$	
Formula weight	968.06	
Crystallization Solvent	Chlorobenzene	
Crystal Habit	Block	
Crystal size	0.27 x 0.22 x 0.19 mm^3	
Crystal color	Yellow	
Data Collection Temperature	100(2) K	
Unit cell dimensions	a = 11.4898(4) Å	a= 80.831(2)°
	b = 13.5141(5) Å	b= 84.498(2)°
	c = 15.1385(5) Å	g = 64.883(2)°
Volume	2100.11(13) $Å^3$	
Z	2	
Crystal system	Triclinic	
Space group	P-1	
Density (calculated)	1.531 Mg/m^3	
q range for data collection	1.68 to 53.10°	
Completeness to θ = 53.10°	94.1 %	
Index ranges	$-24 \le h \le 25, -23 \le k \le 30, -34 \le l \le 34$	
Absorption coefficient	3.045 mm^{-1}	
Absorption correction	Semi-empirical from equivalents	
Refinement method	Full matrix least-squares on F^2	
Data / restraints / parameters	47162 / 0 / 540	
Treatment of hydrogen atoms	Riding	
Goodness-of-fit on F^2	1.413	
Final R indices [I>2s(I), 40639 reflections]	R1 = 0.0243, *w*R2 = 0.0396	
R indices (all data)	R1 = 0.0350, *w*R2 = 0.0405	

Special Refinement Details

The crystal contains chlorobenzene as a solvent of crystallization and occupies a site near a center of symmetry, occupancy = ½. Additionally, the chlorine position is disordered over two sites in a 4:1 ratio and was modeled as such. The benzene ring was constrained to an ideal hexagon and aside from riding hydrogen atoms no other restraints were applied.

Table 2. Atomic coordinates (x 10^4) and equivalent isotropic displacement parameters ($Å^2$x 10^3) for AJMM50 (CCDC 738920). U(eq) is defined at he trace of the orthogonalized U^{ij} tensor.

	x	y	z	U_{eq}	Occ
Re(1)	3818(1)	4048(1)	2615(1)	8(1)	1
P(1)	1838(1)	5510(1)	2043(1)	9(1)	1
P(2)	5815(1)	2700(1)	3303(1)	10(1)	1
O(1)	2332(1)	2840(1)	3843(1)	22(1)	1
O(2)	3809(1)	5574(1)	3901(1)	18(1)	1
O(3)	3967(1)	3220(1)	1424(1)	10(1)	1
O(4)	5521(1)	4971(1)	1244(1)	16(1)	1
B(1)	2861(1)	3221(1)	867(1)	11(1)	1
C(1)	2856(1)	3308(1)	3407(1)	13(1)	1
C(2)	3813(1)	4965(1)	3427(1)	12(1)	1
C(3)	4807(1)	3665(1)	932(1)	13(1)	1
C(4)	4853(1)	4404(1)	1554(1)	11(1)	1

C(5)	5552(1)	5752(1)	1794(1)	20(1)	1
C(6)	1032(1)	5184(1)	1219(1)	12(1)	1
C(7)	1918(1)	4499(1)	507(1)	13(1)	1
C(8)	2129(1)	2560(1)	1504(1)	12(1)	1
C(9)	3102(1)	1418(1)	1905(1)	15(1)	1
C(10)	4032(1)	708(1)	1221(1)	16(1)	1
C(11)	4531(1)	1331(1)	445(1)	14(1)	1
C(12)	3552(1)	2479(1)	63(1)	12(1)	1
C(13)	2529(1)	2420(1)	-491(1)	16(1)	1
C(14)	1607(1)	1997(1)	70(1)	18(1)	1
C(15)	1101(1)	2504(1)	945(1)	17(1)	1
C(16)	1993(1)	6766(1)	1508(1)	13(1)	1
C(17)	2210(1)	7422(1)	2046(1)	21(1)	1
C(18)	2326(1)	8386(1)	1662(1)	28(1)	1
C(19)	2215(1)	8708(1)	746(1)	30(1)	1
C(20)	1984(1)	8073(1)	208(1)	28(1)	1
C(21)	1880(1)	7100(1)	589(1)	19(1)	1
C(22)	533(1)	6112(1)	2854(1)	11(1)	1
C(23)	664(1)	5815(1)	3776(1)	15(1)	1
C(24)	-351(1)	6322(1)	4364(1)	18(1)	1
C(25)	-1518(1)	7117(1)	4036(1)	19(1)	1
C(26)	-1660(1)	7410(1)	3118(1)	19(1)	1
C(27)	-647(1)	6921(1)	2532(1)	16(1)	1
C(28)	6906(1)	3366(1)	3347(1)	13(1)	1
C(29)	6885(1)	3922(1)	4051(1)	15(1)	1
C(30)	7661(1)	4494(1)	4011(1)	20(1)	1
C(31)	8474(1)	4503(1)	3278(1)	22(1)	1
C(32)	8511(1)	3942(1)	2577(1)	24(1)	1
C(33)	7728(1)	3382(1)	2604(1)	19(1)	1
C(34)	5597(1)	2133(1)	4461(1)	14(1)	1
C(35)	6026(1)	995(1)	4709(1)	21(1)	1
C(36)	5828(1)	574(1)	5588(1)	27(1)	1
C(37)	5227(1)	1275(1)	6224(1)	28(1)	1
C(38)	4786(1)	2409(1)	5984(1)	24(1)	1
C(39)	4948(1)	2834(1)	5103(1)	18(1)	1
C(40)	6902(1)	1480(1)	2803(1)	14(1)	1
C(41)	8198(1)	936(1)	3042(1)	24(1)	1
C(42)	9042(1)	60(1)	2612(1)	28(1)	1
C(43)	8622(1)	-298(1)	1945(1)	22(1)	1
C(44)	7334(1)	208(1)	1731(1)	19(1)	1
C(45)	6476(1)	1096(1)	2157(1)	15(1)	1
Cl(1A)	-1382(2)	11699(1)	5630(1)	84(1)	0.403(1)
Cl(1B)	766(3)	11349(3)	4151(3)	42(1)	0.097(1)
C(1A)	-512(2)	10429(1)	5294(1)	41(1)	0.50
C(2A)	-870(1)	9578(2)	5640(1)	44(1)	0.50
C(3A)	-192(2)	8536(1)	5380(1)	45(1)	0.50
C(4A)	843(2)	8345(1)	4772(1)	43(1)	0.50
C(5A)	1200(1)	9195(2)	4426(1)	48(1)	0.50
C(6A)	523(2)	10237(1)	4686(1)	46(1)	0.50

Chapter 4 Crystallographic Tables

$[(Ph_2P(CH_2)_2B(C_8H_{14}))_2Re(CO)_4][BF_4]\bullet(THF)_2$ ($1\bullet(THF)_2$, ajmm49).

Table 1. Crystal data and structure refinement for AJMM49 (CCDC 759590).

Empirical formula	$[C_{56}H_{72}B_2O_6P_2Re]^+ [BF_4]^-$	
Formula weight	1197.71	
Crystallization Solvent	THF/pentane	
Crystal Habit	Block	
Crystal size	0.27 x 0.26 x 0.19 mm^3	
Crystal color	Colorless	
Data Collection Temperature	100(2) K	
Unit cell dimensions	a = 9.7744(4) Å	a= 92.554(2)°
	b = 10.3565(4) Å	b= 104.359(2)°
	c = 14.9063(6) Å	g = 105.481(2)°
Volume	1398.82(10) $Å^3$	
Z	1	
Crystal system	Triclinic	
Space group	P-1	
Density (calculated)	1.422 Mg/m^3	
θ range for data collection	2.25 to 49.35°	
Completeness to θ = 49.35°	98.4 %	
Index ranges	$-20 \le h \le 20$, $-21 \le k \le 22$, $-31 \le l \le 31$	
Absorption coefficient	2.290 mm^{-1}	
Absorption correction	Semi-empirical from equivalents	
Refinement method	Full matrix least-squares on F^2	
Data / restraints / parameters	28016 / 0 / 349	
Treatment of hydrogen atoms	Riding	
Goodness-of-fit on F^2	2.373	
Final R indices [I>2s(I), 27766 reflections]	R1 = 0.0306, *w*R2 = 0.0591	
R indices (all data)	R1 = 0.0311, *w*R2 = 0.0592	

Special Refinement Details

The tetrafluoroborate anion is disordered about a center of symmetry and is modeled with no restraints. The Re atom sits at a center of symmetry.

Table 2. Atomic coordinates (x 10^4) and equivalent isotropic displacement parameters ($Å^2$x 10^3) for AJMM49 (CCDC 759590). U(eq) is defined as the trace of the orthogonalized U^{ij} tensor.

	x	y	z	U_{eq}
Re(1)	5000	5000	5000	13(1)
P(1)	5234(1)	5965(1)	3568(1)	16(1)
O(1)	6268(3)	2696(2)	4500(1)	104(1)
O(2)	1977(2)	2936(2)	3964(1)	80(1)
O(3)	5825(1)	2594(1)	1400(1)	33(1)
B(1)	4152(2)	2772(1)	1366(1)	30(1)
C(1)	5863(2)	3567(2)	4688(1)	45(1)
C(2)	3049(2)	3719(2)	4344(1)	39(1)
C(3)	6713(1)	7536(1)	3723(1)	24(1)
C(4)	8039(2)	7563(2)	3540(1)	49(1)

C(5)	9140(2)	8784(3)	3654(2)	70(1)
C(6)	8929(2)	9963(2)	3955(2)	62(1)
C(7)	7643(2)	9945(2)	4146(2)	59(1)
C(8)	6519(2)	8735(1)	4027(1)	43(1)
C(9)	3681(1)	6478(1)	2901(1)	27(1)
C(10)	3824(2)	7153(1)	2124(1)	43(1)
C(11)	2671(3)	7590(2)	1618(1)	63(1)
C(12)	1402(3)	7403(2)	1881(2)	79(1)
C(13)	1255(2)	6749(3)	2632(3)	84(1)
C(14)	2381(2)	6273(2)	3151(2)	50(1)
C(15)	5560(1)	4868(1)	2699(1)	25(1)
C(16)	4300(2)	3546(1)	2373(1)	30(1)
C(17)	3042(2)	1260(1)	1156(1)	34(1)
C(18)	1497(2)	1378(1)	1146(1)	38(1)
C(19)	934(2)	2314(1)	459(1)	40(1)
C(20)	2098(2)	3651(1)	439(1)	36(1)
C(21)	3655(2)	3537(1)	473(1)	31(1)
C(22)	3698(2)	2794(1)	-437(1)	36(1)
C(23)	2852(2)	1283(1)	-620(1)	41(1)
C(24)	3088(2)	523(1)	245(1)	39(1)
C(25)	7013(2)	3608(1)	1165(1)	38(1)
C(26)	8428(2)	3638(2)	1909(1)	49(1)
C(27)	8097(2)	2189(2)	2134(1)	47(1)
C(28)	6472(2)	1819(1)	2106(1)	41(1)
B(2)	9772(3)	4397(4)	4887(3)	36(1)
F(1)	8569(3)	4842(3)	4623(3)	80(1)
F(2)	9290(4)	3035(3)	4893(4)	121(2)
F(3)	10636(4)	4693(6)	4351(4)	145(2)
F(4)	10567(5)	4993(3)	5779(2)	93(1)

Appendix A Crystallographic Tables

$(C_5Me_4ArNMe_2)Re(CO)_3$ (1, ajmm16)

Table 1. Crystal data and structure refinement for AJMM16 (CCDC 650764).

Empirical formula	$C_{20}H_{22}NO_3Re$	
Formula weight	510.59	
Crystallization Solvent	Hexanes	
Crystal Habit	Block	
Crystal size	0.33 x 0.22 x 0.16 mm^3	
Crystal color	Colorless	
Data Collection Temperature	100(2) K	
Unit cell dimensions	a = 7.9326(2) Å	
	b = 8.3019(2) Å	b= 96.9710(10)°
	c = 14.6614(4) Å	
Volume	958.40(4) $Å^3$	
Z	2	
Crystal system	Monoclinic	
Space group	$P2_1$	
Density (calculated)	1.769 Mg/m^3	
θ range for data collection	2.59 to 47.28°	
Completeness to θ = 47.28°	91.0 %	
Index ranges	$-16 \le h \le 16$, $-15 \le k \le 16$, $-28 \le l \le 28$	
Absorption coefficient	6.357 mm^{-1}	
Absorption correction	Semi-empirical from equivalents	
Refinement method	Full matrix least-squares on F^2	
Data / restraints / parameters	12762 / 1 / 232	
Treatment of hydrogen atoms	Riding	
Goodness-of-fit on F^2	1.293	
Final R indices [I>2s(I), 11217 reflections]	R1 = 0.0368, *w*R2 = 0.0765	
R indices (all data)	R1 = 0.0445, *w*R2 = 0.0783	

Table 2. Atomic coordinates (x 10^4) and equivalent isotropic displacement parameters ($Å^2$x 10^3) for AJMM16 (CCDC 650764). U(eq) is defined as the trace of the orthogonalized U^{ij} tensor.

	x	y	z	U_{eq}
Re(1)	5225(1)	-1475(1)	8099(1)	14(1)
O(1)	2530(4)	-1825(5)	6424(2)	37(1)
O(2)	4378(5)	-4882(4)	8726(3)	37(1)
O(3)	2572(4)	-81(4)	9246(2)	29(1)
N(1)	9292(4)	1775(4)	6432(2)	20(1)
C(1)	3532(4)	-1695(5)	7062(3)	23(1)
C(2)	4683(5)	-3599(4)	8488(3)	22(1)
C(3)	3545(4)	-626(4)	8804(2)	19(1)
C(4)	6977(3)	461(4)	7585(2)	14(1)
C(5)	7522(4)	-1111(3)	7286(2)	16(1)
C(6)	8091(4)	-2027(4)	8088(2)	18(1)
C(7)	7897(4)	-1053(4)	8879(2)	17(1)
C(8)	7214(4)	474(4)	8566(2)	15(1)

C(9)	7634(4)	-1643(5)	6310(2)	19(1)
C(10)	8868(5)	-3681(5)	8093(3)	27(1)
C(11)	8513(4)	-1430(11)	9860(2)	23(1)
C(12)	6976(5)	1896(4)	9170(3)	21(1)
C(13)	6501(4)	1867(4)	6973(2)	15(1)
C(14)	4940(4)	2630(4)	6973(3)	21(1)
C(15)	4454(5)	3919(4)	6401(3)	25(1)
C(16)	5550(5)	4444(5)	5791(3)	26(1)
C(17)	7131(4)	3734(6)	5795(2)	23(1)
C(18)	7660(4)	2469(4)	6400(2)	17(1)
C(19)	10394(4)	2022(5)	7295(3)	25(1)
C(20)	10207(5)	2047(6)	5642(3)	29(1)

[(C5Me4ArNHMe2)Re(CO)3][BF4] (2, ajmm17).

Table 1. Crystal data and structure refinement for AJMM17 (CCDC 650764).

Empirical formula	$[C_{20}H_{23}NO_3Re]^+ [BF_4]^-$
Formula weight	598.40
Crystallization Solvent	Dichloromethane
Crystal Habit	Plate
Crystal size	0.33 x 0.29 x 0.07 mm^3
Crystal color	Colorless
Data Collection Temperature	100(2) K
Unit cell dimensions	a = 11.9180(3) Å b = 14.8020(4) Å c = 12.3664(3) Å
Volume	2181.56(10) $Å^3$
Z	4
Crystal system	Orthorhombic
Space group	$Pca2_1$
Density (calculated)	1.822 Mg/m^3
θ range for data collection	2.19 to 47.16°
Completeness to θ = 47.16°	94.2 %
Index ranges	$-24 \le h \le 24$, $-30 \le k \le 21$, $-25 \le l \le 22$
Absorption coefficient	5.624 mm^{-1}
Absorption correction	Semi-empirical from equivalents
Refinement method	Full matrix least-squares on F^2
Treatment of hydrogen atoms	Riding
Goodness-of-fit on F^2	1.124
Final R indices [I>2s(I), 13046 reflections]	R1 = 0.0334, *w*R2 = 0.0640
R indices (all data)	R1 = 0.0514, *w*R2 = 0.0690

Table 2. Atomic coordinates (x 10^4) and equivalent isotropic displacement parameters ($Å^2$x 10^3) for AJMM17 (CCDC 650764). U(eq) is defined as the trace of the orthogonalized U^{ij} tensor.

	x	y	z	U_{eq}
Re(1)	4851(1)	3842(1)	1191(1)	10(1)
O(1)	5974(3)	3784(2)	-1051(2)	33(1)
O(2)	2830(2)	4908(1)	323(2)	20(1)
O(3)	5942(2)	5646(1)	1821(2)	29(1)
N(1)	6507(2)	1002(1)	3011(2)	16(1)
C(1)	5546(2)	3836(2)	-216(2)	19(1)
C(2)	3593(2)	4510(2)	632(2)	14(1)
C(3)	5547(2)	4973(2)	1544(2)	17(1)
C(4)	5739(2)	2668(2)	2038(2)	12(1)
C(5)	4807(2)	2294(2)	1413(2)	14(1)
C(6)	3797(2)	2655(2)	1860(2)	14(1)
C(7)	4073(2)	3244(2)	2749(2)	14(1)
C(8)	5272(2)	3244(2)	2860(2)	14(1)
C(9)	4897(2)	1603(2)	531(2)	19(1)
C(10)	2620(2)	2393(2)	1535(2)	20(1)
C(11)	3260(2)	3686(2)	3503(2)	20(1)
C(12)	5926(3)	3724(2)	3718(3)	23(1)
C(13)	6947(2)	2397(2)	1978(2)	13(1)
C(14)	7760(2)	2958(2)	1502(2)	16(1)

C(15)	8888(2)	2712(2)	1501(2)	20(1)
C(16)	9227(2)	1906(2)	1958(3)	24(1)
C(17)	8441(2)	1335(2)	2431(3)	22(1)
C(18)	7319(2)	1597(2)	2446(2)	16(1)
C(19)	6743(2)	952(2)	4203(2)	21(1)
C(20)	6455(2)	70(2)	2519(2)	21(1)
B(1)	3795(2)	1078(2)	4207(3)	18(1)
F(1)	3944(2)	347(1)	4895(2)	34(1)
F(2)	2667(2)	1298(1)	4129(2)	29(1)
F(3)	4182(1)	819(1)	3165(1)	24(1)
F(4)	4435(2)	1806(1)	4551(2)	26(1)

[(η^6-$C_5Me_4ArNMe_2$)$Re(CO)_2$][BF_4] (7, ajmm20).

Table 1. Crystal data and structure refinement for (AJMM20) (CCDC 796319).

Empirical formula	$[C_{14}H_{22}N_2O_2Re]^+ [PF_6]^-$	
Formula weight	581.51	
Crystallization Solvent	Not given	
Crystal Habit	Needle	
Crystal size	0.21 x 0.03 x 0.03 mm^3	
Crystal color	Orange	
Data Collection Temperature	100(2) K	
Unit cell dimensions	a = 8.7993(6) Å	a= 90°
	b = 8.7993(6) Å	b= 90°
	c = 23.6102(19) Å	g = 90°
Volume	1828.1(2) $Å^3$	
Z	4	
Crystal system	Tetragonal	
Space group	P 4_3	
Density (calculated)	2.113 Mg/m^3	
θ range for data collection	2.31 to 27.48°	
Absorption coefficient	6.804 mm^{-1}	
Absorption correction	Semi-empirical from equivalents	
Primary solution method	Direct methods	
Secondary solution method	Difference Fourier map	
Hydrogen placement	Geometric positions	
Refinement method	Full matrix least-squares on F^2	
Treatment of hydrogen atoms	Riding	
Goodness-of-fit on F^2	1.340	
Final R indices [I>2s(I), 3549 reflections]	R1 = 0.0379, *w*R2 = 0.0662	
R indices (all data)	R1 = 0.0509, *w*R2 = 0.0686	
Type of weighting scheme used	Sigma	
Weighting scheme used	$w=1/s^2(Fo^2)$	

Special Refinement Details

We were not able to distinguish between carbonyl and nitrosyl positions so the corresponding carbon and nitrogen atoms were refined as a 50:50 mixture.

Table 2. Atomic coordinates (x 10^4) and equivalent isotropic displacement parameters ($Å^2$x 10^3) for AJMM20 (CCDC 796319). U(eq) is defined as the trace of the orthogonalized U^{ij} tensor.

	x	y	z	U_{eq}
Re(1)	4264(1)	934(1)	7501(1)	22(1)
O(1)	7383(7)	523(7)	6984(3)	45(2)
O(2)	3103(7)	3116(7)	6628(3)	40(2)
N(1)	4780(7)	2430(7)	8215(3)	26(2)
C(1A)	6185(9)	792(8)	7181(4)	29(2)
N(2A)	6185(9)	792(8)	7181(4)	29(2)
C(2B)	3591(8)	2316(8)	6974(3)	25(2)
N(2B)	3591(8)	2316(8)	6974(3)	25(2)
C(3)	3161(8)	-310(8)	8239(3)	20(2)

C(4)	2026(9)	-34(8)	7825(4)	24(2)
C(5)	2452(8)	-828(8)	7319(3)	24(2)
C(6)	3839(7)	-1597(7)	7434(4)	21(2)
C(7)	4311(9)	-1302(9)	7993(4)	25(2)
C(8)	511(9)	741(9)	7925(4)	30(2)
C(9)	1519(9)	-925(9)	6785(4)	31(2)
C(10)	4655(9)	-2685(10)	7033(4)	34(2)
C(11)	5679(9)	-1947(10)	8300(4)	36(2)
C(12)	3316(9)	515(8)	8791(4)	26(2)
C(13)	3611(11)	2177(10)	8668(4)	45(2)
C(14)	4830(13)	4049(9)	8074(4)	54(3)
C(15)	6316(10)	2096(11)	8461(4)	50(3)
P(1)	-268(3)	5430(3)	7807(1)	42(1)
F(1)	-1134(6)	4012(6)	7571(4)	64(2)
F(2)	1105(7)	5139(12)	7416(5)	102(3)
F(3)	395(9)	4470(7)	8298(3)	98(3)
F(4)	-1070(10)	6465(10)	7369(5)	138(4)
F(5)	476(10)	6872(7)	8050(3)	106(3)
F(6)	-1688(8)	5700(9)	8198(3)	100(3)

Appendix B Crystallographic Tables

$KHBEt_3$ (ajmm38).

Table 1. Crystal data and structure refinement for AJMM38 (CCDC 796321).

Empirical formula	$[C_6H_{16}B]^- K^+$	
Formula weight	138.10	
Crystallization Solvent	Toluene	
Crystal Habit	Block	
Crystal size	0.19 x 0.11 x 0.11 mm^3	
Crystal color	Colorless	
Data Collection Temperature	100(2) K	
Unit cell dimensions	a = 7.4674(5) Å	a= 90°
	b = 7.6679(6) Å	b= 90°
	c = 14.8055(11) Å	g = 90°
Volume	847.75(11) $Å^3$	
Z	4	
Crystal system	Orthorhombic	
Space group	$P\ 2_12_12_1$	
Density (calculated)	1.082 Mg/m^3	
θ range for data collection	2.75 to 34.95°	
Completeness to θ = 34.95°	98.0 %	
Index ranges	$-11 \le h \le 10, -12 \le k \le 11, -23 \le l \le 23$	
Reflections collected	30389	
Independent reflections	3592 [R_{int}= 0.0800]	
Absorption coefficient	0.536 mm^{-1}	
Absorption correction	None	
Primary solution method	Direct methods	
Secondary solution method	Difference Fourier map	
Hydrogen placement	Difference Fourier map	
Refinement method	Full matrix least-squares on F^2	
Data / restraints / parameters	3592 / 0 / 137	
Treatment of hydrogen atoms	Unrestrained	
Goodness-of-fit on F^2	1.286	
Final R indices [I>2s(I), 3241 reflections]	R1 = 0.0238, *w*R2 = 0.0439	
R indices (all data)	R1 = 0.0289, *w*R2 = 0.0445	
Type of weighting scheme used	Sigma	
Weighting scheme used	$w=1/s^2(Fo^2)$	

Table 2. Atomic coordinates (x 10^4) and equivalent isotropic displacement parameters (Å^{2}x 10^3) for AJMM38 (CCDC 796321). U(eq) is defined as the trace of the orthogonalized U^{ij} tensor.

	x	y	z	U_{eq}
K(1)	2231(1)	6266(1)	5707(1)	17(1)
B(1)	2627(1)	8873(1)	4027(1)	13(1)
C(1)	1429(1)	10264(1)	4615(1)	18(1)
C(2)	2467(1)	11737(1)	5076(1)	26(1)
C(3)	1319(1)	7365(1)	3595(1)	14(1)
C(4)	2246(2)	5955(1)	3036(1)	25(1)
C(5)	3825(1)	9836(1)	3244(1)	15(1)
C(6)	2754(2)	10701(1)	2485(1)	24(1)

18c6/KHBEt3 (ajmm34)

Table 1. Crystal data and structure refinement for AJMM34 (CCDC 796320).

Empirical formula	$[C_{12}H_{24}KO_6]^+ [C_6H_{16}B]^-$	
Formula weight	402.41	
Crystallization Solvent	Chlorobenzene	
Crystal Habit	Block	
Crystal size	0.26 x 0.25 x s0.23 mm^3	
Crystal color	Colorless	
Data Collection Temperature	100(2) K	
Unit cell dimensions	a = 15.2147(8) Å	a= 90°
	b = 38.660(2) Å	b= 90.331(3)°
	c = 15.5890(9) Å	g = 90°
Volume	9169.3(9) $Å^3$	
Z	16	
Crystal system	Monoclinic	
Space group	P $2_1/c$	
Density (calculated)	1.166 Mg/m^3	
θ range for data collection	1.31 to 30.31°	
Completeness to θ = 30.31°	93.1 %	
Index ranges	$-21 \le h \le 21$, $-54 \le k \le 30$, $-21 \le l \le 21$	
Reflections collected	104729	
Independent reflections	25606 [R_{int}= 0.0801]	
Absorption coefficient	0.259 mm^{-1}	
Absorption correction	None	
Primary solution method	Direct methods	
Secondary solution method	Difference Fourier map	
Hydrogen placement	Geometric positions	
Refinement method	Full matrix least-squares on F^2	
Data / restraints / parameters	25606 / 0 / 950	
Treatment of hydrogen atoms	Riding	
Goodness-of-fit on F^2	1.579	
Final R indices [I>2s(I), 15131 reflections]	R1 = 0.0621, *w*R2 = 0.0888	
R indices (all data)	R1 = 0.1169, *w*R2 = 0.0955	
Type of weighting scheme used	Sigma	
Weighting scheme used	$w=1/s^2(Fo^2)$	

Special Refinement Details

This crystal is a twin that mimics orthorhombic. The twin law employed was -1 0 0 0 -1 0 0 0 1 with a batch scale factor of 0.389.

Table 2. Atomic coordinates (x 10^4) and equivalent isotropic displacement parameters ($Å^2$x 10^3) for AJMM34 (CCDC 796320). U(eq) is defined as the trace of the orthogonalized U^{ij} tensor.

	x	y	z	U_{eq}
K(1)	2538(1)	2629(1)	3988(1)	27(1)
O(1A)	4171(1)	2812(1)	3342(1)	27(1)
O(2A)	3936(2)	2152(1)	4160(1)	29(1)
O(3A)	2208(2)	1903(1)	4119(1)	31(1)
O(4A)	810(1)	2382(1)	4078(1)	27(1)

O(5A)	1058(2)	3042(1)	3319(1)	30(1)
O(6A)	2784(2)	3304(1)	3331(1)	30(1)
B(1)	2940(3)	3003(1)	6046(2)	24(1)
C(1A)	4854(2)	2623(1)	3778(2)	33(1)
C(2A)	4692(2)	2245(1)	3681(2)	33(1)
C(3A)	3735(2)	1793(1)	4060(2)	32(1)
C(4A)	2900(2)	1714(1)	4519(2)	36(1)
C(5A)	1377(2)	1830(1)	4476(2)	36(1)
C(6A)	686(2)	2019(1)	3968(2)	32(1)
C(7A)	123(2)	2572(1)	3658(2)	37(1)
C(8A)	281(2)	2950(1)	3777(2)	35(1)
C(9A)	1236(2)	3402(1)	3373(2)	33(1)
C(10A)	2064(3)	3474(1)	2901(2)	37(1)
C(11A)	3588(2)	3354(1)	2897(2)	34(1)
C(12A)	4309(2)	3174(1)	3385(2)	34(1)
C(13A)	2071(2)	3156(1)	5548(2)	28(1)
C(14A)	1522(2)	3413(1)	6075(2)	32(1)
C(15A)	3517(2)	3310(1)	6498(2)	28(1)
C(16A)	3805(2)	3596(1)	5890(2)	32(1)
C(17A)	2686(2)	2707(1)	6760(2)	33(1)
C(18A)	2416(3)	2358(1)	6379(2)	45(1)
K(2)	2523(1)	134(1)	3935(1)	26(1)
O(1B)	2331(1)	-591(1)	4178(1)	25(1)
O(2B)	863(1)	-150(1)	4088(1)	27(1)
O(3B)	1004(1)	522(1)	3340(1)	28(1)
O(4B)	2735(1)	792(1)	3251(1)	28(1)
O(5B)	4172(1)	342(1)	3308(1)	25(1)
O(6B)	4006(1)	-281(1)	4252(1)	24(1)
B(2)	2350(2)	502(1)	5904(2)	26(1)
C(1B)	1484(2)	-692(1)	4459(2)	29(1)
C(2B)	800(2)	-510(1)	3921(2)	30(1)
C(3B)	126(2)	39(1)	3752(2)	30(1)
C(4B)	291(2)	416(1)	3876(2)	30(1)
C(5B)	1209(2)	878(1)	3463(2)	31(1)
C(6B)	1981(2)	968(1)	2916(2)	30(1)
C(7B)	3504(2)	852(1)	2764(2)	29(1)
C(8B)	4277(2)	708(1)	3245(2)	28(1)
C(9B)	4896(2)	184(1)	3757(2)	26(1)
C(10B)	4761(2)	-198(1)	3765(2)	25(1)
C(11B)	3872(2)	-648(1)	4291(2)	27(1)
C(12B)	3022(2)	-719(1)	4720(2)	28(1)
C(13B)	3083(2)	750(1)	5462(2)	30(1)
C(14B)	3628(2)	978(1)	6081(2)	34(1)
C(15B)	2857(2)	174(1)	6387(2)	29(1)
C(16B)	2264(2)	-89(1)	6800(2)	42(1)
C(17B)	1724(2)	716(1)	6552(2)	29(1)
C(18B)	1272(2)	1037(1)	6153(2)	32(1)
K(3)	2506(1)	9853(1)	9095(1)	27(1)
O(1C)	4160(1)	10159(1)	9082(1)	27(1)
O(2C)	3980(1)	9475(1)	8435(1)	26(1)
O(3C)	2260(1)	9186(1)	8436(1)	28(1)
O(4C)	831(1)	9647(1)	8433(1)	28(1)

O(5C)	992(1)	10302(1)	9216(1)	26(1)
O(6C)	2669(2)	10589(1)	9098(1)	29(1)
B(3)	2873(3)	9482(1)	11109(2)	30(1)
C(1C)	4866(2)	9967(1)	8714(2)	31(1)
C(2C)	4726(2)	9590(1)	8910(2)	27(1)
C(3C)	3798(2)	9119(1)	8577(2)	30(1)
C(4C)	3004(2)	9019(1)	8068(2)	30(1)
C(5C)	1471(2)	9120(1)	7964(2)	30(1)
C(6C)	717(2)	9281(1)	8425(2)	31(1)
C(7C)	101(2)	9817(1)	8799(2)	34(1)
C(8C)	234(2)	10202(1)	8732(2)	32(1)
C(9C)	1129(2)	10668(1)	9152(2)	31(1)
C(10C)	1995(2)	10757(1)	9561(2)	30(1)
C(11C)	3524(2)	10707(1)	9337(2)	30(1)
C(12C)	4186(2)	10514(1)	8840(2)	32(1)
C(13C)	2013(2)	9288(1)	10672(2)	32(1)
C(14C)	1465(2)	9065(1)	11286(2)	37(1)
C(15C)	2617(2)	9805(1)	11740(2)	40(1)
C(16C)	2373(2)	10134(1)	11292(2)	48(1)
C(17C)	3476(2)	9211(1)	11664(2)	33(1)
C(18C)	3800(2)	8892(1)	11193(2)	37(1)
K(4)	2442(1)	7637(1)	4108(1)	26(1)
O(1D)	1064(1)	7145(1)	4280(1)	26(1)
O(2D)	780(1)	7807(1)	3463(1)	25(1)
O(3D)	2132(1)	8311(1)	3492(1)	30(1)
O(4D)	3871(2)	8070(1)	3450(1)	30(1)
O(5D)	4189(1)	7405(1)	4171(1)	28(1)
O(6D)	2803(2)	6915(1)	4216(1)	29(1)
B(4)	2073(3)	8002(1)	6171(2)	26(1)
C(1D)	302(2)	7233(1)	3784(2)	28(1)
C(2D)	112(2)	7612(1)	3884(2)	33(1)
C(3D)	612(2)	8169(1)	3537(2)	30(1)
C(4D)	1310(2)	8361(1)	3065(2)	34(1)
C(5D)	2818(2)	8497(1)	3078(2)	31(1)
C(6D)	3668(2)	8428(1)	3526(2)	31(1)
C(7D)	4668(2)	7979(1)	3883(2)	34(1)
C(8D)	4843(2)	7601(1)	3743(2)	36(1)
C(9D)	4313(2)	7043(1)	4039(2)	32(1)
C(10D)	3659(2)	6845(1)	4555(2)	31(1)
C(11D)	2134(2)	6717(1)	4628(2)	31(1)
C(12D)	1288(2)	6790(1)	4179(2)	32(1)
C(13D)	2940(2)	8155(1)	5695(2)	28(1)
C(14D)	3512(2)	8404(1)	6245(2)	34(1)
C(15D)	2329(2)	7699(1)	6884(2)	37(1)
C(16D)	2563(3)	7352(1)	6505(2)	48(1)
C(17D)	1506(2)	8306(1)	6612(2)	28(1)
C(18D)	1225(2)	8600(1)	6017(2)	32(1)

1. van der Sluis, P.; Spek, A. L. *Acta Crystallogr A* **1990**, *46*, 194.